



**US Army Corps
of Engineers®**
Engineer Research and
Development Center

ERDC
INNOVATIVE SOLUTIONS
for a safer, better world

Airfield Damage Repair Modernization Program

AM2 Opposite Lay Evaluation

Lyan Garcia, Wipawi Vanadit-Ellis, Timothy W. Rushing,
Jeb S. Tingle, and Craig A. Rutland

June 2015



The US Army Engineer Research and Development Center (ERDC) solves the nation's toughest engineering and environmental challenges. ERDC develops innovative solutions in civil and military engineering, geospatial sciences, water resources, and environmental sciences for the Army, the Department of Defense, civilian agencies, and our nation's public good. Find out more at www.erdc.usace.army.mil.

To search for other technical reports published by ERDC, visit the ERDC online library at <http://acwc.sdp.sirsi.net/client/default>.

AM2 Opposite Lay Evaluation

Lyan Garcia , Wipawi Vanadit-Ellis, Timothy W. Rushing,
and Jeb S. Tingle

*Geotechnical and Structures Laboratory
U.S. Army Engineer Research and Development Center
3909 Halls Ferry Road
Vicksburg, MS 39180-6199*

Craig A. Rutland, PhD

*Engineering Division
Civil Engineering Branch
Air Force Civil Engineer Center
139 Barnes Drive, Suite 1
Tyndall AFB, FL 32403*

Final report

Approved for public release; distribution is unlimited.

Abstract

AM2 airfield matting has a long history of successful performance as an expeditionary airfield surfacing system. It has been used to form runways, vertical takeoff and landing pads, taxiways, and aircraft parking areas. A test program was initiated by the Naval Air Systems Command to evaluate and identify optimal AM2 lay patterns under different traffic conditions, and to validate a Dynamic Interface Model by feeding it mat breakage, deformation, and recorded strain data. The testing efforts discussed in this report focused on understanding the performance of AM2 when installed in the brickwork pattern on a weak subgrade and trafficked in a direction perpendicular to typical traffic operations. The mat test section was subjected to simulated F-15E and C-17 traffic until predetermined failure criteria were reached. The system became highly unstable after a limited number of F-15E and C-17 passes. Test results and discussions related to the stability of the system and structural integrity of the mat panels during traffic are provided.

DISCLAIMER: The contents of this report are not to be used for advertising, publication, or promotional purposes. Citation of trade names does not constitute an official endorsement or approval of the use of such commercial products. All product names and trademarks cited are the property of their respective owners. The findings of this report are not to be construed as an official Department of the Army position unless so designated by other authorized documents.

DESTROY THIS REPORT WHEN NO LONGER NEEDED. DO NOT RETURN IT TO THE ORIGINATOR.

Contents

Abstract	ii
Figures and Tables.....	v
Preface	viii
Unit Conversion Factors	ix
1 Introduction.....	1
1.1 Background.....	1
1.1.1 Naval Air Systems Command Dynamic Interface Model	1
1.1.2 AM2 certified configuration lay patterns	1
1.1.3 AM2 opposite lay test	3
1.2 Objective and scope	3
2 Experimental Program.....	5
2.1 Materials	5
2.1.1 AM2 airfield mat.....	5
2.1.2 High-plasticity clay (CH) subgrade.....	6
2.2 Test section general description.....	6
2.3 Test section construction	9
2.3.1 Subgrade construction and posttest forensics	9
2.3.2 AM2 strain gauge instrumentation	16
2.3.3 AM2 mat installation.....	20
2.4 Traffic application	22
2.4.1 F-15E load cart.....	22
2.4.2 C-17 load cart.....	23
2.5 Data collection.....	24
2.5.1 Centerline profile.....	26
2.5.2 Unloaded cross sections.....	26
2.5.3 Loaded cross sections	27
2.5.4 Strain measurements	27
2.5.5 Borescope observation	27
2.6 Failure criteria.....	28
2.6.1 Mat breakage	28
2.6.2 Permanent deformation	29
3 Test Results.....	31
3.1 Behavior of mat under traffic (visual observations)	31
3.1.1 F-15E test item.....	31
3.1.2 C-17 test item.....	31
3.2 Permanent deformation	31
3.3 Strain gauge data	37

3.3.1	<i>F-15E item</i>	38
3.3.2	<i>C-17 item</i>	38
4	Analysis of Results	54
4.1	Mat behavior	54
4.1.1	<i>F-15E item</i>	54
4.1.2	<i>C-17 item</i>	54
4.2	Permanent deformation	55
4.2.1	<i>Centerline profile</i>	55
4.2.2	<i>Cross sections</i>	55
4.3	Strain gauge readings	56
5	Conclusions and Recommendations	60
5.1	Conclusions.....	60
5.2	Recommendations	61
References		62
Appendix A: Strain gauge data for F-15E item		64
Appendix B: Strain gauge data for C-17 item		120
Report Documentation Page		

Figures and Tables

Figures

Figure 1. (a) F71 and (b) F72 mat packages.....	5
Figure 2. Gradation curve for Vicksburg Buckshot high-plasticity clay (CH).....	7
Figure 3. Dry density vs. moisture content for CH subgrade material.....	7
Figure 4. CBR vs. moisture content for CH subgrade material.....	8
Figure 5. Test section profile.....	8
Figure 6. AM2 mat opposite lay panel layout.....	9
Figure 7. Test section excavation.....	10
Figure 8. Test pit lined with impervious sheeting	10
Figure 9. Pulverizing CH.....	11
Figure 10. Addition of water to adjust moisture content.	12
Figure 11. Leveling CH material in test pit prior to compaction.....	12
Figure 12. Compacting CH subgrade with pneumatic roller.	13
Figure 13. Nuclear moisture-density gauge test.....	13
Figure 14. Field CBR test.....	14
Figure 15. Strain gauge on lower overlap region of AM2 panel end connector.	16
Figure 16. Strain gauge locations at F-joint.....	17
Figure 17. Strain gauge location on the female hinge connector of AM2.	17
Figure 18. Typical strain gauge placement on female hinge connector of AM2 panel.	18
Figure 19. Modification to male hinge of AM2 panel.....	18
Figure 20. Test section instrumentation layout.....	19
Figure 21. Insertion of aluminum locking bar between adjacent panels.....	21
Figure 22. Installation of AM2 panel on the test section subgrade.....	21
Figure 23. Final assembled test section.....	22
Figure 24. F-15E test load cart.....	23
Figure 25. Plan view showing F-15E normally distributed traffic lanes.....	23
Figure 26. C-17 test load cart.....	24
Figure 27. Plan view showing C-17 normally distributed traffic lanes.....	25
Figure 28. Data collection layout for each test item.....	26
Figure 29. Surveying centerline profile.....	27
Figure 30. Typical survey of loaded cross section.	28
Figure 31. Subgrade centerline profile in the F-15E item after 524 passes.....	32
Figure 32. Centerline profile on the subgrade in the C-17 item after 392 passes.	33
Figure 33. Centerline profile on the mat surface in the F-15E item.	33
Figure 34. Centerline profile on the mat surface in the C-17 item.....	34
Figure 35. Average deformation on the subgrade in the F-15E after 524 passes.	34

Figure 36. Average deformation on the subgrade in the C-17 item after 392 passes.....	35
Figure 37. Average deformation on the loaded mat surface in the F-15E item.....	35
Figure 38. Average deformation on the loaded mat surface in the C-17 item.....	36
Figure 39. Average deformation on the unloaded mat surface in the F-15E item.....	36
Figure 40. Average deformation on the unloaded mat surface in the C-17 item.....	37
Figure 41. F-15E item, gauge C90F1, passes 17-32.....	39
Figure 42. F-15E item, gauge C90F2, passes 17-32.....	40
Figure 43. F-15E item, gauge C91F1, passes 17-32.....	40
Figure 44. F-15E item, gauge C91F2, passes 17-32.....	41
Figure 45. F-15E item, gauges C95C1, passes 17-32.....	41
Figure 46. F-15E item, gauge C95C2, passes 17-32.....	42
Figure 47. Maximum tensile strain for panel C87 at F-joint.....	42
Figure 48. Maximum compressive strain for panel C87 at F-joint.....	43
Figure 49. Maximum tensile strain for panels C90 and C91 at F-joint.....	43
Figure 50. Maximum compressive strain for panels C90 and C91 at F-joint.....	44
Figure 51. Maximum tensile strain for panels C94 and C95 at F-joint.....	44
Figure 52. Maximum compressive strain for panels C94 and C95 at F-joint.....	45
Figure 53. Max tensile strain for panels C82, C94 and C95 at C-joint.....	45
Figure 54. Max compressive strain for panels C82, C94 and C95 at C-joint.....	46
Figure 55. C-17 item, gauge C30F1, passes 13-24.....	46
Figure 56. C-17 item, gauge C30F2, passes 13-24.....	47
Figure 57. C-17 item, gauge C31F1, passes 13-24.....	47
Figure 58. C-17 item, gauge C31F2, passes 13-24.....	48
Figure 59. C-17 item, gauge C39C1, passes 13-24.....	48
Figure 60. C-17 item, gauge C39C2, passes 13-24.....	49
Figure 61. Maximum tensile strain for panels C30 and C31 at F-joint.....	49
Figure 62. Maximum compressive strain for panels C30 and C31 at F-joint.....	50
Figure 63. Maximum tensile strain for panels C34 and C35 at F-joint.....	50
Figure 64. Maximum compressive strain for panels C34 and C35 at F-joint.....	51
Figure 65. Maximum tensile strain for panels C38 and C39 at F-joint.....	51
Figure 66. Maximum compressive strain for panels C38 and C39 at F-joint.....	52
Figure 67. Maximum tensile strain for panels C26,C38 and C39 at C-joint.....	52
Figure 68. Maximum compressive strain for panels C26,C38 and C39 at C-joint.....	53
Figure 69. Maximum strains for F-15E Test Item.....	57
Figure 70. Maximum strains for C-17 test item.....	58

Tables

Table 1. AM2 testing program.....	2
Table 2. Summary of AM2 brickwork pattern subgrade sensitivity testing results.....	3
Table 3. Mat properties.....	6

Table 4. Average in situ properties of the subgrade in each test item.....	15
Table 5. Strain gauge installation locations.....	19
Table 6. Data collection intervals for F-15E traffic.....	25
Table 7. Data collection intervals for the C-17 test item.	25
Table 8. Maximum values of measured permanent deformation for each test item.....	32

Preface

This study was conducted for the U.S. Naval Air Systems Command (NAVAIR) Expeditionary Airfield (EAF) team and the U.S. Air Force Civil Engineer Center (AFCEC). Technical oversight was provided by Jeb S. Tingle.

The work was performed by the Airfields and Pavements Branch (GMA) of the Engineering Systems and Materials Division (GM), U.S. Army Engineer Research and Development Center, Geotechnical and Structures Laboratory (ERDC-GSL). At the time the research was conducted, Dr. Gary L. Anderton was Chief, CEERD-GMA; Dr. Larry N. Lynch was Chief, CEERD-GM; and Dr. David A. Horner, CEERD-GVT, was the Technical Director for Force Projection and Maneuver Support. The Deputy Director of ERDC-GSL was Dr. William P. Grogan, and the Director was Dr. David W. Pittman.

At the time the research was conducted, COL Jeffrey R. Eckstein was the Commander of ERDC, and Dr. Jeffery P. Holland was the Director.

Unit Conversion Factors

Multiply	By	To Obtain
cubic feet	0.02831685	cubic meters
feet	0.3048	meters
inches	0.0254	meters
kip-inches	112.948	newton-meters
pounds (force)	4.448222	newtons
pounds (force) per square foot	47.88026	pascals
pounds (force) per square inch	6.894757	kilopascals
pounds (mass)	0.45359237	kilograms
square feet	0.09290304	square meters
square inches	6.4516 E-04	square meters

1 Introduction

1.1 Background

1.1.1 Naval Air Systems Command Dynamic Interface Model

AM2 aluminum matting has been the primary temporary airfield matting system used by the U.S. military since the late 1960s. AM2 was developed by the U.S. Navy but has been adopted for use by the U.S. Air Force (USAF) and U.S. Army for fixed-wing and rotary-wing operational surfaces. Over the years, AM2 has been modified to address limiting structural concerns. The current production version of AM2 is modification (Mod) 5.

An AM2 surface is comprised of interlocking 2-ft by 12-ft full panels and 2-ft by 6-ft half-panels that are 1.5 in. thick. An AM2 mat expanse can be assembled to form runways, vertical takeoff and landing (VTOL) pads, taxiways, and aircraft parking areas. The Naval Air Systems Command (NAVAIR) developed a Dynamic Interface Model (DIM) to analyze aircraft landings and takeoffs on AM2. The model was validated through laboratory subscale tests, but additional development and validation was required to accurately model the matting-soil interaction for various installation patterns. Therefore, a program was initiated to validate the model through full-scale testing using simulated fighter and cargo aircraft loads. The NAVAIR Expeditionary Airfield Team (EAF) partnered with the Air Force Civil Engineer Support Center (AFCEC) to sponsor the evaluations listed in Table 1.

1.1.2 AM2 certified configuration lay patterns

Descriptions of the placement or lay patterns in Table 1 (brickwork, 2-1, and 3-4) are provided in NAWCADLKE-MISC-48J200-0011. The individual patterns were established as part of an initiative to optimize the use of 6-ft half-panels. The original AM2 shipping package, F44, contained sixteen 12-ft panels and four 6-ft panels. Each package was designed to allow assembly of two 108-ft-wide rows or four 54-ft-wide rows in a brickwork configuration with no continuous longitudinal joints. The brickwork pattern improves the load-carrying capability of the system. Since 6-ft panels are used only for the row ends, more 12-ft panels are required for assembly. However, ship transportation of the mats across the globe led to a need for the mats to be shipped on an International

Organization for Standardization (ISO) flat rack for compatibility with other containerized goods. A decision was made by the U.S. Navy to re-package AM2 into new shipping packages, resulting in the F71 and F72 shipping configurations.

Table 1. AM2 testing program.

Test sequence	Test Name	AM2 lay pattern	Condition of AM2 mat	F-15E traffic	C-17 traffic
1	In-plane bow on asphalt surface	Brickwork	New	N/A	N/A
2	Vehicle braking test on asphalt surface	Brickwork	New	N/A	N/A
3	Brickwork on voided subgrade (CBR of 6)	Brickwork	New and Refurbished	Yes	-
4	Brickwork on CBR of 6	Brickwork	New and Refurbished	Yes	Yes
5	In-plane bow on CBR of 6	Brickwork	New	N/A	N/A
6	Opposite Lay on CBR of 6*	Brickwork	New	Yes	Yes
7	3-4 Lay on CBR of 6	3-4	New	Yes	Yes
8	2-1 Lay on CBR of 6	2-1	New	Yes	Yes
9	Brickwork on voided subgrade (CBR of 6)	Brickwork	New	Yes	-
10	Brickwork on CBR of 6	Brickwork	New	Yes	Yes

*Traffic applied parallel to long dimension of AM2 panels

The F71 contains eighteen 12-ft mats, and the F72 contains eighteen 6-ft mats. The new configurations allow one F71 and one F72 to be placed end-to-end on a 20-ft ISO flat rack and optimize use of the available space. The new package configuration also reduced confusion when designing a mat surface. In some instances, F44 packages were re-bundled with different numbers of 6-ft panels inside the 12-ft mat packages. Separating the panels into the F71 and F72 packages eliminated the need to include mixed sizes in packages and improved the accuracy of panel inventories.

The optimization of packaging and shipping of AM2 required equal numbers of 12-ft and 6-ft mat panels to be delivered with each AM2 order. Since only a fraction of the available 6-ft panels are needed to assemble a brickwork pattern, many extra 6-ft panels were unused. To optimize mat use, NAVAIR EAF created an allowance for two alternate assembly patterns, the 2-1 and the 3-4 lay patterns. Although the two patterns were approved by NAVAIR EAF, they had not been evaluated under simulated aircraft

loading conditions to determine if any reduction in the number of allowable passes was caused by the allowance of continuous longitudinal joints. Therefore, they were included in the test program. Results for the 3-4 lay pattern are reported in ERDC/GSL TR-14-38 (Rushing et al. 2014). Results for the 2-1 lay pattern are being analyzed.

1.1.3 AM2 opposite lay test

Although the brickwork pattern has been evaluated over different subgrade materials and strengths (Table 2), information obtained from these tests was not sufficient to validate the DIM. Therefore, NAVAIR and AFCEC included testing of the brickwork pattern in the program with appropriate strain gauge instrumentation at the end connector joint to use as input for the DIM. NAVAIR EAF was also interested in gathering information for the condition where an aircraft would traffic parallel to the long dimension of the mat (90 deg to the typical direction of traffic), which could routinely occur on aprons and large VTOL pads. There was concern as to the stability of the panels and the effect the different traffic conditions would have on roughness and rutting of the system. It was decided to include the opposite lay test, assembled in the brickwork pattern, in the testing program. The brickwork pattern was chosen to make an accurate assessment by comparing to the results in Table 2.

Table 2. Summary of AM2 brickwork pattern subgrade sensitivity testing results.

Sustained Traffic Passes			
Subgrade Strength (CBR)	F-15E	C-17	Reference
6	1,500	1,500	Rushing and Tingle (2007)
10	3,000	6,000	Rushing et al. (2008)
15	4,100	7,000	Rushing and Mason (2008)
25	6,300	10,000*	Garcia et al. (2014a)
100	23,000	-	Garcia et al. (2014b)

* Failure was not achieved. Trafficking was stopped because of time constraints.

1.2 Objective and scope

The objectives of this effort were to evaluate AM2 mat turned 90 deg to typical traffic application, referred to as opposite lay, under simulated aircraft traffic over a weak subgrade to determine the number of allowable passes and to record strain and subgrade deformation data to calibrate the DIM. To accomplish these objectives, a full-scale test section was

constructed with a 36-in.-deep high-plasticity clay (CH) subgrade processed to a CBR of 6. The subgrade was surfaced with AM2 mat panels installed in a brickwork lay pattern and trafficked with load carts simulating F-15E and C-17 aircraft traffic until pre-defined failure criteria were achieved.

2 Experimental Program

The following sections describe the AM2 airfield mat, construction of the full-scale test section, traffic application, data collection, and the failure criteria.

2.1 Materials

2.1.1 AM2 airfield mat

AM2 airfield mat was developed in the 1960s under a program sponsored by the Naval Air Engineering Center, Philadelphia, PA. Various versions of AM2 were tested under simulated aircraft loads at the U.S. Army Engineer Waterways Experiment Station in Vicksburg, MS, from 1961 through 1971, with major procurements beginning in 1965. The original AM2 mat has been modified through the years to address limiting structural concerns. The current production version of AM2, modification version 5, was obtained from NAVAIR, Lakehurst, NJ. Photographs of the AM2 F71 and F72 packages similar to those used in this test are shown in Figure 1.

Figure 1. (a) F71 and (b) F72 mat packages.



(a)

(b)

Pertinent properties of the AM2 mat used in this evaluation are shown in Table 3. Each full panel was 24 in. by 144 in. by 1.5 in. and fabricated from a single 6061-T6 aluminum alloy extrusion with end connectors welded to the 24-in. ends to form a complete panel. The core of the extruded panels was comprised of vertical stiffeners spaced 1.75 in. apart in the 12-ft direc-

tion. The panels were joined along the two 144-in. edges by a hinge-type male/female connection (C-joint). The adjacent 24-in. ends were joined by an overlap/underlap connection secured by an aluminum locking bar (F-joint). The panels were coated with a nonskid material to increase the surface friction. The AM2 panels were delivered in F71 and F72 packages and were in new condition. The panels were visually inspected to ensure that they had not been damaged prior to testing and to make certain they met procurement specifications for AM2 matting.

Table 3. Mat properties.

	Full panel	Half-panel
Length (in.)	144.0	72.0
Width (in.)	24.0	24.0
Thickness (in.)	1.5	1.5
Panel Weight (lbf)	145.5	74.4
Unit Weight (lbf/ft ²)	6.1	6.3

2.1.2 High-plasticity clay (CH) subgrade

The CH material used for subgrade construction was procured from a local source in Vicksburg and was subjected to laboratory tests including a grain-size analysis (hydrometer), Atterberg Limits, modified-Proctor compaction, and un-soaked CBR testing. Classification data for the subgrade soil is shown in Figure 2. The moisture-density and CBR-moisture content relationships are shown in Figures 3 and 4, respectively. These data were used to determine the target moisture content and dry density required to obtain the target CBR of 6.

2.2 Test section general description

The tests were conducted on a full-scale test section constructed and trafficked under shelter in the Hangar 4 pavement test facility at the ERDC. AM2 mat panels were placed directly over a 36-in.-deep CH subgrade prepared to a target CBR of 6 over an existing silt foundation, as shown in Figure 5. The mat panels were trafficked until failure, as described later in this chapter.

Figure 2. Gradation curve for Vicksburg Buckshot high-plasticity clay (CH).

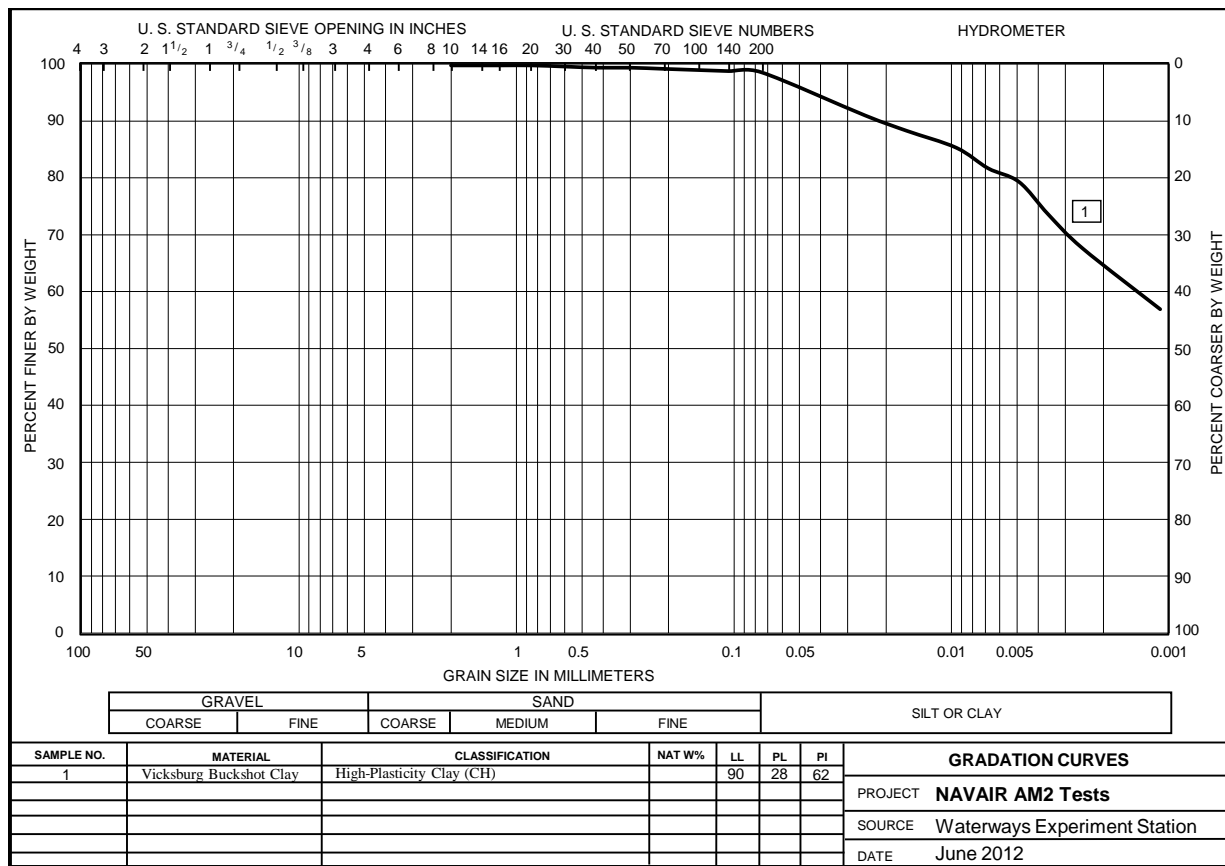


Figure 3. Dry density vs. moisture content for CH subgrade material.

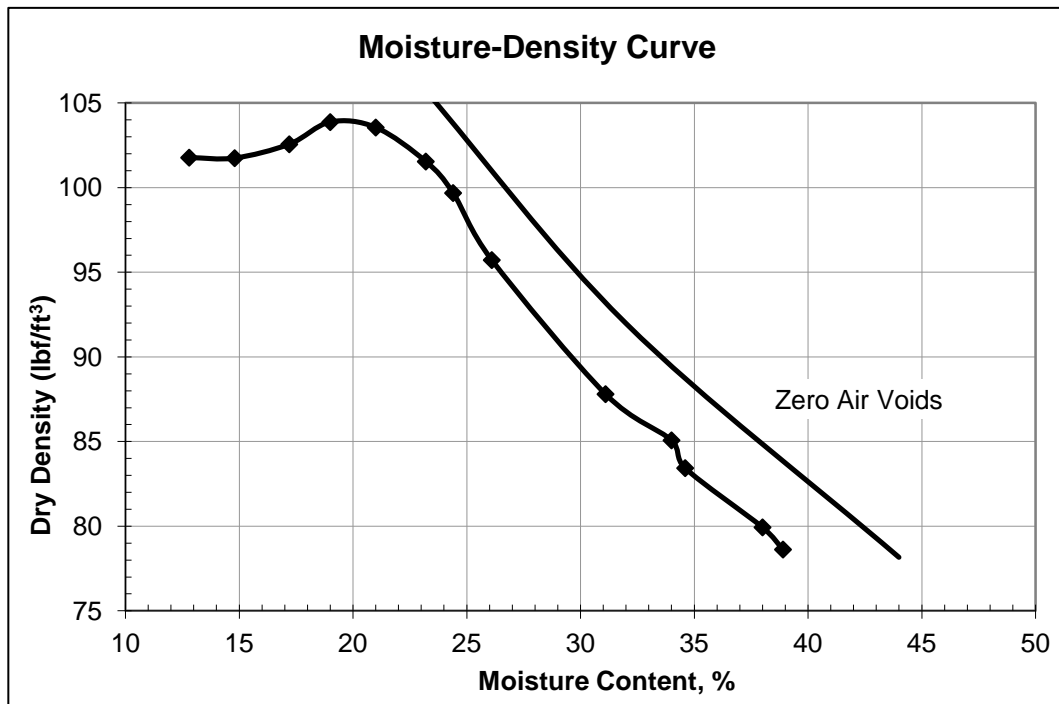


Figure 4. CBR vs. moisture content for CH subgrade material.

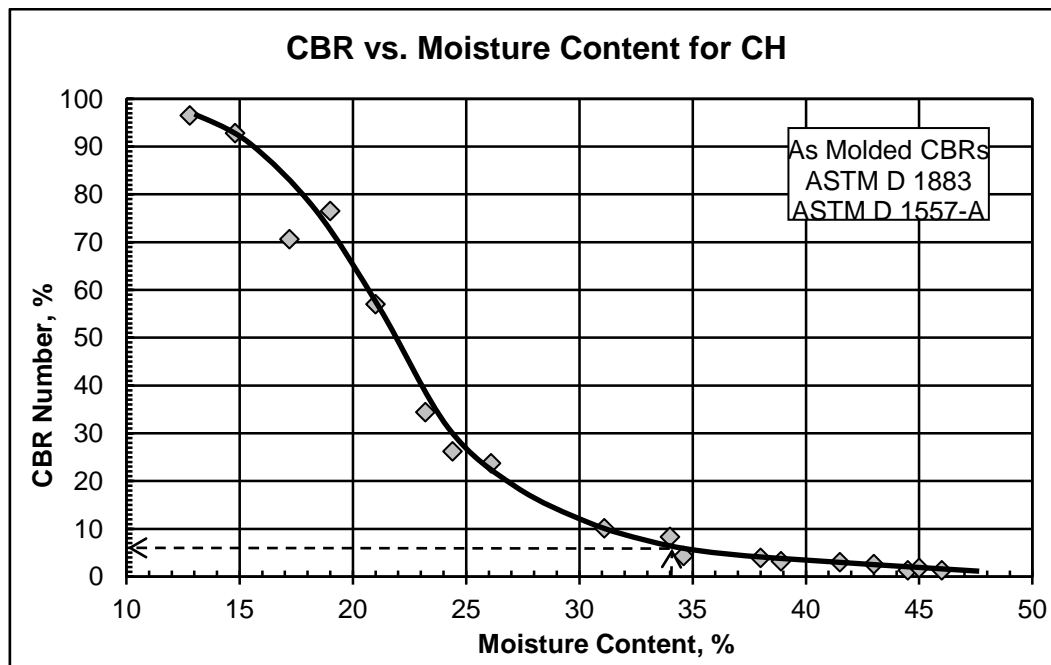
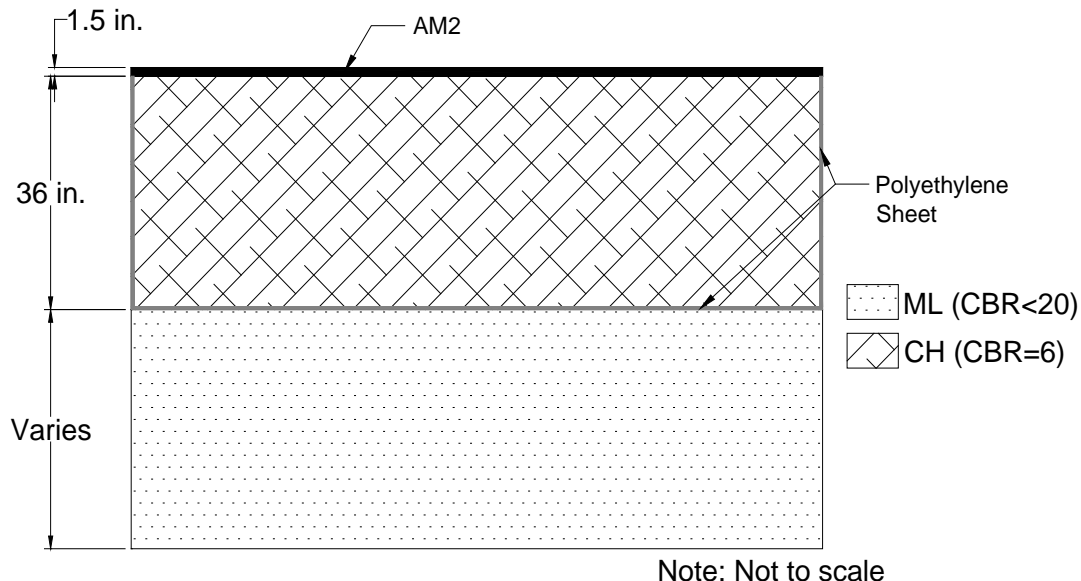


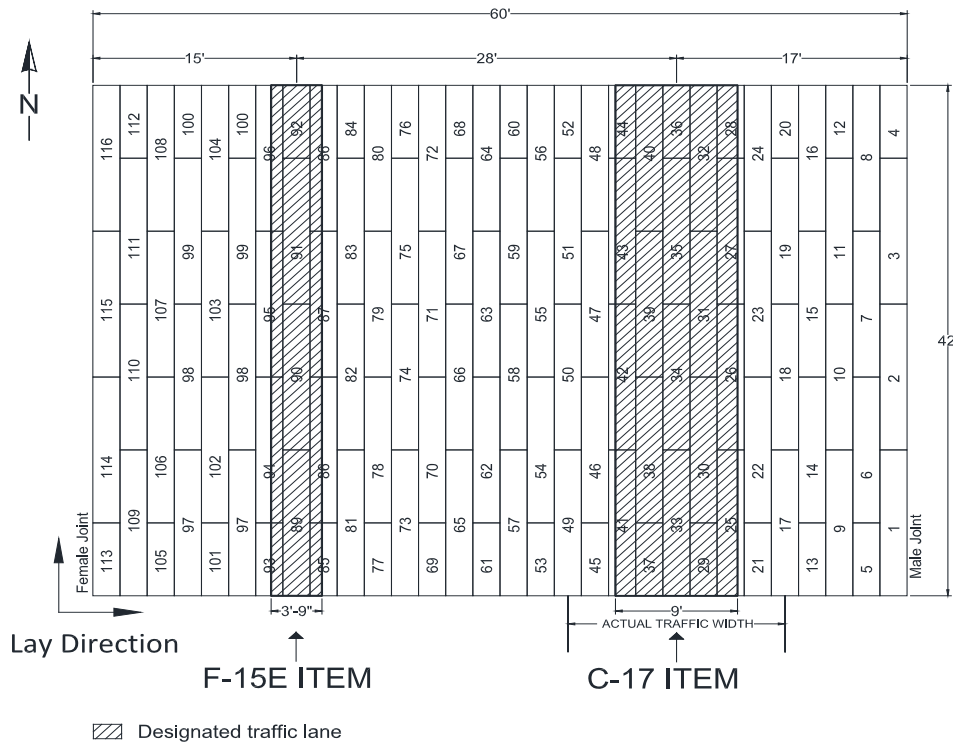
Figure 5. Test section profile.



A general layout of the test section, along with panel designations, is shown in Figure 6. Each panel was identified with a number to track damage during trafficking. The test section consisted of a 60-ft-wide by 42-ft-long section of matting that was subsequently divided into two test items. An area centered 15 ft from the west edge of the test section had a 3.75-ft-wide lane designated for simulated F-15E traffic, and an area

centered 17 ft from the east edge had a 9-ft-wide lane designated for simulated C-17 traffic. Lanes for the F-15E and C-17 items were trafficked according to normally distributed wander patterns associated with the F-15E and C-17 aircrafts, which are described later in this chapter.

Figure 6. AM2 mat opposite lay panel layout.



2.3 Test section construction

The following sections describe the construction of the foundation subgrade and the AM2 mat installation. Field and laboratory soil testing data used to determine the moisture, density, and bearing capacity in terms of CBR are also included.

2.3.1 Subgrade construction and posttest forensics

The test section subgrade was built using in-place material from the “In Plane Bow” test section constructed to a CBR of 6 (Table 1). The original subgrade was constructed by excavating a 60-ft-wide by 42-ft-long test pit to a minimum 36-in. depth below the existing finished grade in Hangar 4, as shown in Figure 7. The soil at the bottom of the excavation was a silt material (ML) having a CBR less than 20. The existing ML material was leveled with a bulldozer and compacted with a pneumatic roller and a

vibratory steel-wheel compactor to ensure that the remainder of the test section was constructed over a stable foundation. The bottom and sides of the test pit were lined with impervious 6-mil polyethylene sheeting to minimize moisture migration from the 36 in. of new CH soil serving as the test section subgrade, as shown in Figure 8.

Figure 7. Test section excavation.



Figure 8. Test pit lined with impervious sheeting.



The CH was processed at a nearby preparatory site by spreading the material to a uniform 12-in. depth, pulverizing the material with a rotary mixer, adjusting the moisture content, and pulverizing the material again, as shown in Figures 9 and 10. This was an iterative process necessary to achieve a uniform distribution of moisture throughout the material. Once the CH had been processed to the target moisture content, the material was placed in the test section, spread and leveled by a bulldozer in 8-in. lifts, and then compacted with a pneumatic roller to a compacted thickness of 6 in., as shown in Figures 11 and 12.

Each compacted lift was subjected to nuclear moisture/density tests (ASTM D 6938), as shown in Figure 13, in addition to convection oven moisture determination tests (ASTM D 4643) to verify that target values had been met. In situ CBR tests (CRD-C654-95), as shown in Figure 14, were conducted at four locations on every 6-in. compacted lift to verify that the target CBR of 6 had been reasonably achieved. If the average pretest CBR of a lift differed from the target value by more than +1.0 or -0.5 CBR, the lift was reconstituted. Each lift was surveyed to obtain an average thickness. After data collection, the surface was scarified with a rotary mixer to an average depth of 1 in. prior to placement of the following lift to facilitate bonding at the interface.

Figure 9. Pulverizing CH.



Figure 10. Addition of water to adjust moisture content.



Figure 11. Leveling CH material in test pit prior to compaction.



Figure 12. Compacting CH subgrade with pneumatic roller.

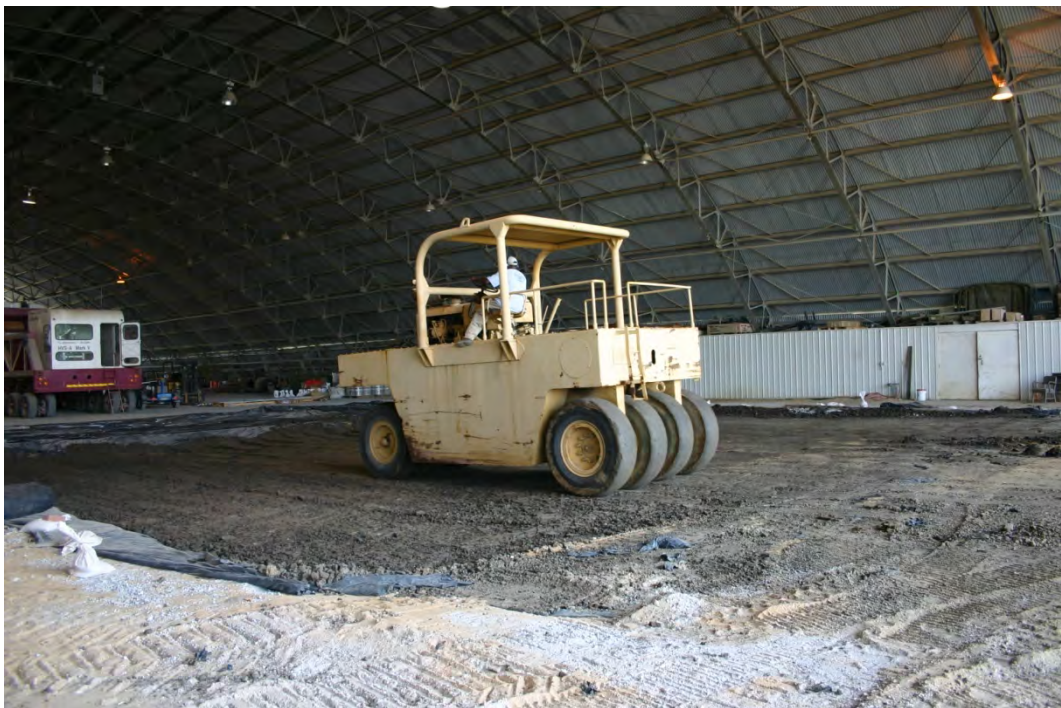


Figure 13. Nuclear moisture-density gauge test.



Figure 14. Field CBR test.



For the opposite lay test section, the upper 12 in. of the existing test bed were removed and reprocessed. Field CBR tests indicated that the existing material from 12 in. to 36 in. retained a CBR of approximately 6; therefore, reconstruction of the entire depth was unnecessary. The reprocessed material was replaced in two 6-in. lifts. Field CBR tests were performed on each lift at stations 10 and 30 along the centerline of each test item to ensure the target CBR of 6 was achieved.

After the mat testing had been completed, the in situ CBR, moisture, and density measurements were used to determine the depth of subgrade that might have undergone gradual drying and possible densification under traffic. The results of the CBR, moisture, and density tests during construction (pretest) and after trafficking (posttest) for both test items are shown in Table 4. Some increase in CBR was expected because of thixotropic properties of clay structures and gradual drying and densification during trafficking. Based on historic testing data, surface increases less than 5 CBR and 6-in.-deep increases less than 3 CBR are common and, therefore, acceptable (Rushing and Tingle, 2007; Rushing and Torres, 2007; Rushing et al., 2011; Garcia et al., 2012; Rushing et al., 2012).

Table 4. Average in situ properties of the subgrade in each test item.

Test Depth	Wet Density ^a (lbf/ft ³)	Dry Density ^a (lbf/ft ³)	Moisture ^a (%)	Oven Moisture (%)	In Situ CBR (%)	Change in CBR (%)
Pretest F-15E Item						
Surface ^b	119.2	91.5	30.5	-	6.7	-
6 in. ^b	119.7	93.2	28.5	30.8	6.1	-
12 in.	118.8	92.3	28.7	29.1	6.2	-
18 in.	118.1	91.4	29.3	31.3	6.1	-
24 in.	116.3	87.6	32.7	27.2	5.7	-
30 in.	117.5	88.9	32.0	32.6	6.2	-
Posttest F-15E Item						
Surface	120.0	92.1	30.3	27.6	9.6	2.9
Pretest C-17 Item						
Surface ^b	119.7	92.0	29.5	-	6.2	-
6 in. ^b	119.2	91.7	30.0	29.8	5.5	-
12 in.	116.1	88.7	30.8	32.2	5.8	
18 in.	117.1	90.1	29.9	30.8	6.0	
24 in.	115.1	88.5	30.2	27.5	5.9	
30 in.	115.2	86.9	32.7	33.2	6.1	
Posttest C-17 Item						
Surface	121.1	93.5	29.5	29.5	8.2	2.0

^a Readings are from nuclear density gauge.

^b New compacted lift.

The pretest moisture content and density measurements presented in Table 4 generally follow the trends found from laboratory measurements presented in Figures 3 and 4. However, previous experience has shown that the field moisture content required to construct a CBR of 6 typically ranges from 30% to 32% instead of 34% as suggested in Figure 4. This occurs because of the higher compaction energy used in the field compared to laboratory compaction effort.

For the F-15E test item, the posttest CBR measurements at the surface increased from 6.7 to 9.6 CBR during trafficking. For the C-17 test item, the posttest CBR measurements at the surface increased from 6.2 to 8.2. Since surface CBR increases were less than 5 CBR and remained within

acceptable limits throughout testing, additional testing 6 in. below the surface was not required.

2.3.2 AM2 strain gauge instrumentation

Prior to installation of the test mat, 14 individual mat panels were instrumented with a total of 24 foil strain gauges on the upper underlap or lower overlap regions of the 2-ft end connectors. A total of 12 foil strain gauges were installed in female hinge connectors. Gauge locations on the F-joint (underlap and overlap end connection) and C-joint (male and female hinge connection) and typical placement on a panel section are shown in Figures 15 through 18. A small section of the rim of the male joint was removed to ensure proper housing for a strain gauge placed on the joining female connector, as shown in Figure 19. The gauges were installed by the Applied Research Laboratory (ARL) at Pennsylvania State University (PSU) under a contract with NAVAIR. The mats with gauges were delivered to the ERDC for this evaluation. The locations of gauged panels in the test array are shown in Figure 20. The number and location of gauges installed on each panel are detailed in Table 5.

Figure 15. Strain gauge on lower overlap region of AM2 panel end connector.



Figure 16. Strain gauge locations at F-joint.

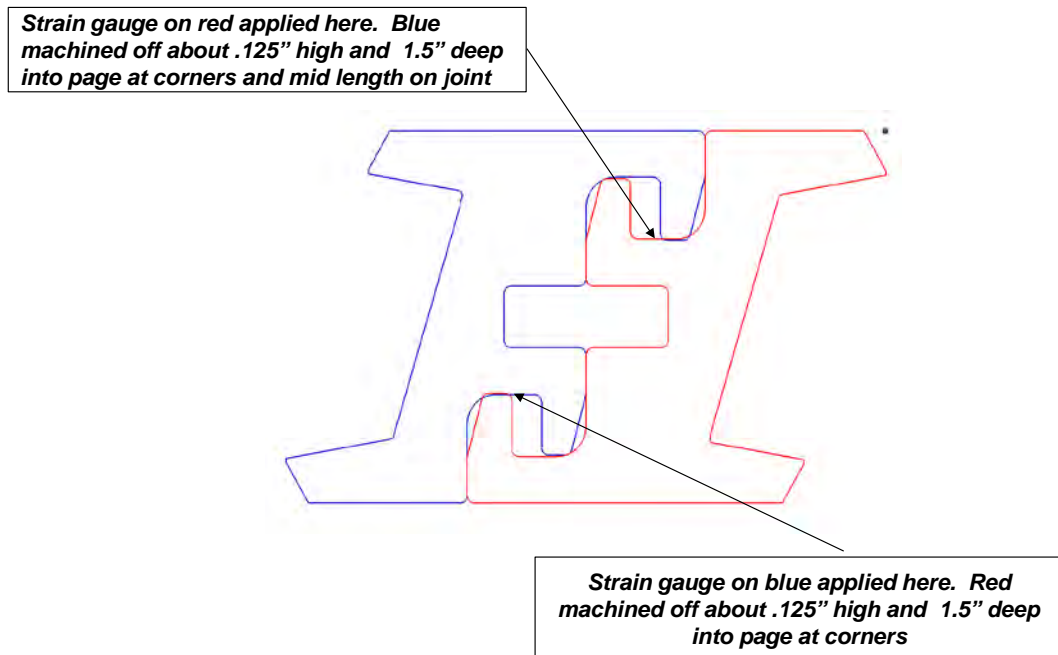


Figure 17. Strain gauge location on the female hinge connector of AM2.

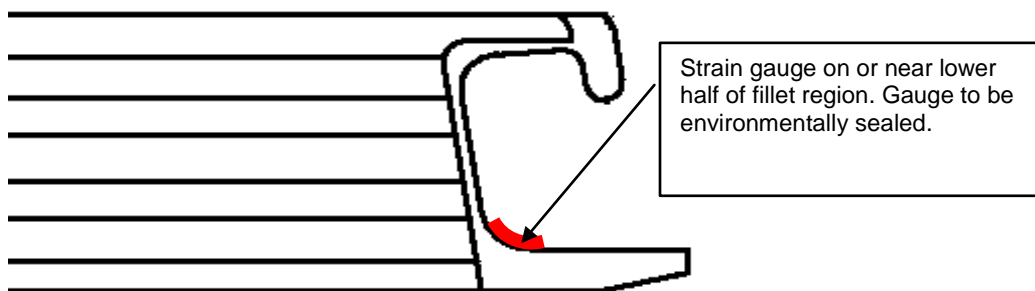


Figure 18. Typical strain gauge placement on female hinge connector of AM2 panel.



Figure 19. Modification to male hinge of AM2 panel.



Figure 20. Test section instrumentation layout.

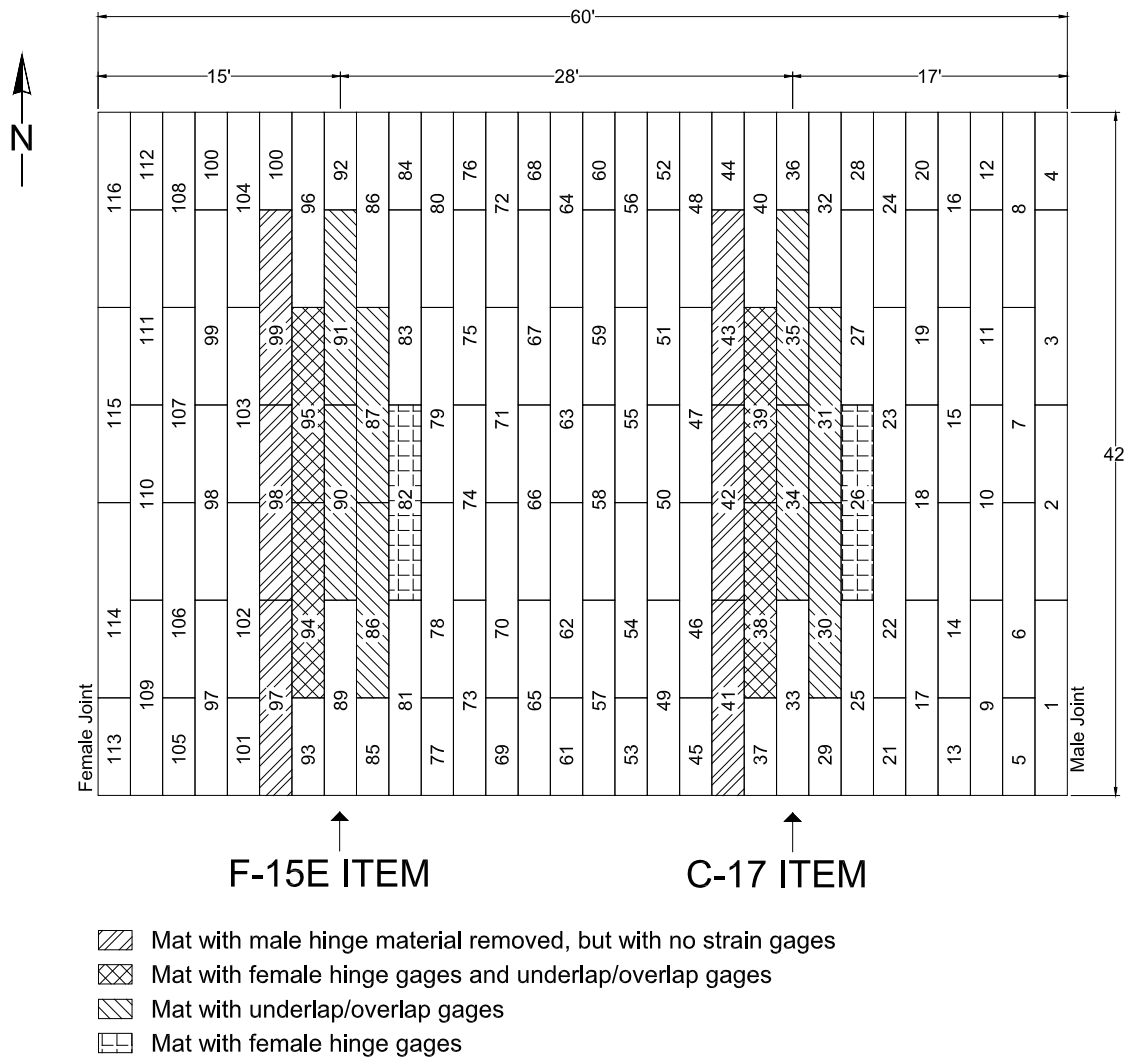


Table 5. Strain gauge installation locations.

Gauge Installation Location	Test item	C-joint	F-joint	
		Female hinge	Upper Underlap	Lower Overlap
Panel number (gauge count)	F-15E	82 (2)	94 (2)	95 (2)
		94 (2)	90 (2)	91 (2)
		95 (2)	86 (2)	87 (2)
	C-17	26 (2)	38 (2)	39 (2)
		38 (2)	34 (2)	35 (2)
		39 (2)	30 (2)	31 (2)

The strain gauges were used to gather critical strain information for calibrating the DIM. The DIM showed the installation regions on the prongs of the F-joint to be the component most susceptible to breaking. These regions have also been shown to be the predominant failure regions in full-scale tests of AM2 reported by Rushing and Tingle (2007), Rushing and Torres (2007), Rushing et al. (2008), Rushing and Mason (2008), and Garcia and Rushing (2013). The data gathered will be used to validate the DIM for NAVAIR and future modeling efforts by the ERDC.

2.3.3 AM2 mat installation

The AM2 airfield mat system was placed on the surface of the prepared test section subgrade by an experienced labor crew. The mat bundles were placed on the test section with a forklift, and the individual panels were carried by two men and placed into position.

For the opposite lay, the first mat panel was placed flat on the ground with the long dimensions parallel to the direction of traffic and with the male hinge connector facing east. The second panel was positioned adjacent to the 2-ft end of the first, allowing the overlapping end connector of the second panel to drop into position over the underlapping end connector of the first panel. A rectangular slot was formed between the two end connector rails, and an aluminum locking bar was inserted into the slot, as shown in Figure 21. This locking bar prevented the ends of the mat panels from separating. This process was continued until the first row was installed. For the second row, the 12-ft female hinge connector was attached to the male hinge connector of panels from the first row, and the panel was pivoted into place. The next panel was installed by attaching the female hinge connector to the male hinge connector of panels in the first row and allowing the overlapping end connector rail to pivot over and connect to the underlapping end connector rail of the adjacent panel (Figure 22). An aluminum locking bar was inserted into the space provided to keep the panels from separating. This process was repeated until the entire mat test section was assembled in the brickwork configuration.

Once assembly was complete, full-panels of AM2 were installed along the ends of the traffic lanes to facilitate the entrance and exit of the test vehicles. H-connectors were attached to the ends of the panels in the north and south edges of the test section to facilitate ramp installation. A photograph of the final assembled test section is shown in Figure 23. Once the mats had been installed, 1,000-lb steel weights were placed along the edges of the test section to anchor the mats and simulate the resistance to movement provided by a large expanse of matting.

Figure 21. Insertion of aluminum locking bar between adjacent panels.



Figure 22. Installation of AM2 panel on the test section subgrade.



Figure 23. Final assembled test section.



2.4 Traffic application

This section describes the application of simulated aircraft traffic on the AM2 airfield mat system. Pertinent data concerning the test load carts are provided.

2.4.1 F-15E load cart

A specially designed single-wheel load cart was used to simulate F-15E aircraft traffic. The load cart was equipped with a 36-in.-by-11-in., 30-ply tire inflated to 325 lbf/in.² and loaded such that the test wheel was supporting 35,235 lb. The F-15E load cart was equipped with an outrigger wheel to prevent overturning and was powered by the prime mover of a Case vibratory steel-wheel roller as shown in Figure 24.

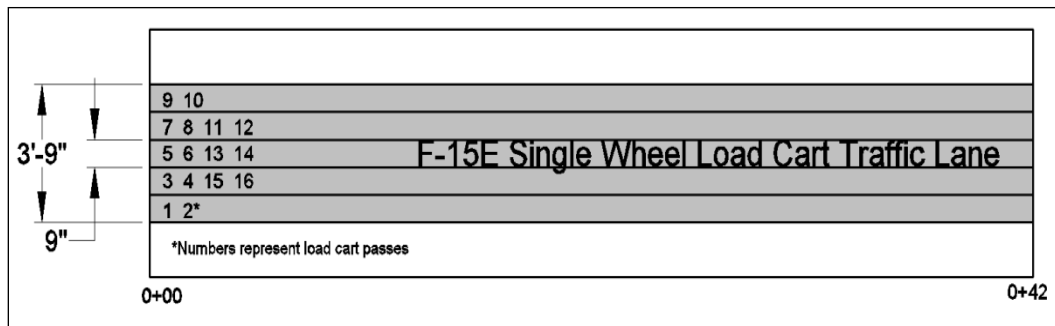
A normally distributed pattern of simulated traffic was applied in a 3.75-ft-wide traffic area for the F-15E test item, as shown in Figure 25. The traffic area was broken into five lanes that were designed to simulate the traffic distribution pattern, or wander width, of the main landing-gear wheel on a mat surface when taxiing to and from an active runway. The width of each lane corresponded to the measured contact width, 9 in., of the F-15E tire when fully loaded and not the overall published tire width of 11 in. The normally distributed traffic patterns were simplified for ease-of-use by the

load cart operator. Traffic was applied by driving the load cart forward and then backward over the length of the test item and then shifting the path of the load cart laterally approximately one tire width on each forward path. This procedure was continued until one pattern of traffic was completed. One pattern resulted in 16 passes, or 4 coverages.

Figure 24. F-15E test load cart.



Figure 25. Plan view showing F-15E normally distributed traffic lanes.



2.4.2 C-17 load cart

The multiple-wheel C-17 load cart was designed to exactly match one-half main gear of a C-17. The multiple-wheel C-17 load cart was equipped with six 50-in.-by-21-in., 20-ply tires inflated to 142 lbf/in.² and loaded such that the test gear was supporting 269,560 lb, with estimated individual wheel loads of 44,930 lb. The test cart was powered by the front half of a Fiat scraper as shown in Figure 26.

Figure 26. C-17 test load cart.



A simulated normally distributed traffic pattern was applied in a 9-ft-wide traffic area for the C-17 test item, as shown in Figure 27. The traffic area was divided into individual lanes that were designed to simulate the traffic distribution pattern, or wander width, of the main landing-gear wheels on a mat surface when taxiing to and from an active runway. The width of each lane corresponded to the measured contact width, 18 in., of the C-17 tires when fully loaded and not the overall published tire width of 21 in. The normally distributed traffic patterns were simplified for ease-of-use by the load cart operator. Traffic was applied by driving the load cart forward and then backward over the length of the C-17 test item and then shifting the path of the load cart laterally approximately one tire width on each forward pass. Tracking guides were attached to assist the driver in shifting the load cart the proper amount for each forward pass. This procedure was continued until one pattern of traffic was completed. For the C-17 test item, one pattern resulted in 28 passes, or 25 coverages.

2.5 Data collection

Data collection included robotic total station measurements of centerline profiles, cross sections, dynamic strain measurements, and borescope observation videos. The data collection traffic intervals are shown in Tables 6 and 7, and the layout is shown in Figure 28. The mat surface was inspected for damage periodically during trafficking.

Figure 27. Plan view showing C-17 normally distributed traffic lanes.

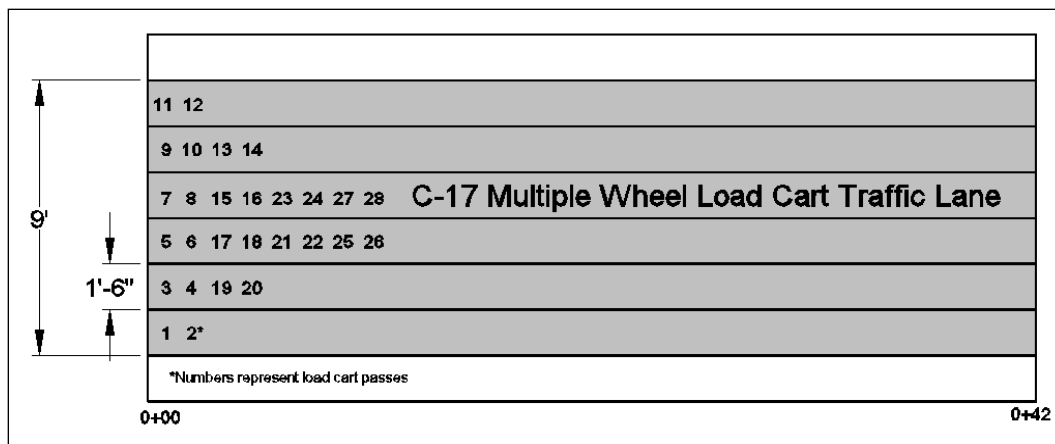


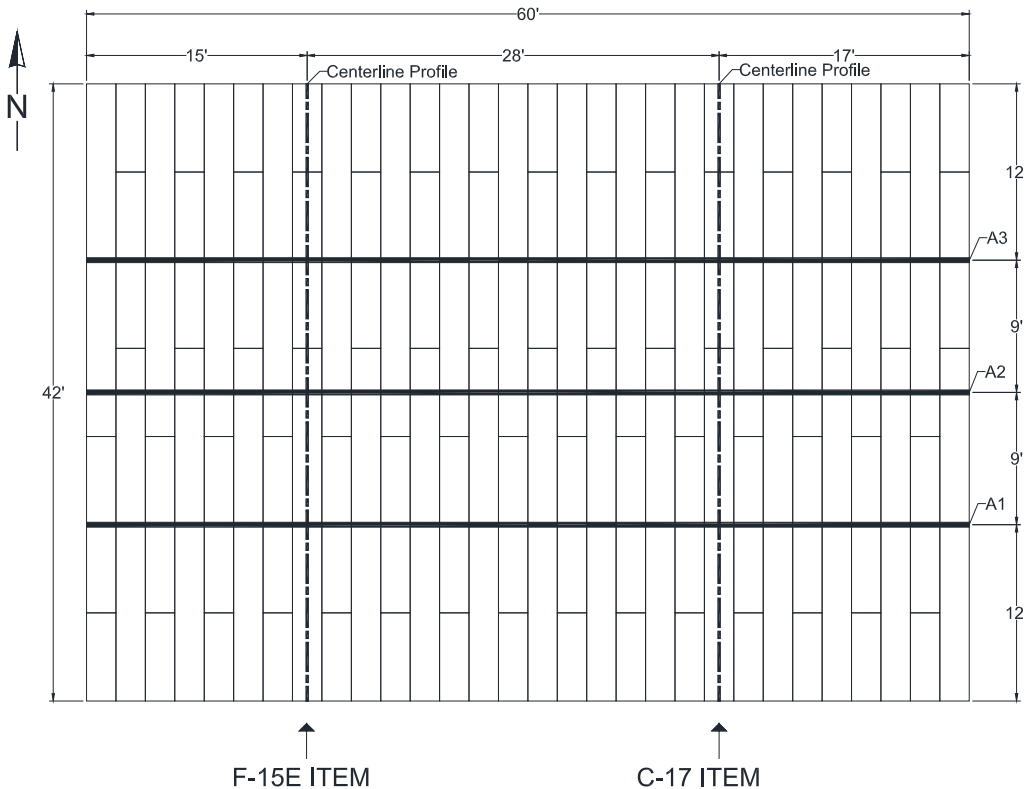
Table 6. Data collection intervals for F-15E traffic.

Total Passes	Profile	Unloaded Cross sections	Loaded Cross sections	Strain Gauges
Pretest Subgrade	X	X		
0	X	X	X	X
10	X	X	X	X
16	X	X	X	X
32	X	X	X	X
48	X	X	X	X
112	X	X	X	X
240	X	X	X	X
496	X	X	X	X
524	X	X	X	X
Posttest Subgrade	X	X		

Table 7. Data collection intervals for the C-17 test item.

Total Passes	Profile	Unloaded Cross sections	Loaded Cross sections	Strain Gauges
Pretest Subgrade	X	X		
0	X	X	X	X
12	X	X	X	X
24	X	X	X	X
26	X	X	X	X
56	X	X	X	X
84	X	X	X	X
168	X	X	X	X
308	X	X	X	X
392	X	X	X	X
Posttest Subgrade	X	X		

Figure 28. Data collection layout for each test item.



2.5.1 Centerline profile

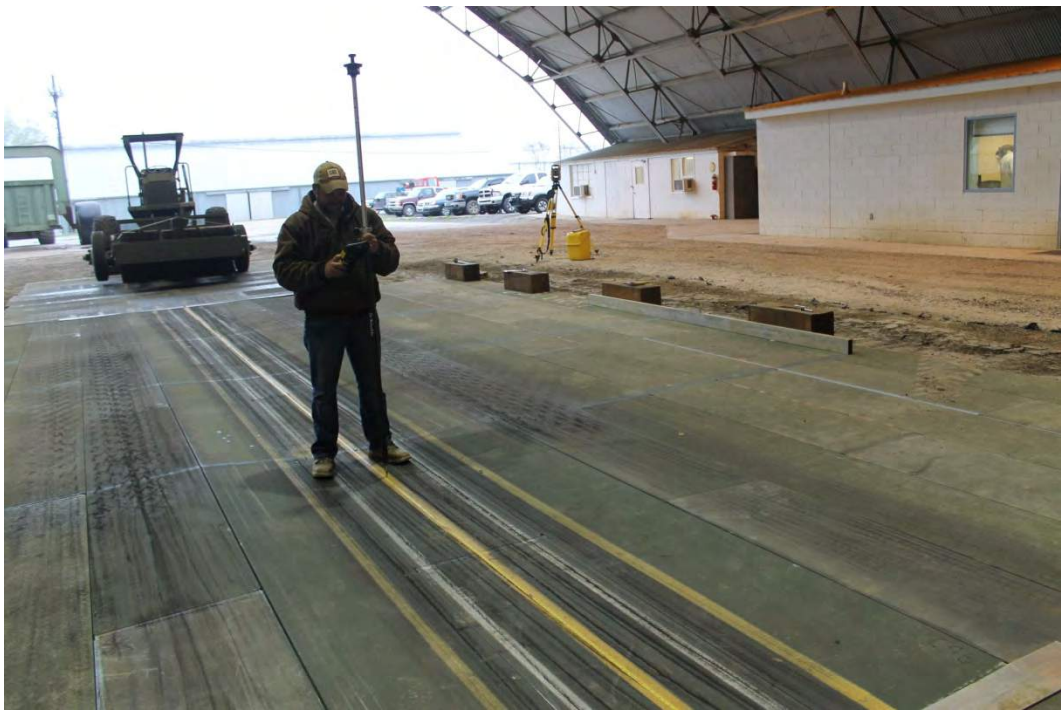
Data collected on the subgrade prior to, at scheduled pass levels during, and after trafficking along the traffic centerline are labeled “centerline profiles” in this report. Robotic total station elevation data were collected at 1-ft intervals on both the subgrade and mat surface (Figure 29).

2.5.2 Unloaded cross sections

Data collected on the subgrade prior to, at scheduled pass levels during, and after trafficking at the locations labeled A1, A2, and A3 (Figure 28) are called “cross sections” in this report. The locations of perpendicular lines A1, A2, and A3 were selected near the quarter-points of the test items to characterize the average performance while avoiding potential end effects associated with boundary conditions at the ends of the test sections.

Robotic total station elevation data were collected at 1-ft intervals from 2 ft to 12 ft offset from the centerline and at 6-in. intervals up to 2 ft offset from the centerline for the F-15E item. For the C-17 item, data were recorded at 1-ft intervals from 8 ft to 16 ft offset from the centerline and at 6-in. intervals up to 8 ft offset from the centerline.

Figure 29. Surveying centerline profile.



2.5.3 Loaded cross sections

In an attempt to measure the permanent deformation of the subgrade underneath the mat surface, a forklift carrying two 2,000-lb lead weights was parked on the mat surface adjacent to each cross section, and elevation data were once again recorded at the same intervals (Figure 30). The wheel load applied was approximately 6,000 lb. These data are noted as “loaded cross sections” in this report. The goal of the load application was to deflect the mat enough to contact the subgrade but not so much as to induce elastic deflections in the subgrade.

2.5.4 Strain measurements

National Instruments NI SCXI data acquisition hardware was used to collect data points at a rate of 100 Hz. Data were collected continuously and were paused only at the pass levels shown in Tables 6 and 7 and when traffic stopped temporarily for inspection of the mat surface.

2.5.5 Borescope observation

Observation holes were installed in panels 34, 35, 90, and 91 in an attempt to monitor the deformation progression of the subgrade underneath the mats. Concentric circles were drawn on the underside of these panels with

radii of 3, 6, and 9 in., and two flexible tapes were laid orthogonally across the subgrade to assist in scaling during video review. Panel locations are shown in Figure 20. Videos of the borescope observations have been retained for archiving, but no measurements are reported in this document.

Figure 30. Typical survey of loaded cross section.



2.6 Failure criteria

The failure criteria established were (1) 10% mat breakage or (2) the development of 1.25 in. of permanent surface deformation for the F-15E or 3.0 in. of permanent surface deformation for the C-17. These failure criteria were developed based upon previous testing of airfield matting and USAF requirements. Failure criteria values were recorded and monitored for compliance.

2.6.1 Mat breakage

Mat breakage percentages were calculated by dividing the area of the failed panel (or half-panel) by the total area influenced by the simulated traffic application in the assembled test item. Individual panels were considered failed if damage posed a significant tire hazard or caused instability of the load cart. Tire hazards were defined as damage that could not be reasonably maintained by simple field maintenance procedures. A typical example was

a top skin tear in excess of 10 to 12 in., representing significant structural damage to the surface skin with sharp edges that could endanger an aircraft tire.

2.6.2 Permanent deformation

The permanent surface deformation limits of 1.25 in. and 3.0 in. are based on roughness limitations for the F-15E and C-17 aircrafts, respectively. An abrupt change in elevation or the development of a rut in the wheel path greater than the allowable values may exceed roughness limits. The rut depth limit is required since many connecting taxiways and aprons intersect at an angle of 90 deg; crossing perpendicular to a pre-formed rut may cause an abrupt change in elevation, exceeding aircraft limits. Permanent surface deformation was determined from robotic total station elevation measurements of cross sections and centerline profiles. Each of the following data collection categories were analyzed for compliance with the failure criterion.

1. centerline profile deformation,
2. loaded surface deformation, and
3. unloaded surface deformation.

2.6.2.1 *Centerline profile deformation*

The difference in elevation one or two stations apart (1 ft or 2 ft apart) was analyzed from plots of the centerline profile data to determine if an abrupt change in elevation reached failure limits during trafficking.

2.6.2.2 *Loaded surface deformation*

Loaded surface deformation was determined from data collected in accordance with procedures described in section 2.5.3. The maximum deformation at each location was determined as the difference in elevation from the average height of the elevated material on each side of the trough to the deepest point in the bottom of the trough. Measurements were averaged to obtain a single value for comparison to the failure criterion.

2.6.2.3 *Unloaded surface deformation*

Unloaded surface deformation was determined from data collected in accordance with the procedures described in section 2.5.2. The maximum deformation at each location was determined as the difference in elevation

from the average height of the elevated material on each side of the trough to the deepest point in the bottom of the trough. Measurements were averaged to obtain a single value for comparison to the failure criterion.

3 Test Results

3.1 Behavior of mat under traffic (visual observations)

The following sections describe the behavior of the AM2 airfield mat under simulated F-15E and C-17 traffic.

3.1.1 F-15E test item

Trafficking of the F-15E test item began April 2, 2013. After 240 passes, no mat breakage was evident. However, the loaded surface deformation had reached 1.30 in. on the mat surface, exceeding the permanent deformation limit of 1.25 in. Subsequently, the test item was rated as failed. Trafficking was continued to 524 passes to collect additional data. At that point, the loaded surface deformation had nearly reached 3.0 in., and trafficking was concluded to prevent instability of the load cart.

3.1.2 C-17 test item

Trafficking of the C-17 test item began April 8, 2013. The only damage noted was minor corner curls. Trafficking was terminated after 392 passes when the loaded surface deformation was 3.0 in. Test item was rated as failed since it reached the permanent deformation limit of 3.0 in.

3.2 Permanent deformation

To show only the changes that occurred because of trafficking, the pre-traffic data were subtracted from all subsequent data collected after trafficking began to normalize the data. The discussions that follow are based on normalized data. Table 8 summarizes maximum deformation values measured on each item from data collected along the centerline profile and cross sections. Each of these values was compared to the failure criteria.

Plots of the centerline profile data, as determined from robotic total station recordings, for the F-15E and C-17 test items are shown in Figures 31 through 34. When determining the maximum roughness value in each item, boundary conditions were ignored (i.e., first two and last two stations along the centerline). This was done because of the different properties at the interface of the test section subgrade and the surrounding material (much

stronger). Plots of the average cross-section elevation data, collected along lines A1, A2, and A3 shown in Figure 28 for each test item, are shown in Figures 35 through 40.

Table 8. Maximum values of measured permanent deformation for each test item.

Test Item	F-15E	C-17
Pass Number	524	392
Subgrade Profile Max Abrupt Change in Elevation (in.)	0.29	0.35
Mat Surface Profile Max Abrupt Change in Elevation (in.)	0.11	0.08
Subgrade Permanent Deformation (in.)	3.17	2.83
Loaded Deformation on Mat Surface (in.)	2.95	3.00
Unloaded Deformation on Mat Surface (in.)	1.69	2.96

Figure 31. Subgrade centerline profile in the F-15E item after 524 passes.

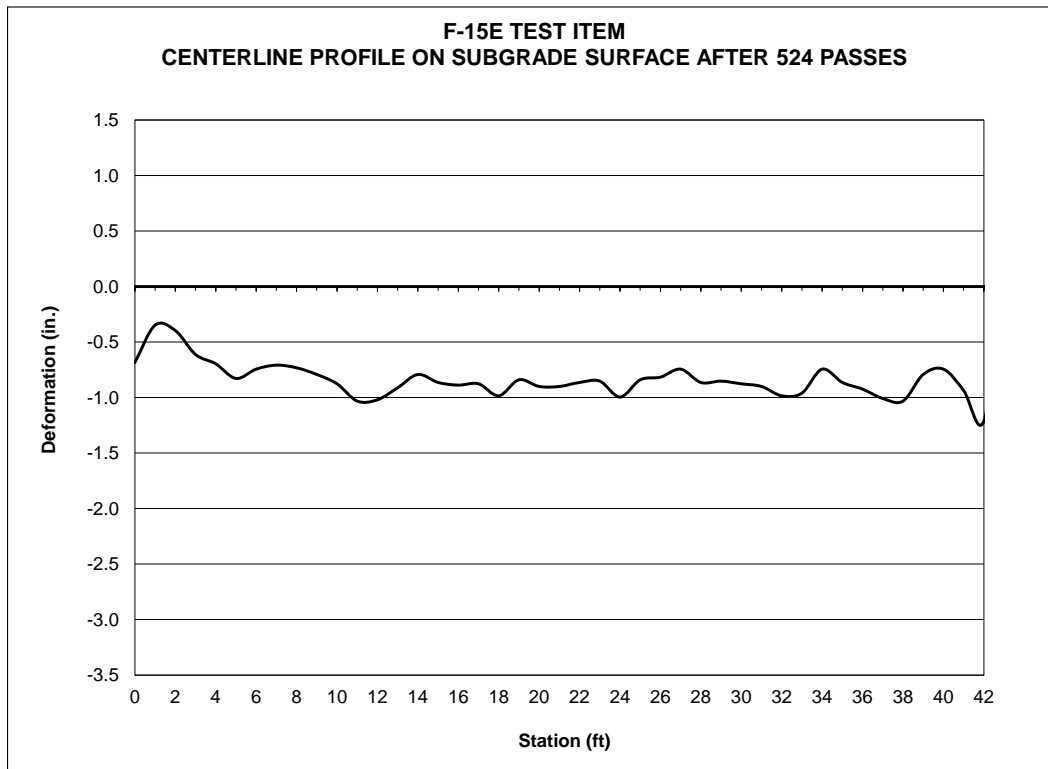


Figure 32. Centerline profile on the subgrade in the C-17 item after 392 passes.

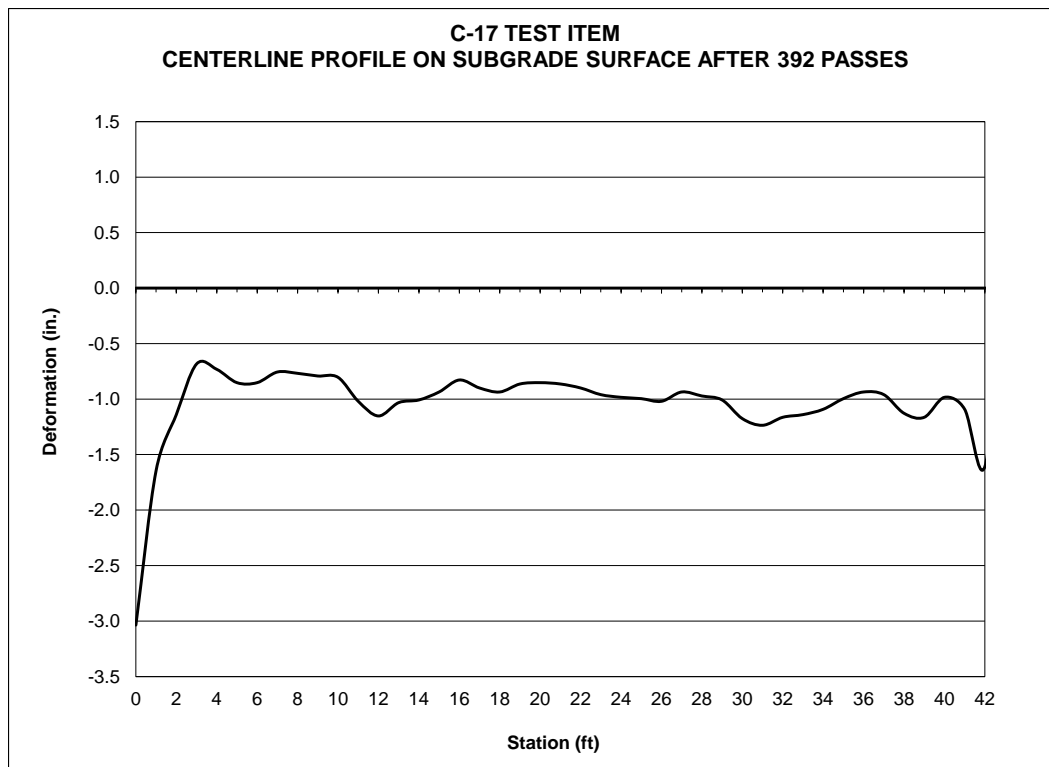


Figure 33. Centerline profile on the mat surface in the F-15E item.

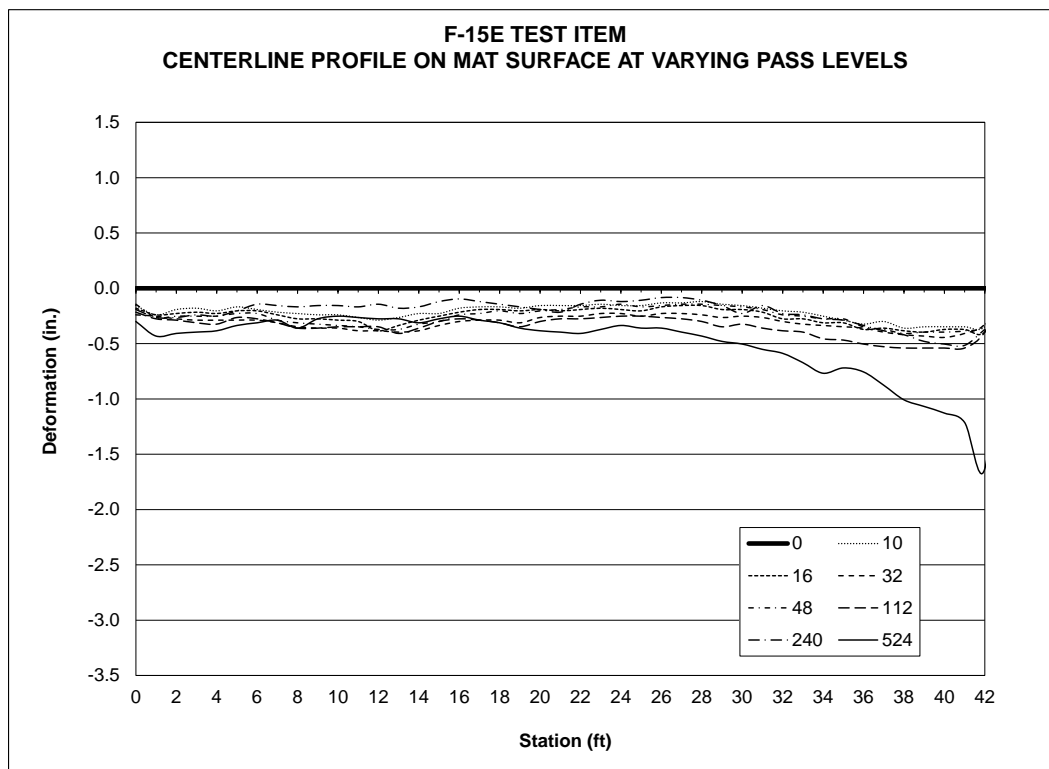


Figure 34. Centerline profile on the mat surface in the C-17 item.

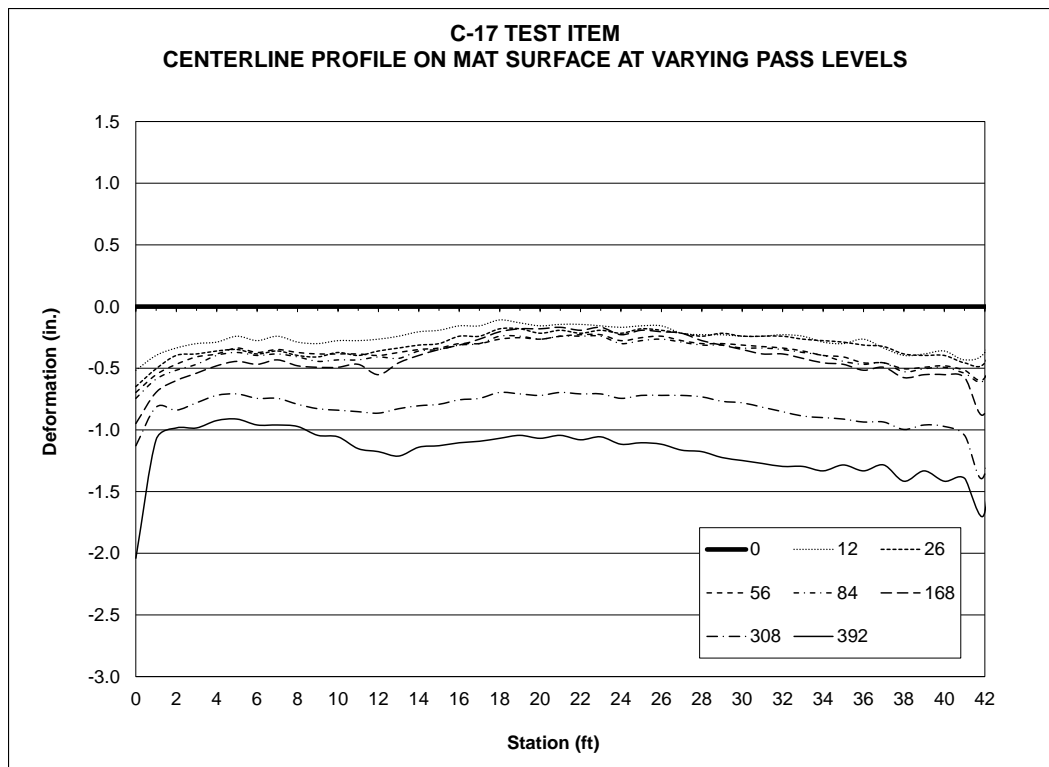


Figure 35. Average deformation on the subgrade in the F-15E after 524 passes.

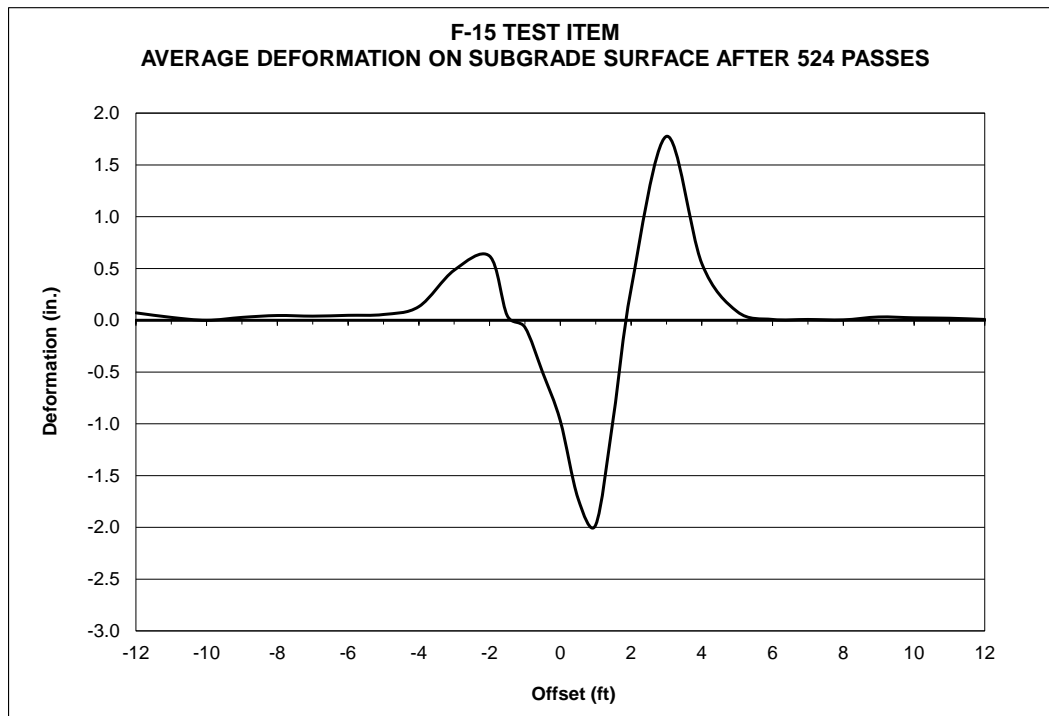


Figure 36. Average deformation on the subgrade in the C-17 item after 392 passes.

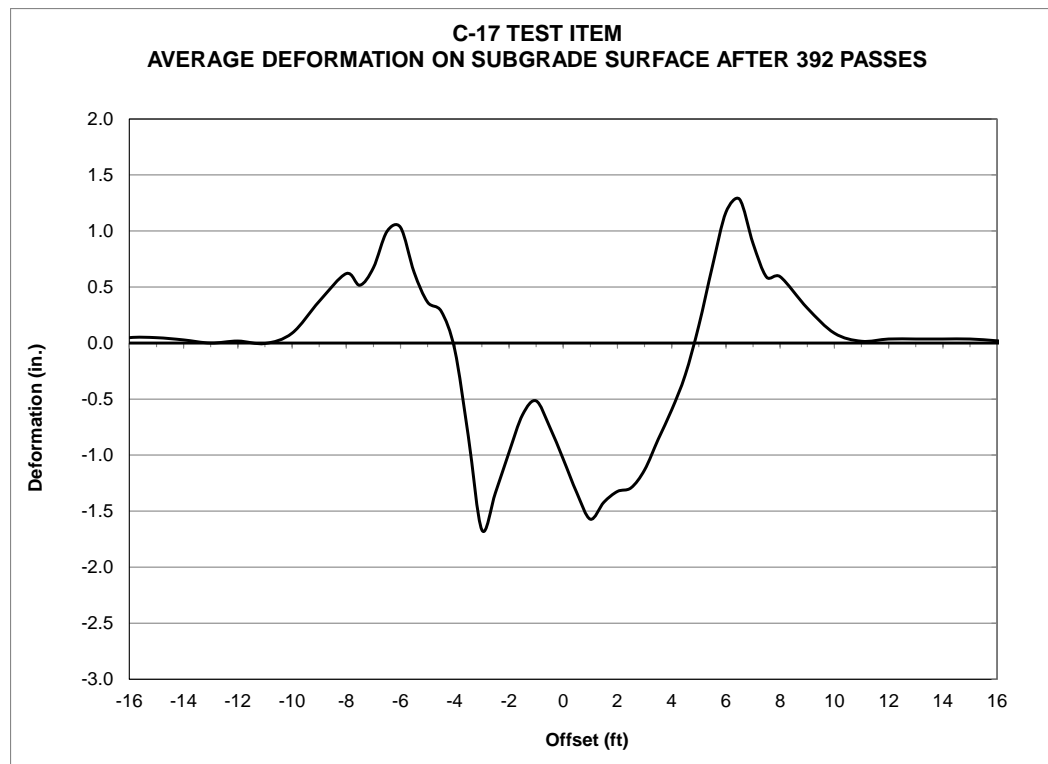


Figure 37. Average deformation on the loaded mat surface in the F-15E item.

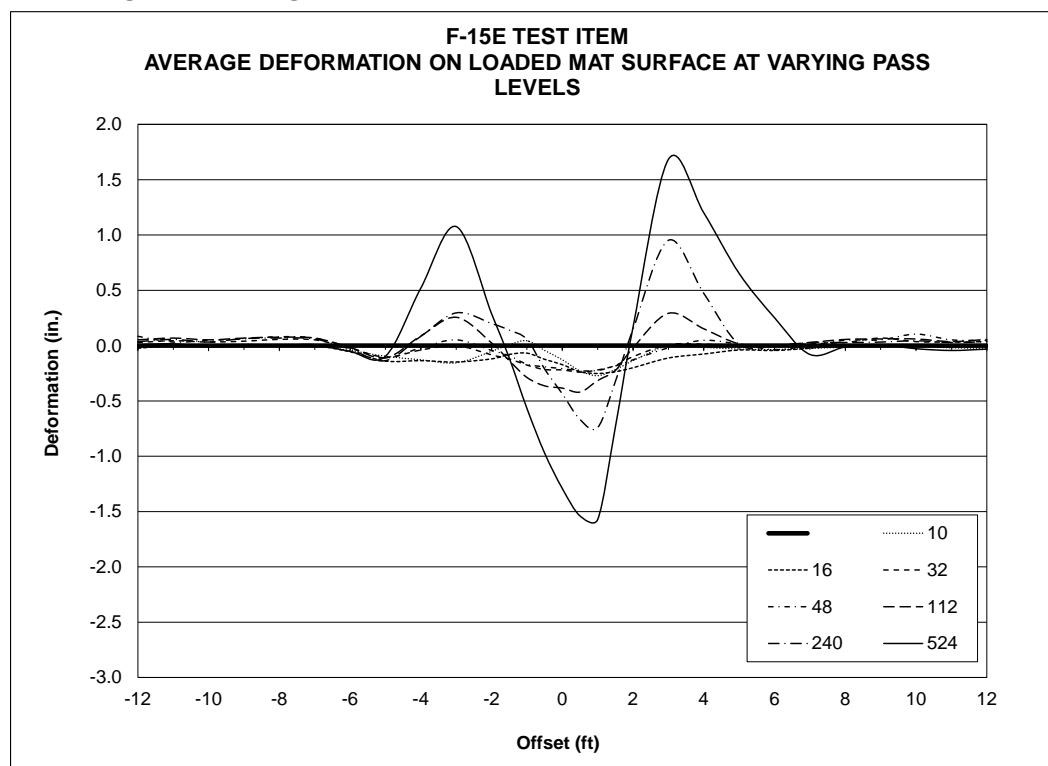


Figure 38. Average deformation on the loaded mat surface in the C-17 item.

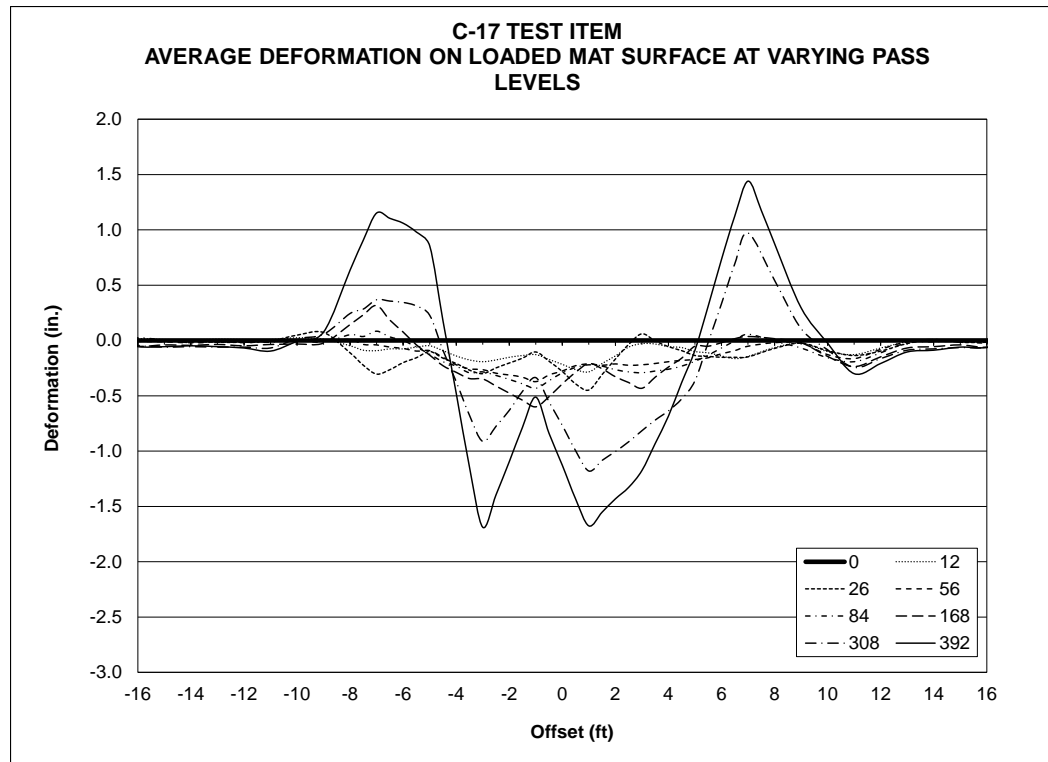


Figure 39. Average deformation on the unloaded mat surface in the F-15E item.

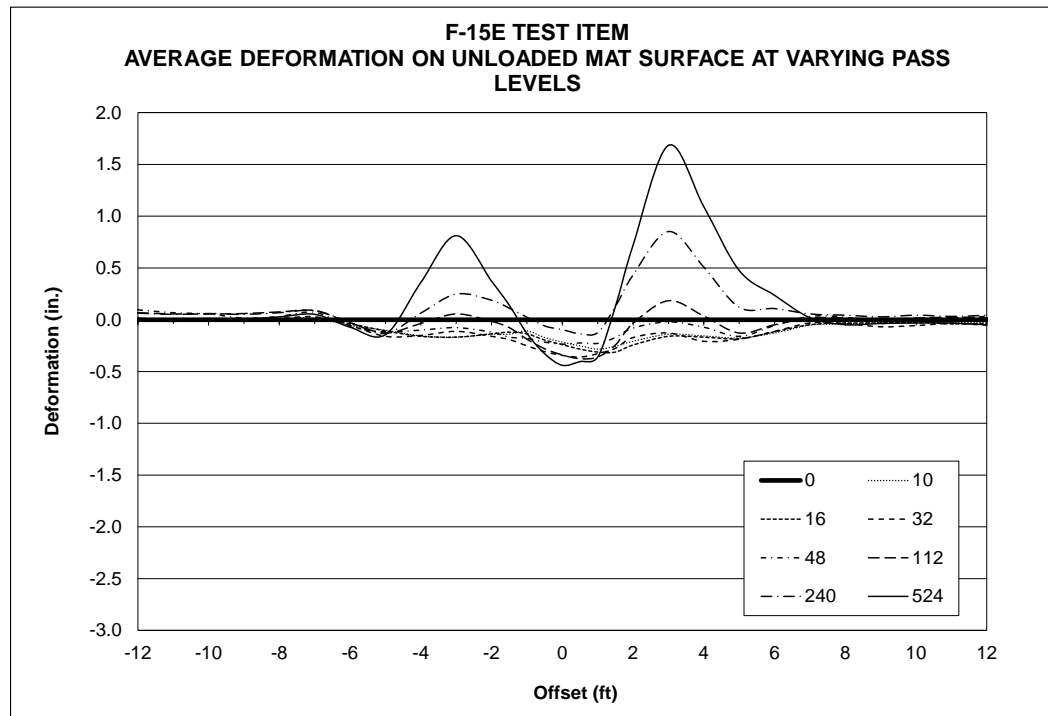
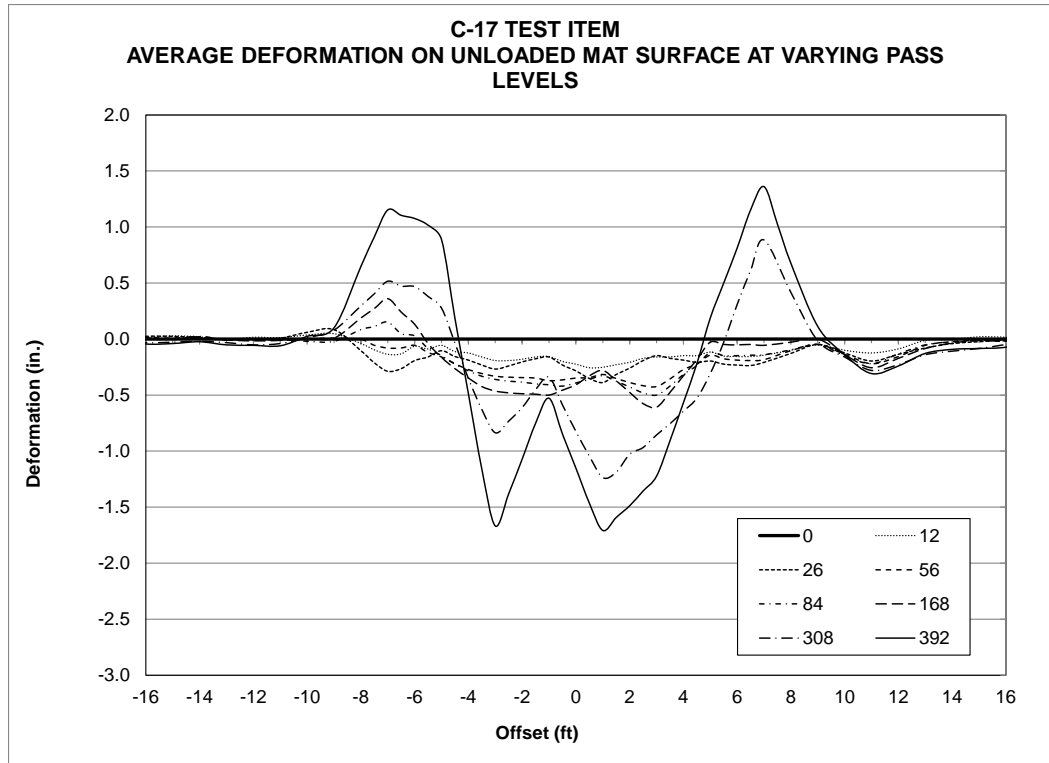


Figure 40. Average deformation on the unloaded mat surface in the C-17 item.



3.3 Strain gauge data

Example plots of the strain data recorded are shown in the following sections. The strain gauge data examples are presented in groups based on their comparable locations on the F-15E and C-17 test items. In each plot, the x-axis represents the elapsed time (during the recording period) in seconds, and the y-axis is the strain measurement in microstrain (10^{-6}). Each of the positive peaks represents tensile strains, and the negative peaks represent compressive strains. The changing magnitude of the peaks was caused by the wander pattern used to simulate a normal distribution of traffic over the test section. The prominent peaks indicate that the load cart was located directly above, or adjacent to, the strain gauge.

From the raw data, the maximum tensile strains and the absolute value of the compressive strains were captured for each gauge throughout trafficking and are reported in the following sections. Data respective to the C-joint were plotted separately from that recorded at the F-joint. For the latter, the plots were organized to report data for joining panels in the same figure. Gauge malfunction in both test items is marked by the disappearance of data. Since mat breakage was not observed, gauge malfunction could not be attributed to failure of a rail or cracking at the

connection. Gauges that malfunctioned in the F-15E item at different pass levels were C94C1, C95C1, and C95C2. Gauges C94C2, C87F2, C86F1, and C86F2 failed to report usable data from the beginning of the test. Gauges C38C1 and C39C1 malfunctioned during trafficking of the C-17 item, and gauge C39F2 failed to report usable data from the onset of testing. The remainder of the full data set is archived at the ERDC and may be made available upon request. Plots of the measured data are shown in Appendix A and Appendix B for the F-15E and C-17 items, respectively.

3.3.1 F-15E item

Figures 41 through 44 are plots showing strain response at the F-joint of Panels C90 and C91 in F-15E test item during pass interval 17-32. Each of the large peaks represents one pass by the single-wheel load cart. According to Figure 41, strain gauge C90F1 showed very little response to the applied load. The response coincides with strain recorded at the gauge opposite to its location (gauge C91F1), with the prominent peaks occurring at 145, 160, 380, and 400 seconds. According to Figures 42 and 44, C90F2 and C91F2 show some elastic strain between the elapsed time of 230 and 325 seconds. The strain recorded by gauge C91F2 also mirrors the response of gauge C90F2. Figures 45 and 46 are plots of the strain responses at the C-joint of Panel C95 during passes 17-32. According to Figure 45, gauge C95C1 recorded higher tensile strains than gauge C95C2 during passes 17-32. This may have contributed to the earlier malfunction of C95C1.

Figure 47 through 54 show the absolute value of the maximum tensile and compressive strain measured by each gauge at each pass interval of recorded data. It is evident from the data that larger strains were measured at the F-joints than at the C-joints. Strain measured at the F-joint of panels C90 and C91 was comparably much larger than strain measured at other locations, an expected outcome since the centerline of traffic was at the center of these panels.

3.3.2 C-17 item

Figures 55 through 58 are plots showing the responses at the F-joint for Panels C30 and C31 in the C-17 test item during passes 13-24. Each pair of large peaks represents a single pass of the load cart, since the six-wheel gear has two load-carrying axles. The smaller peaks represent the drive wheels of the load tractor. Gauge C31F1 (lower overlap rail) generally measured higher tensile strains than C30F1 (upper underlap rail). C31F1

also experienced permanent deformation after 180 seconds, as marked in Figures 57. Gauges C30F2 and C31F2 both measured high compressive strains at an elapsed time of 140 seconds, but C31F2 also showed permanent deformation along with a tensile strain at an elapsed time of 150 seconds. The data from these panels show that larger compressive strains were measured at the lower overlap rail (C31F1 and C31F2). Figures 59 and 60 are plots of the data recorded by strain gauges installed at the C-joint of Panel C39 during passes 13-24. Similar responses were recorded at both locations of the female hinge.

Figures 61 through 68 show the absolute values of the maximum tensile and compressive strains for each working gauge during each pass interval. At the C-joint, both tensile and compressive strains remained below 6,000 microstrain, but tensile strains were generally higher than compressive strains. At the F-joint, compressive strains reached as high as 11,000 microstrain, and tensile strains were below 6,000 microstrain. Strain measured in the C-17 item was comparatively much higher than in the F-15E item.

Figure 41. F-15E item, gauge C90F1, passes 17-32.

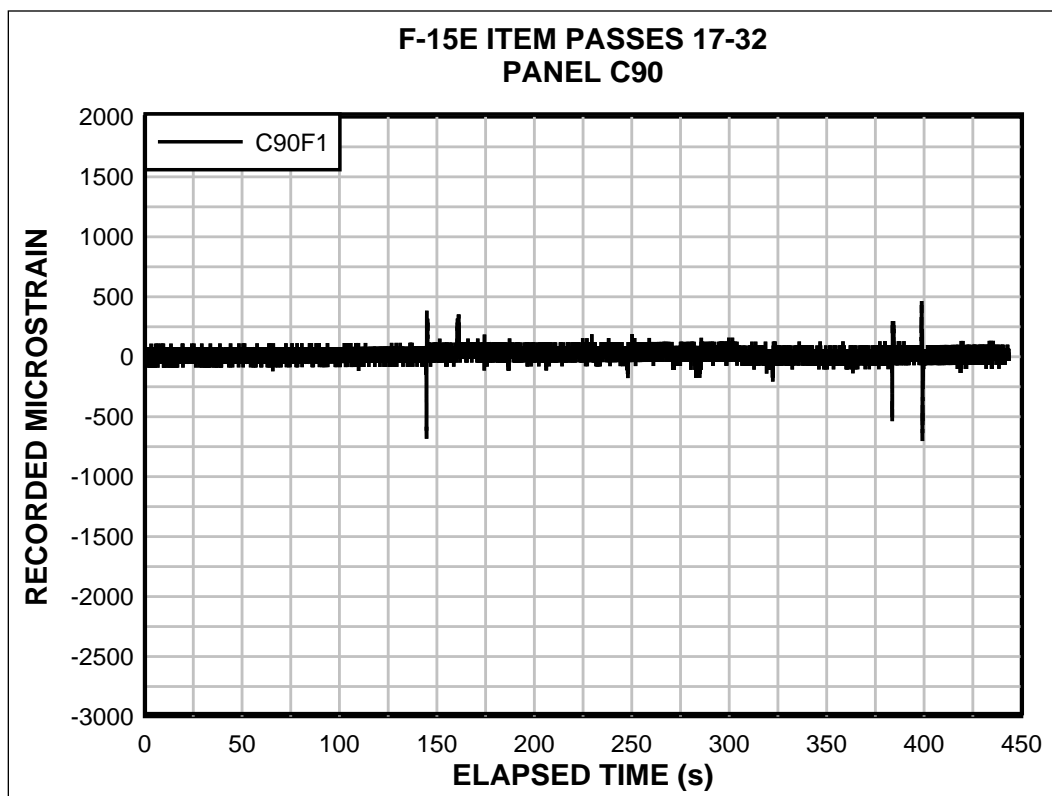


Figure 42. F-15E item, gauge C90F2, passes 17-32.

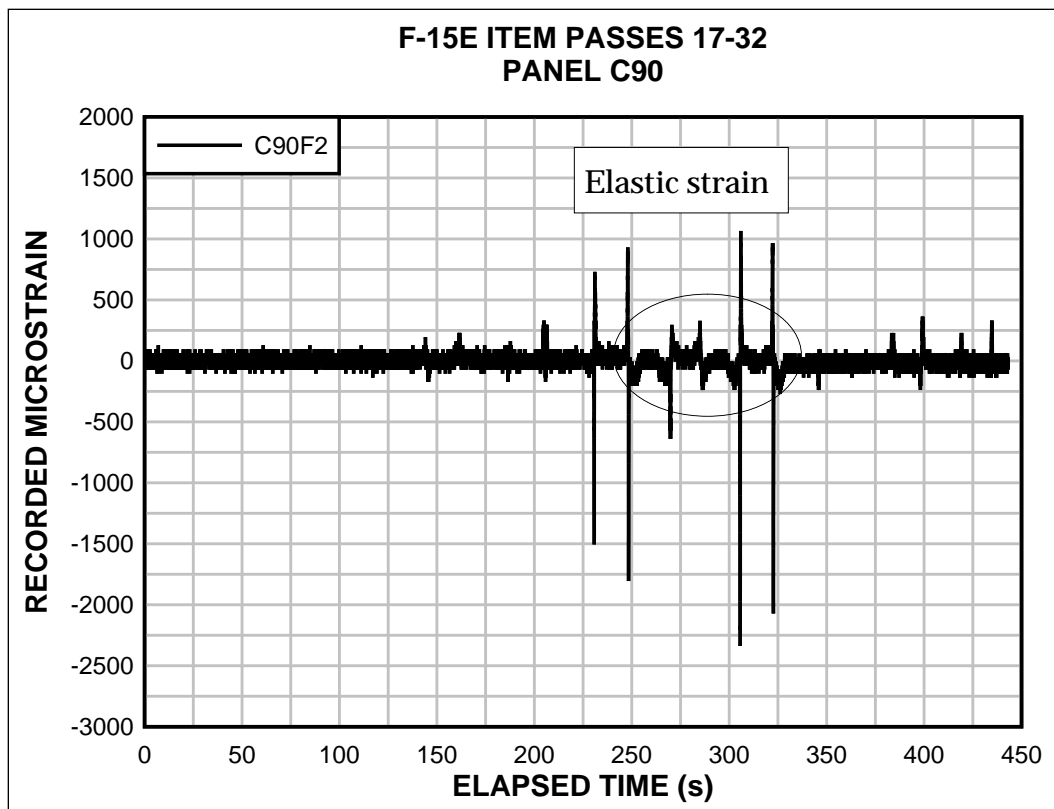


Figure 43. F-15E item, gauge C91F1, passes 17-32.

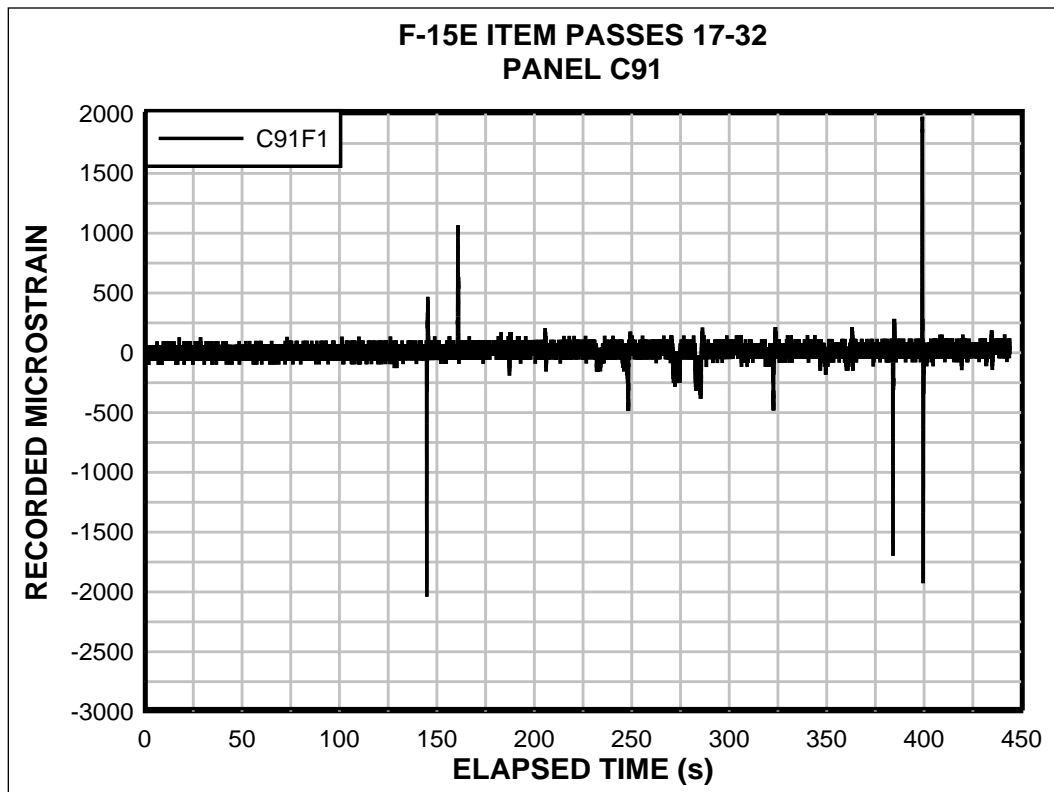


Figure 44. F-15E item, gauge C91F2, passes 17-32.

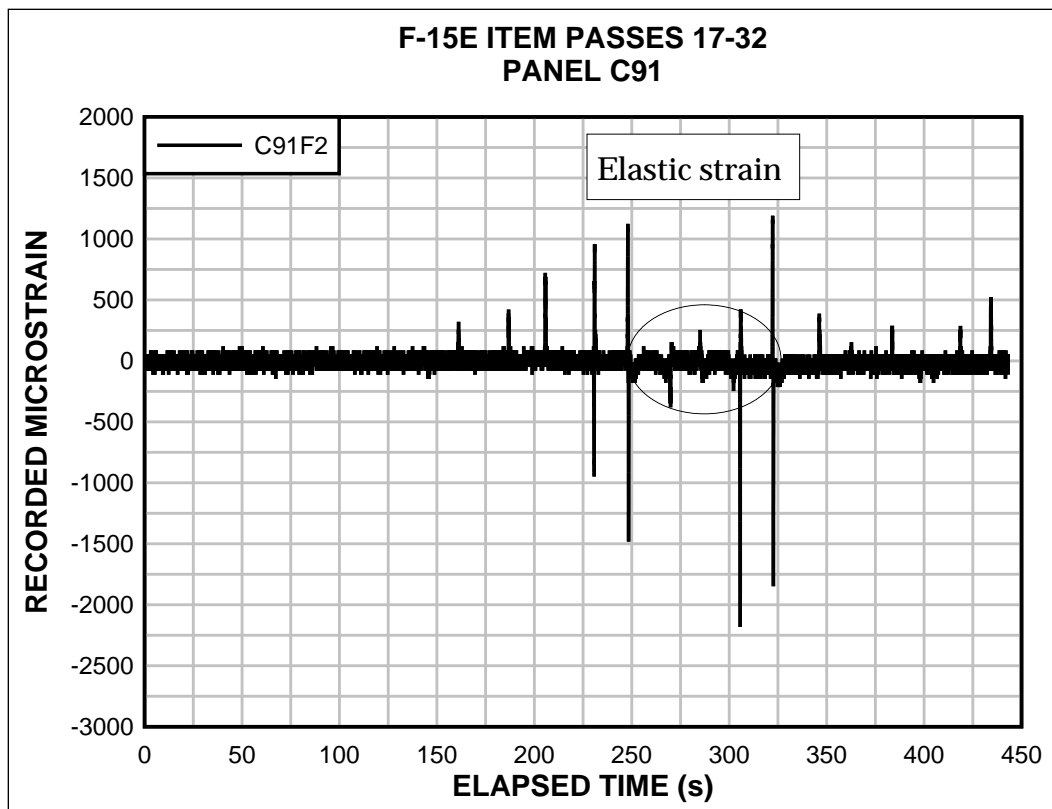


Figure 45. F-15E item, gauges C95C1, passes 17-32.

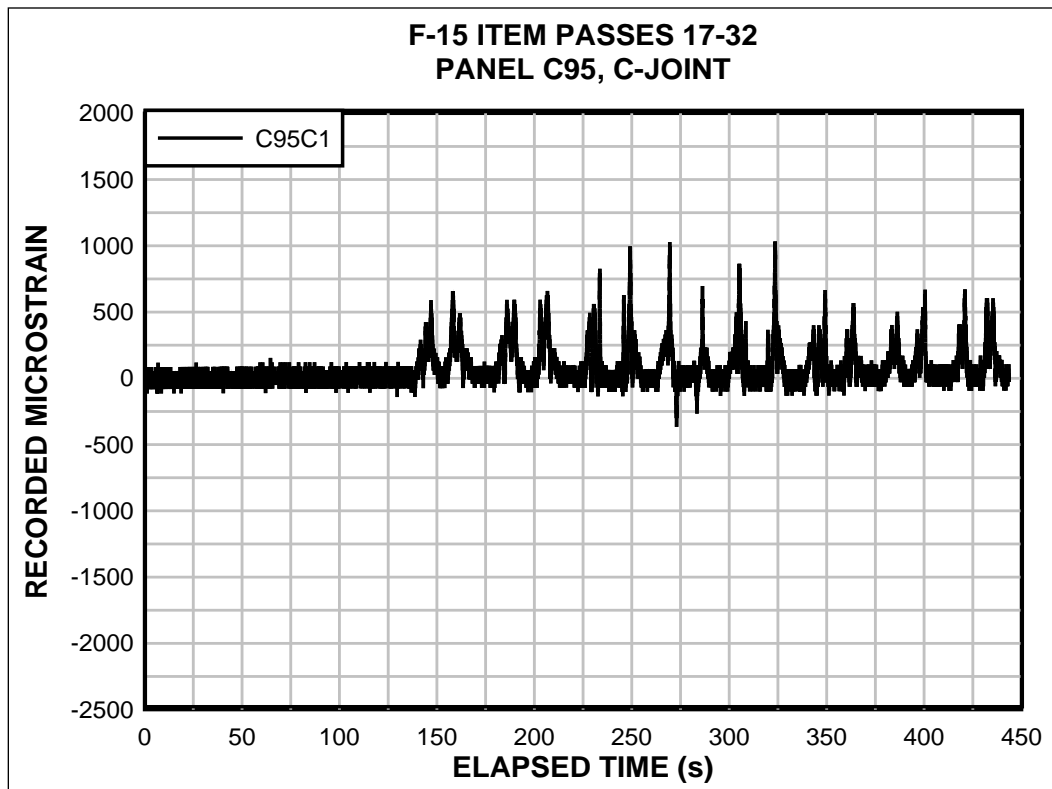


Figure 46. F-15E item, gauge C95C2, passes 17-32.

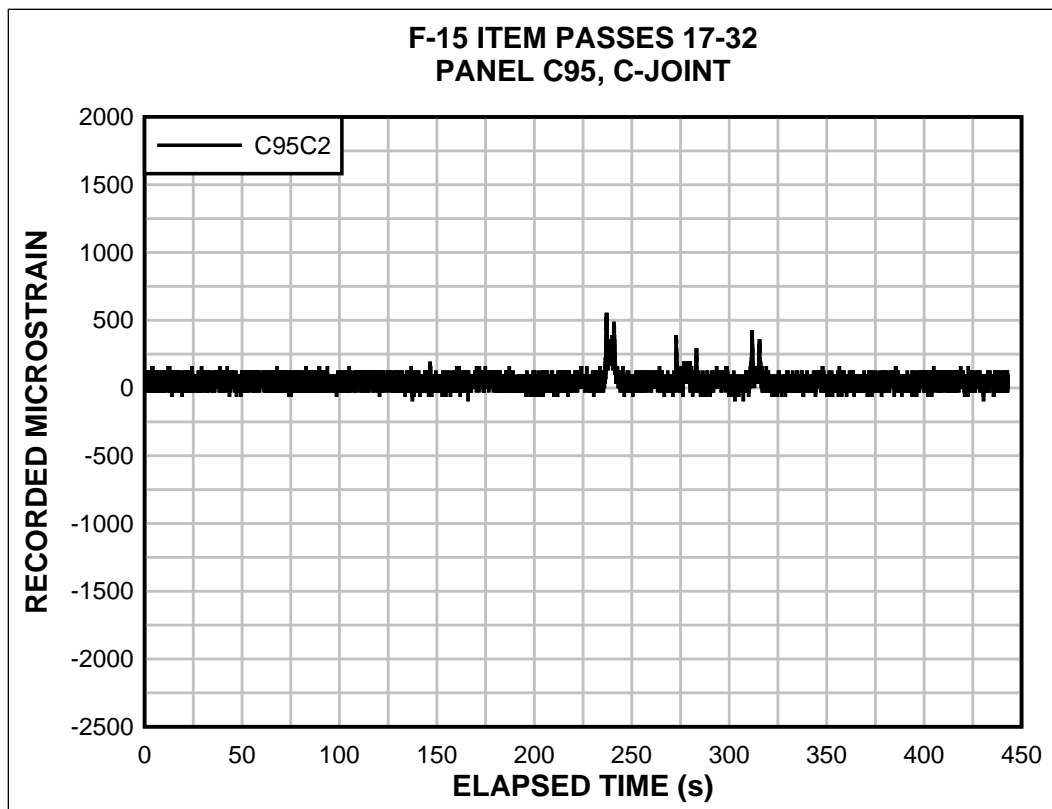


Figure 47. Maximum tensile strain for panel C87 at F-joint.

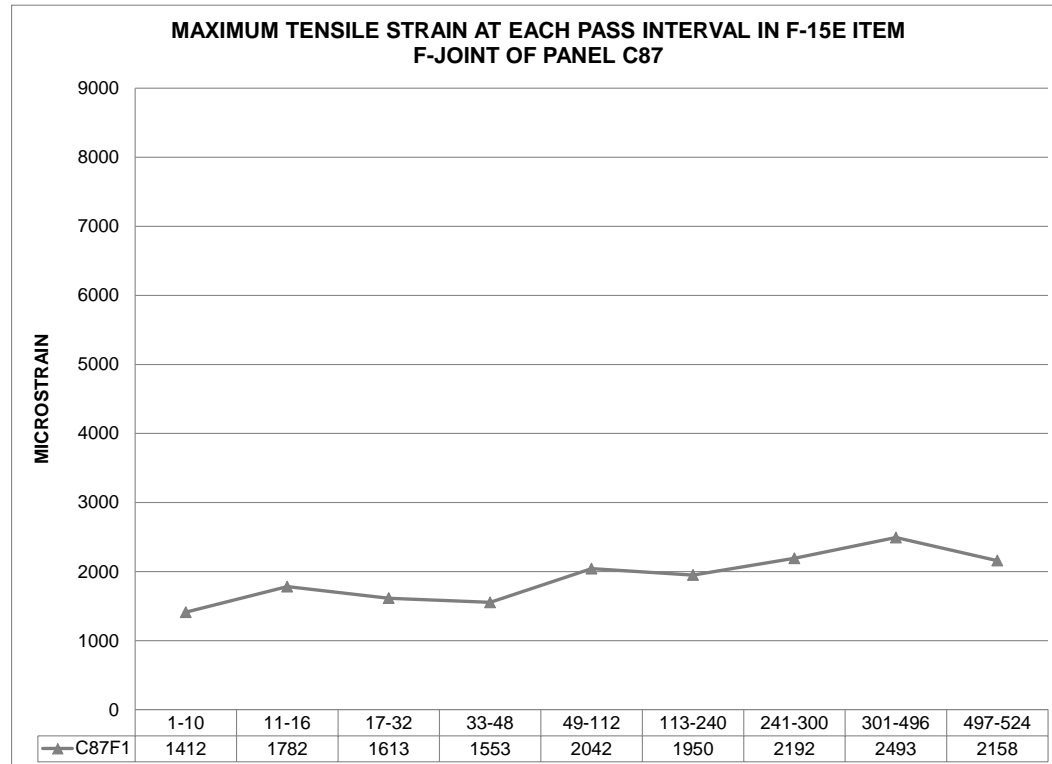


Figure 48. Maximum compressive strain for panel C87 at F-joint.

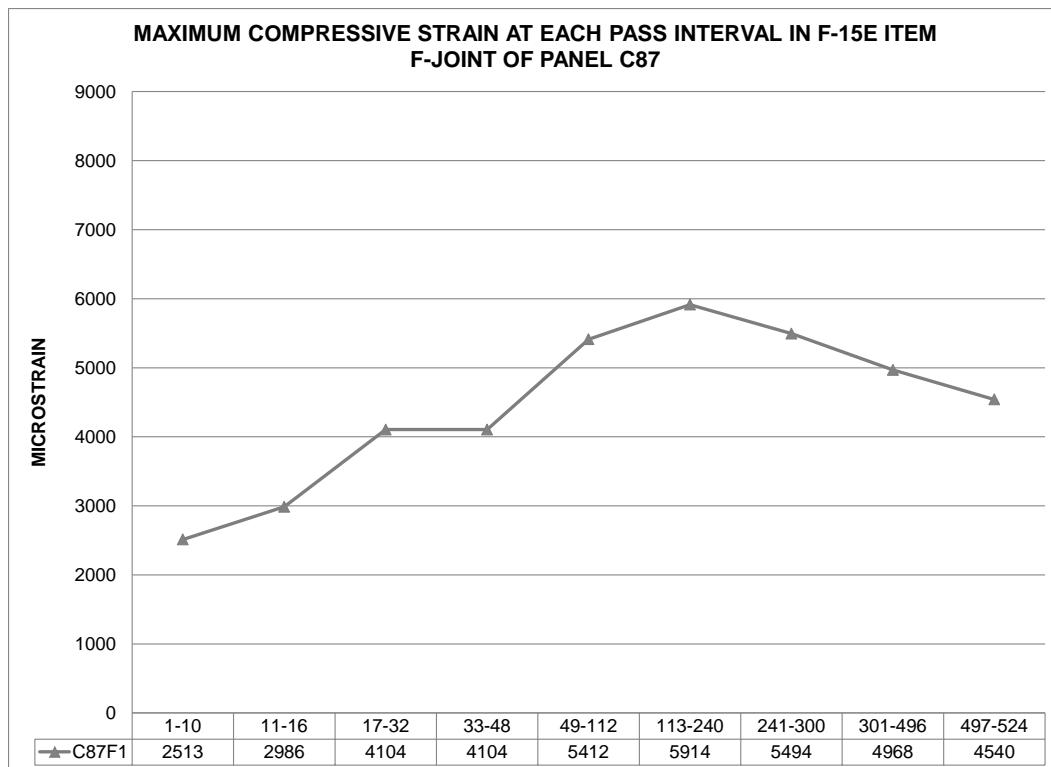


Figure 49. Maximum tensile strain for panels C90 and C91 at F-joint.

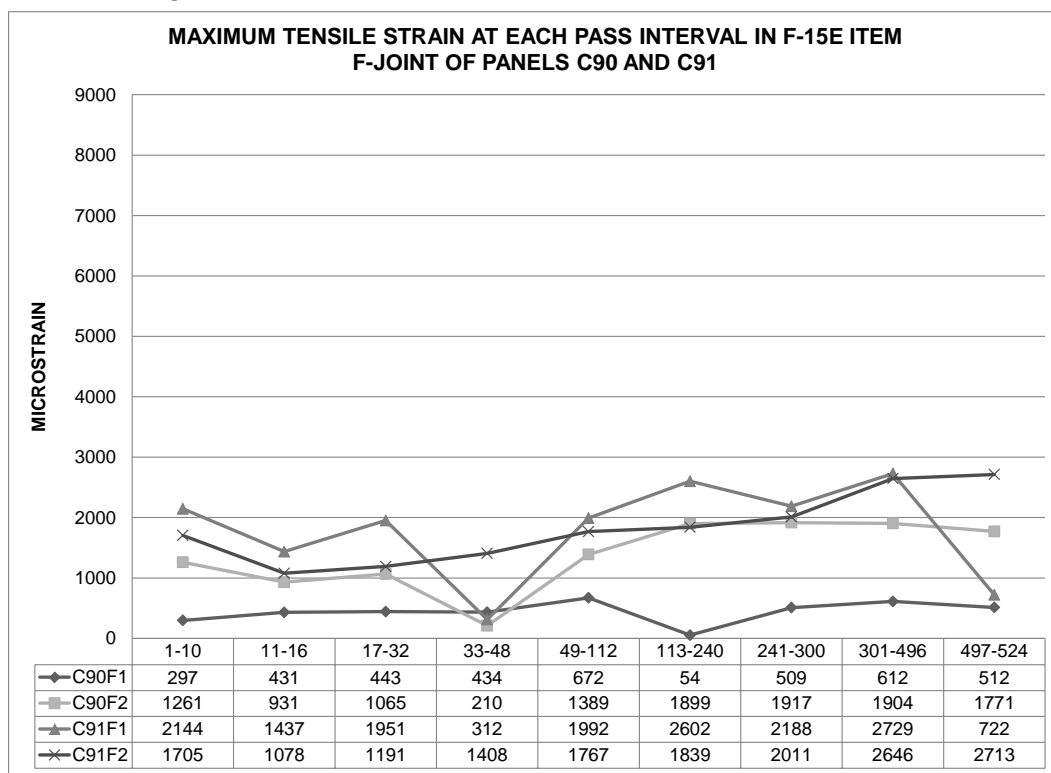


Figure 50. Maximum compressive strain for panels C90 and C91 at F-joint.

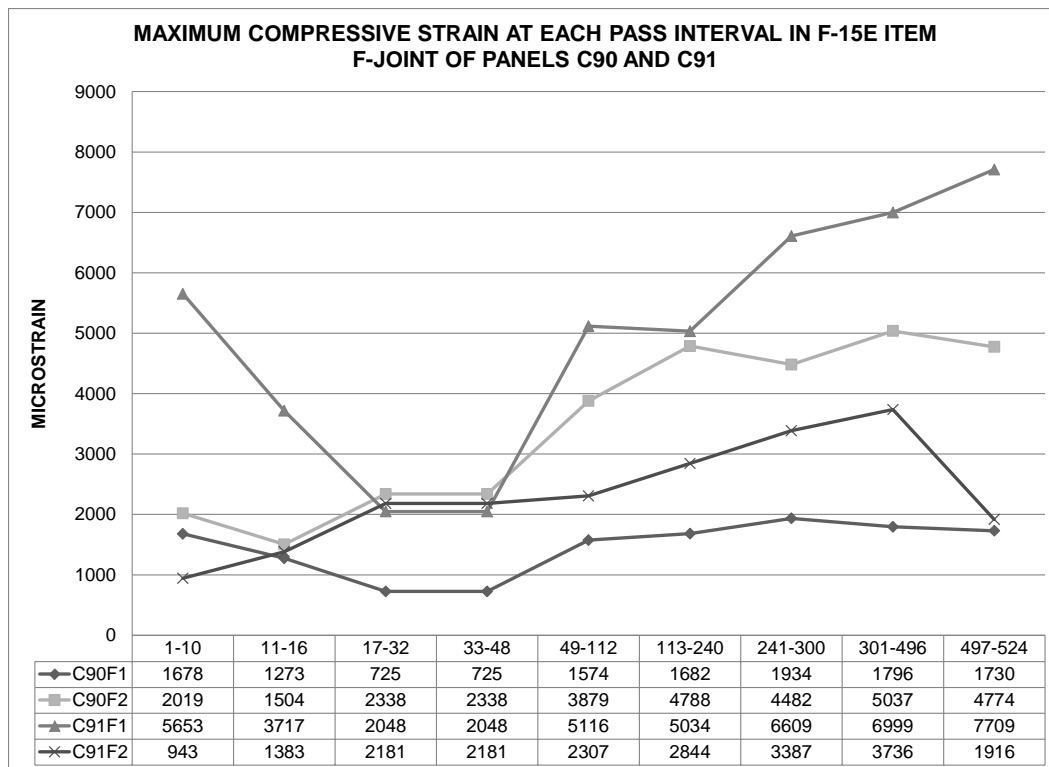


Figure 51. Maximum tensile strain for panels C94 and C95 at F-joint.

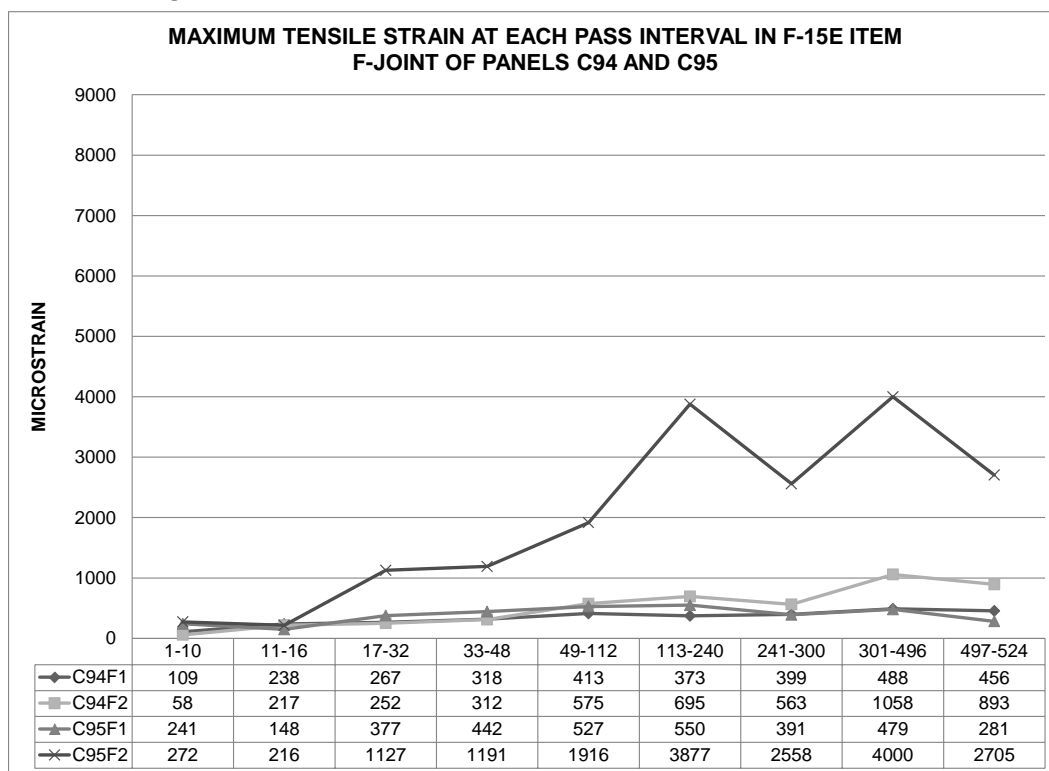


Figure 52. Maximum compressive strain for panels C94 and C95 at F-joint.

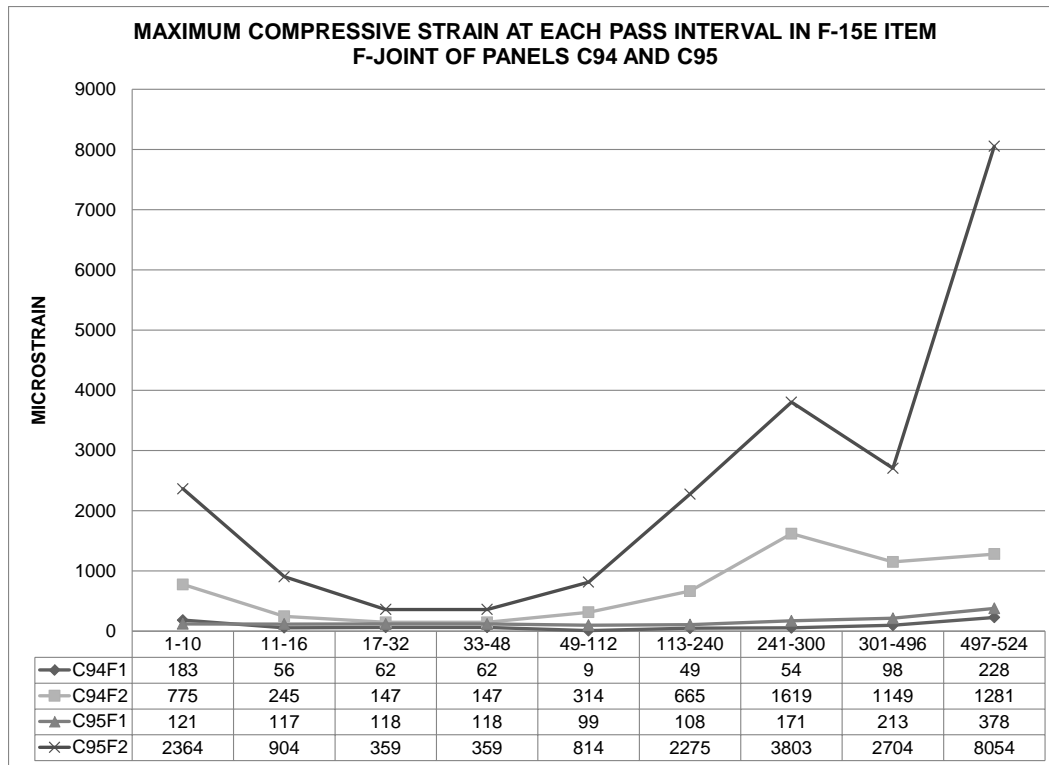


Figure 53. Max tensile strain for panels C82, C94 and C95 at C-joint.

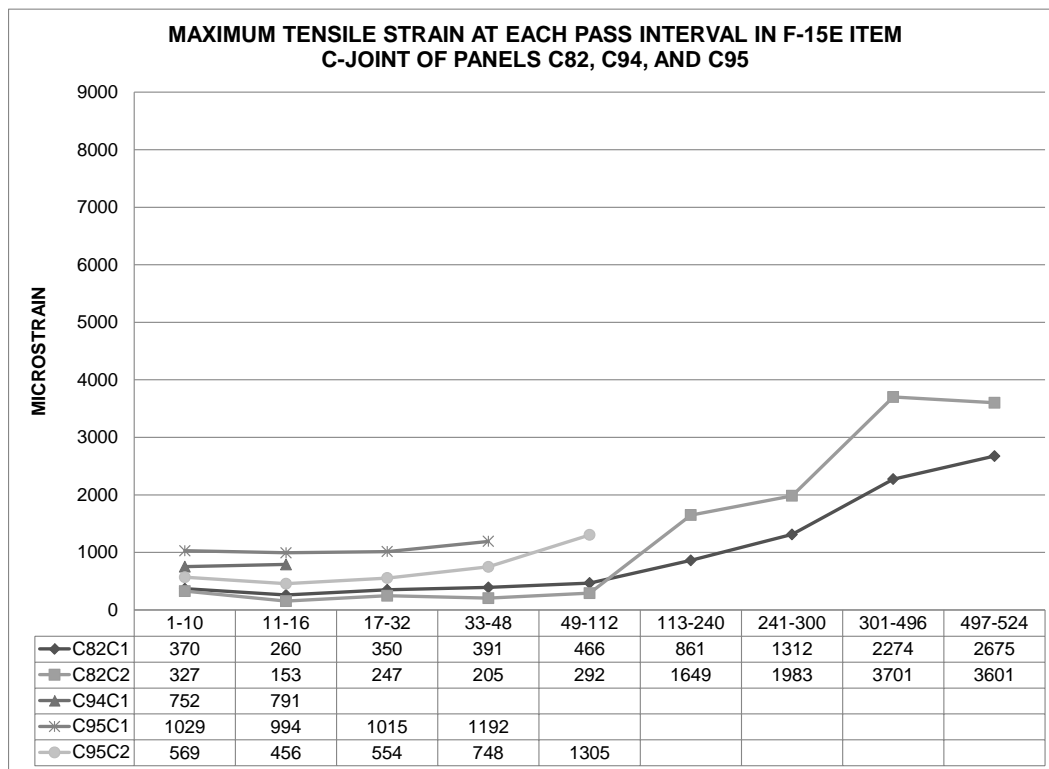


Figure 54. Max compressive strain for panels C82, C94 and C95 at C-joint.

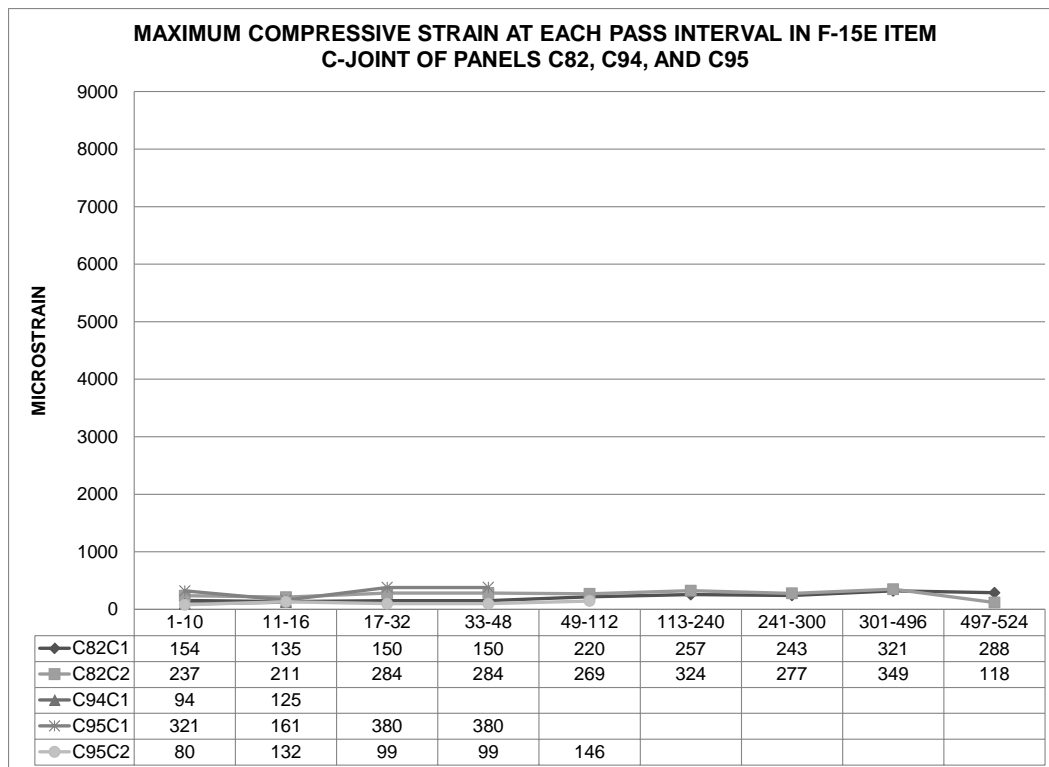


Figure 55. C-17 item, gauge C30F1, passes 13-24.

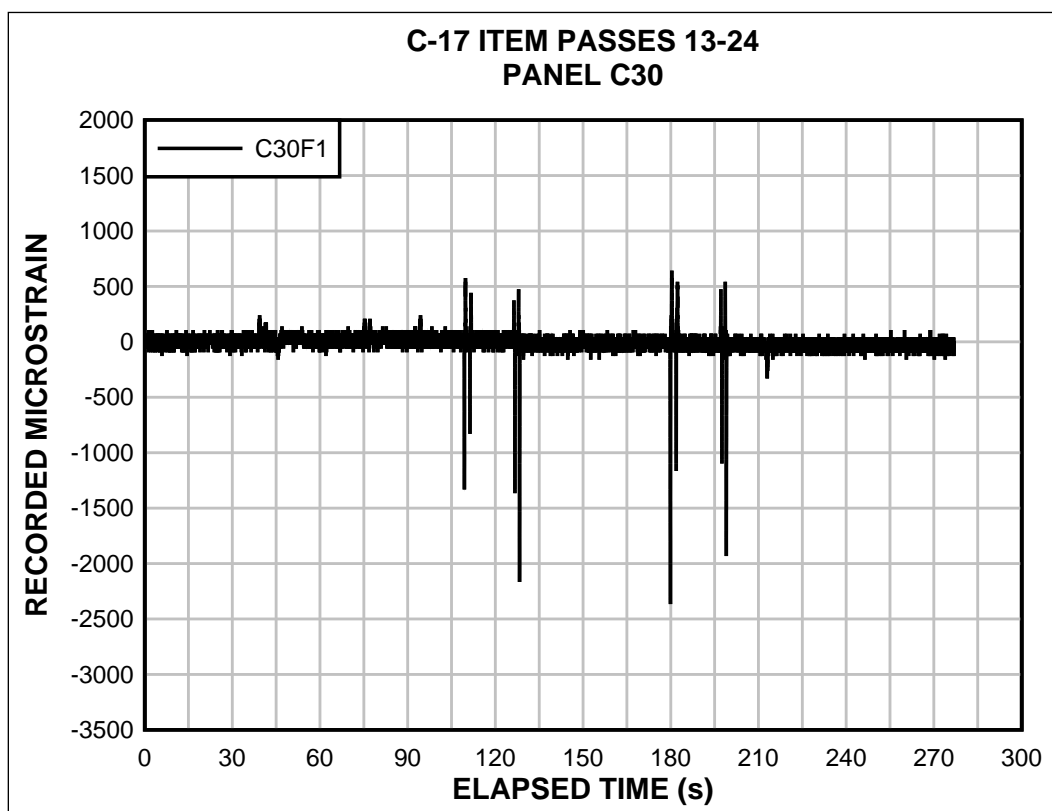


Figure 56. C-17 item, gauge C30F2, passes 13-24.

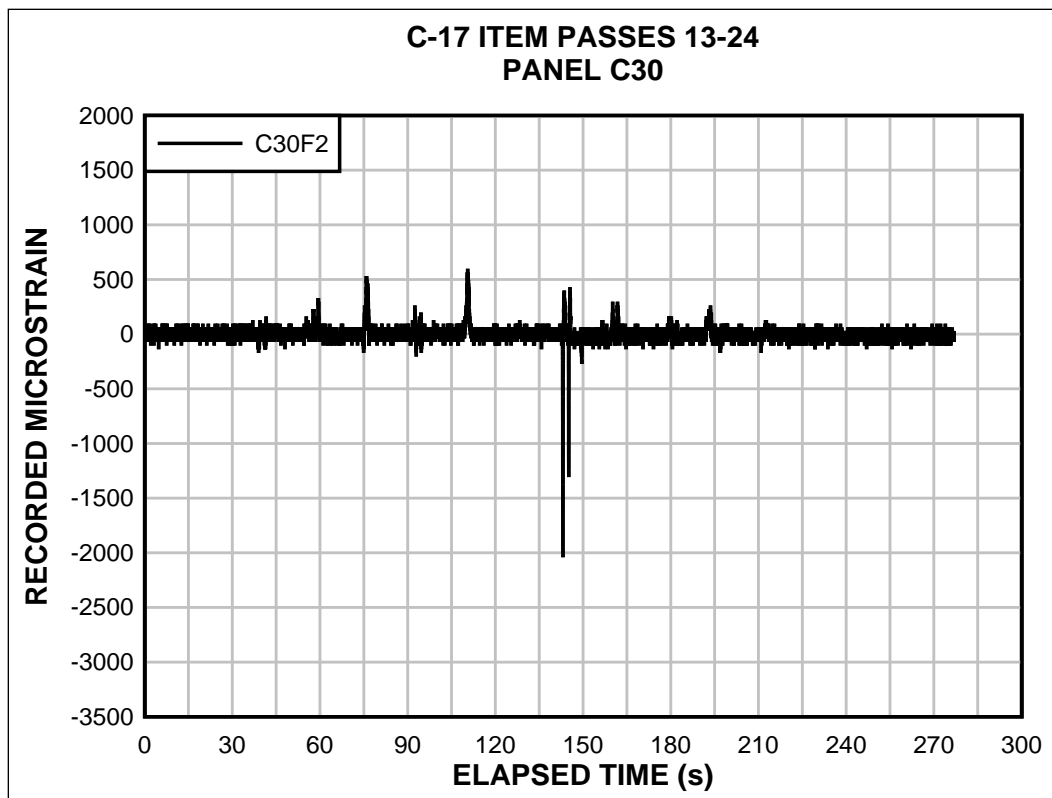


Figure 57. C-17 item, gauge C31F1, passes 13-24.

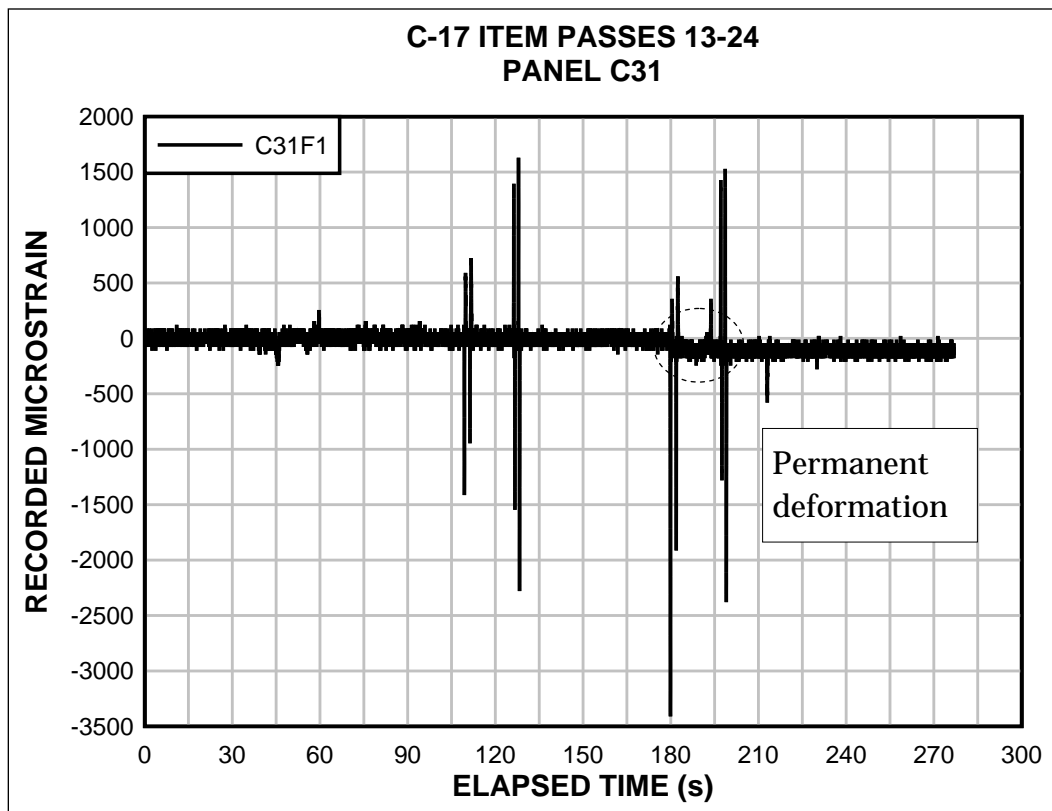


Figure 58. C-17 item, gauge C31F2, passes 13-24.

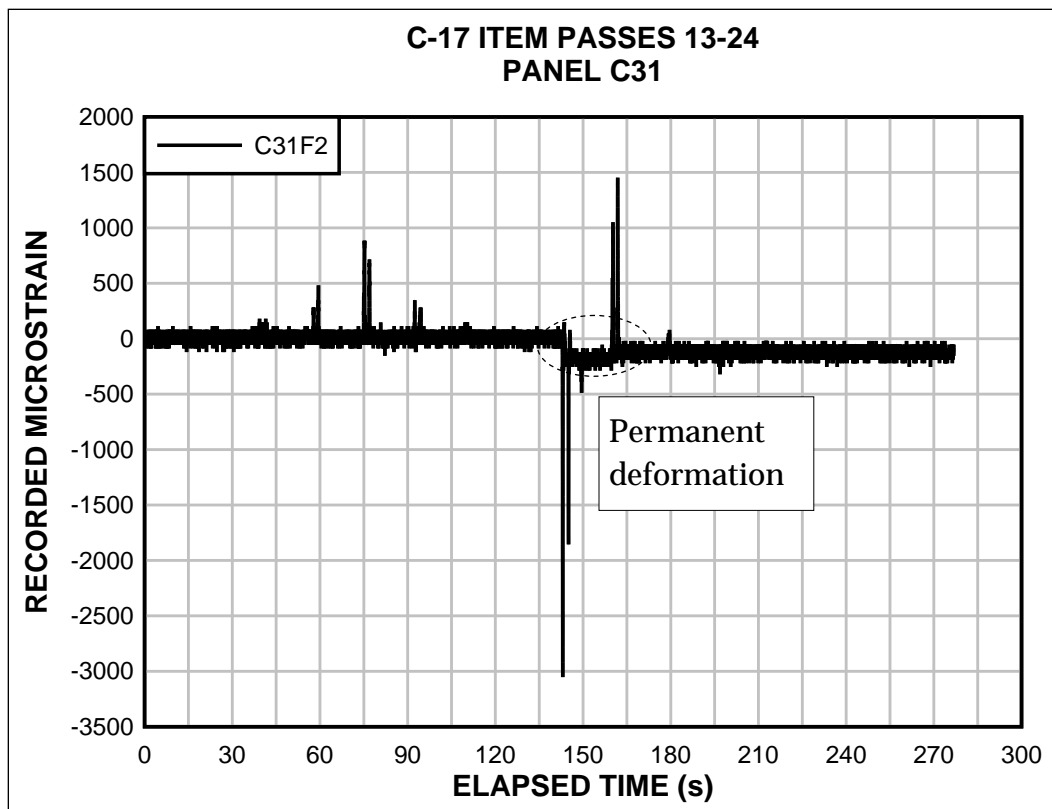


Figure 59. C-17 item, gauge C39C1, passes 13-24.

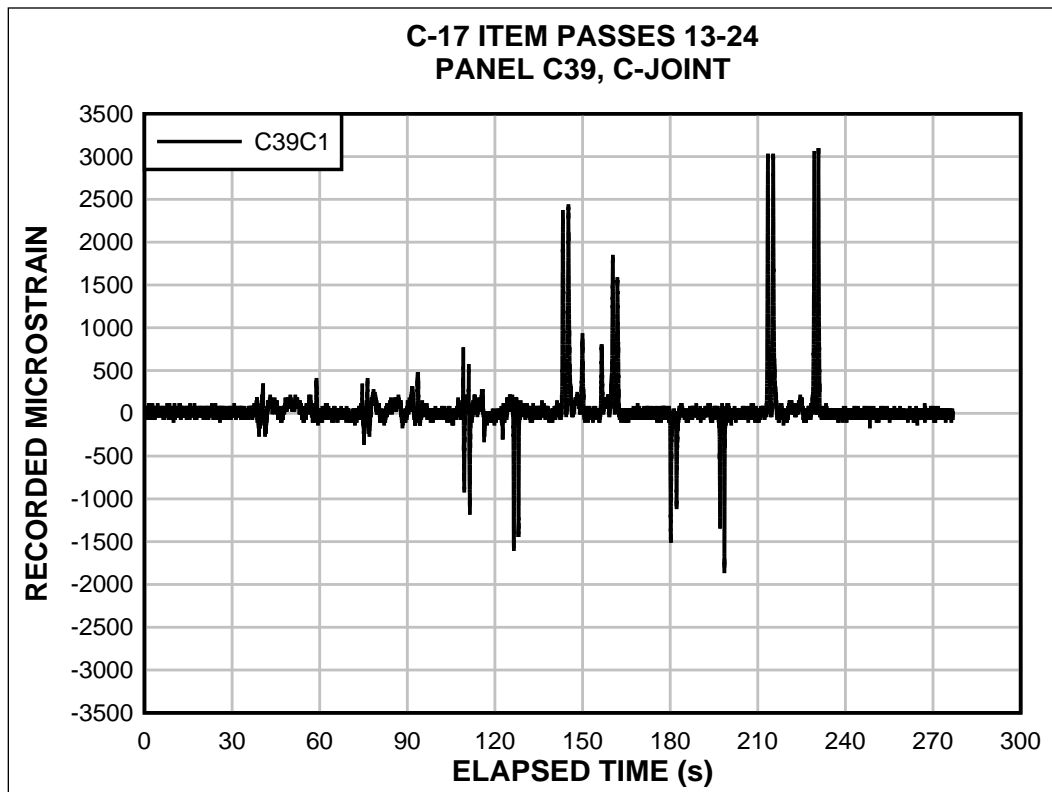


Figure 60. C-17 item, gauge C39C2, passes 13-24.

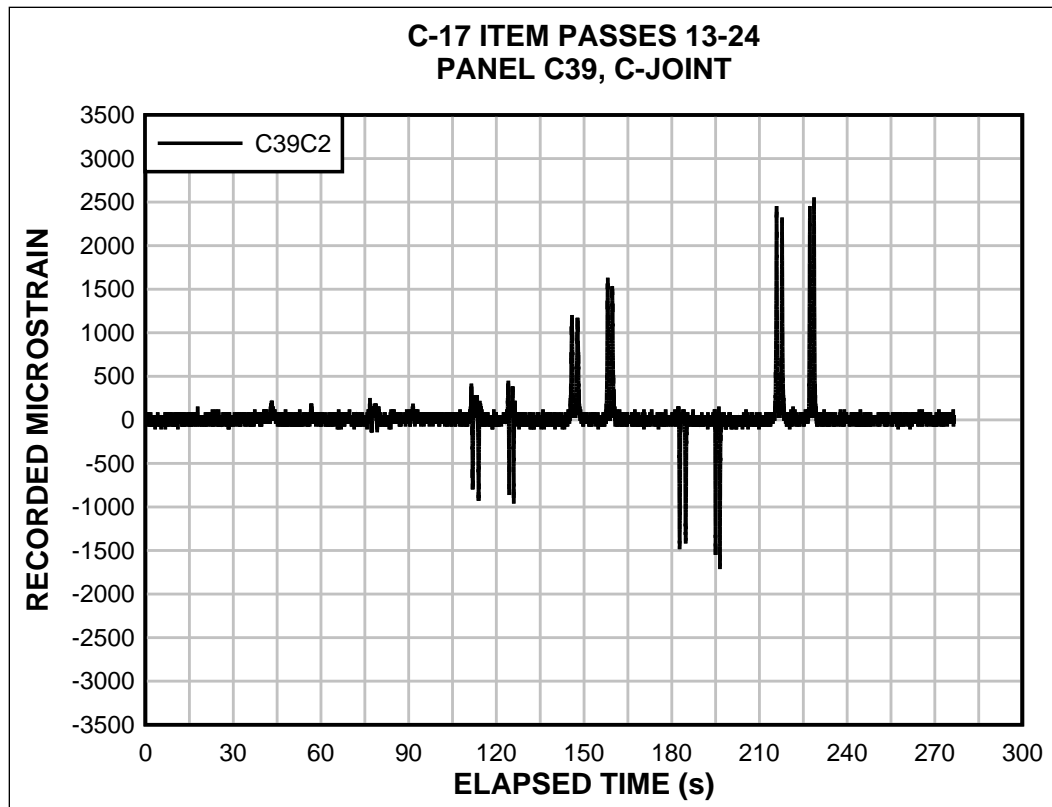


Figure 61. Maximum tensile strain for panels C30 and C31 at F-joint.

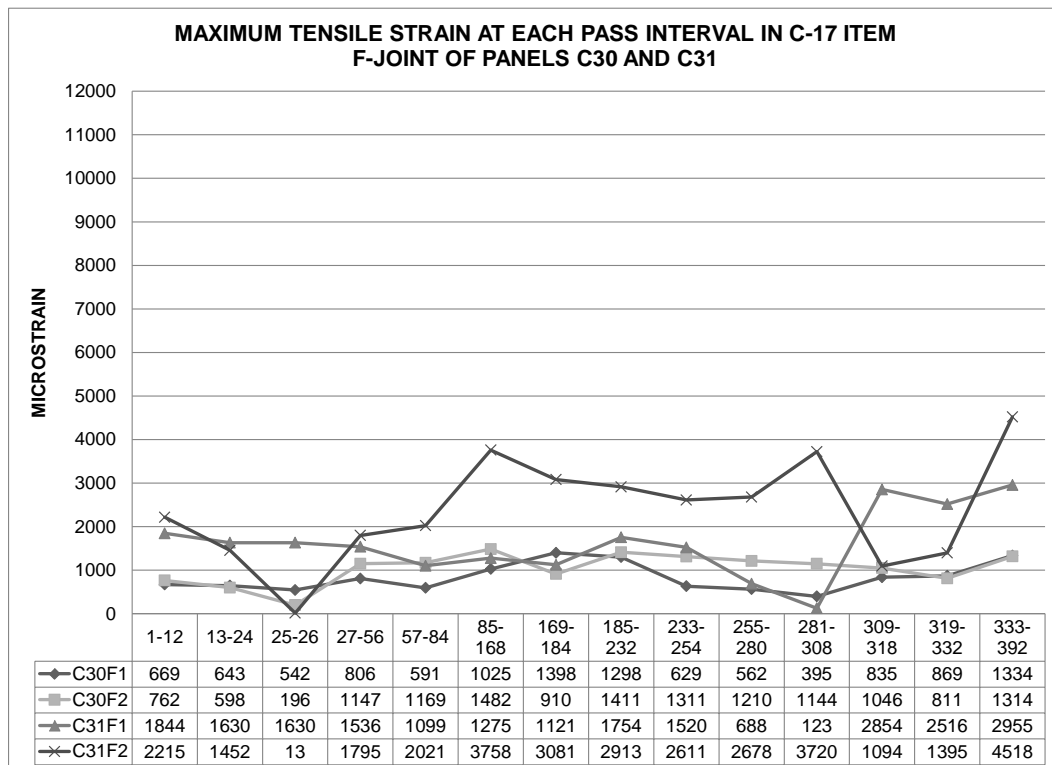


Figure 62. Maximum compressive strain for panels C30 and C31 at F-joint.

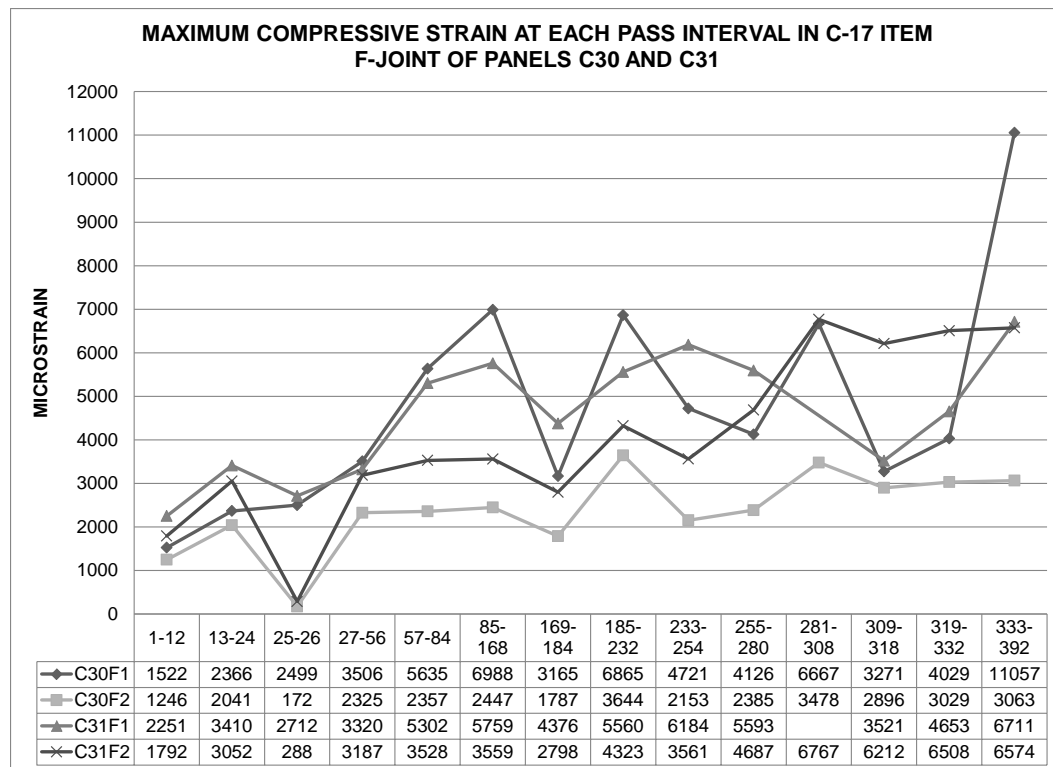


Figure 63. Maximum tensile strain for panels C34 and C35 at F-joint.

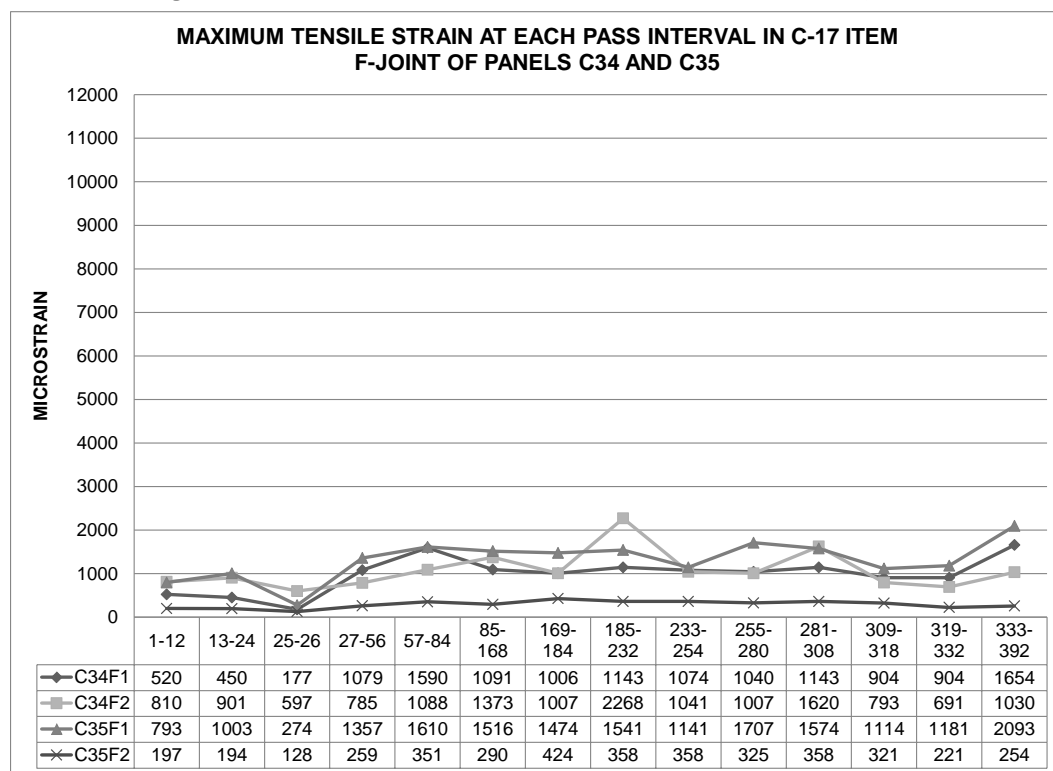


Figure 64. Maximum compressive strain for panels C34 and C35 at F-joint.

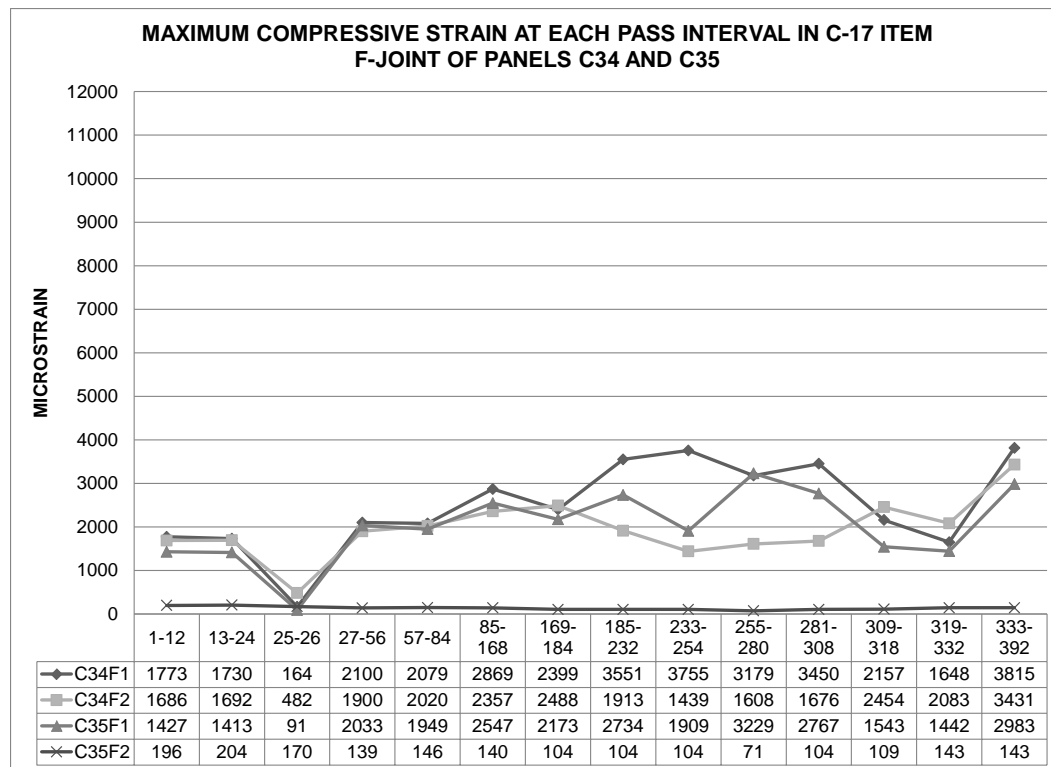


Figure 65. Maximum tensile strain for panels C38 and C39 at F-joint.

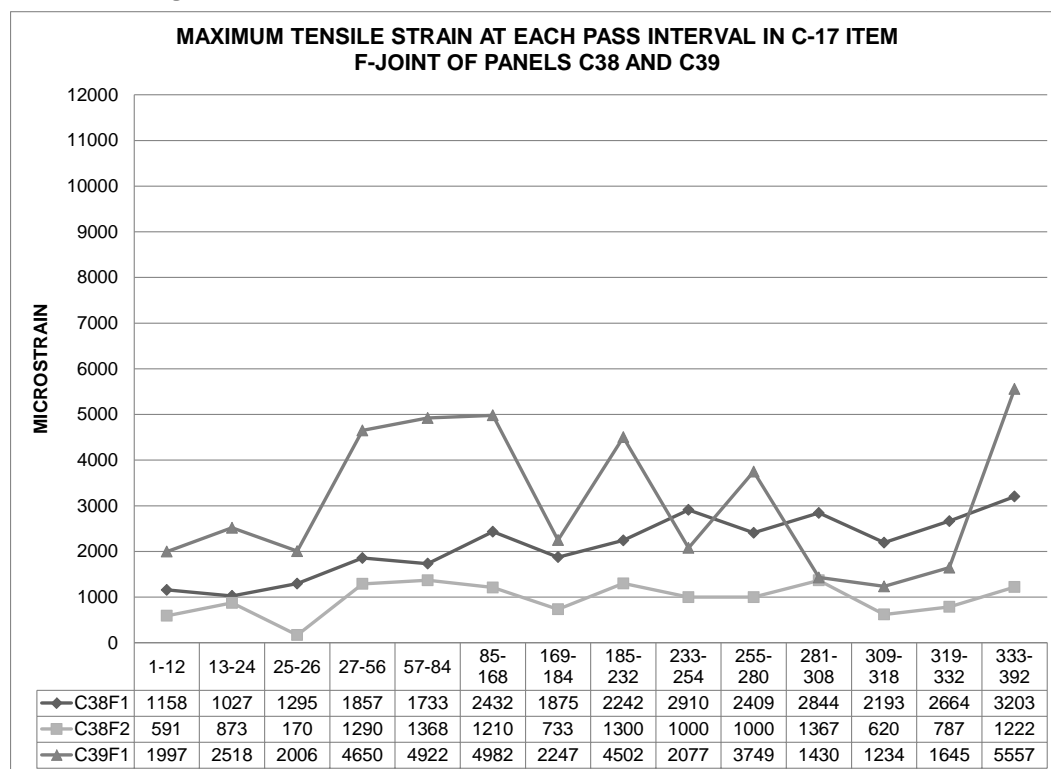


Figure 66. Maximum compressive strain for panels C38 and C39 at F-joint.

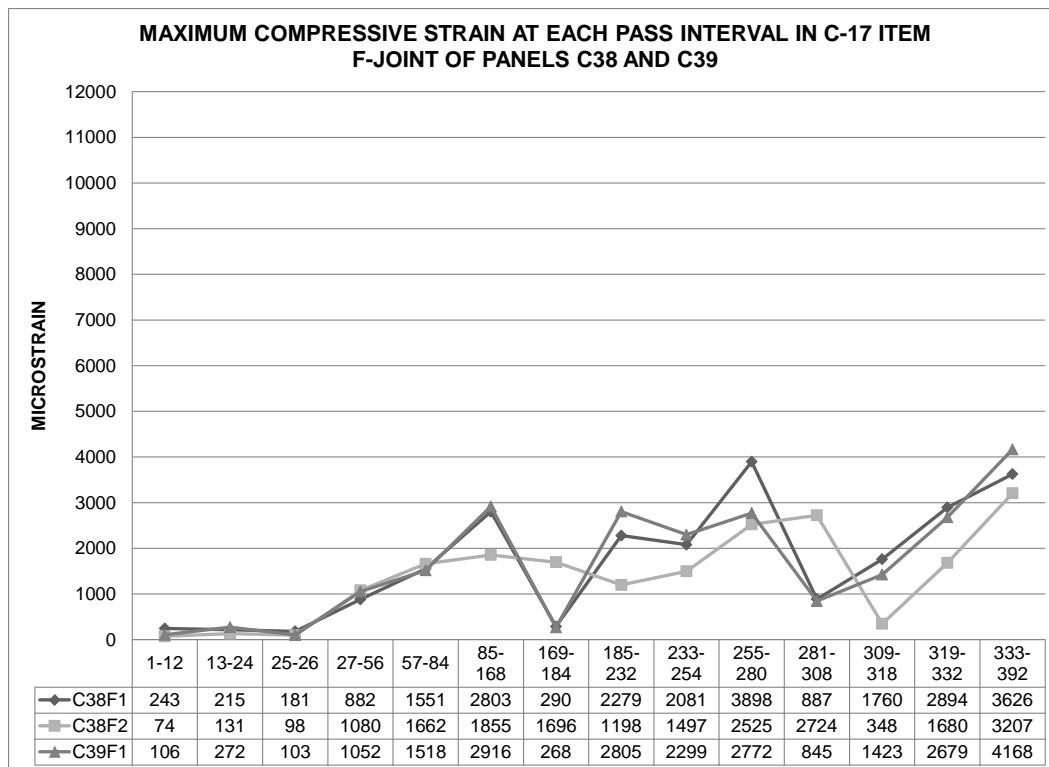


Figure 67. Maximum tensile strain for panels C26, C38 and C39 at C-joint.

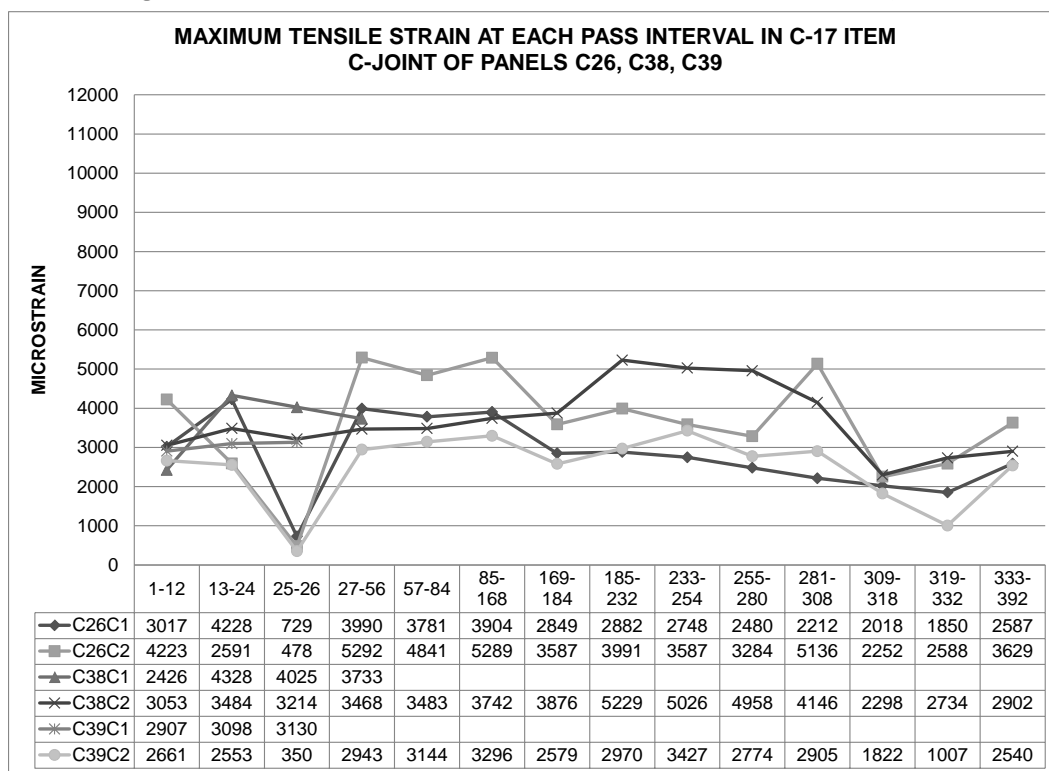
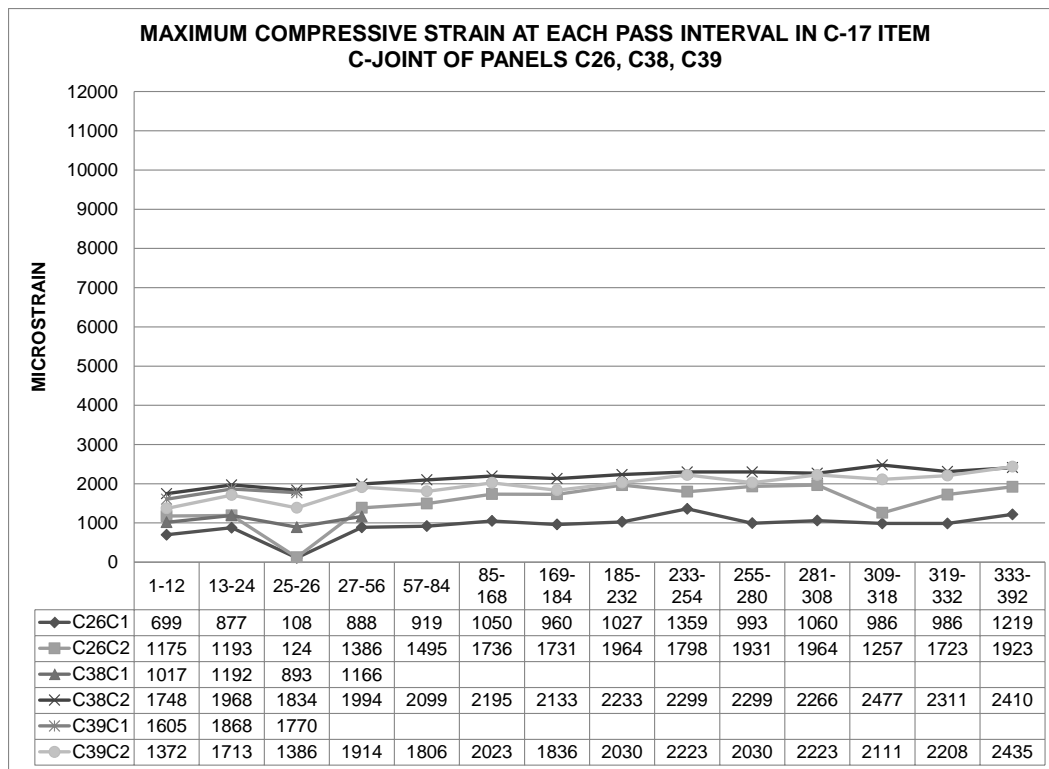


Figure 68. Maximum compressive strain for panels C26, C38 and C39 at C-joint.



4 Analysis of Results

4.1 Mat behavior

4.1.1 F-15E item

The F-15E test item sustained 240 passes (60 coverages) of simulated F-15E aircraft traffic before failure by exceeding the permanent deformation criterion. No mat breakage was noted on the test item at any point during the test, and trafficking was continued to 524 passes to capture additional data. As reported by Rushing and Tingle (2007), Rushing and Torres (2007), Rushing et al. (2008), Rushing and Mason (2008), and Garcia and Rushing (2013), most AM2 mat failures over medium strength to soft subgrades are associated with the end connectors, specifically at the upper underlap rails and the lower overlap rails. Core crushing due to buckling of the core vertical stiffeners has also been reported. Damage at the C-joint is usually a crack that propagates along the face of the female hinge, but is known to be associated with the cyclic movement at the F-joint of the panels with connecting male hinges. However, this is all common to traffic that is parallel to the short end connectors, with the majority of the load being imposed along the F-joint. In this test, traffic was conducted parallel to the long dimension of the mat, and most of the load was applied along the vertical stiffeners and along the male/female hinges. Since the C-joint has the ability to rotate easily, as opposed to the F-joint, which has increased stiffness properties, the applied load had little effect to the integrity of the mat. Since the hinge was able to rotate freely, the permanent deformation criterion was exceeded quickly, and the mat was only able to sustain approximately 15 % of the traffic applied during the AM2 baseline test over a CBR of 6 (Rushing and Tingle 2007). The system became highly unstable after a relatively limited numbers of coverages by the load cart.

4.1.2 C-17 item

The C-17 test item was trafficked until 392 passes (350 coverages) were completed. No mat breakage occurred in the test item. Typically, when AM2 mat panels are placed on medium to soft soil and subjected to simulated C-17 traffic, they tend to fail at the F-joint. The weld of the end connector breaks or one of the rails breaks free, causing separation at the joint. Cracking that propagates along the female hinge is also very common (Rushing and Tingle 2007; Rushing et al. 2008; Rushing and Mason 2008;

Garcia and Rushing 2013). However, this behavior has been associated with typical traffic operations, which occur parallel to the short end connectors. As discussed in section 4.1.1, the ability of the C-joint to rotate freely with the moving loads in this test caused premature permanent deformation. The mat system was able to sustain approximately 25% of the traffic applied during the AM2 baseline test over a CBR of 6 (Rushing and Tingle 2007). Although mat damage did not occur, instability of the system makes it unsafe to conduct many traffic operations perpendicular to the normal traffic direction, which is parallel to the short end of the mat.

4.2 Permanent deformation

4.2.1 Centerline profile

The centerline profiles for the post-traffic subgrade and the surface of the mat at various traffic intervals were analyzed to determine whether the roughness criteria were exceeded.

4.2.1.1 F-15E item

The maximum change in elevation between one or two stations along the centerline profile was less than 0.5 in. on both the subgrade and mat surface. The 1.25-in.-deep maximum value established for roughness for F-15E aircraft traffic was not exceeded. Therefore, the system performed adequately to prevent excessive roughness from occurring along the profile. This behavior was also documented in previous tests listed in Table 2.

4.2.1.2 C-17 item

The maximum change in elevation between one or two stations along the centerline profile was below the 3.0-in.-deep maximum value established for roughness for C-17 aircraft traffic. Therefore, the system performed adequately to prevent excessive roughness from occurring along the profile. This behavior was also documented in previous tests listed in Table 2.

4.2.2 Cross sections

The permanent deformations on the subgrade, the loaded mat surface, and the unloaded mat surface were analyzed to determine whether the deformation criteria were exceeded. The deformation at each location was determined as the difference in elevation from the average height of the elevated material on each side of the trough to the deepest point in the

bottom of the trough. On the subgrade, the trough values were about 2 in. and 1.6 in. for the F-15E and C-17 items, respectively. However, as shown in Figures 31 and 32, the change in the elevation of the centerline profile on the subgrade from the pretest measurements was only about 1 in. throughout the length of both test items (ignoring boundary conditions). As shown in Figures 35 through 40, the trough was not located on the centerline. In the F-15E item, it was located about 1 ft offset from the centerline. In the C-17 item, it was offset about 3 ft from the centerline. The centerline of traffic was located along the center of panels C89, C90, C91, and C92 in the F-15E item. Since these panels were rotating about their C-joints during traffic, which were located 1 ft offset from centerline, most deformation on the subgrade occurred 1 ft offset from the centerline. In the C-17 item, the centerline was located along panels C33, C34, C35, and C36. The distributed load caused the C-joints 3 ft offset from the centerline to rotate increasingly during traffic; thus, most subgrade deformation occurred 3 ft offset from the centerline.

4.2.2.1 F-15E item

For the F-15E test item, the maximum permanent deformation after 524 passes was 3.17 in., 2.95 in., and 1.69 in. on the subgrade, loaded, and unloaded mat surface, respectively. The maximum permanent deformation on the mat and subgrade exceeded the 1.25-in. limit. Therefore, the system did not perform adequately to prevent excessive roughness from occurring.

4.2.2.2 C-17 item

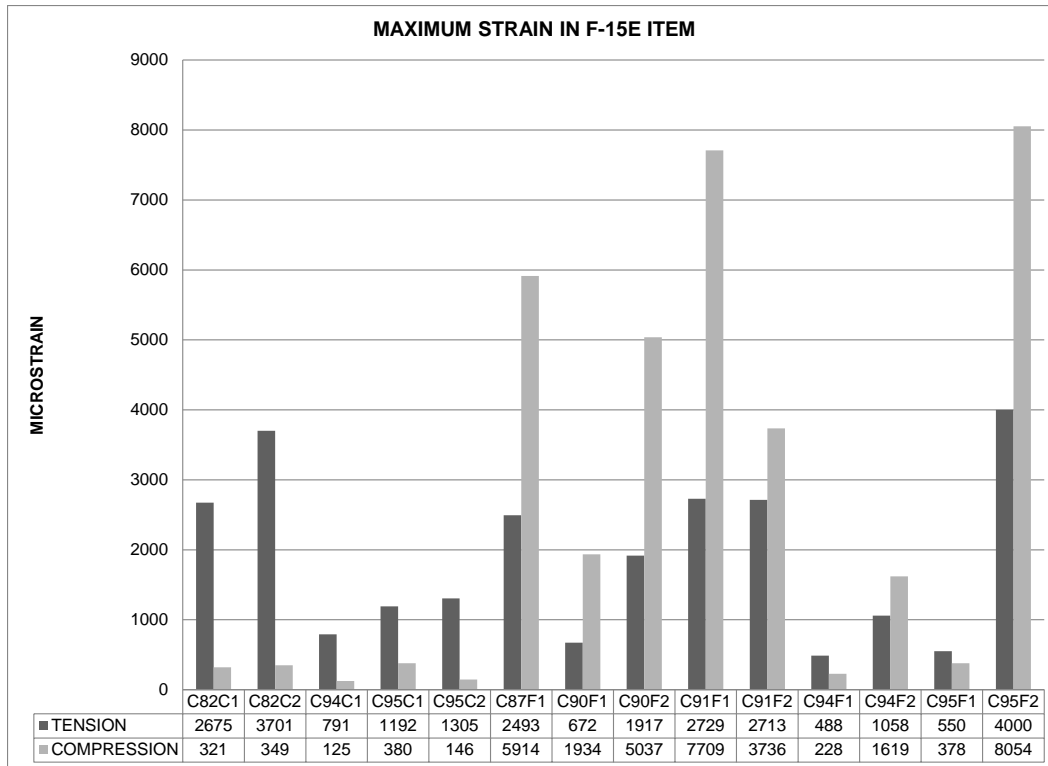
For the C-17 test item, the maximum permanent deformations after 392 passes were 2.83 in., 3.00 in., and 2.96 in. on the subgrade, loaded, and the unloaded mat surface, respectively. The failure criteria state that the permanent deformation on the mat surface must not exceed 3.0 in. for C-17 traffic. Therefore the test item wasn't able to prevent excessive permanent deformation before the baseline performance criteria of 1,500 passes was reached (Rushing and Tingle 2007).

4.3 Strain gauge readings

Mat breakage did not occur in the F-15E item; therefore, failure of a panel could not be linked to a measured strain at a particular location. Larger strains were measured at the F-joint than at the C-joint. This behavior is

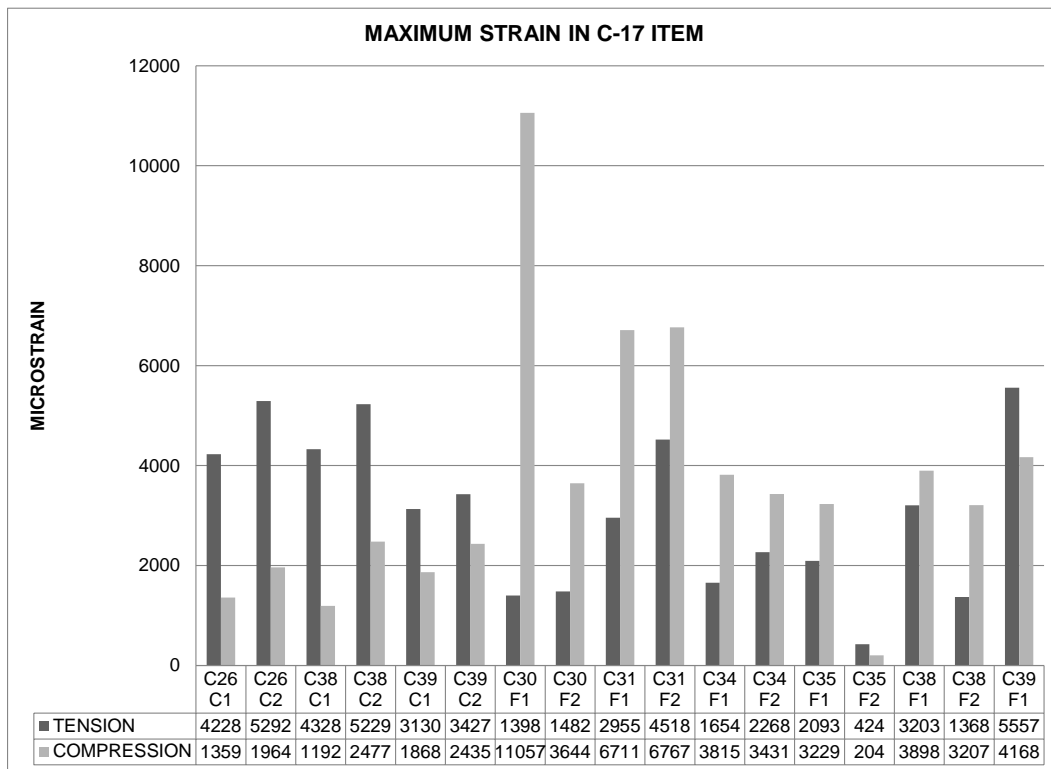
understandable since the locking bar at the F-joint causes a greater resistance to cyclic movement, whereas the C-joint is free to rotate with the moving load without straining the female hinge. Compressive strains tended to accumulate throughout the test and were typically higher than tensile strains at the F-joint. The opposite was true at the C-joint; tensile strains were generally higher than compressive strains and tended to accumulate towards the end of the test. The single-wheel load applied on panels C94 and C95 likely triggered the panels to bow in a clockwise rotation, causing the female hinge of both panels to pull at the bottom flange. When the load was applied on panels C86 and C87, both panels bowed upward in a counterclockwise rotation. This rotation created tensile strains at the female hinge of panel C82. As deformation increased in the traffic area and the system became more unstable, panels C94, C95, C86, and C87 were able to bow upward in increasing amounts, causing higher tensile strains at the female hinges of C94, C95, and C82. A summary of the maximum strain measured by each working gauge in the F-15E item is plotted in Figure 69.

Figure 69. Maximum strains for F-15E Test Item.



Unlike the F-15E item, the magnitudes of the tensile strains at the C-joint of panels in the C-17 item were generally higher than at the F-joint. It is possible that, since the multiple-wheel load cart distributes the load over a much wider area, a series of connected panels was allowed to bow, instead of just one panel attempting to rotate at the C-joint. Since both the male and female hinges of an instrumented C-joint were trying to rotate in opposite directions with the moving load, high tensile strains were measured at the female hinge. Compressive strains were generally larger than tensile strains at the F-joint. A clear pattern could not be established as to whether compressive strain was predominant at the lower overlap or the upper underlap rail. A summary of the maximum strain measured by each working gauge in the C-17 item is plotted in Figure 70.

Figure 70. Maximum strains for C-17 test item.



Compared to the F-15E item, tensile and compressive strains measured at the F-joints and C-joints were higher in the C-17 item. At the C-joint of panels in the C-17 item, tensile and compressive strains reached maximum values of more than 3,000 and 1,000 microstrain, respectively, at each gauge. At the C-joint of panels in the F-15E item, maximum tensile strains remained mostly under 3,000 microstrain, and maximum compressive strains were well below 1,000 microstrain for each gauge. At the F-joint of

panels in the C-17 item, maximum tensile strains were greater than 1,000 microstrain, with the exception of one gauge (C35F2). Maximum compressive strains were mostly greater than 3,000 microstrain. In the F-15E item, maximum tensile strains at the F-joints were under 3,000 microstrain, with the exception of gauge C95F2. Compressive strains were more comparable to those measured in the C-17 item, but were still generally less than 3,000 microstrain.

5 Conclusions and Recommendations

5.1 Conclusions

The purpose of this investigation was to evaluate the ability of the AM2 airfield mat to sustain simulated F-15E and C-17 aircraft traffic when placed in the opposite lay direction (90 deg) over a CH subgrade with a CBR of 6. Permanent deformation and mat breakage were monitored to determine the number of passes to predetermined failure criteria, and strain data were recorded continuously. The results from both test items were compared to those documented in previous tests where AM2 was installed in the brickwork pattern. The information obtained from these tests will be used to feed the NAVAIR DIM.

The following conclusions were derived from accelerated traffic testing of the AM2 airfield matting system installed in the opposite lay direction conducted April 2013:

1. The AM2 mat system was able to sustain 240 passes of simulated F-15E traffic before failure by permanent deformation. Mat breakage did not occur. In terms of number of passes to failure, the performance reduced by approximately 85% when compared to tests conducted under typical traffic operations on a CBR of 6.
2. The AM2 mat system was able to sustain 392 passes of C-17 traffic before failure by permanent deformation. Mat breakage did not occur. In terms of number of passes to failure, the performance reduced by approximately 75% when compared to tests conducted under typical traffic operations on a CBR of 6.
3. The strain gauges placed on the F-joints and C-joints functioned as designed to monitor strains during trafficking. Initial data analysis showed that the gauge responses correctly followed the expected load paths. Strain magnitude varied depending on the location and position of the aircraft simulator. Sufficient data were gathered for input to the DIM.
4. Although panel failures did not occur, an accumulation of compressive strain was typical at the F-joint. An accumulation of tensile strain was typical at the C-joint. Since AM2 mat failures are associated with high compressive strain, it is possible that failure would have been noted at the F-joint before any damage occurred at the C-joint if trafficking had continued. This follows the general failure mechanisms of AM2 mat

panels, which tend to have breakage at the end connector rails when installed on soft soils.

5.2 Recommendations

Traffic in the opposite lay direction of the AM2 mat system should be limited to a small number of operations. Instability of the system can cause damage to aircraft and risk the safety of personnel operating the aircraft.

References

ASTM International. 2008. *Standard test method for determination of water (moisture) content of soil by microwave oven heating*. Designation: D 4643-08. West Conshohocken, PA: ASTM.

ASTM International. 2010. *Standard test method for in-place density and water content of soil and soil-aggregate by nuclear methods (shallow depth)*. Designation: D 6938-10. West Conshohocken, PA: ASTM.

Garcia, L. T. and T. W. Rushing. 2013. *AM2 sand subgrade sensitivity test*. ERDC/GSL TR-13-10. Vicksburg, MS: U.S. Army Engineer Research and Development Center.

Garcia, L., T. W. Rushing, and Q. S. Mason. 2012. *Evaluation of Webcore prototype AMX mat system*. ERDC/GSL TR-12-14. Vicksburg, MS: U.S. Army Engineer Research and Development Center.

Garcia, L., T. W. Rushing, and Q. S. Mason. 2014a. *AM2 25 CBR subgrade sensitivity test*. ERDC TR-14-7. Vicksburg, MS: U.S. Army Engineer Research and Development Center.

Garcia, L. , T. W. Rushing, B. A. Williams, and C. A. Rutland. 2014b. *AM2 100 CBR subgrade sensitivity test*. ERDC TR-14-37. Vicksburg, MS: U.S. Army Engineer Research and Development Center.

Naval Air Warfare Center, Aircraft Division. 2006. *Expeditionary airfield AM2 mat certification requirements*. NAWCADLKE-MISC-48J200-0011. Lakehurst, NJ: NAWCAD.

Rushing, T. W., and J. S. Tingle. 2007. *AM2 and M19 airfield mat evaluation for the Rapid Parking Ramp Expansion Program*. ERDC/GSL TR-07-5. Vicksburg, MS: U.S. Army Engineer Research and Development Center.

Rushing, T. W., and N. Torres. 2007. *Prototype mat system evaluation*. ERDC/GSL TR-07-29. Vicksburg, MS: U.S. Army Engineer Research and Development Center.

Rushing, T. W., and Q. S. Mason. 2008. *AM2 15 CBR subgrade sensitivity test for the Rapid Parking Ramp Expansion Program*. ERDC/GSL TR-08-25. Vicksburg, MS: U.S. Army Engineer Research and Development Center.

Rushing, T. W., L. Garcia, and Q. S. Mason. 2011. *Large-scale 6-CBR prototype mat system evaluation for the AMX program*. ERDC/GSL TR-11-37. Vicksburg, MS: U.S. Army Engineer Research and Development Center.

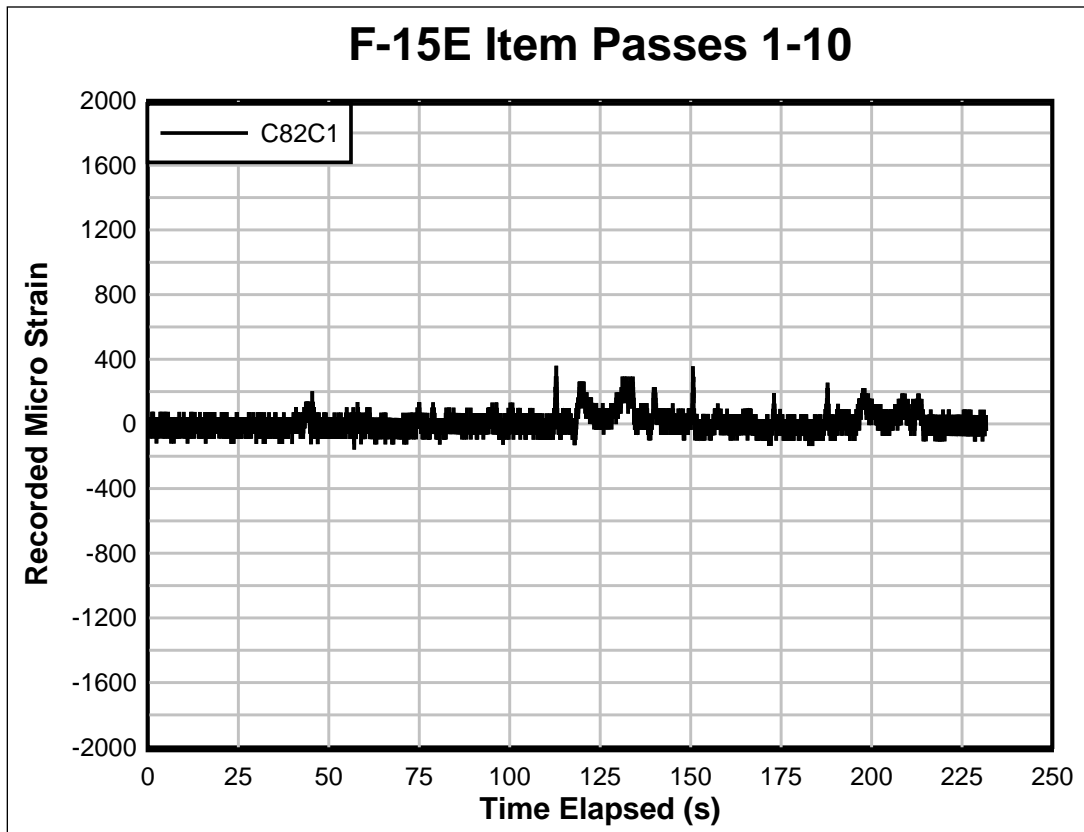
Rushing, T. W., L. Garcia, and Q. S. Mason. 2012. *Evaluation of Faun aluminum mat systems*. ERDC/GSL TR-12-32, Vicksburg, MS: U.S. Army Engineer Research and Development Center.

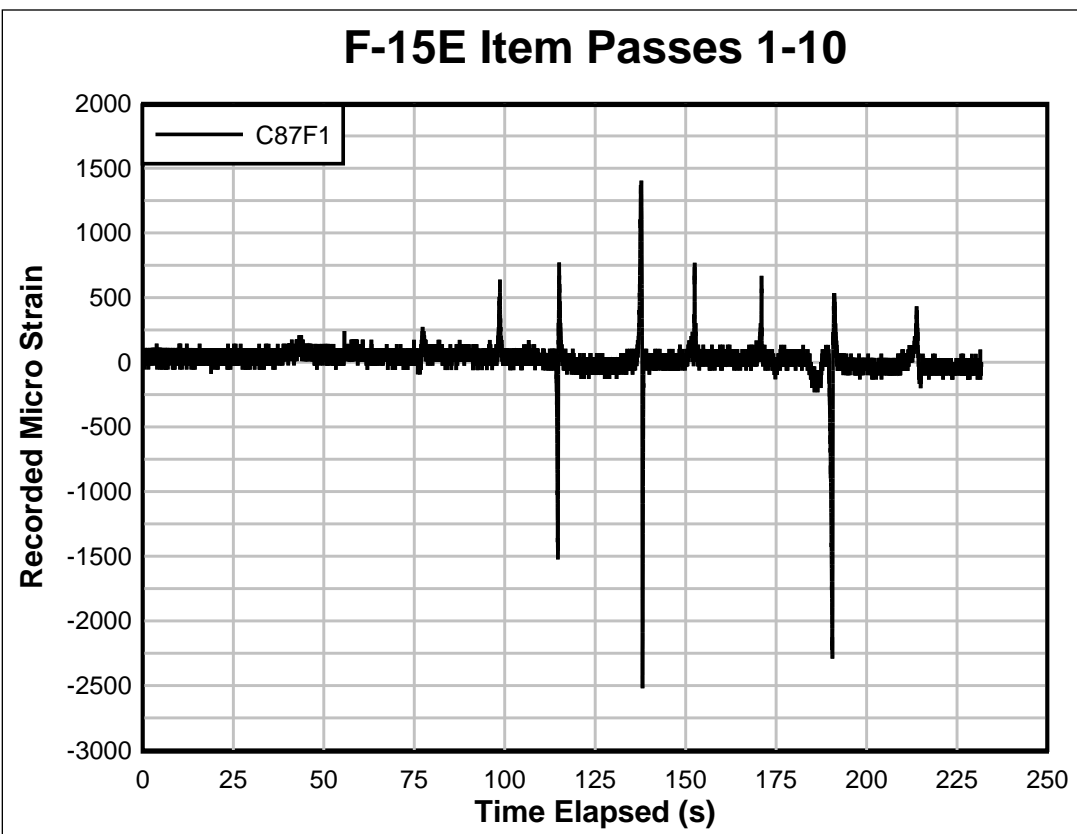
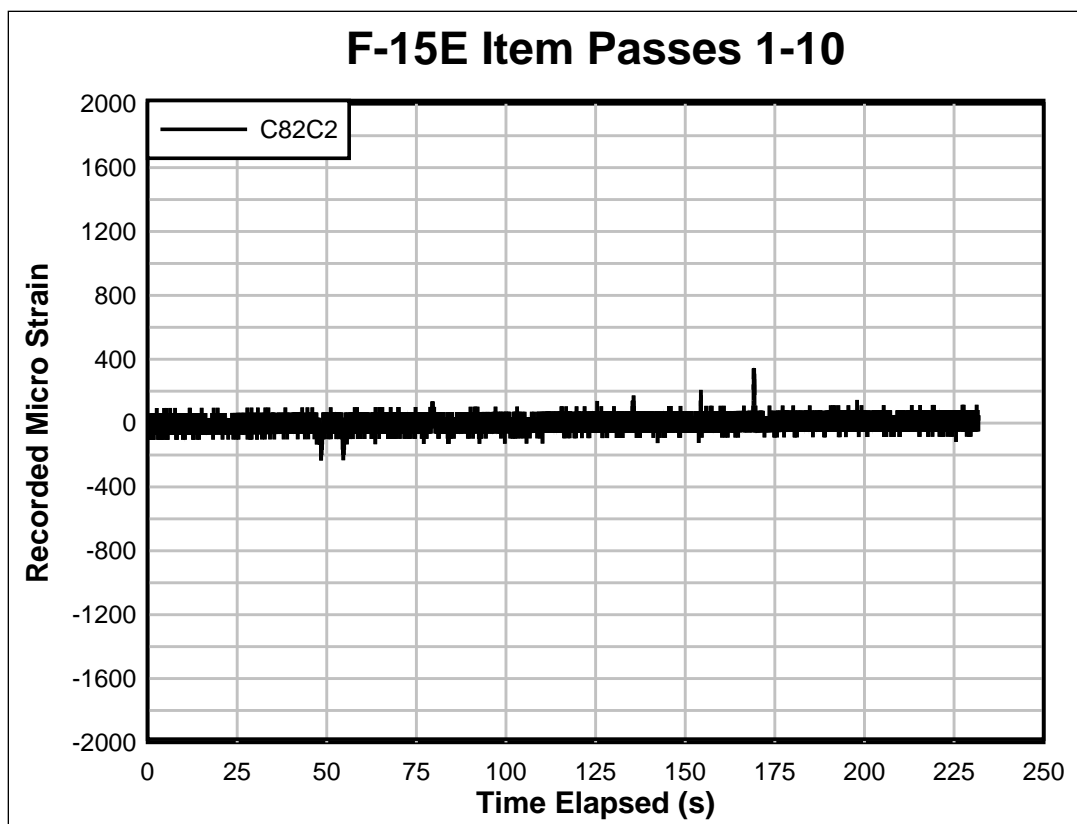
Rushing, T. W., N. Torres, and Q. Mason. 2008. *AM2 10 CBR subgrade sensitivity test for the Rapid Parking Ramp Expansion Program*. ERDC/GSL TR-08-13. Vicksburg, MS: U.S. Army Engineer Research and Development Center.

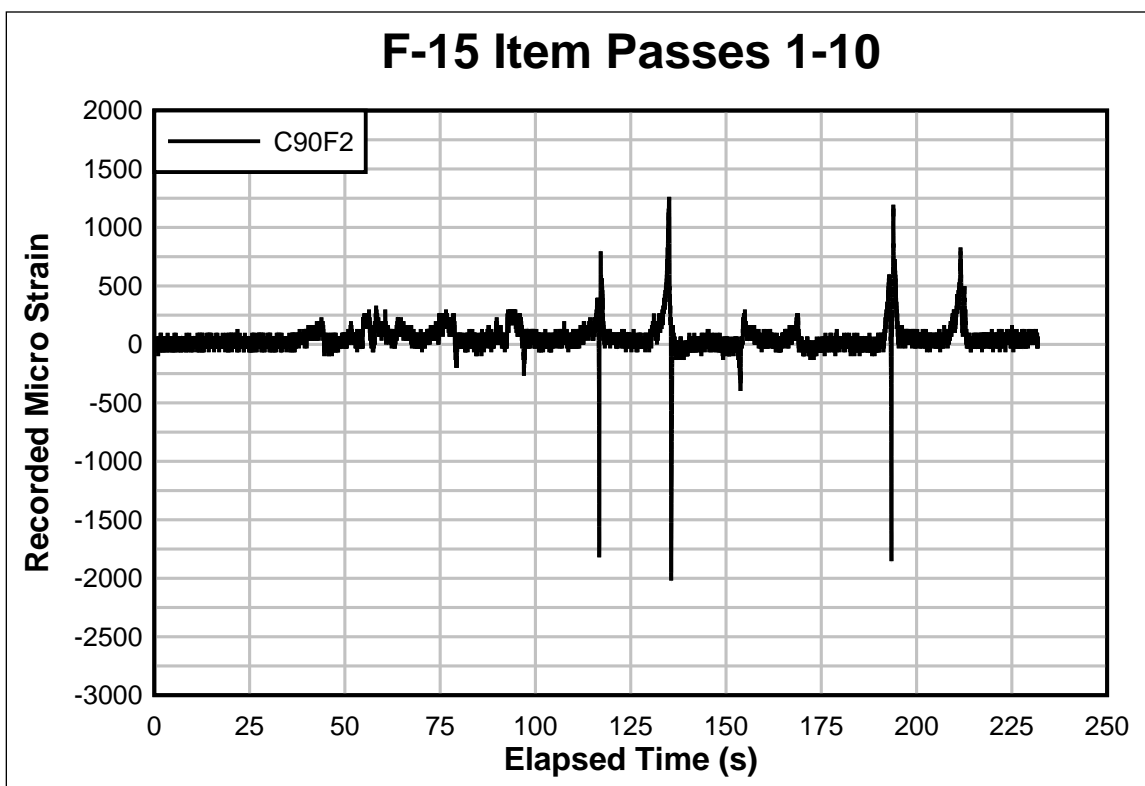
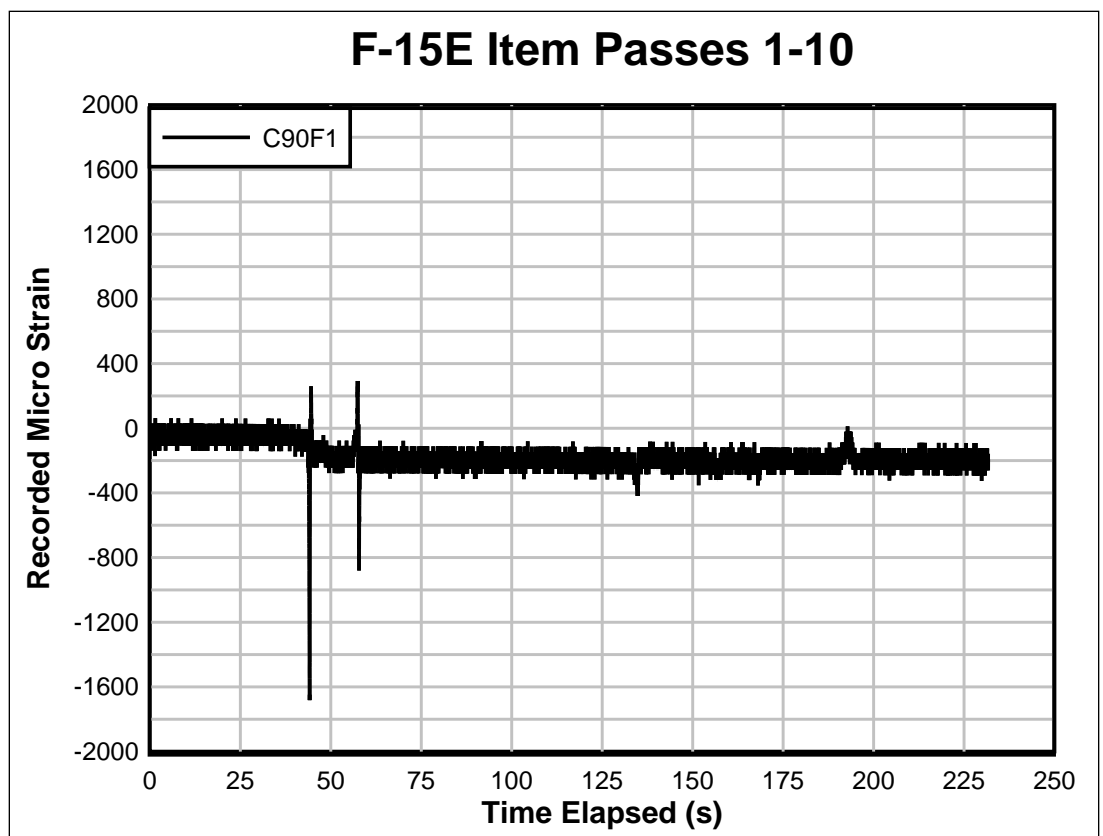
Rushing, T. W., L. Garcia, J. S. Tingle, P. G. Allison, and C. A. Rutland. 2014. *AM2 3-4 alternate lay pattern evaluation*. ERDC/GSL TR-14-38. Vicksburg, MS: U.S. Army Engineer Research and Development Center.

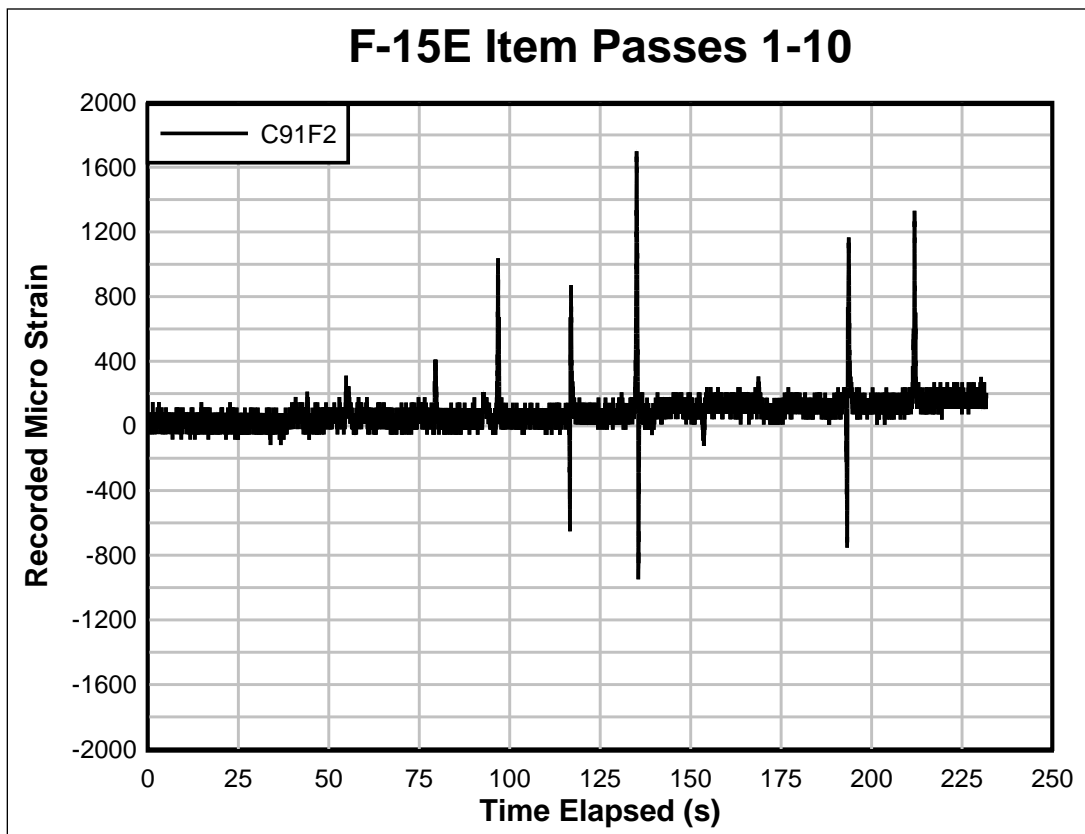
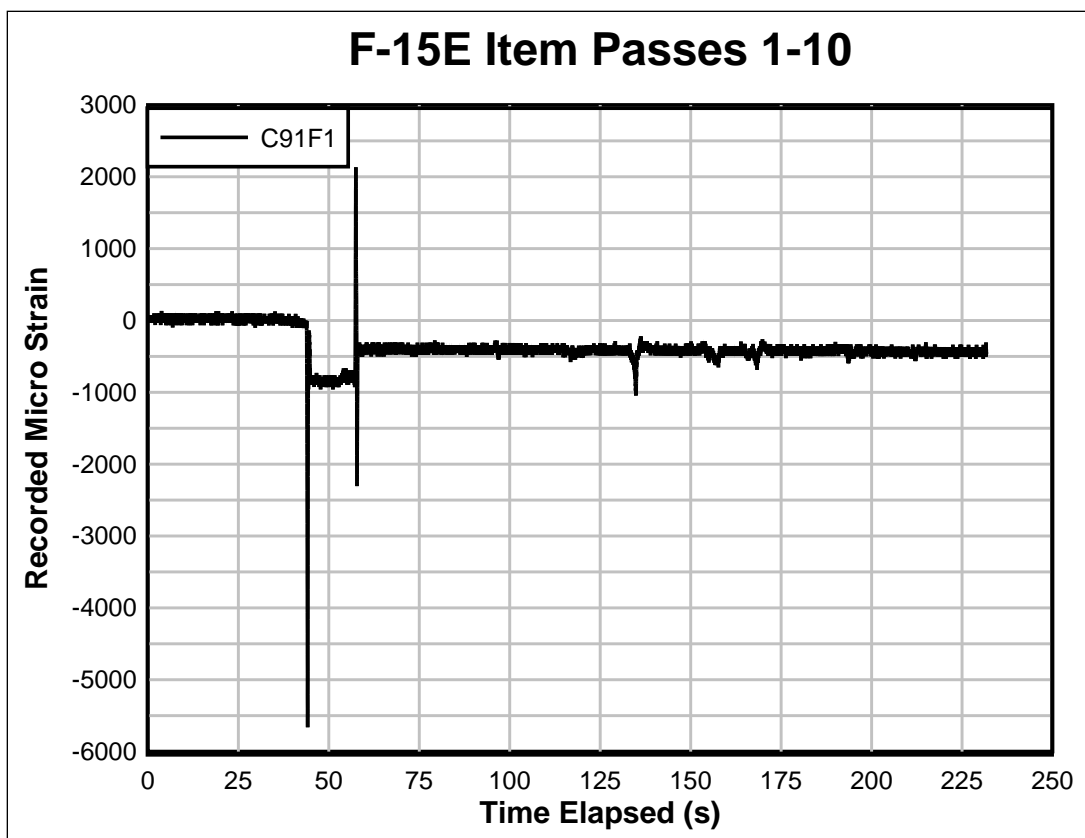
U.S. Army Engineer Research and Development Center. 1995. *Standard test method for California Bearing Ratio of soils in place*. Designation: CRD-C654-95. Vicksburg, MS: ERDC.

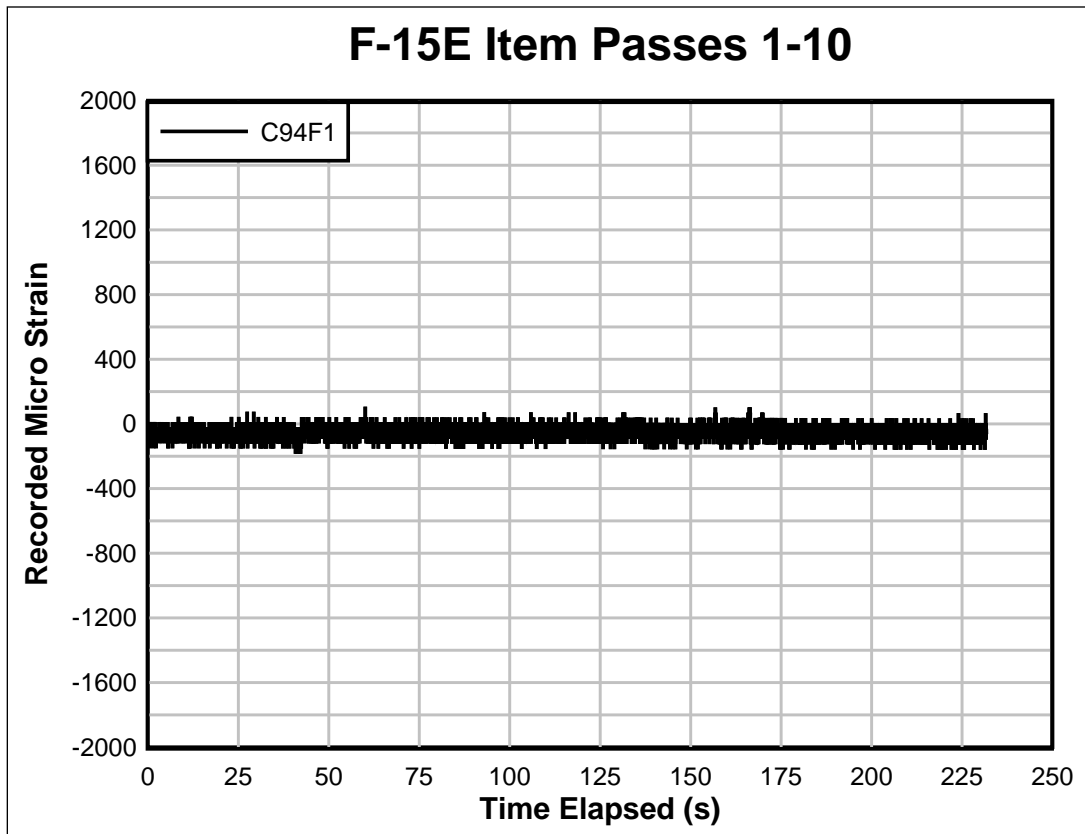
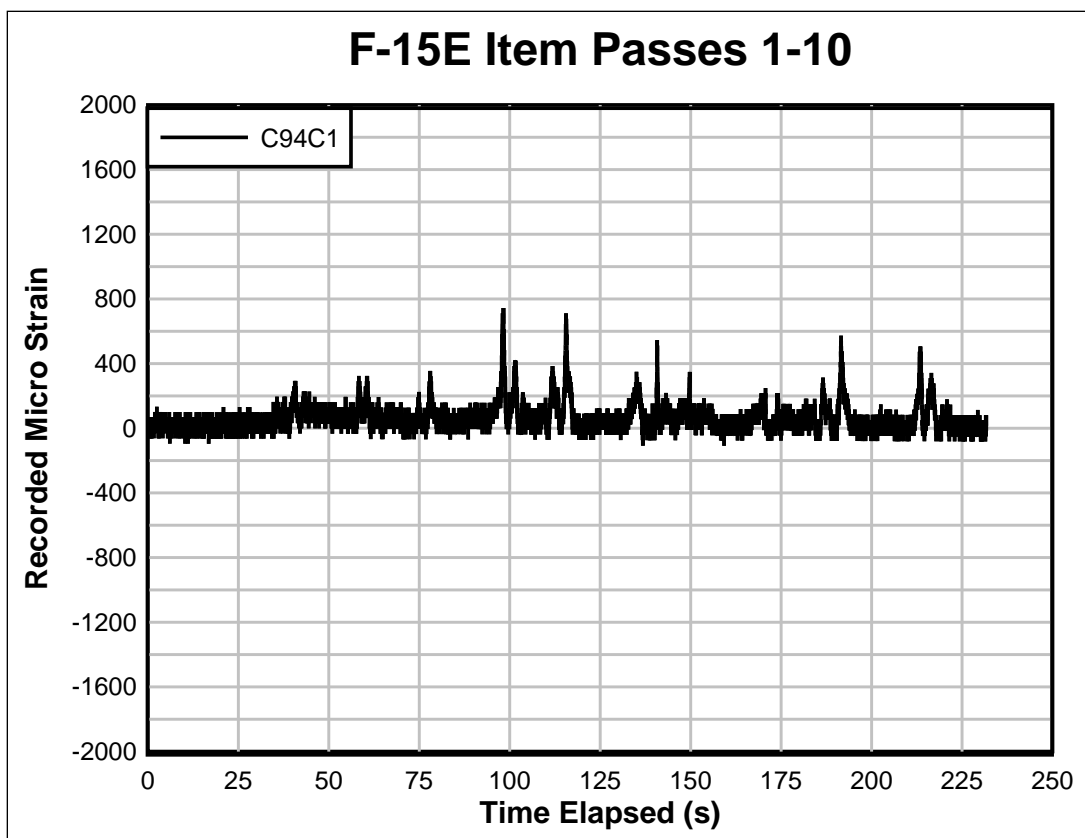
Appendix A: Strain gauge data for F-15E item

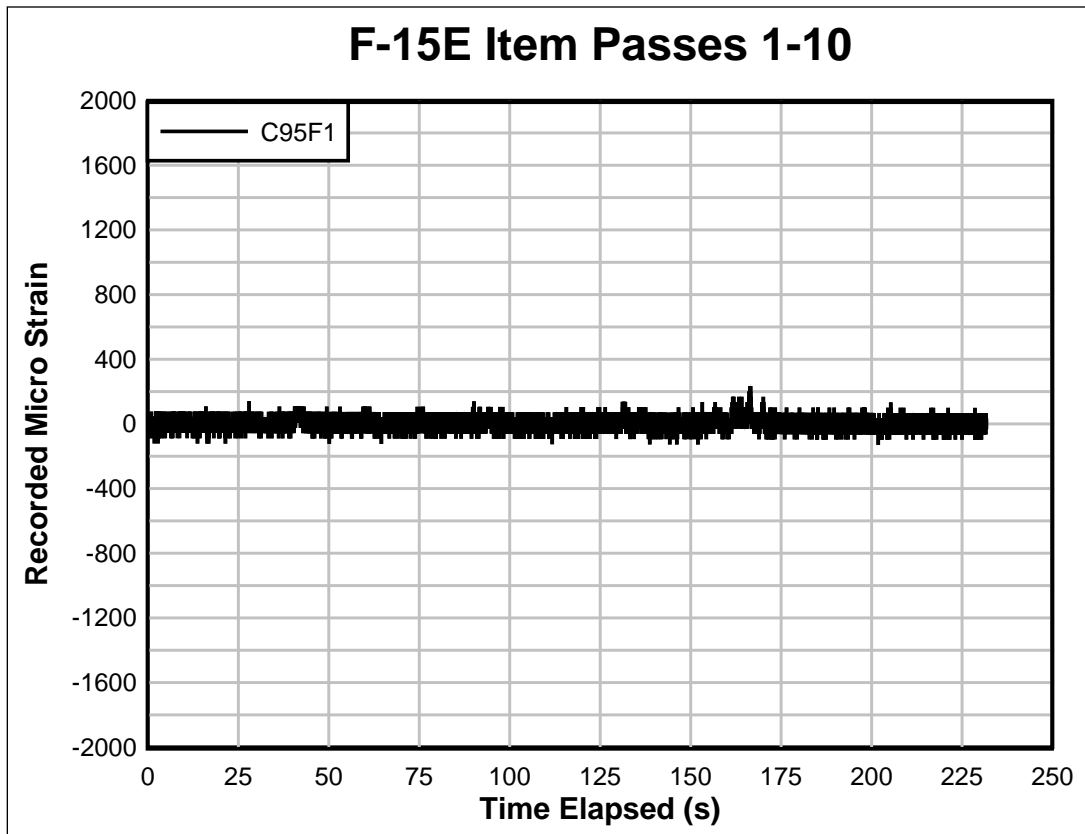
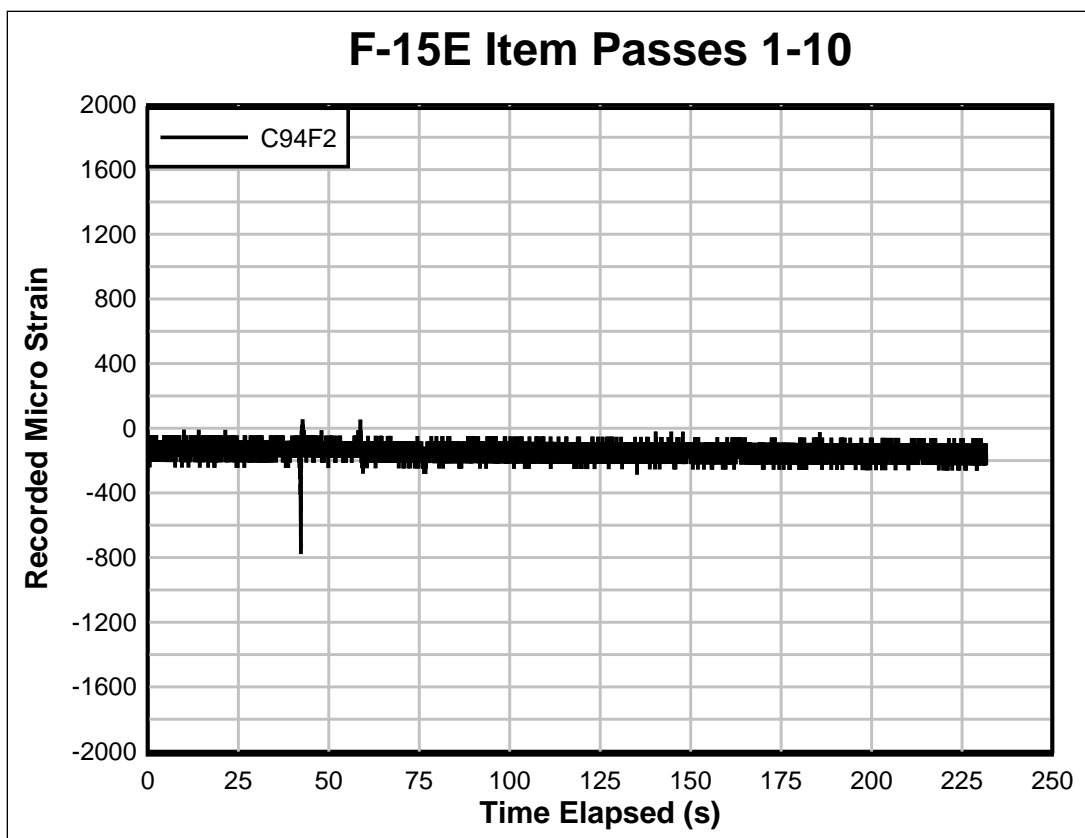


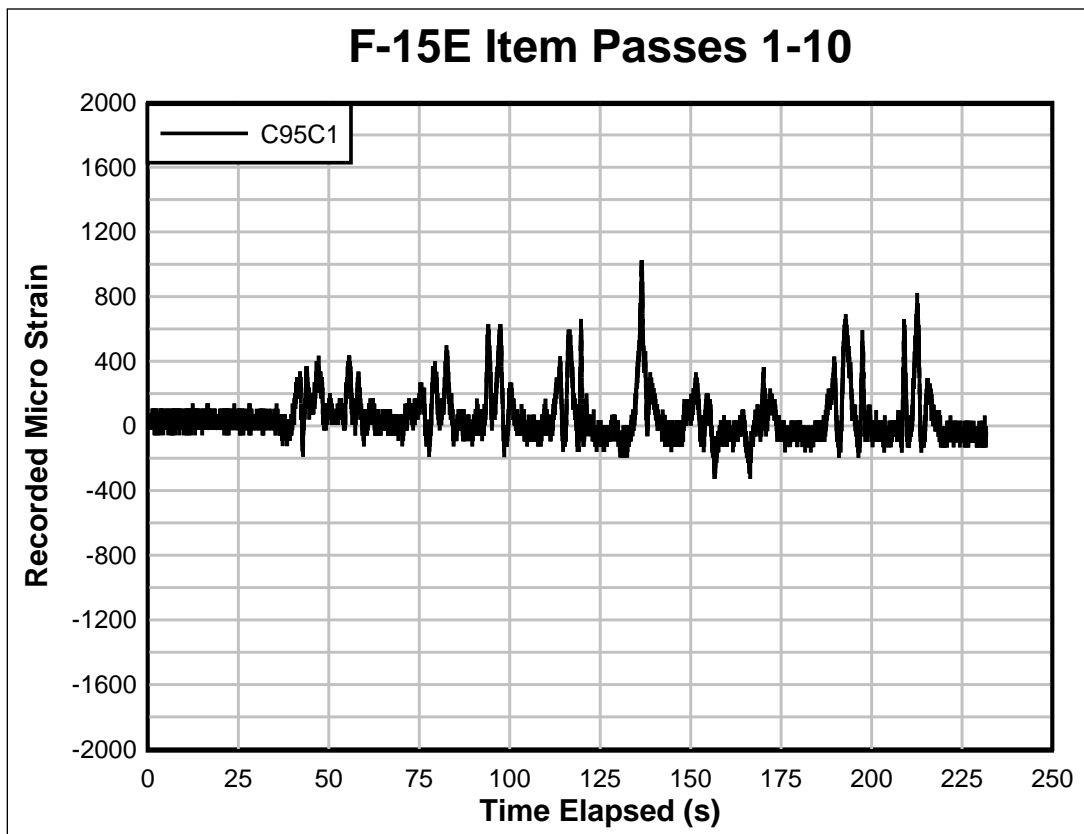
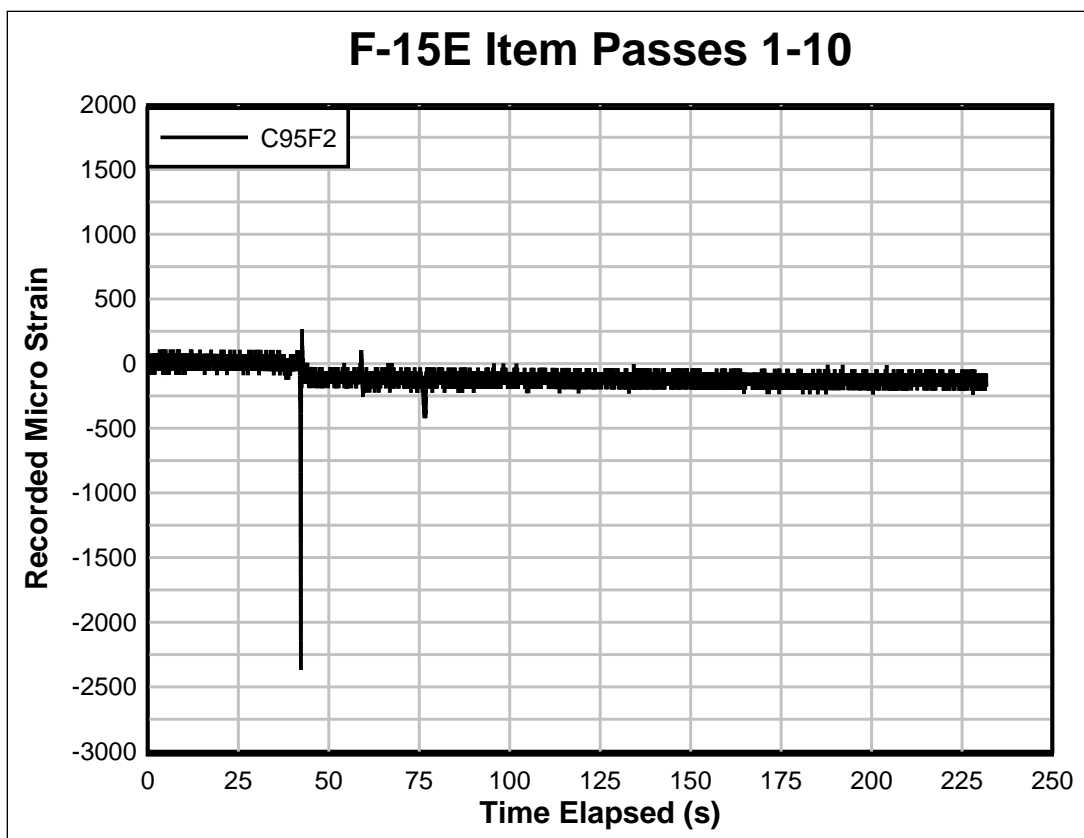


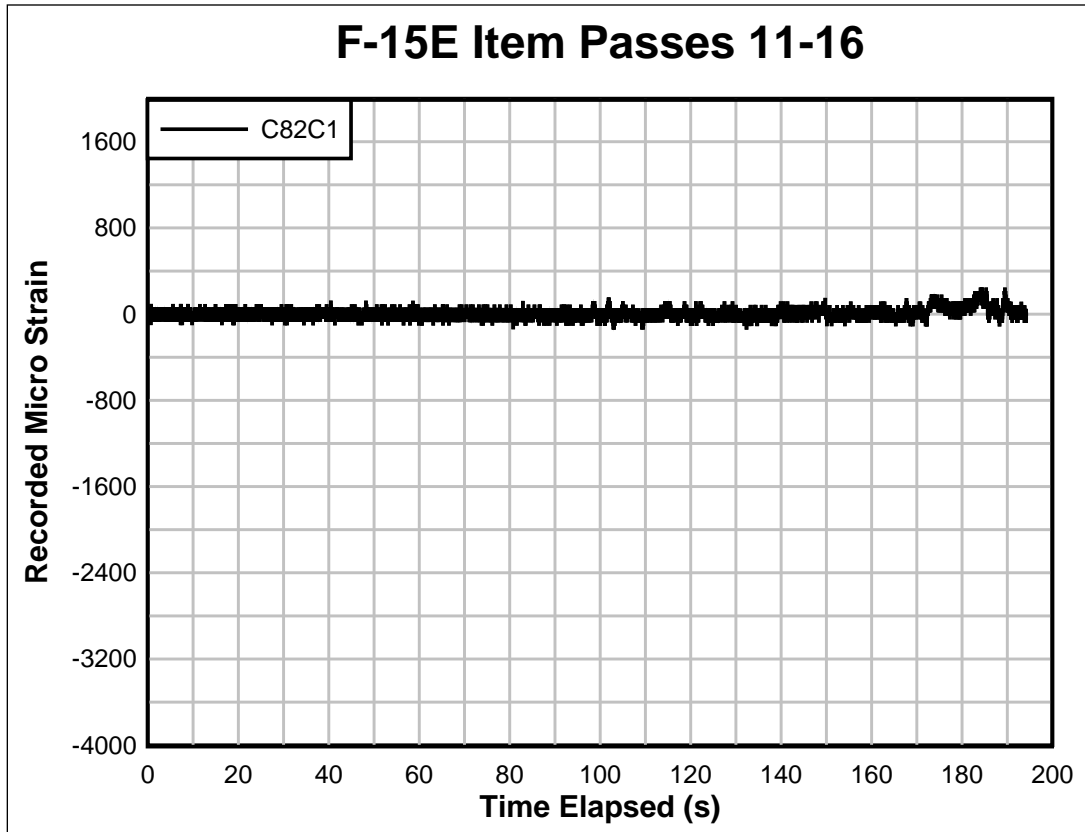
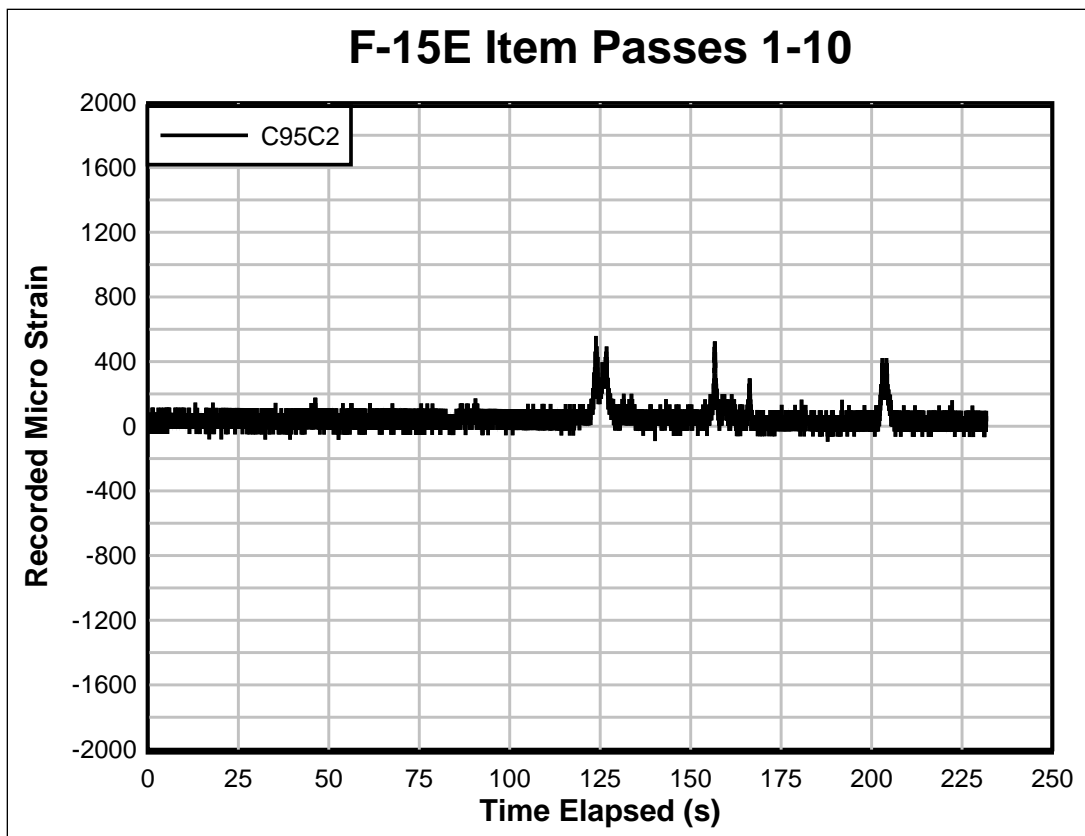


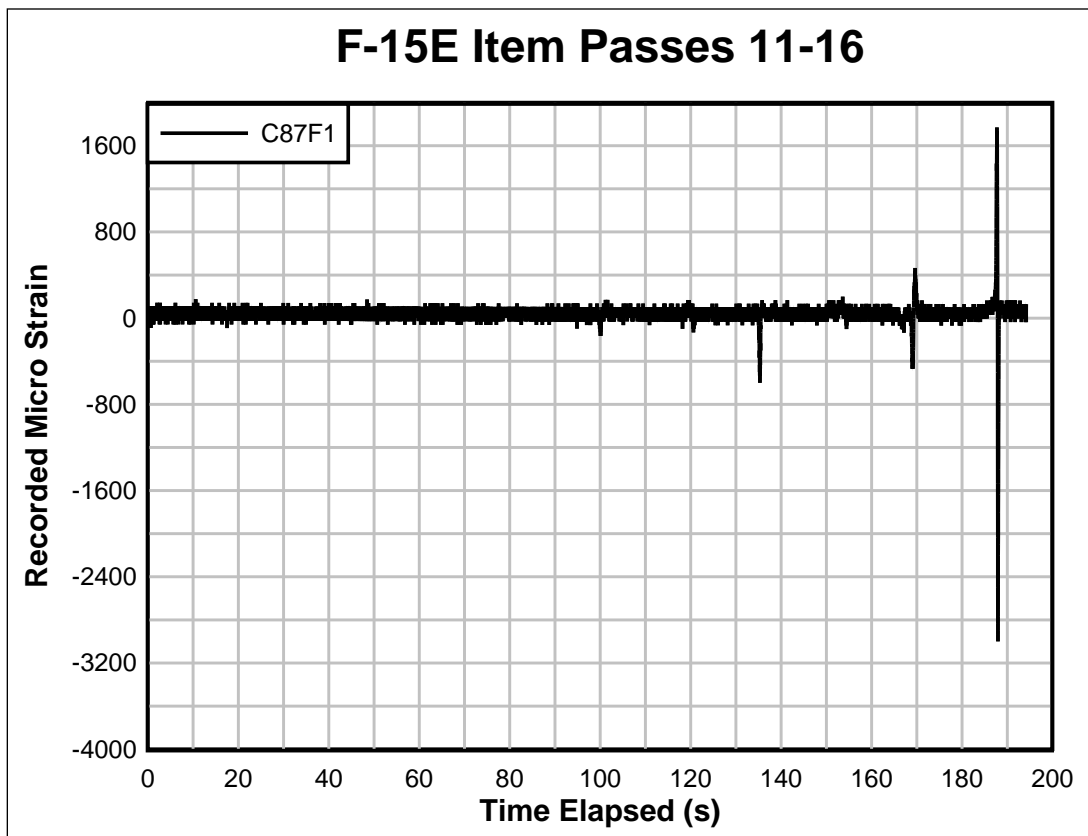
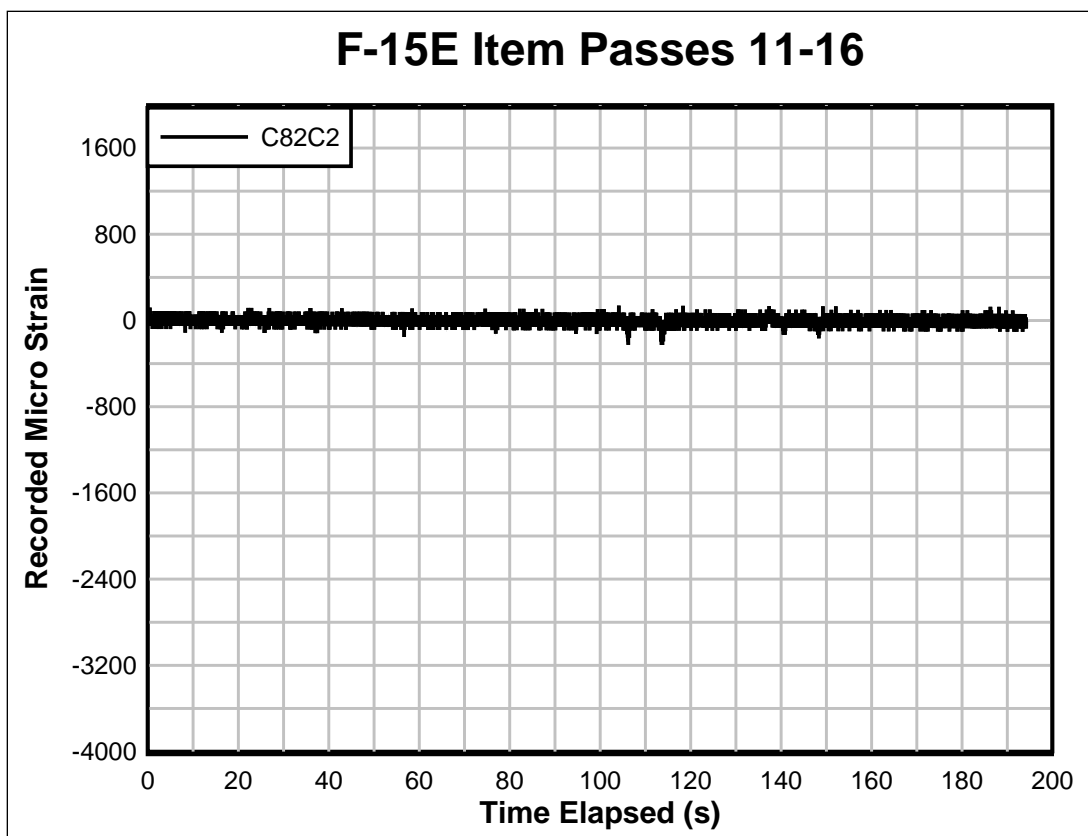


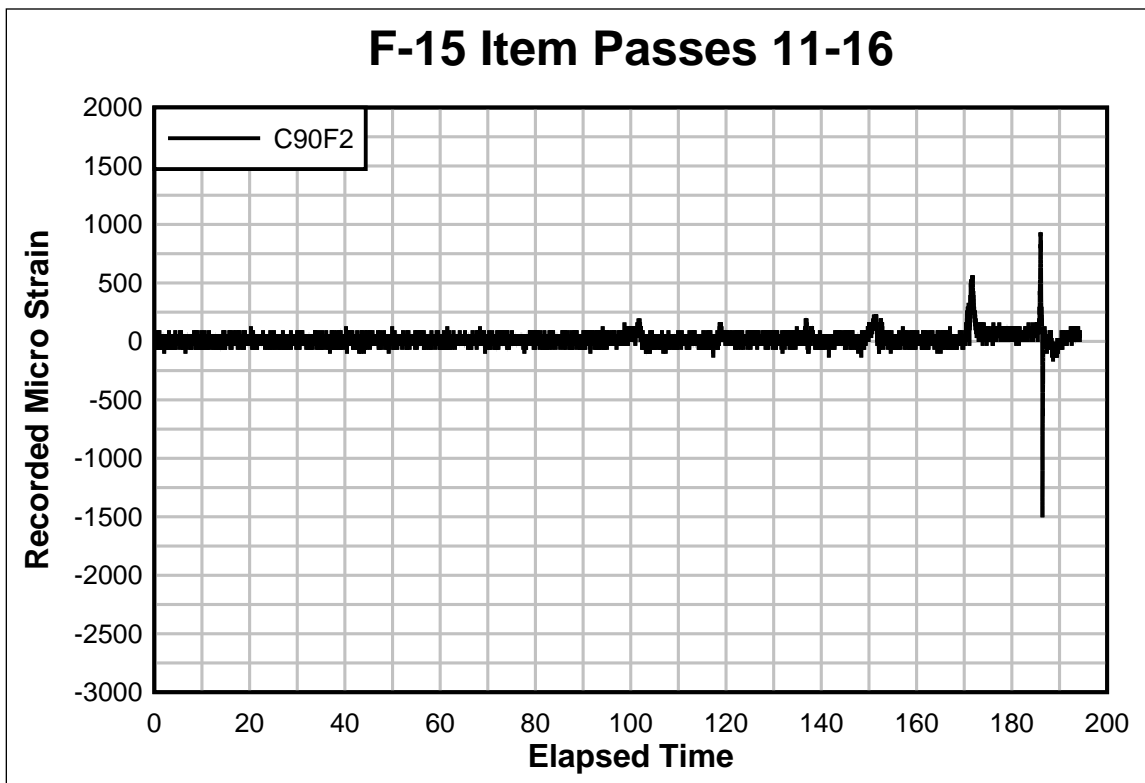
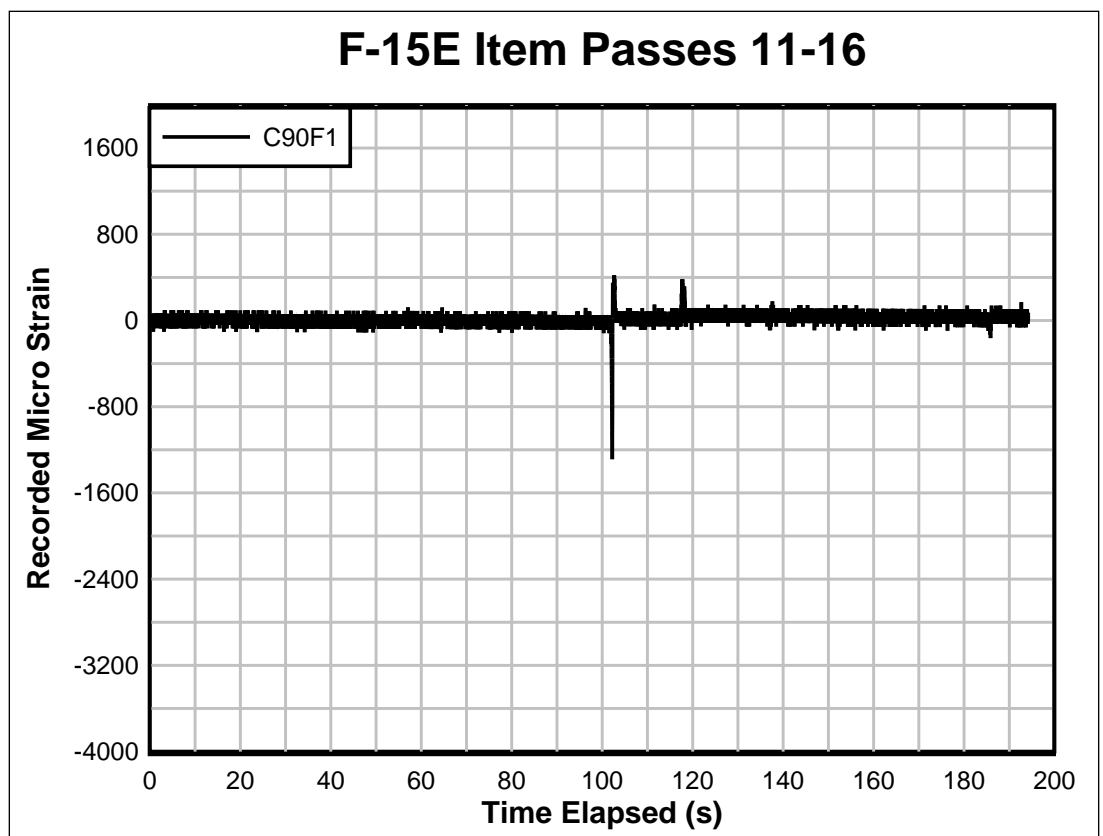


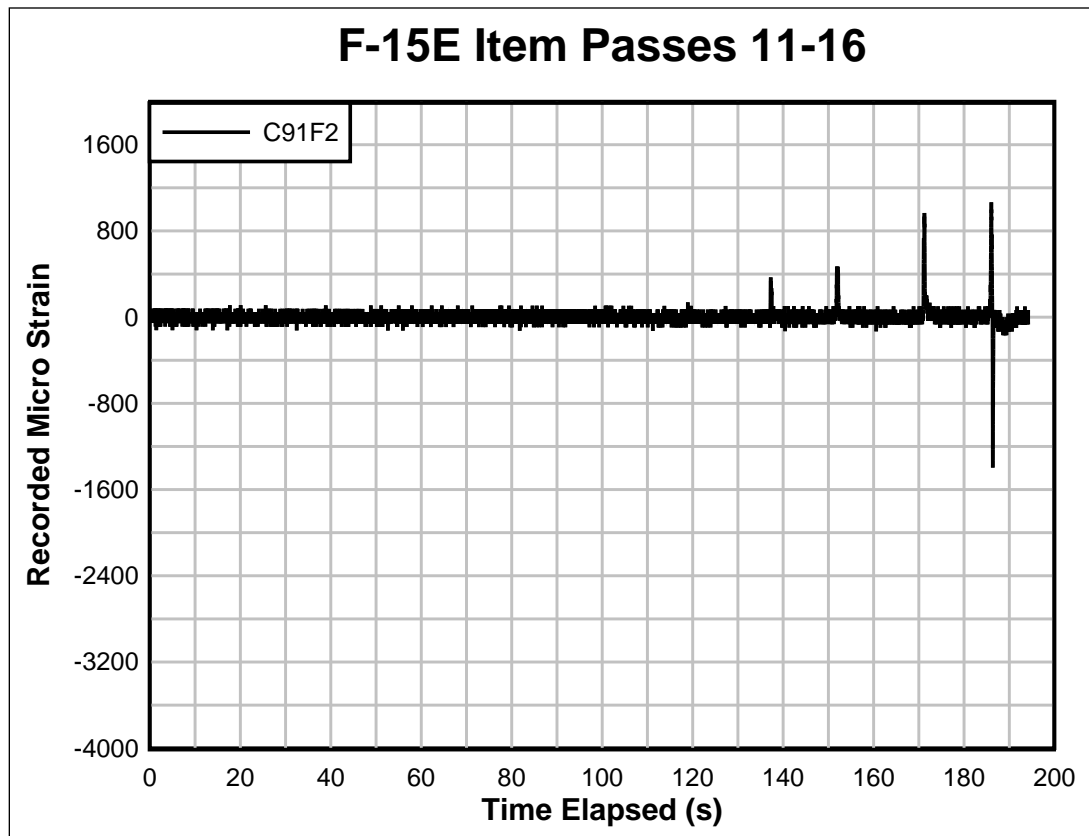
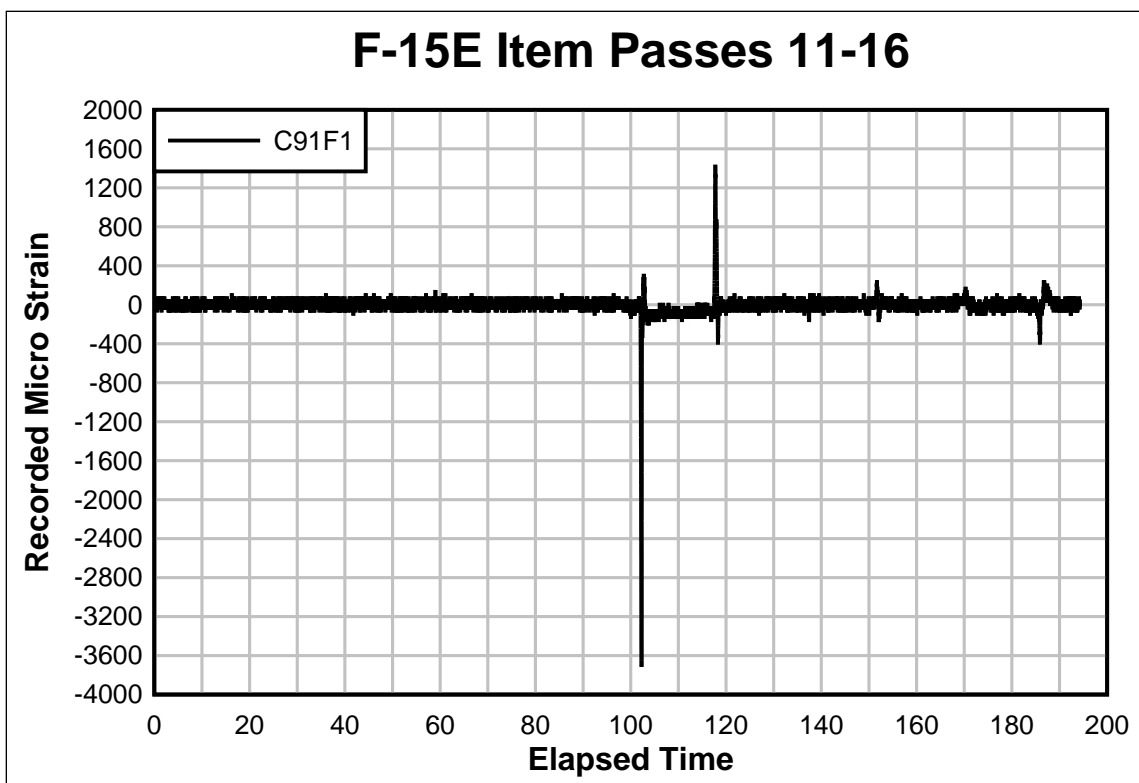


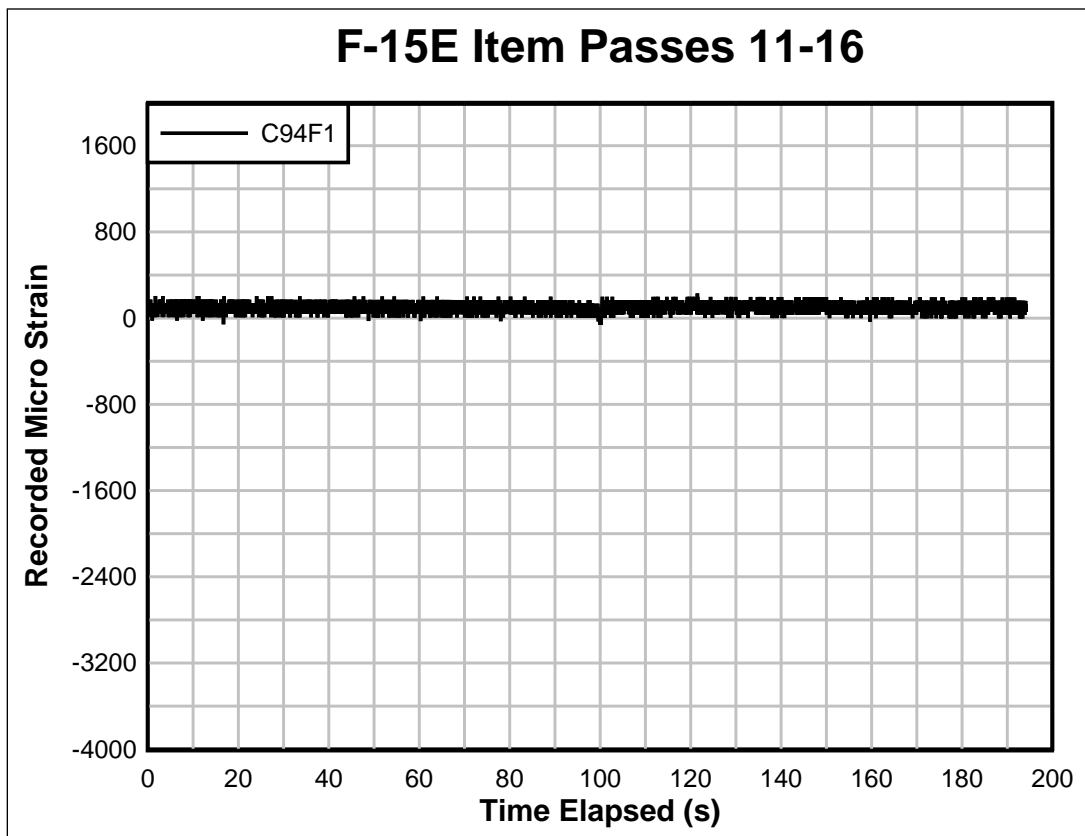
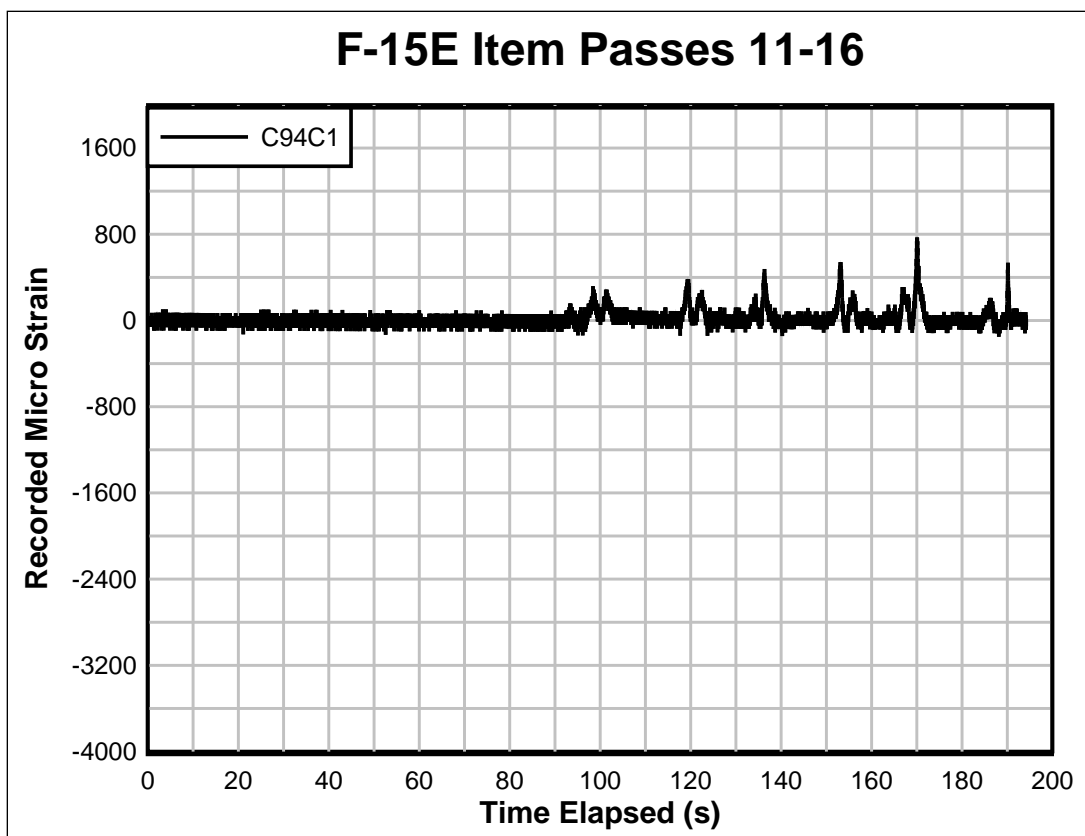


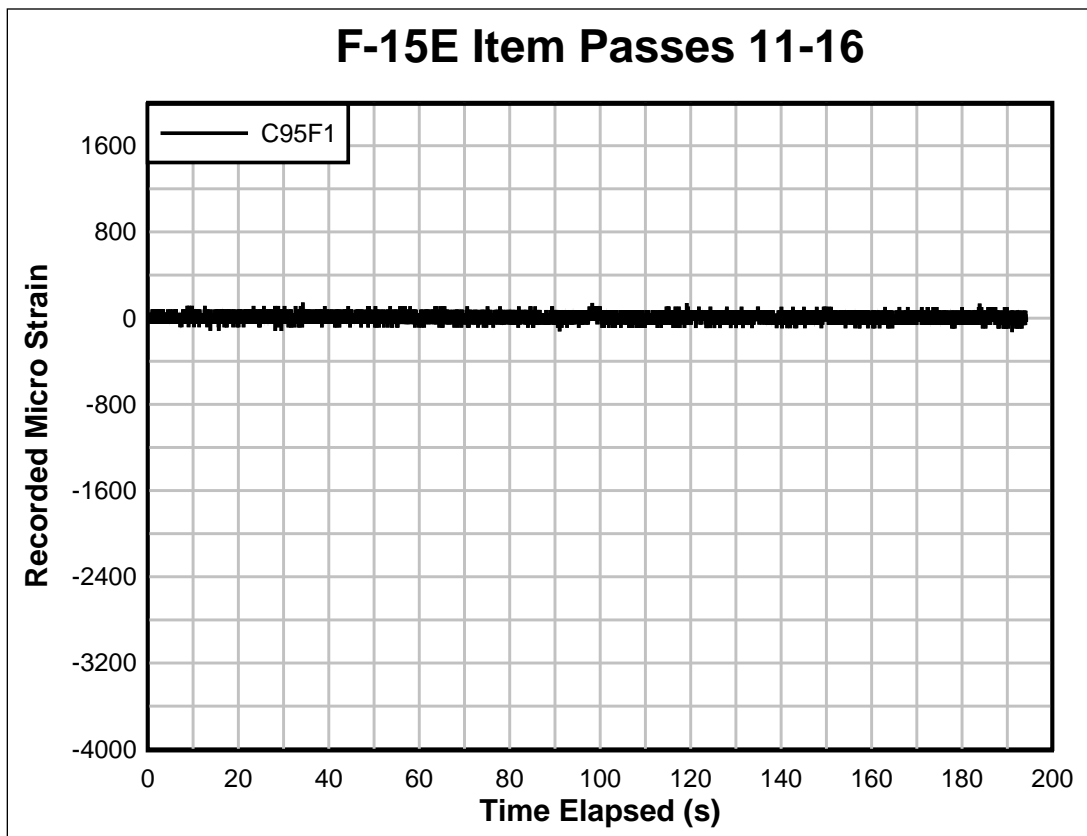
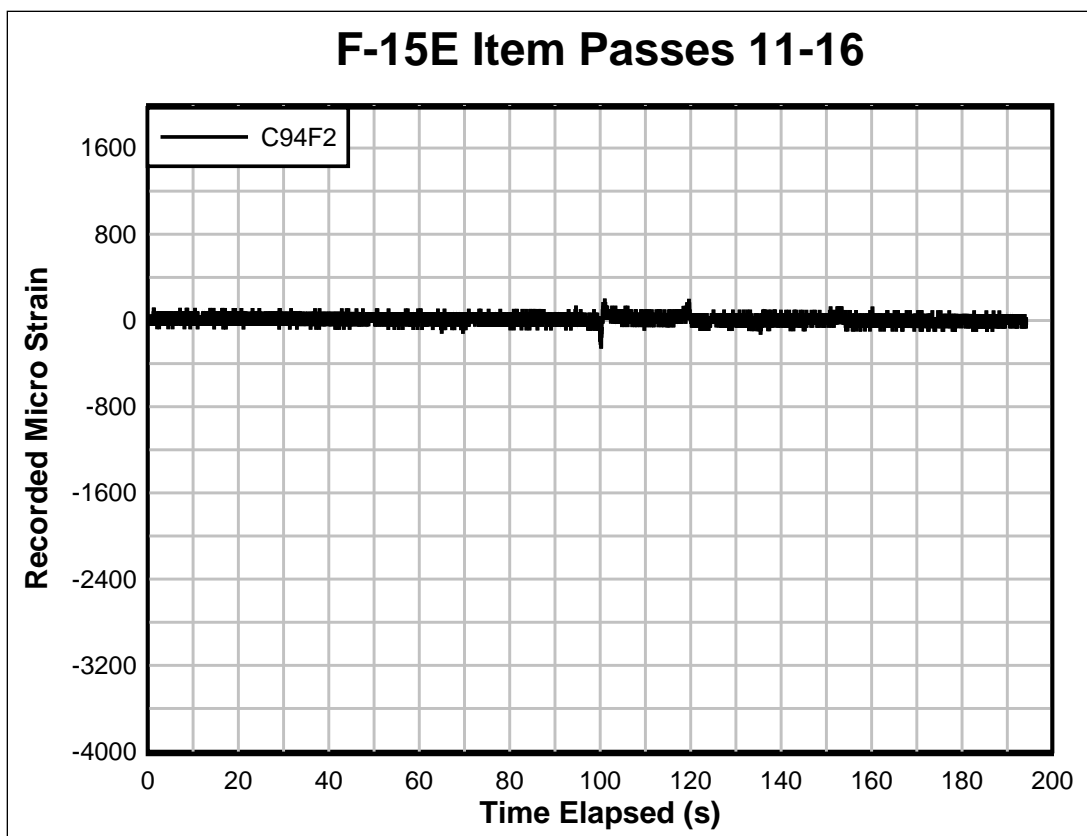


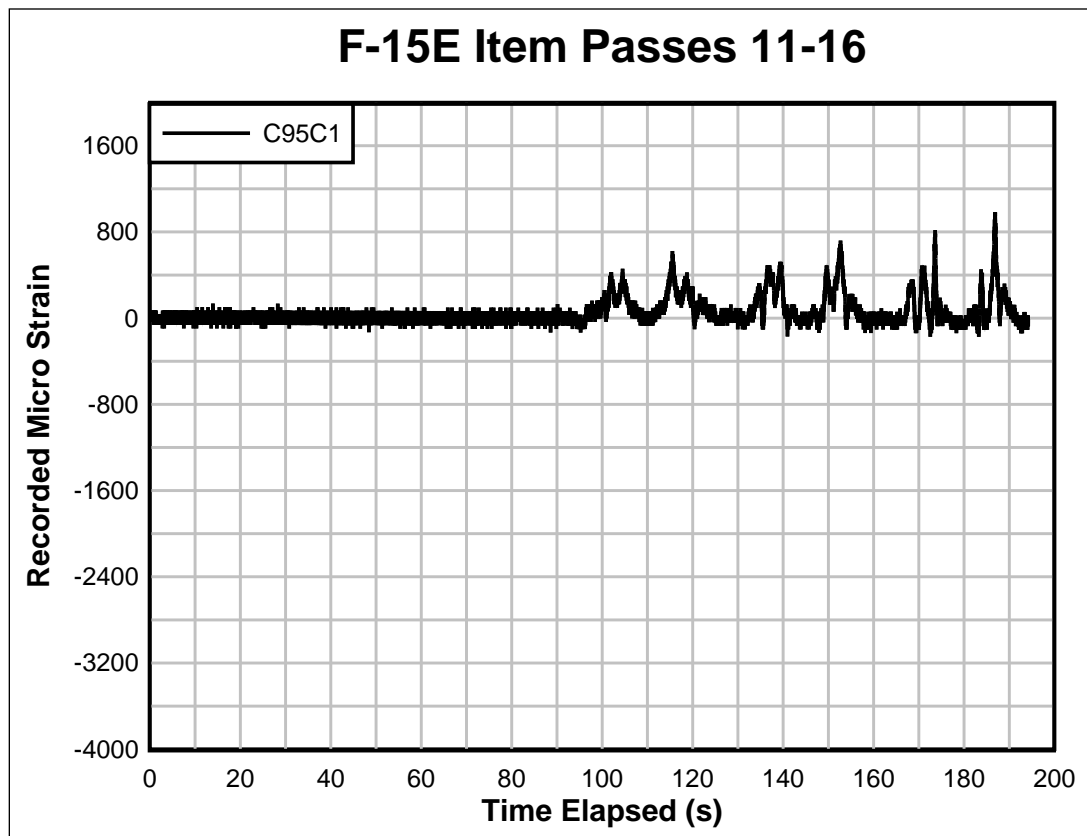
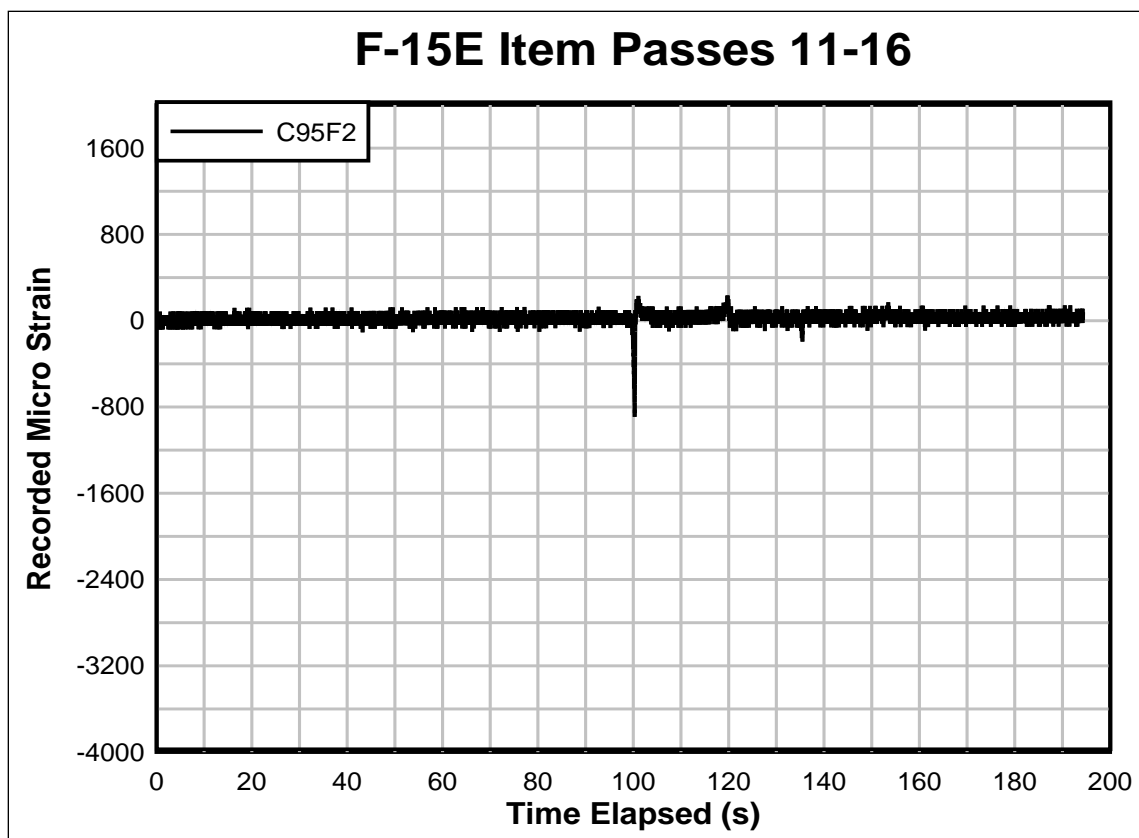


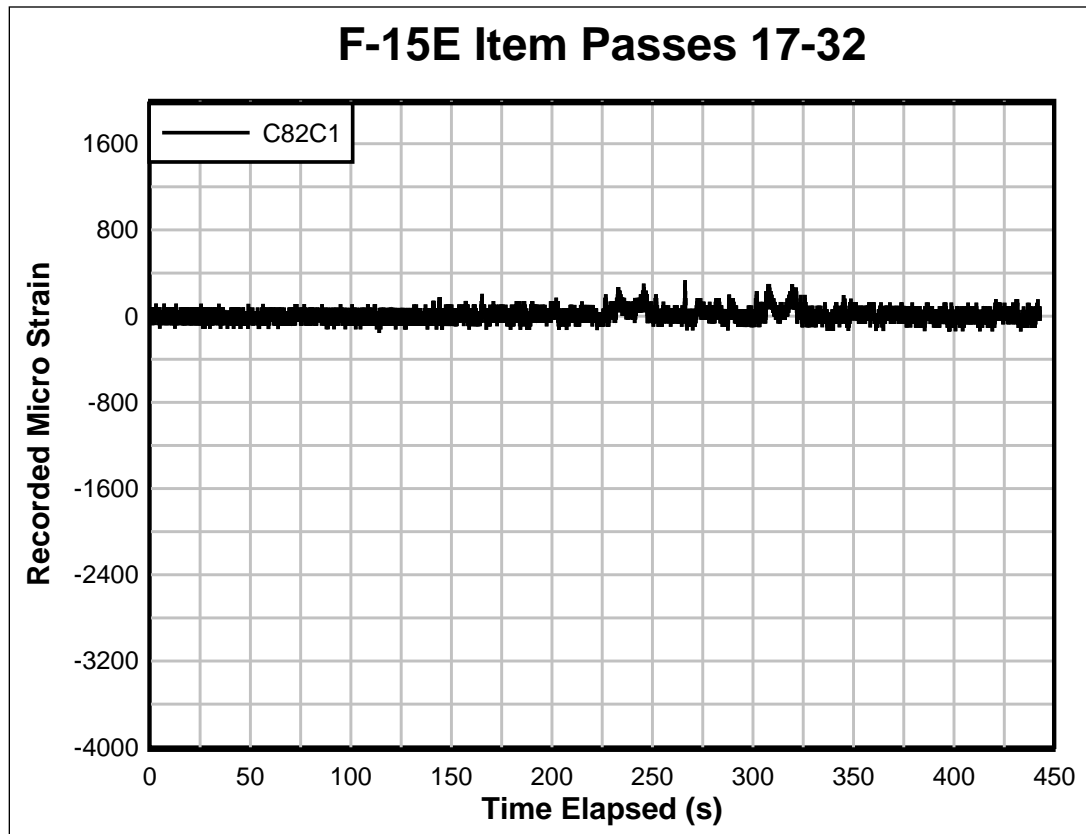
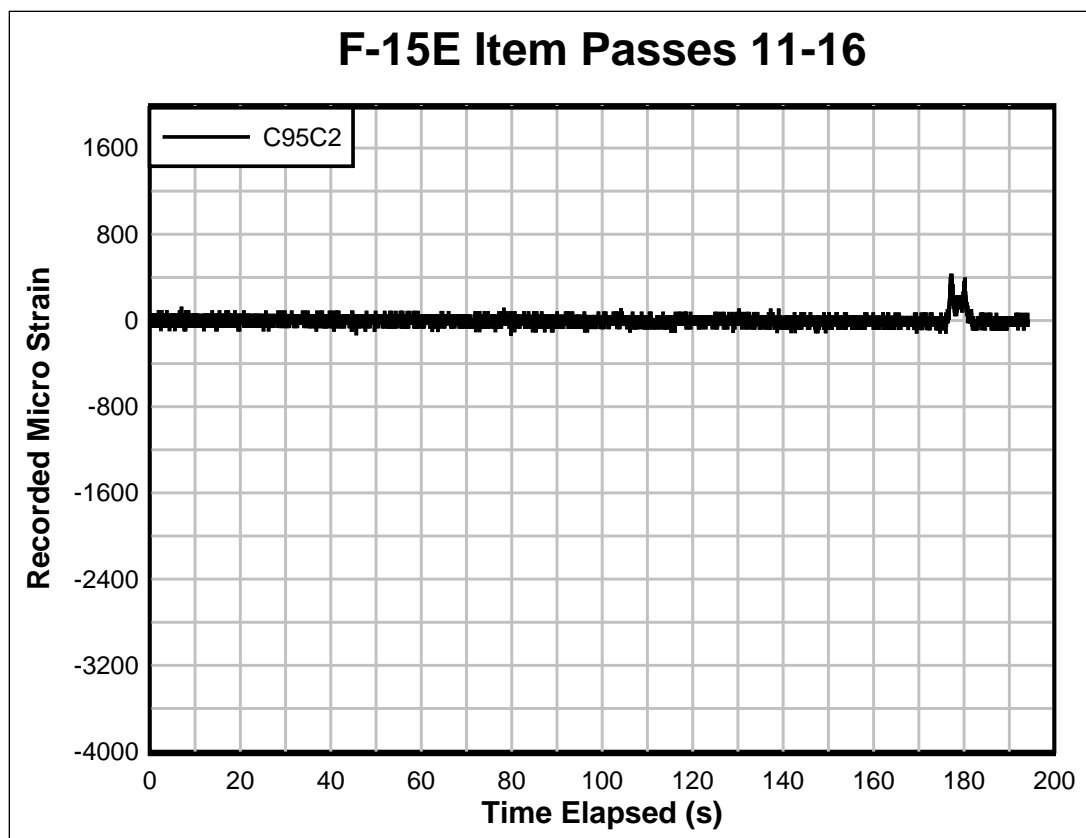


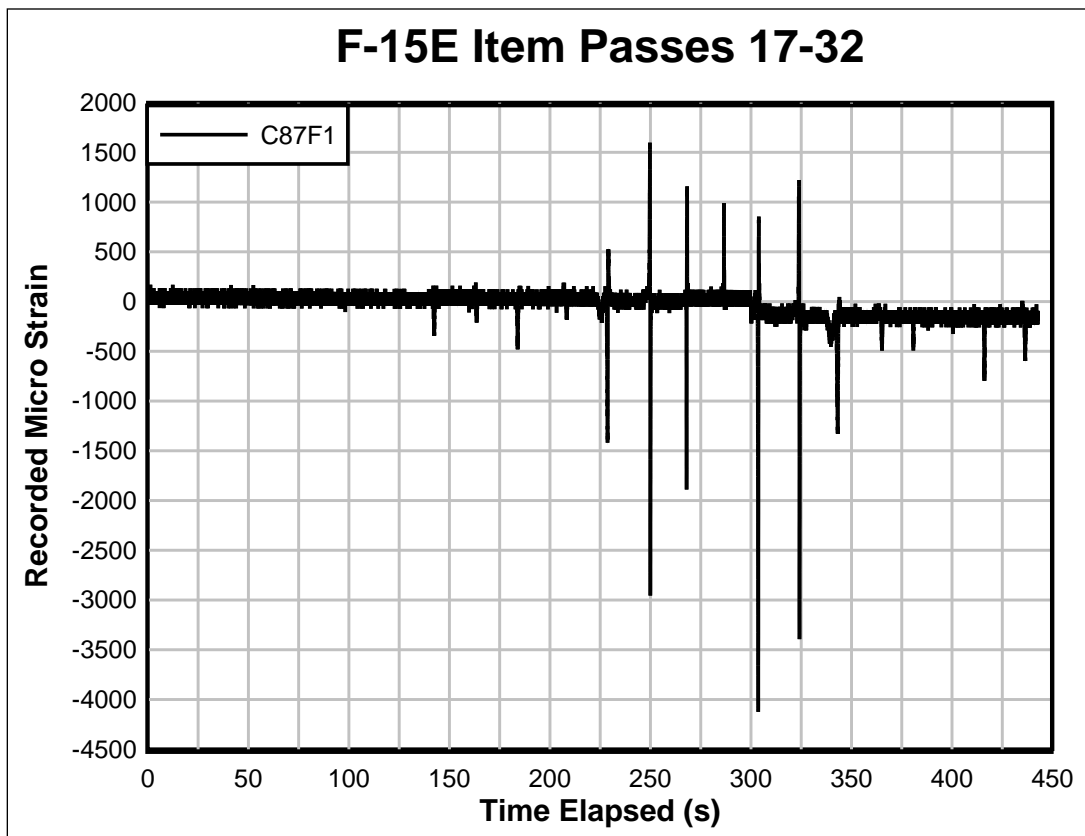
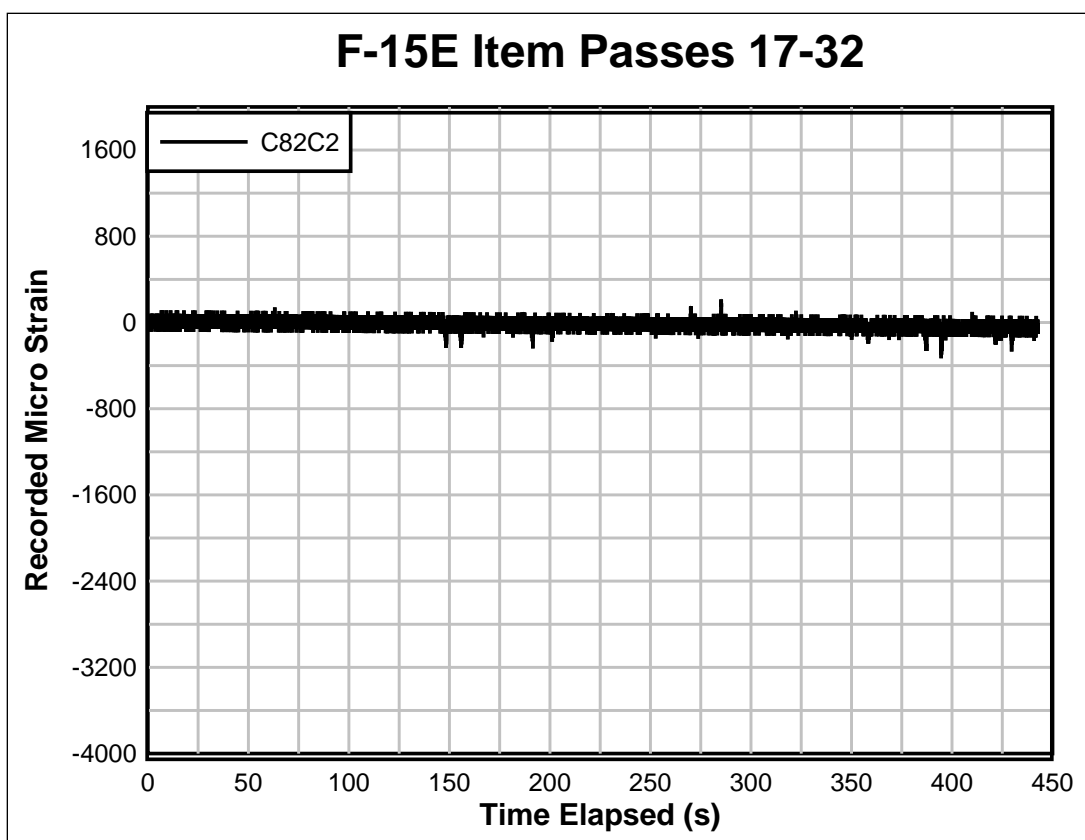


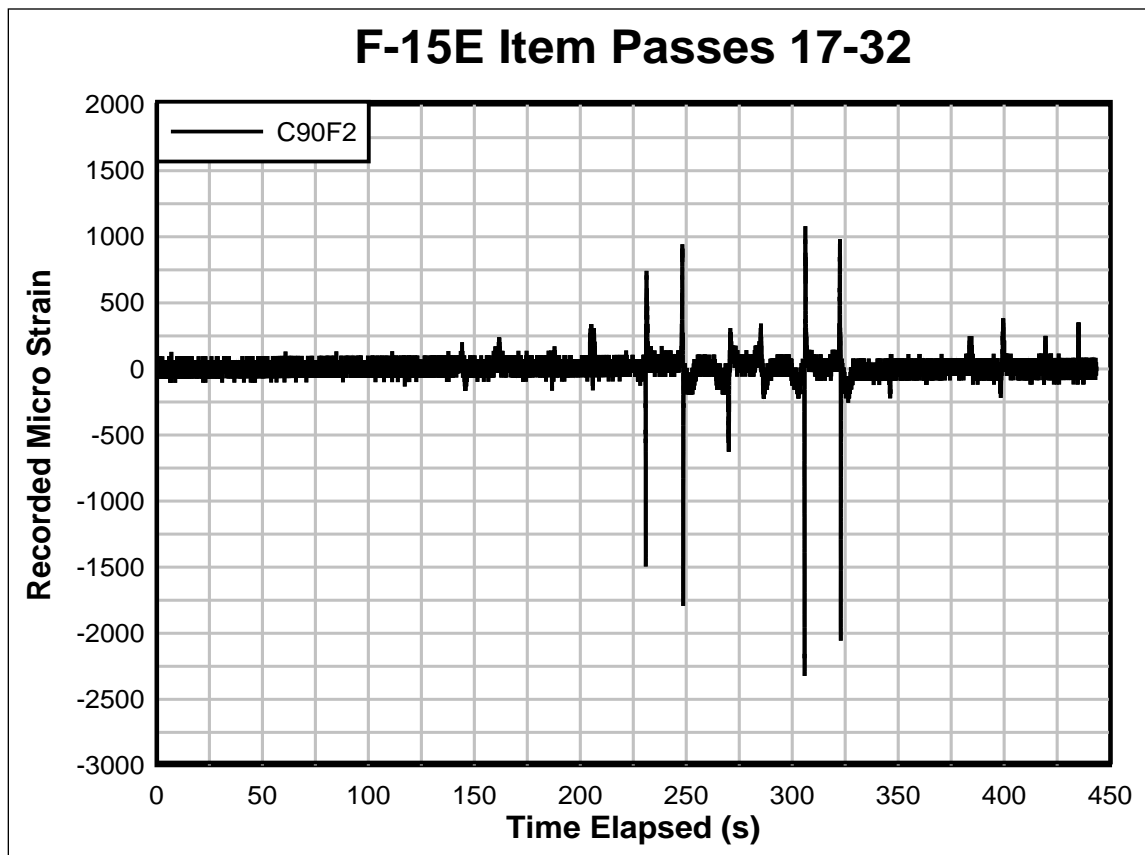
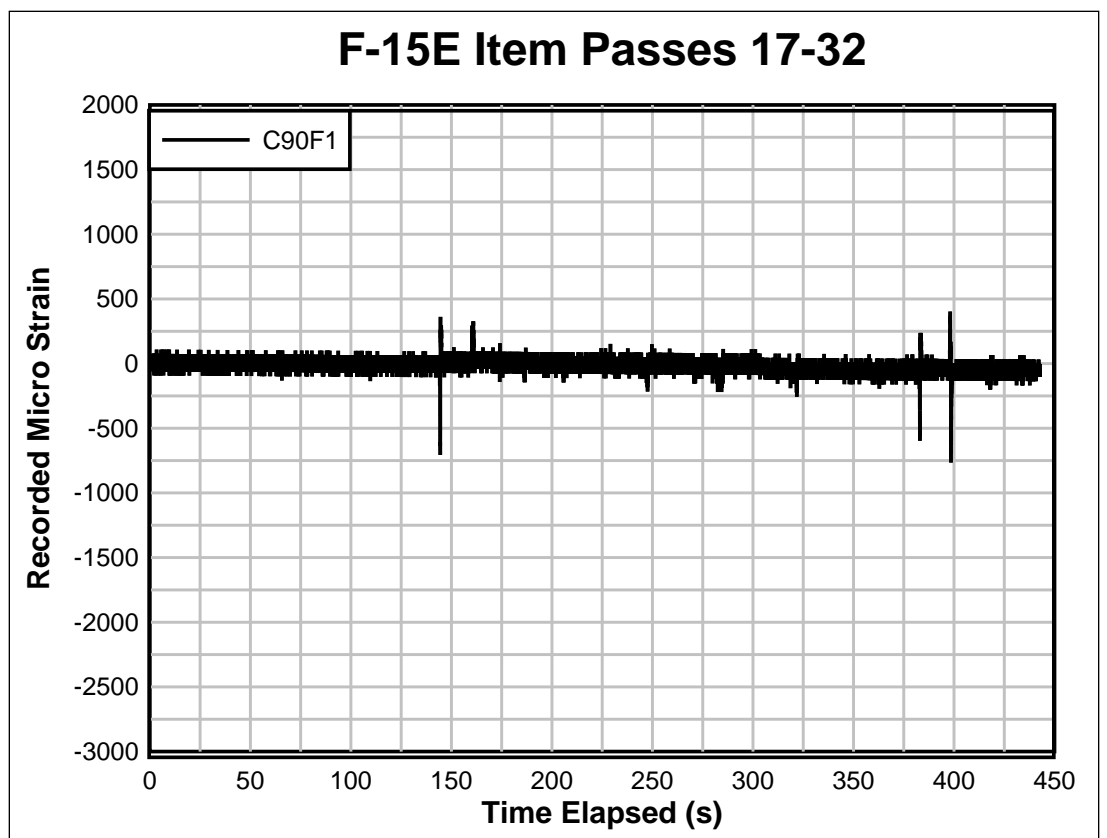


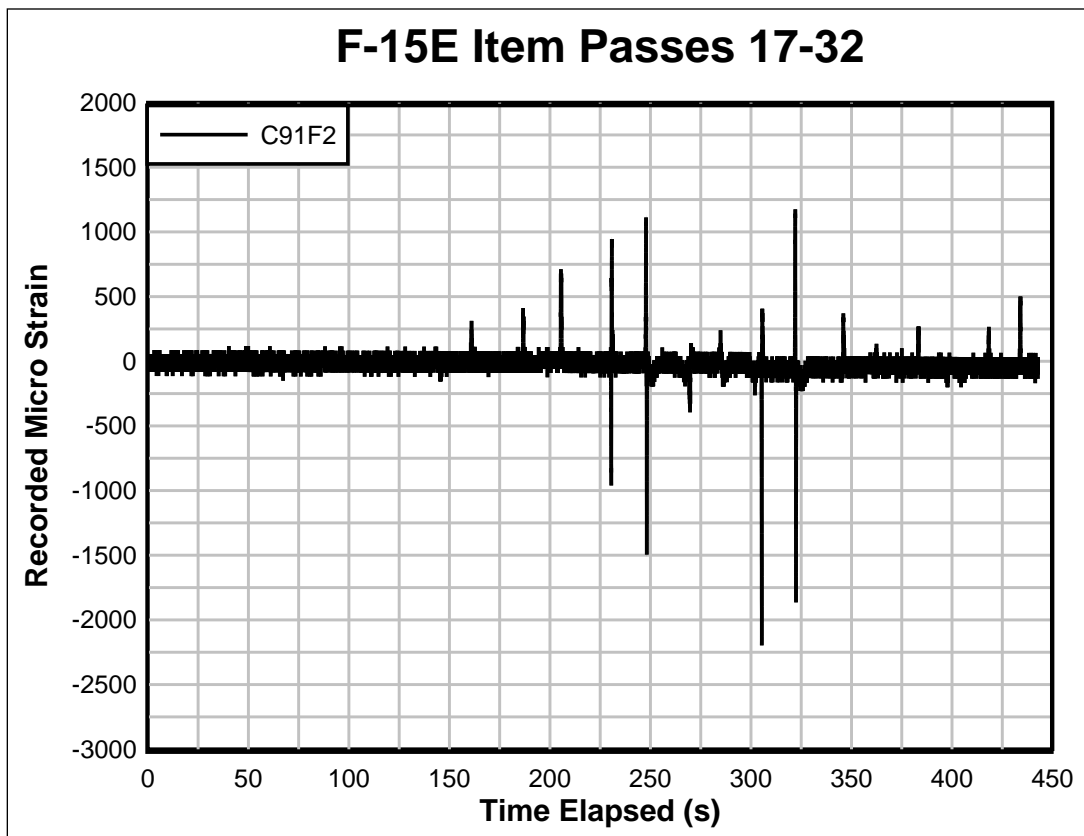
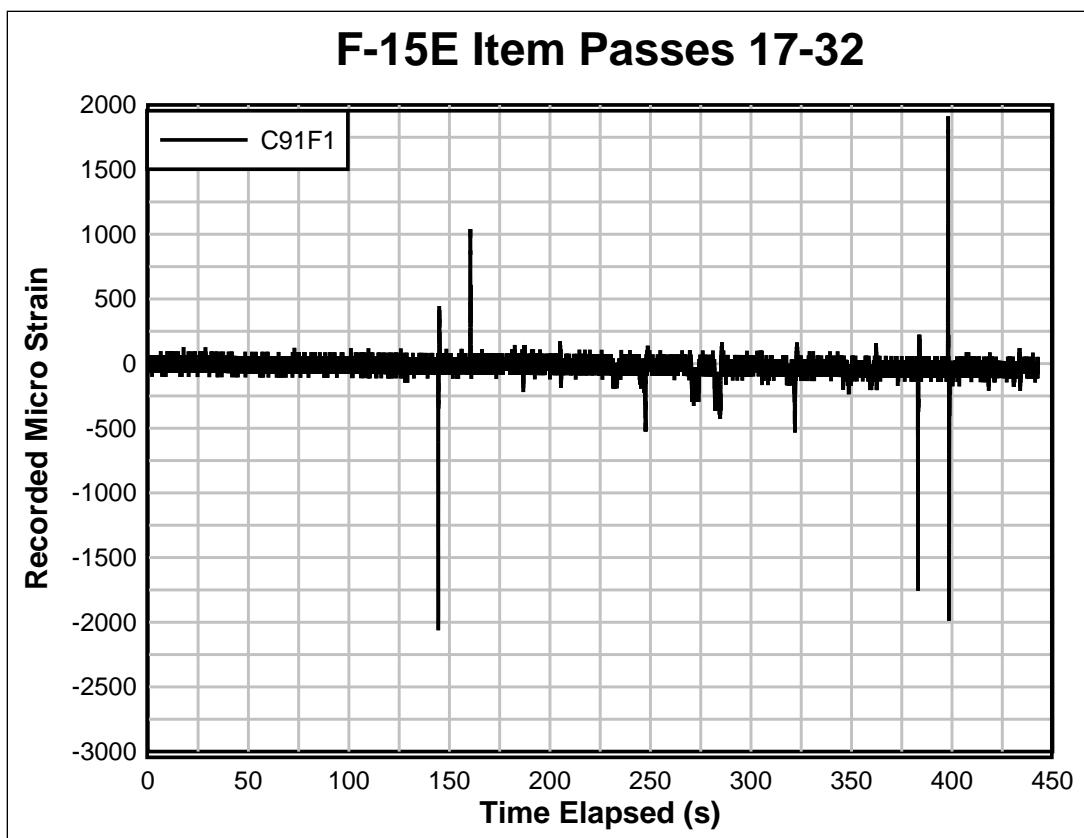


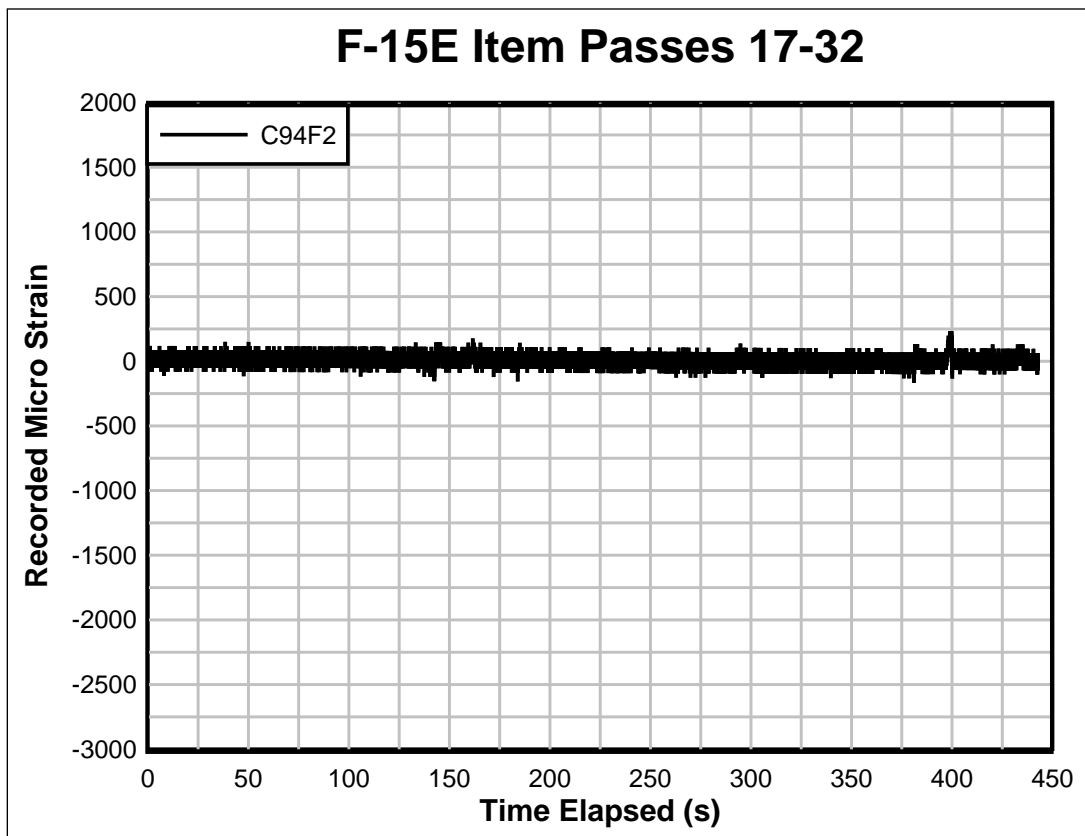
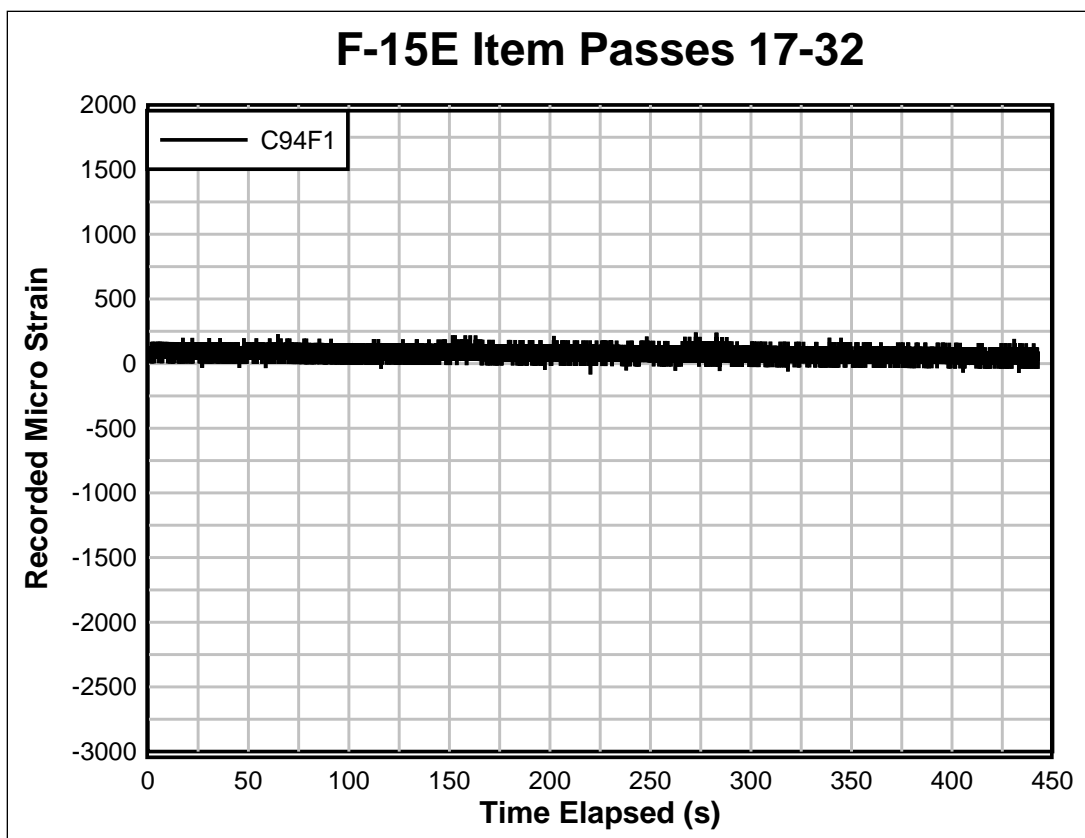


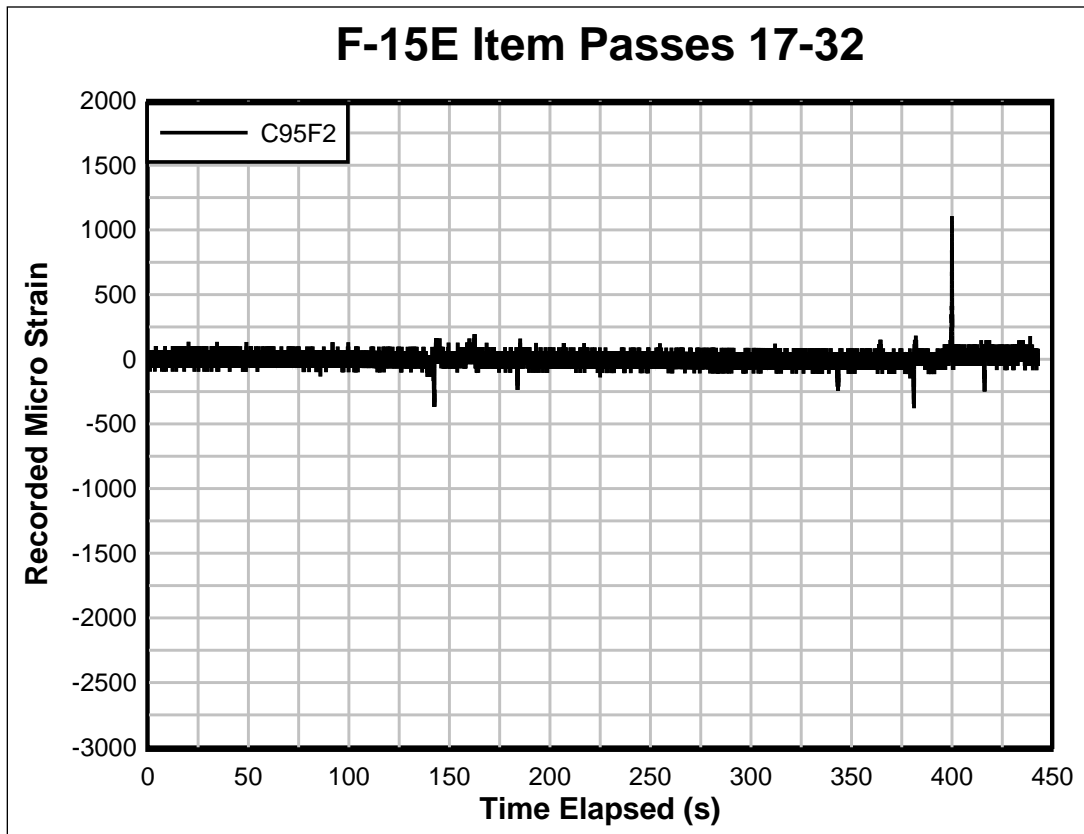
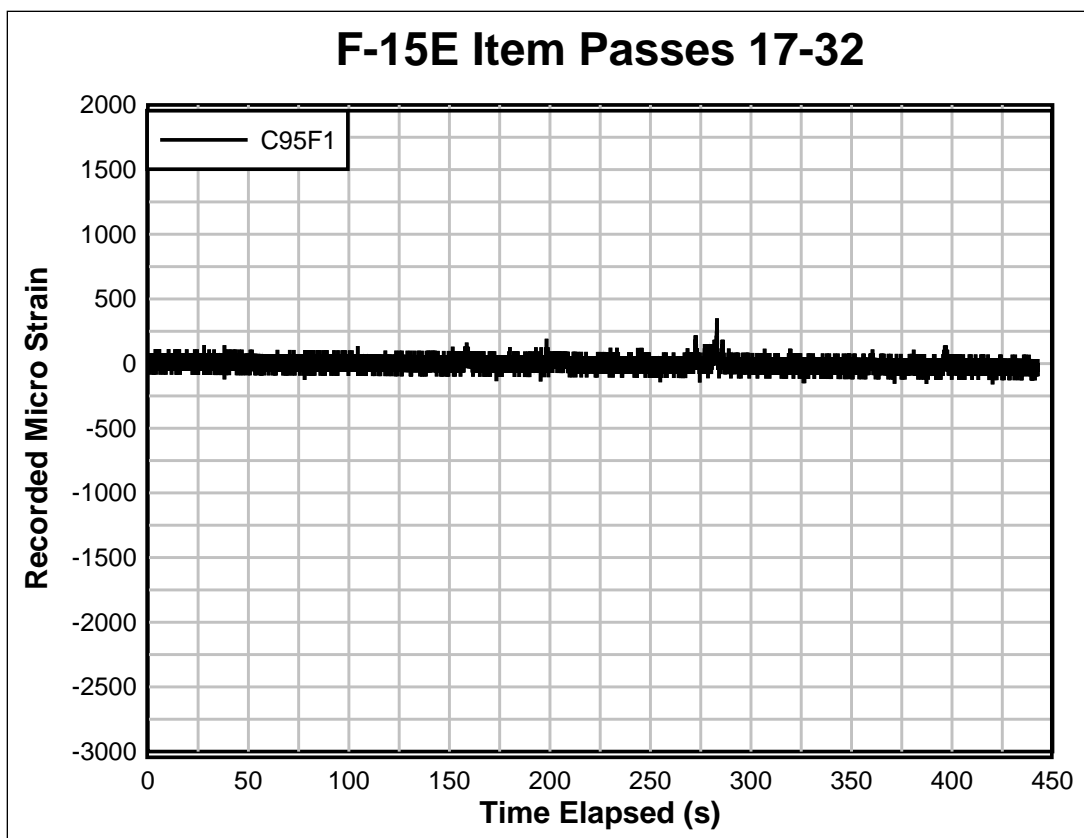


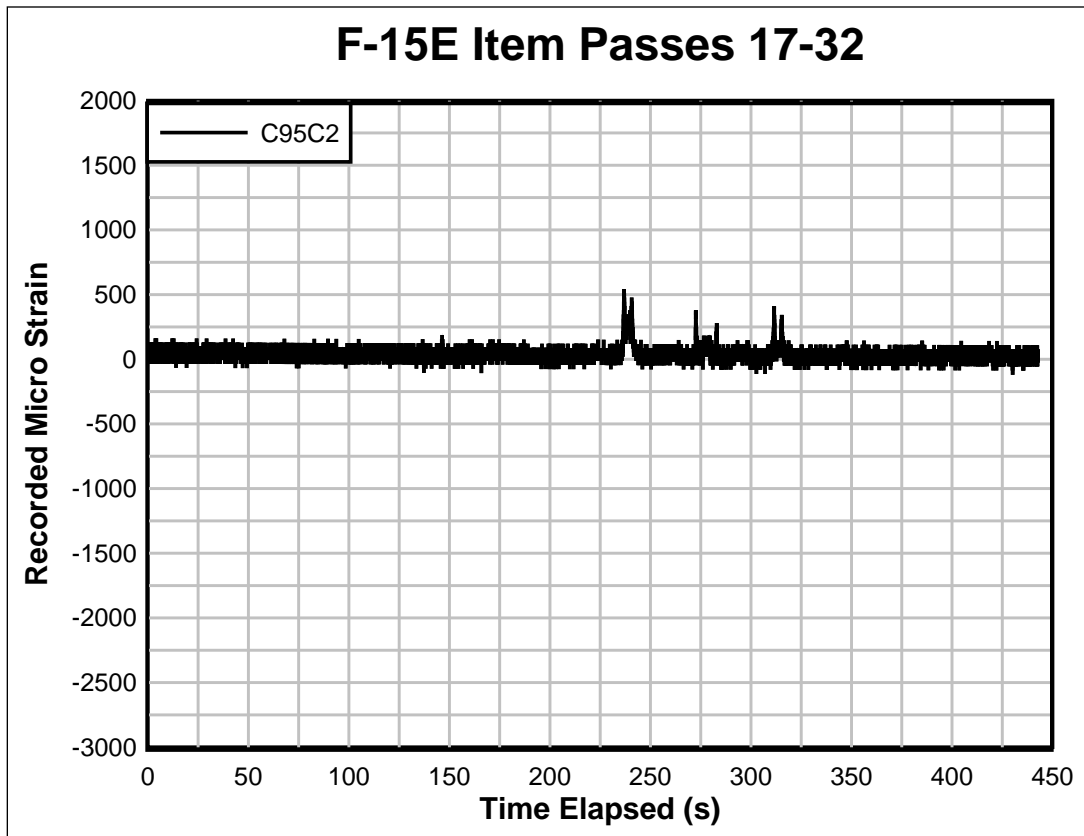
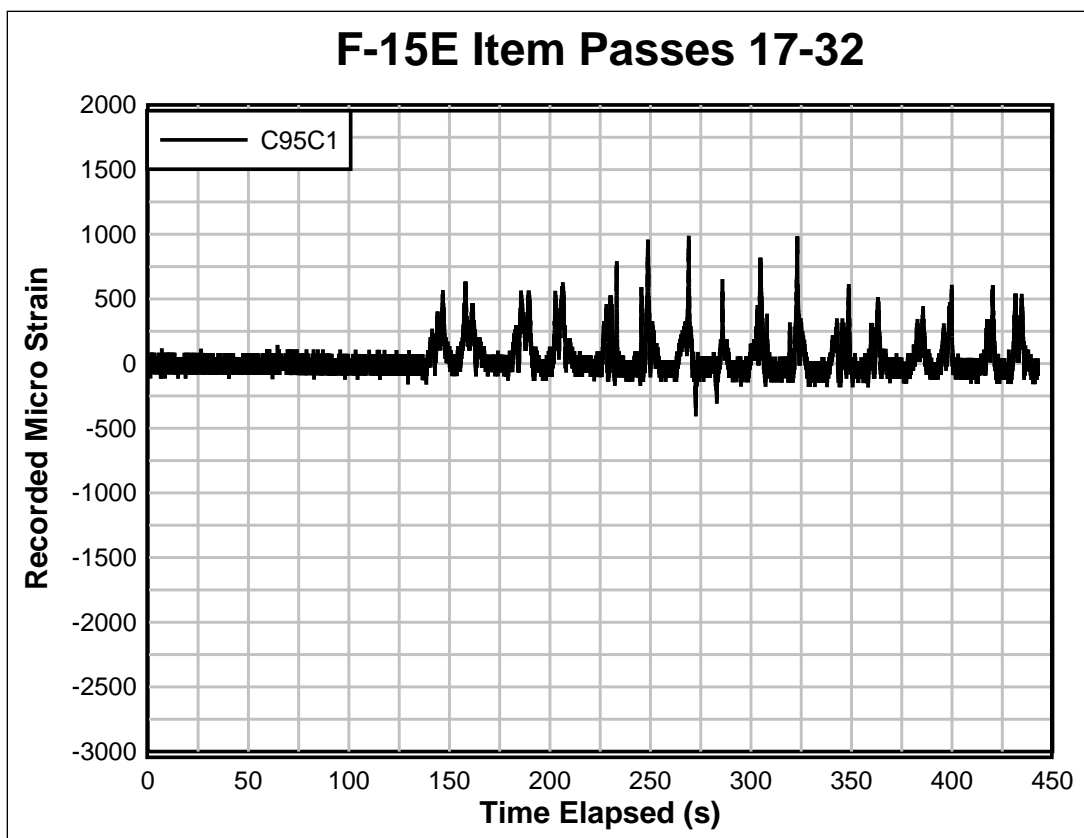


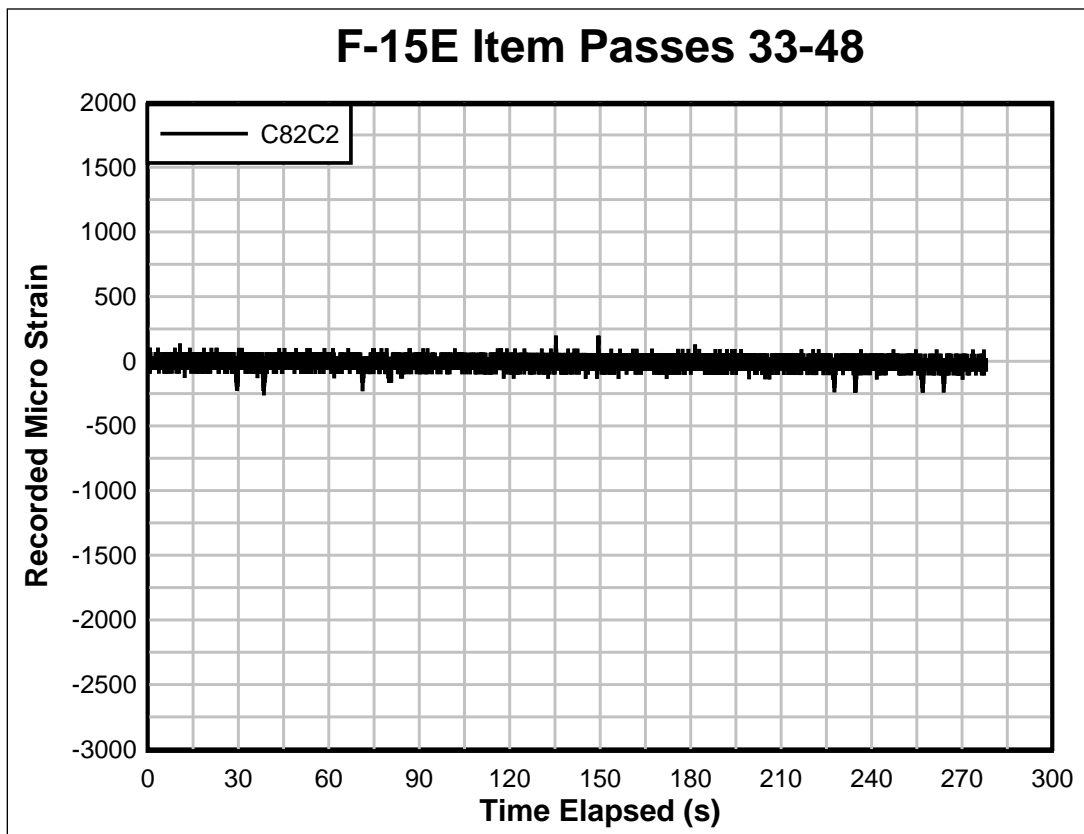
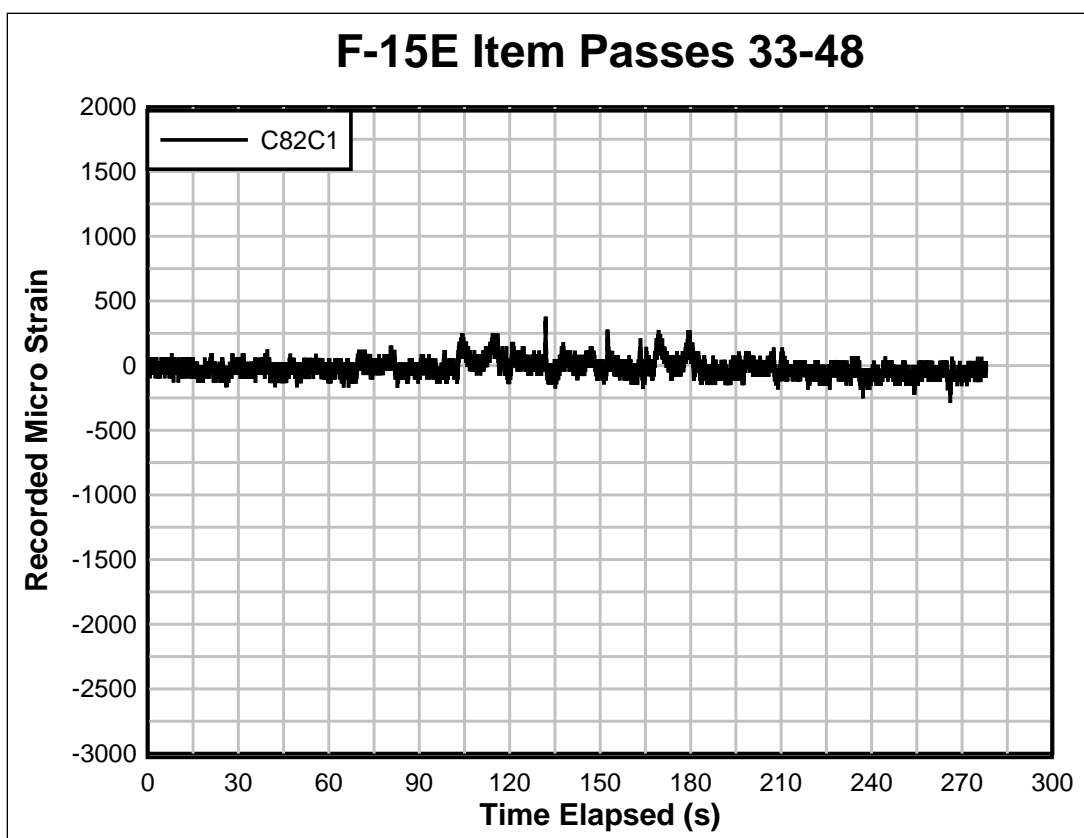


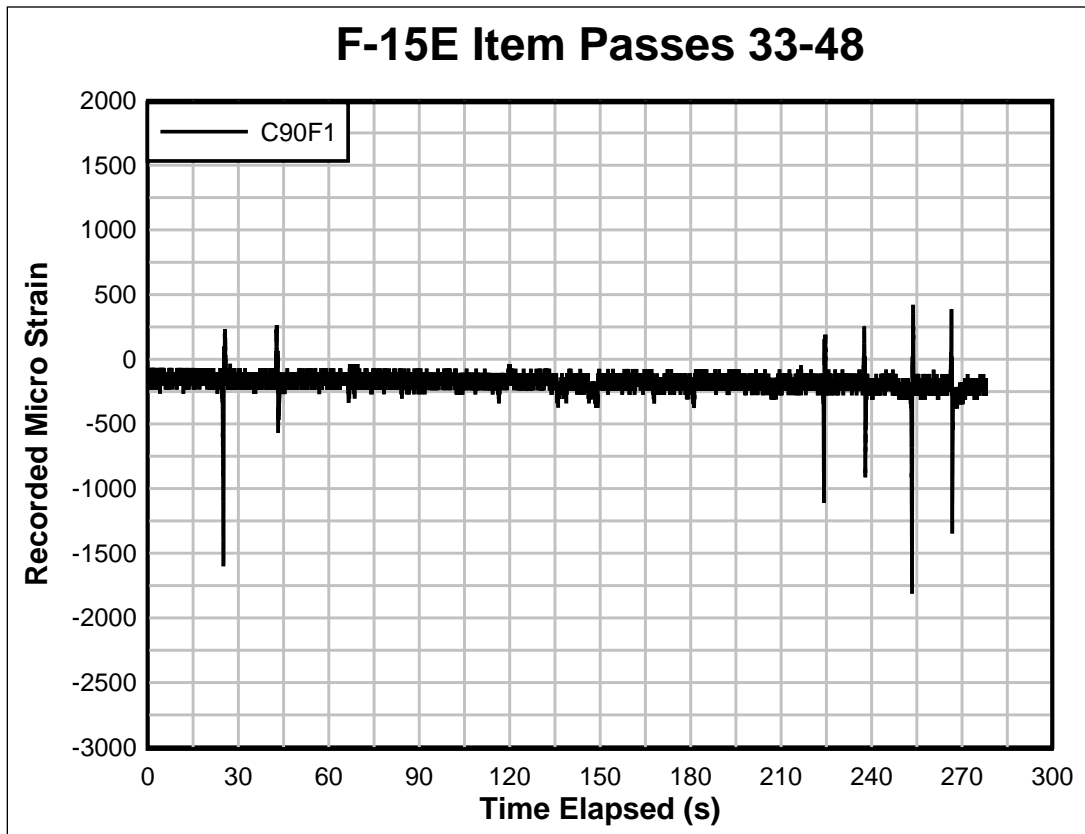
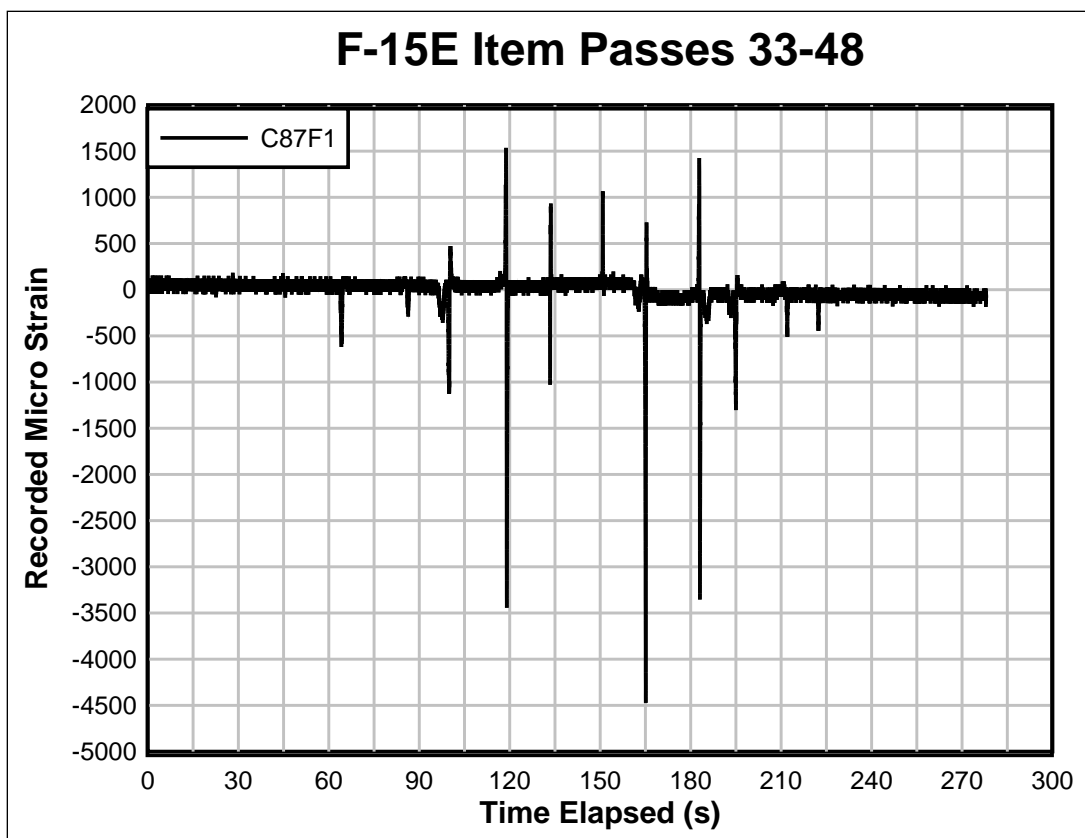


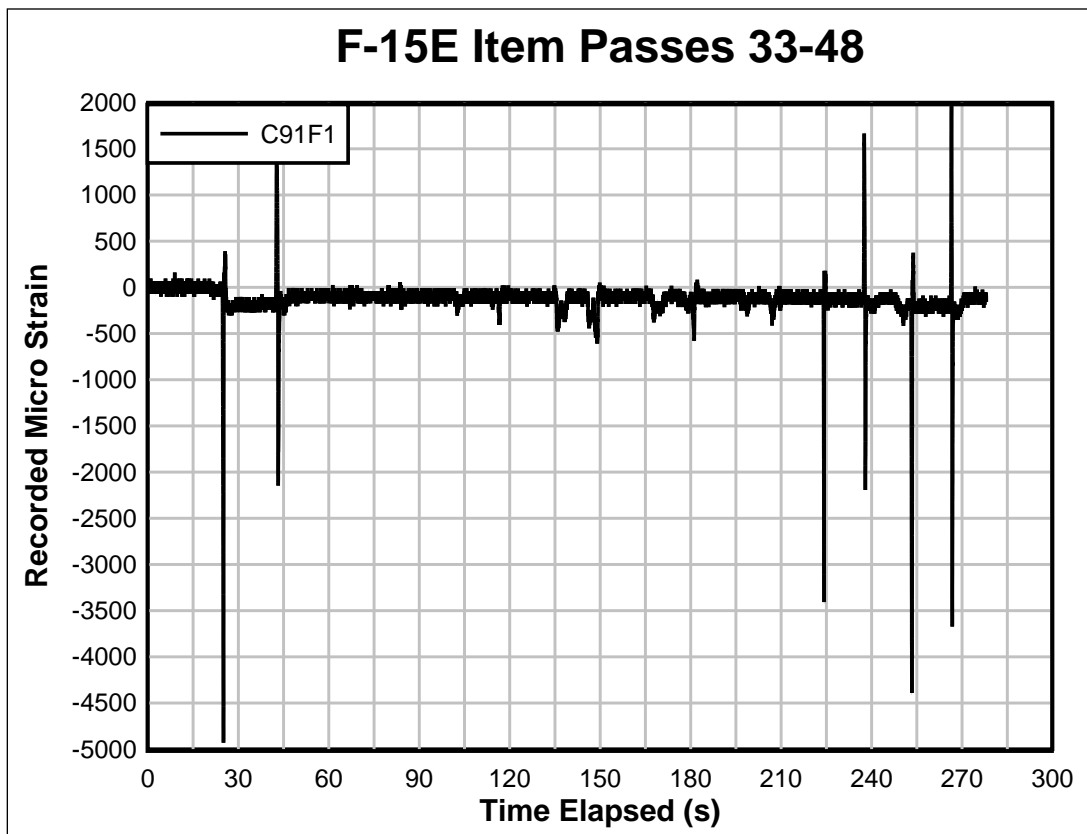
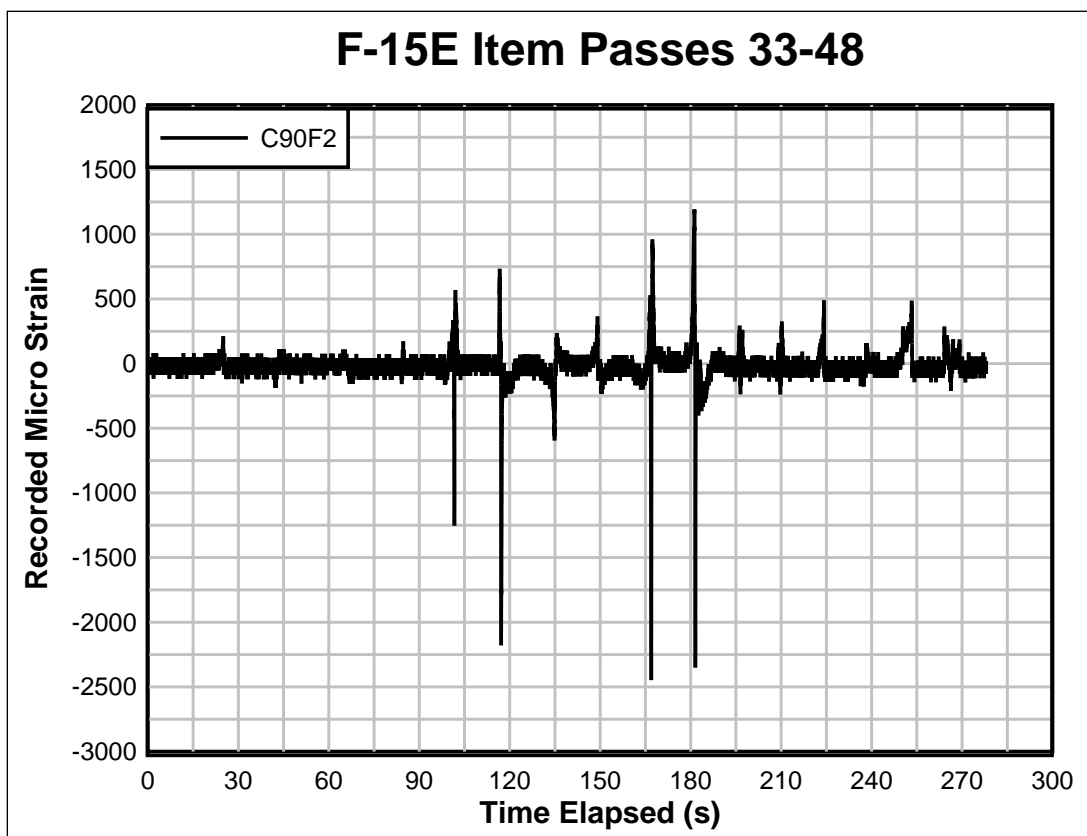


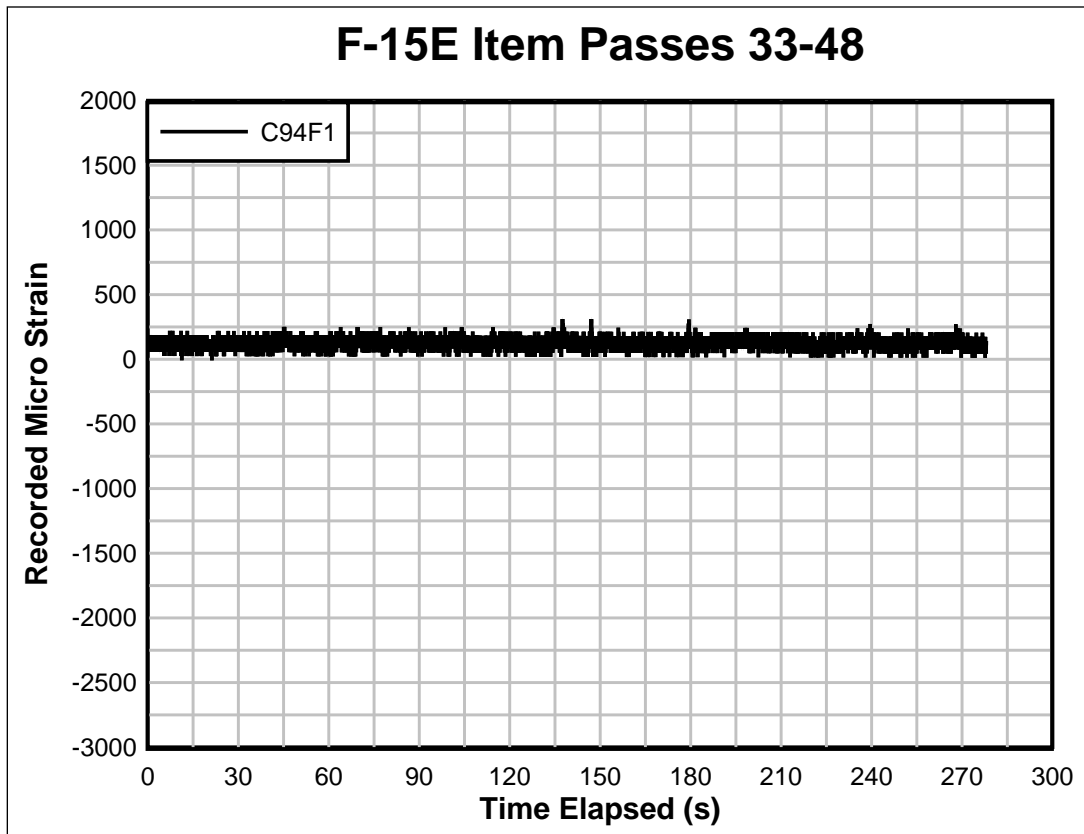
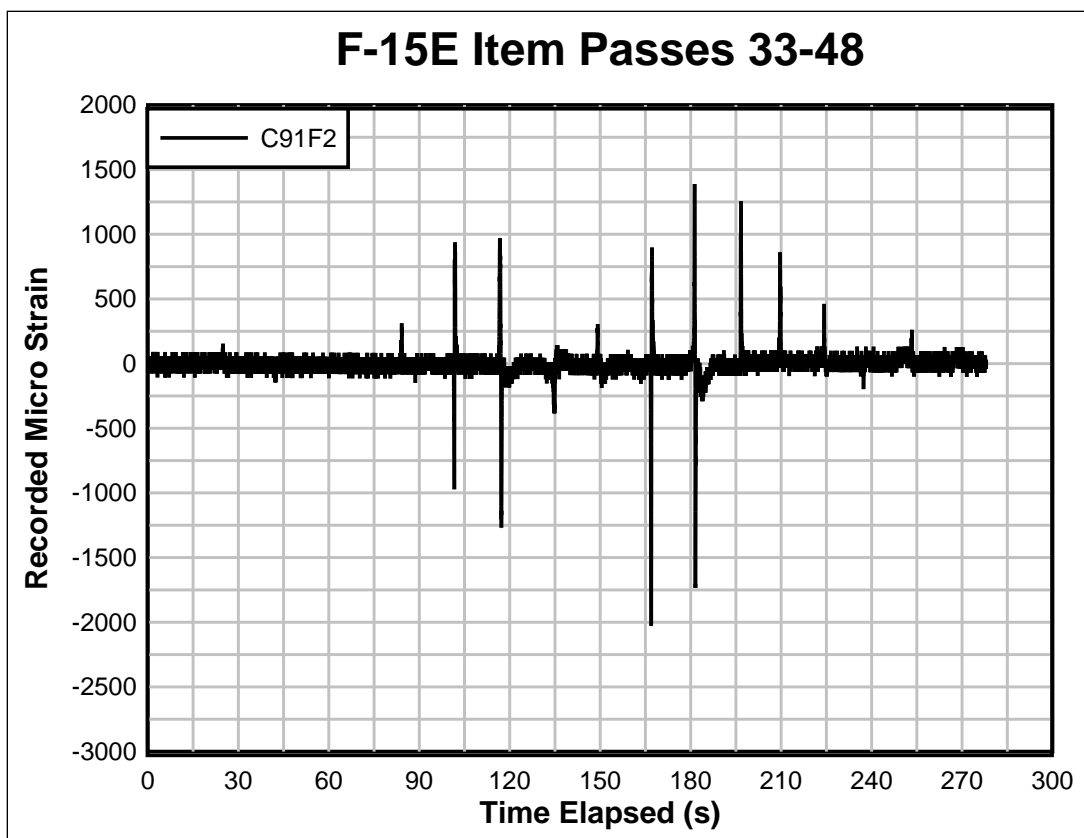


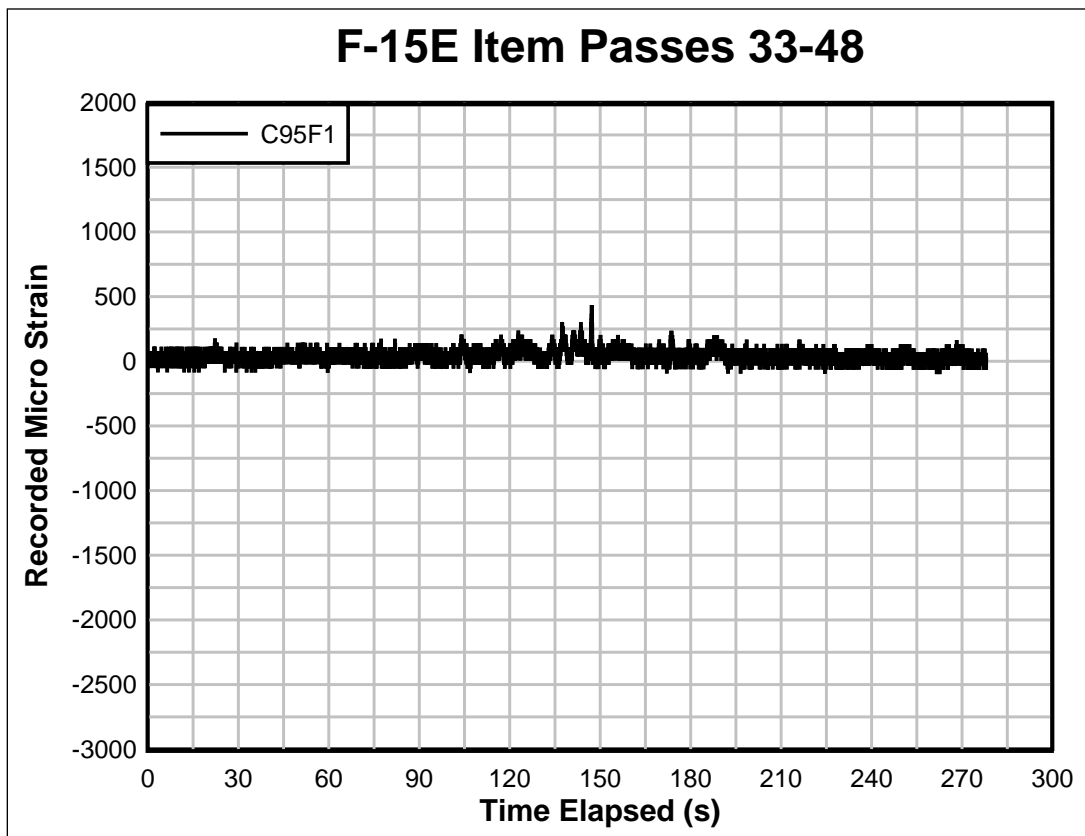
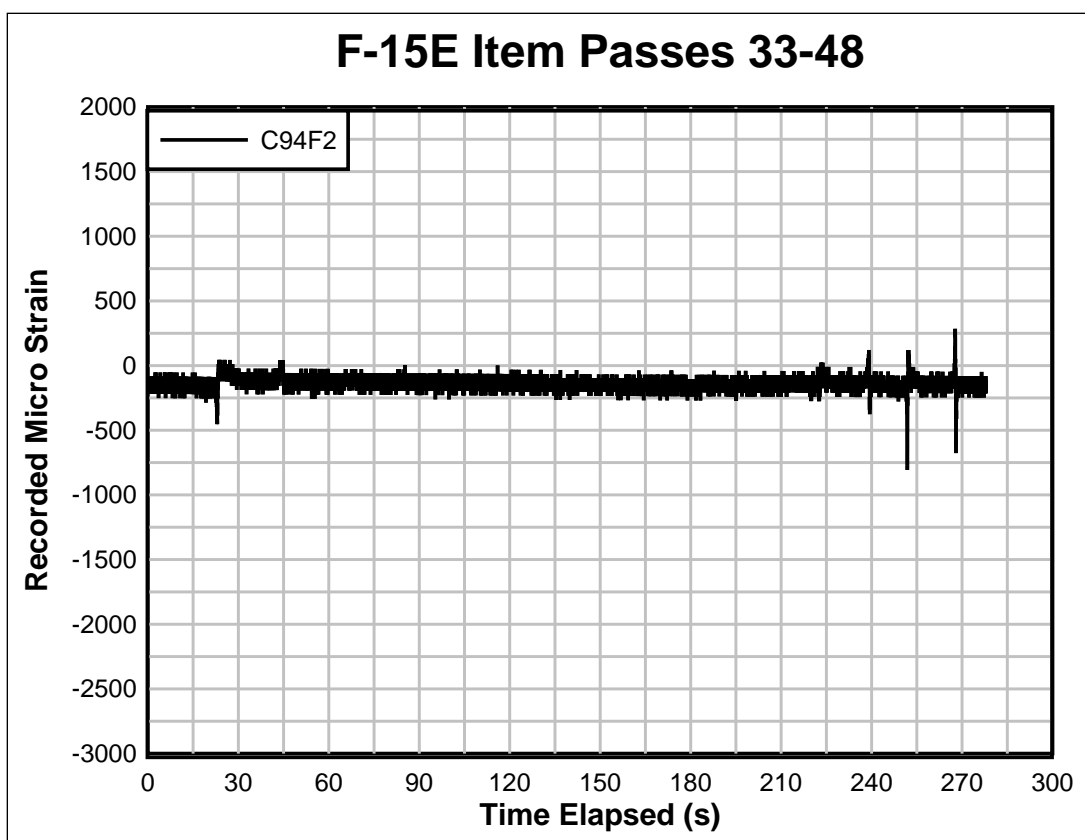


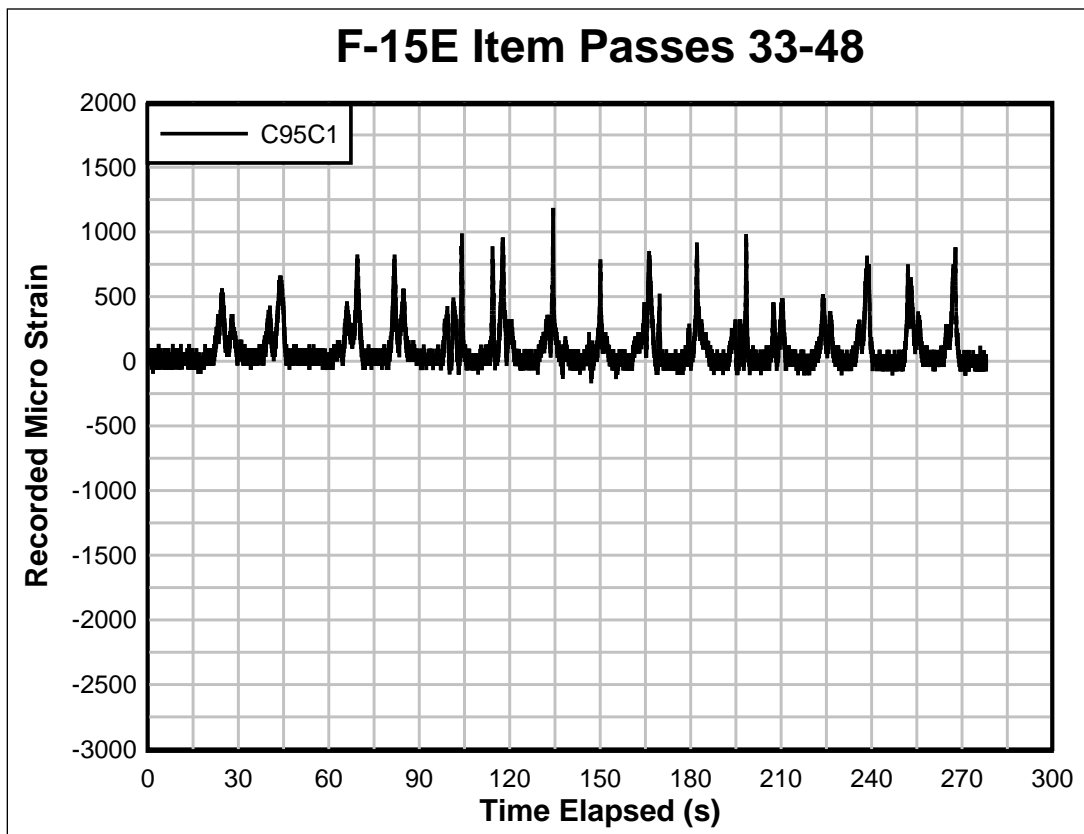
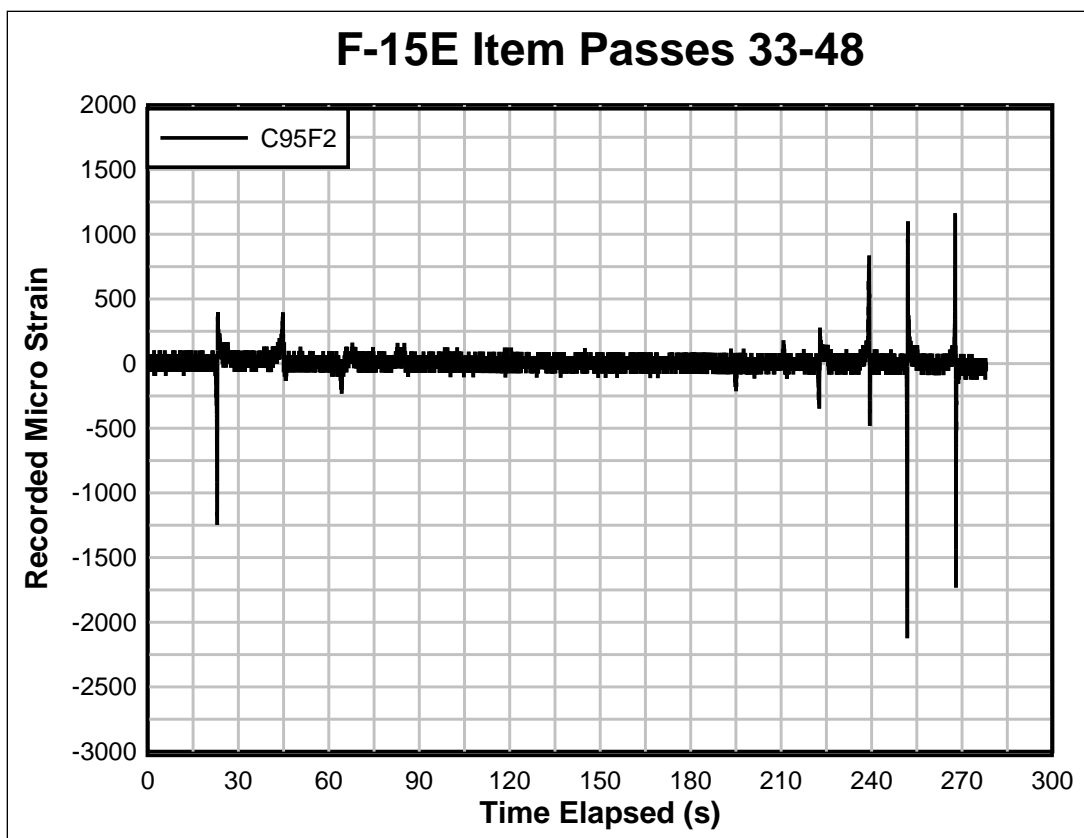


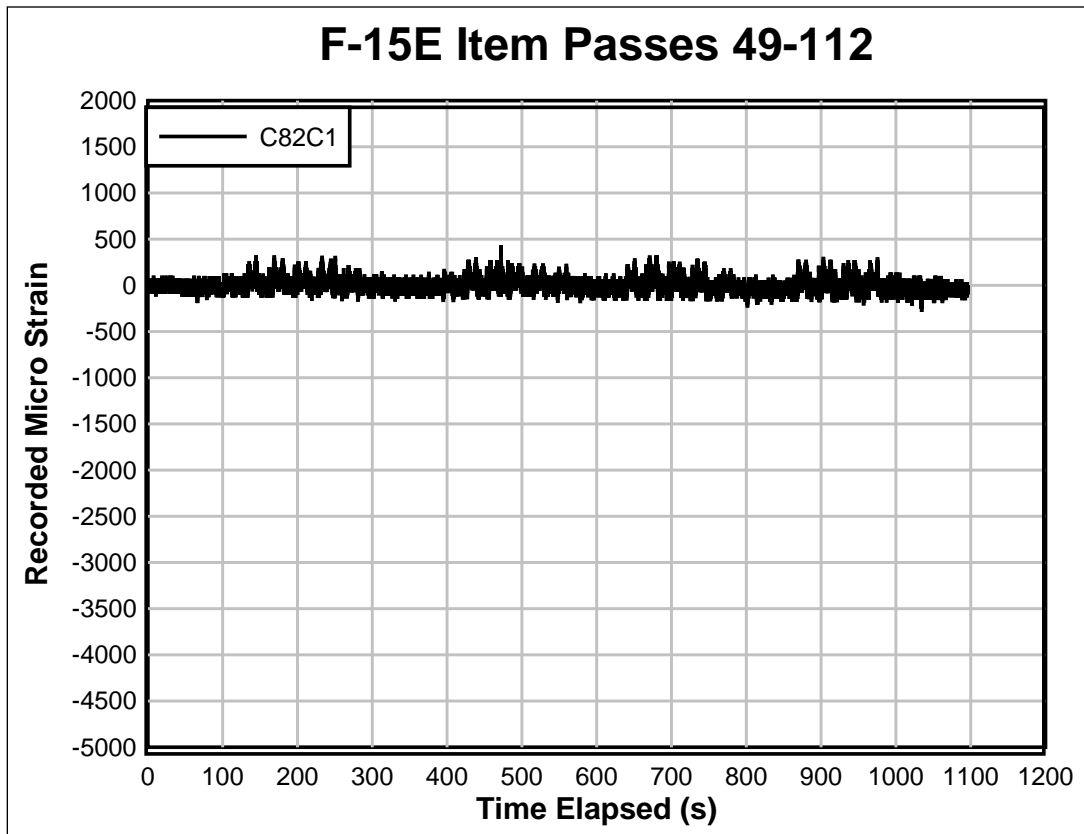
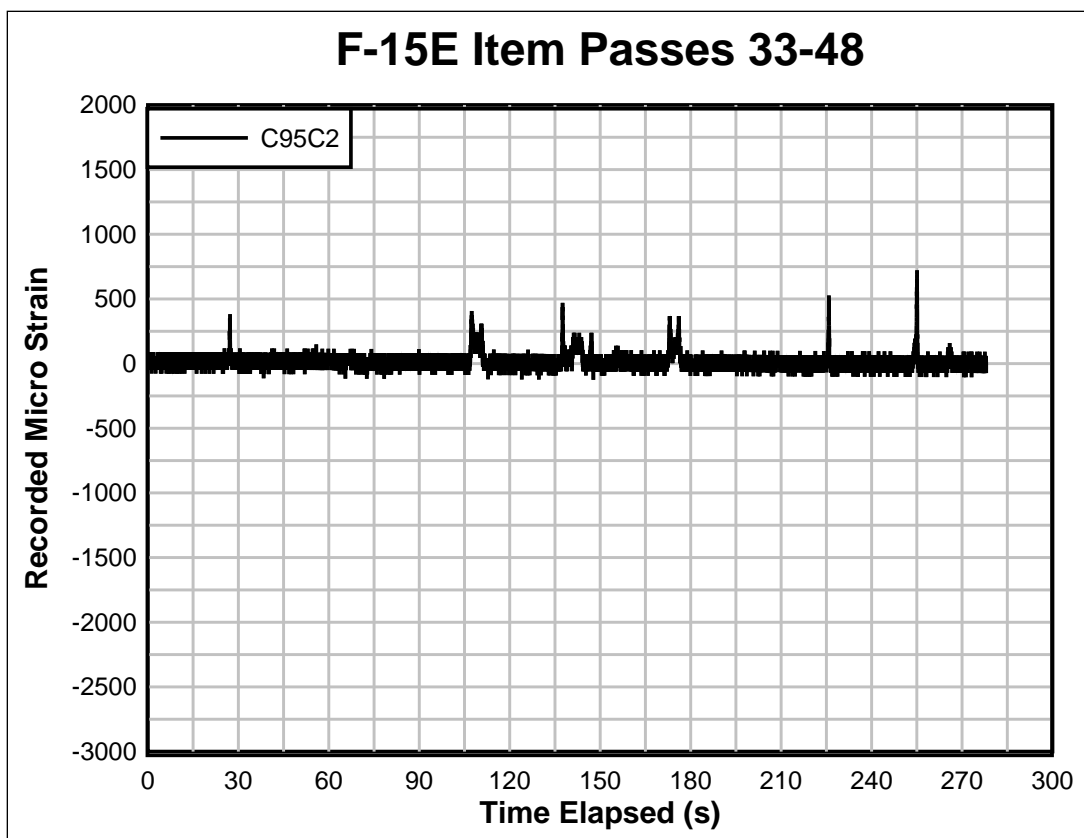


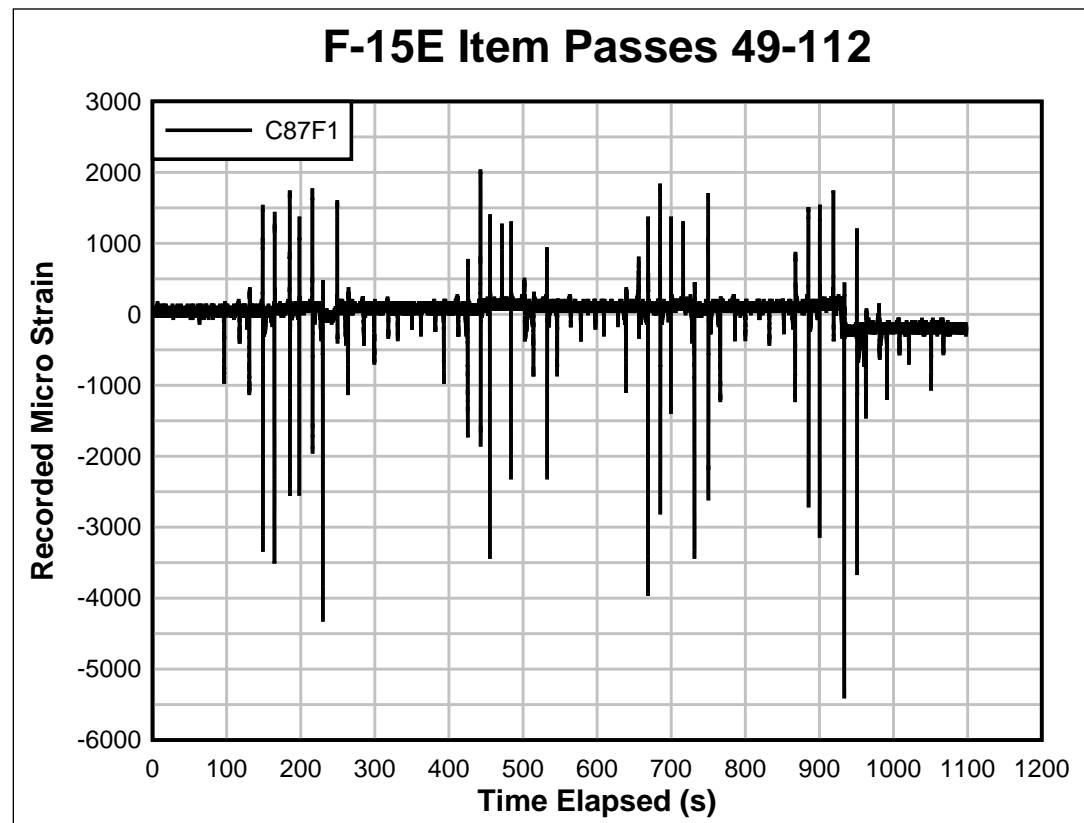
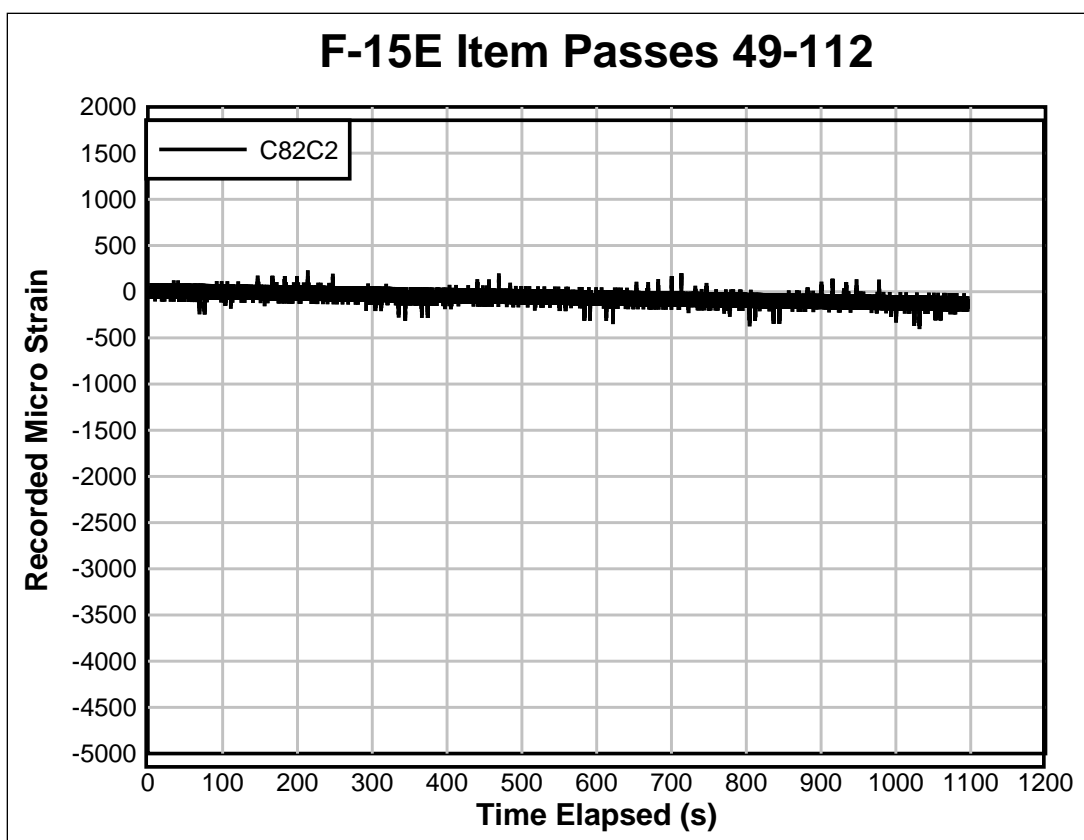


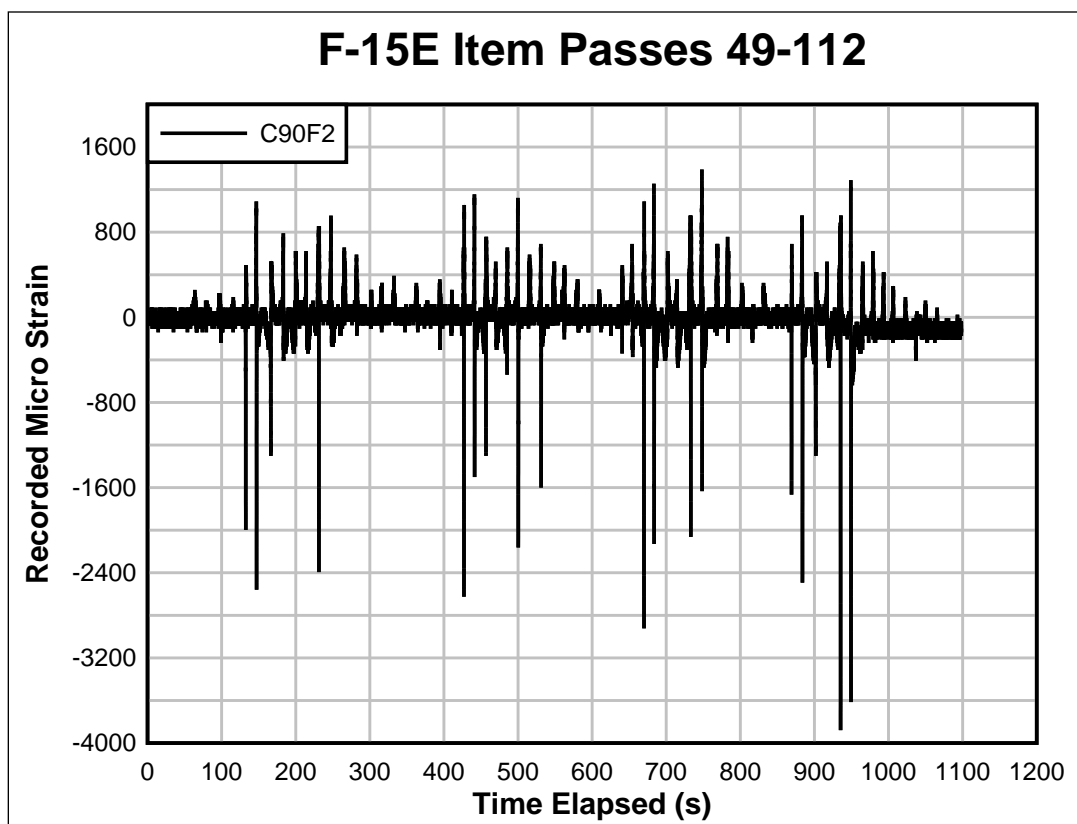
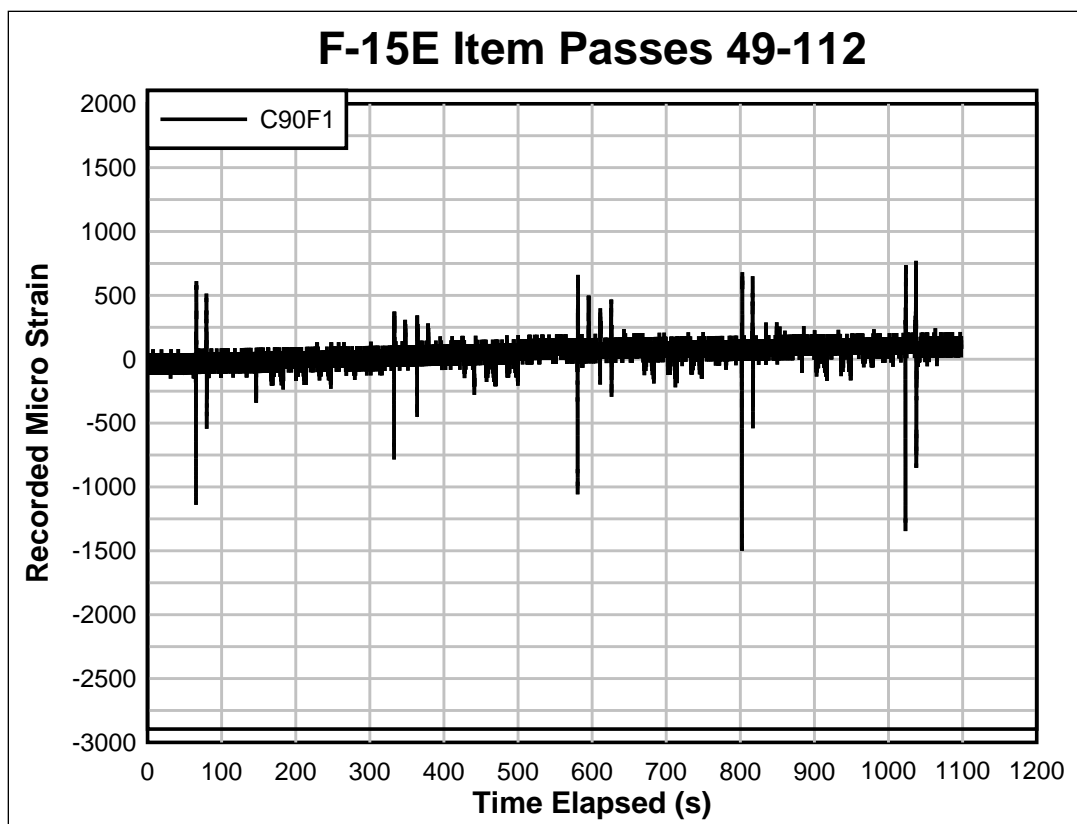


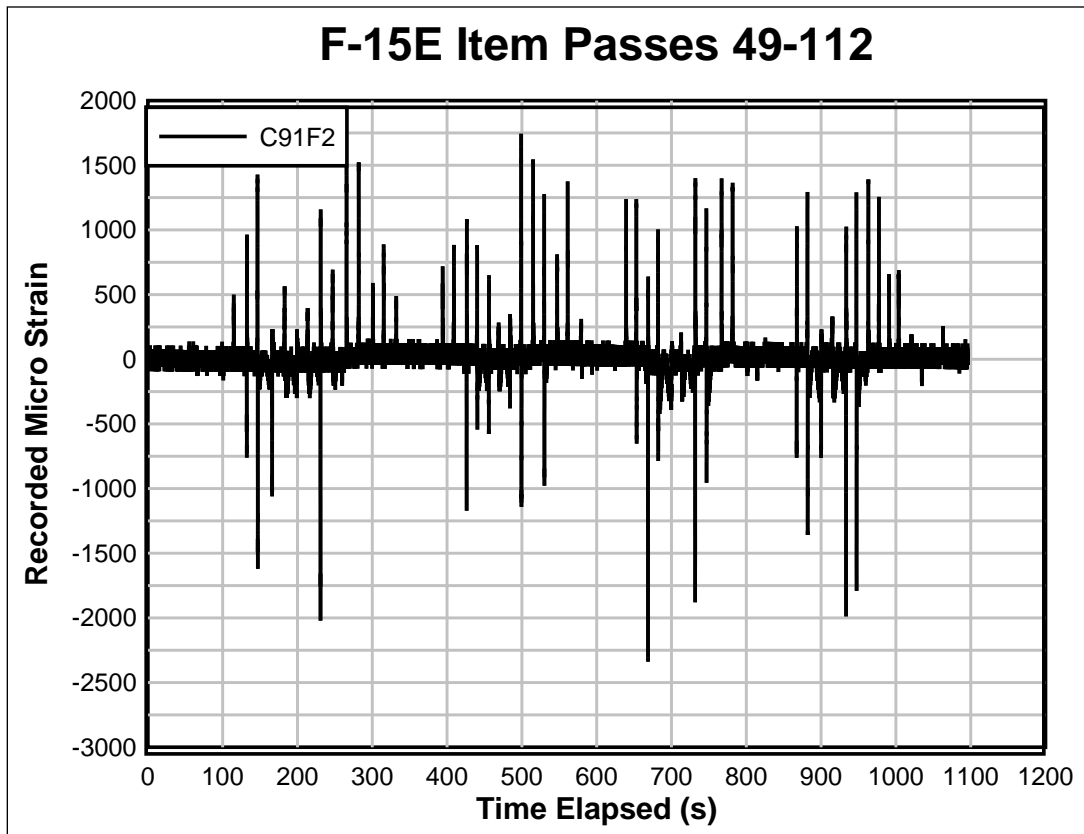
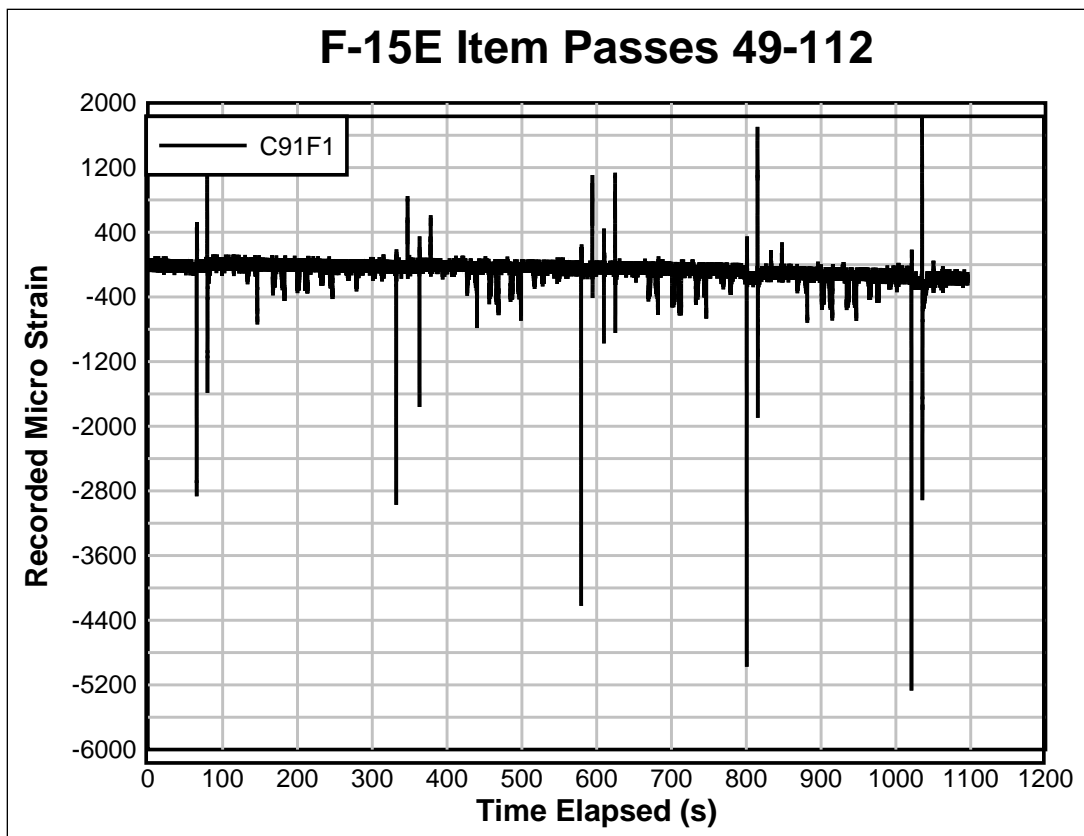


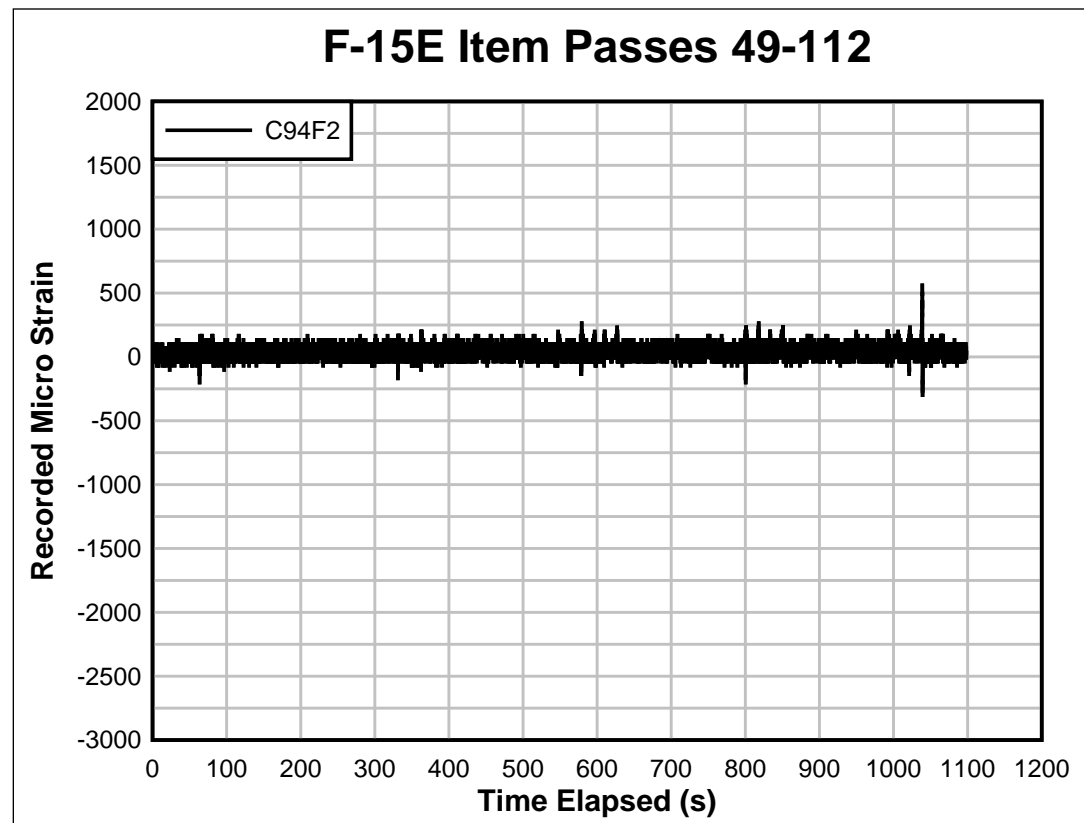
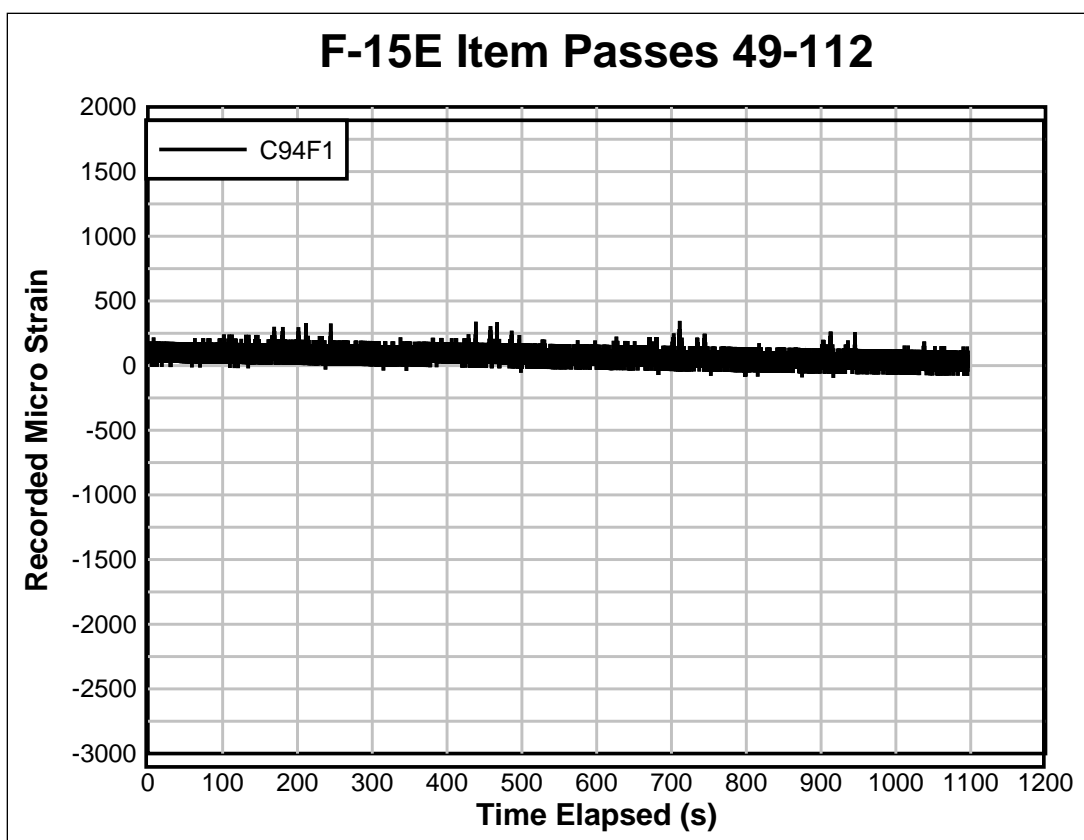


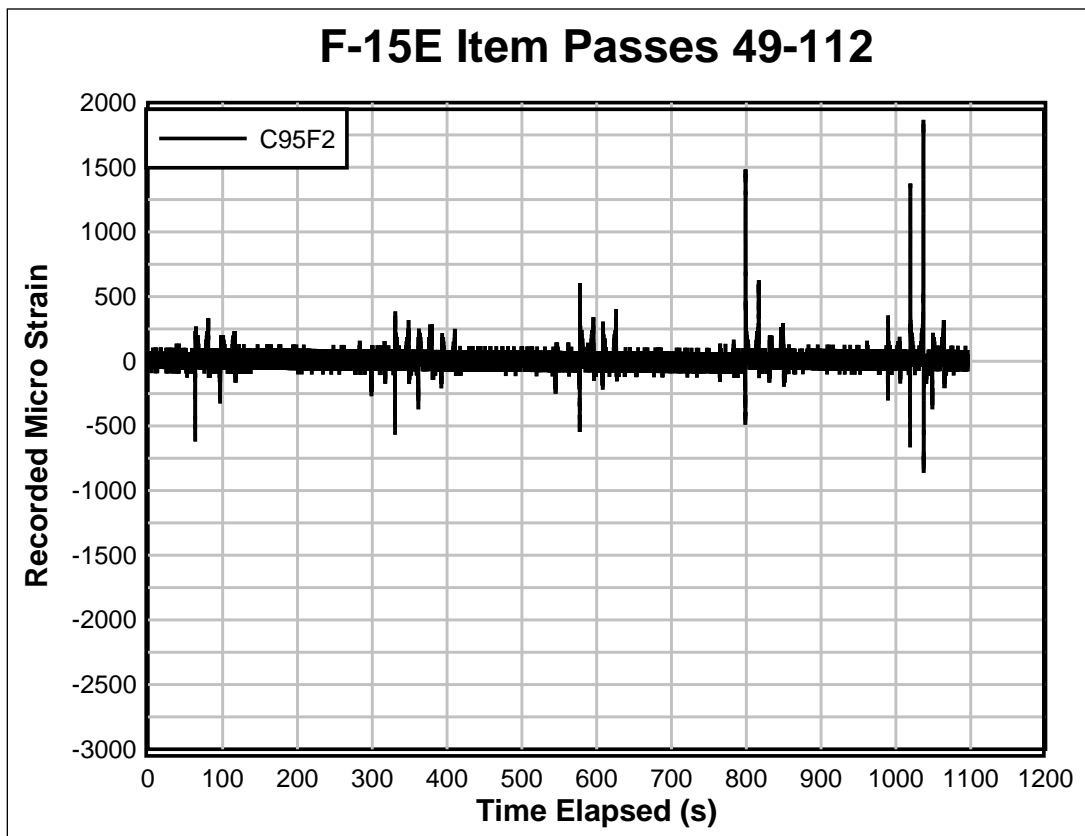
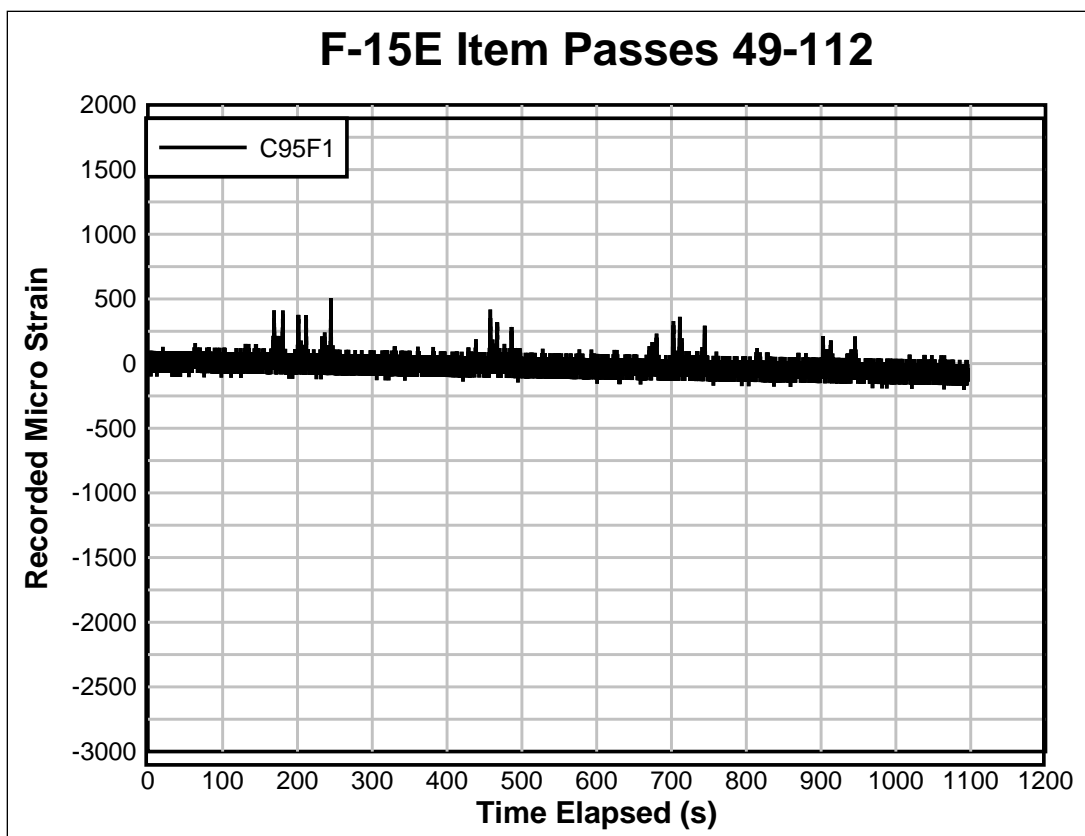


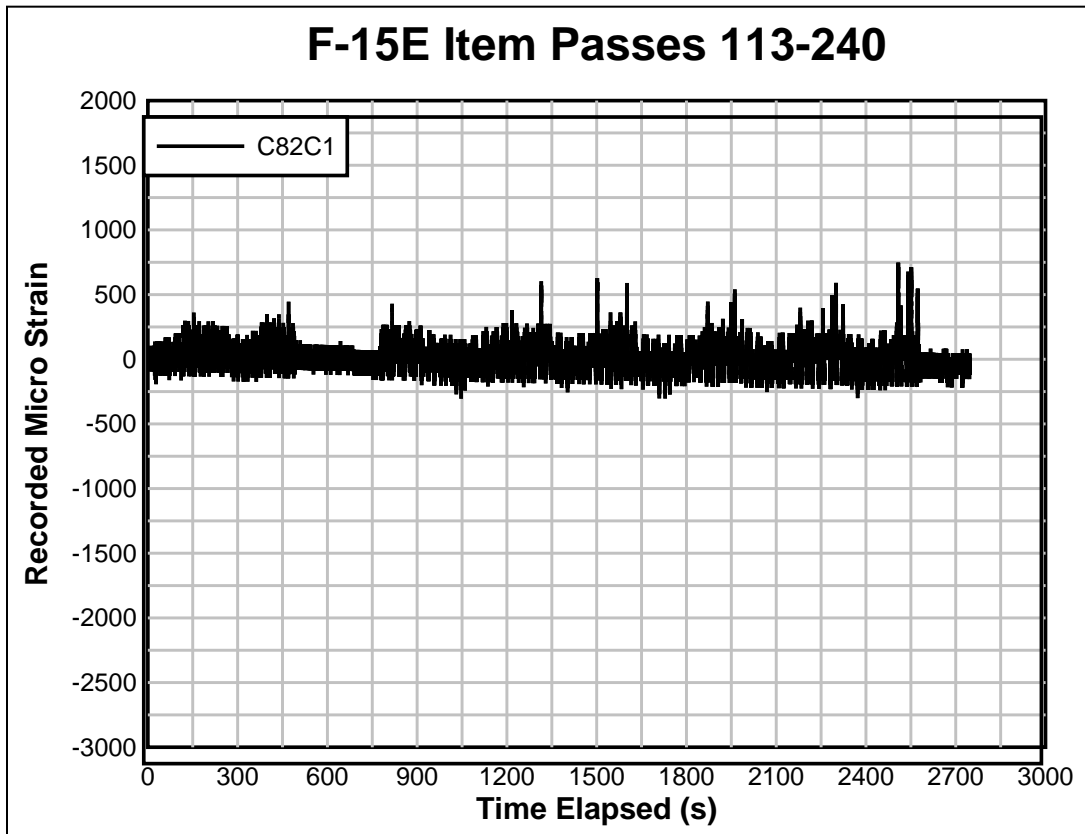
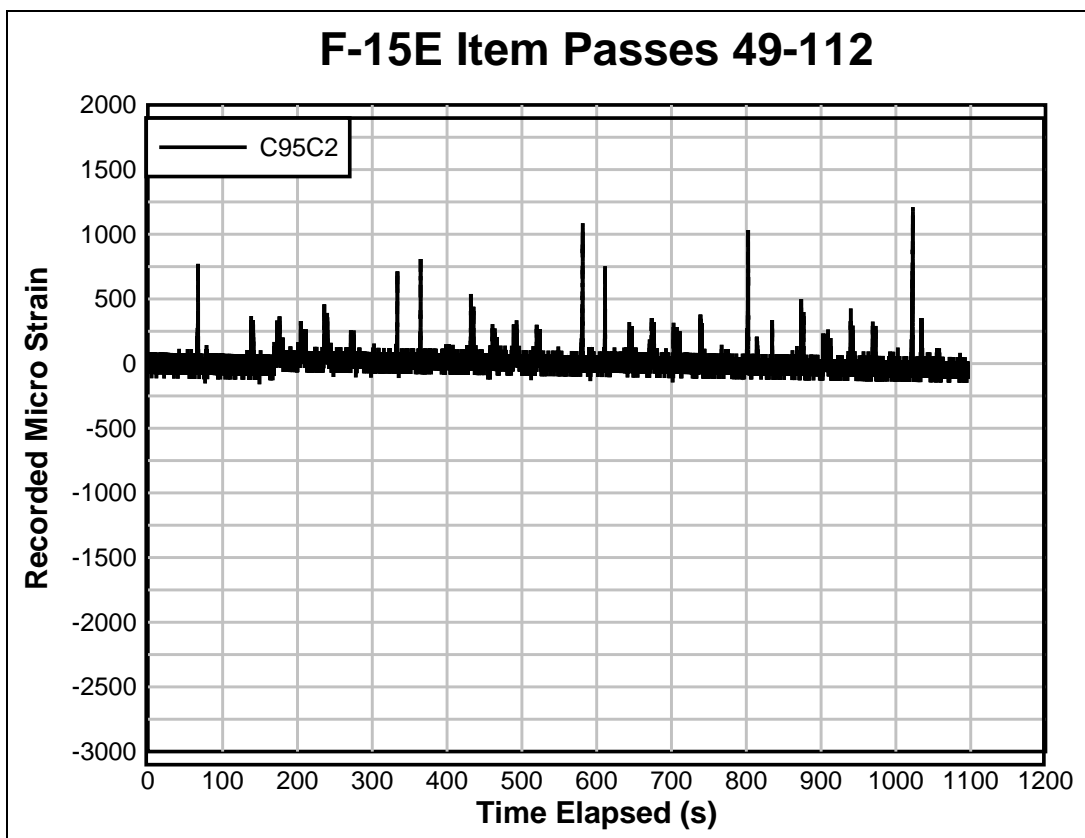


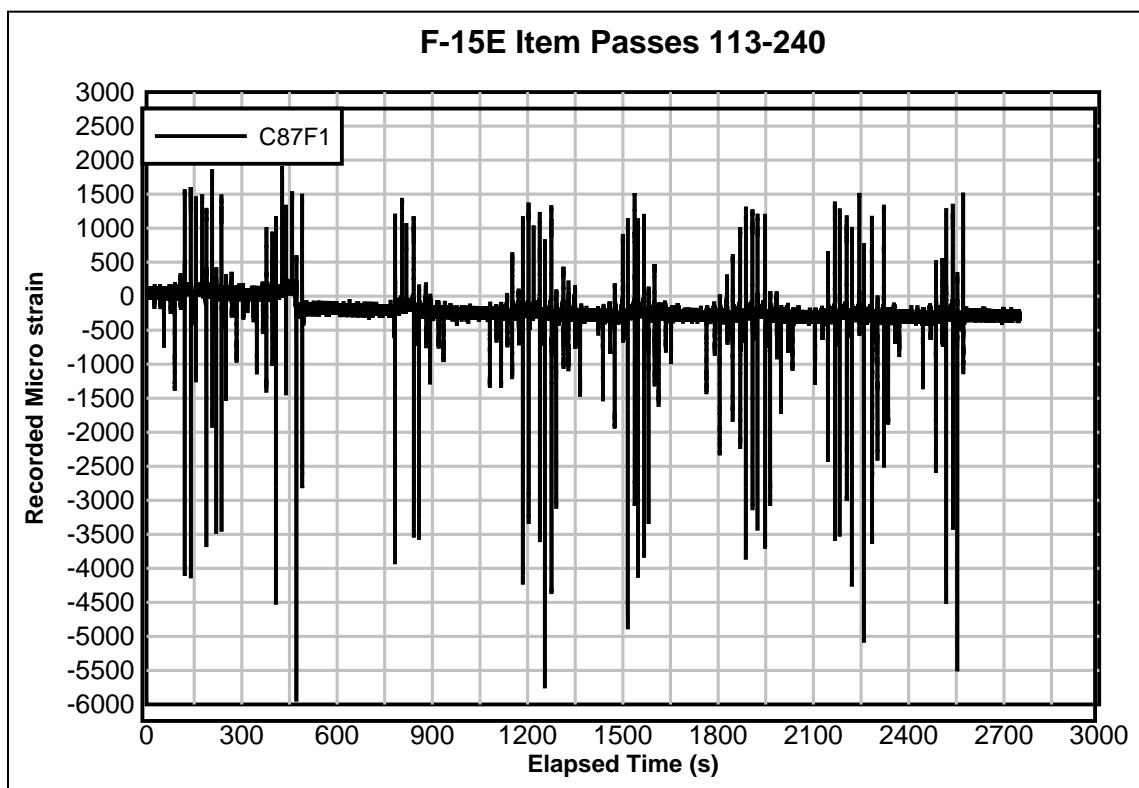
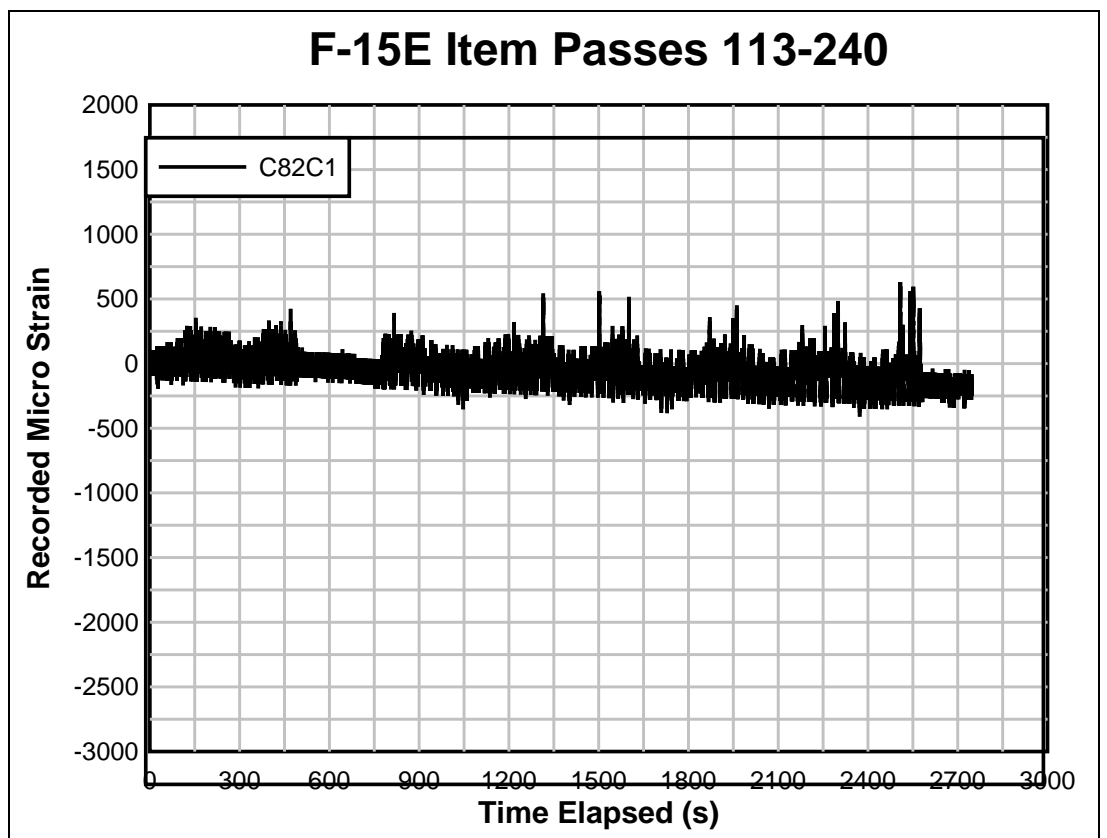


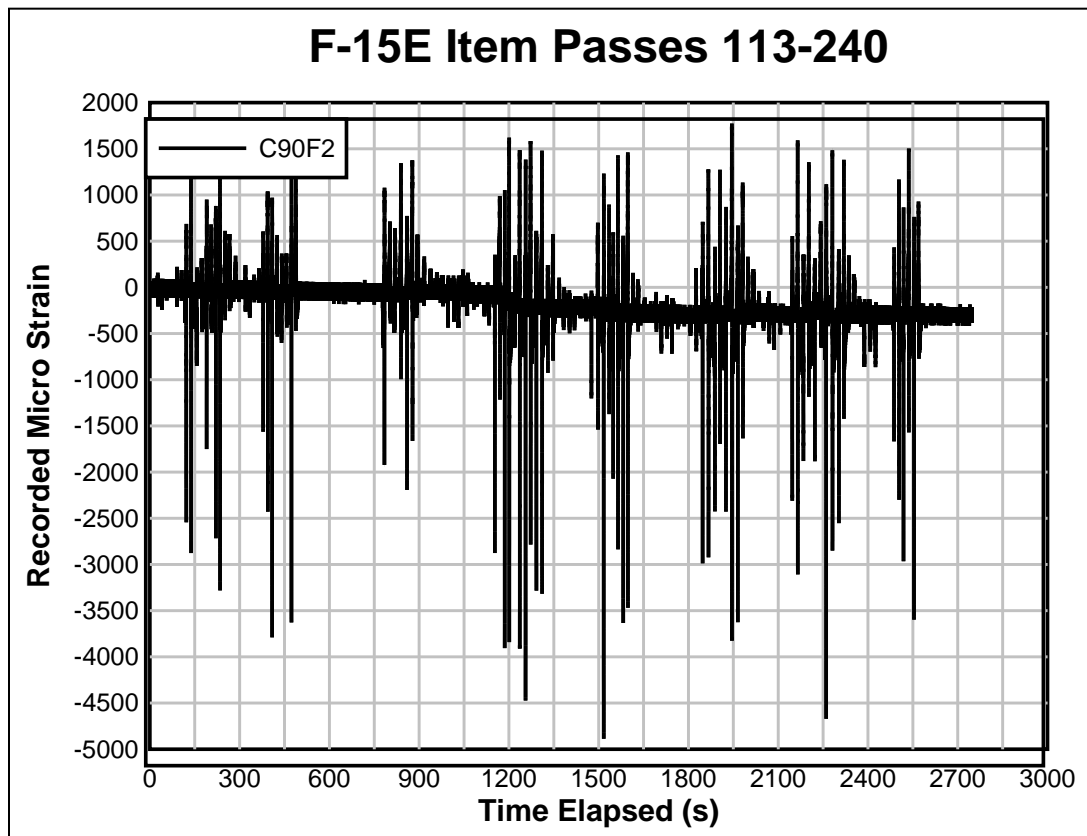
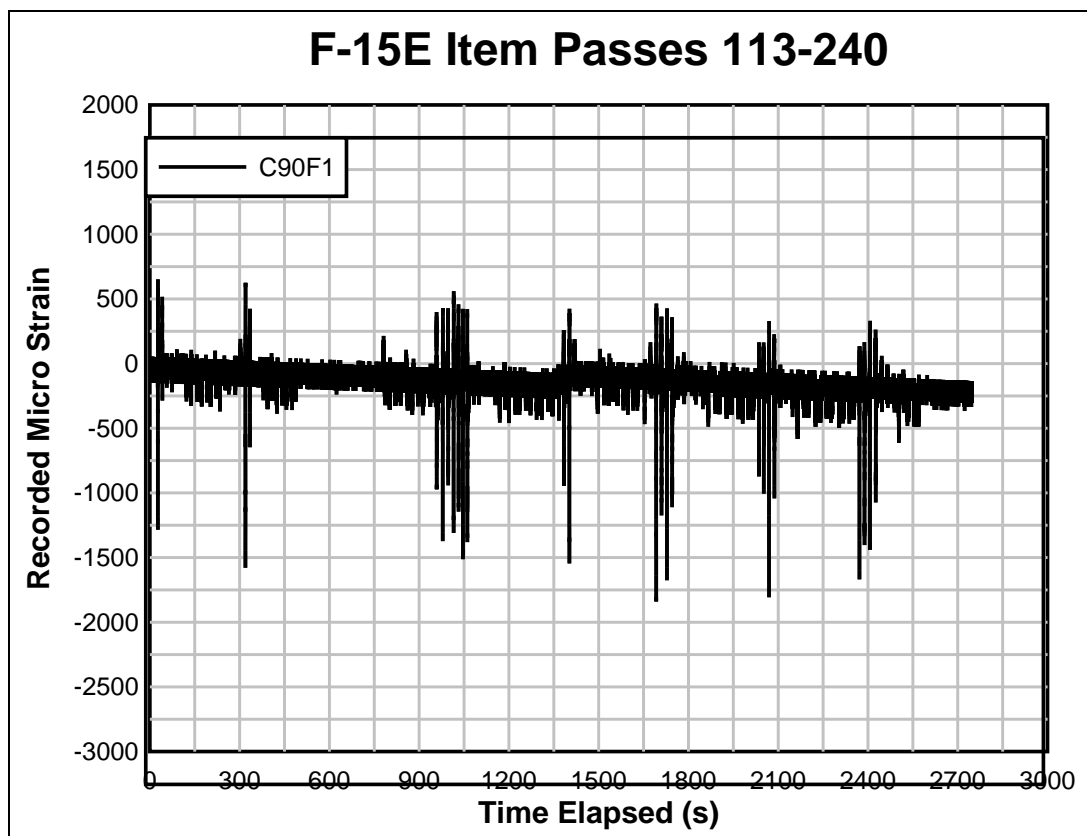


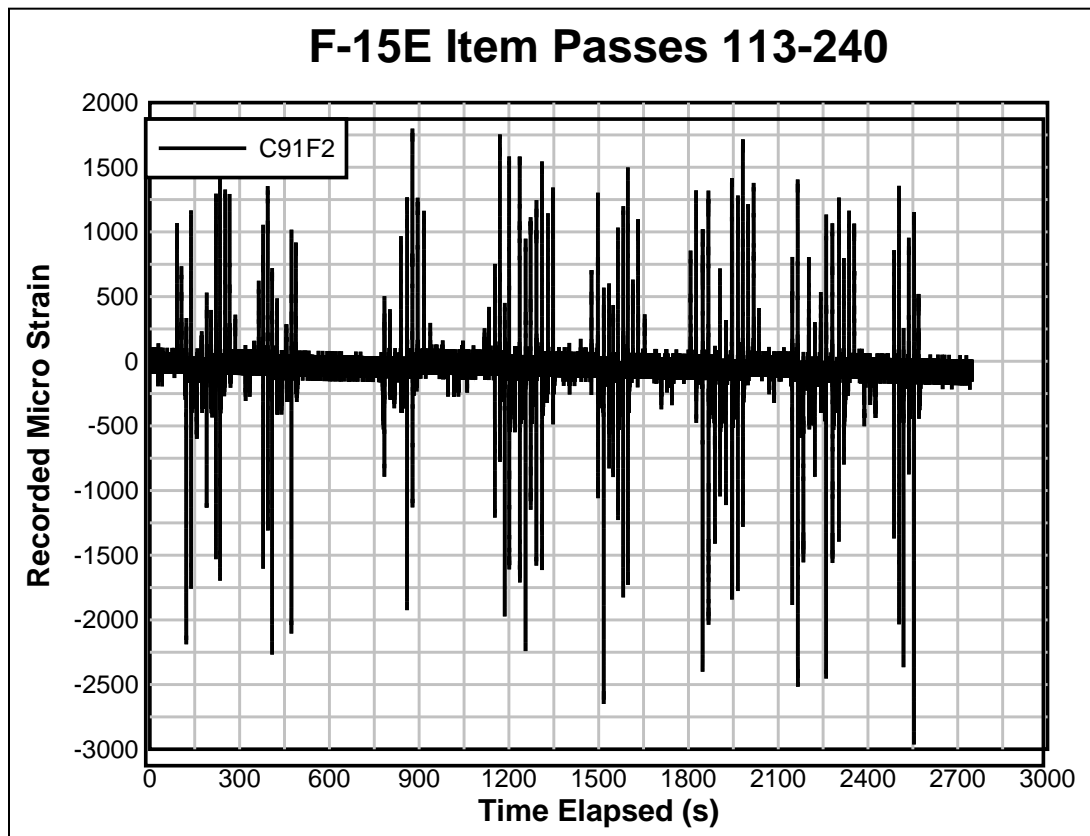
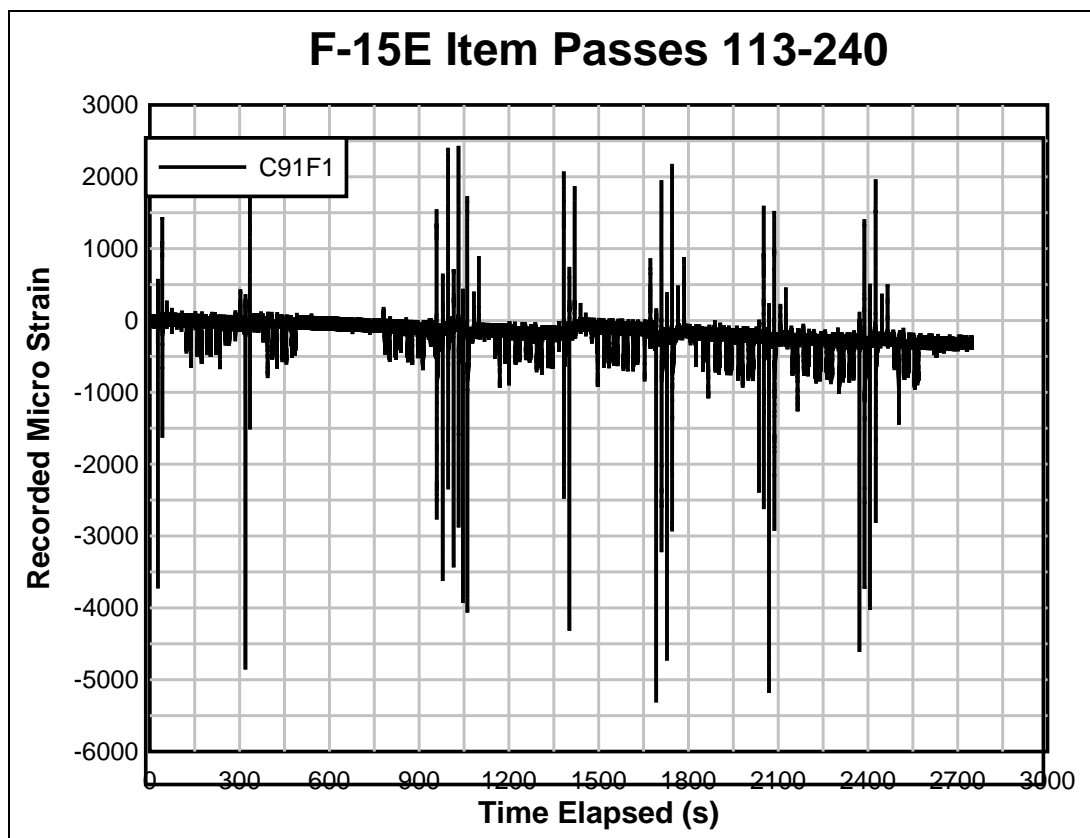


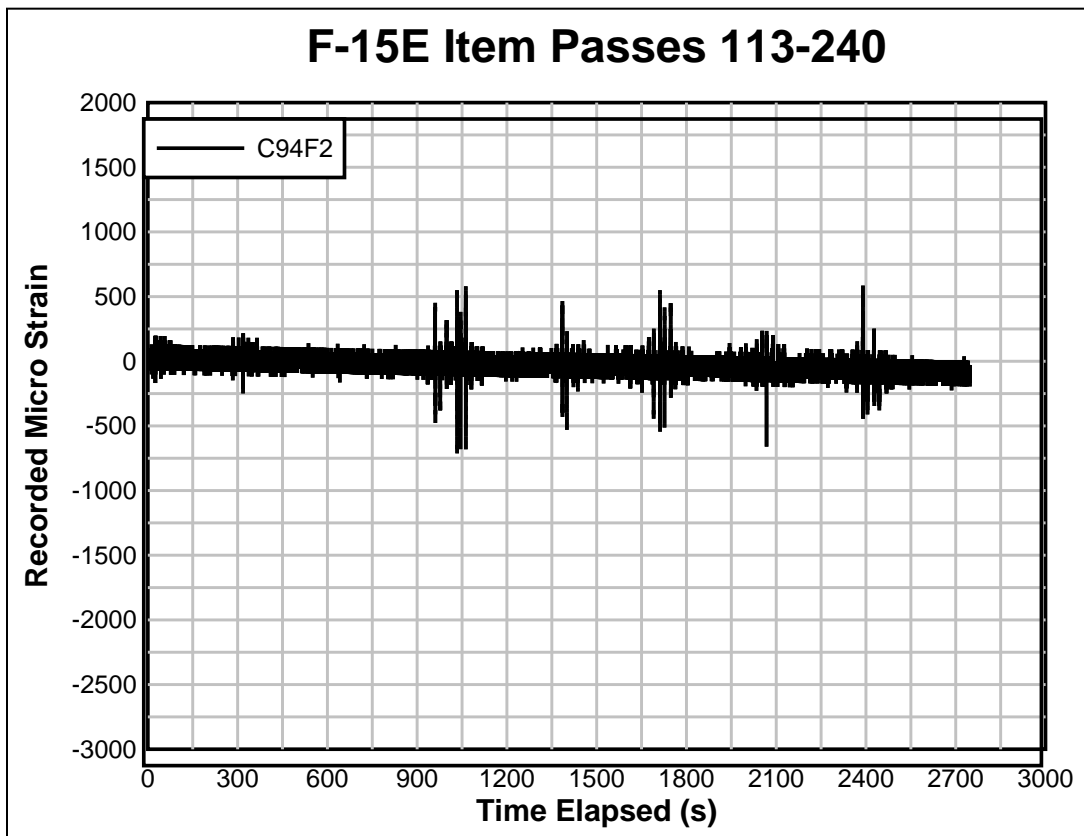
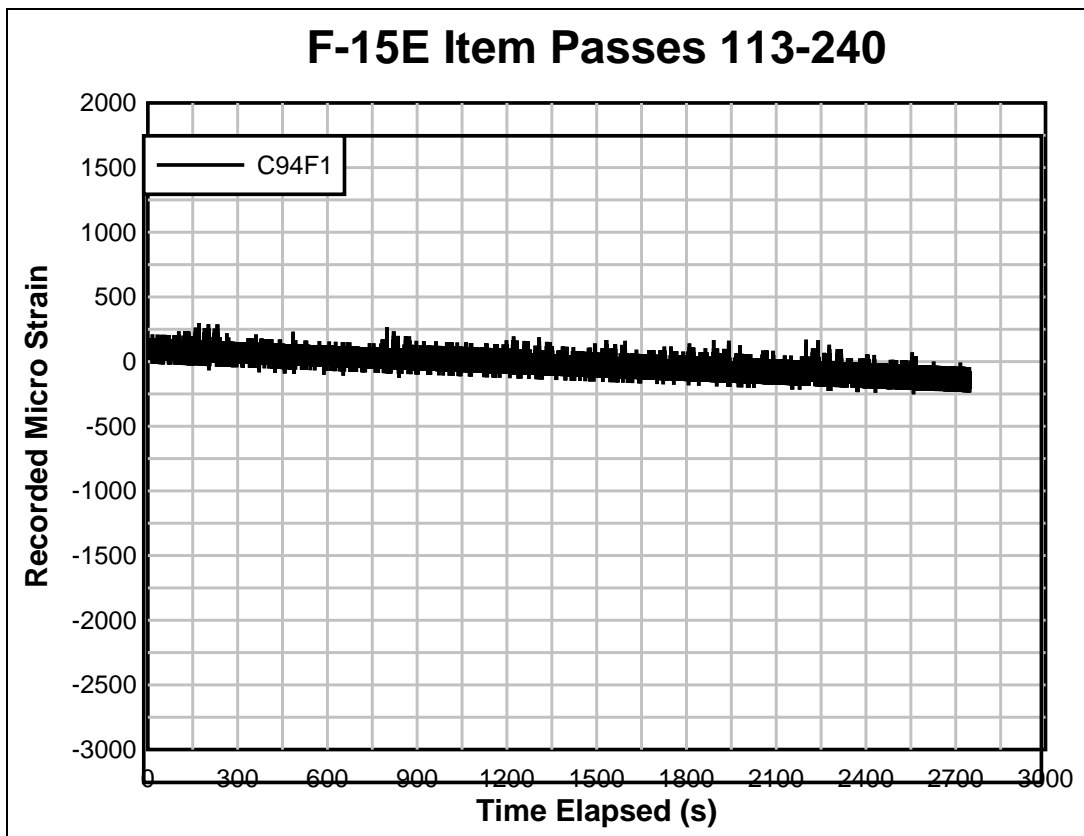


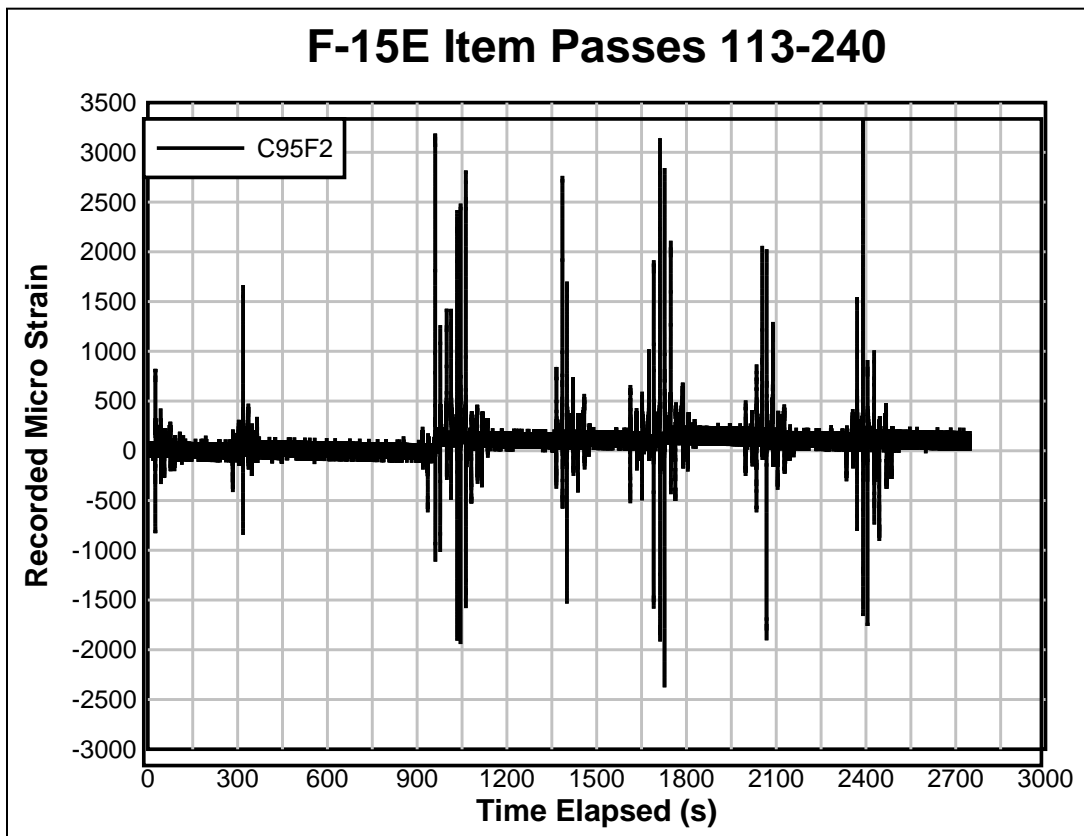
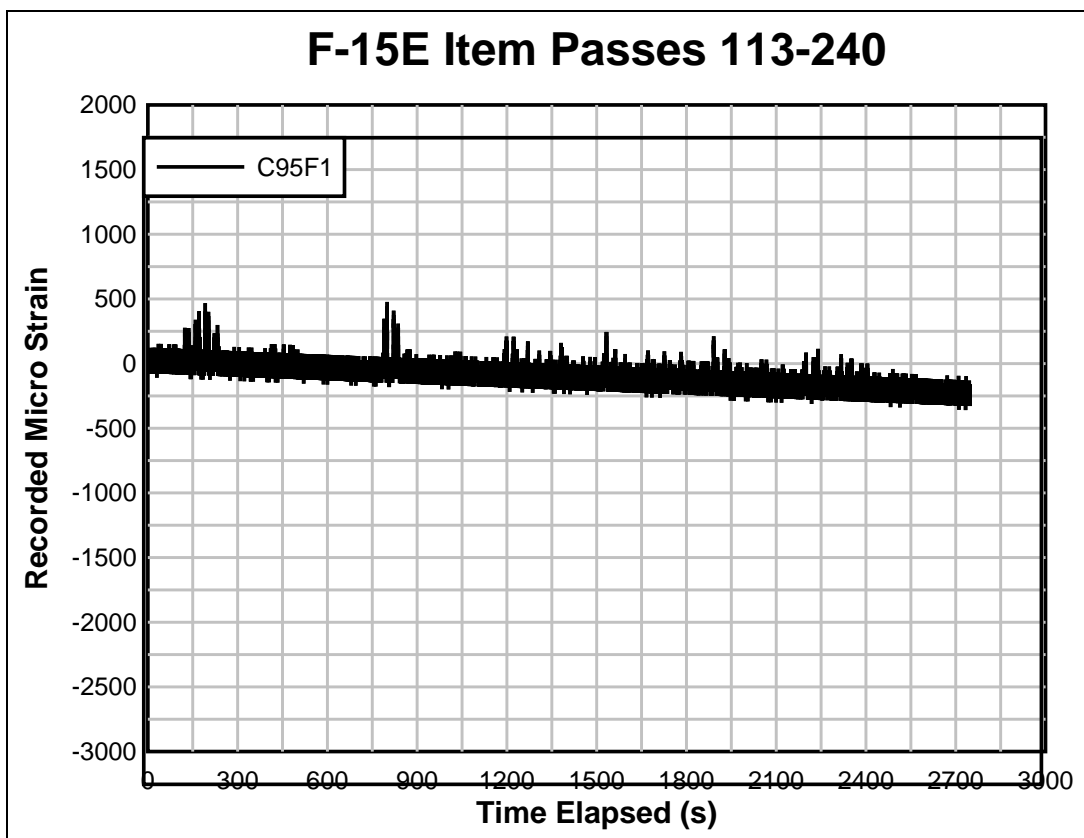


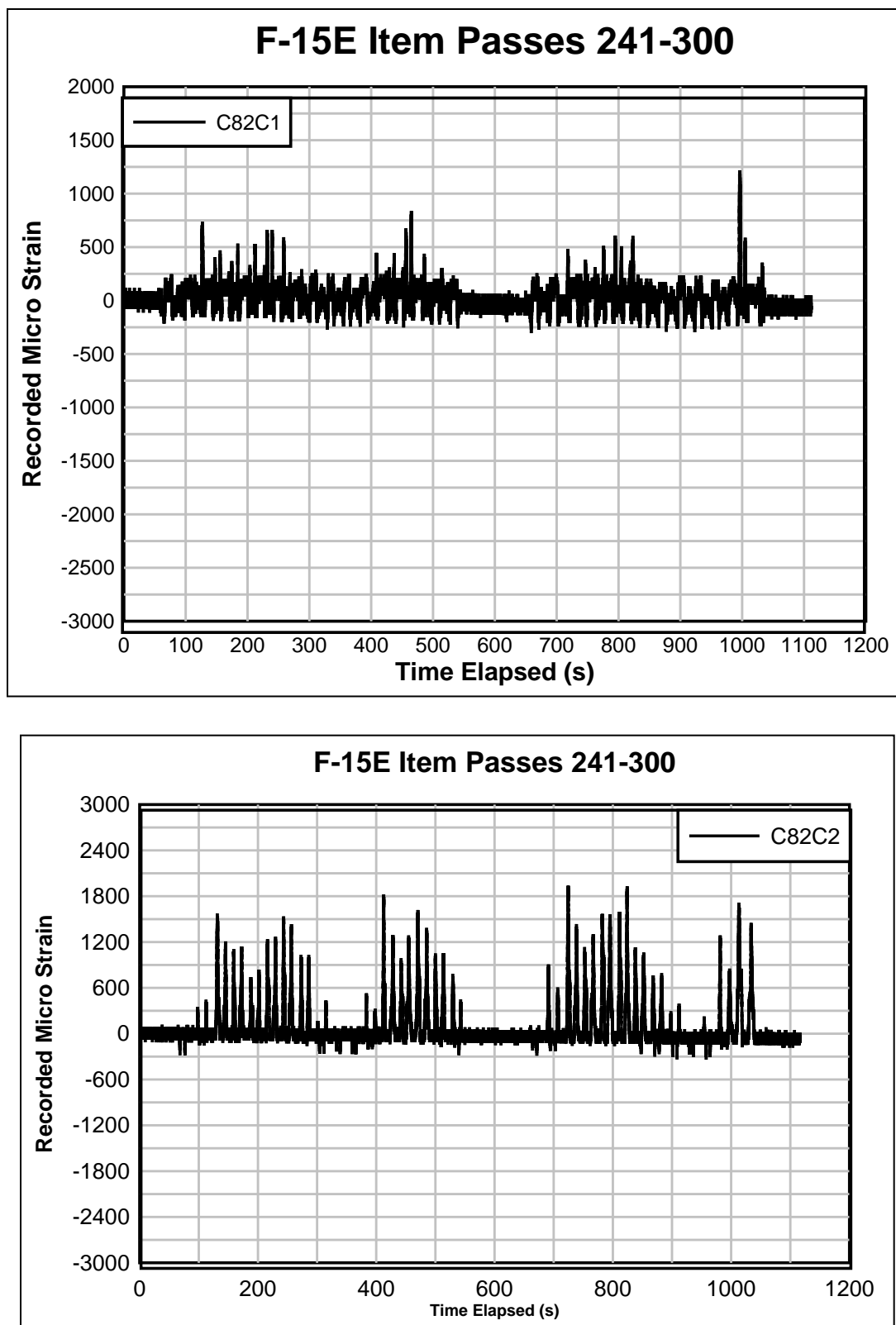


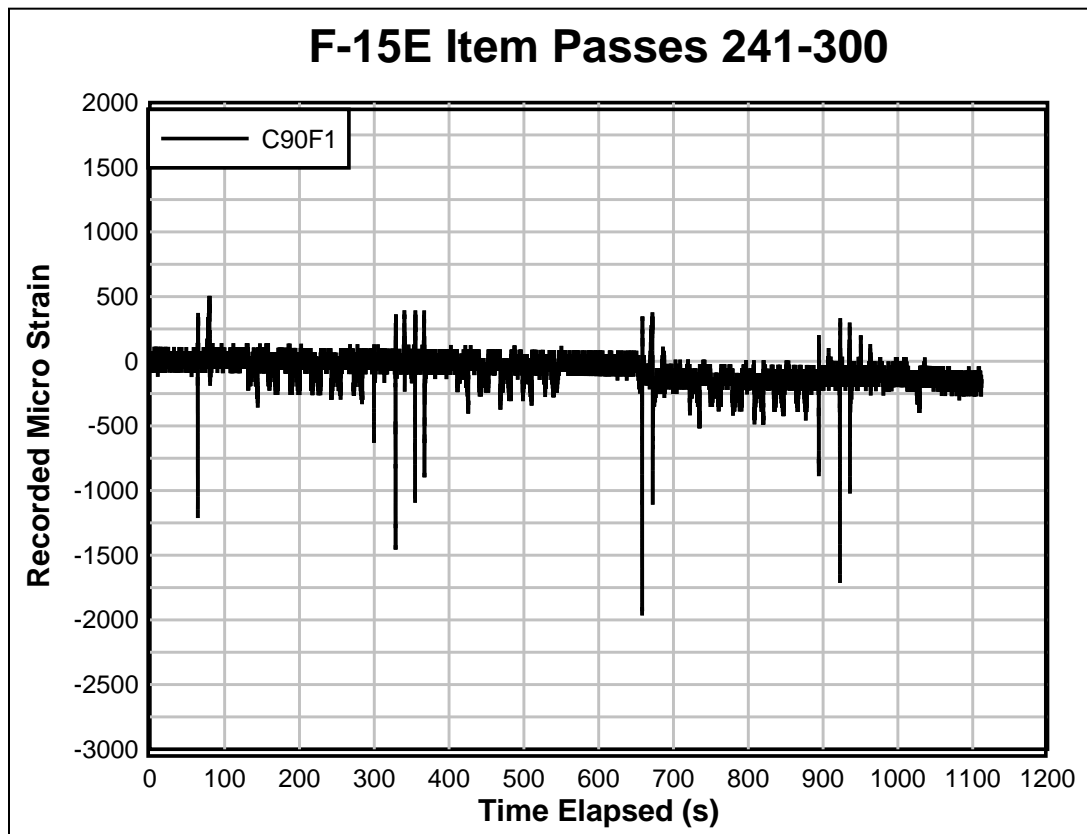
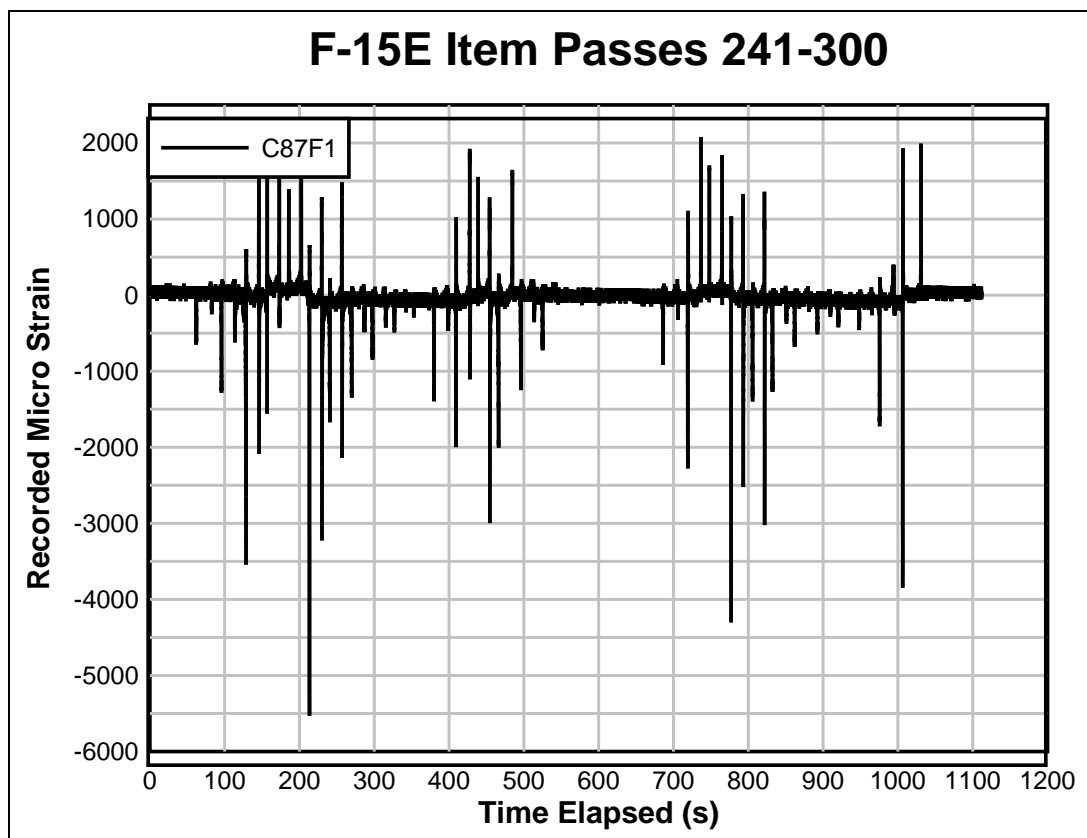


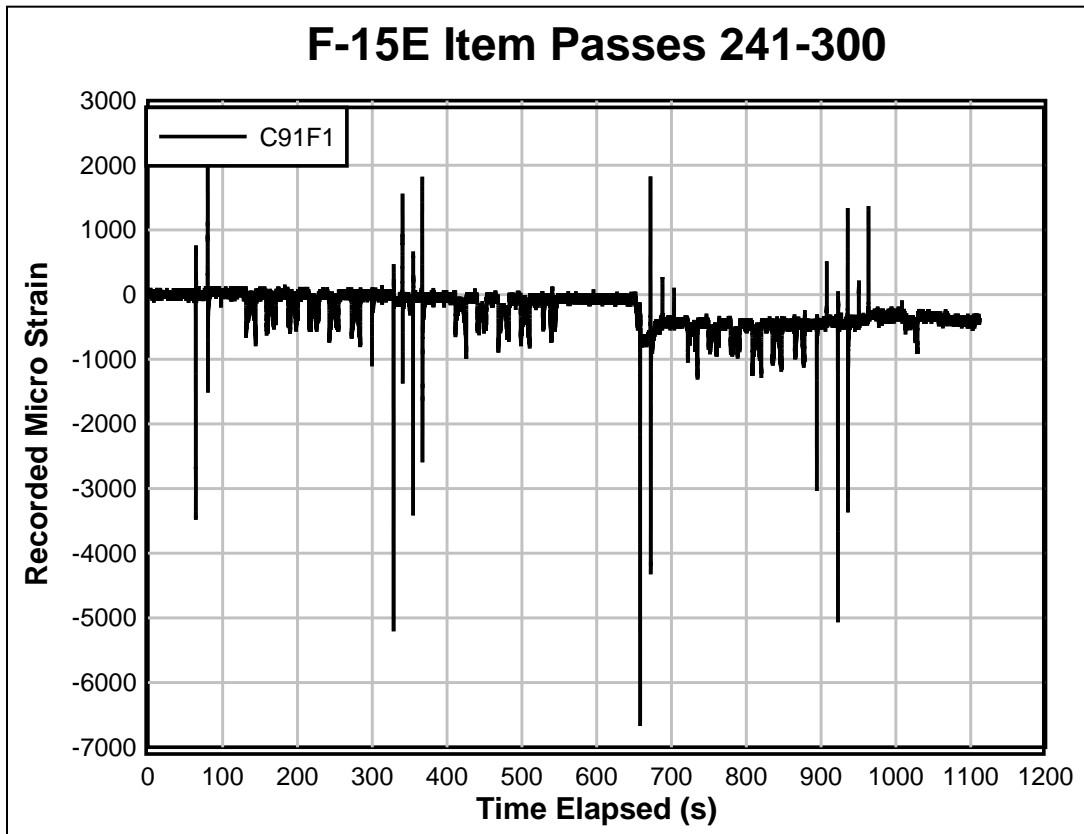
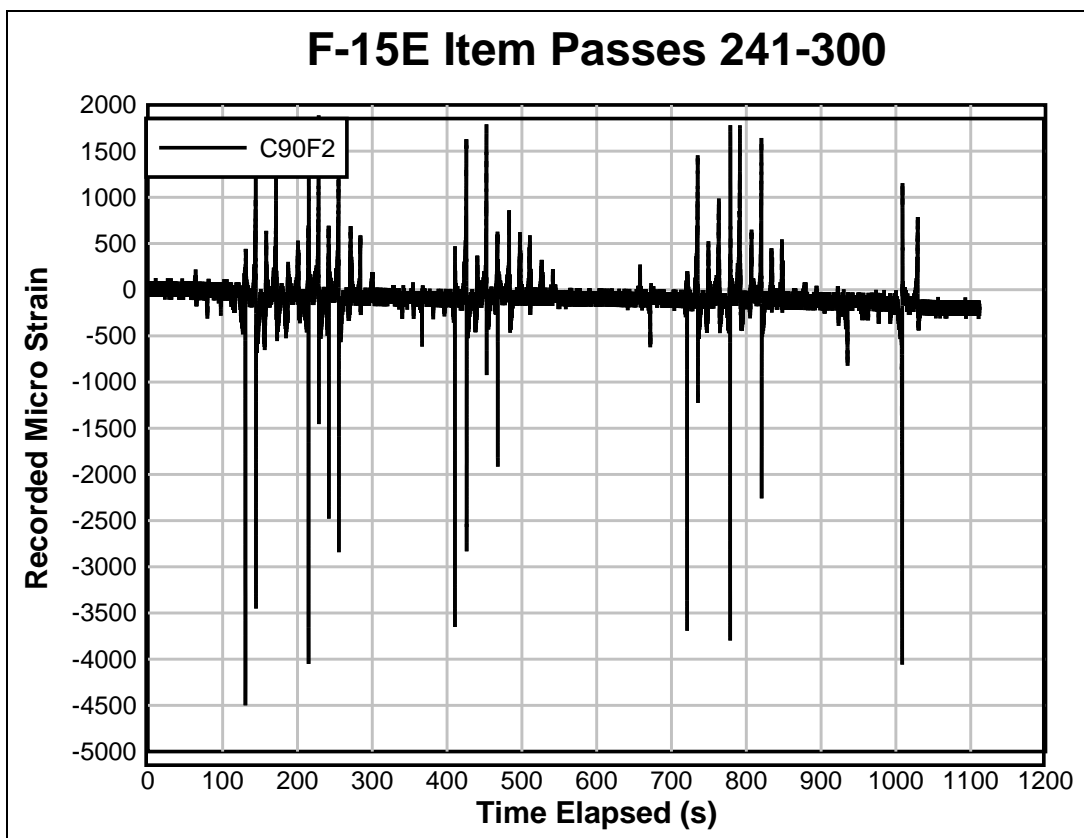


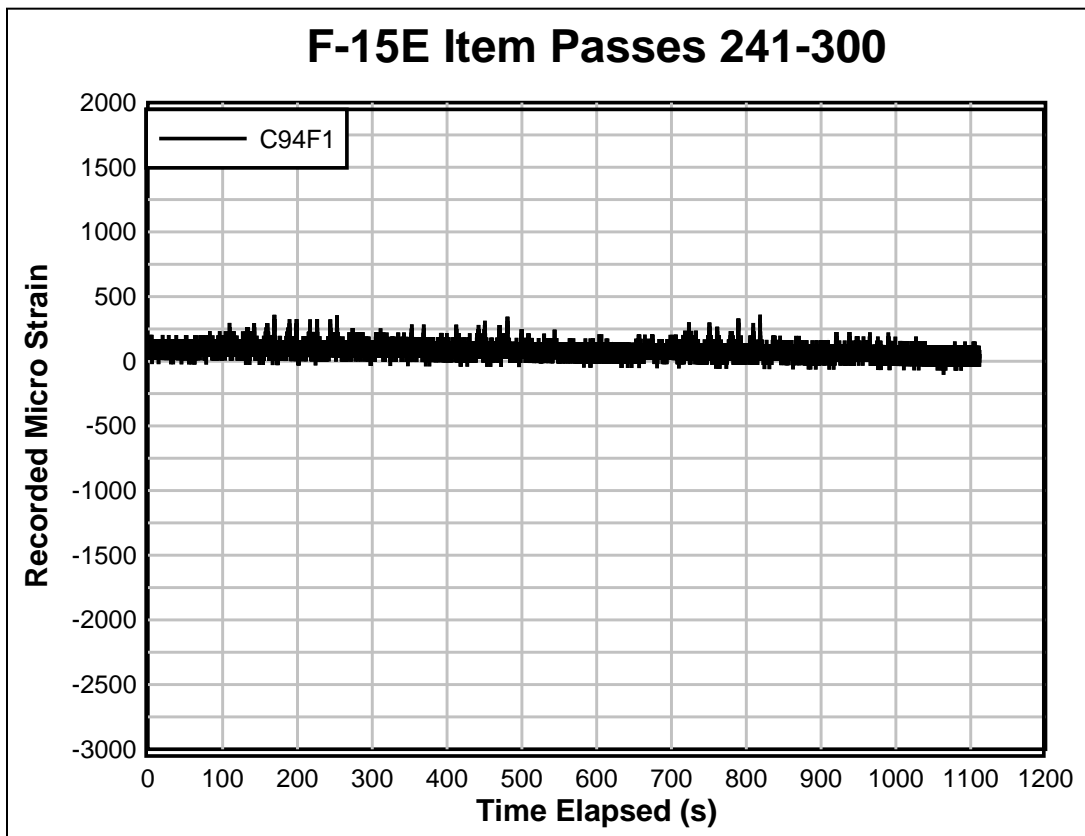
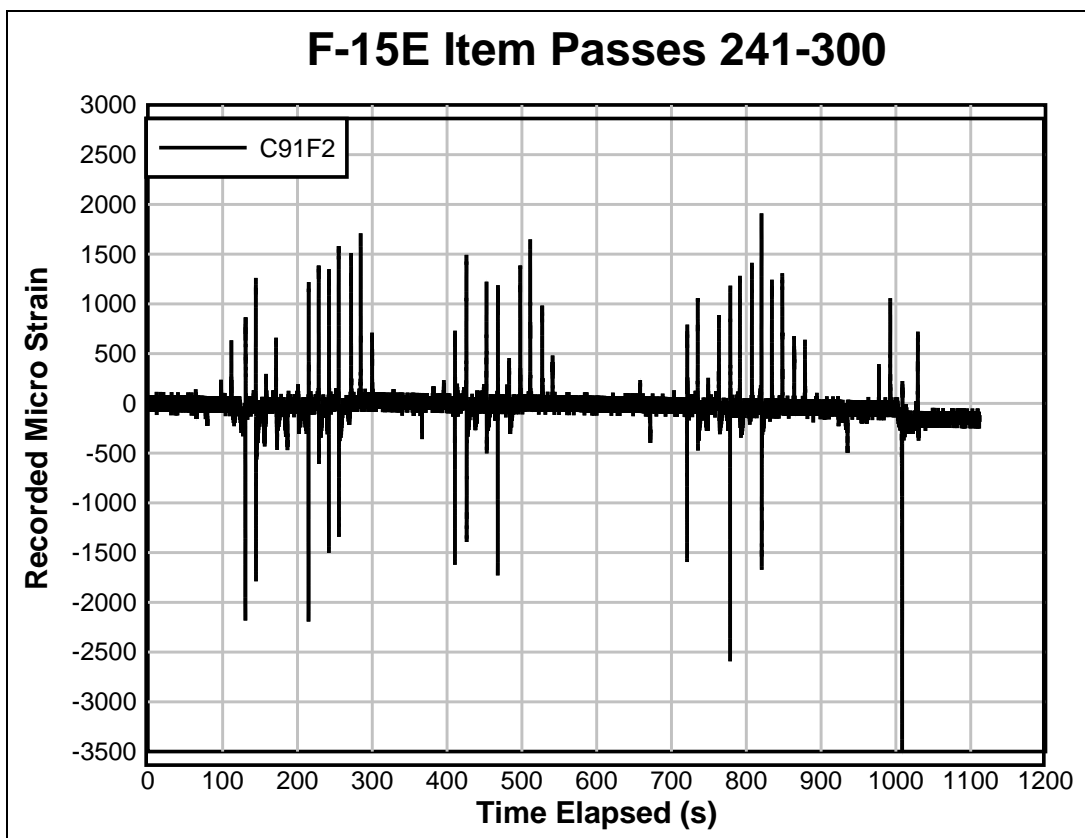


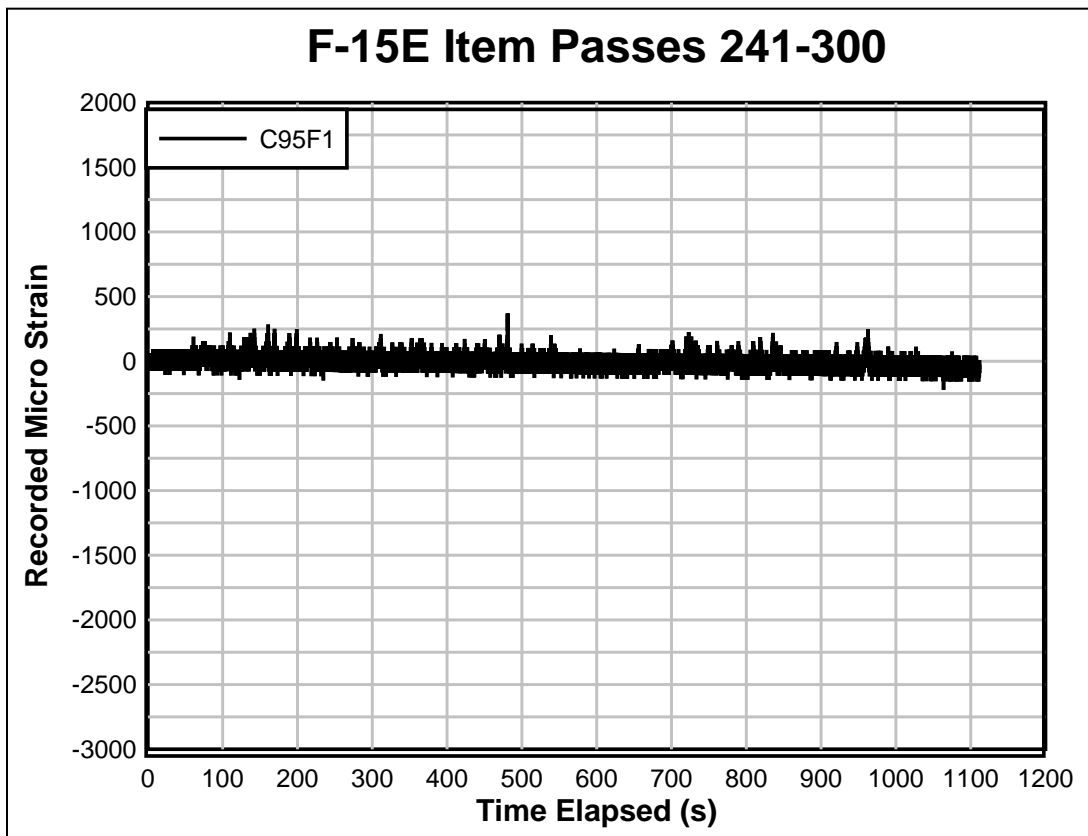
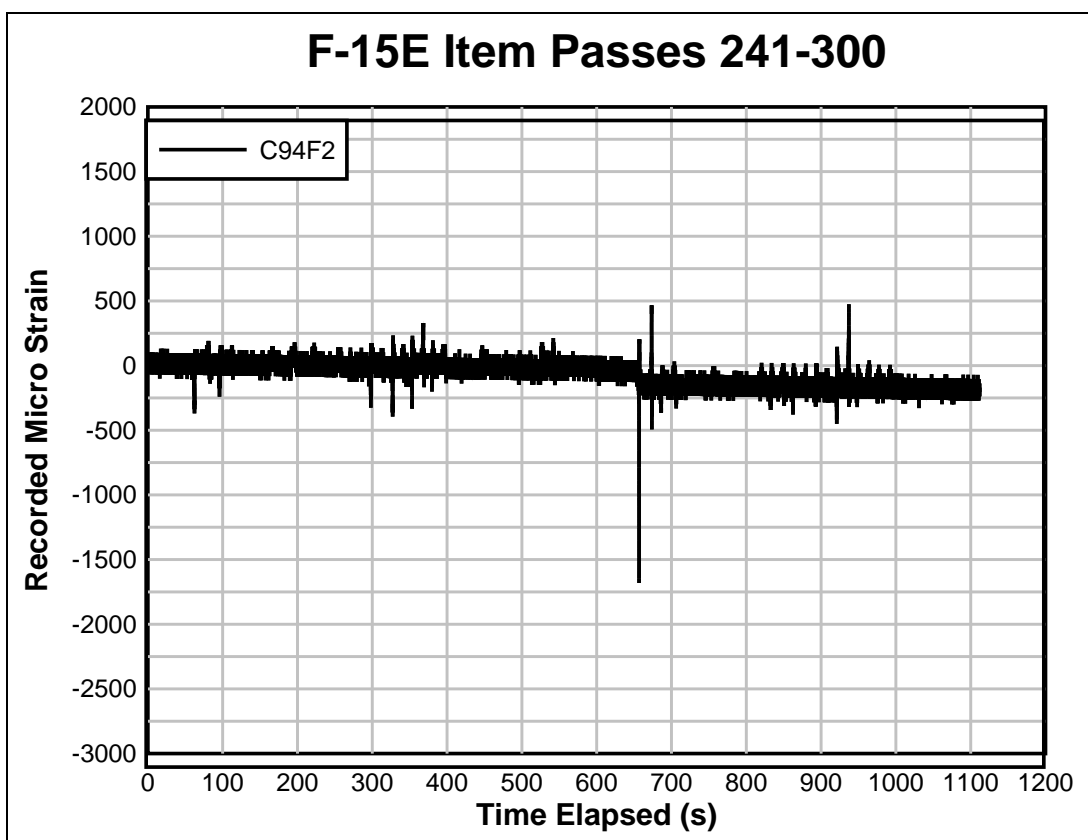


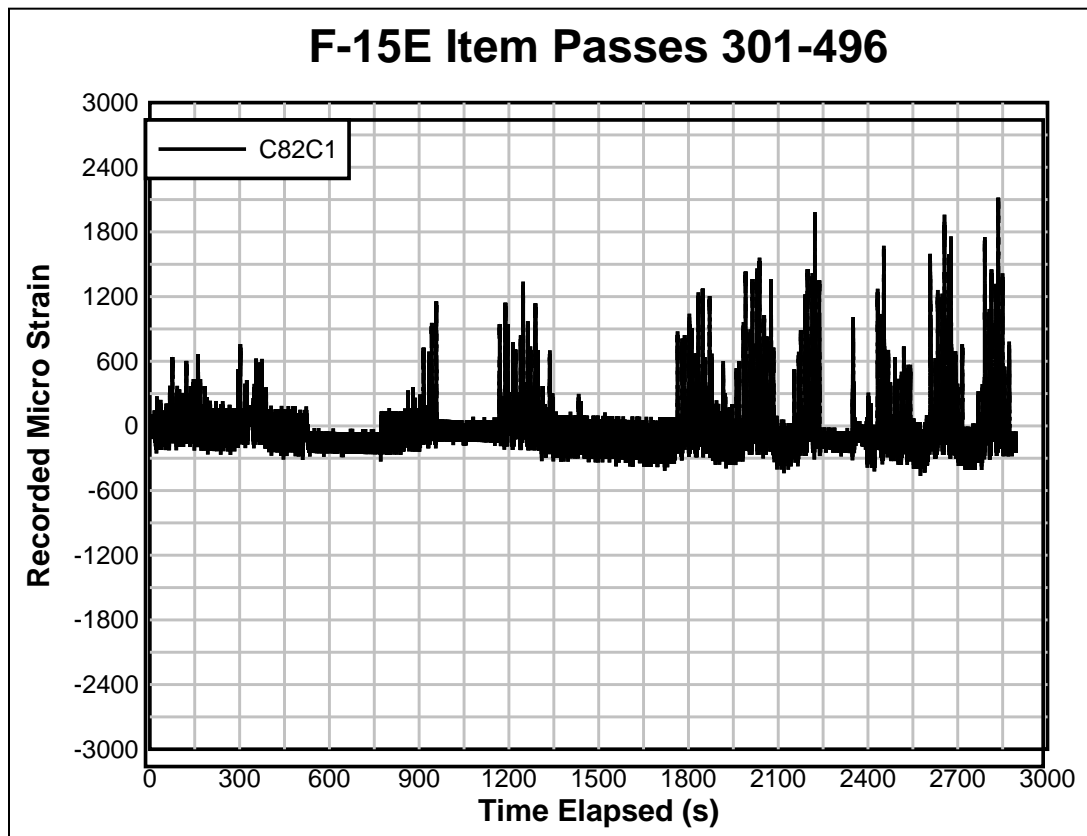
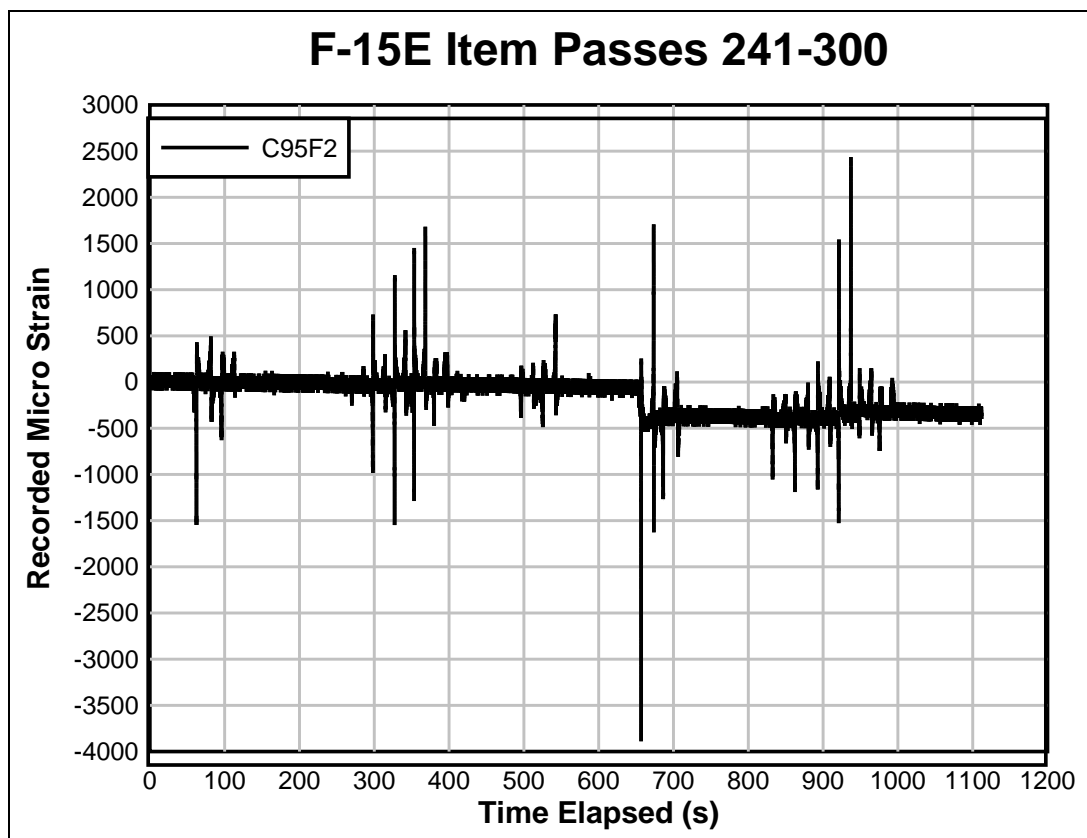


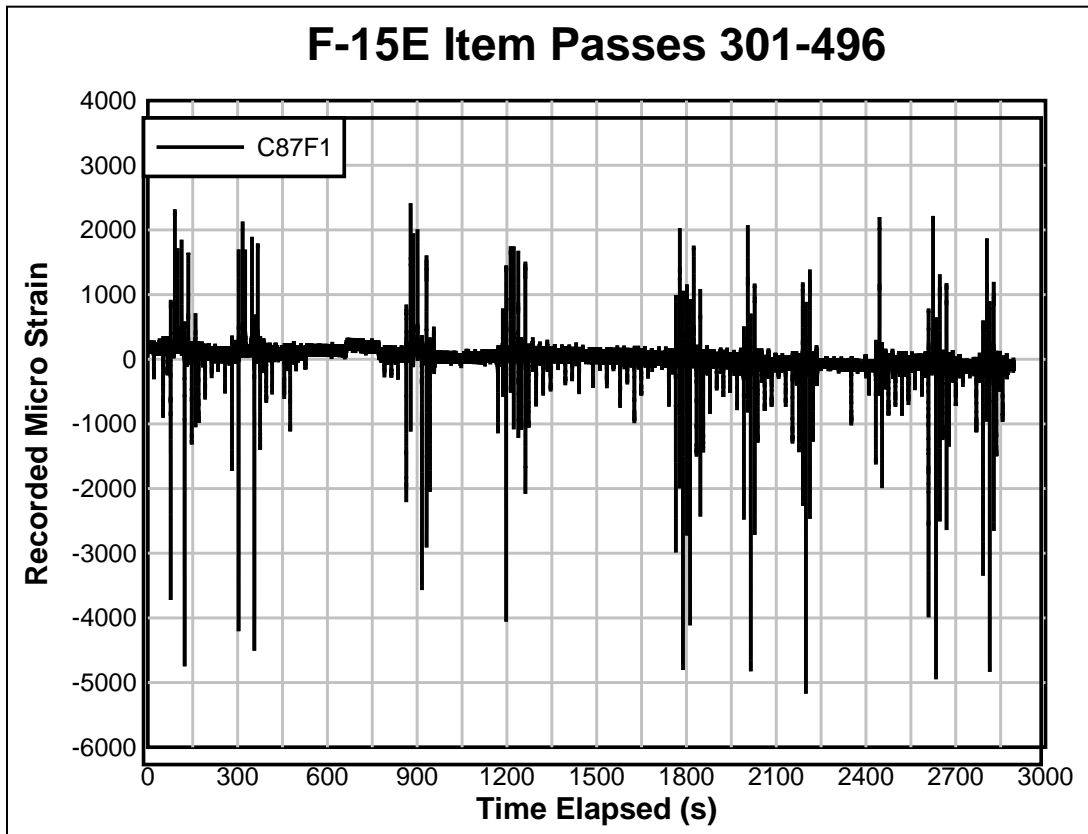
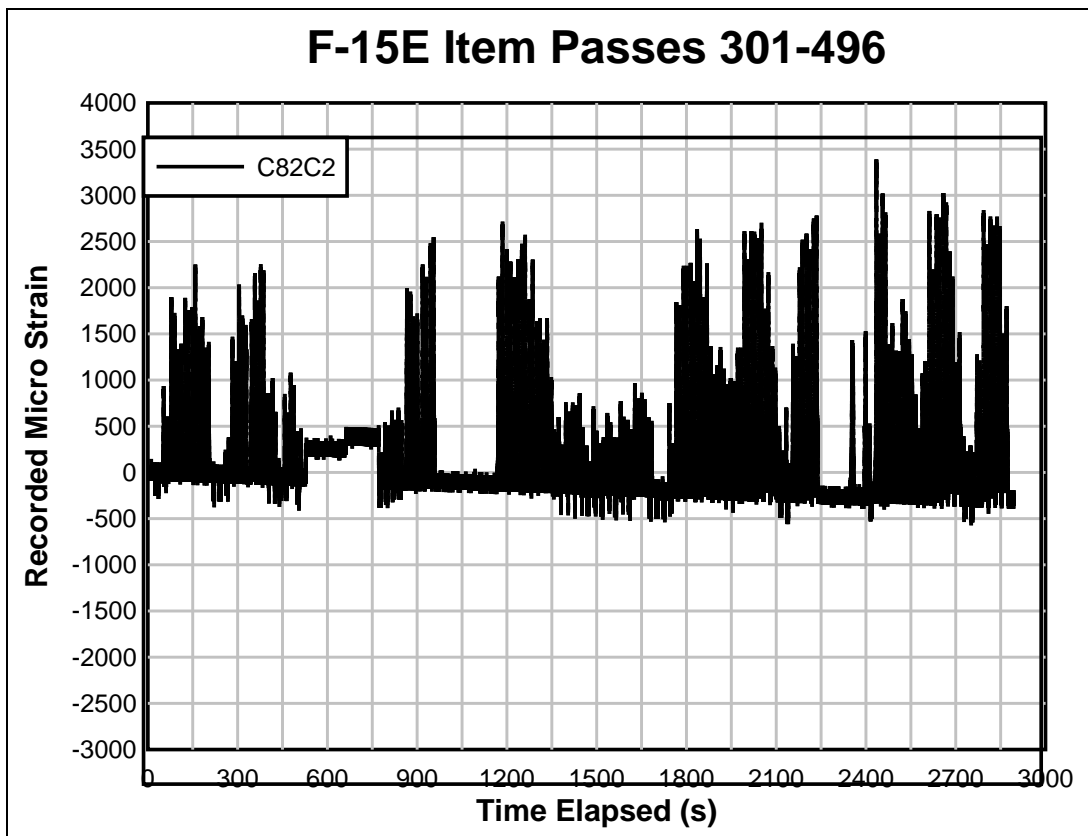


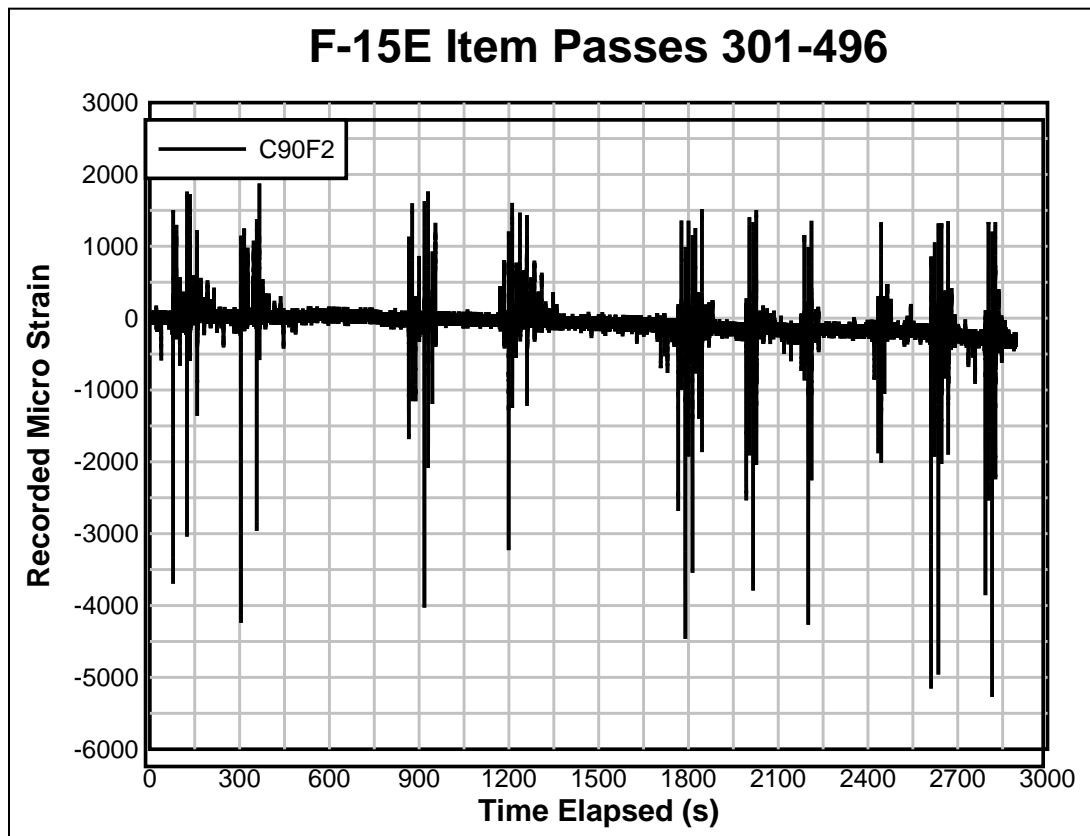
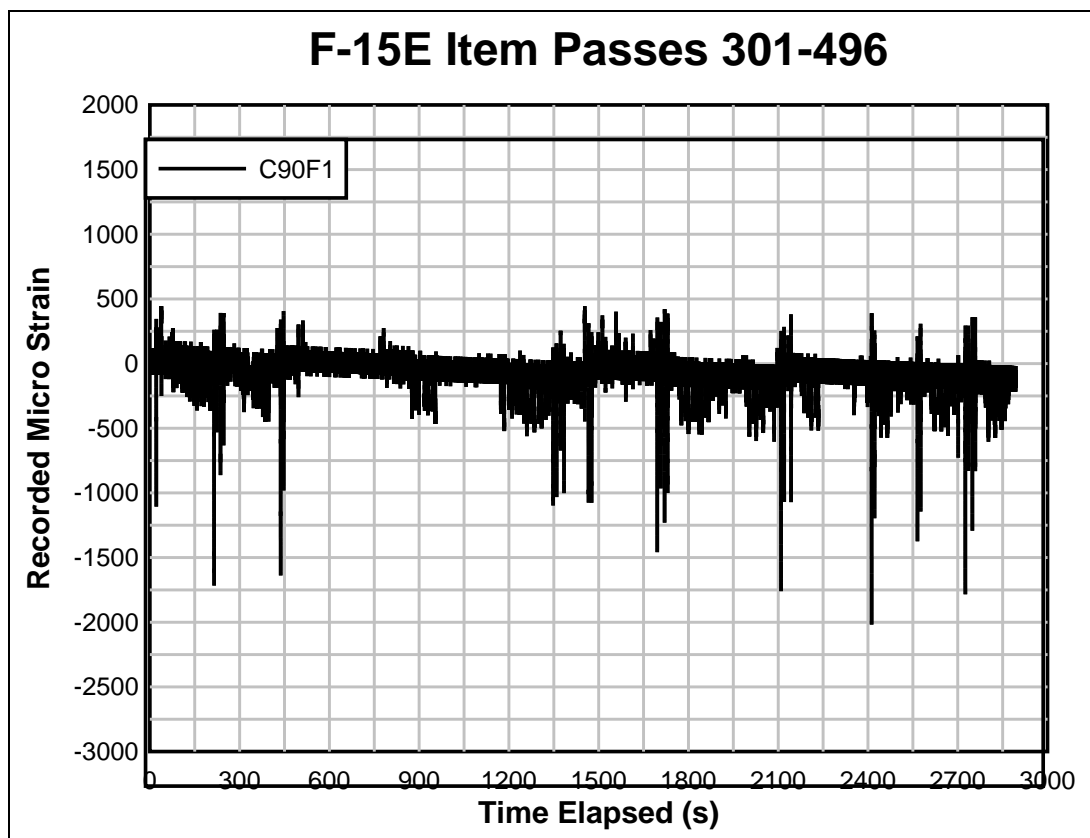


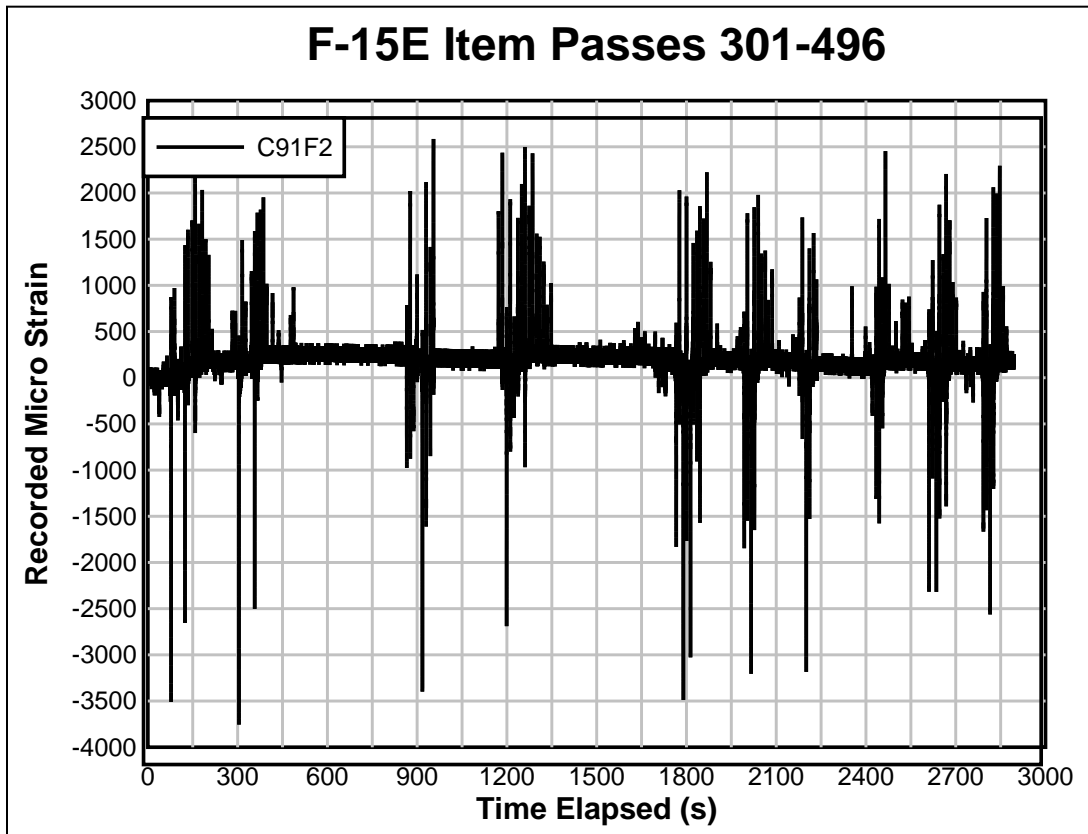
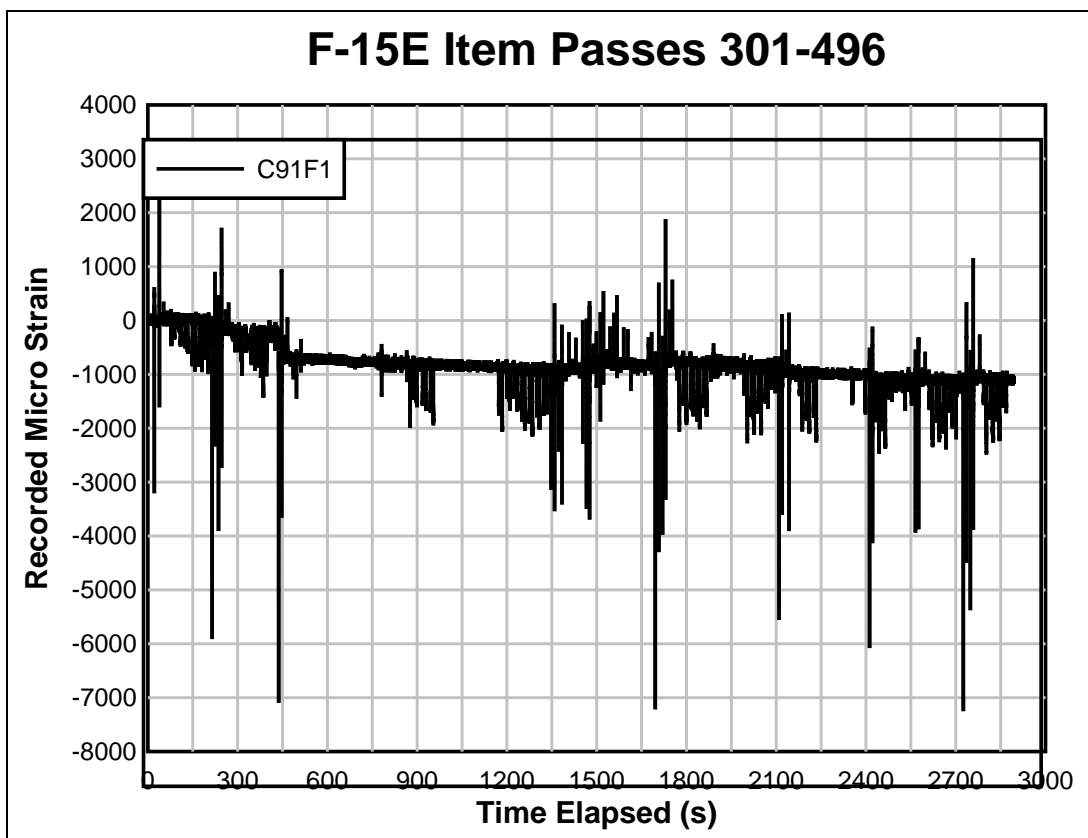


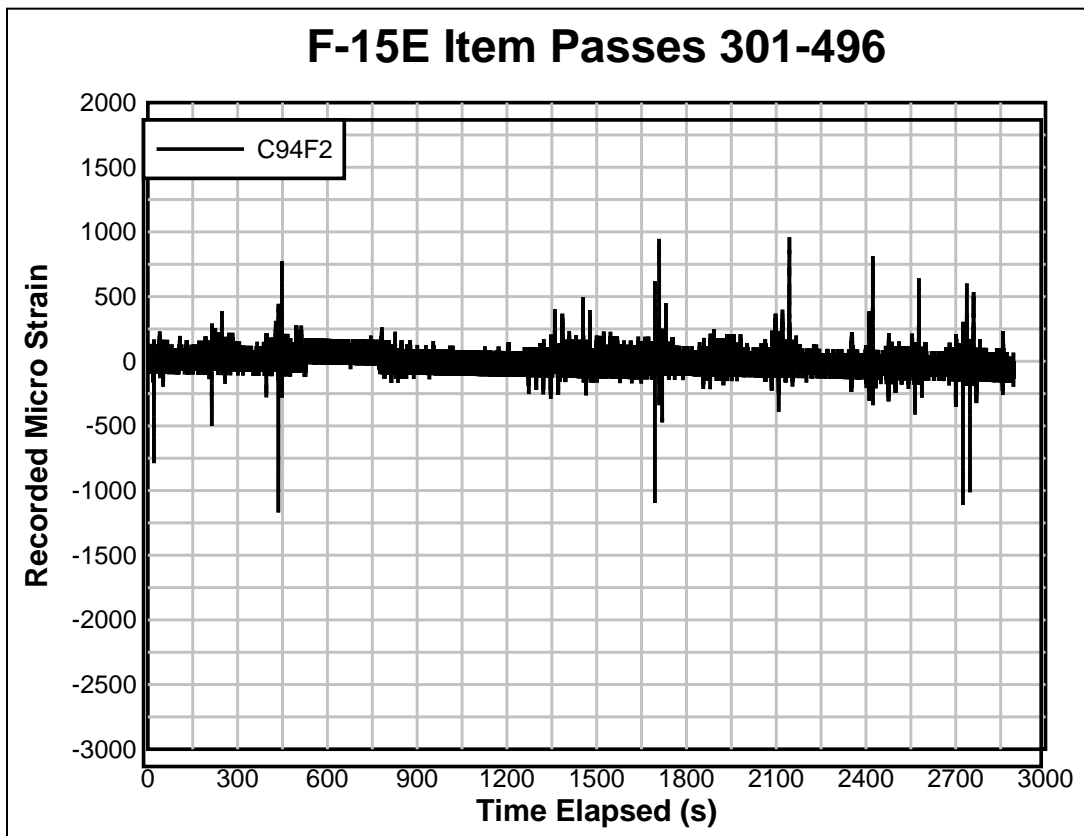
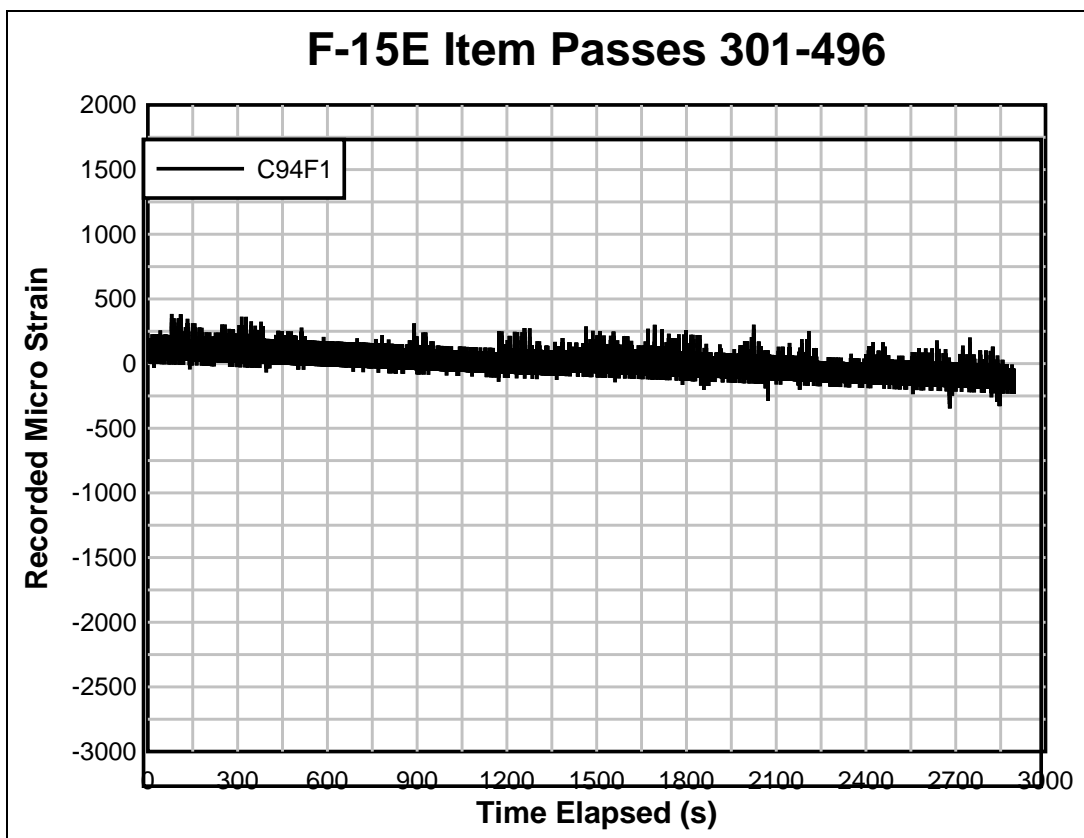


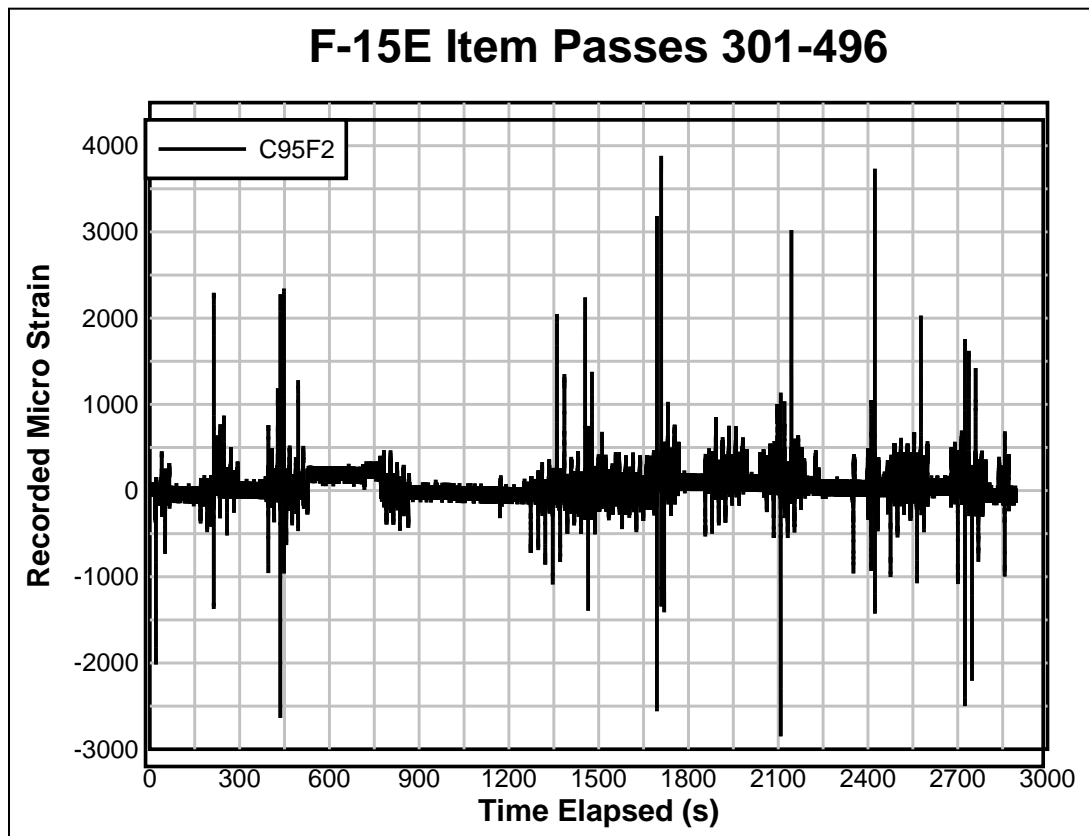
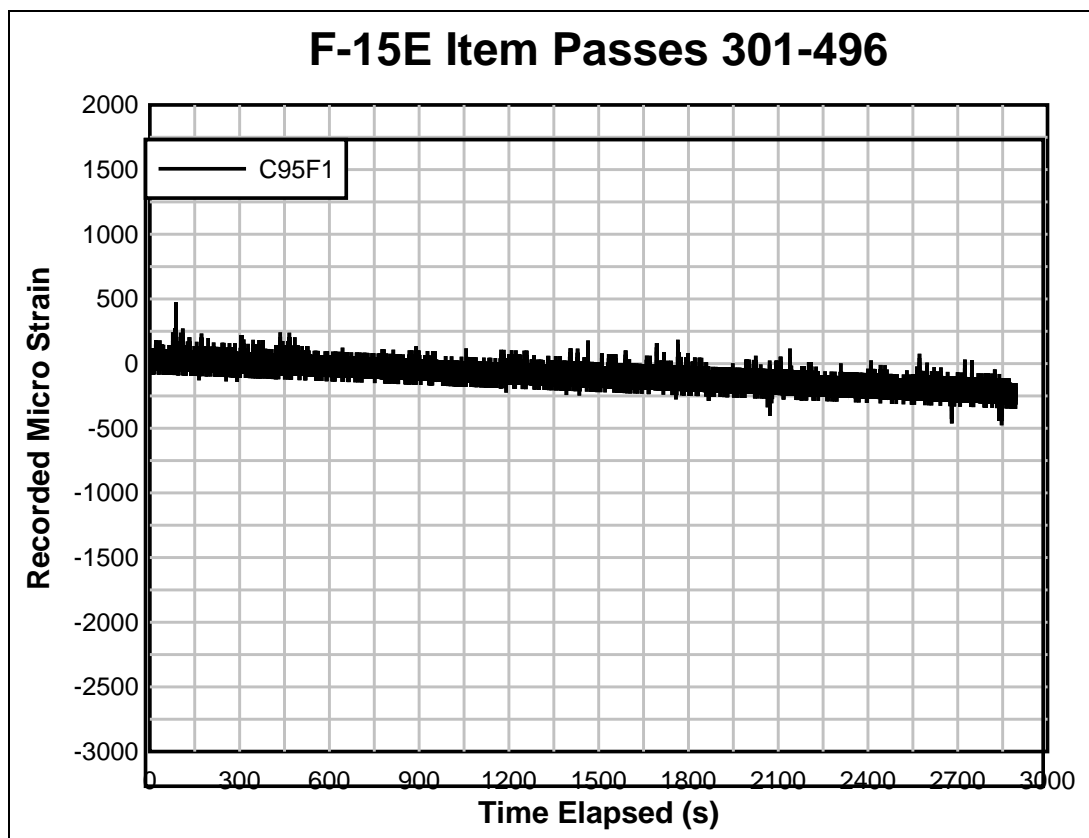


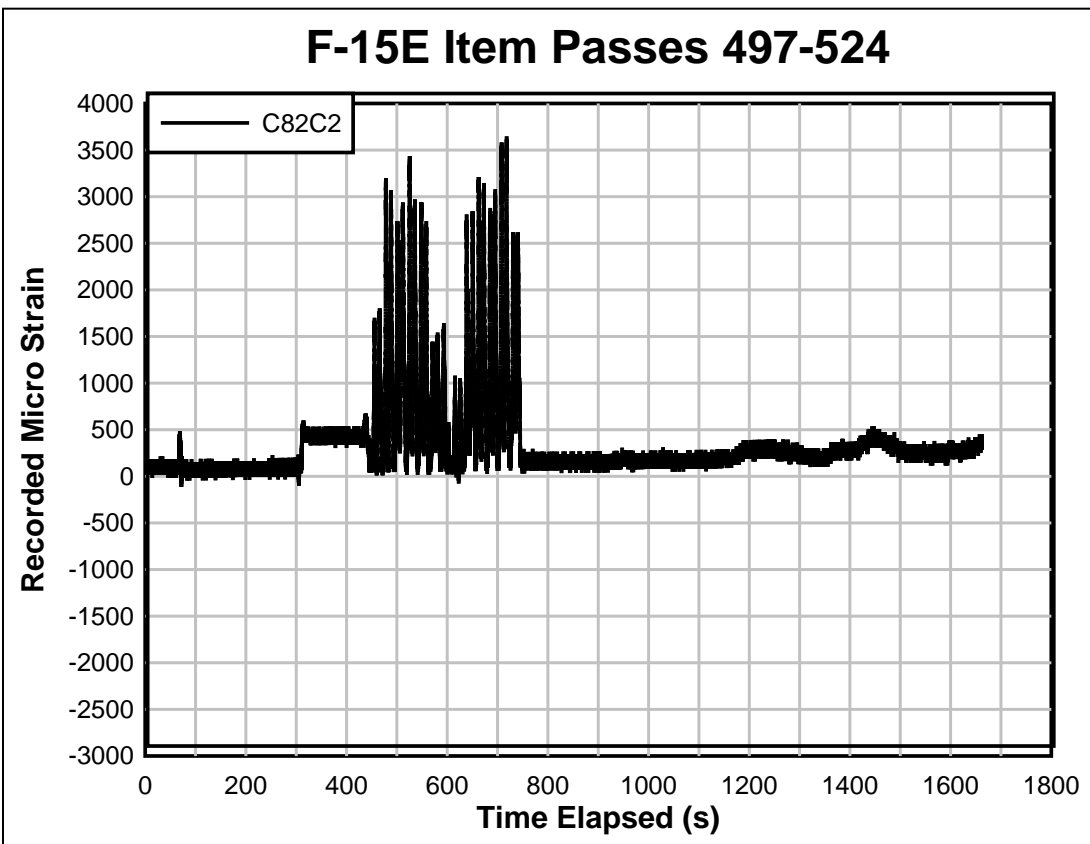
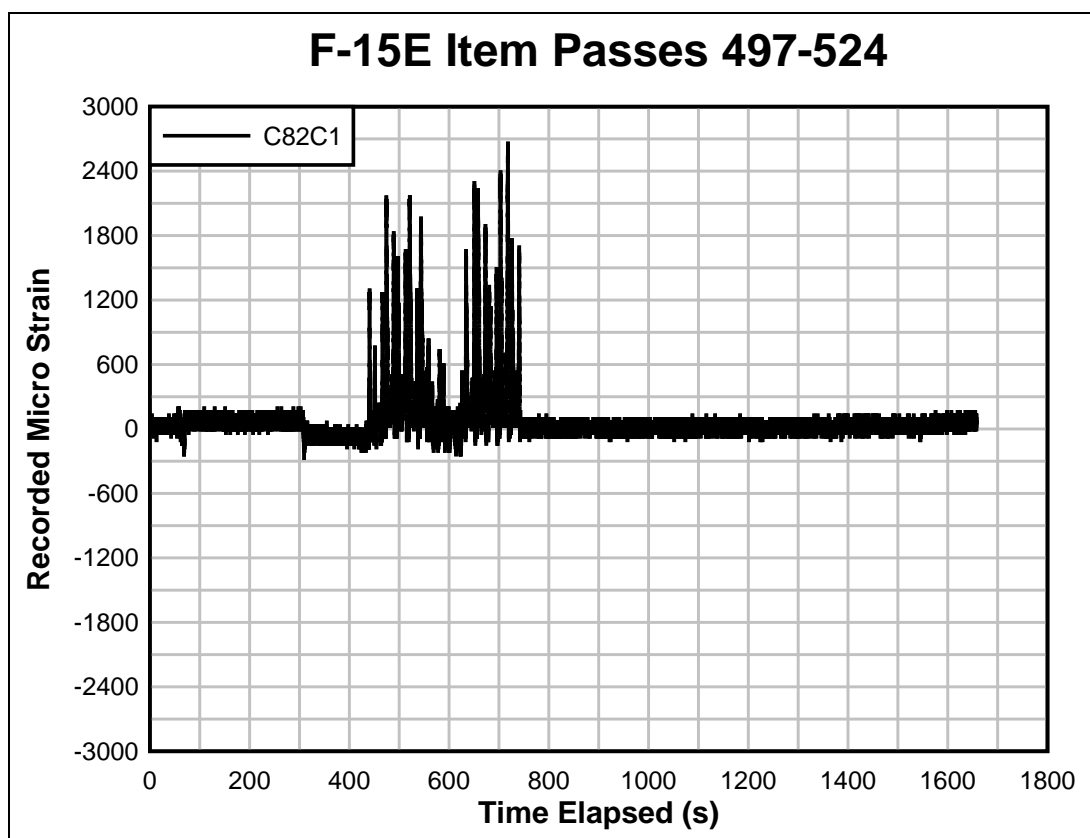


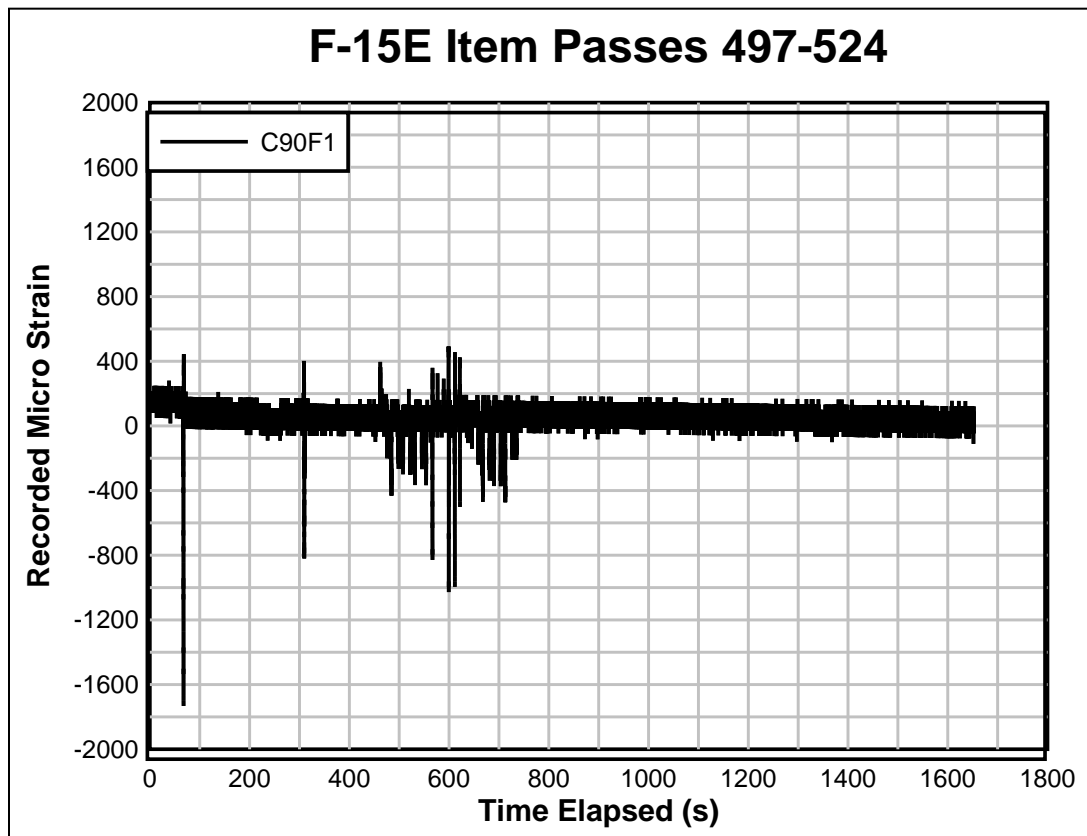
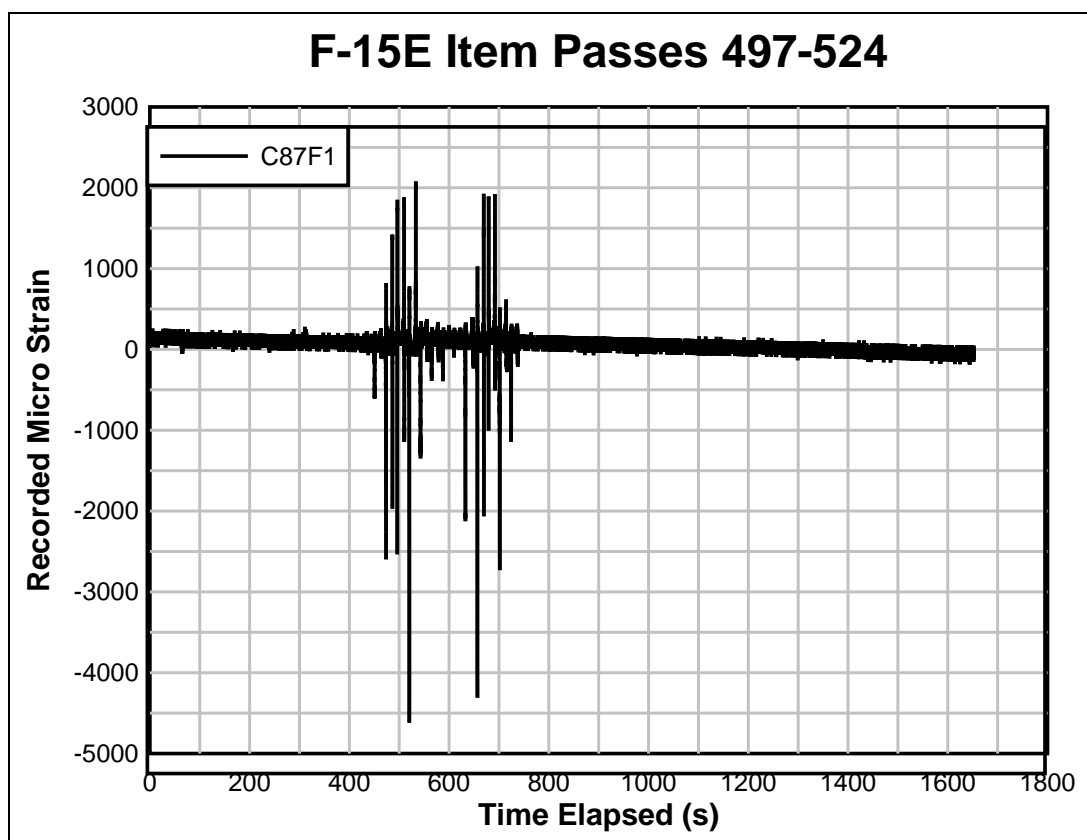


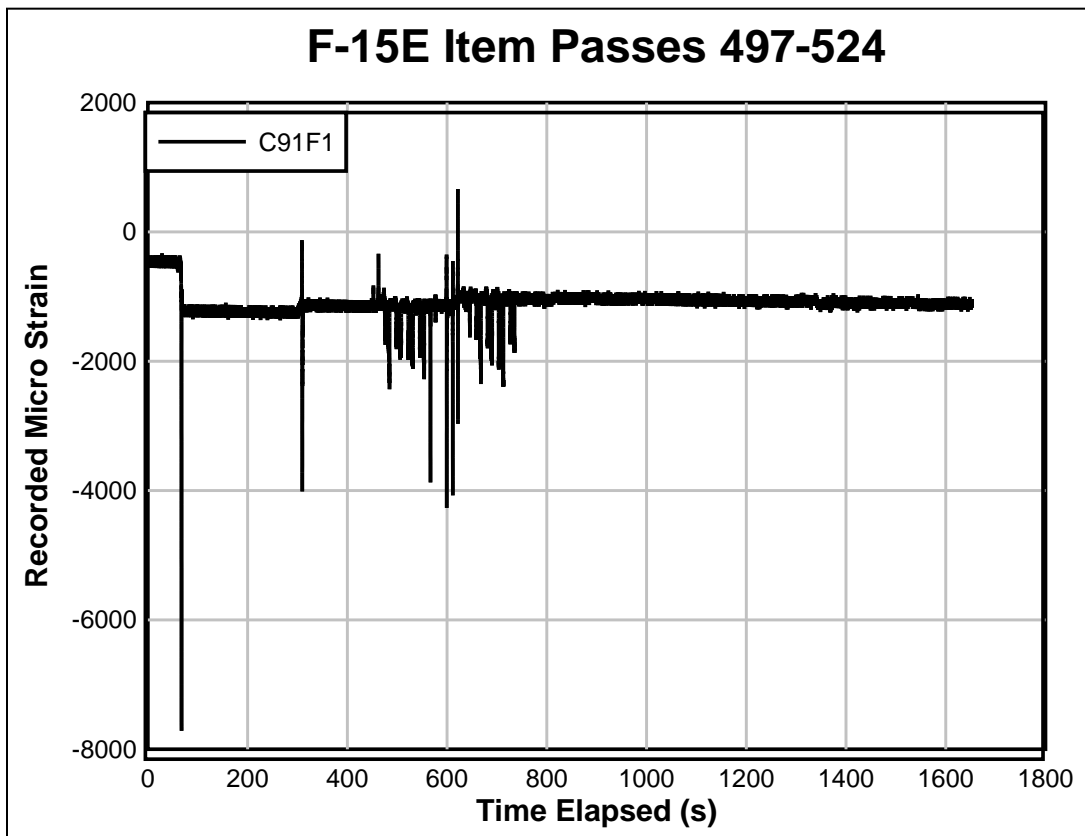
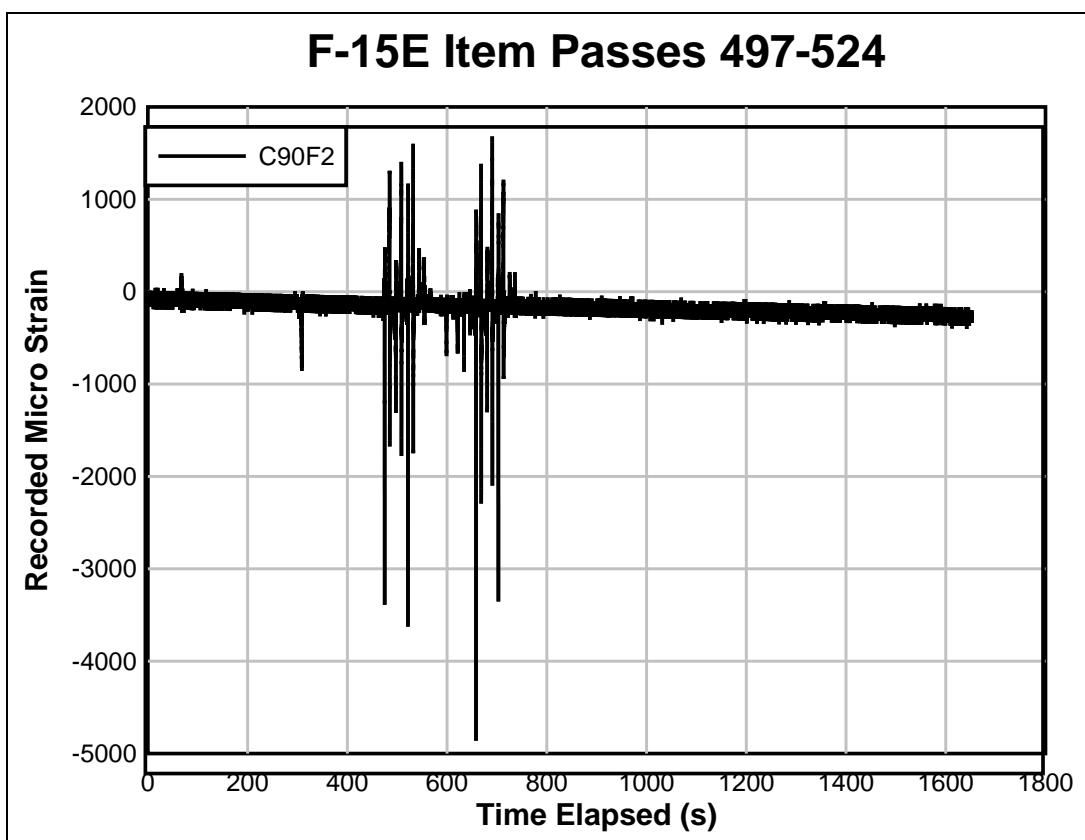


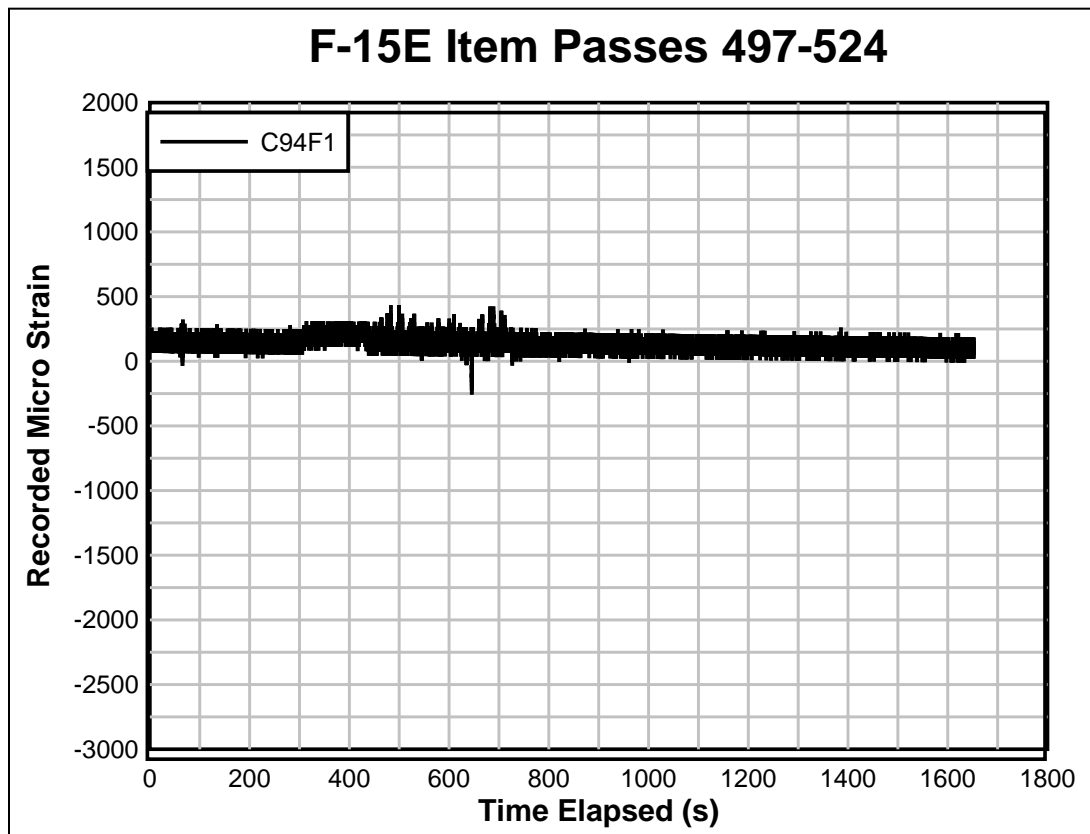
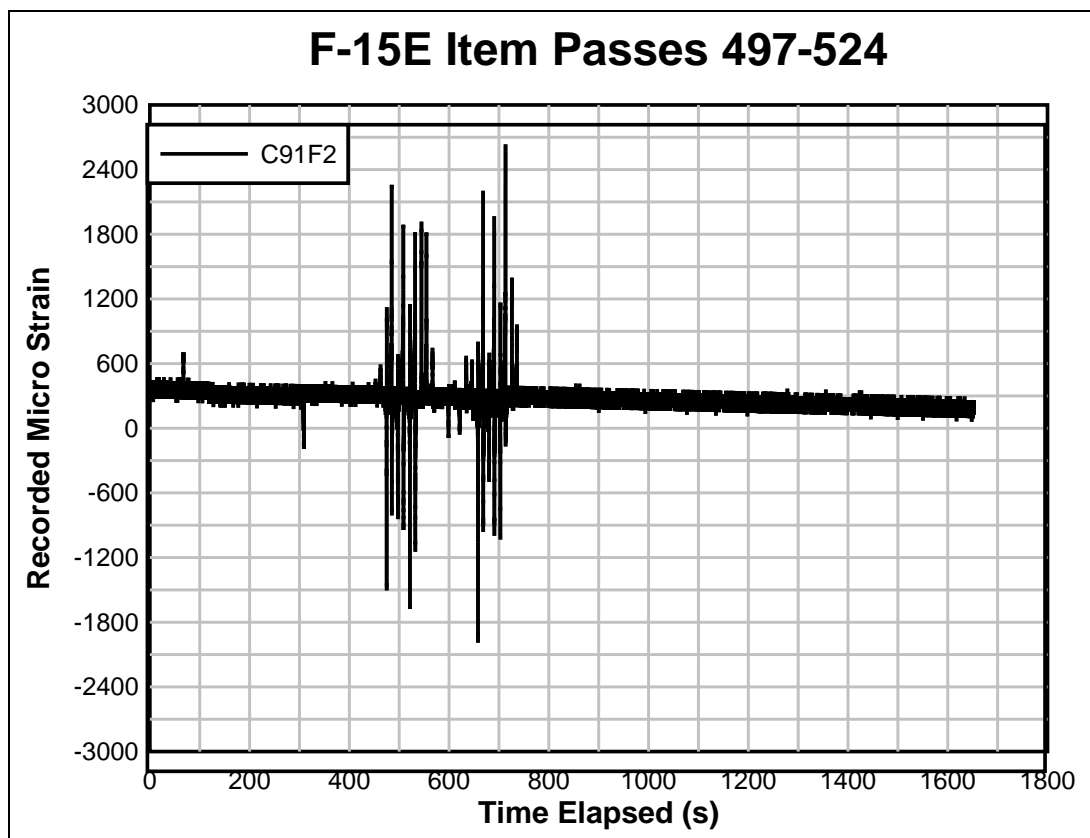


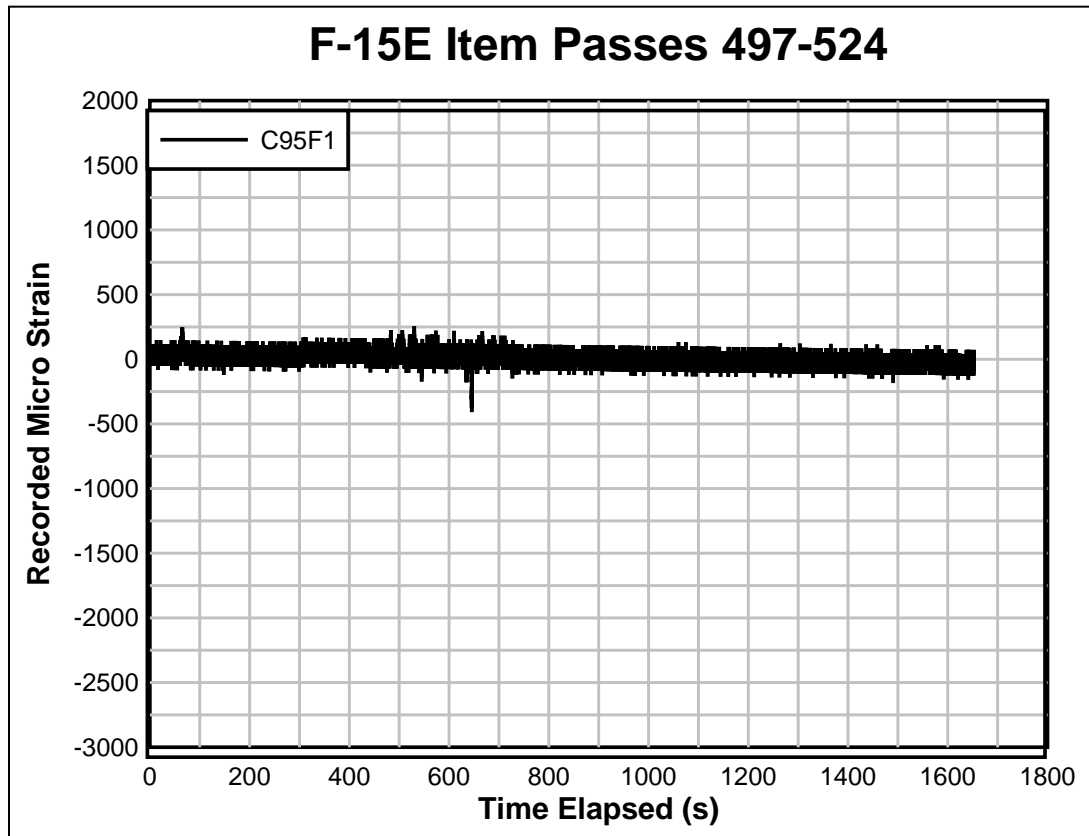
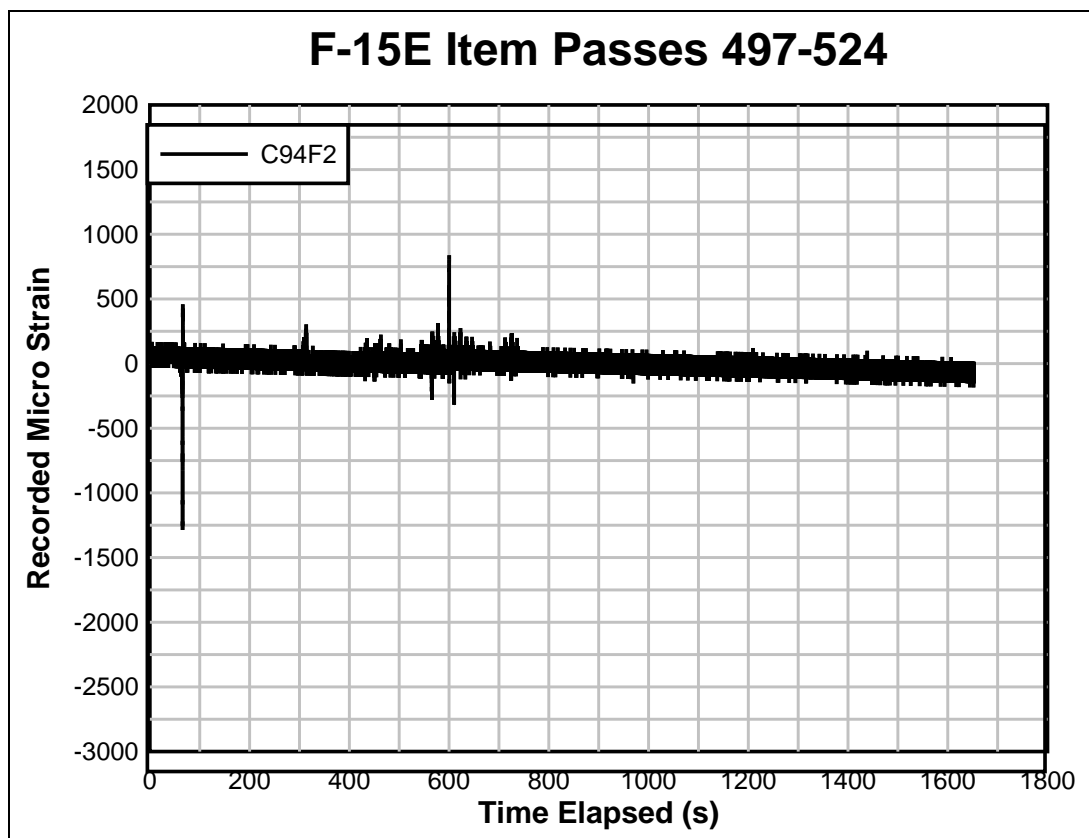


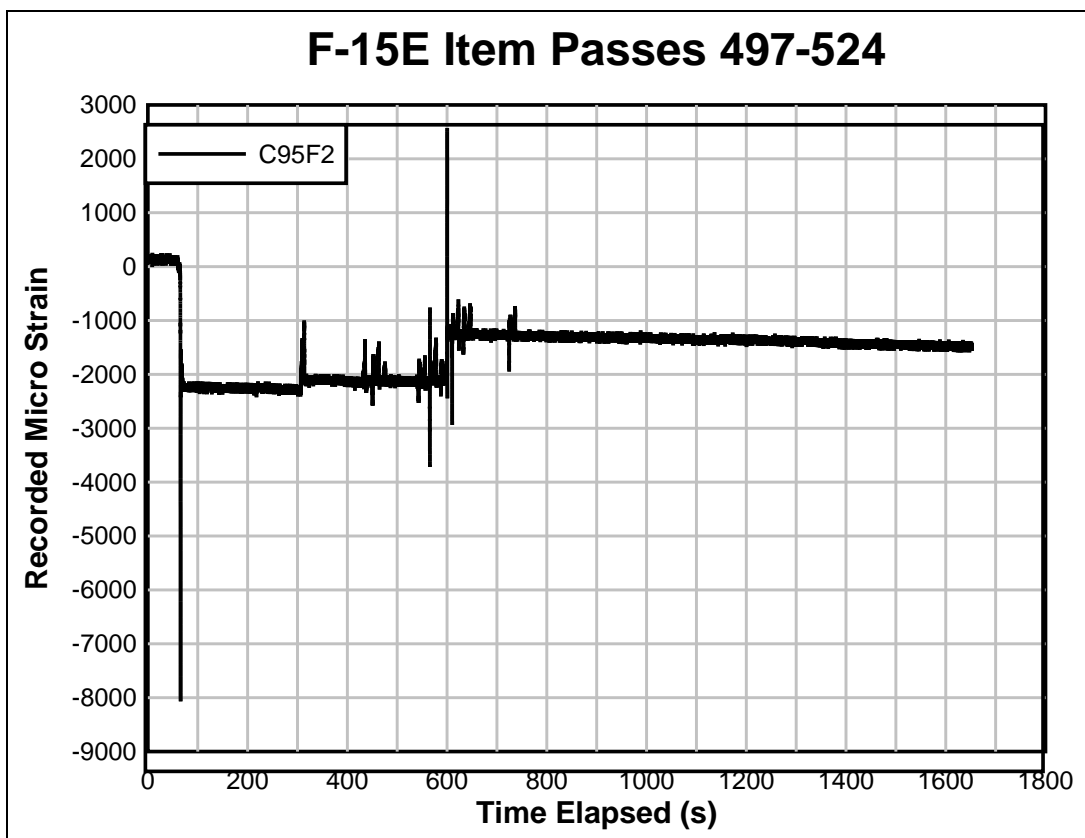




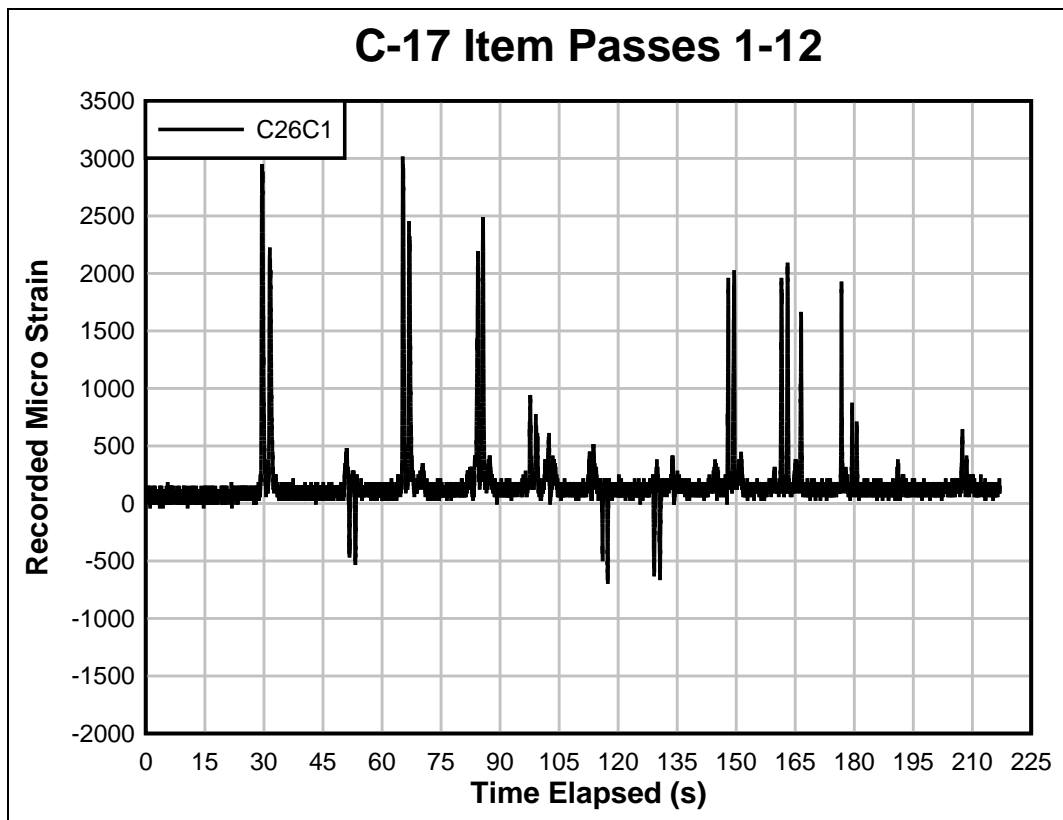


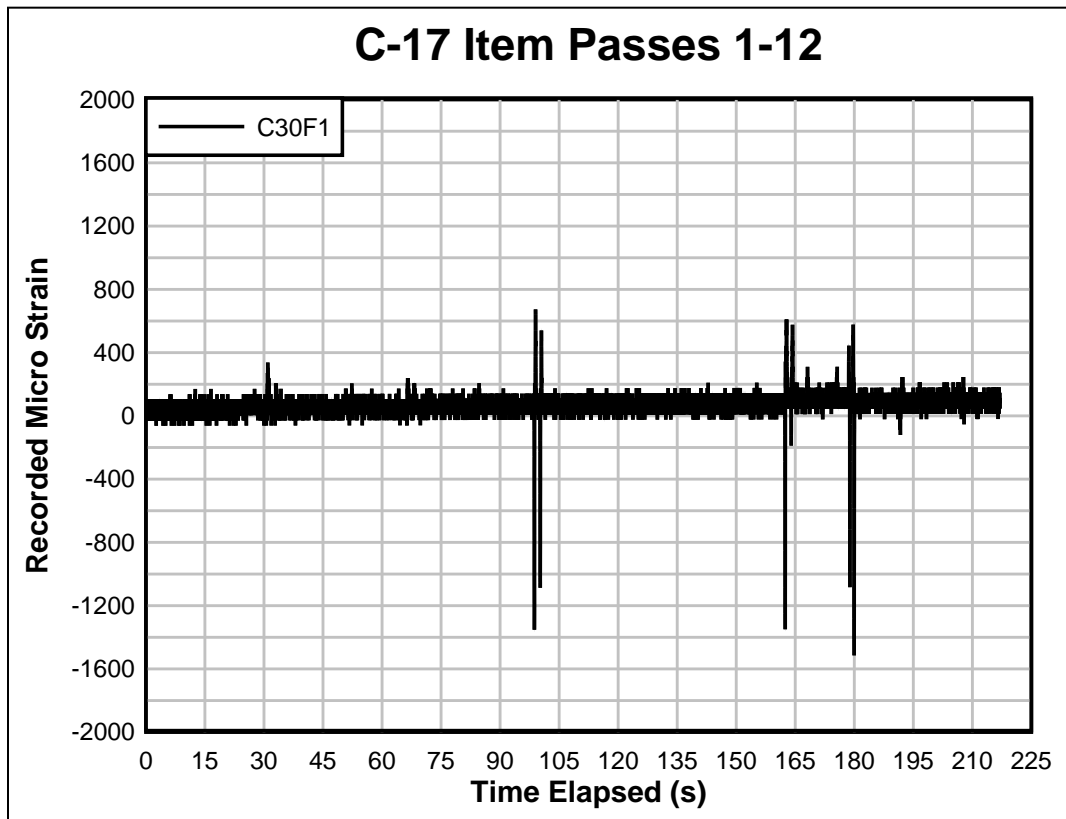
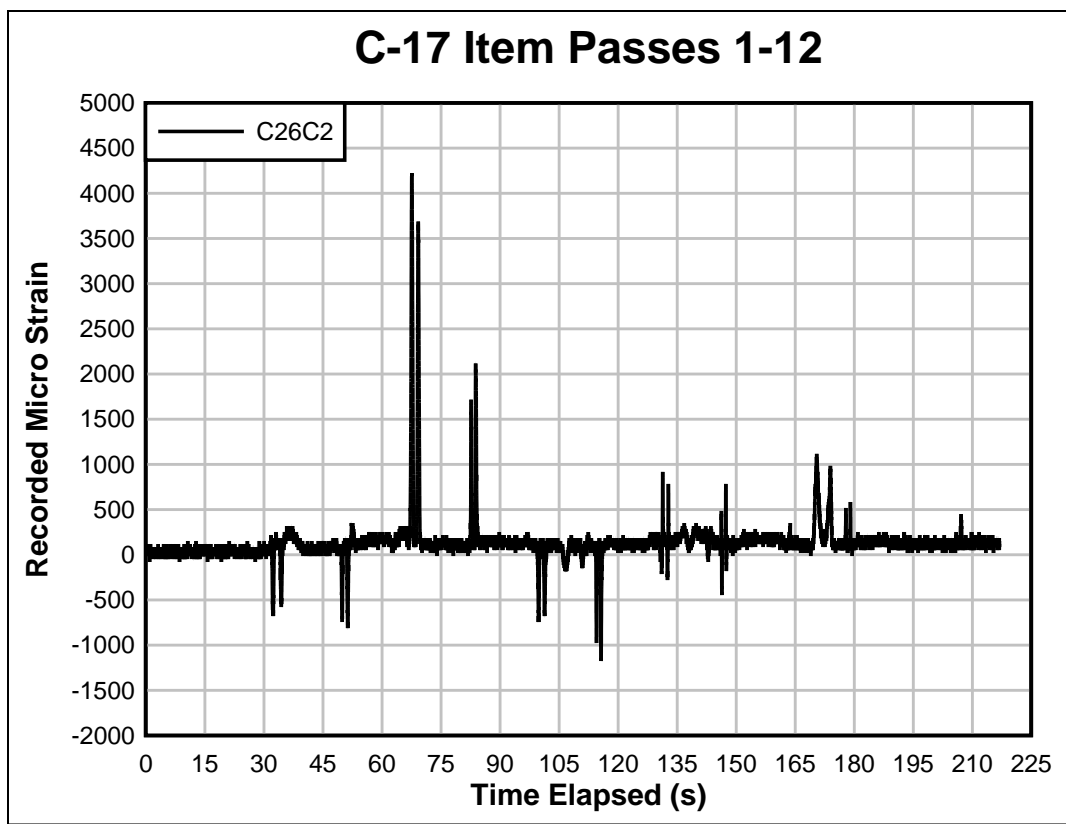


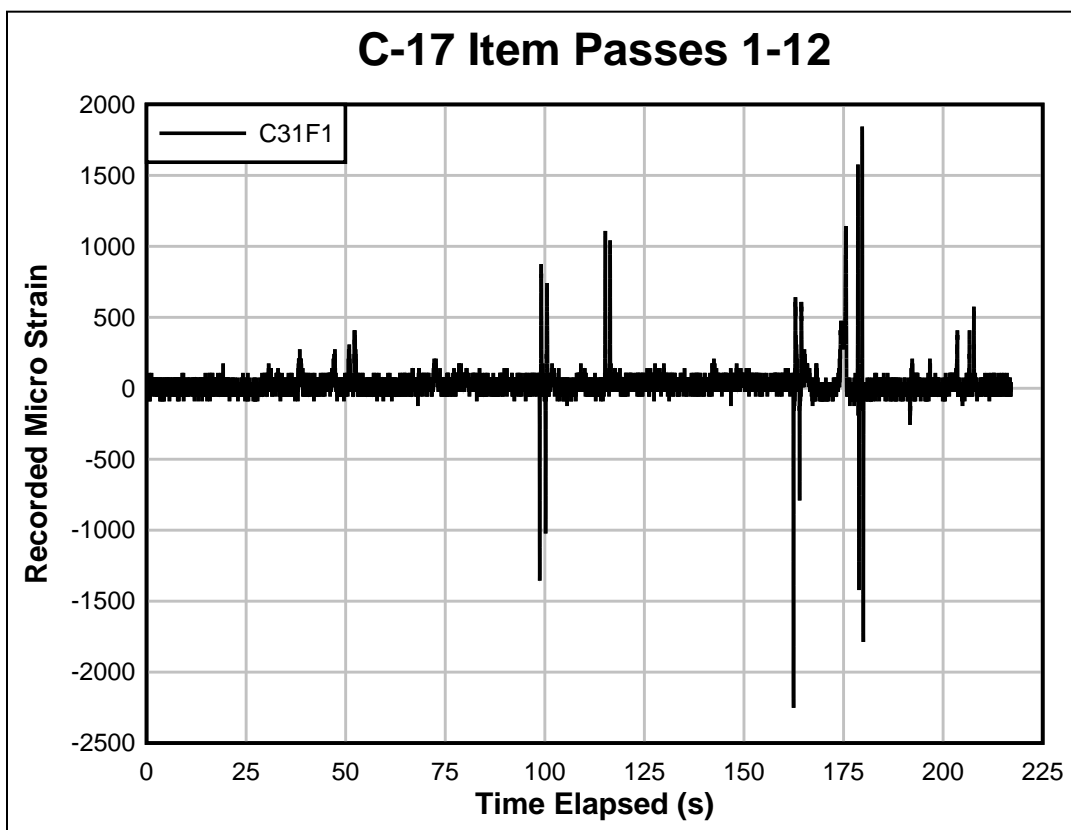
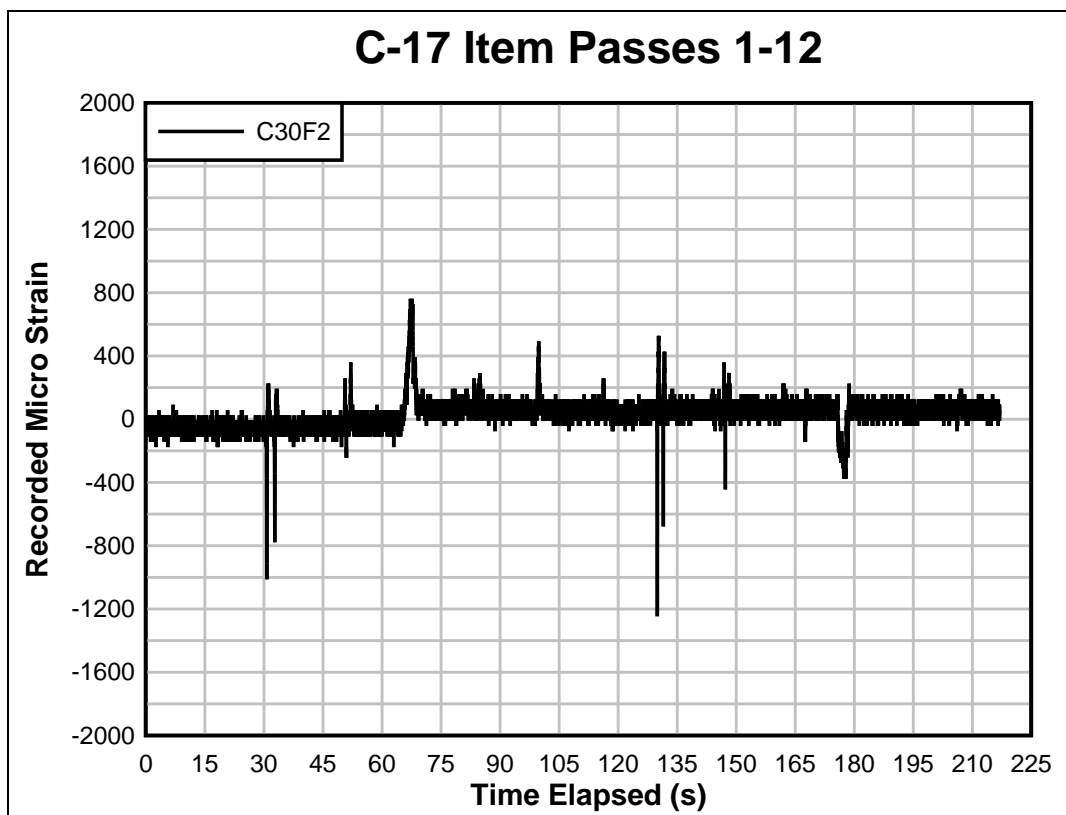


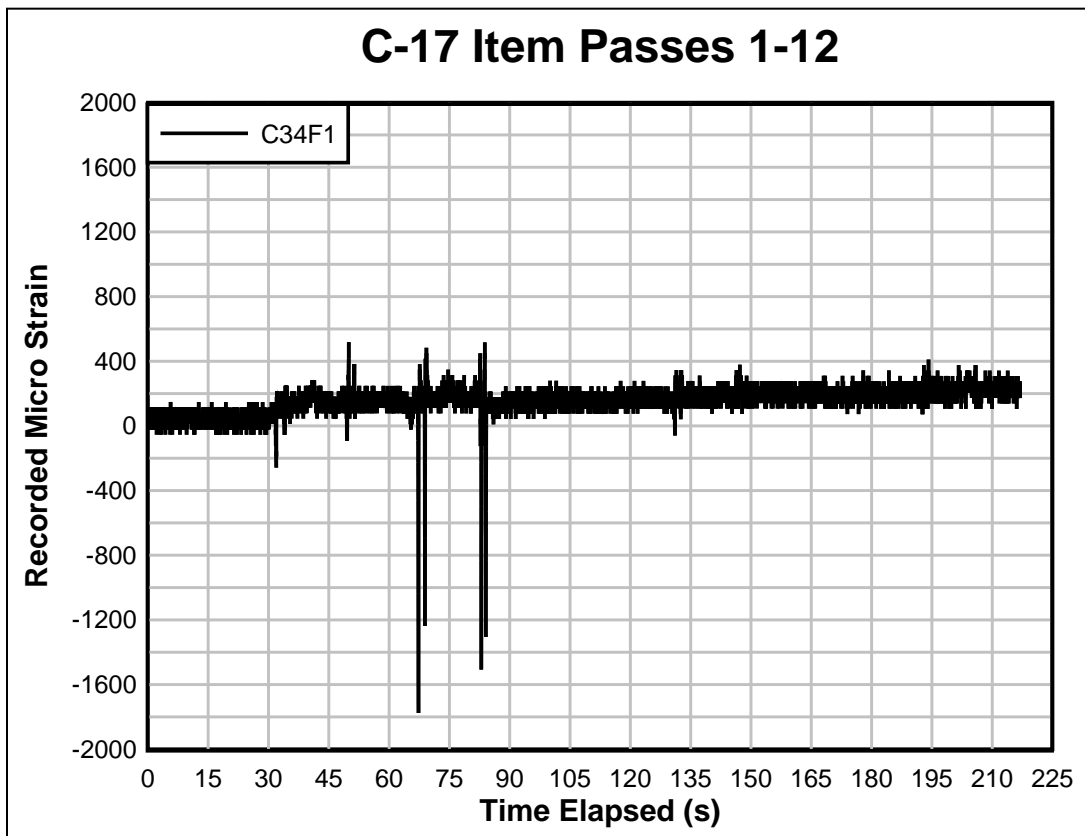
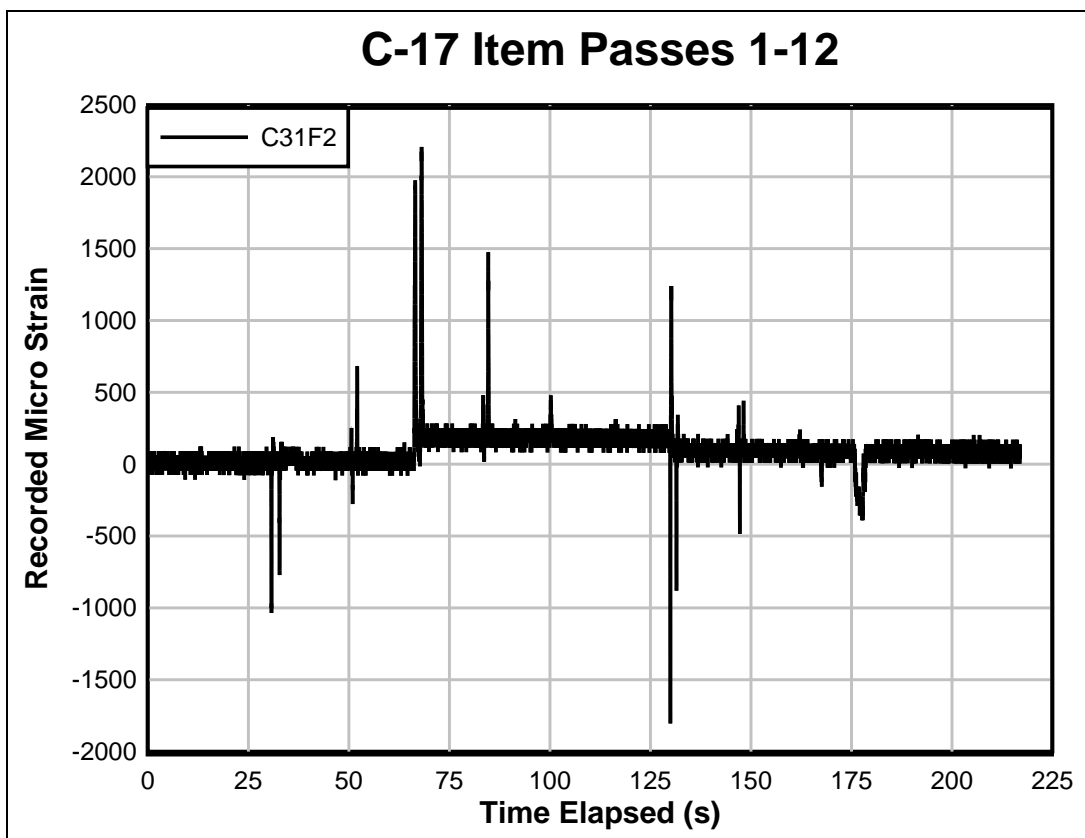


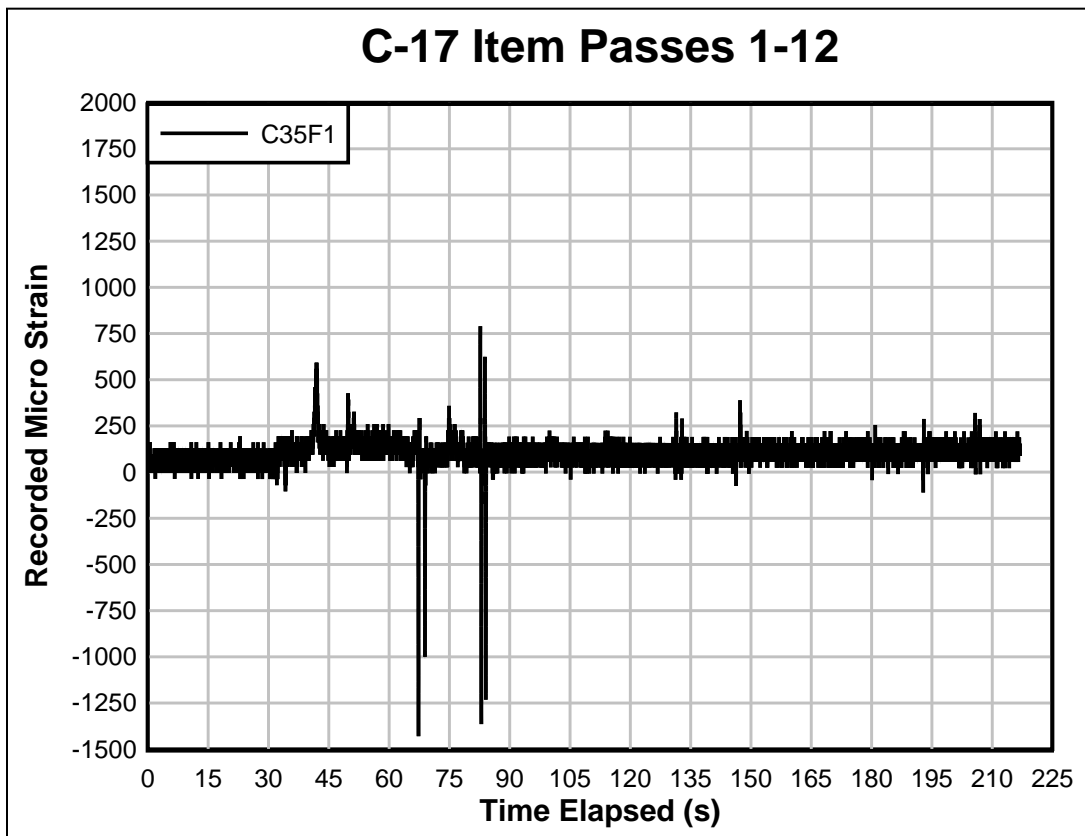
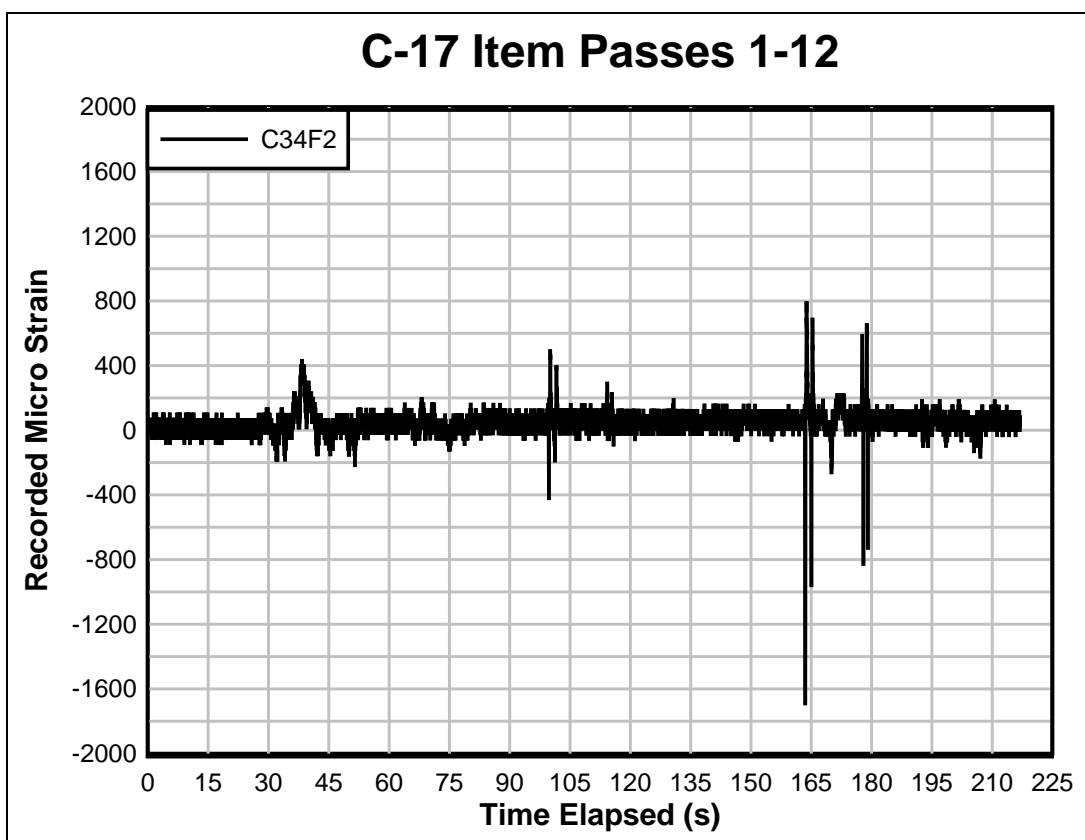
Appendix B: Strain gauge data for C-17 item

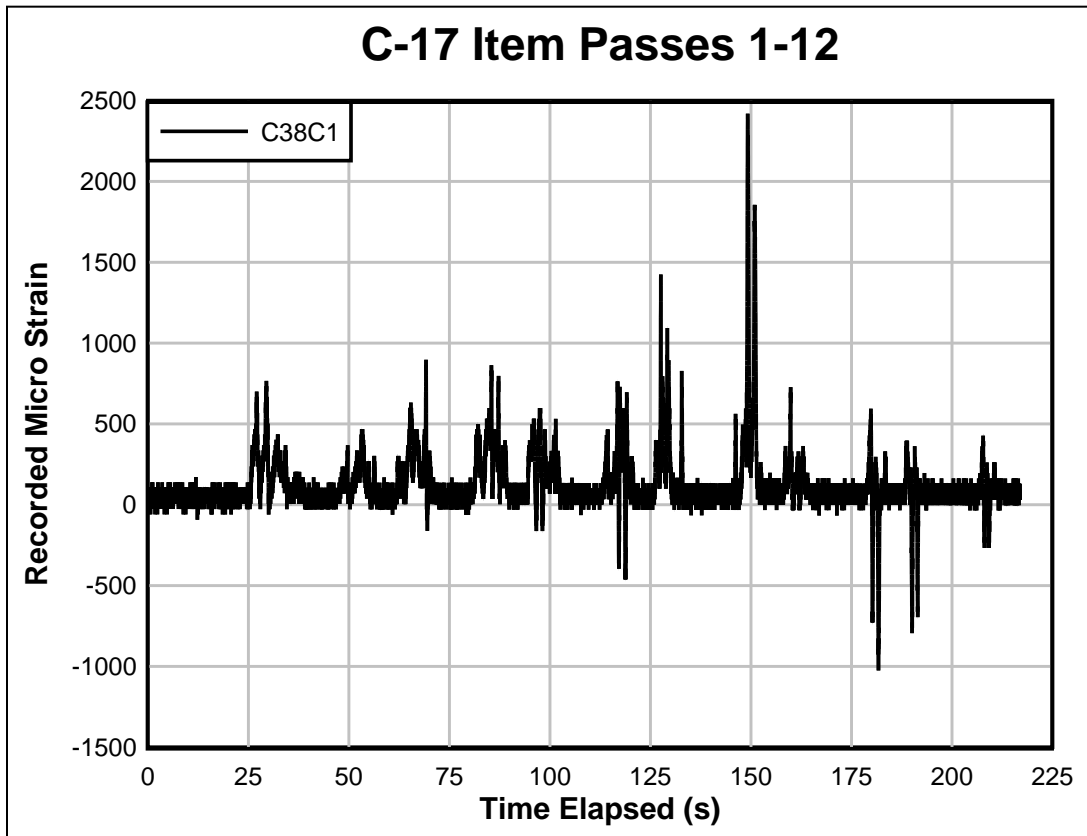
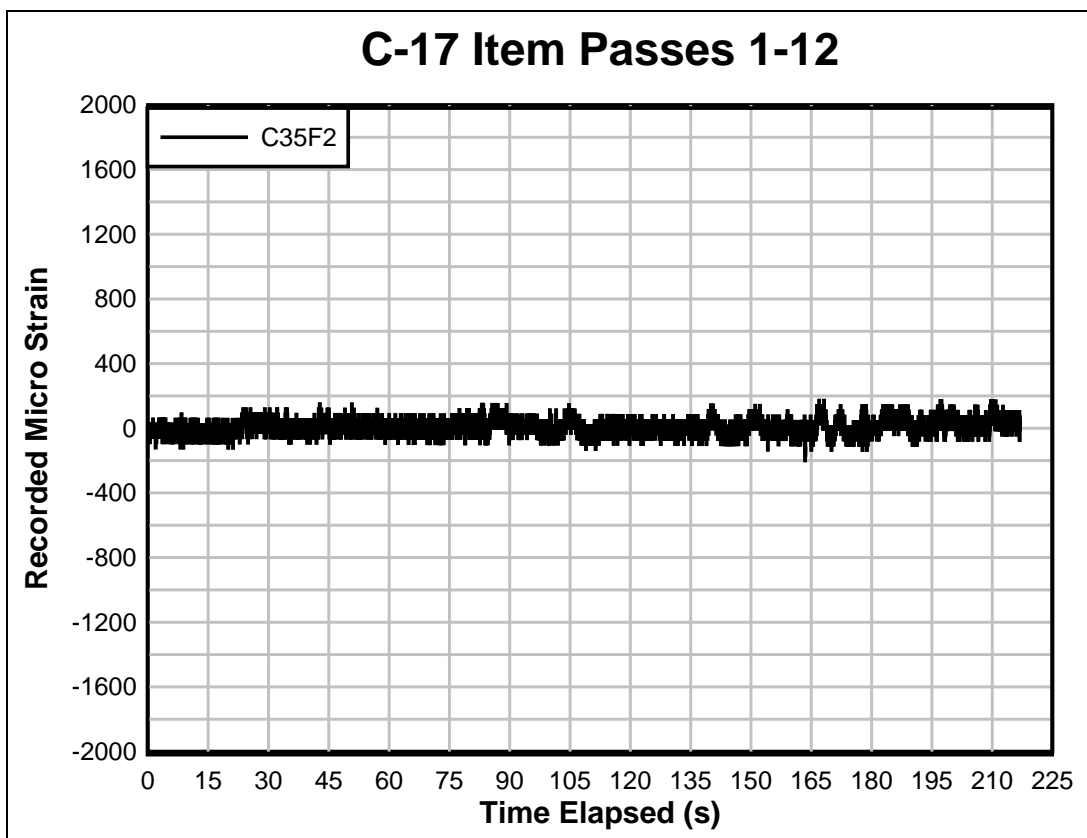


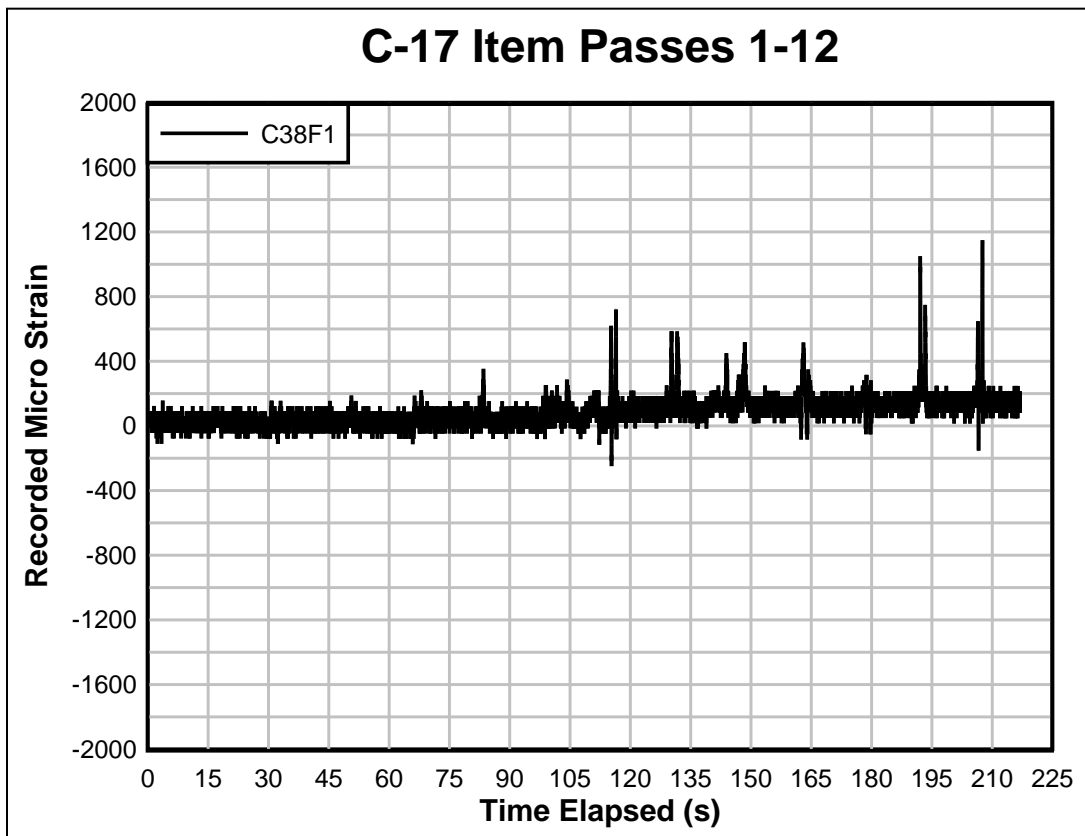
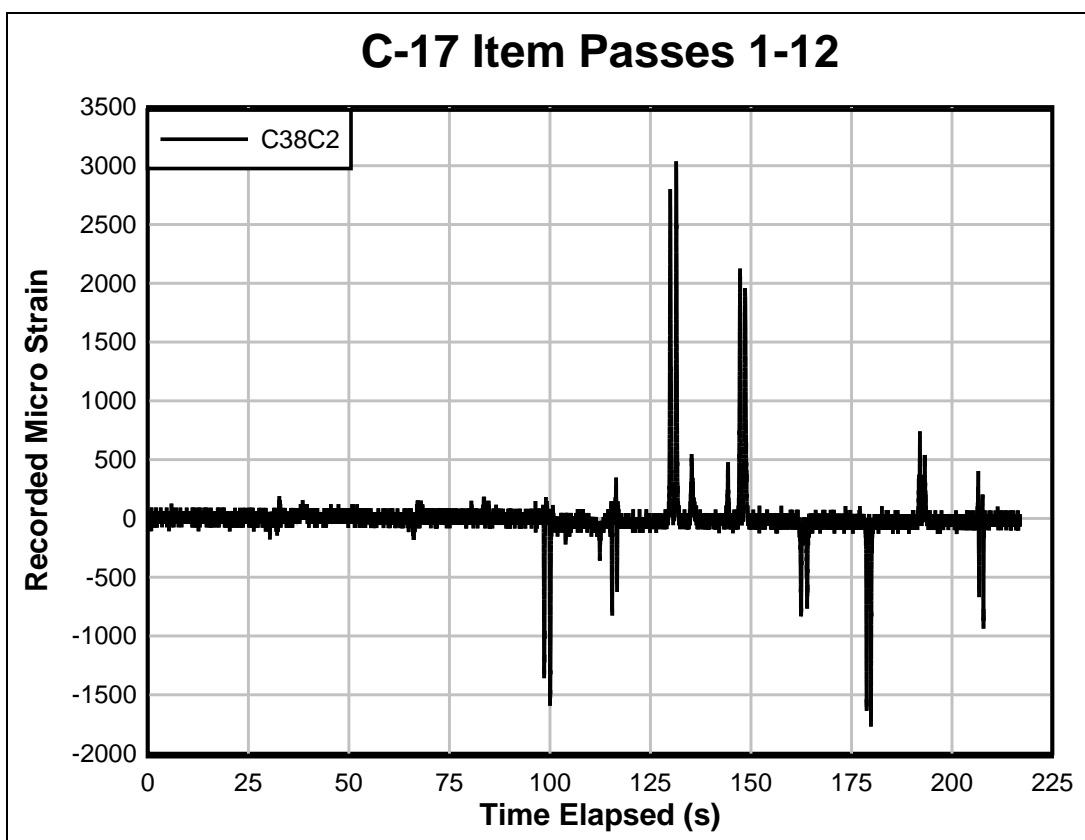


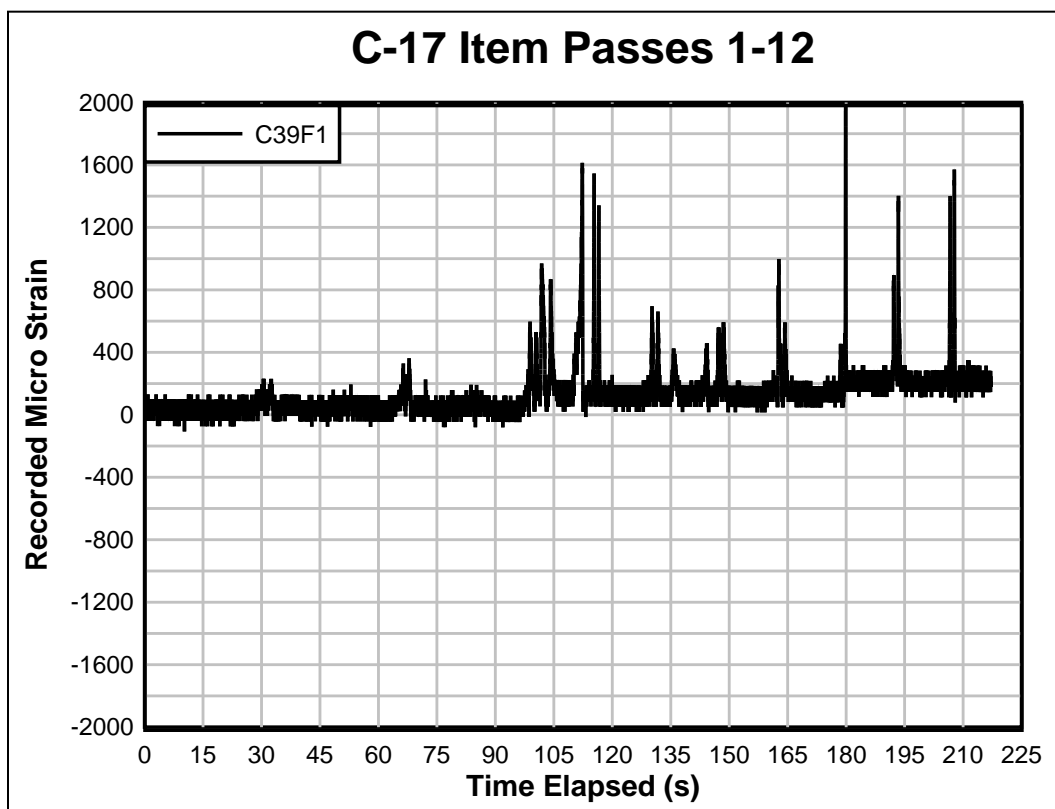
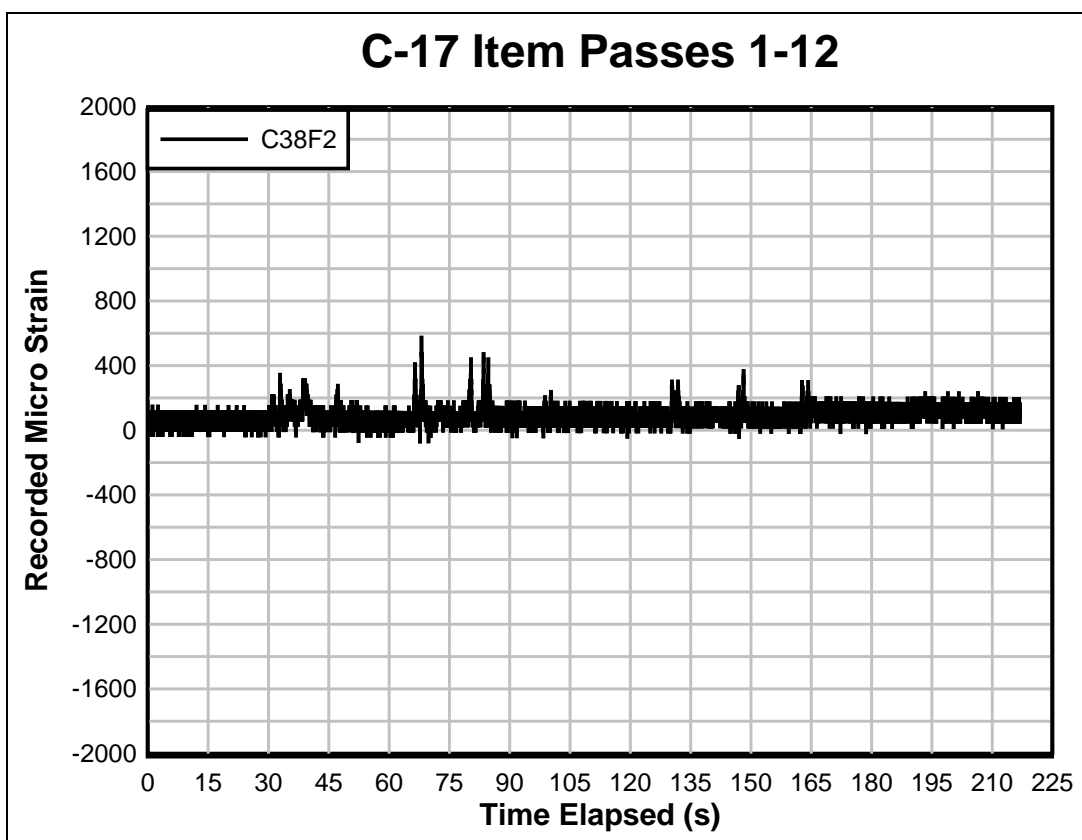


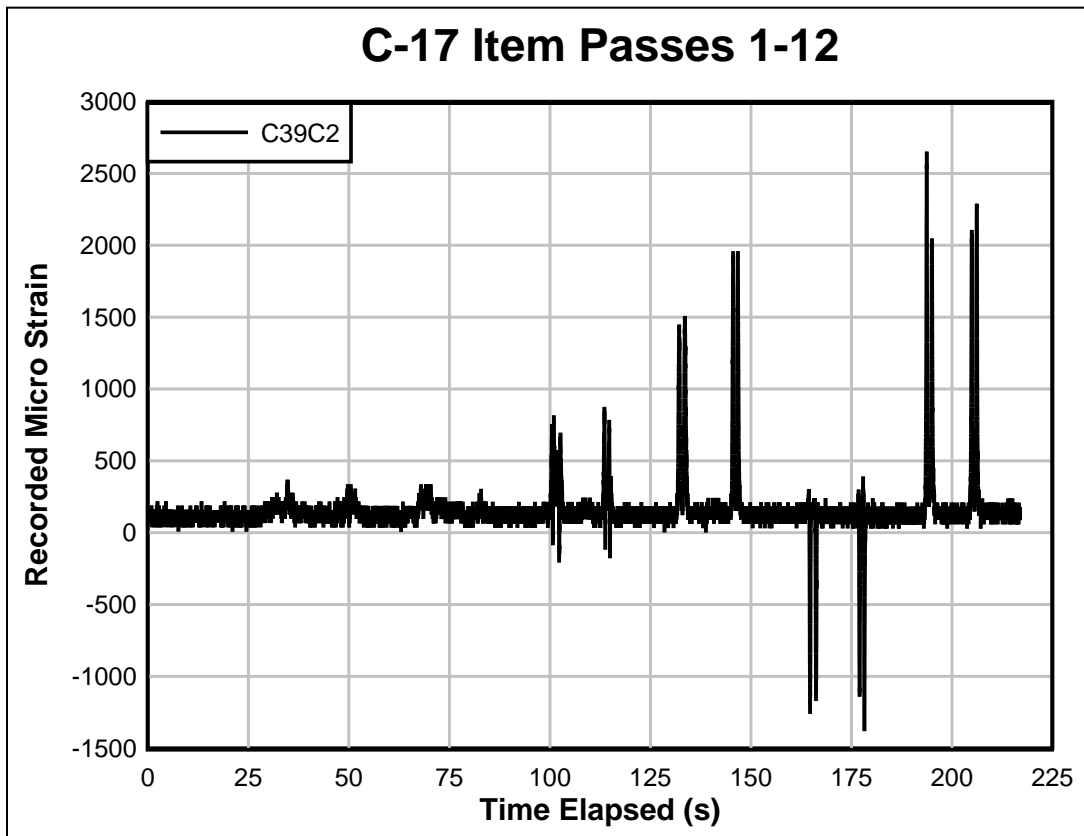
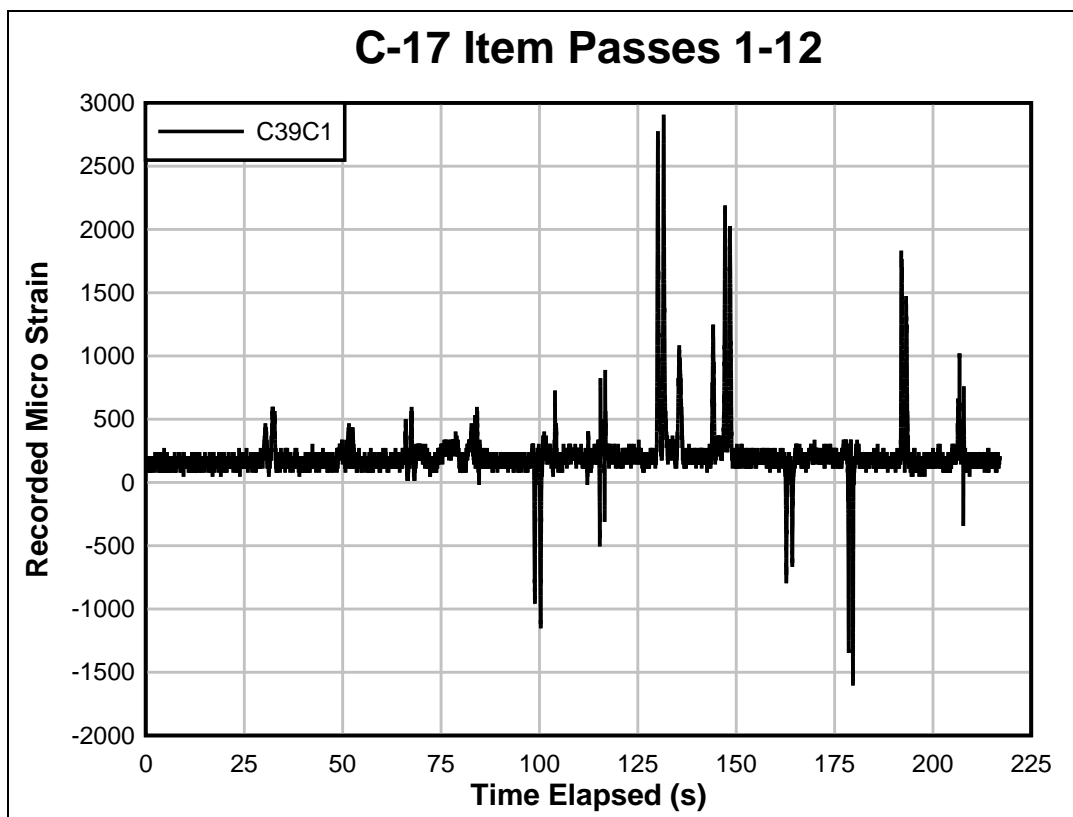


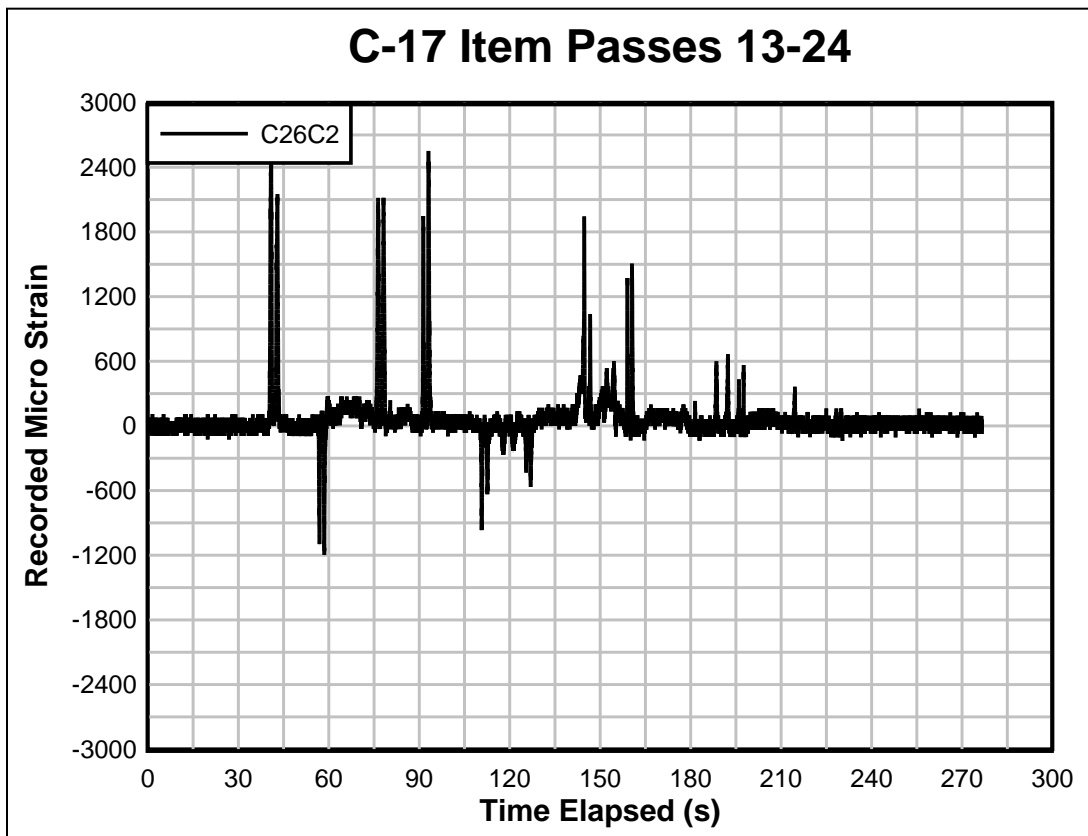
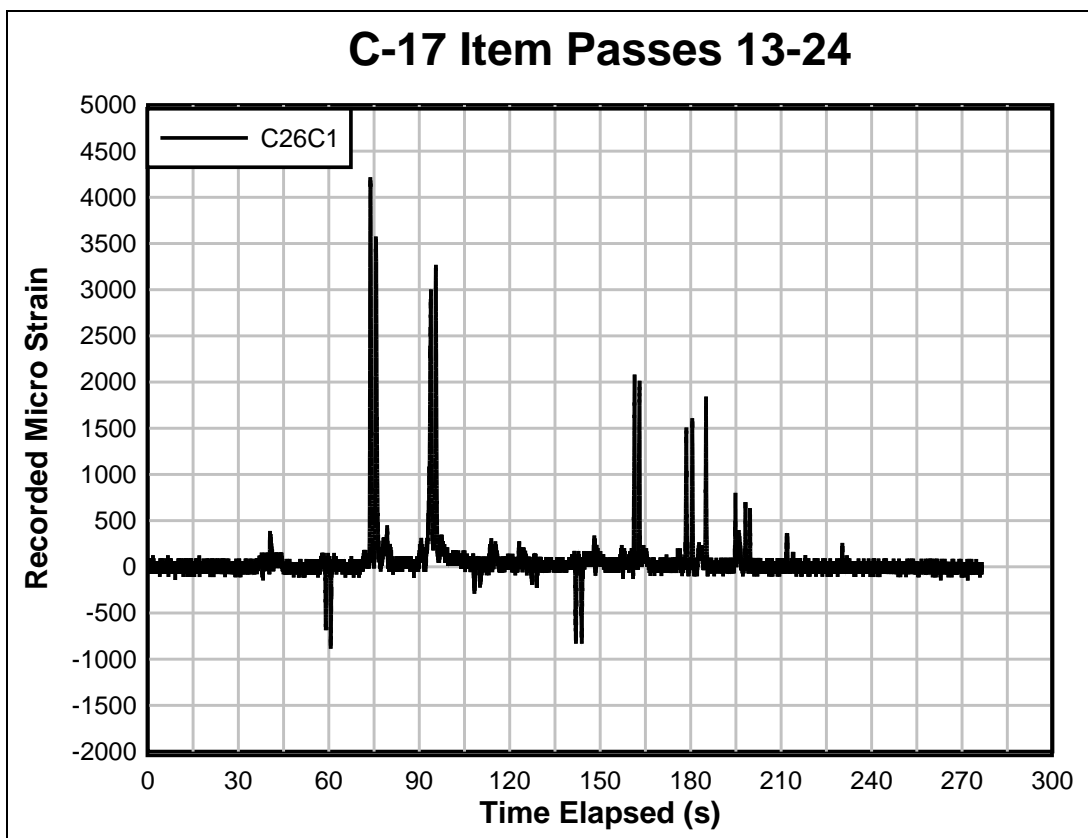


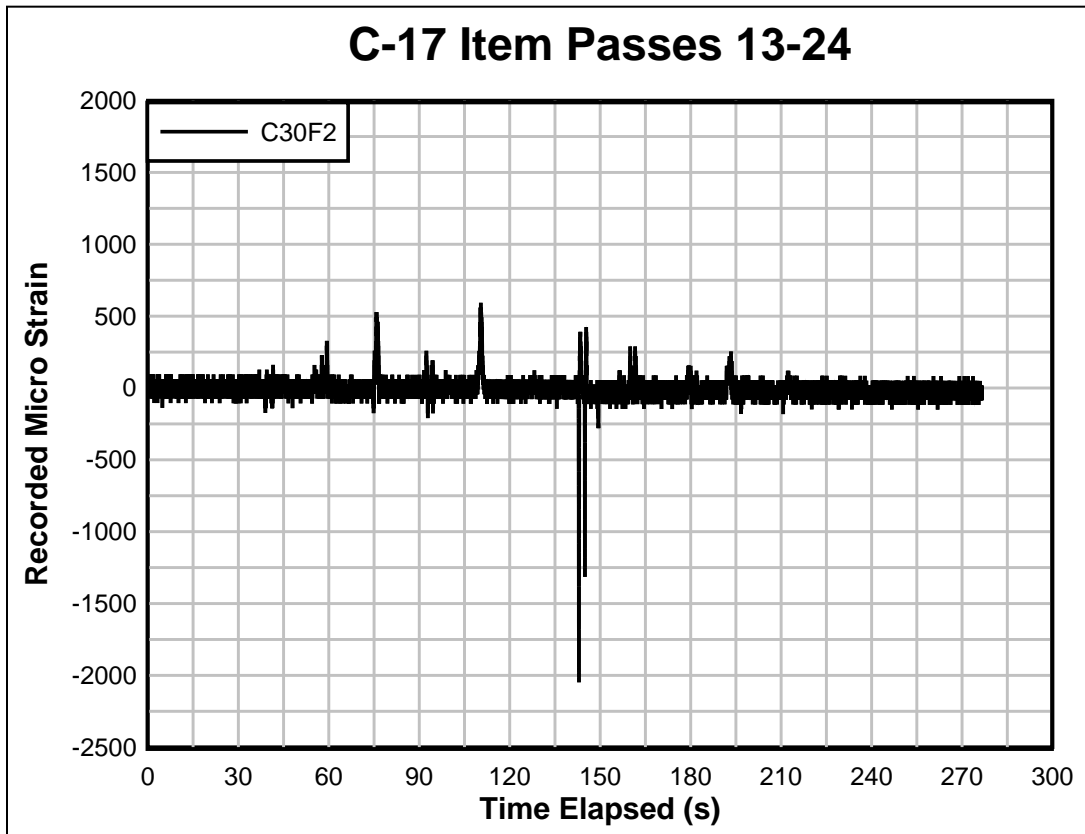
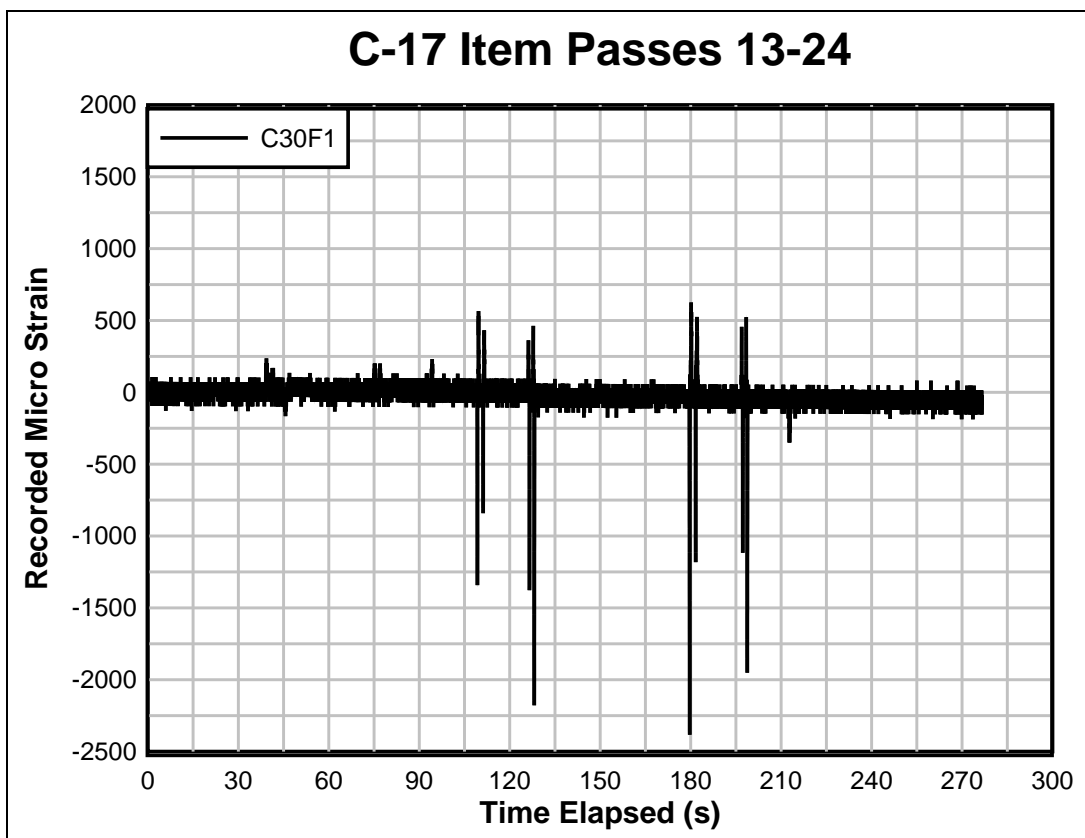


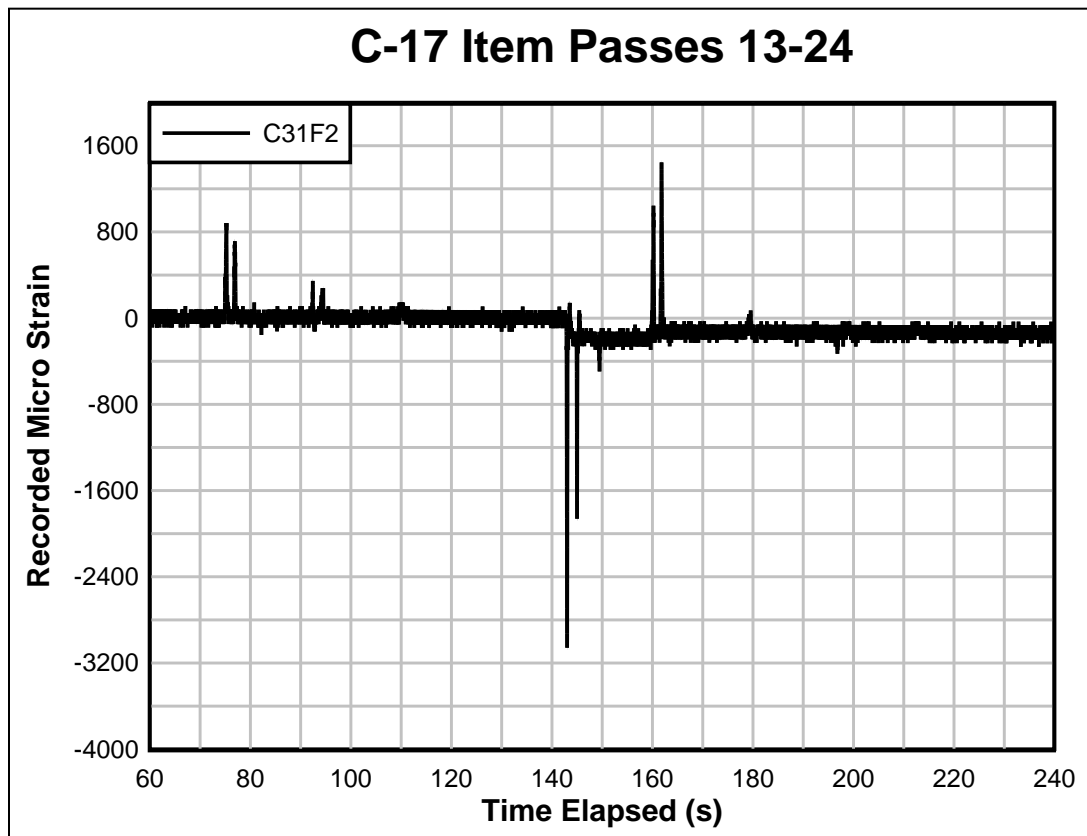
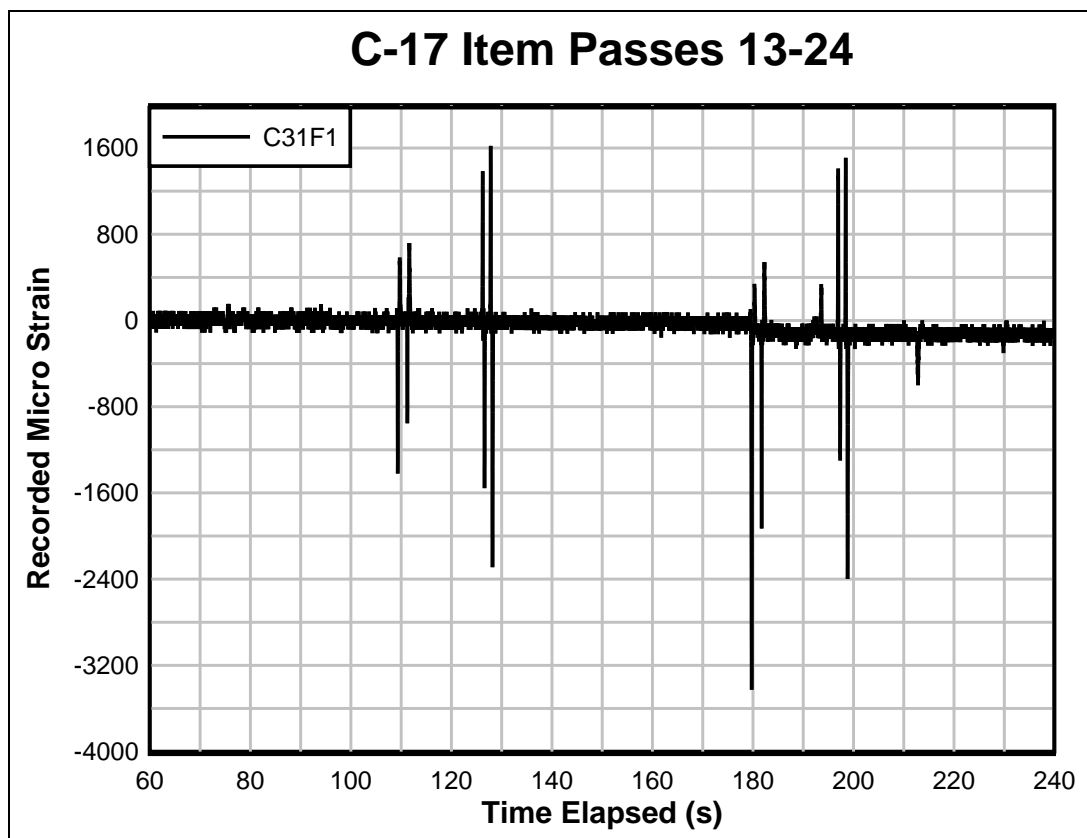


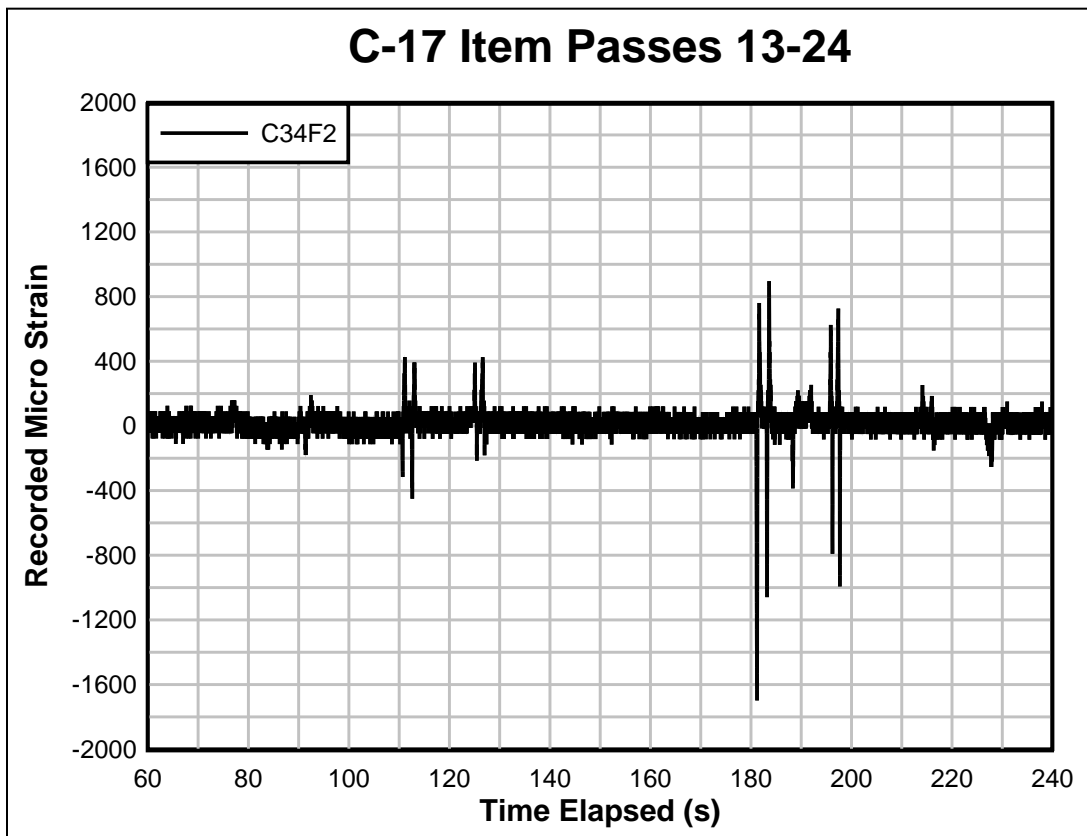
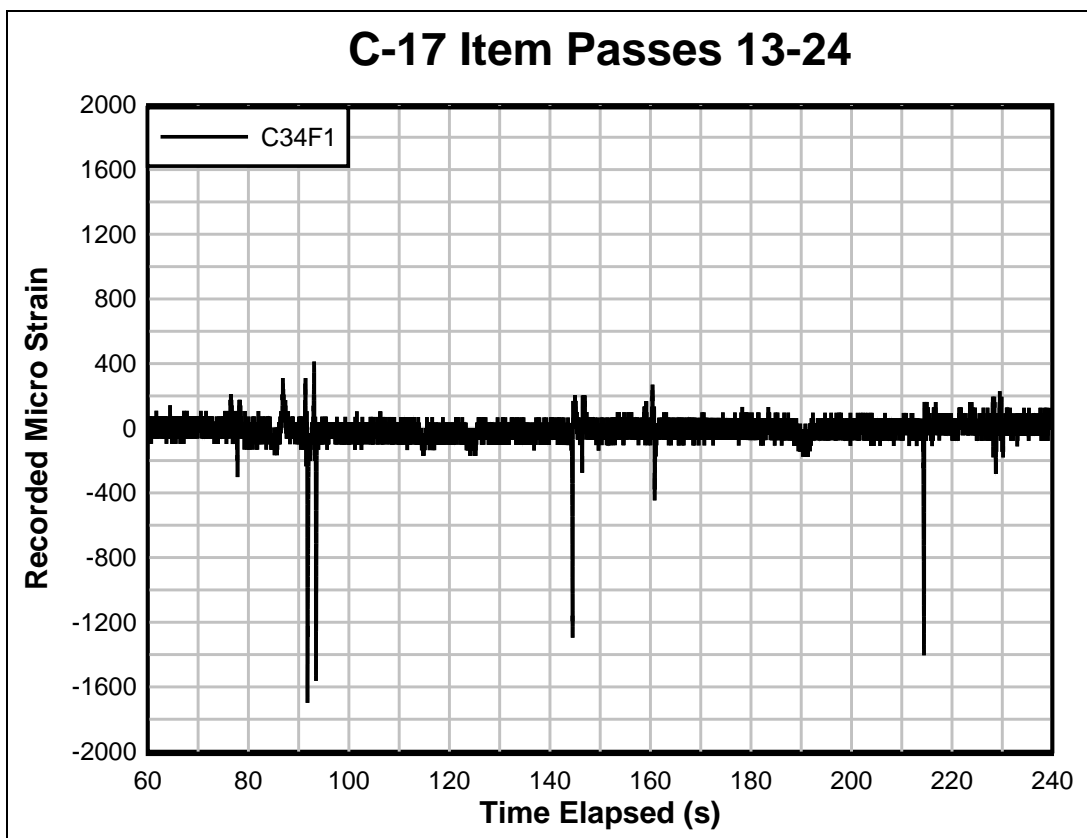


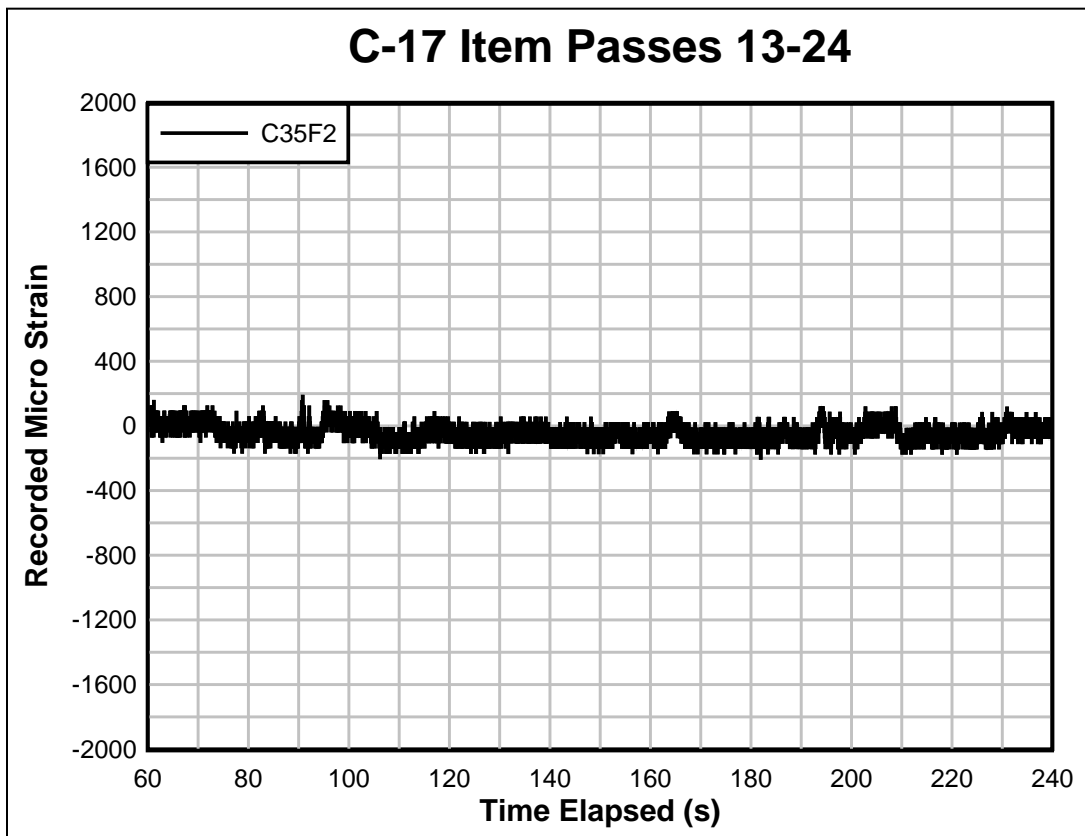
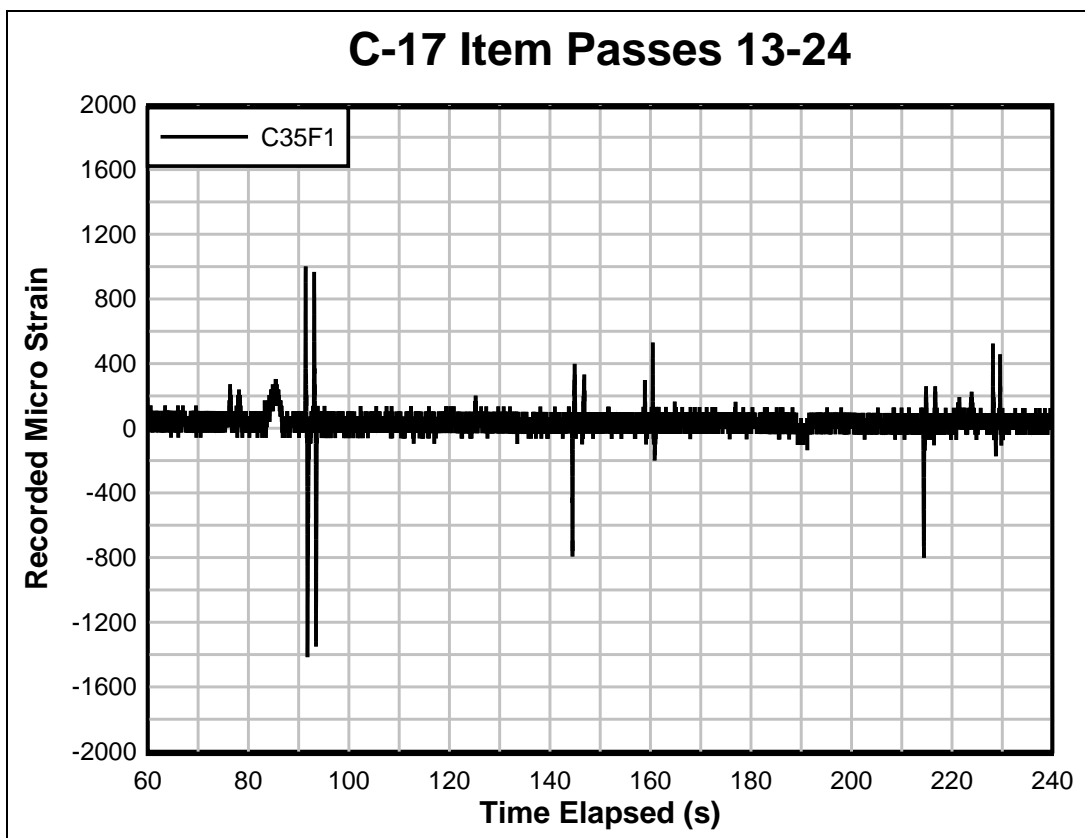


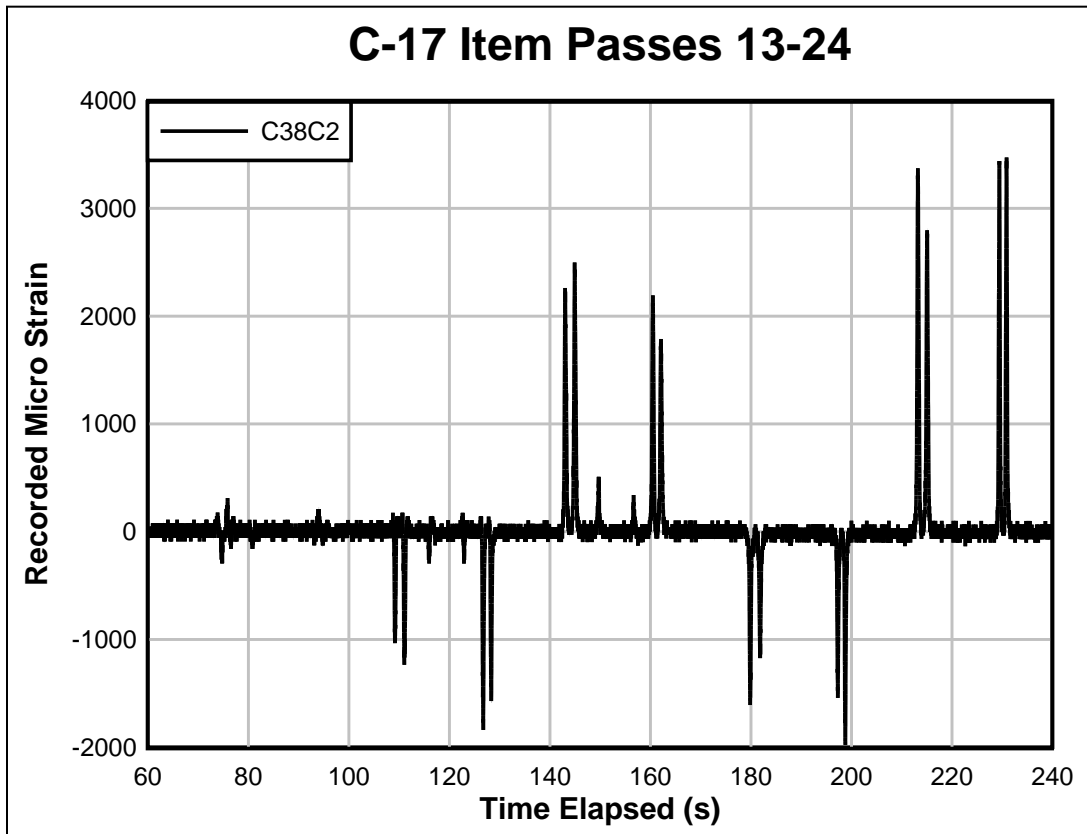
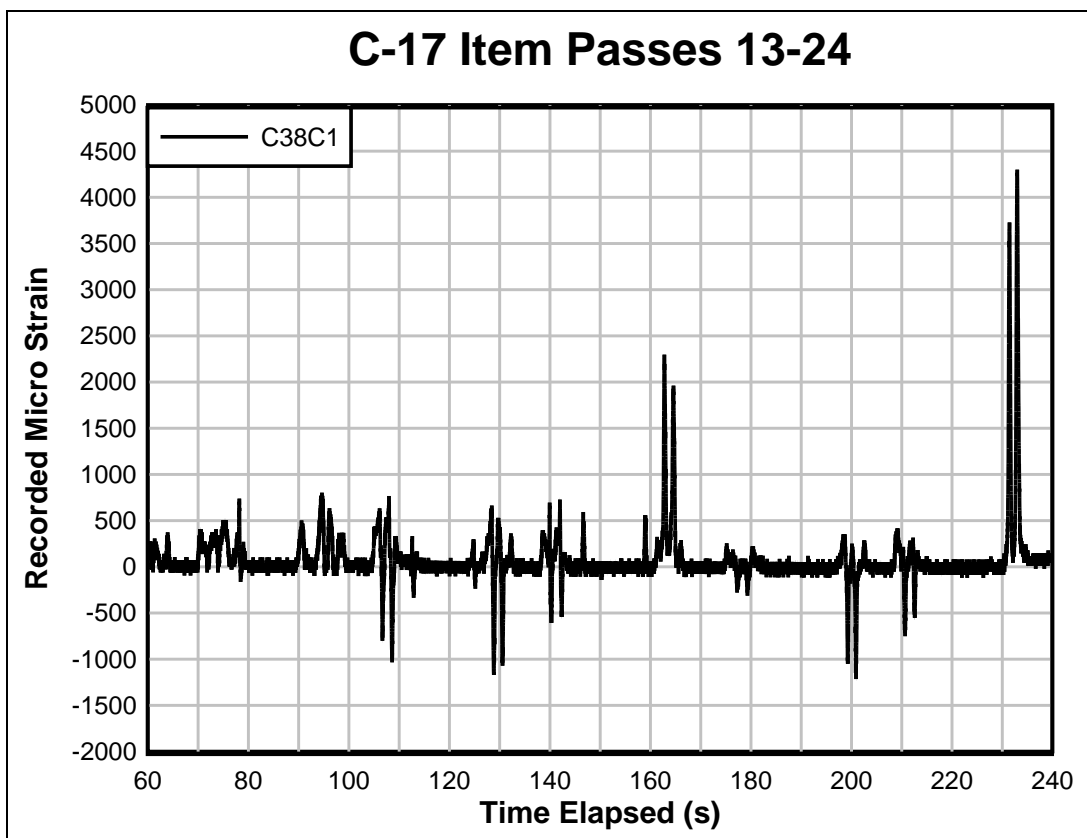


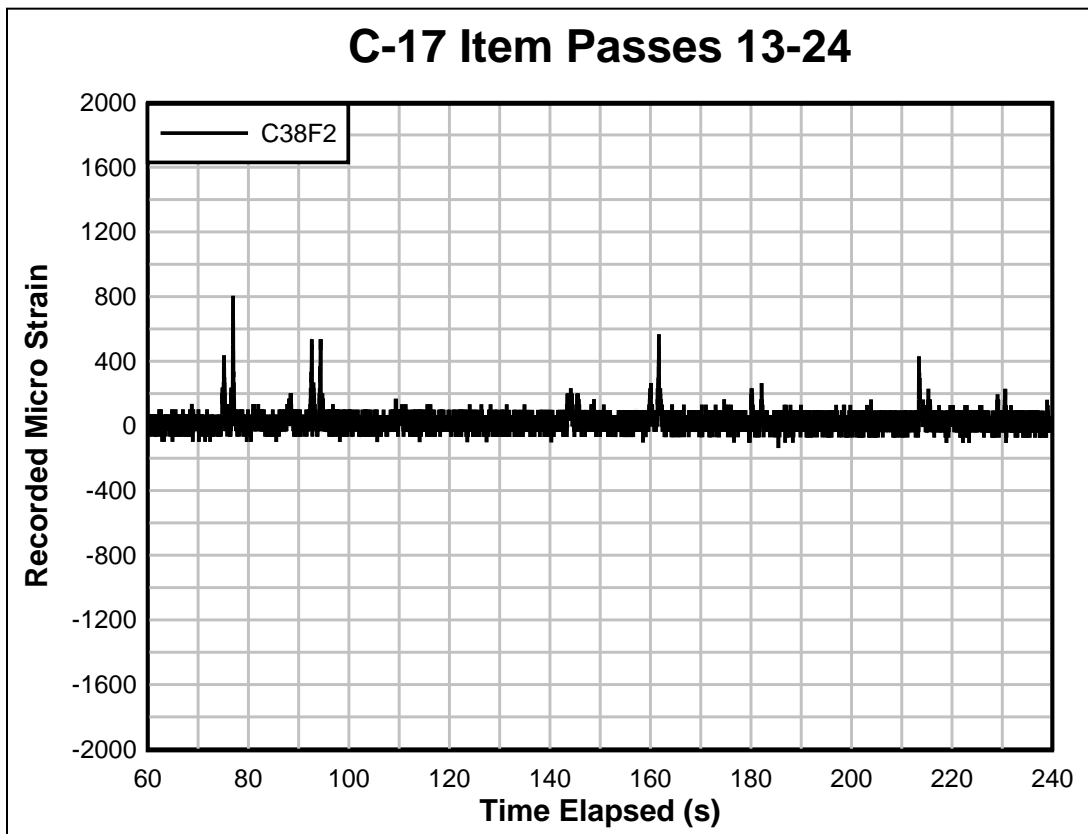
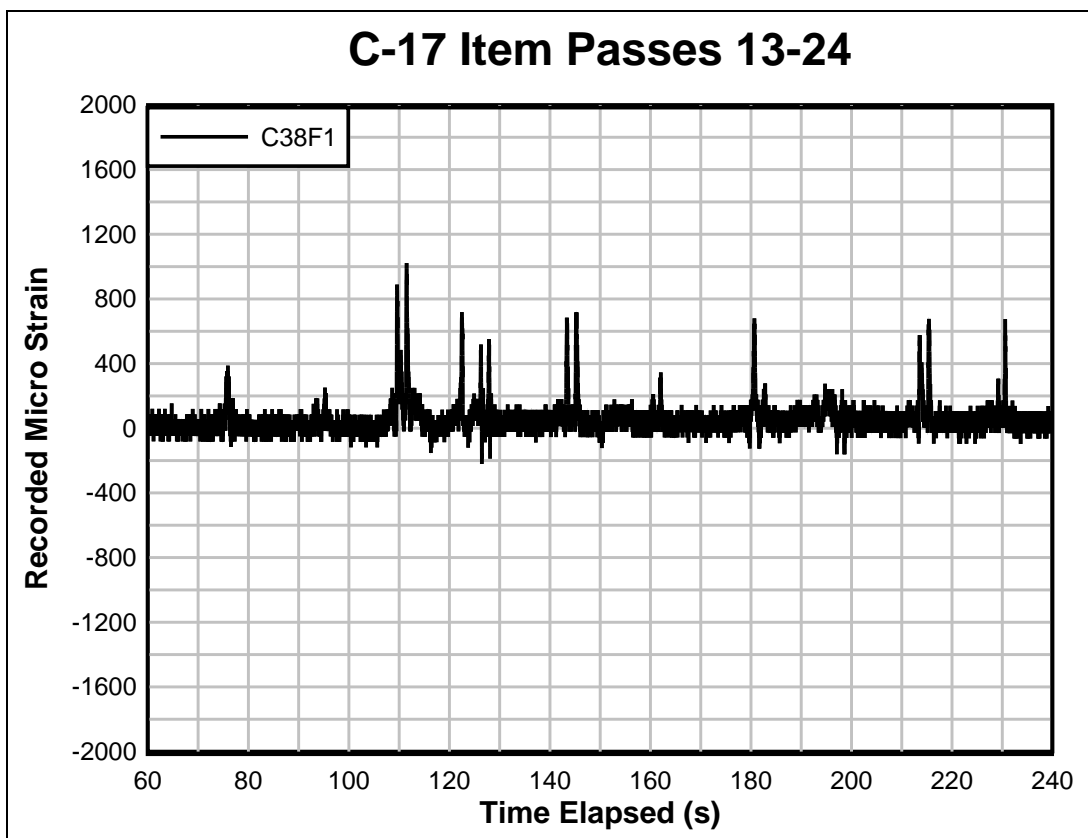


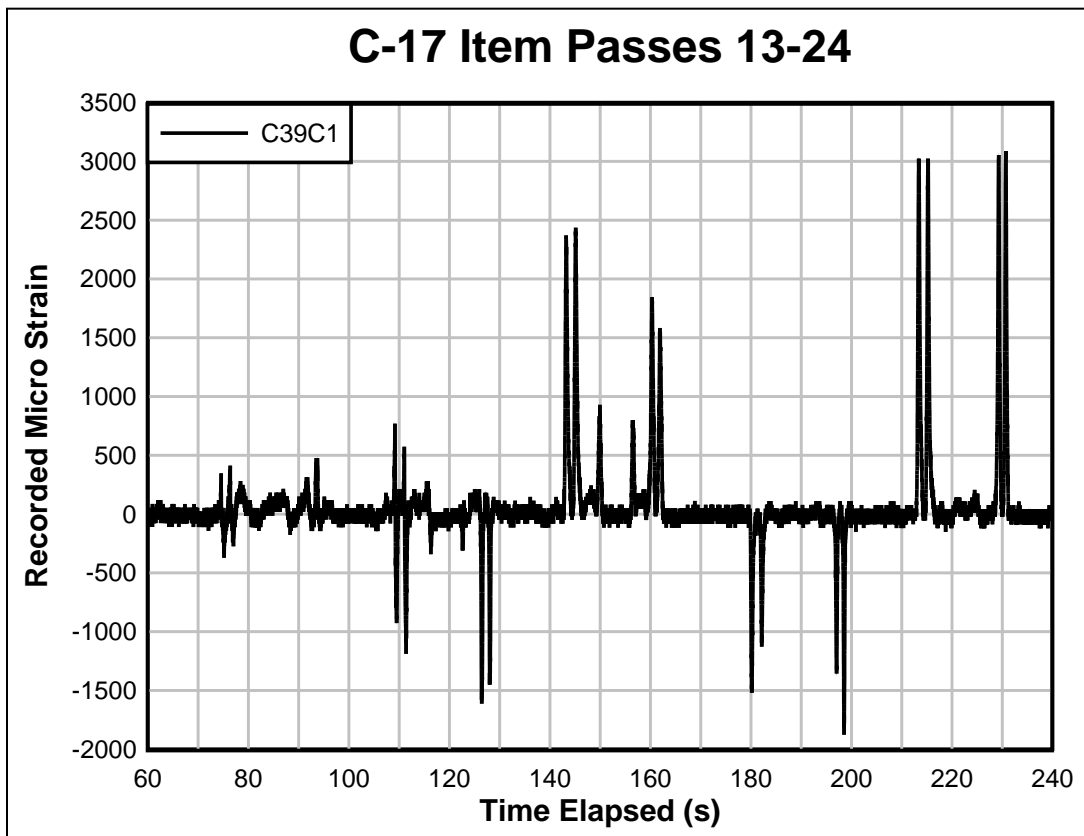
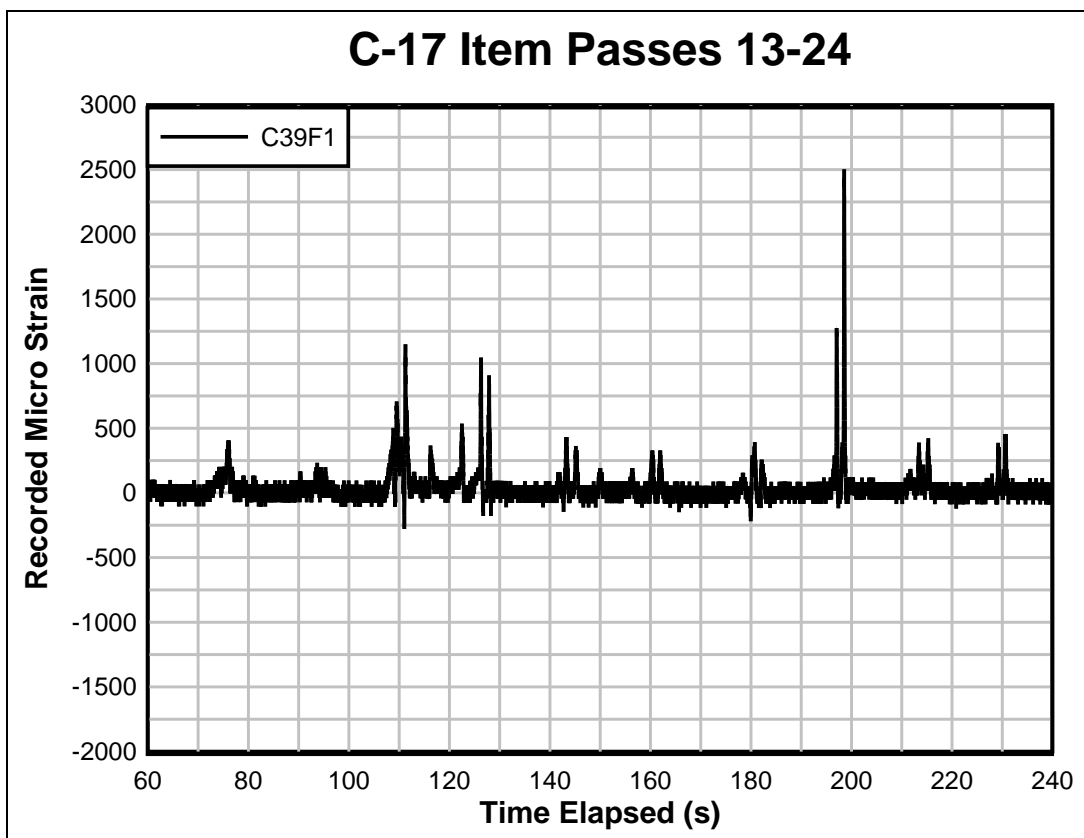


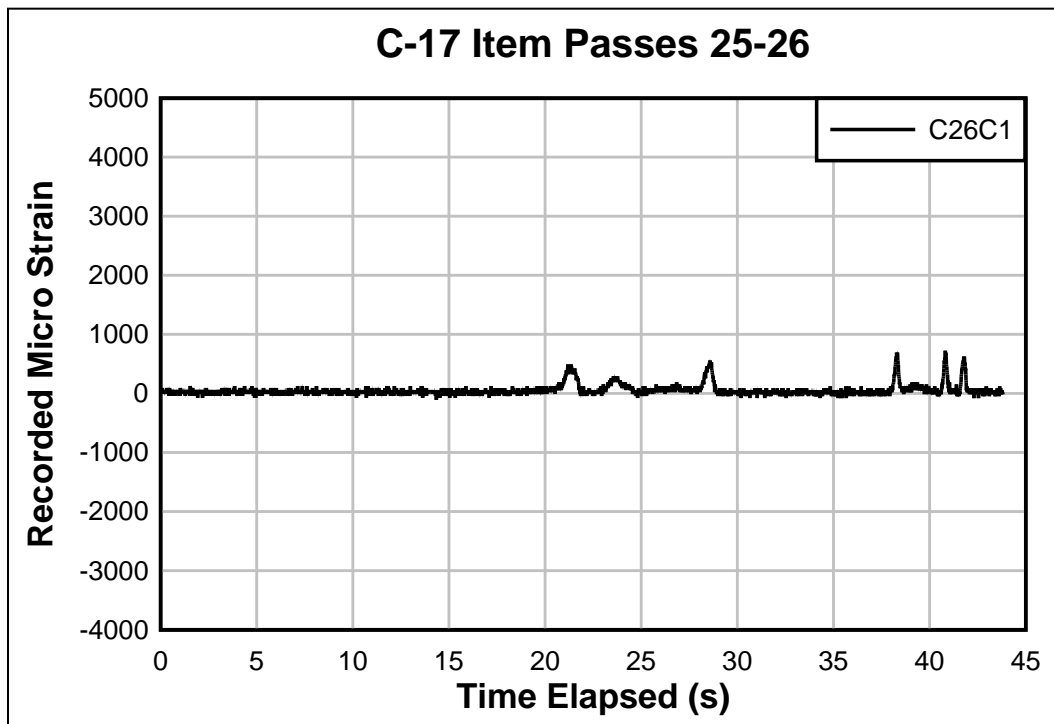
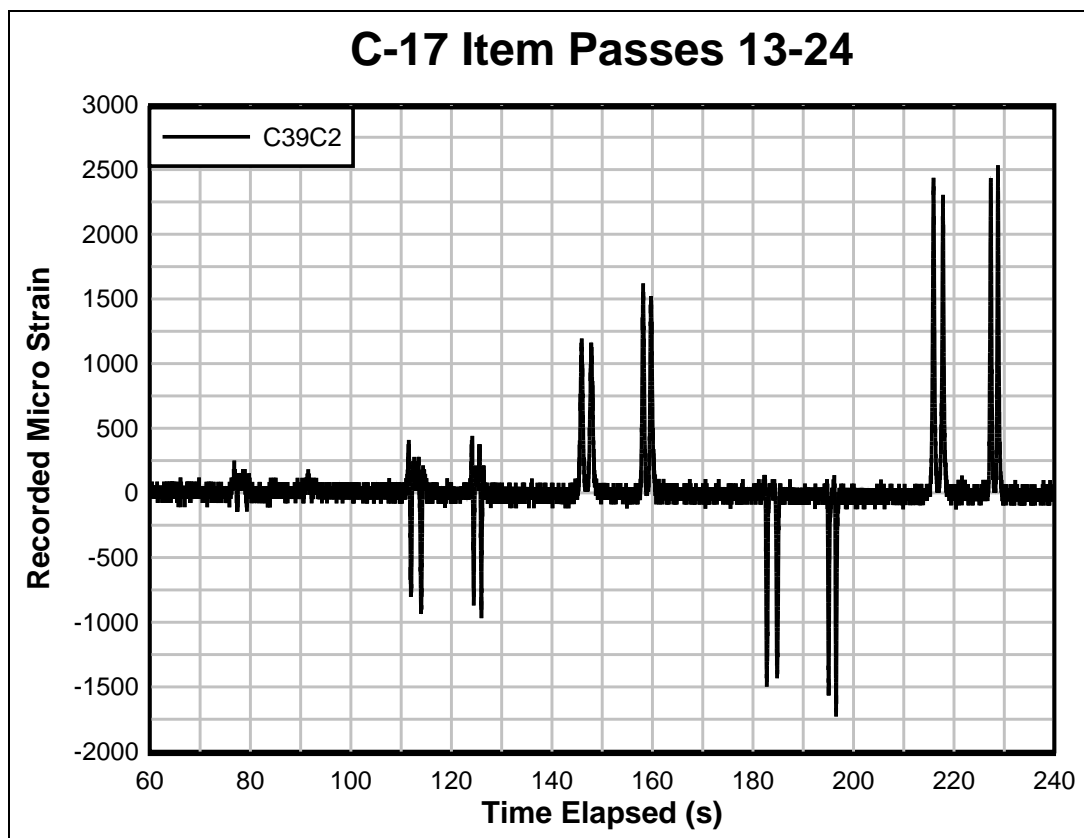


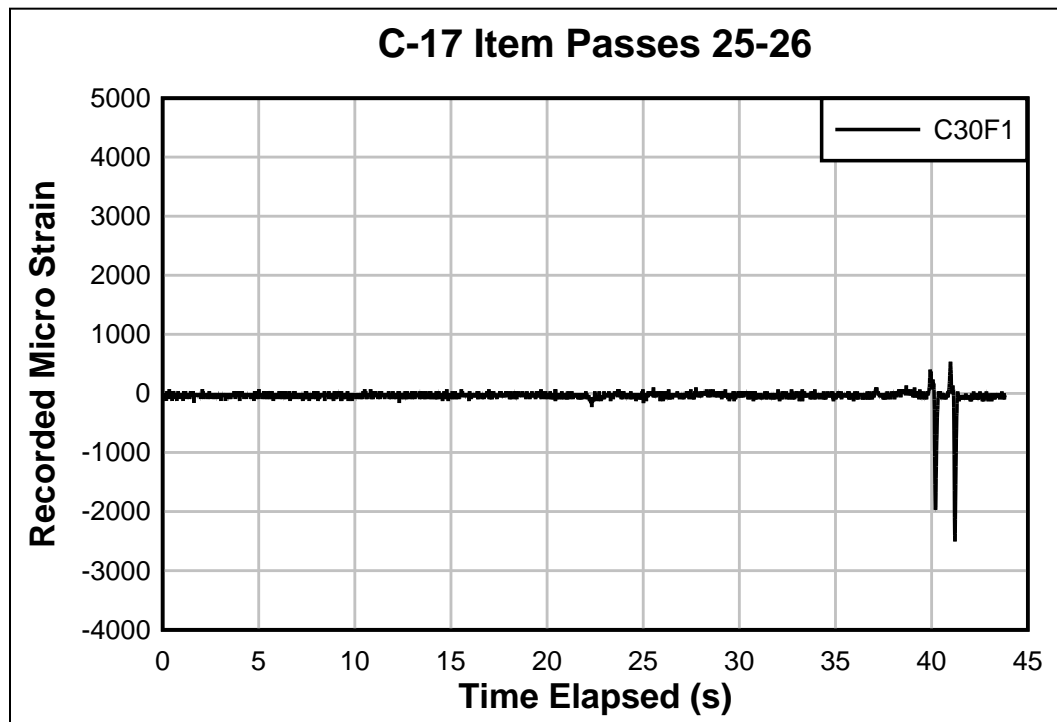
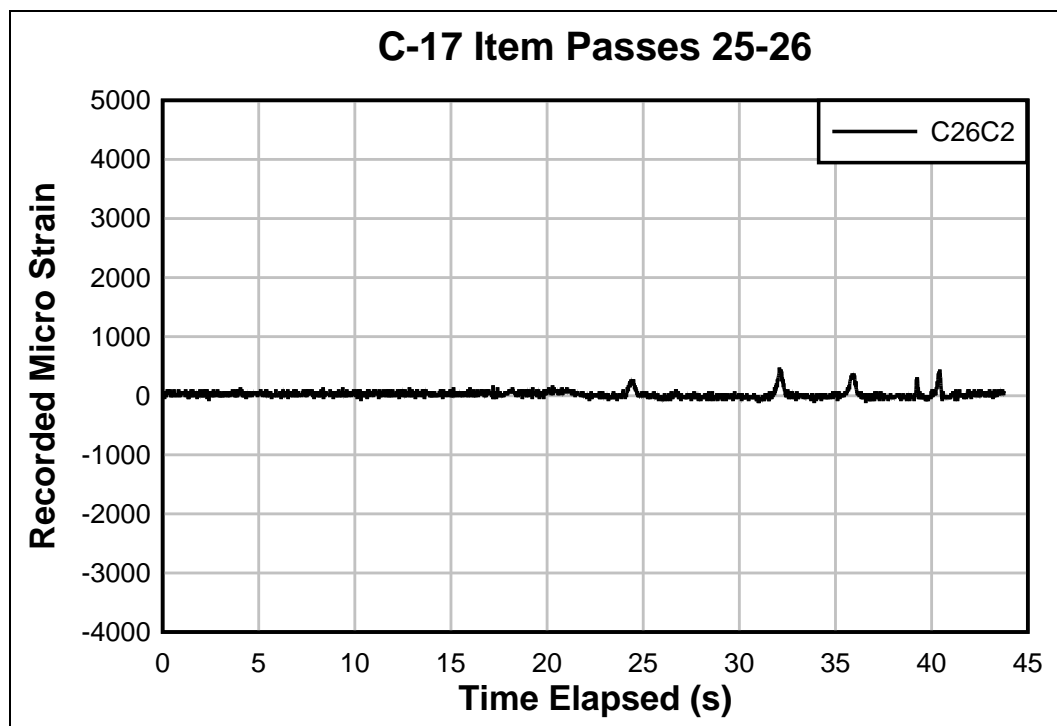


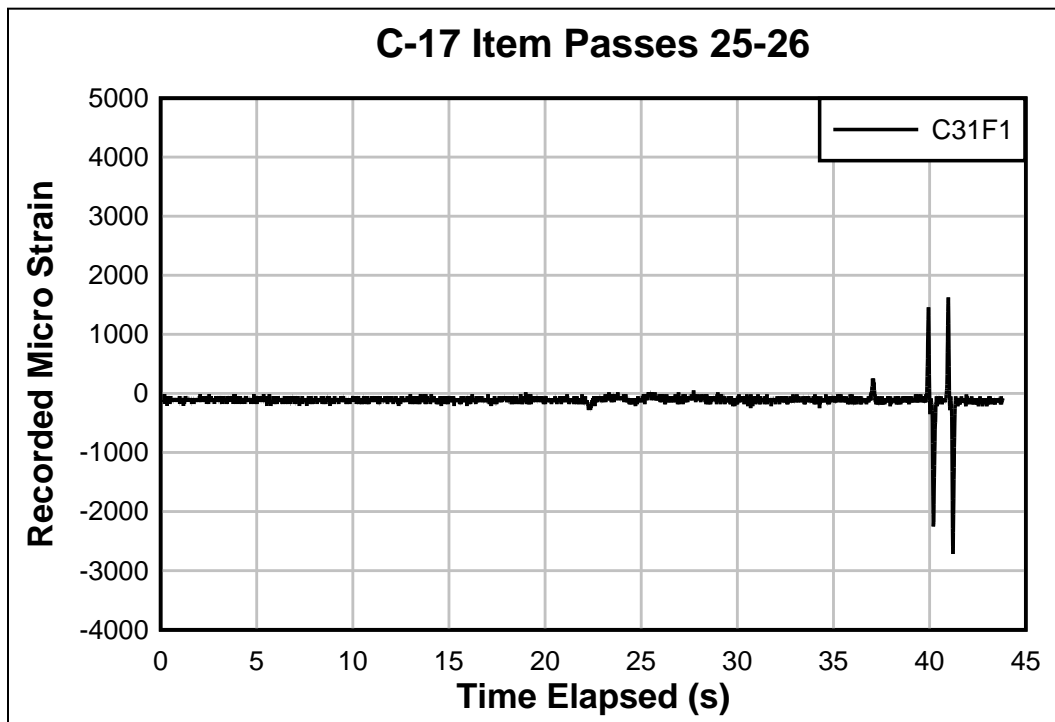
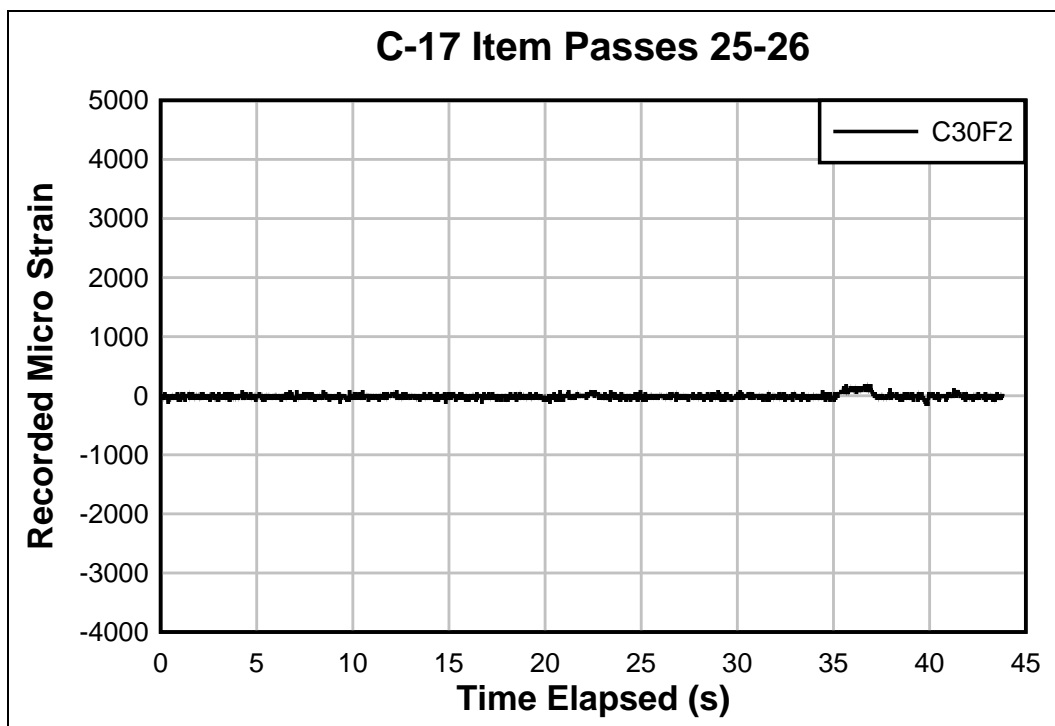


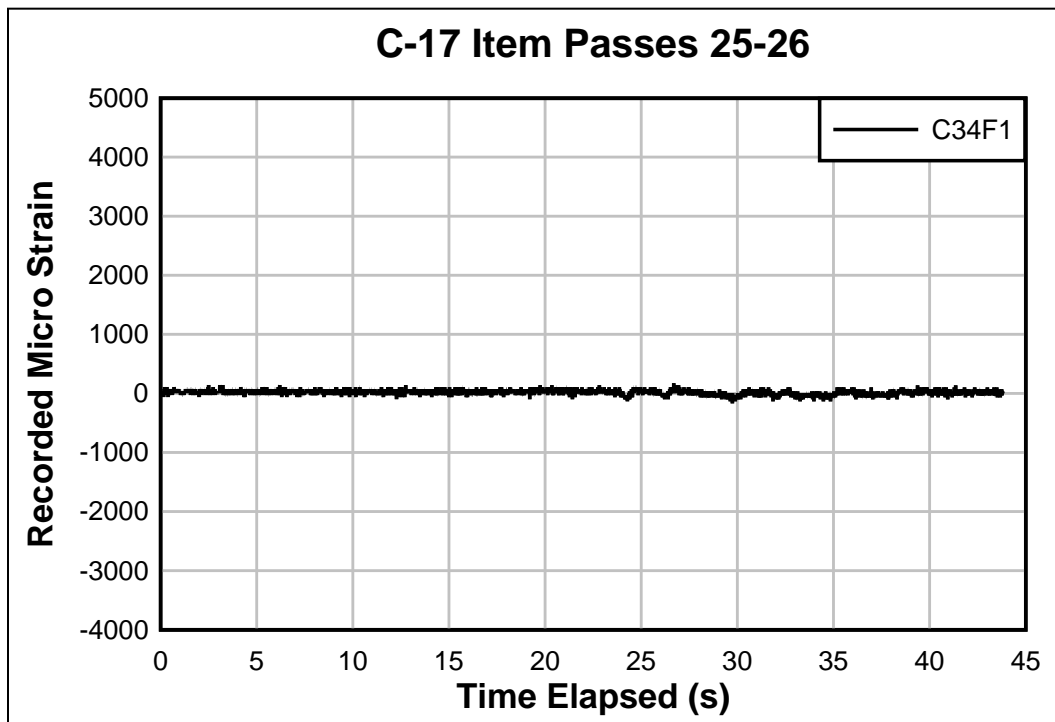
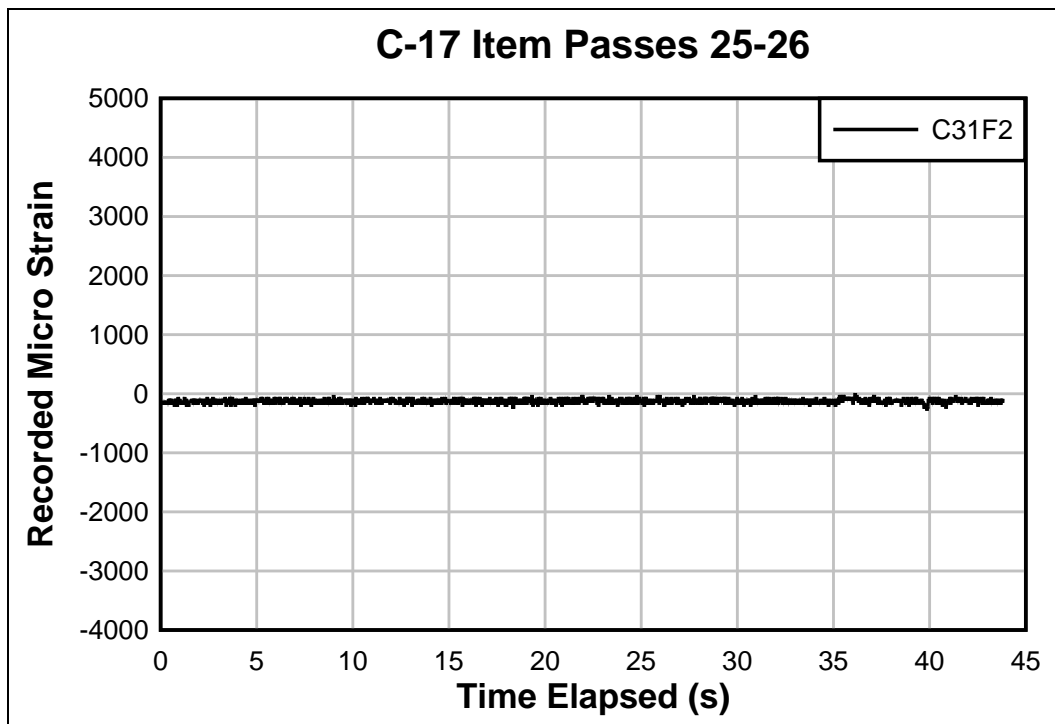


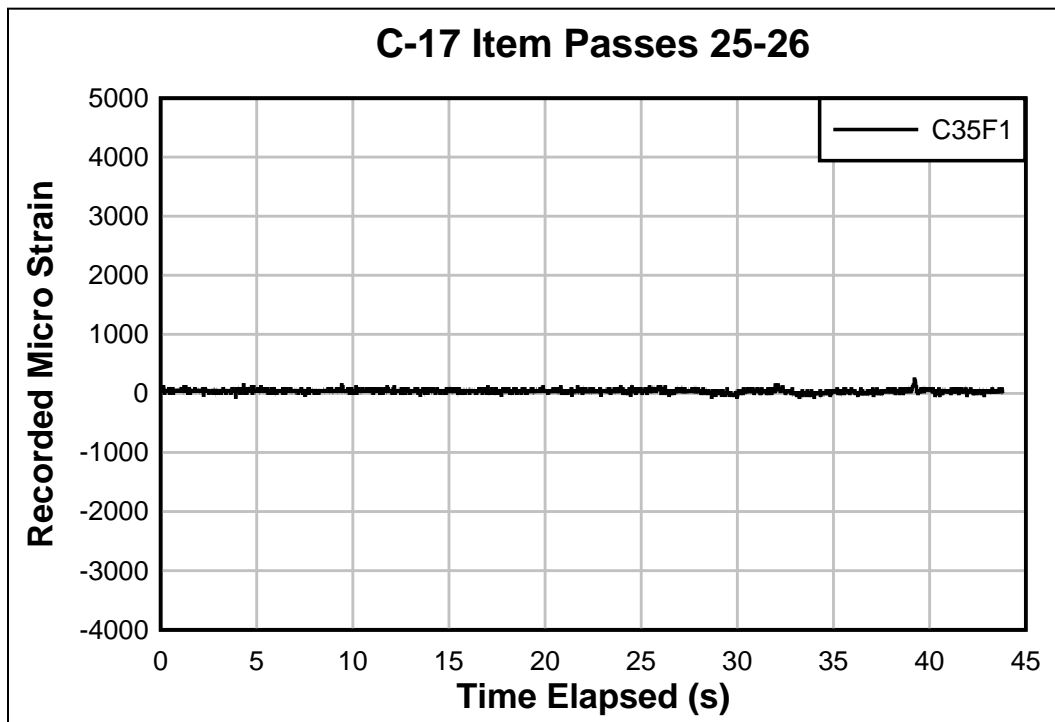
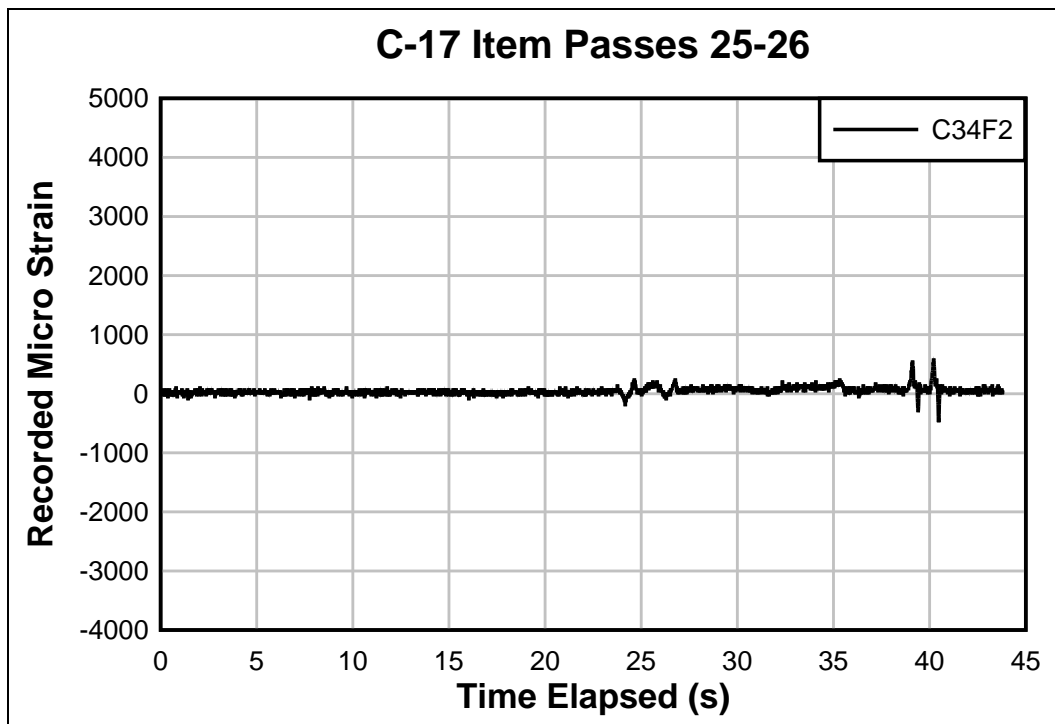


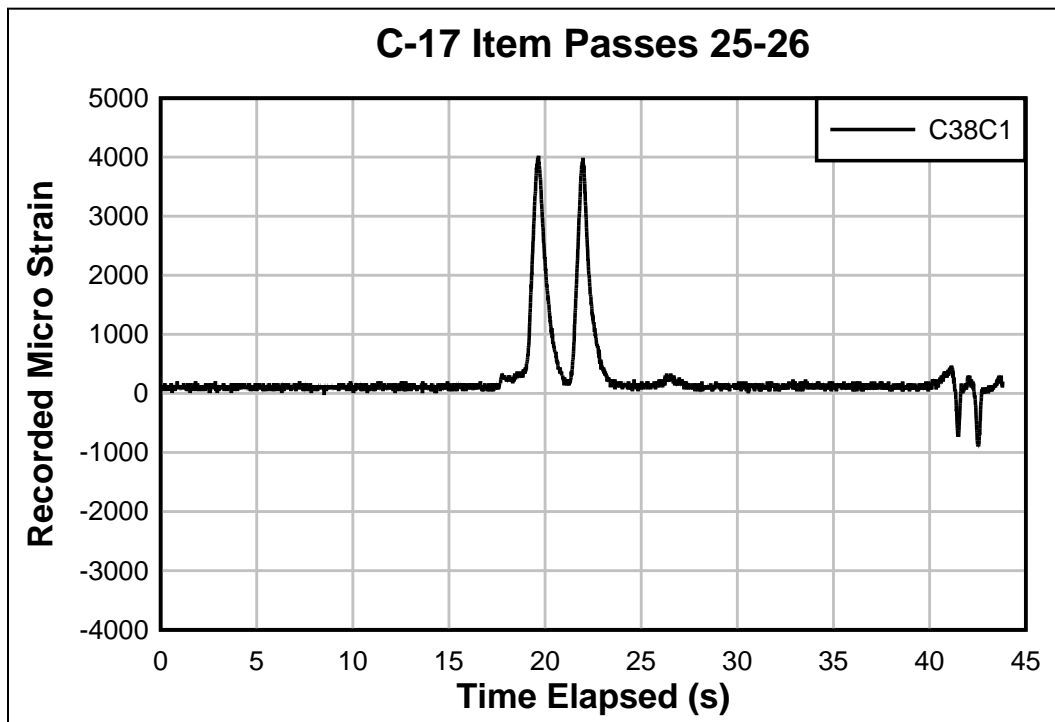
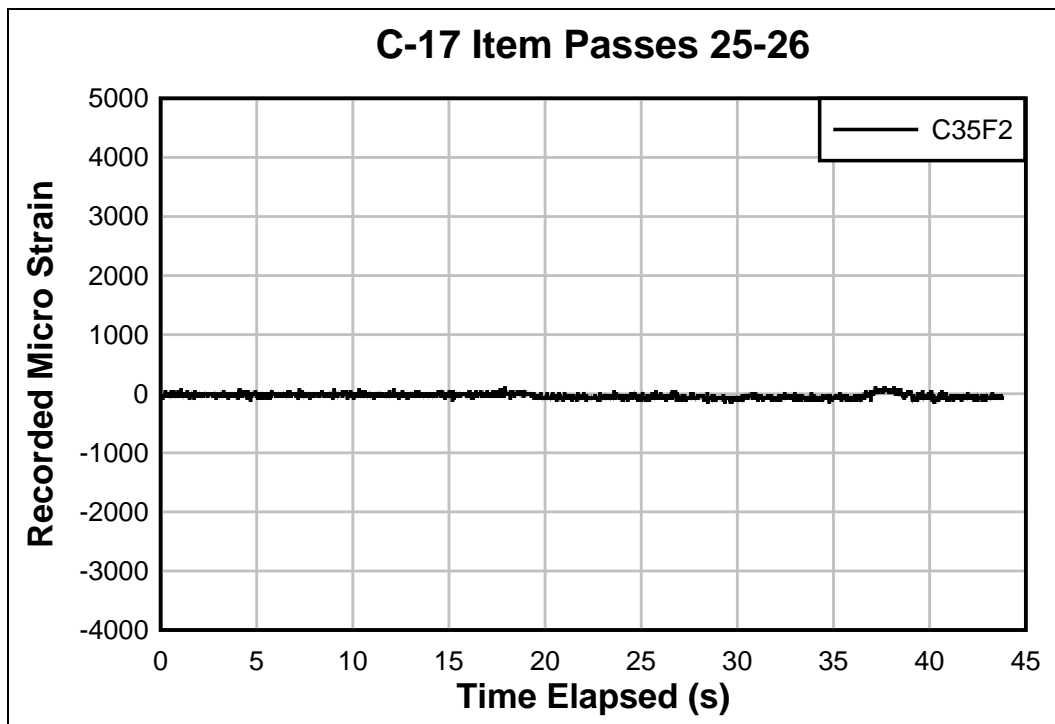


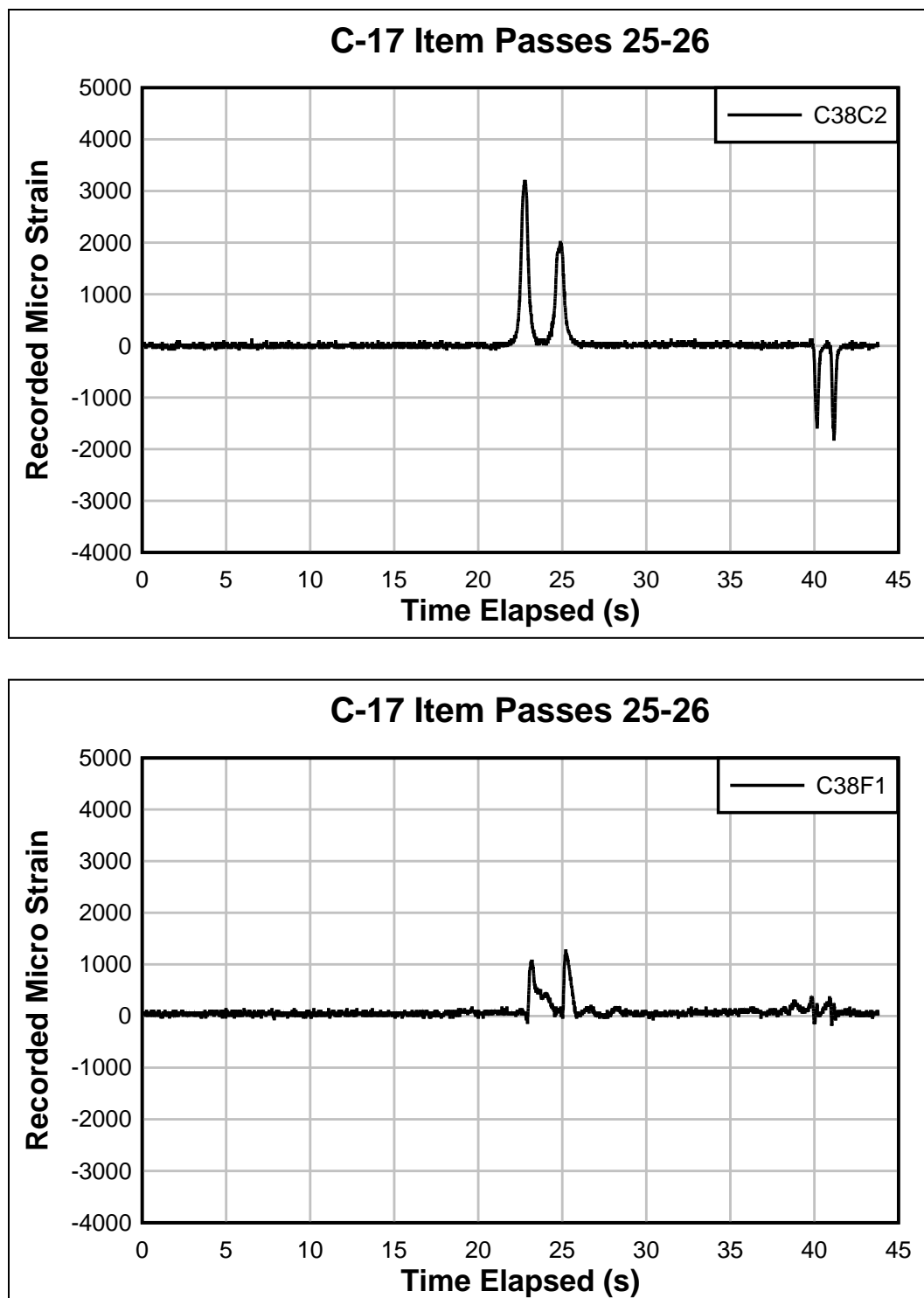


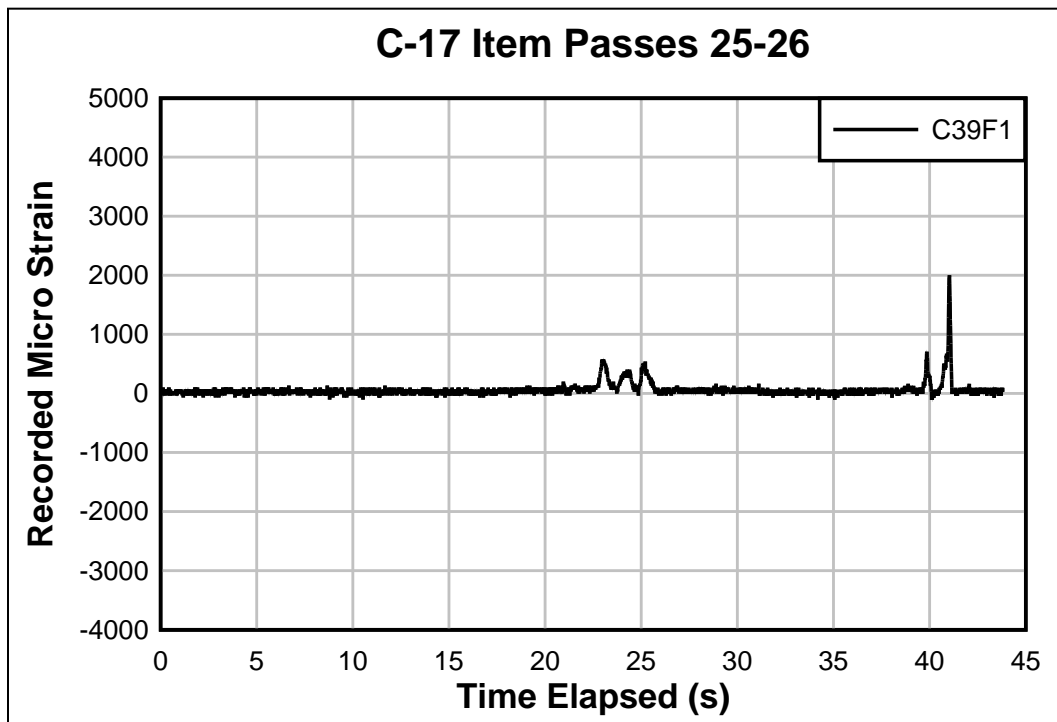
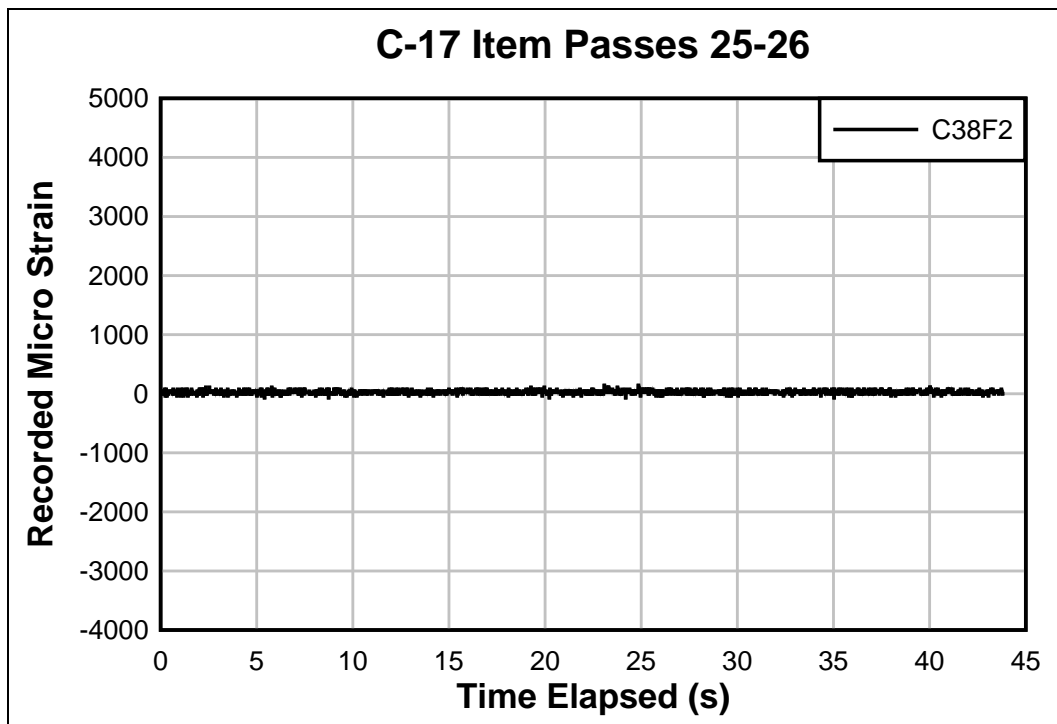


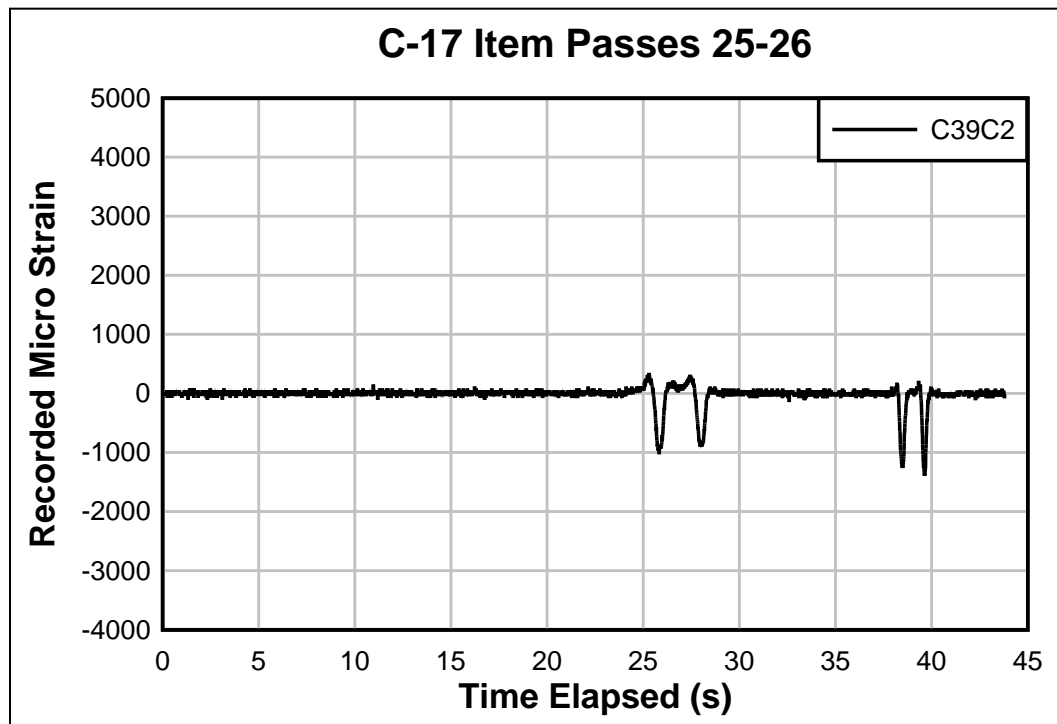
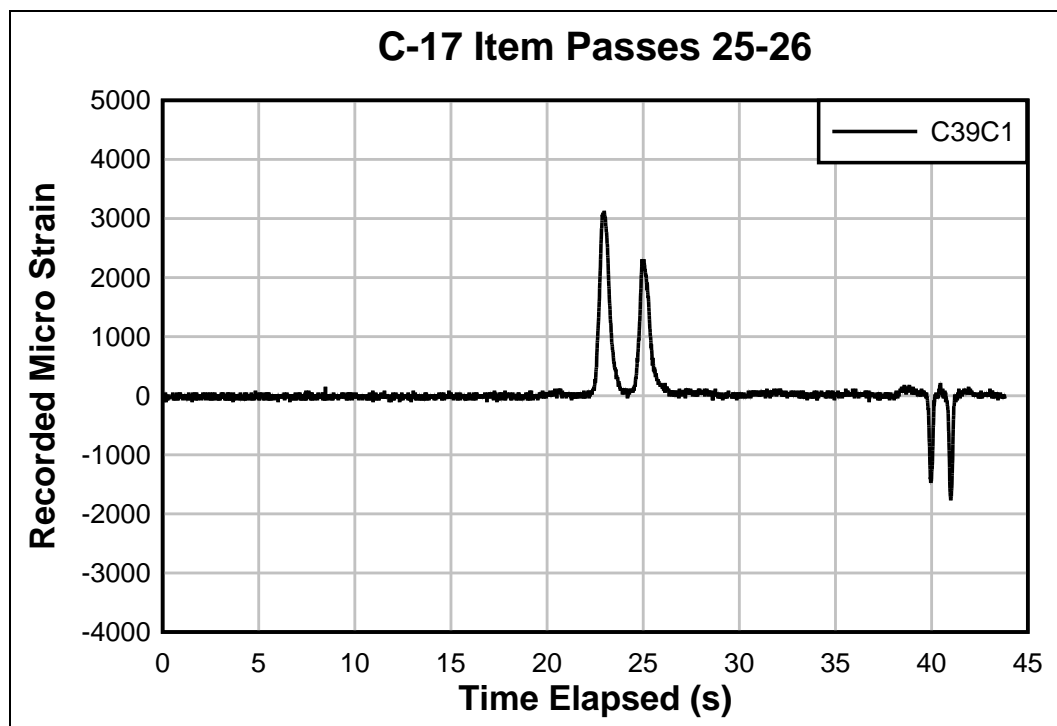


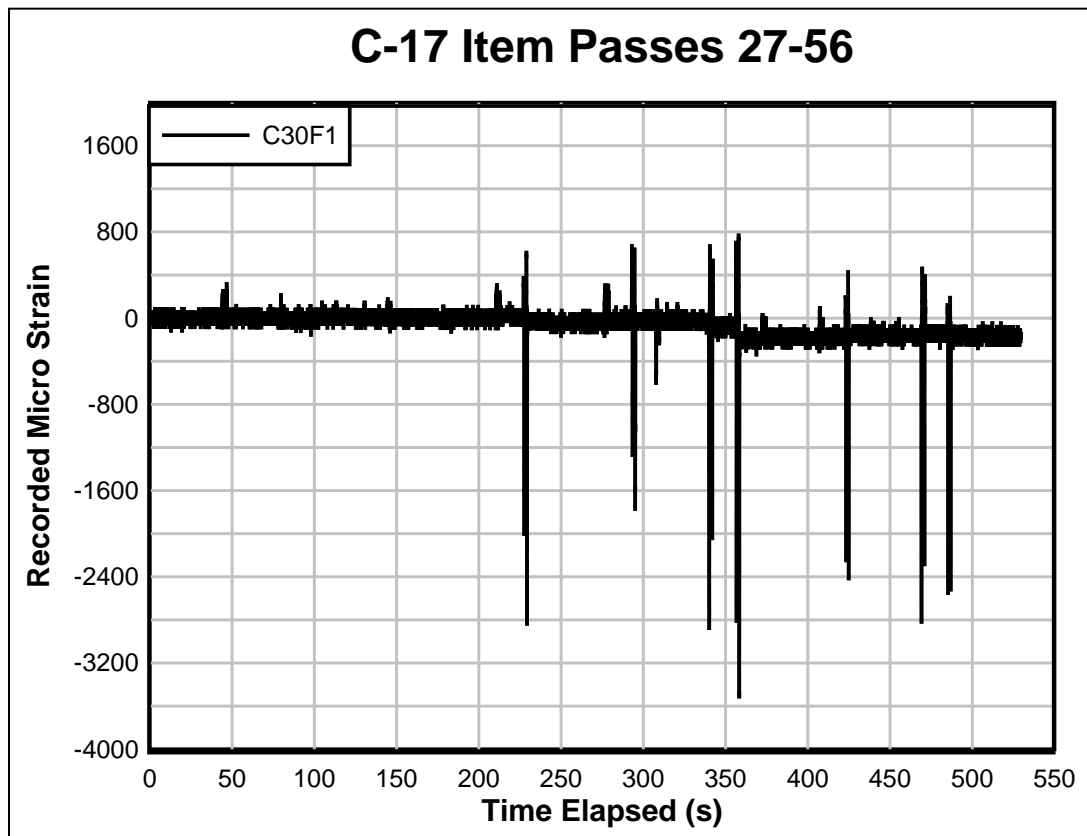
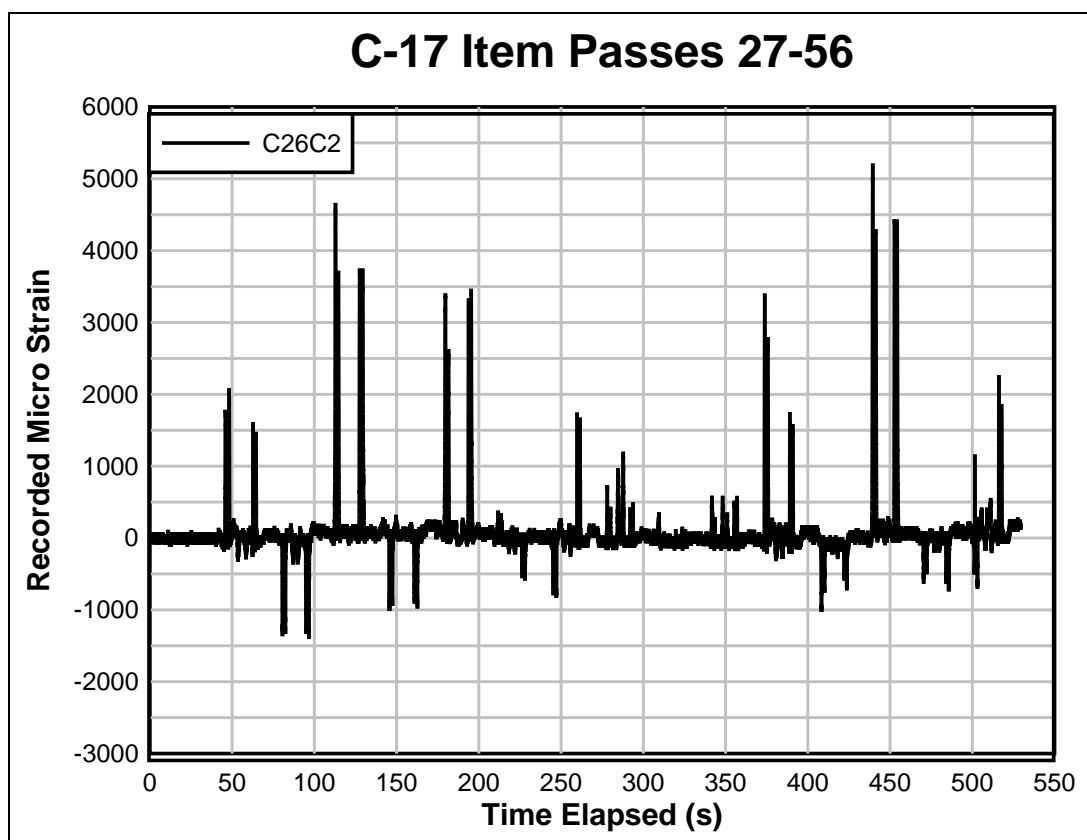


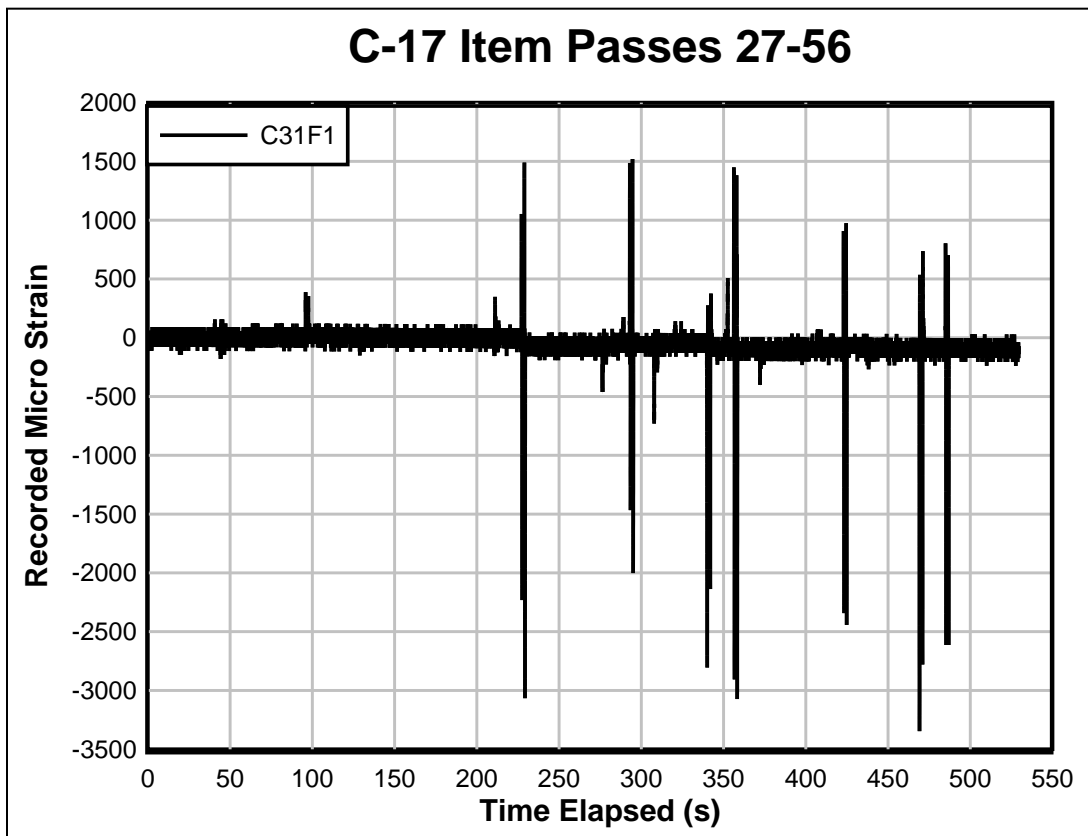
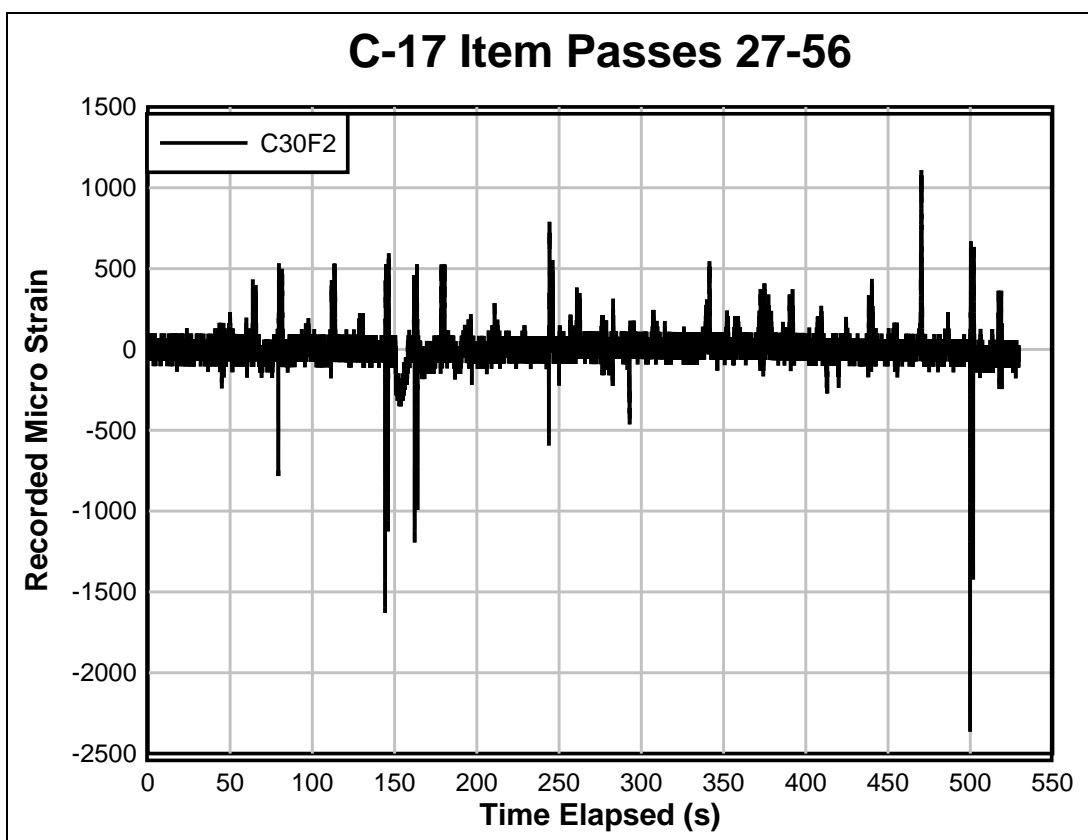


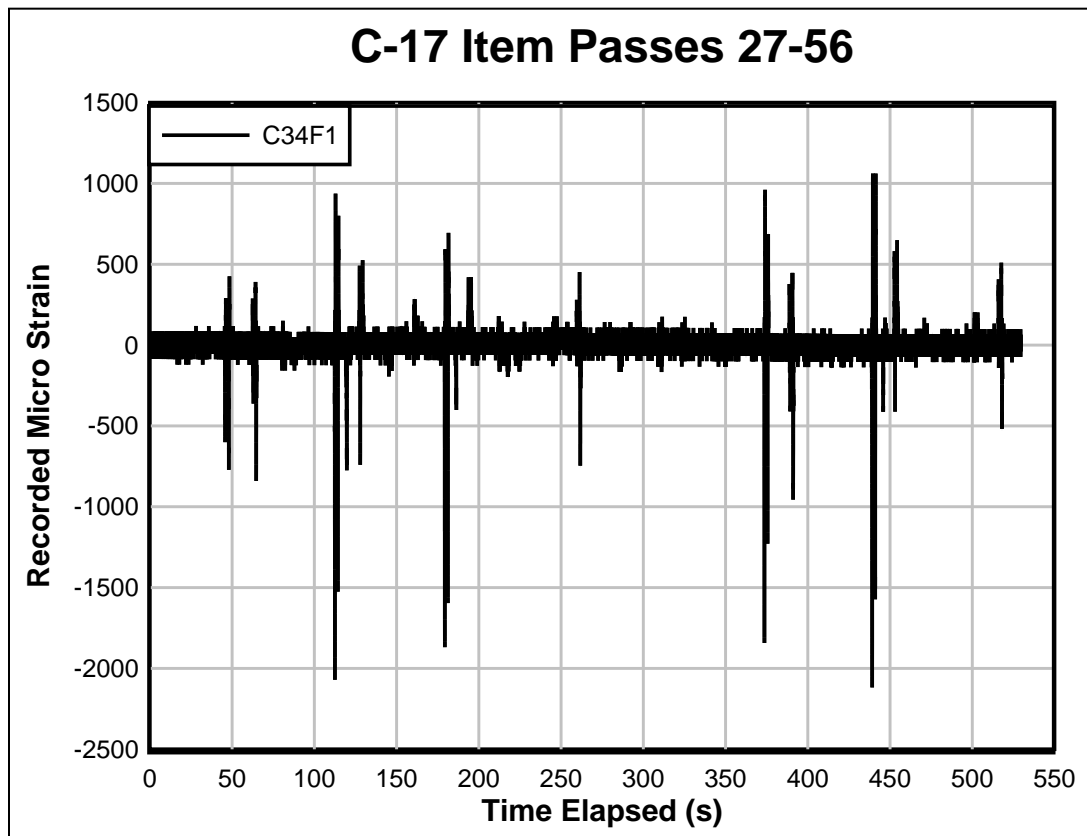
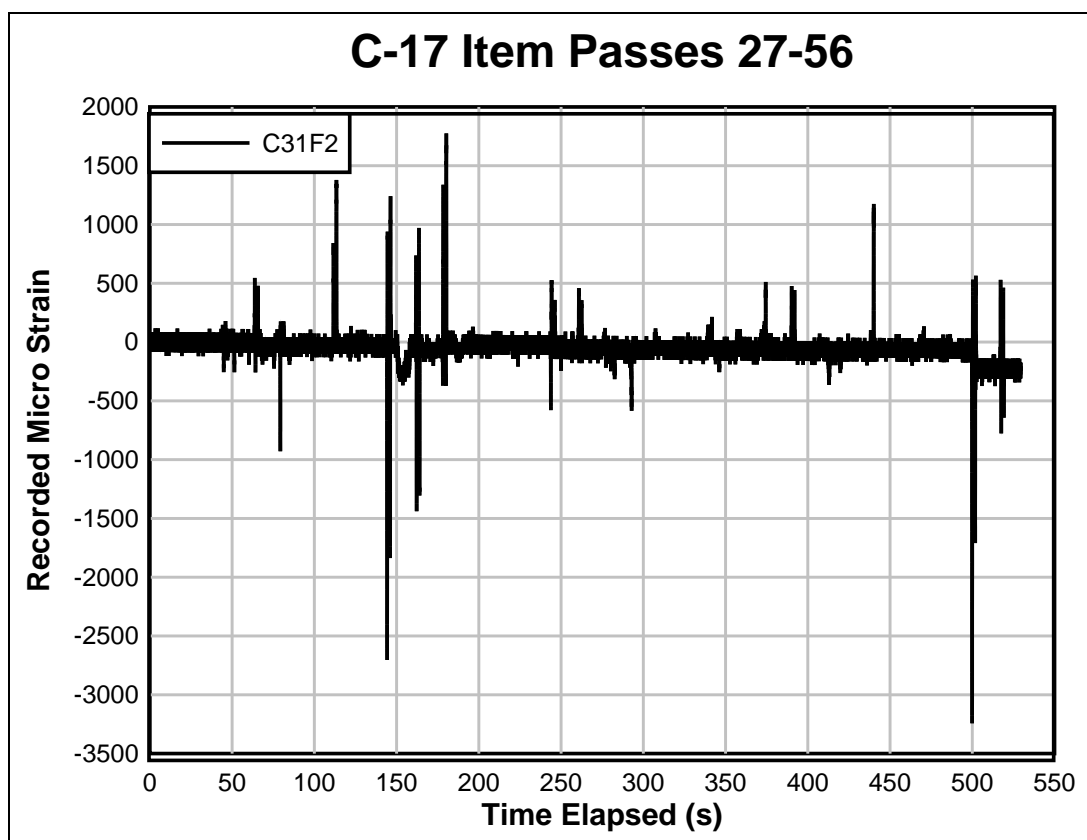


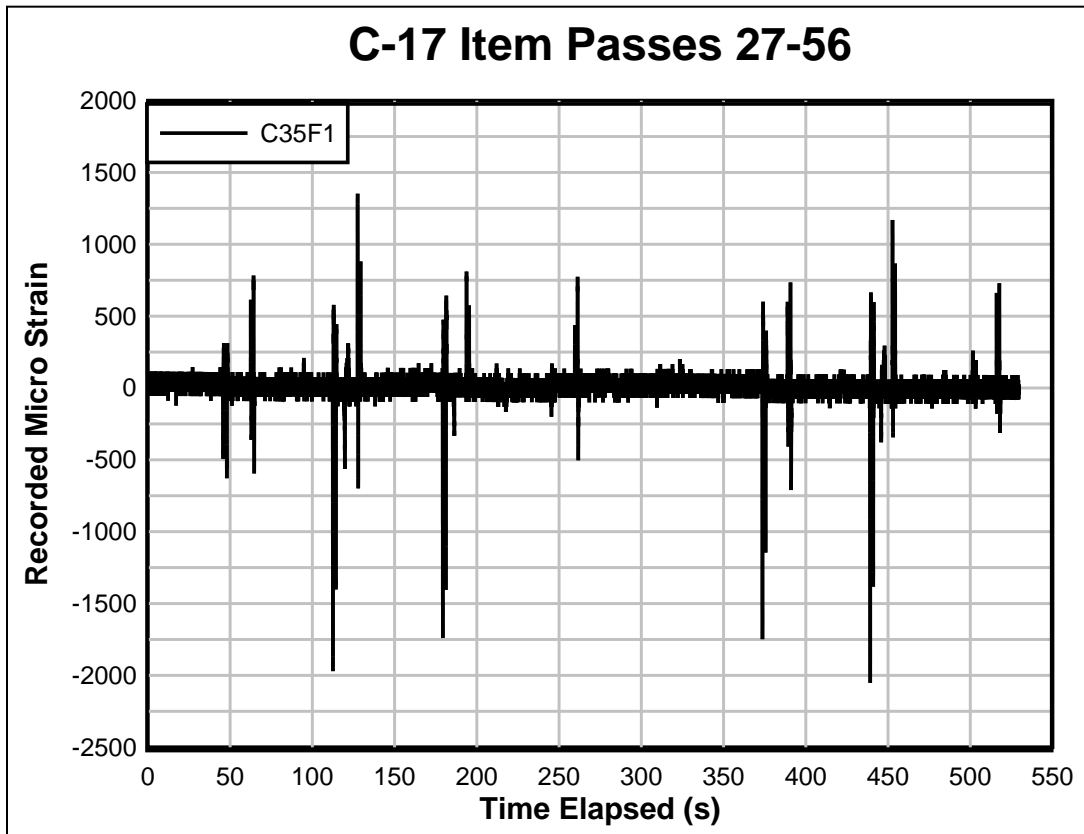
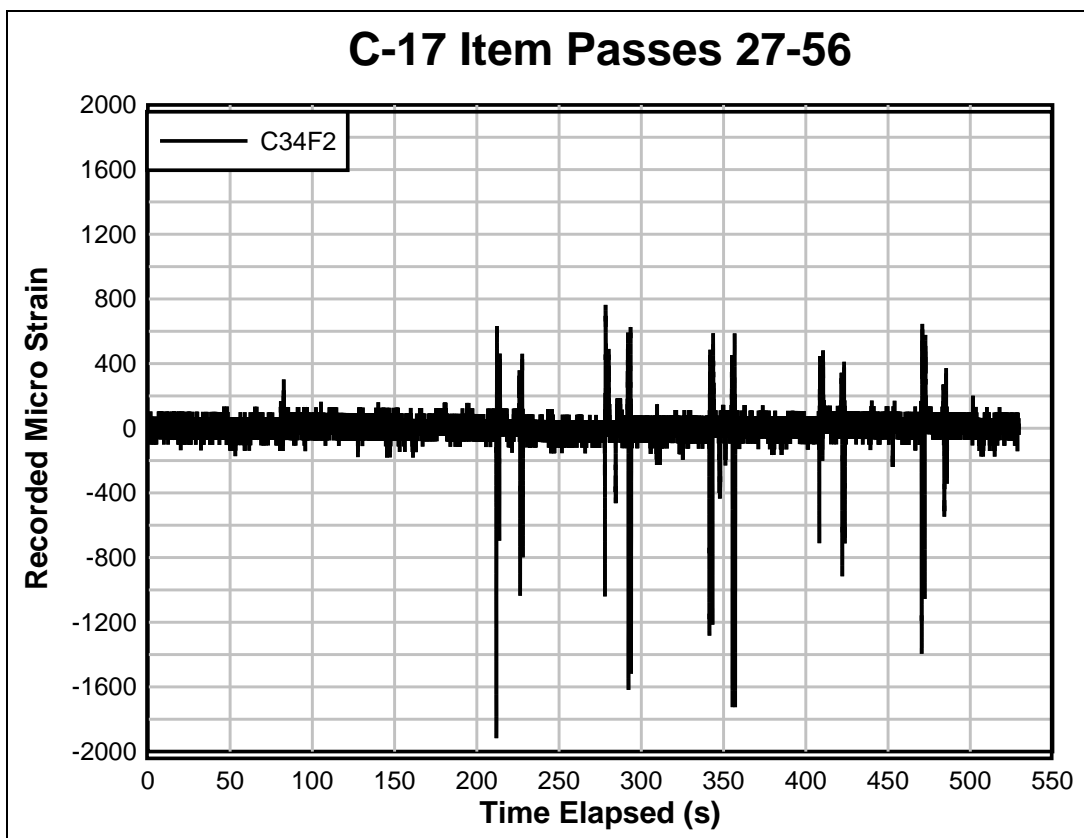


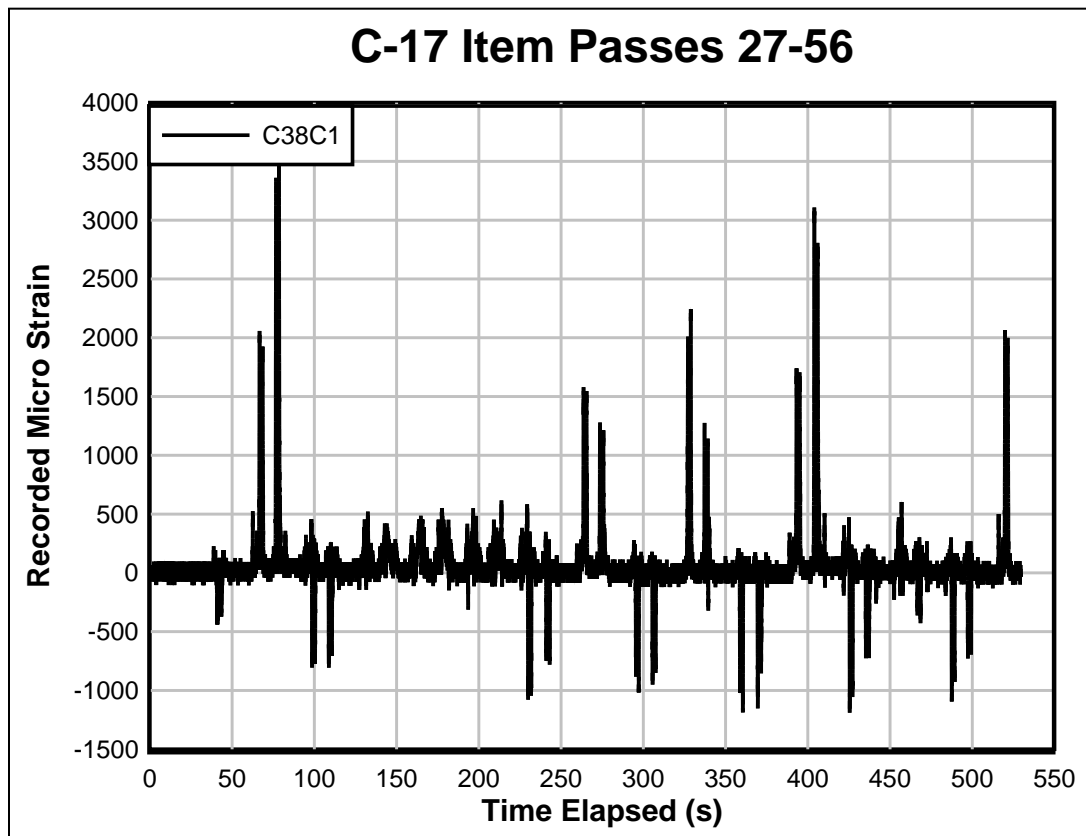
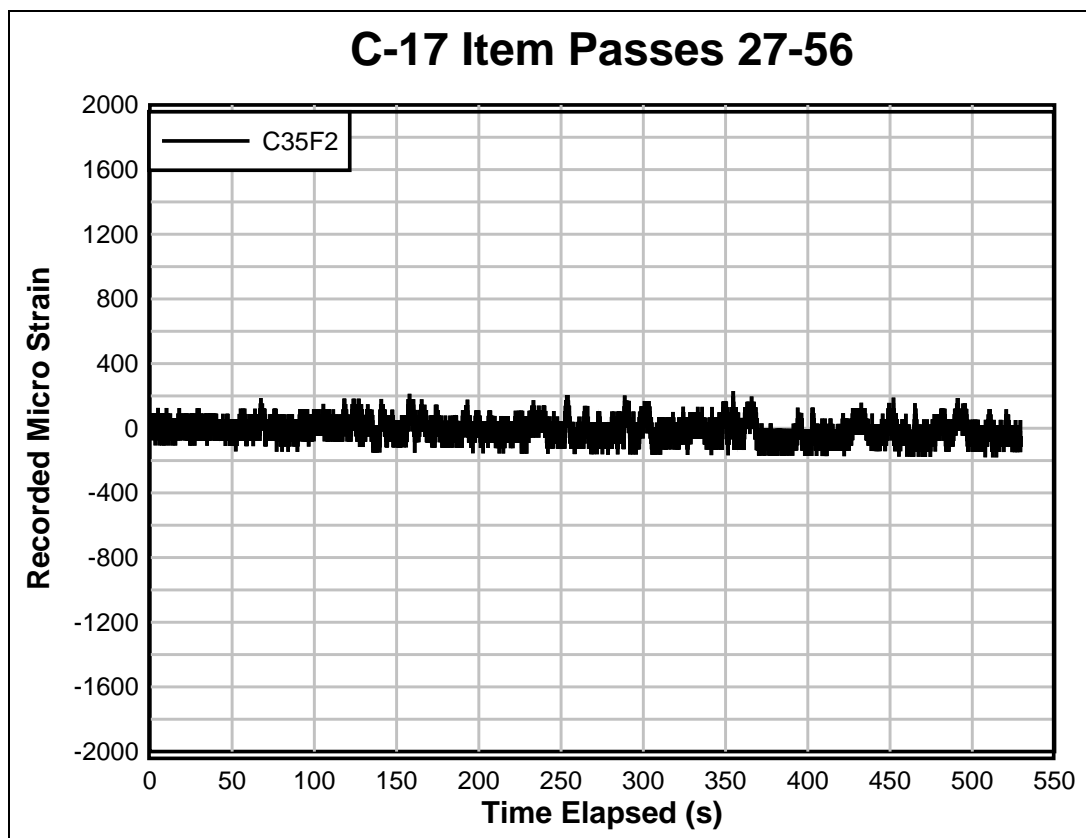


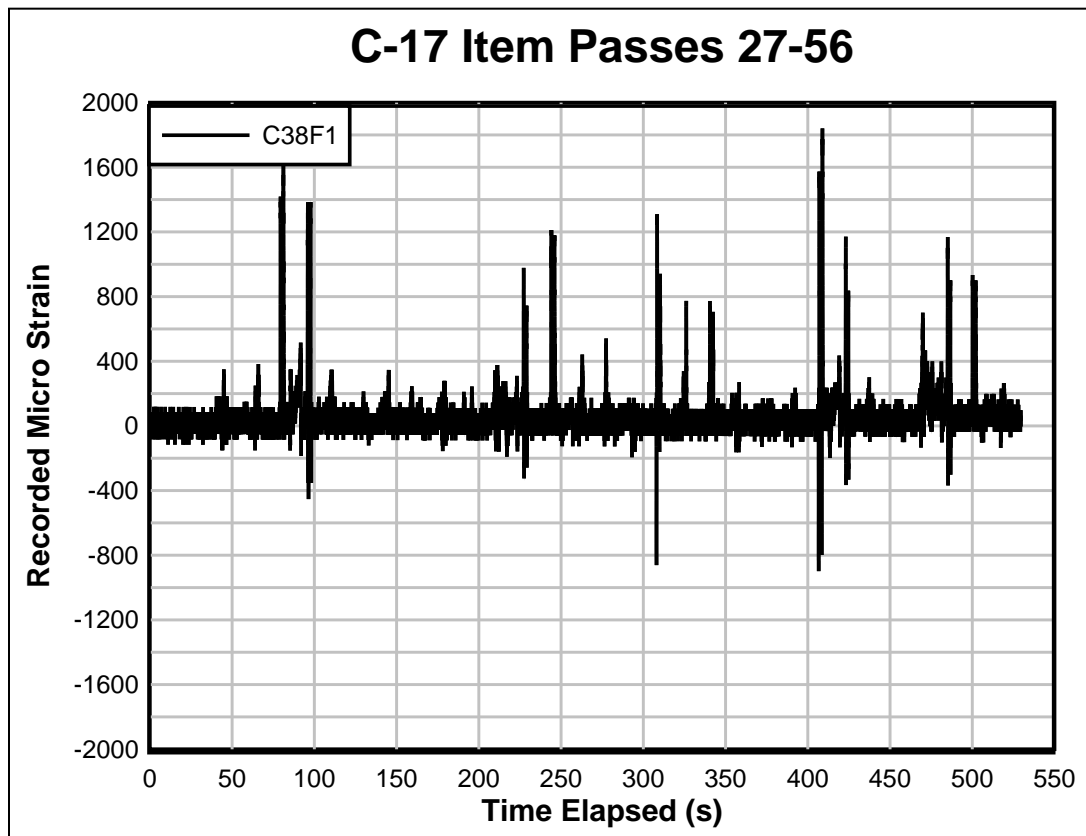
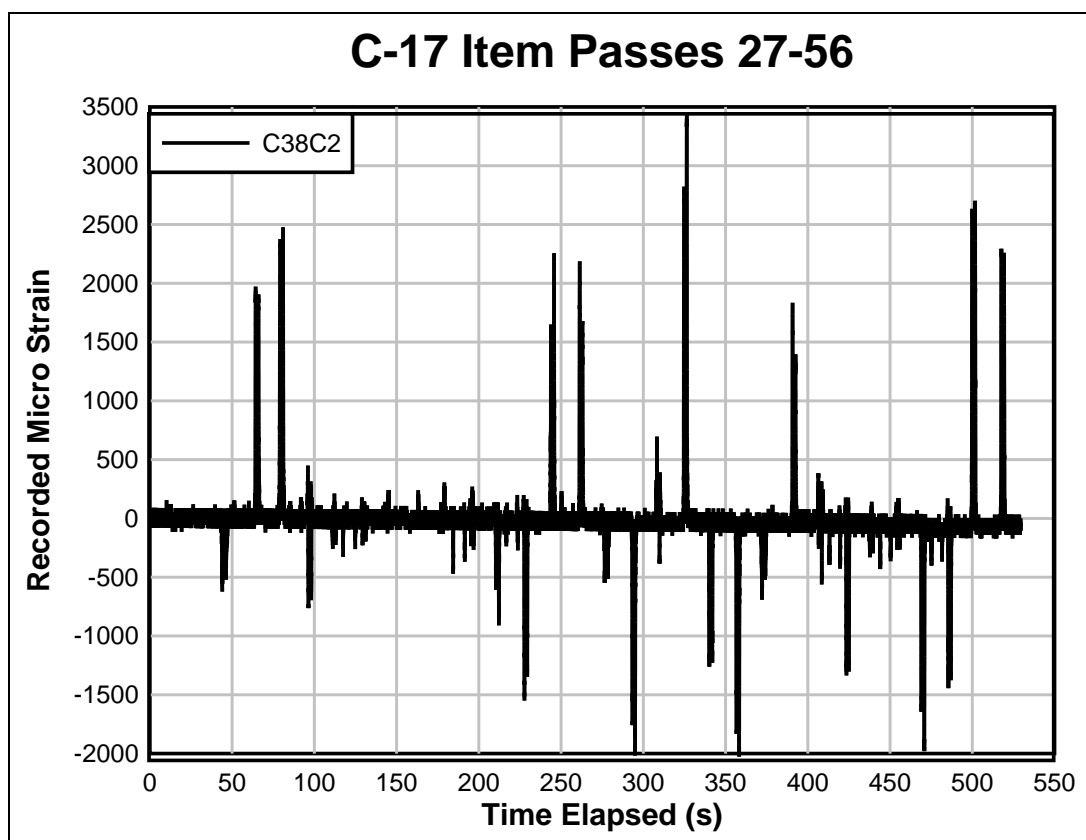


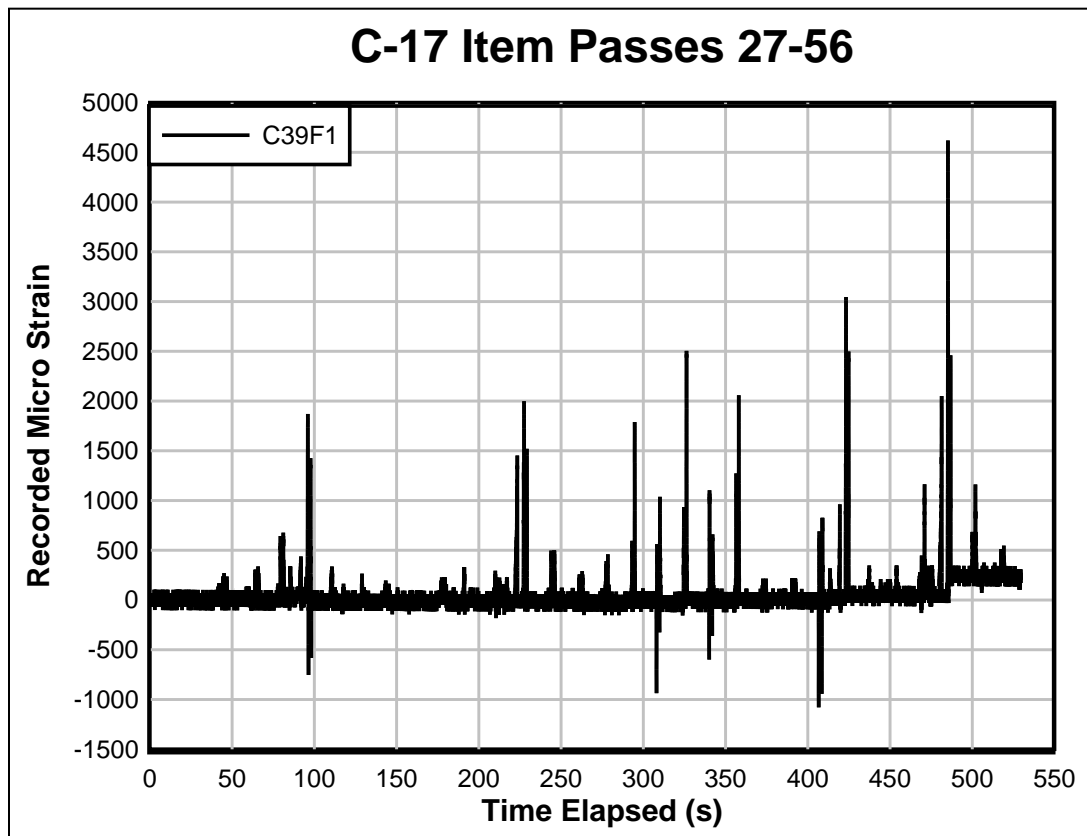
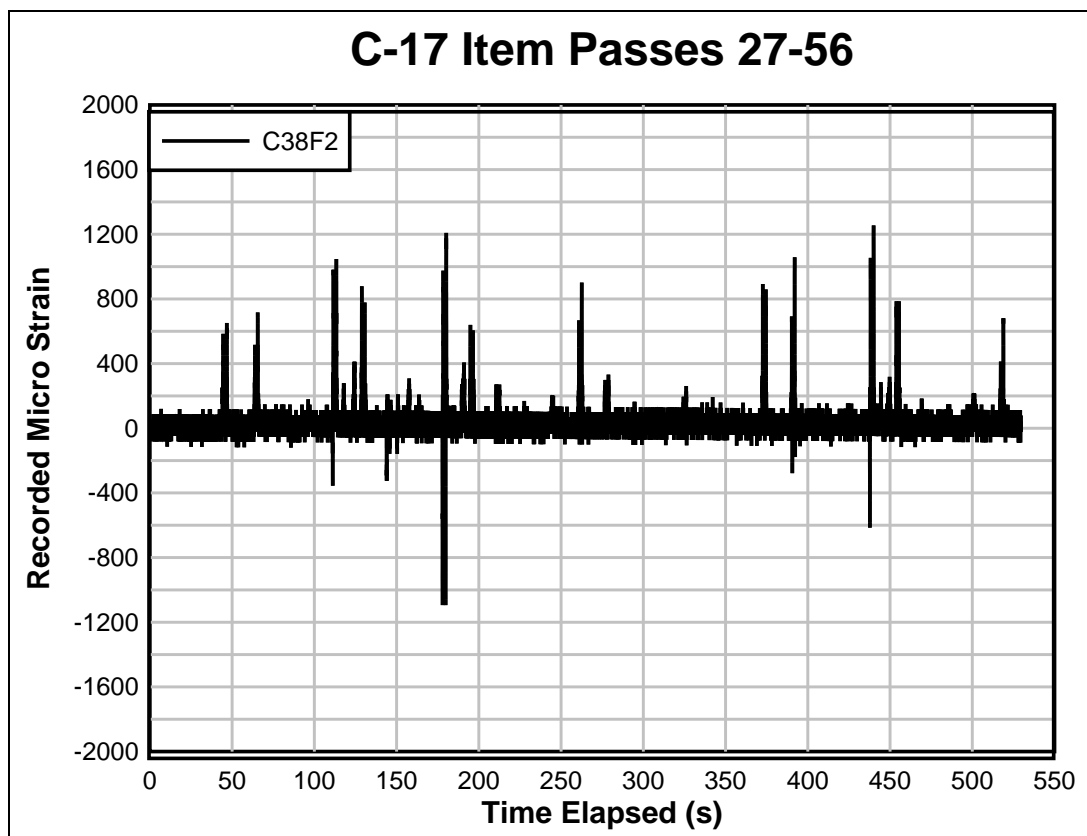


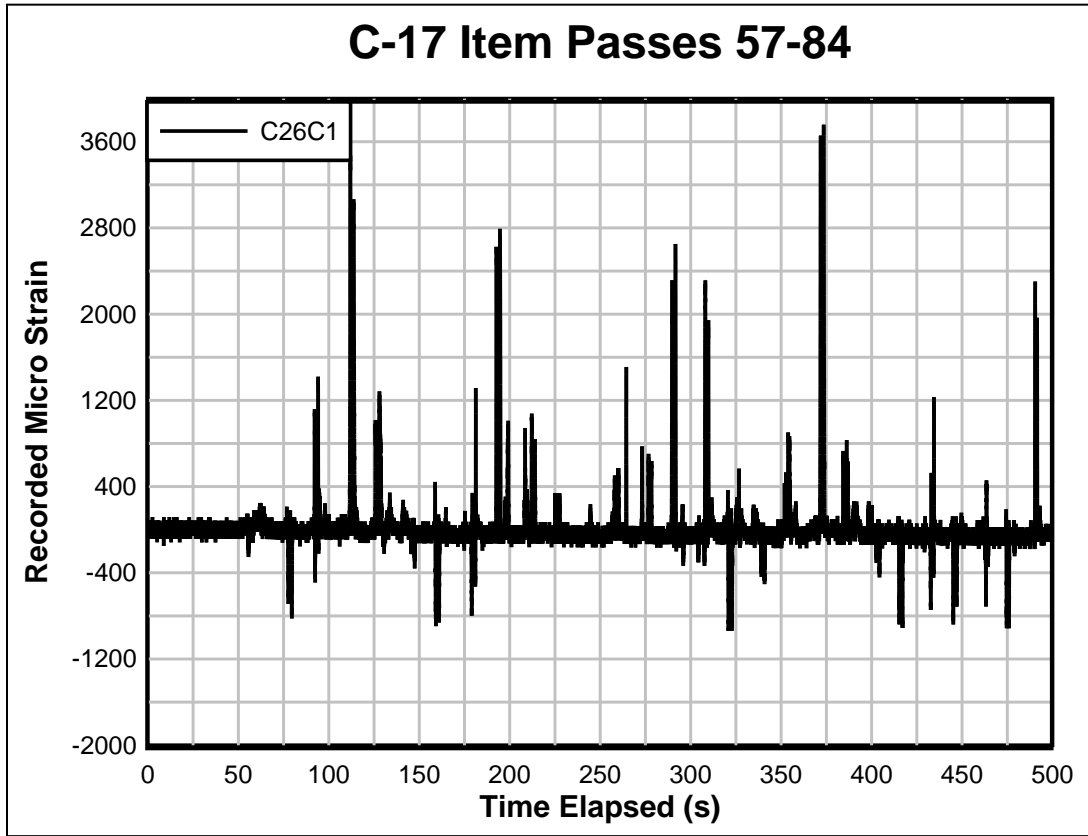
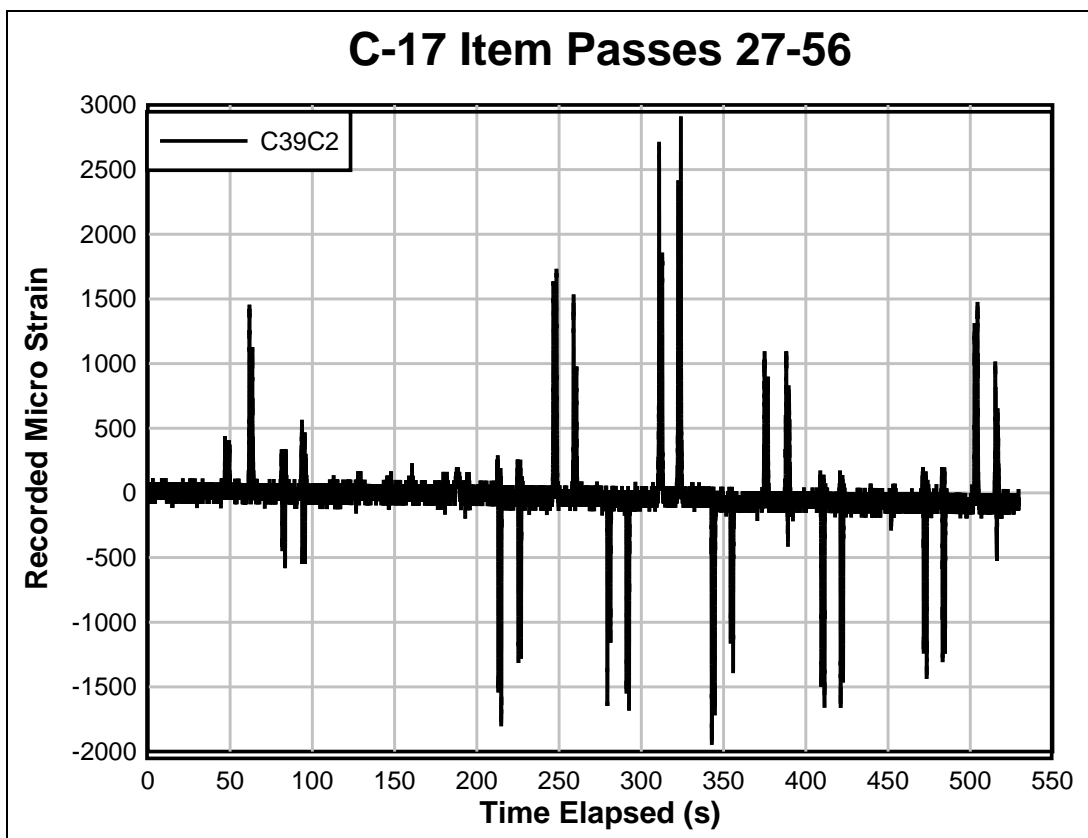


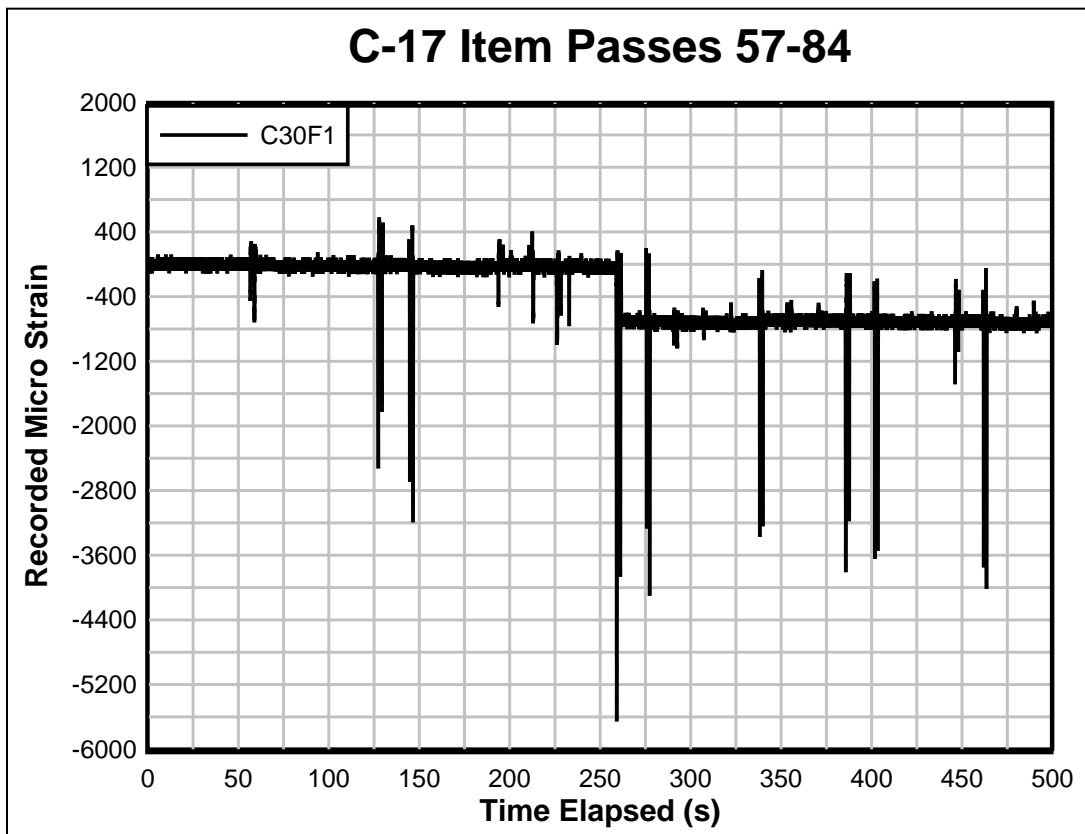
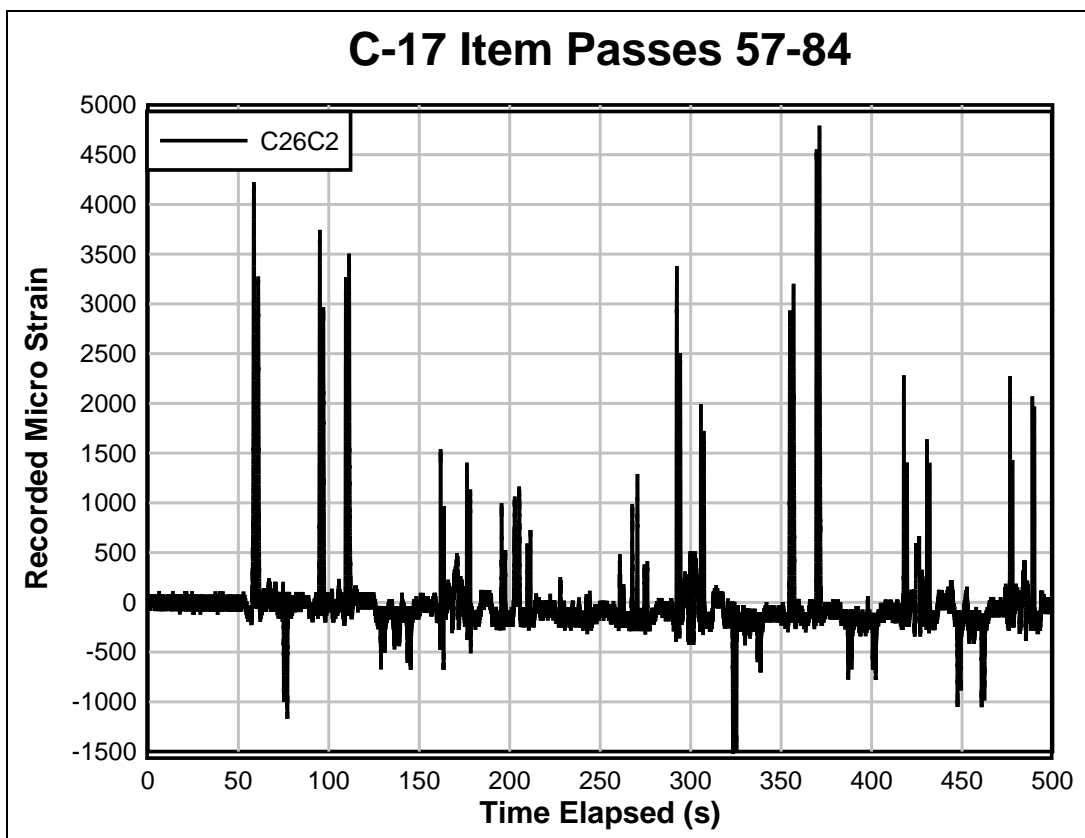


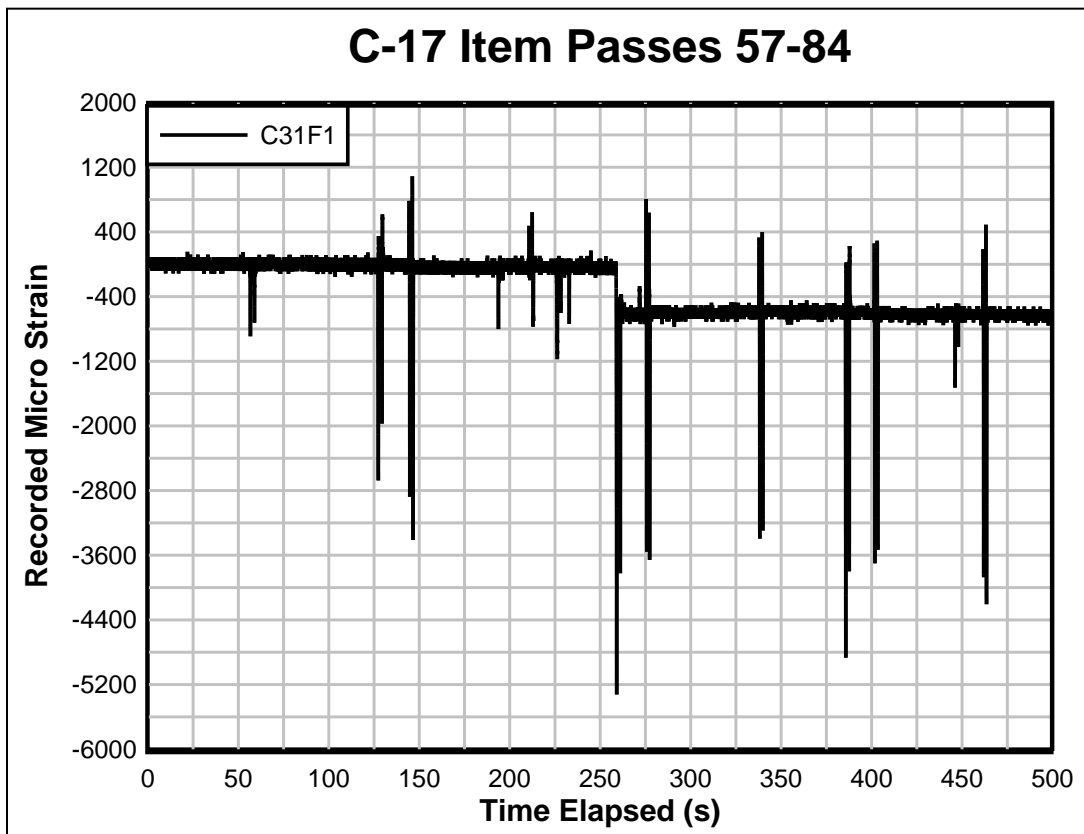
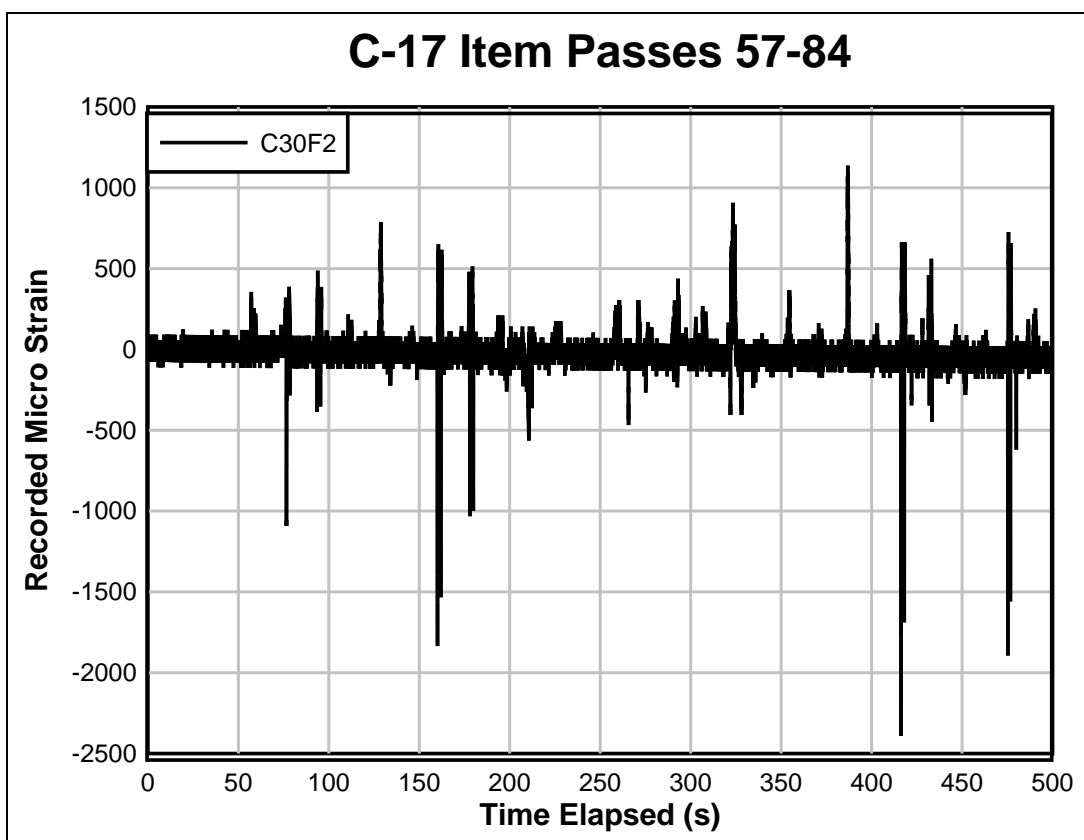


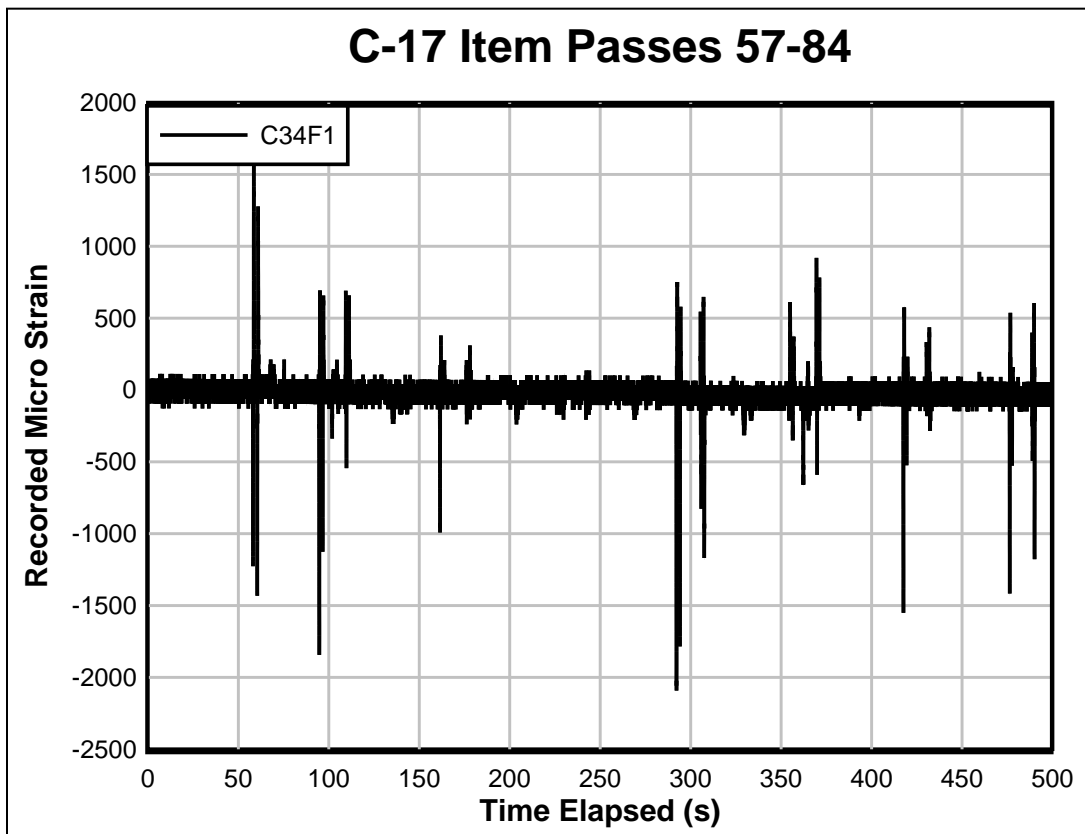
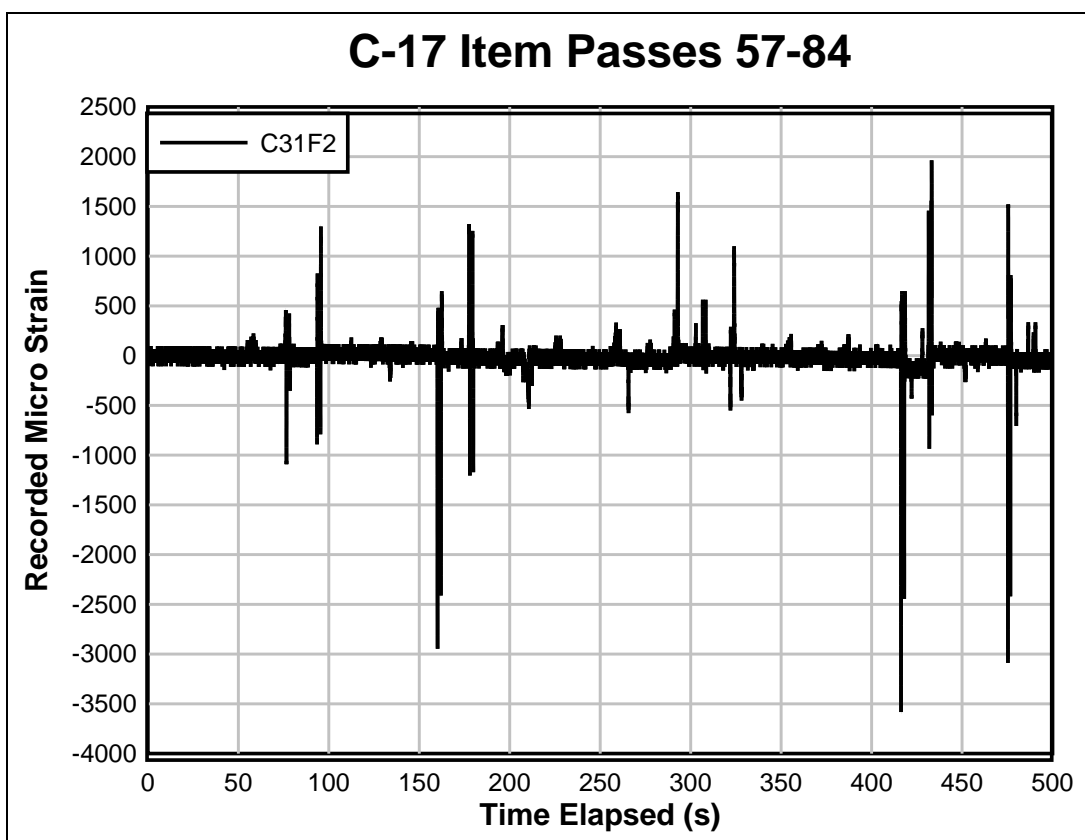


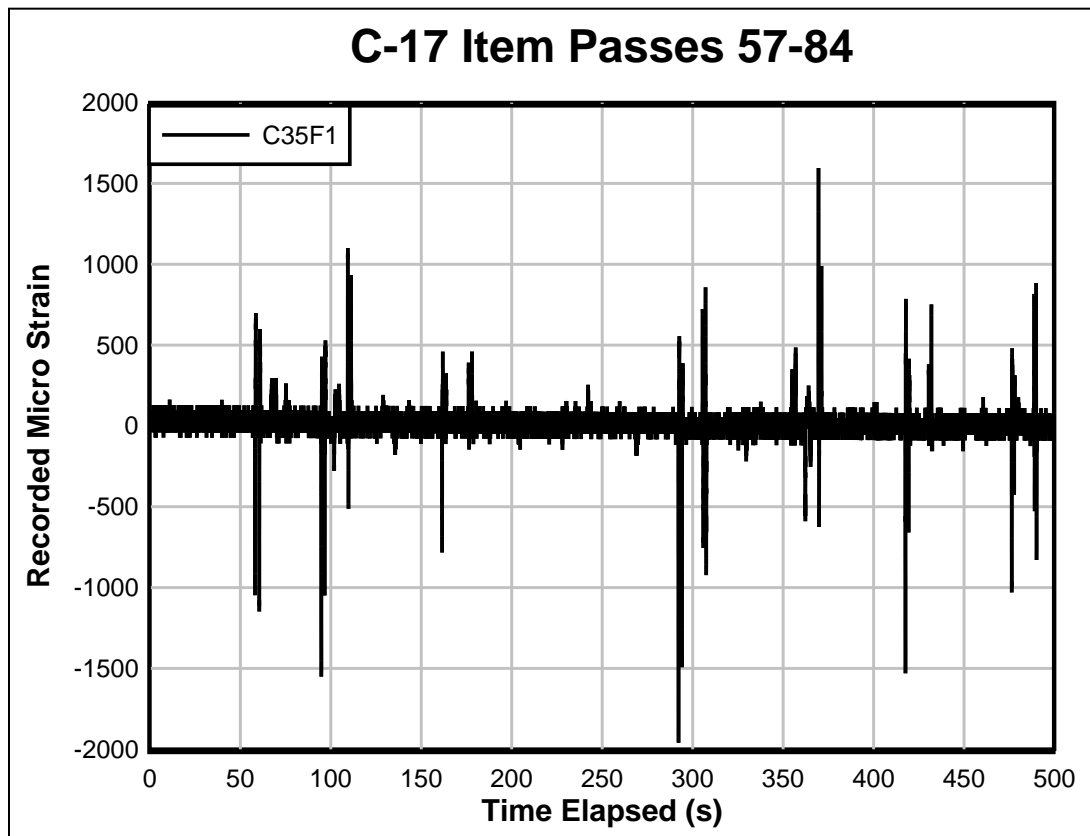
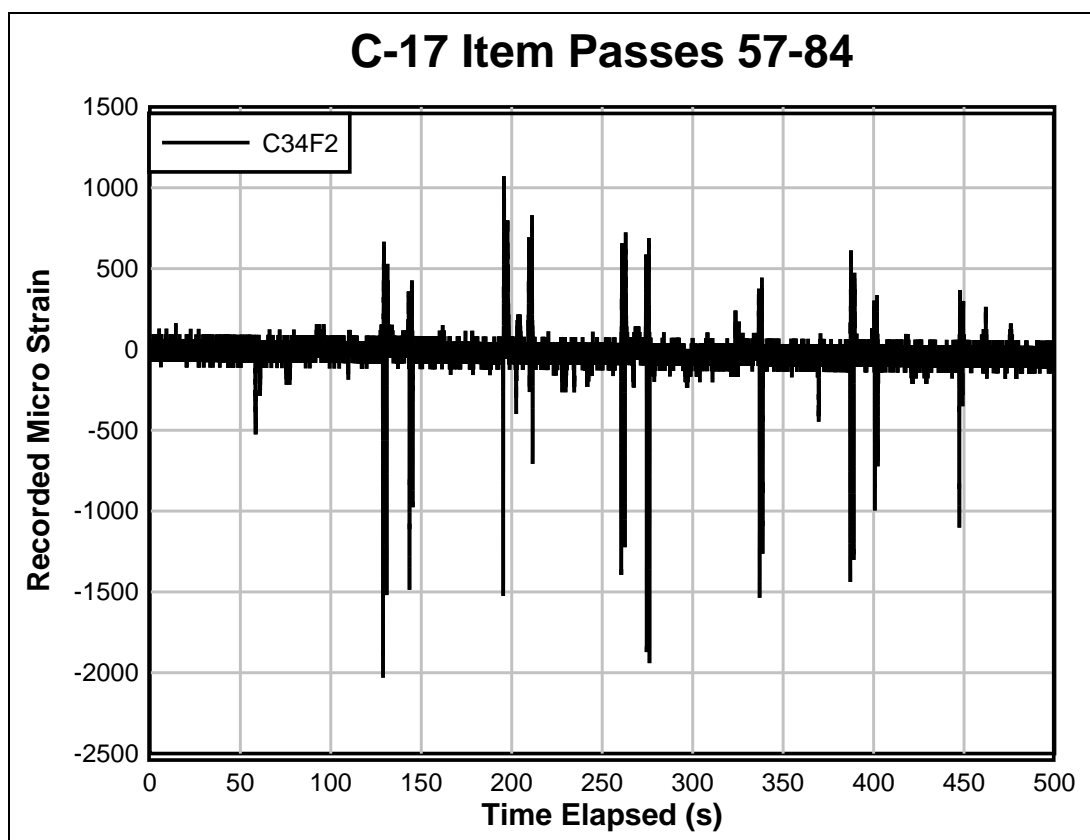


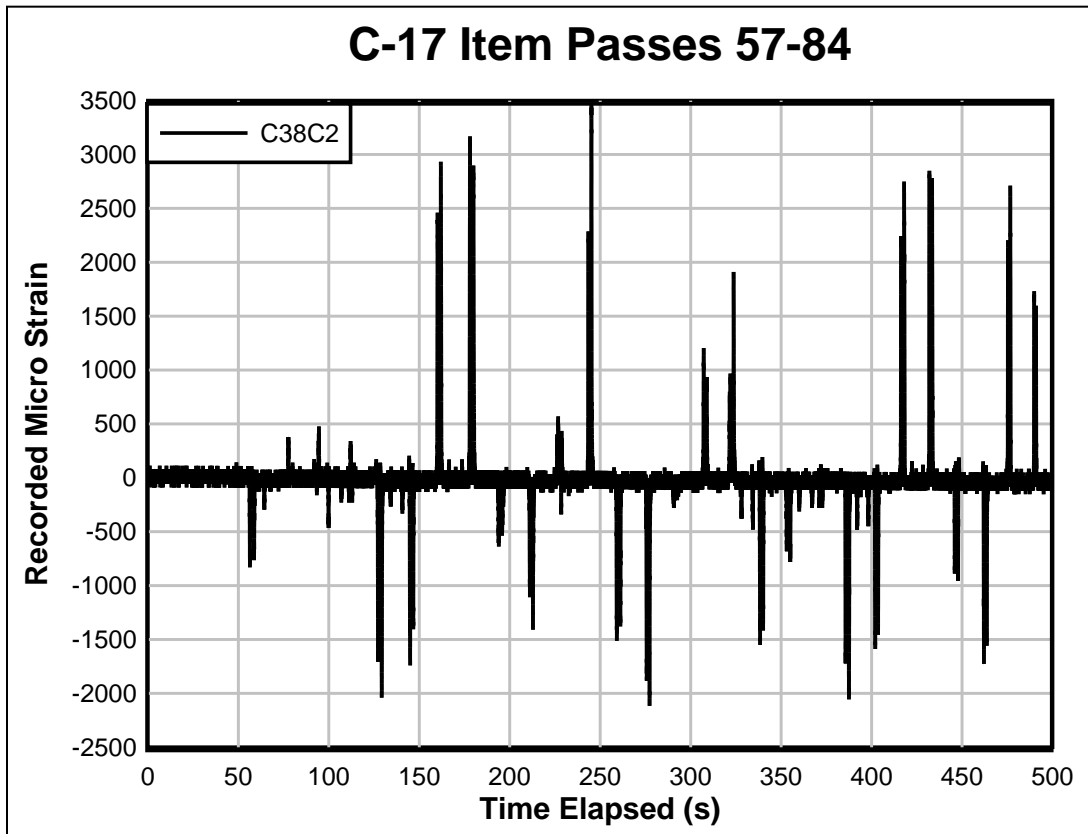
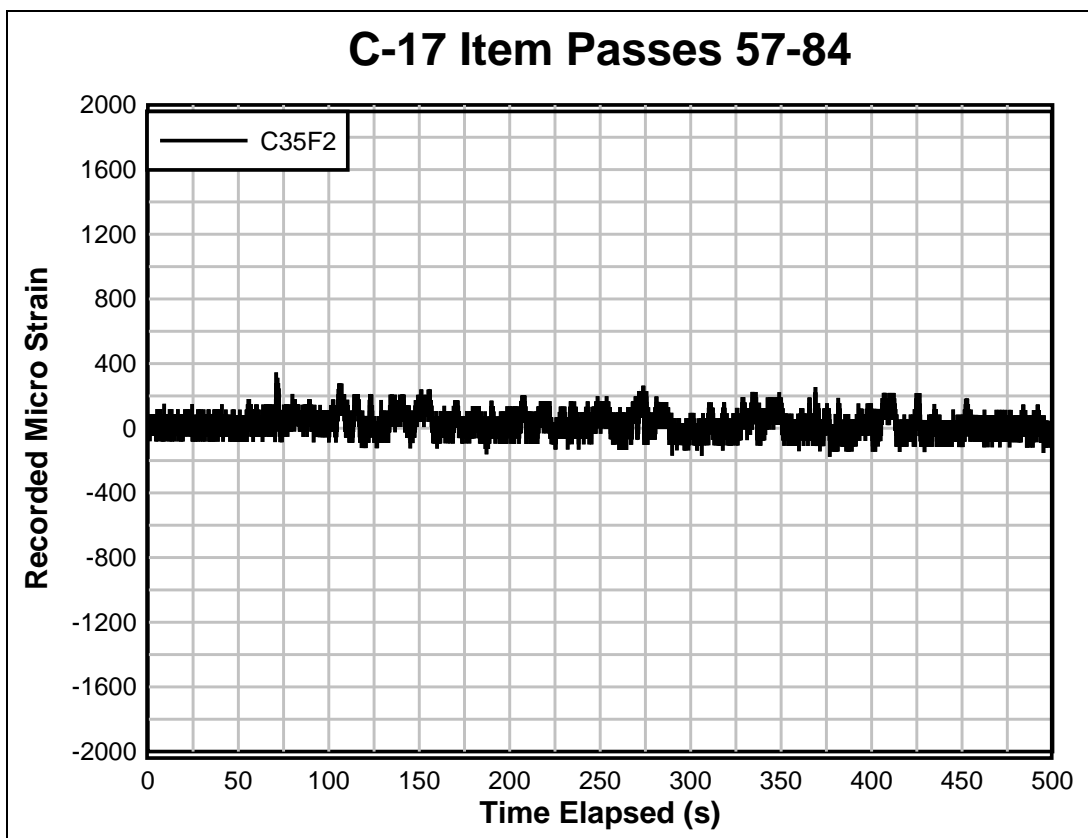


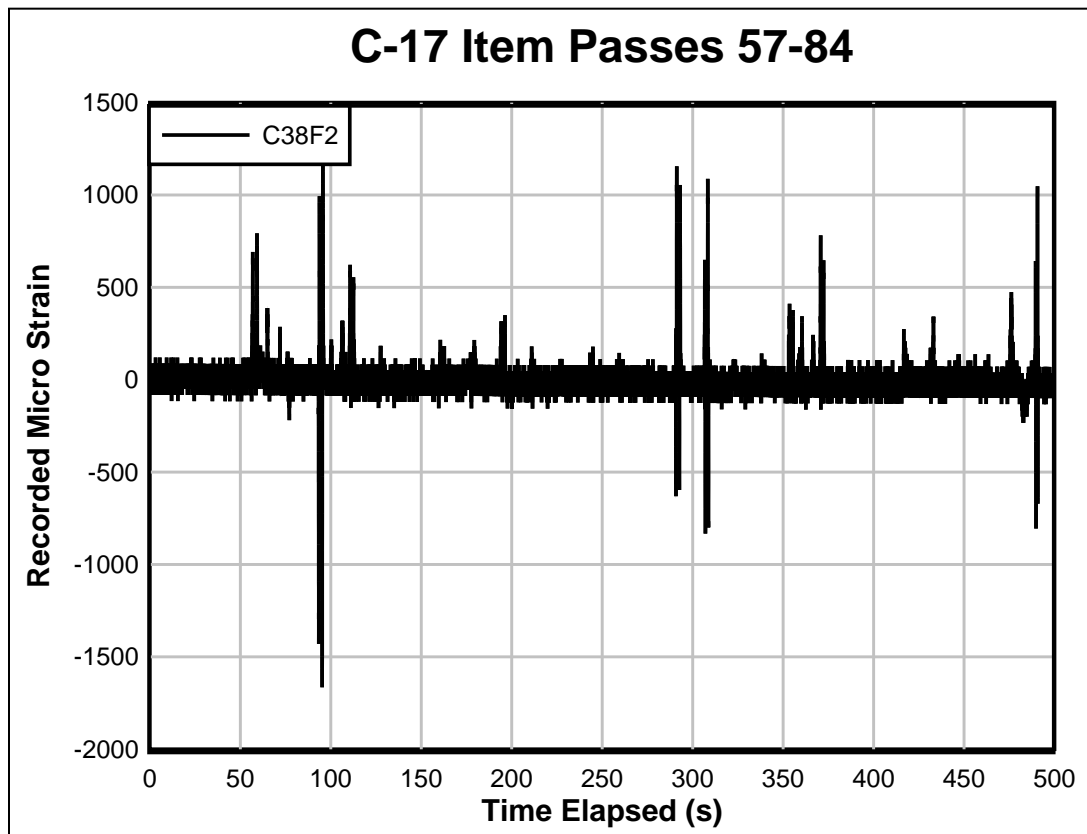
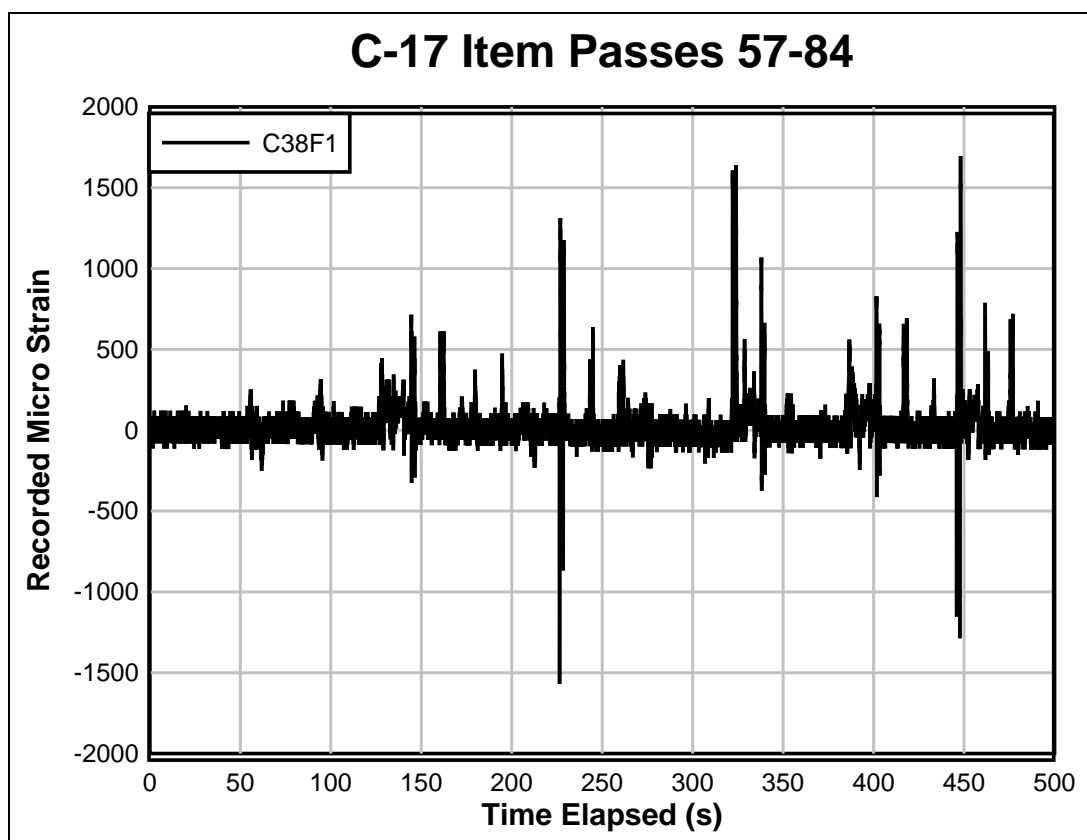


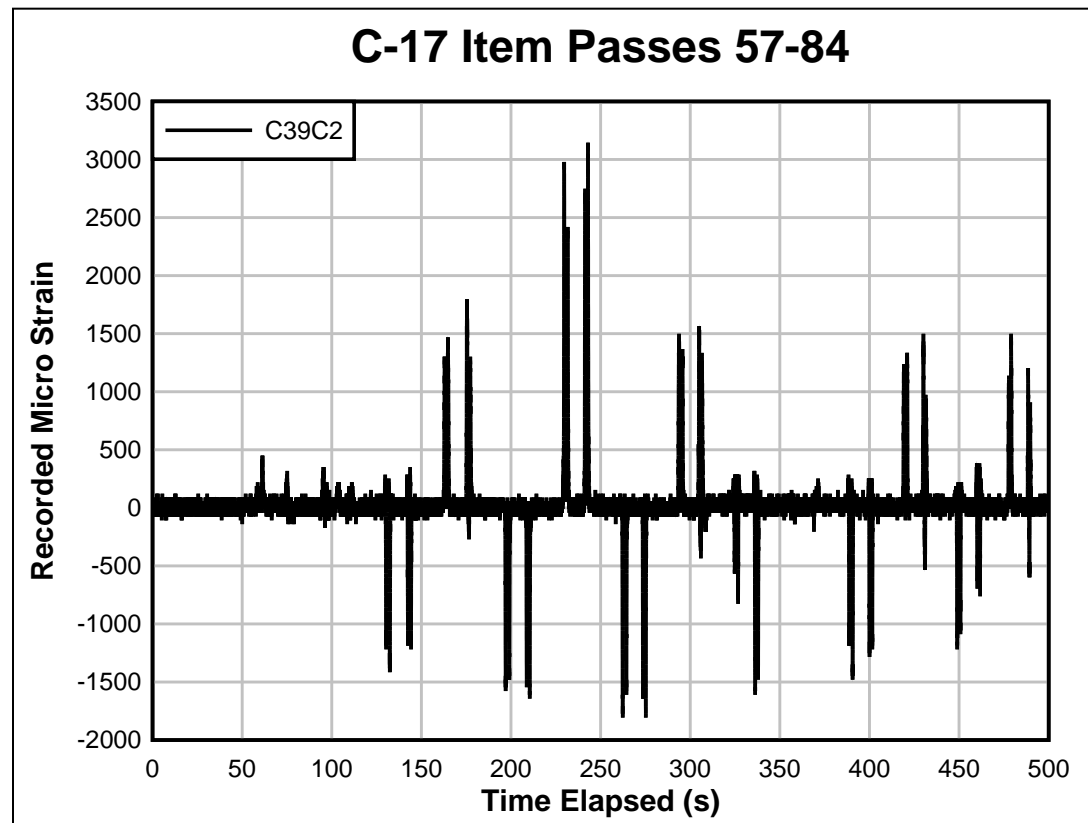
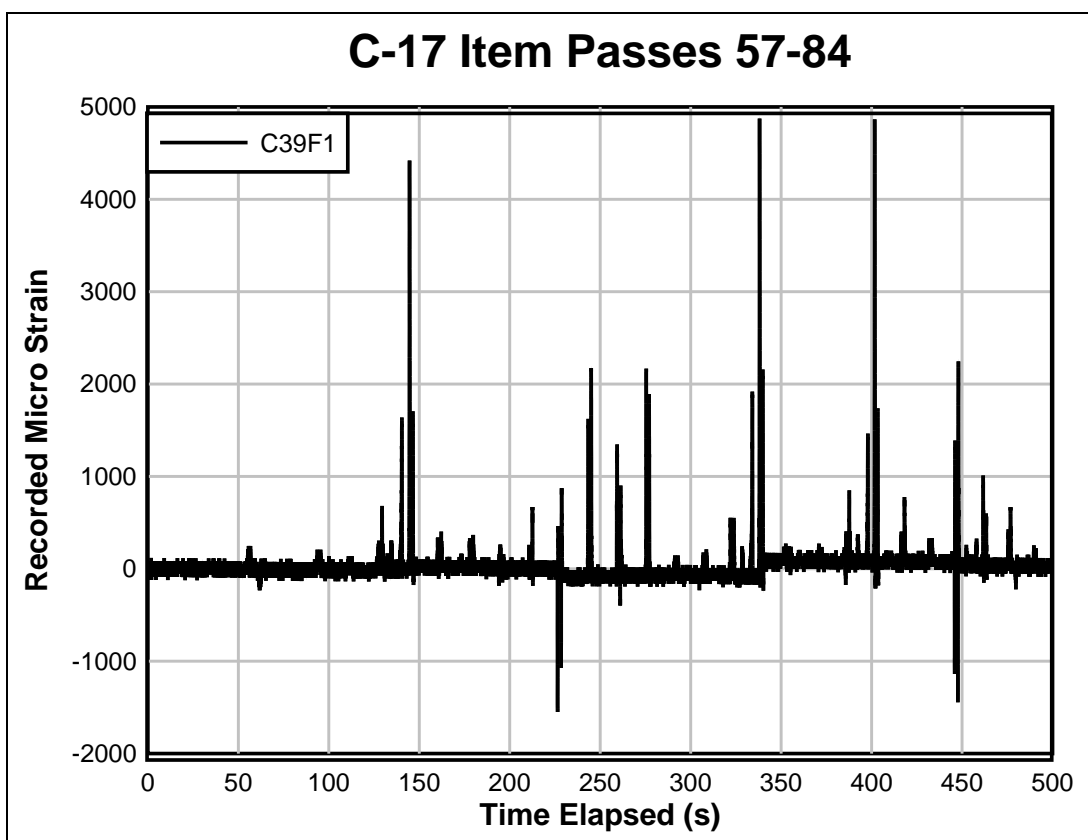


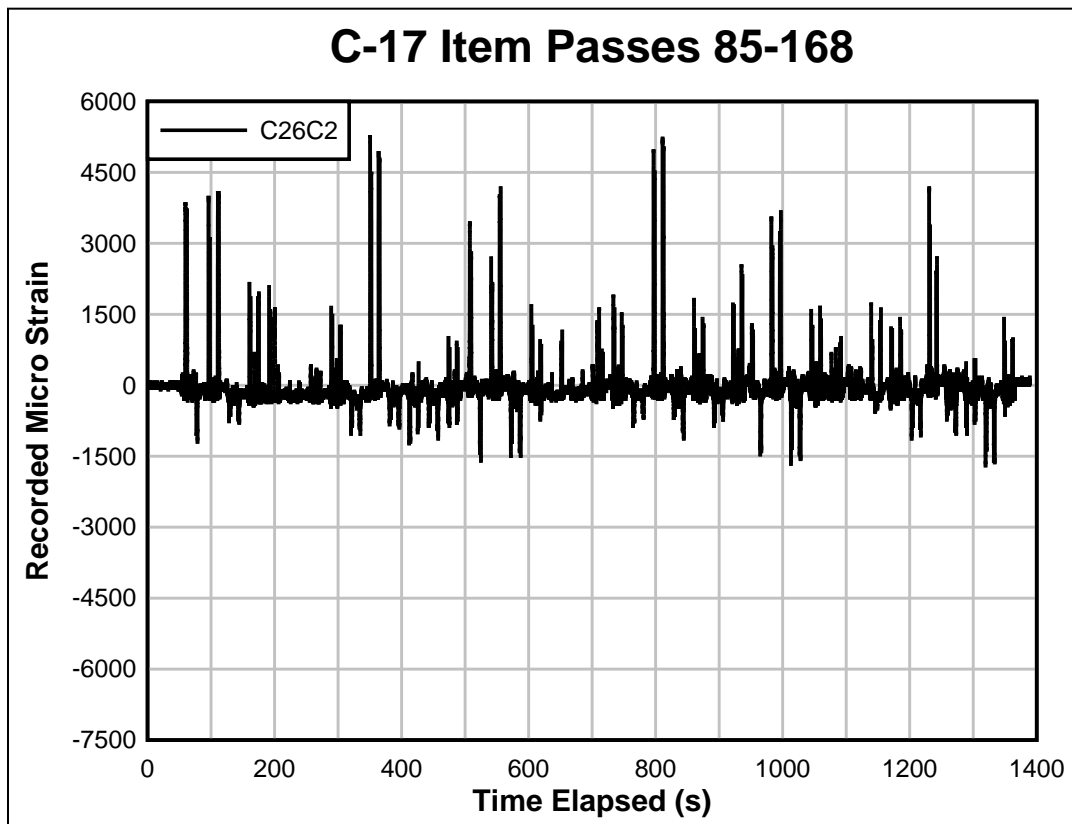
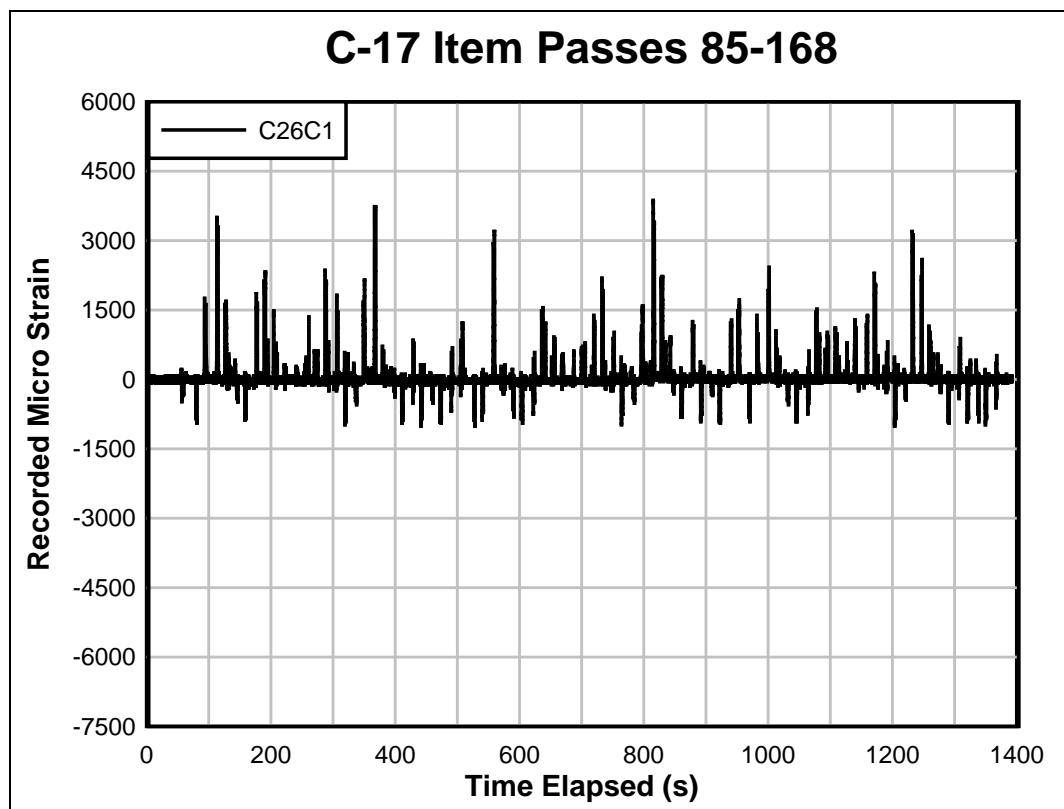


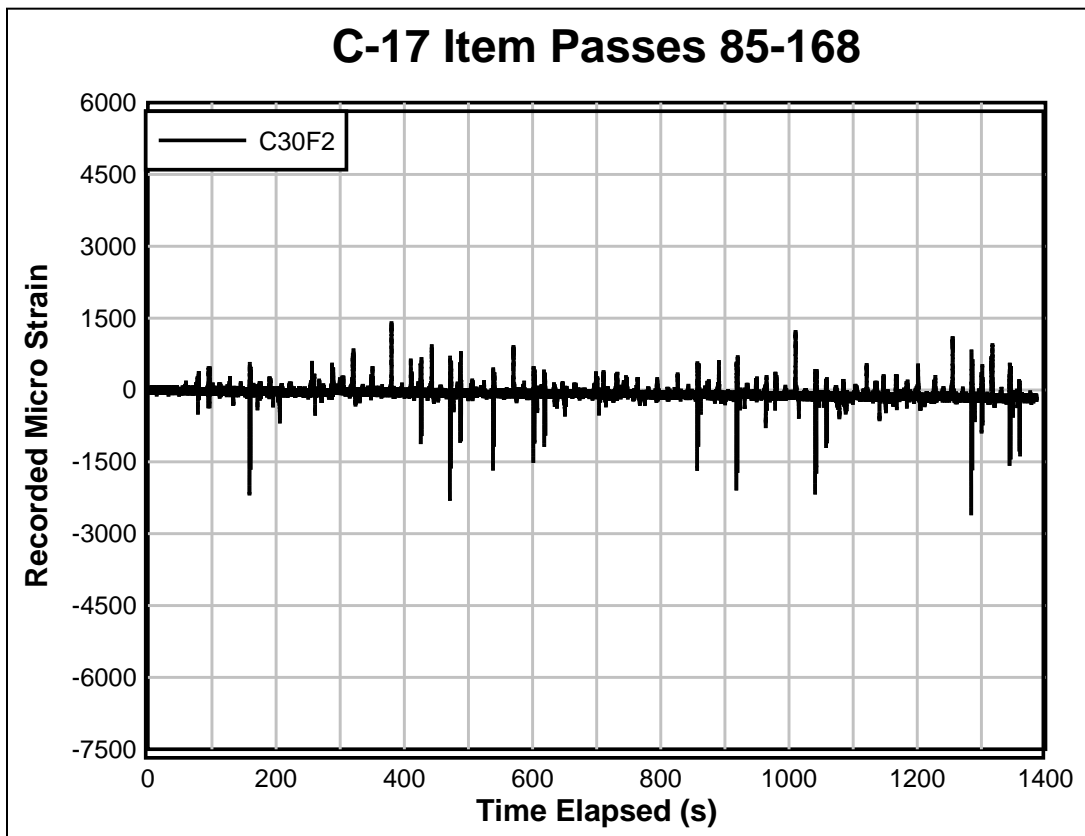
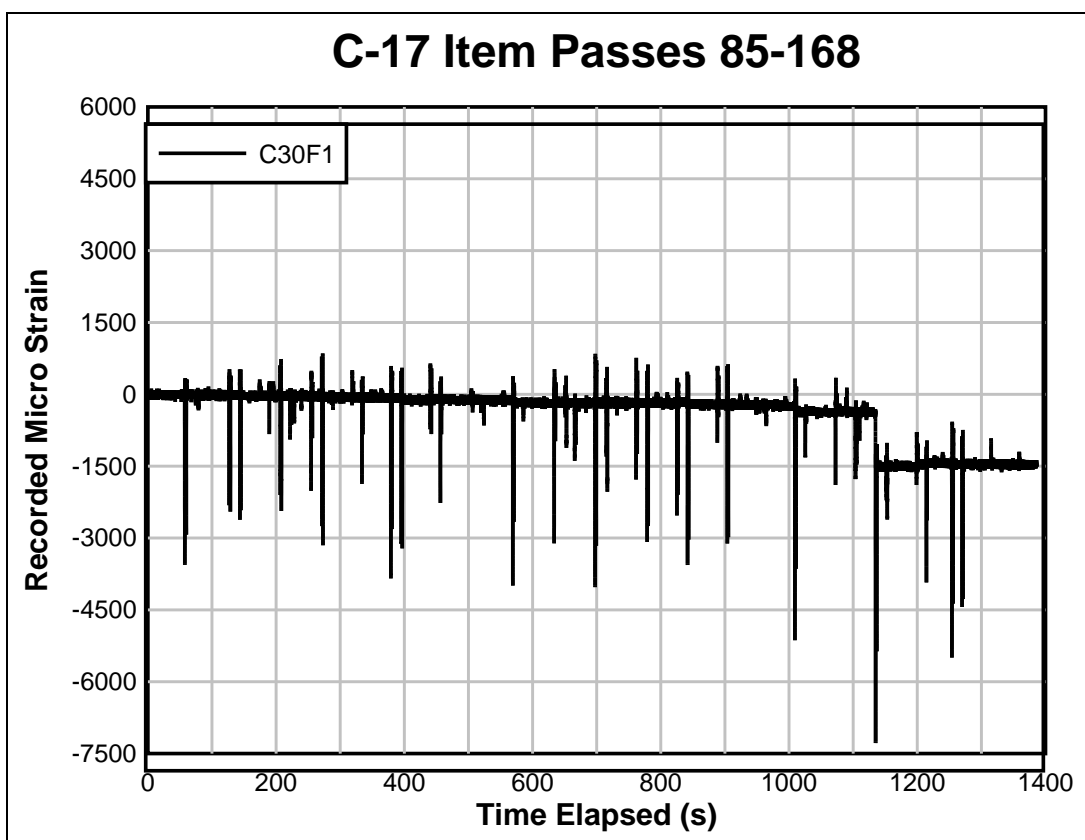


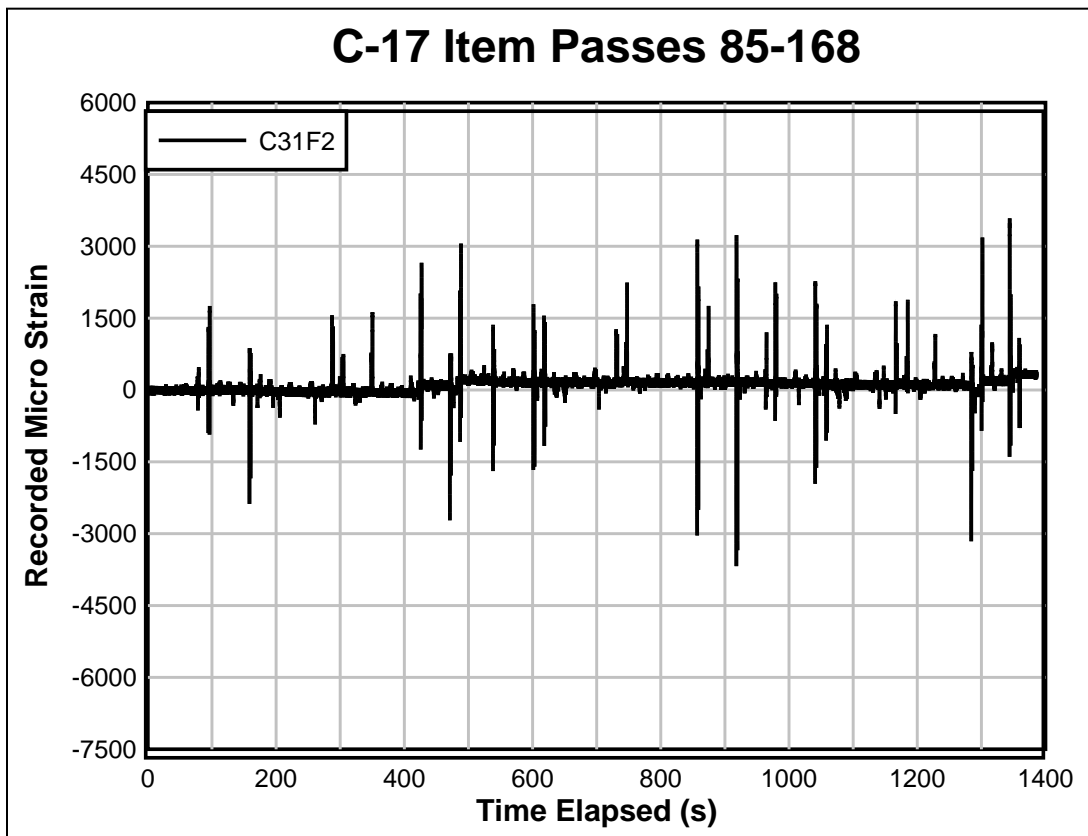
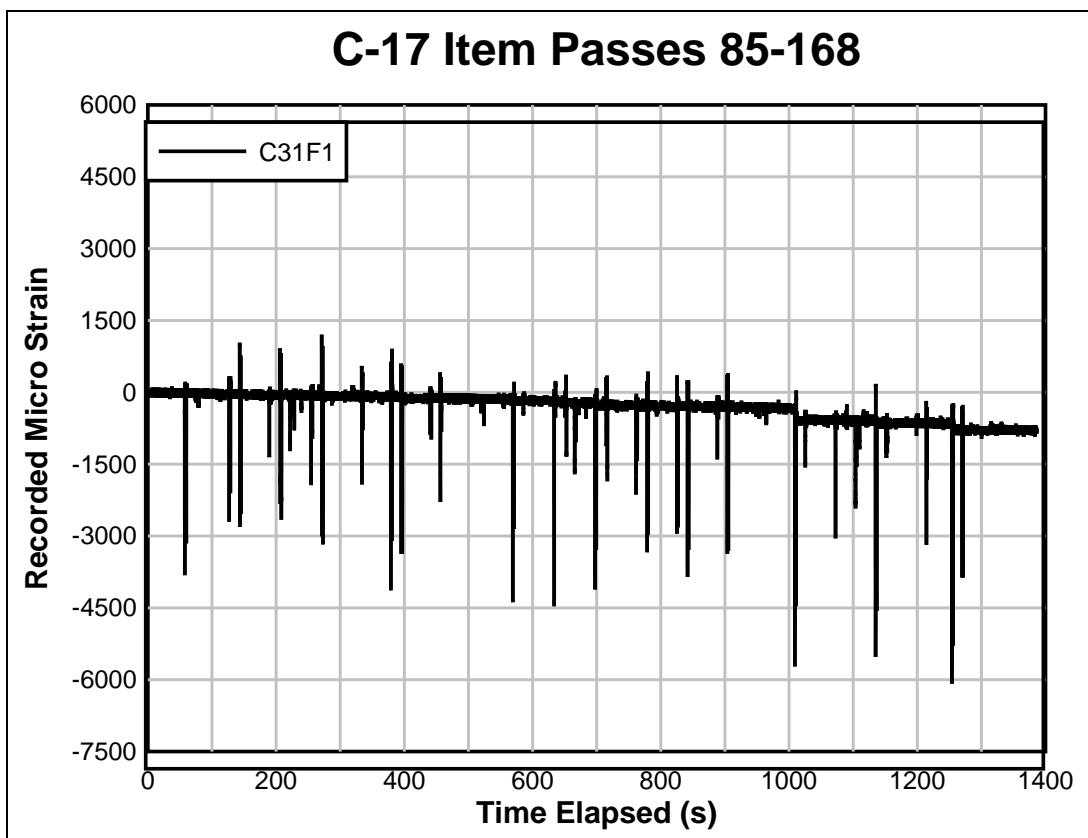


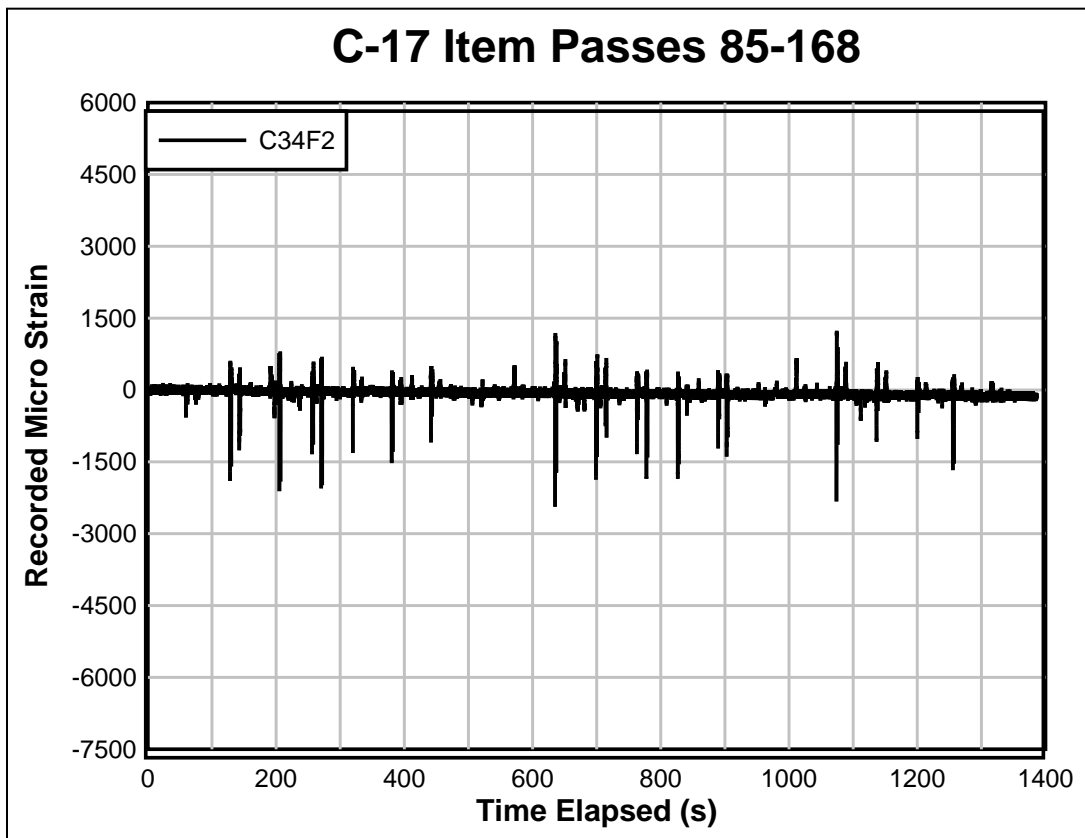
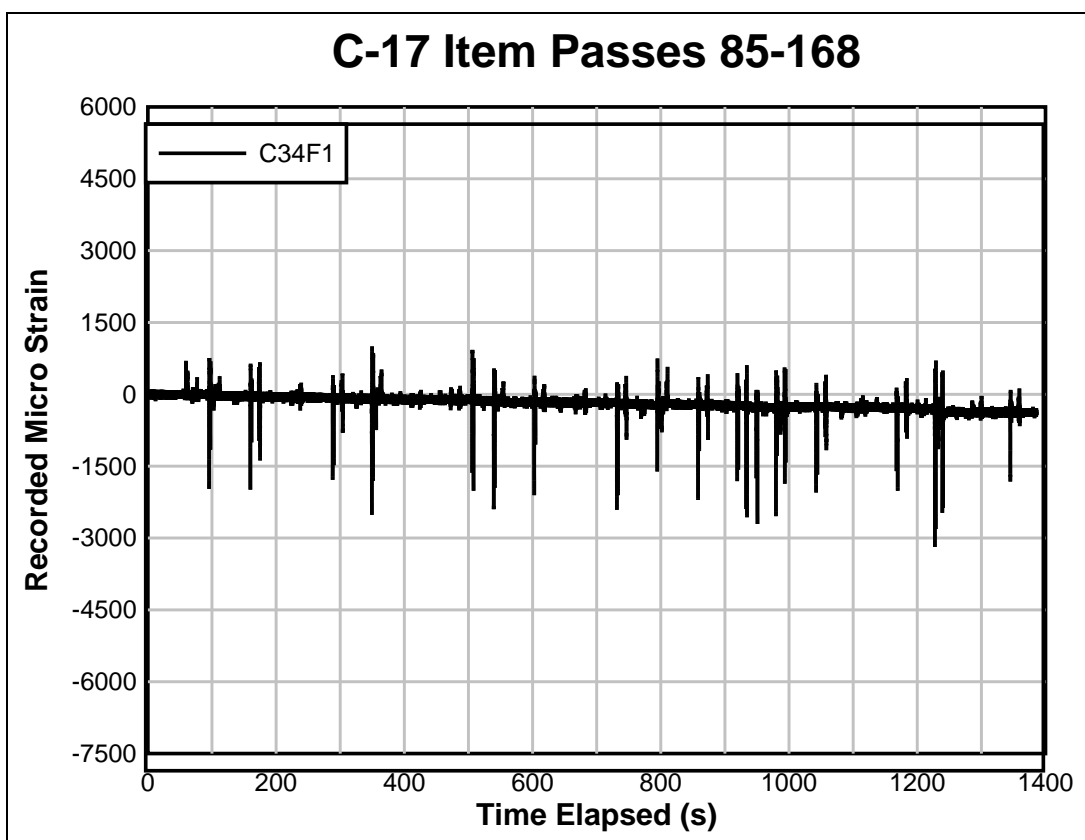


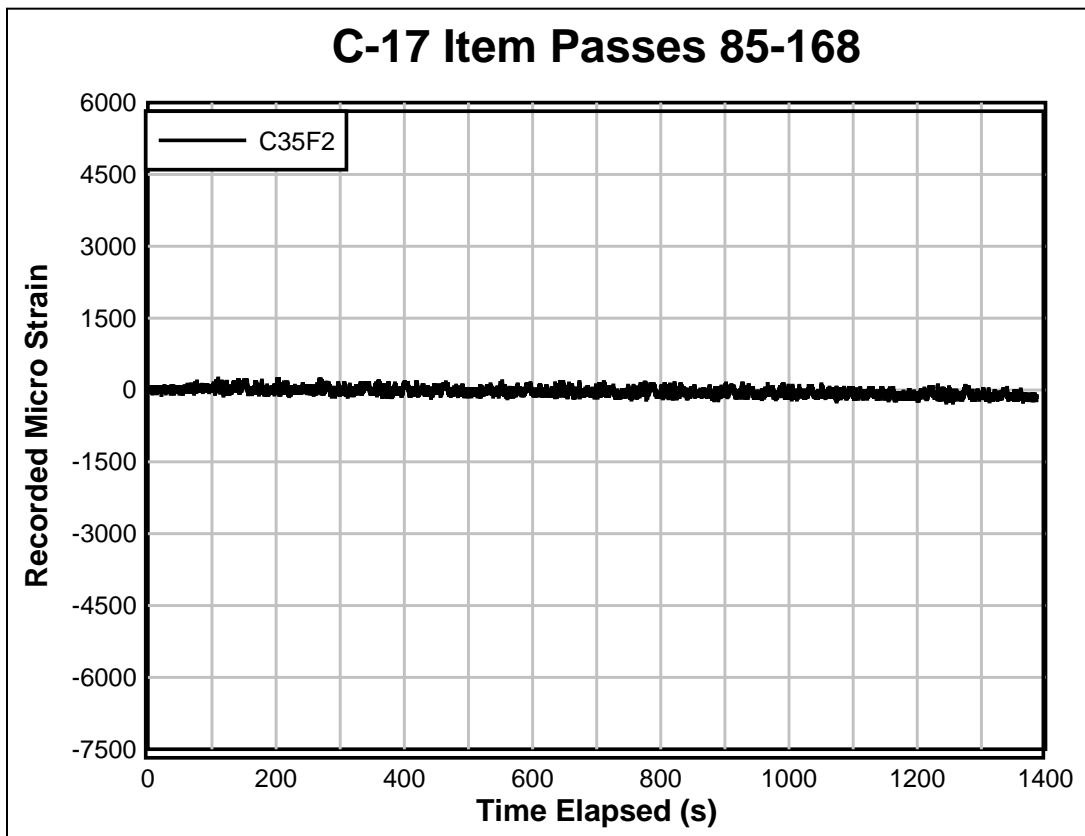
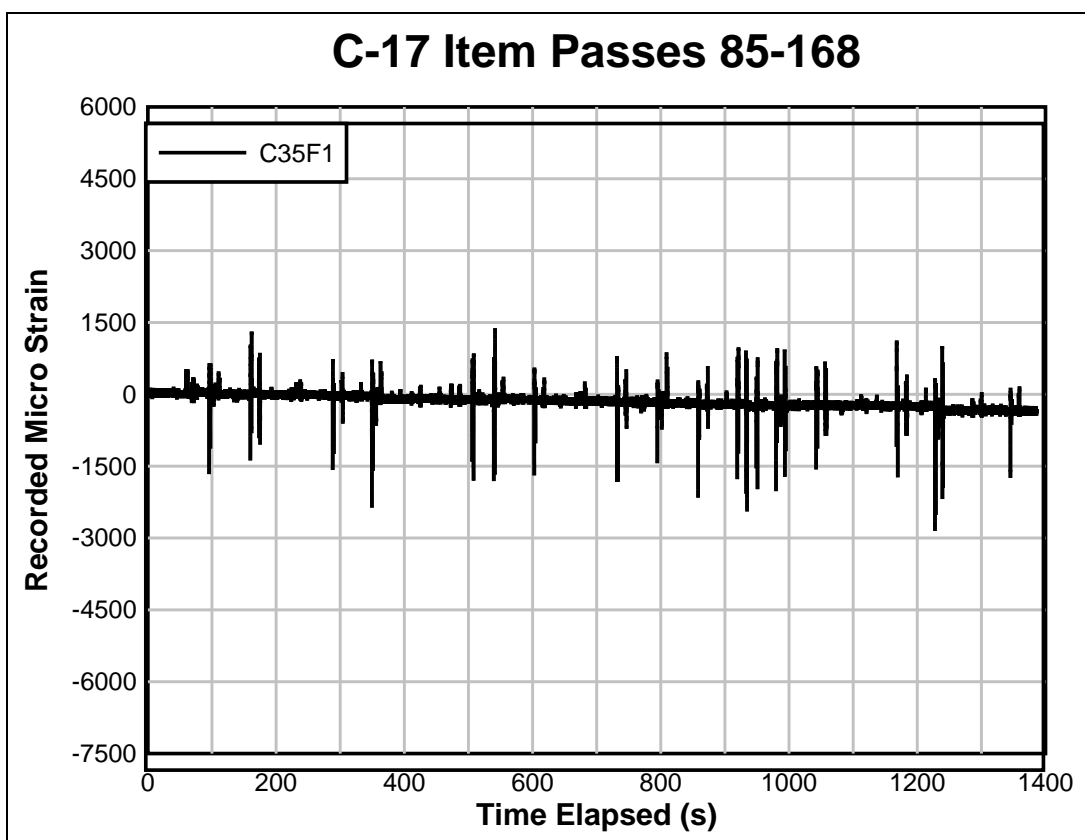


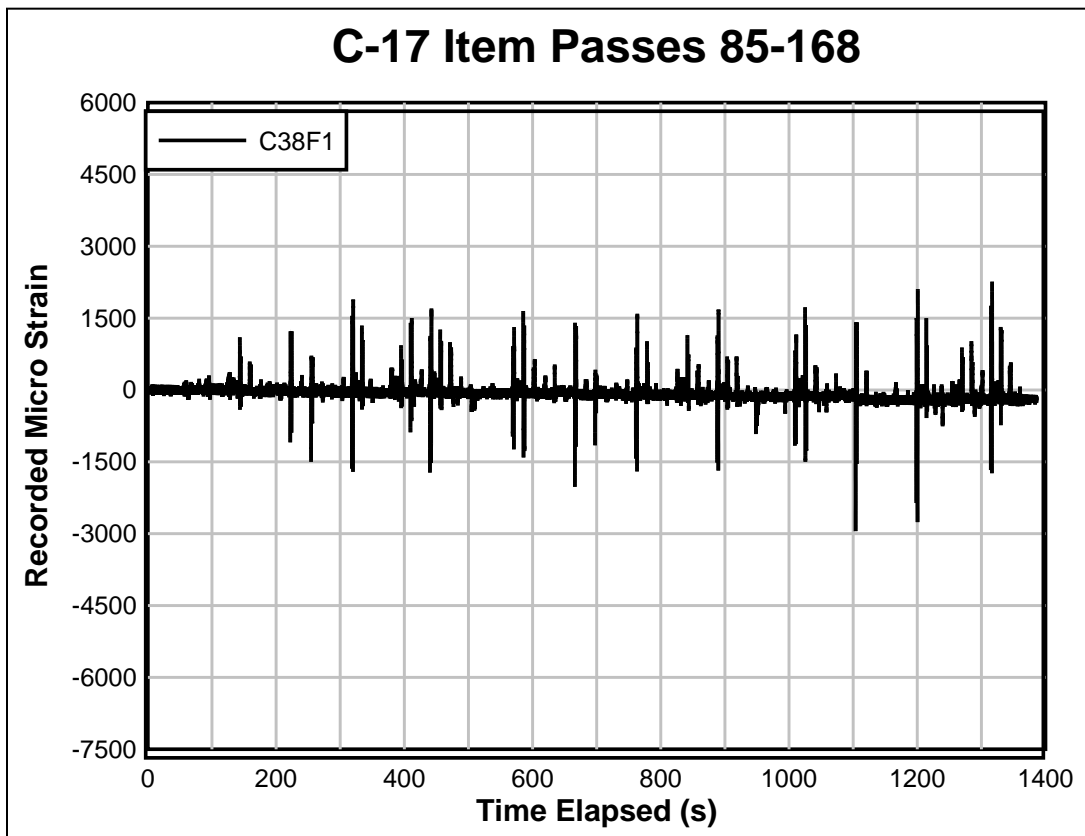
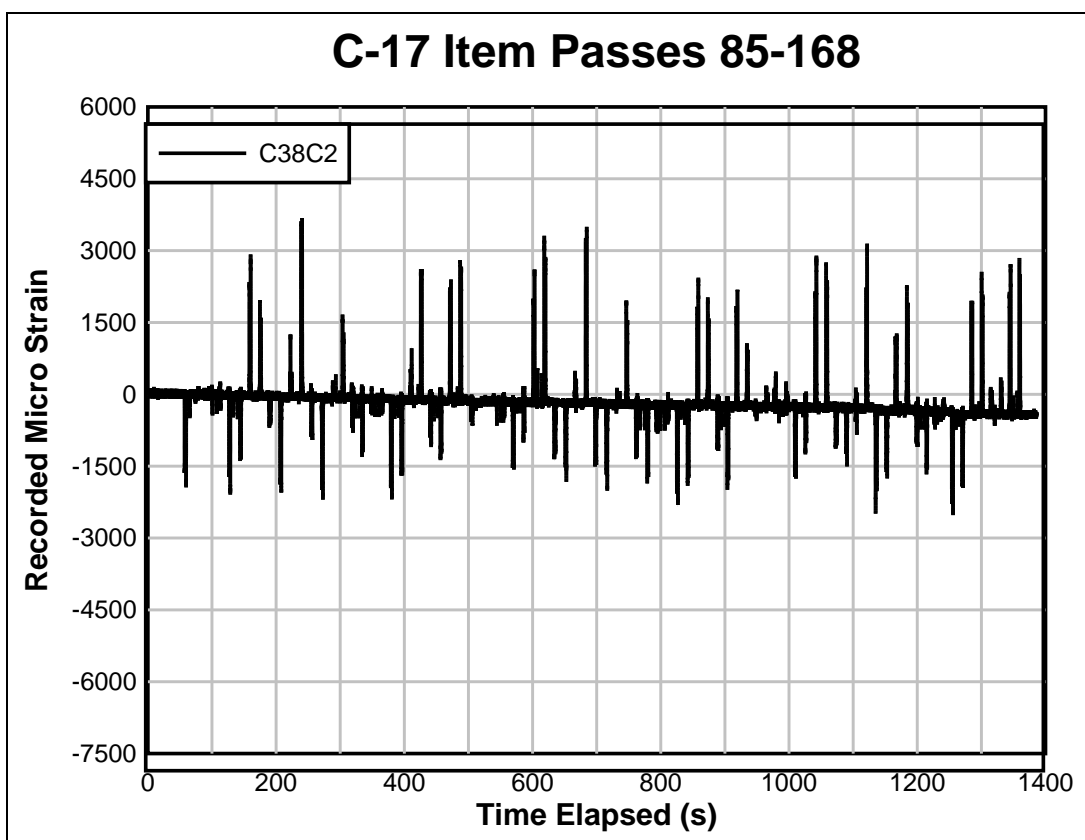


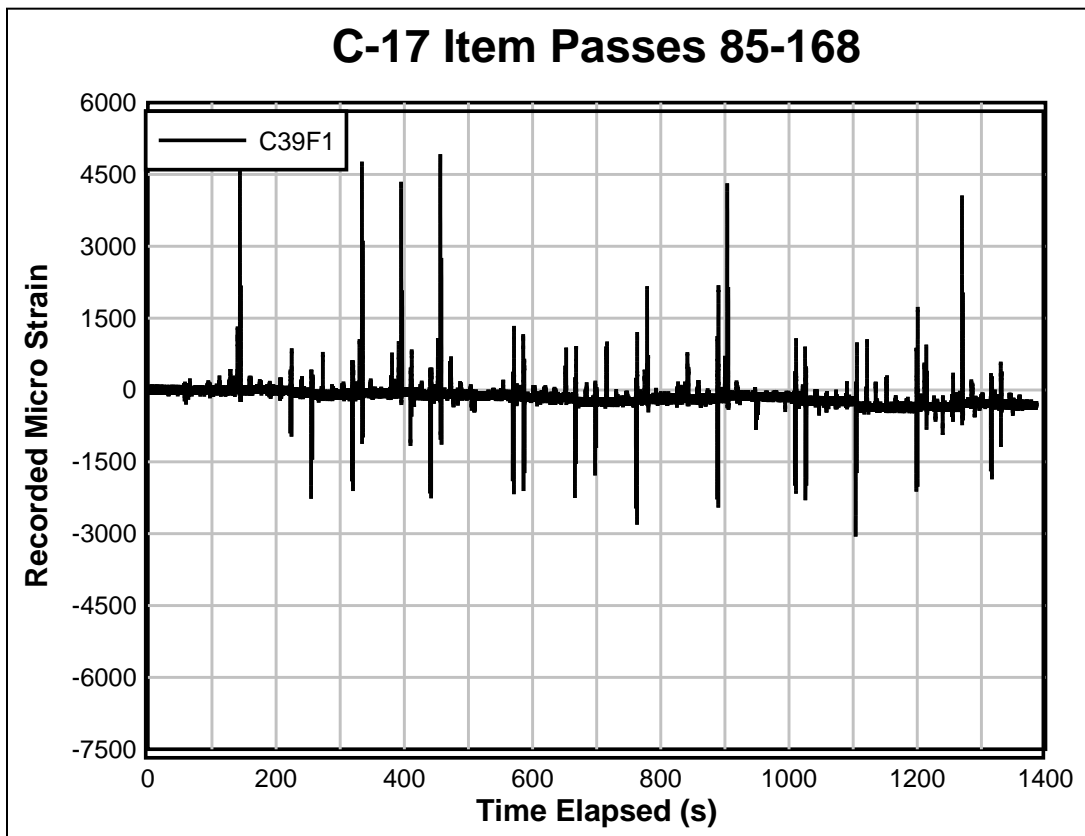
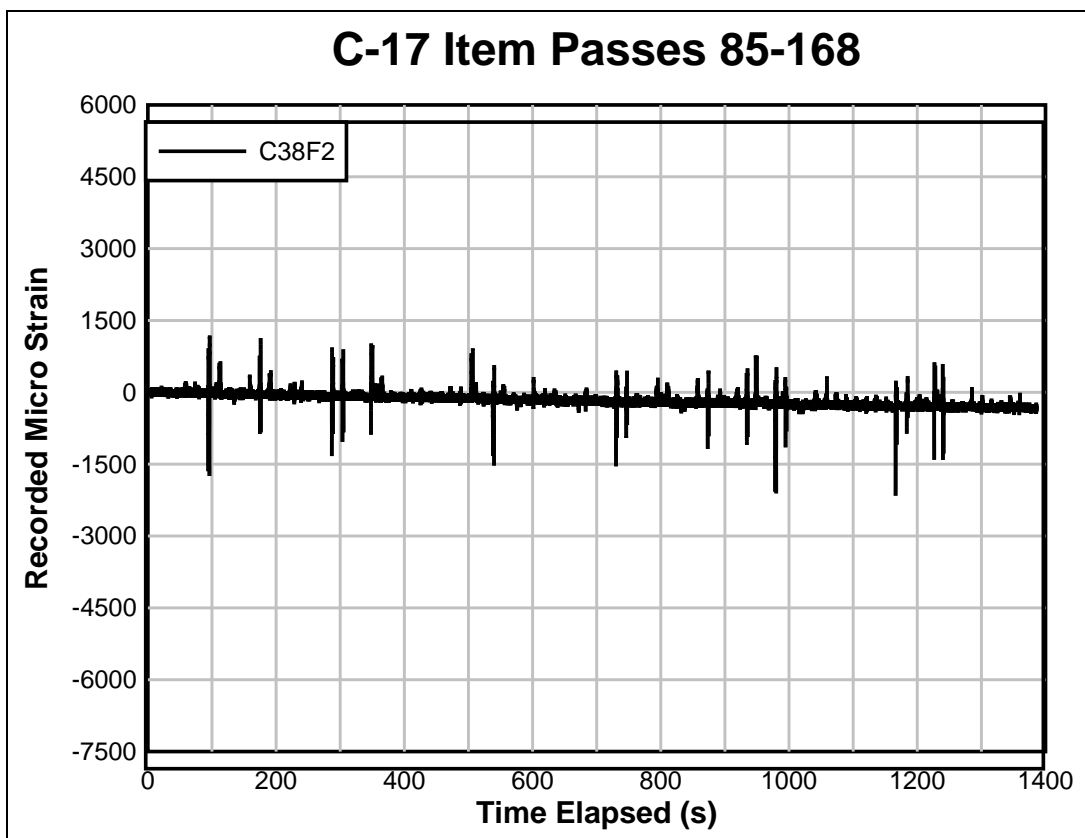


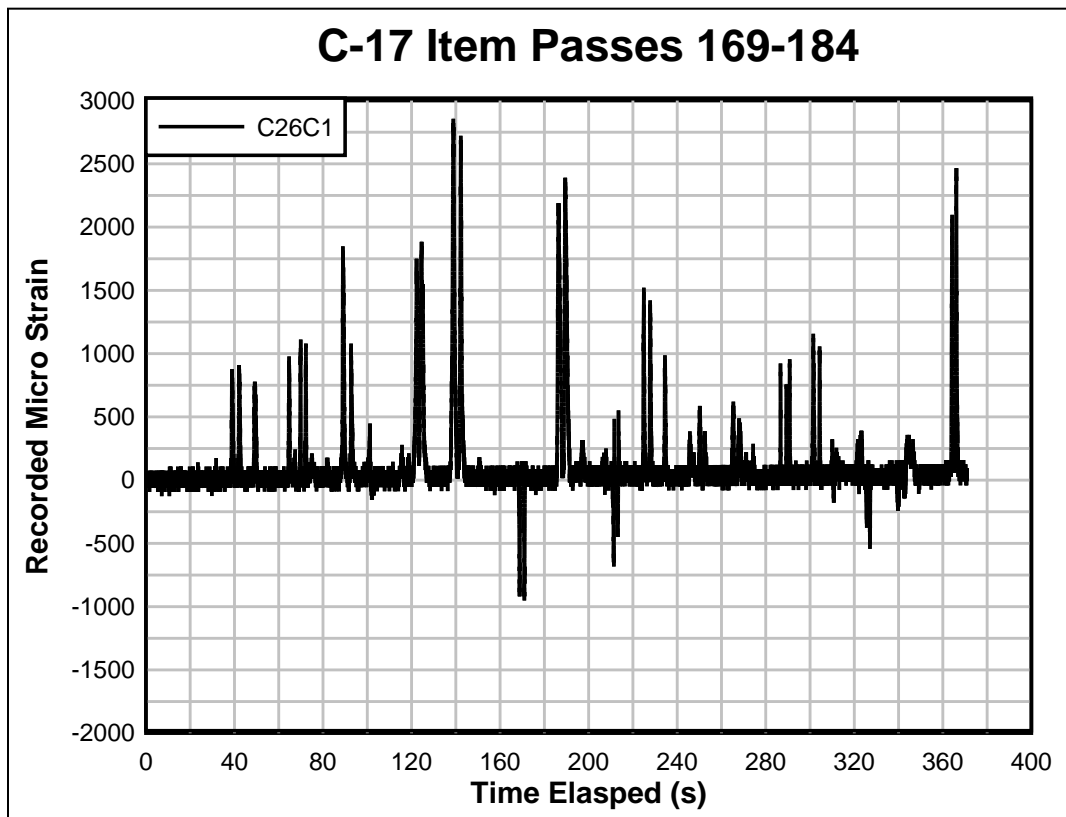
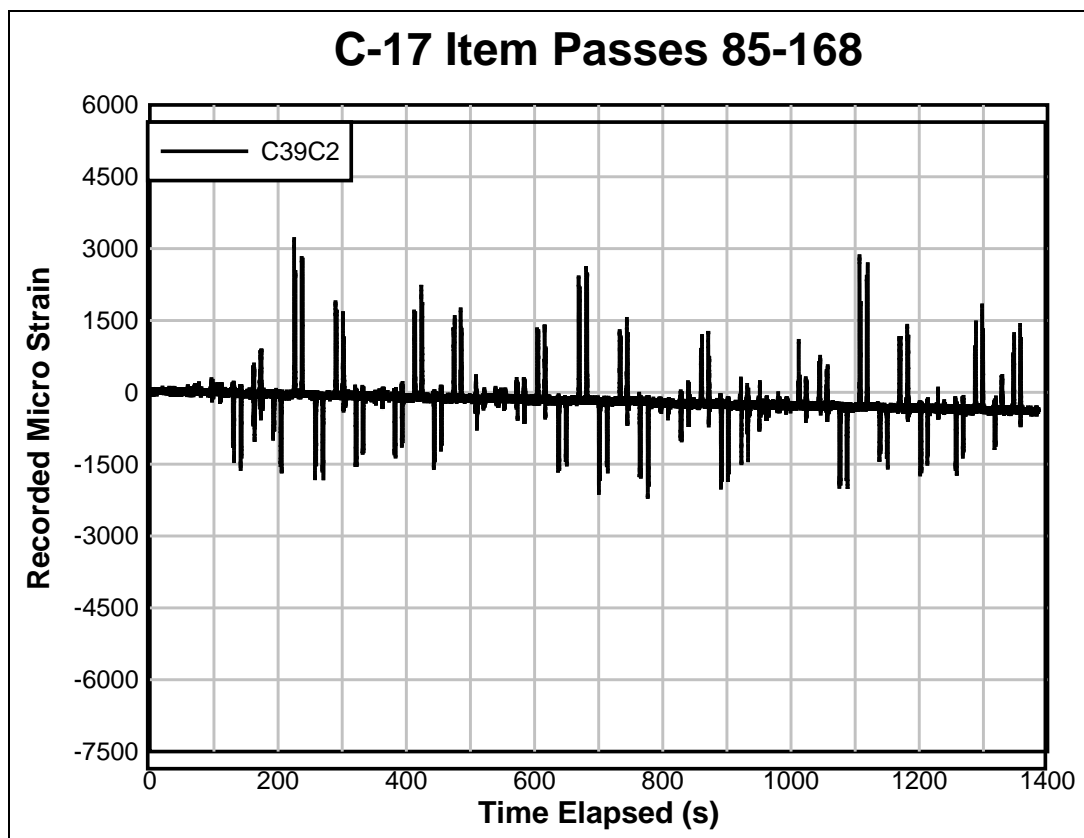


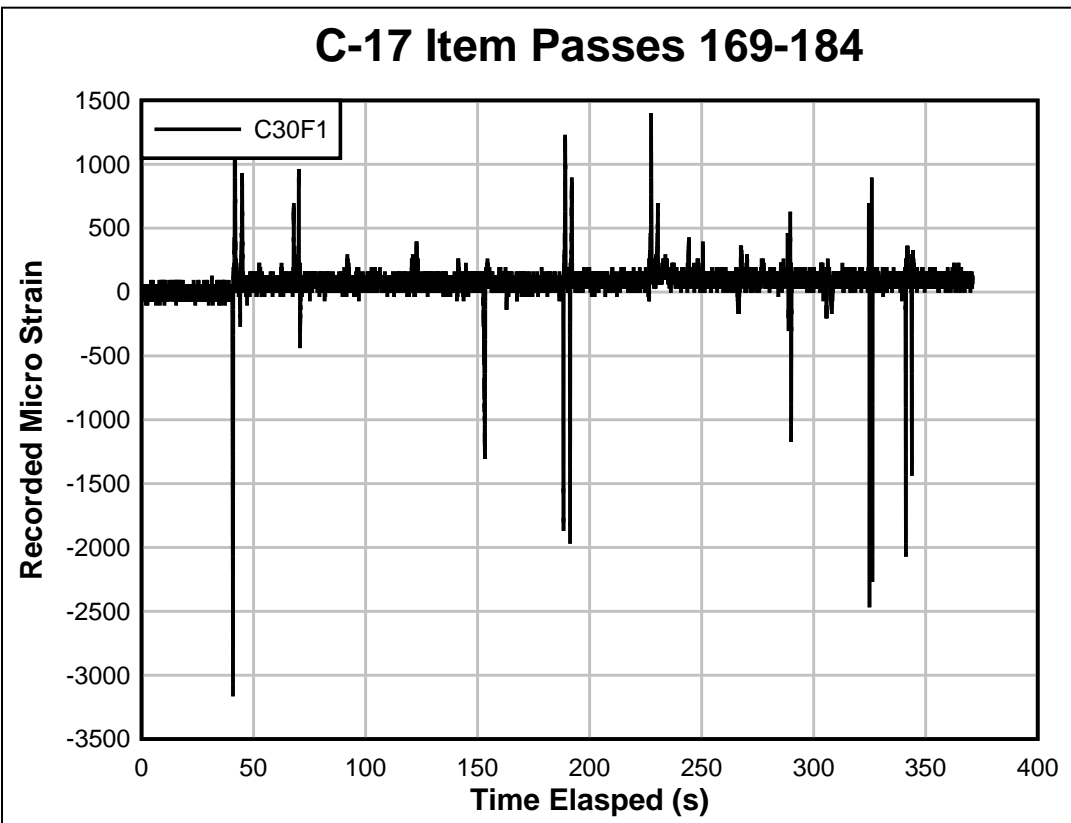
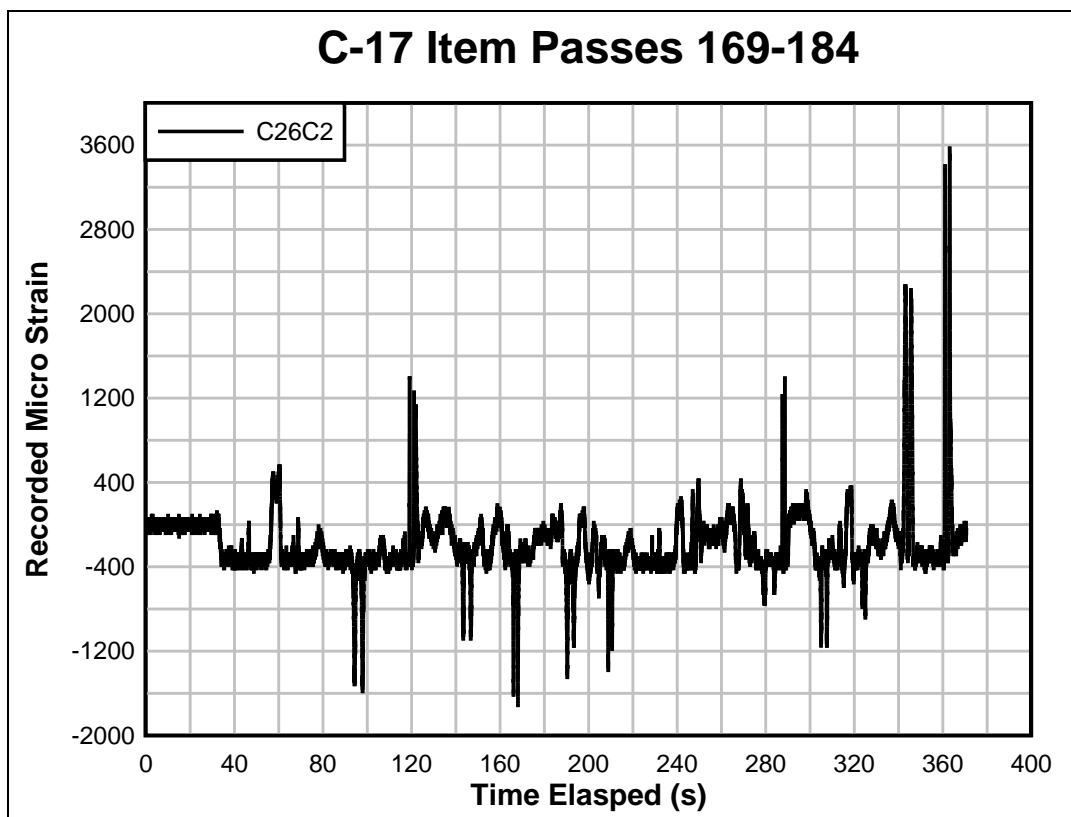


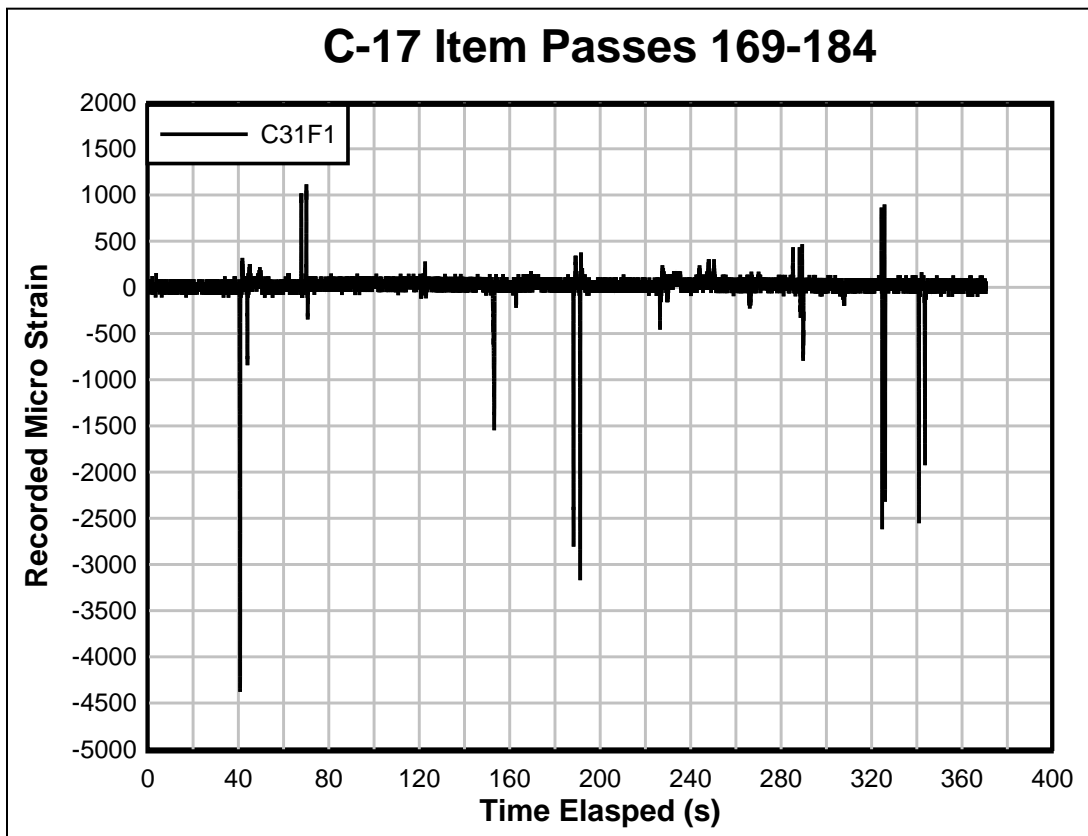
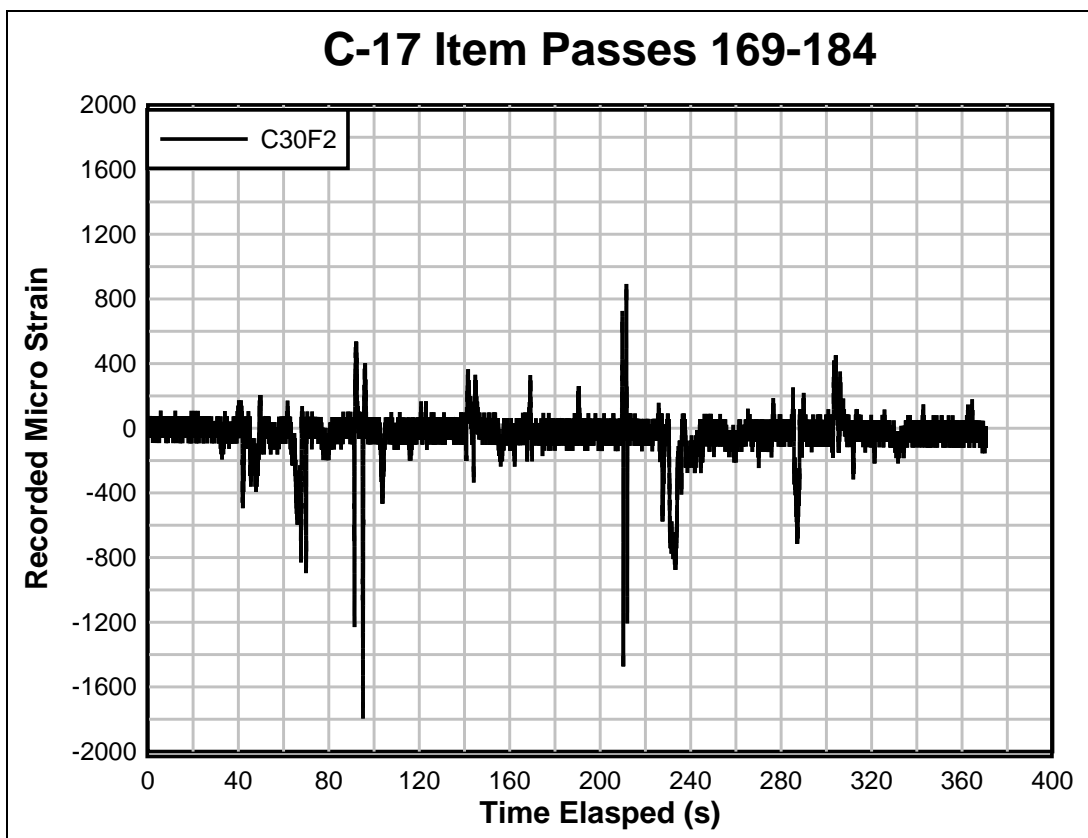


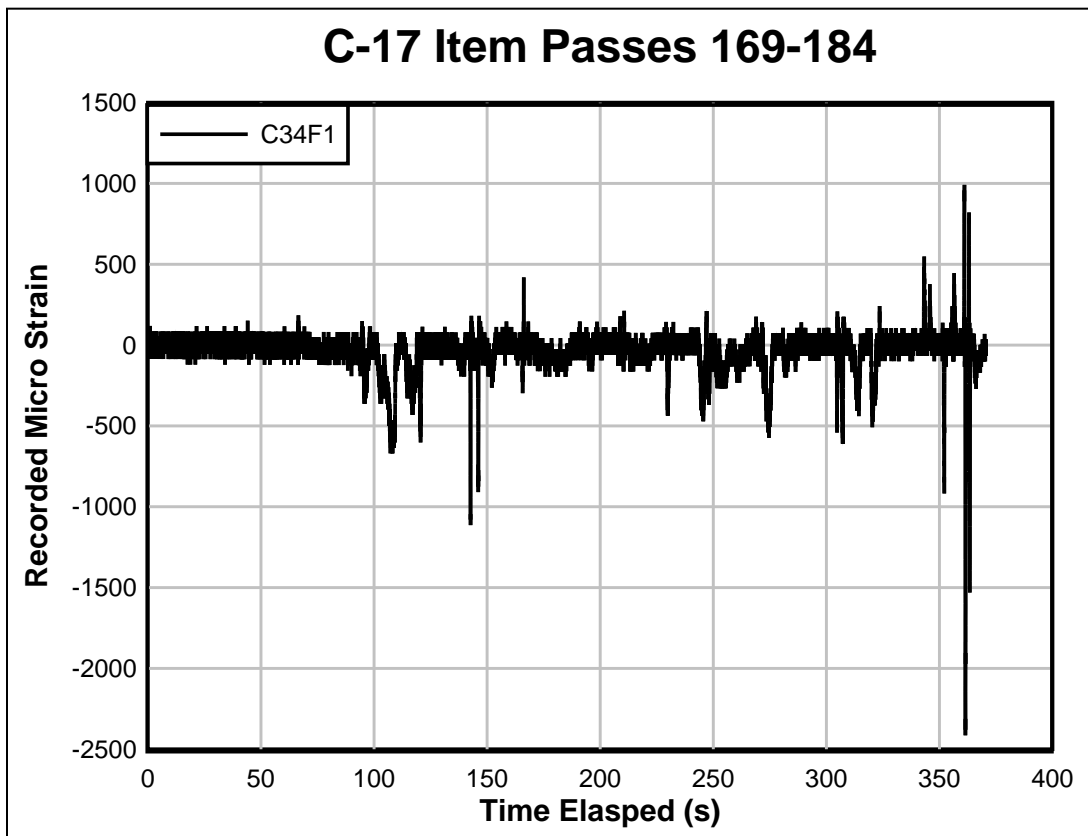
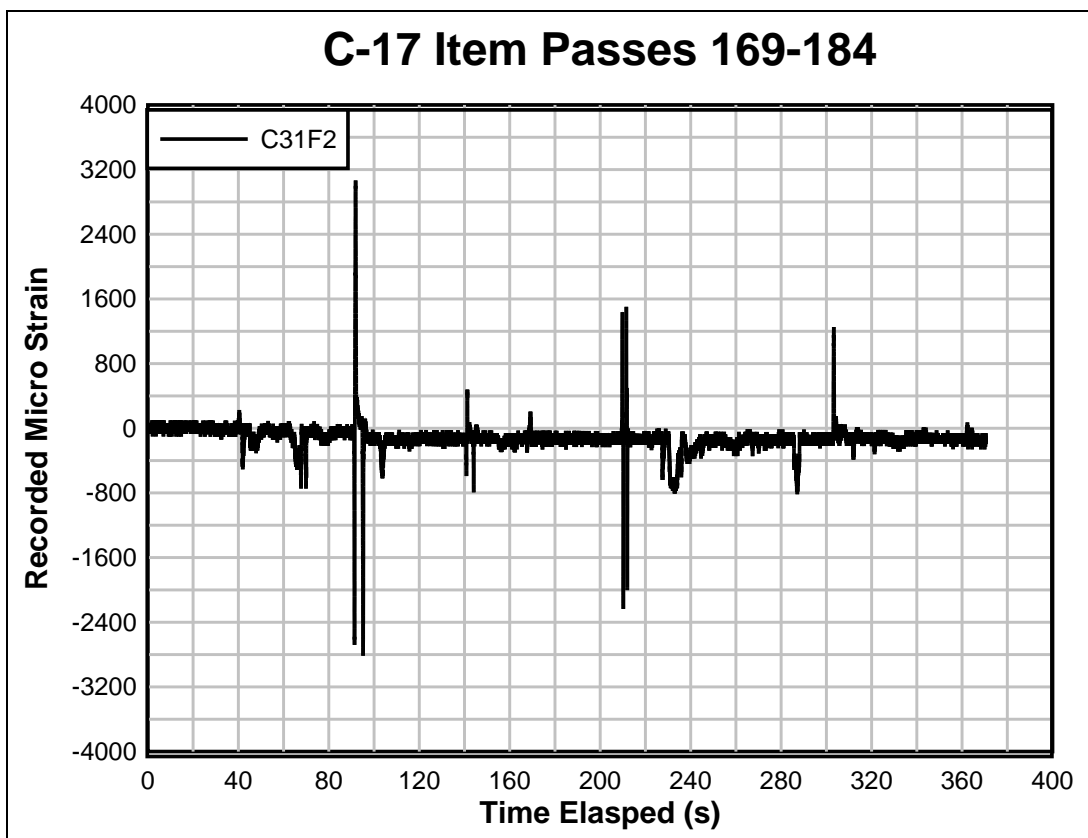


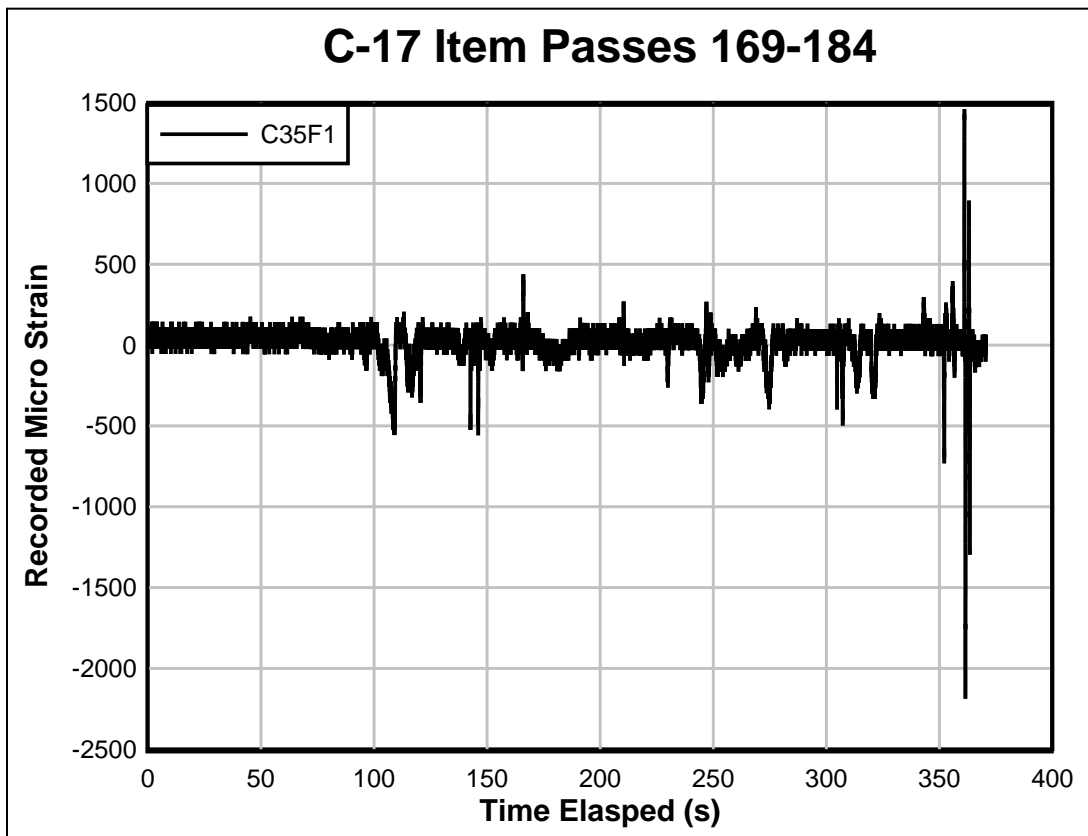
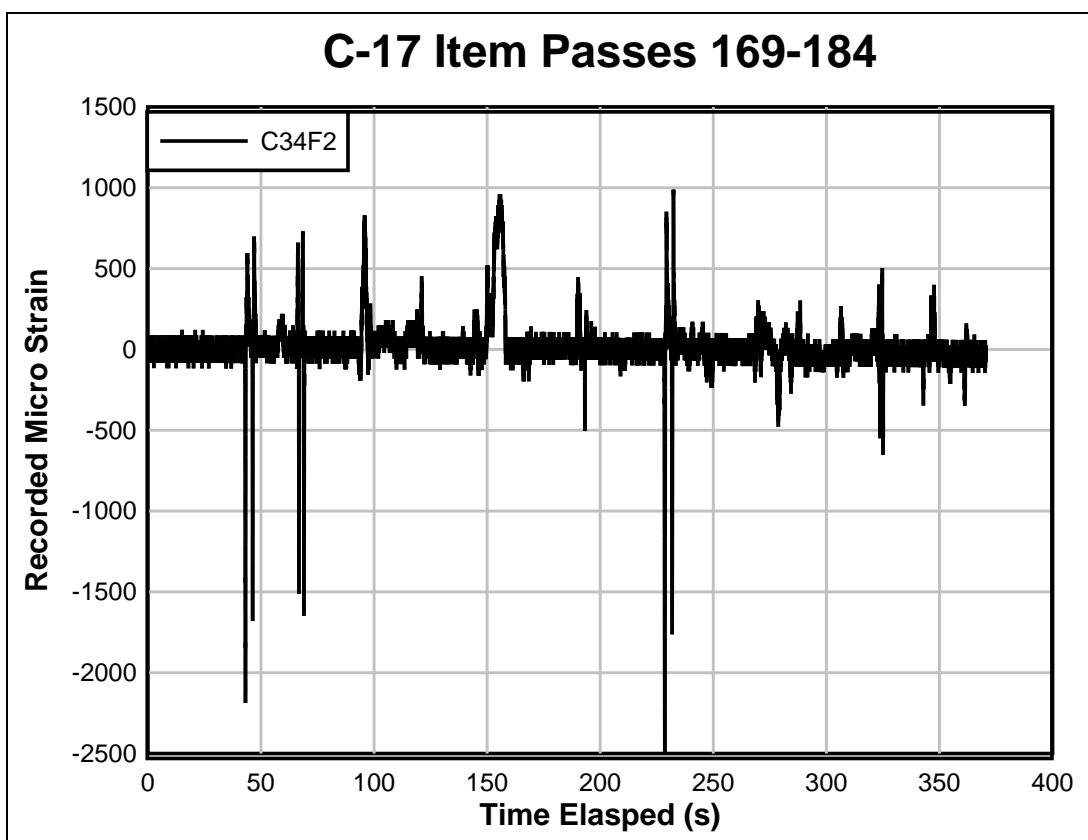


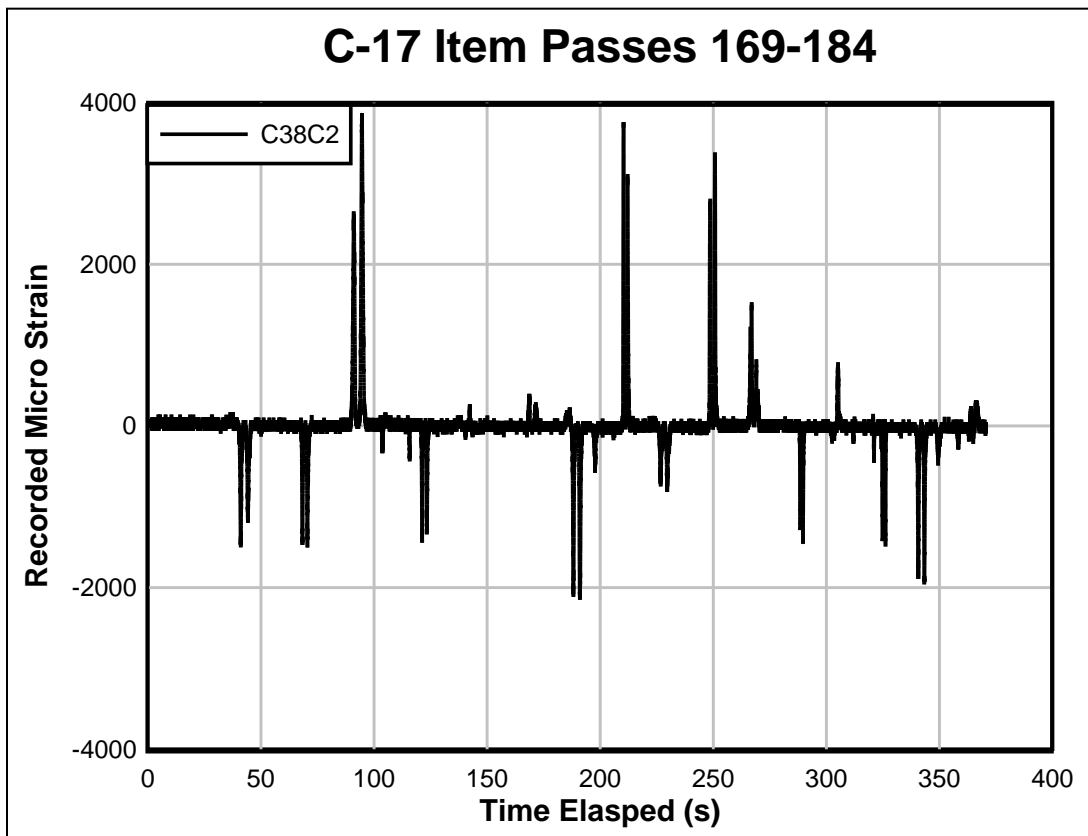
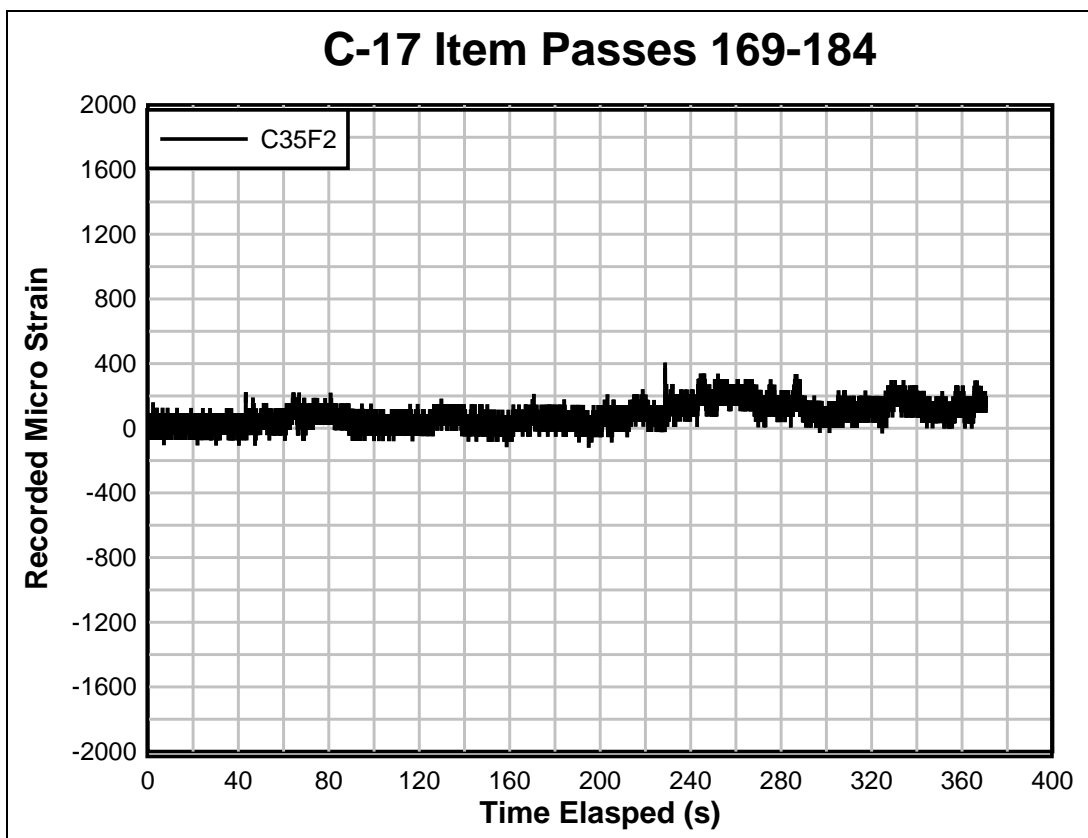


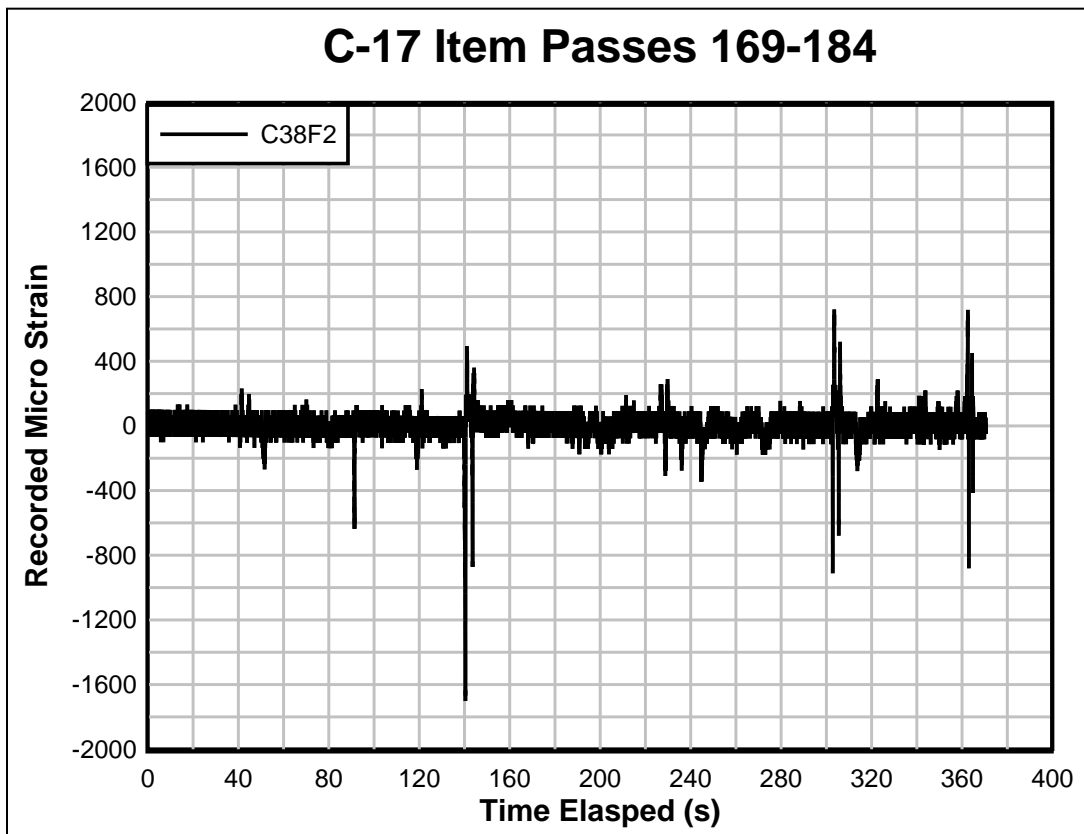
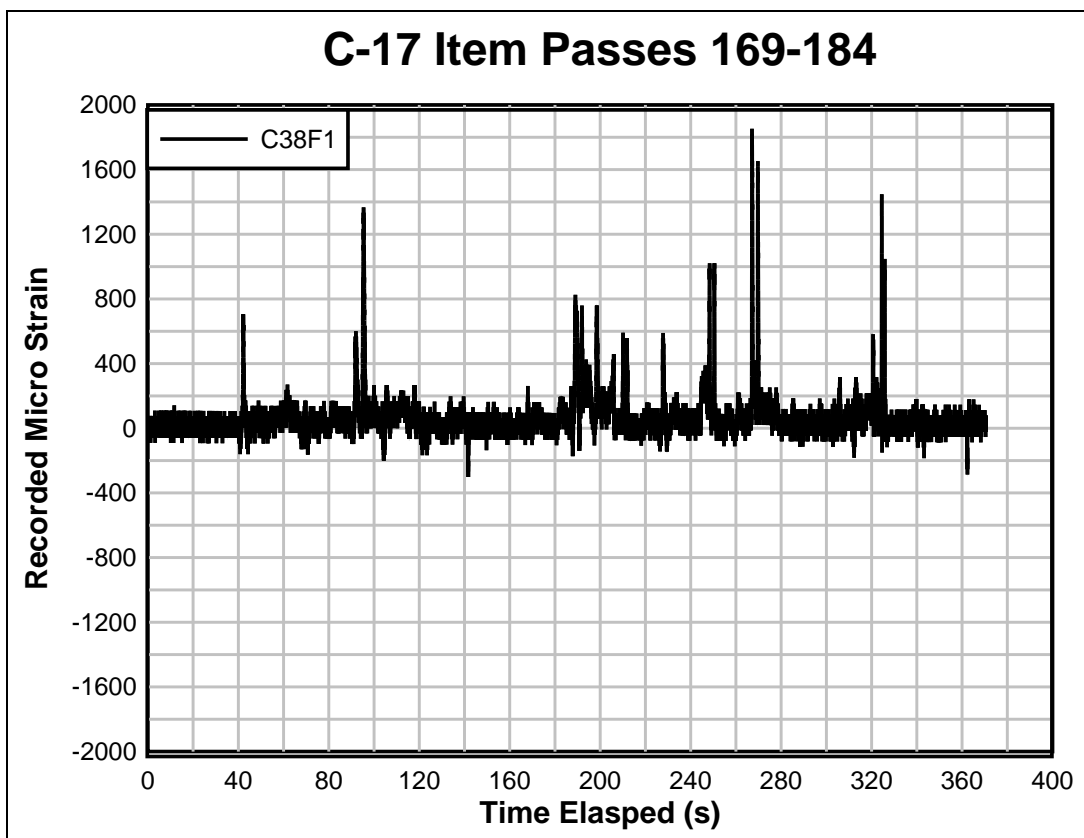


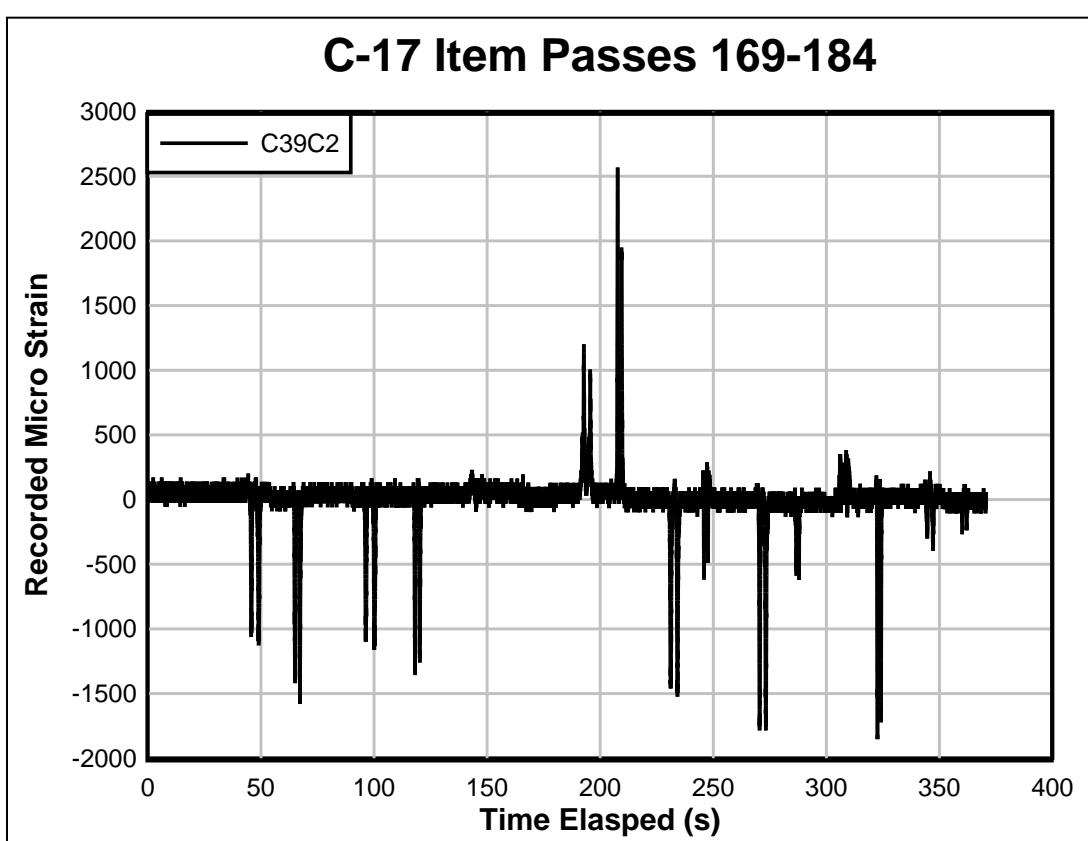
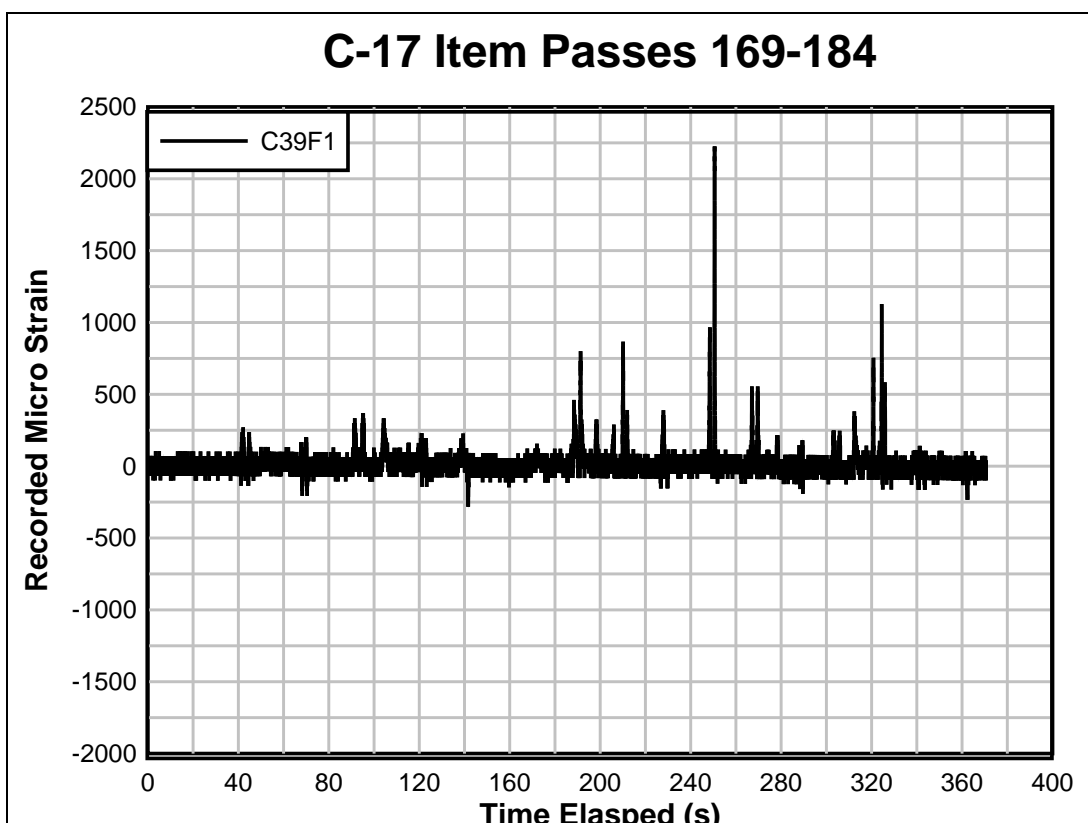


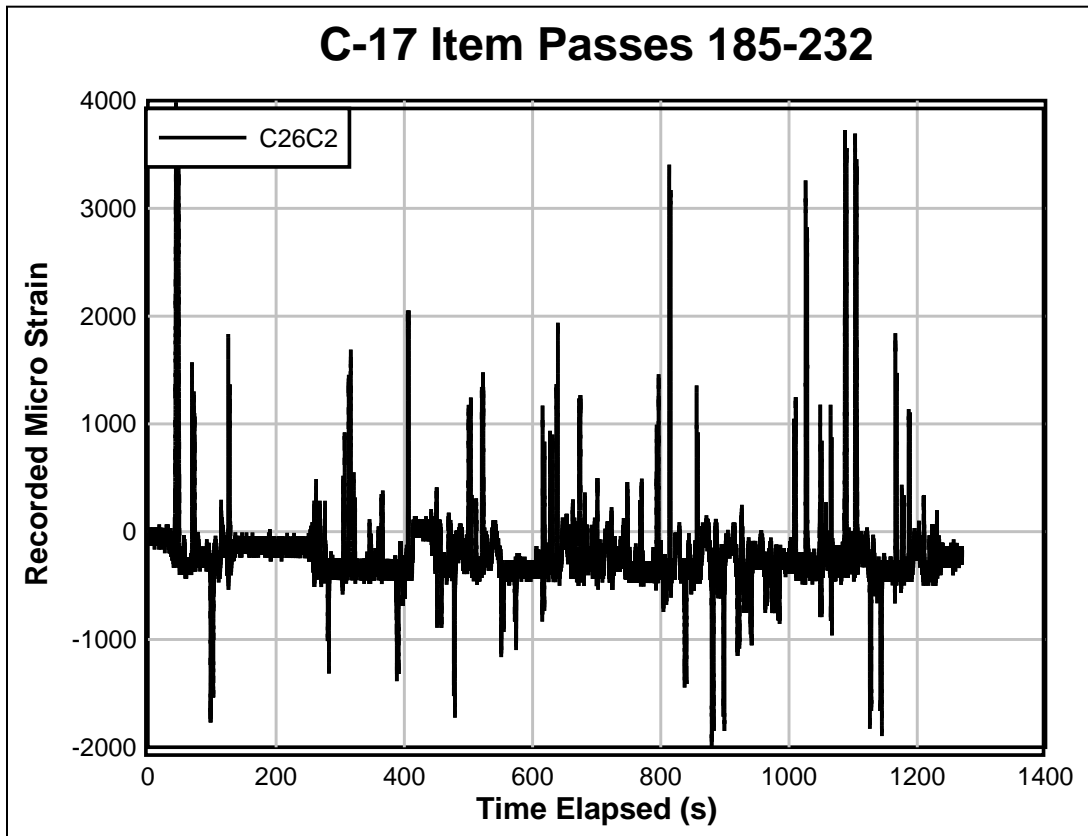
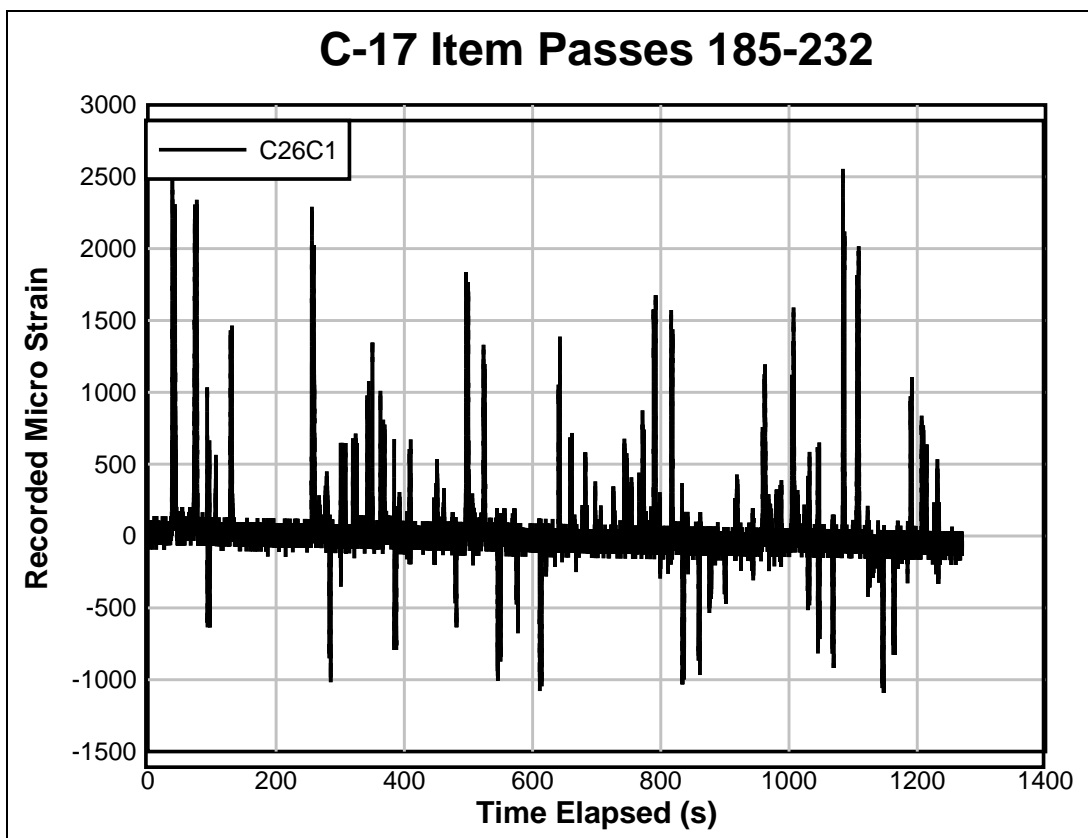


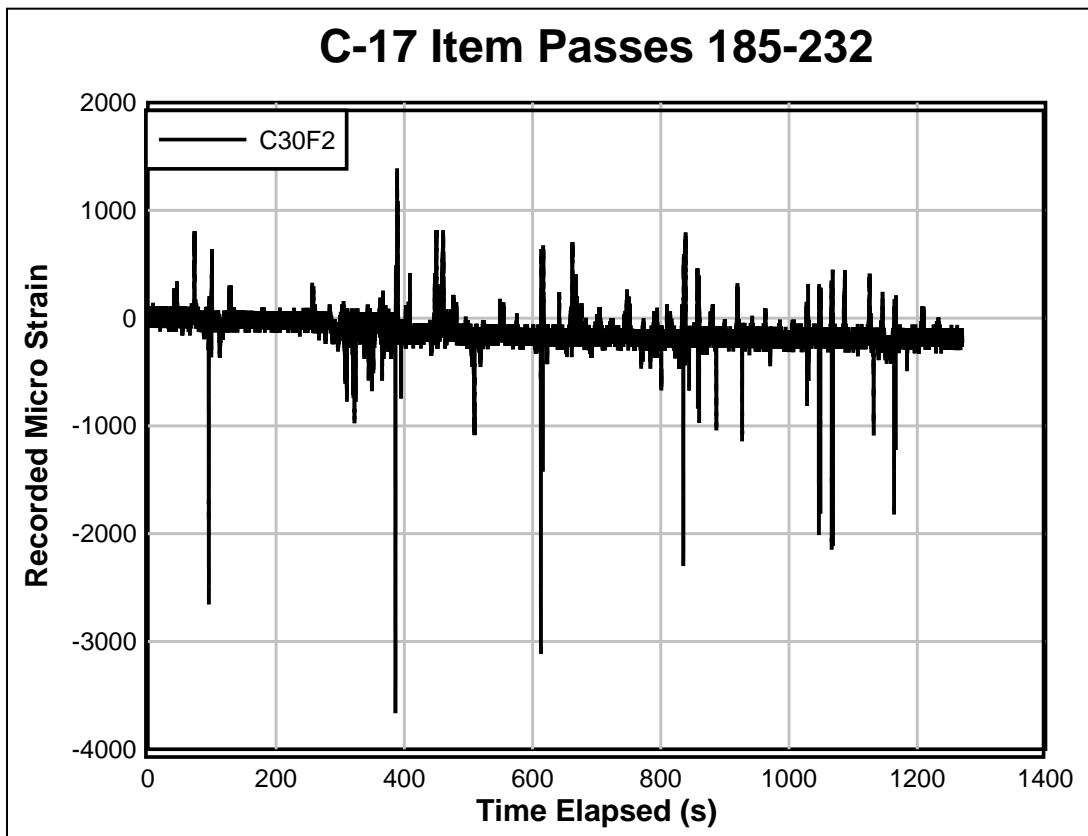
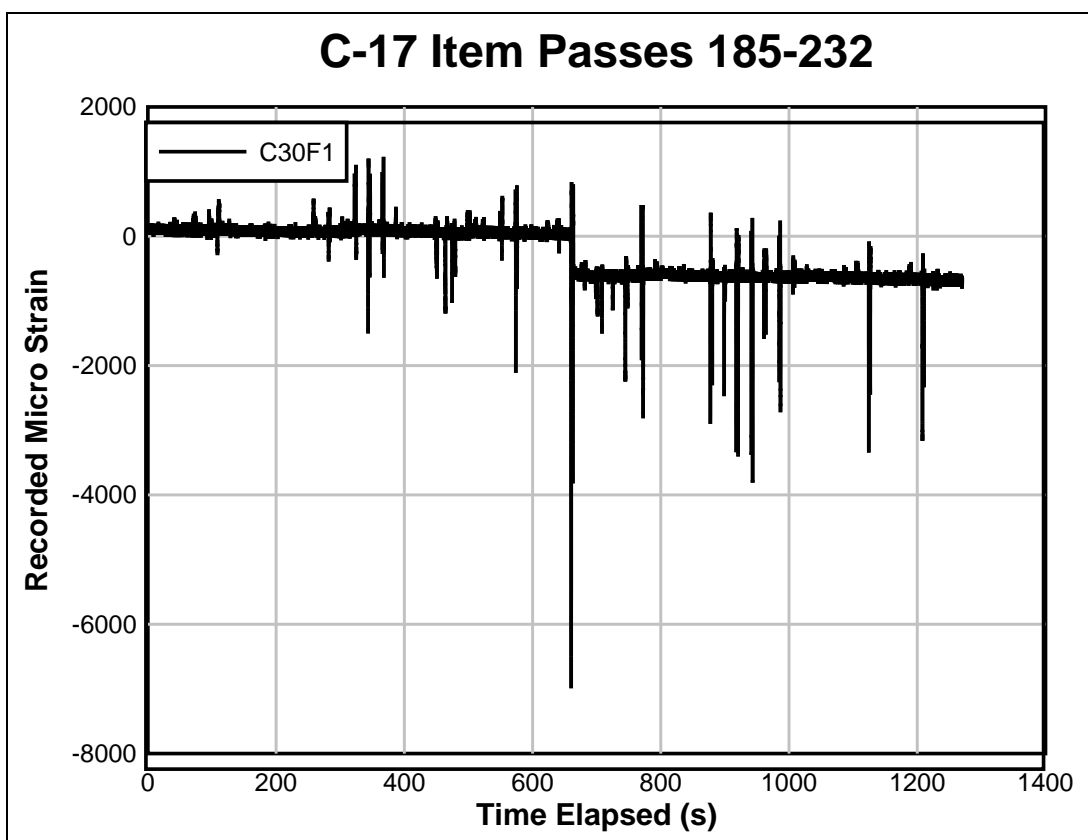


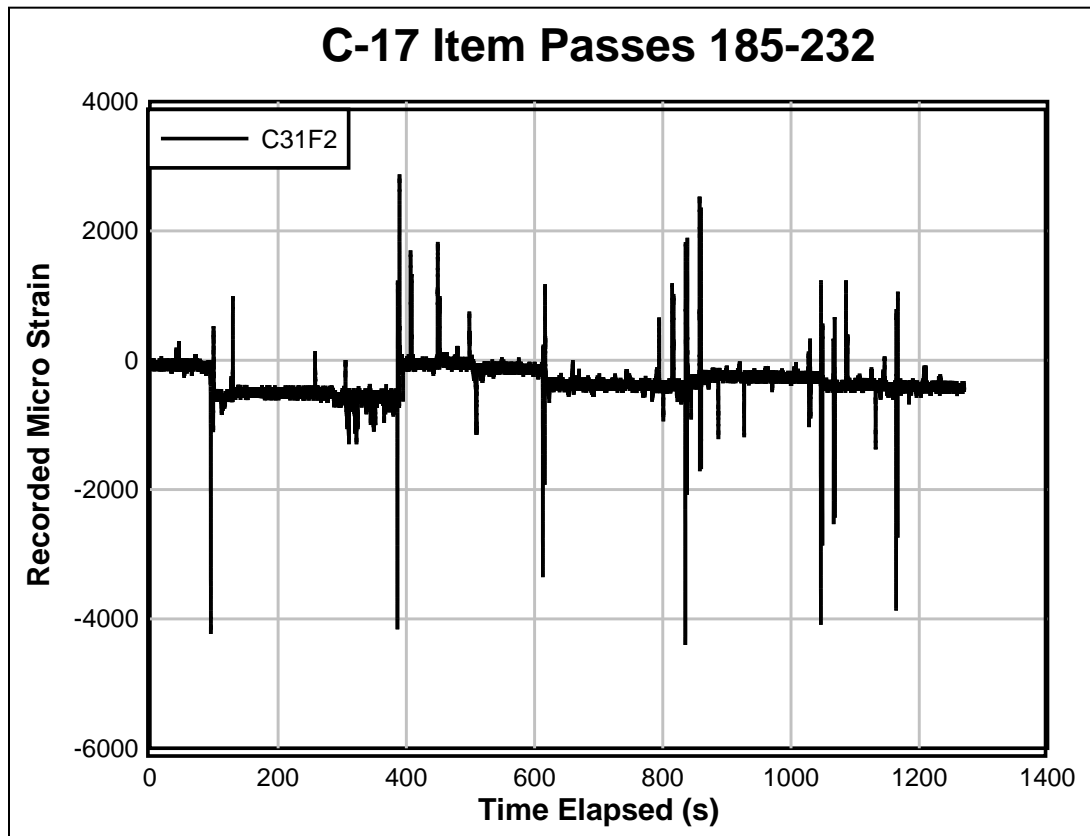
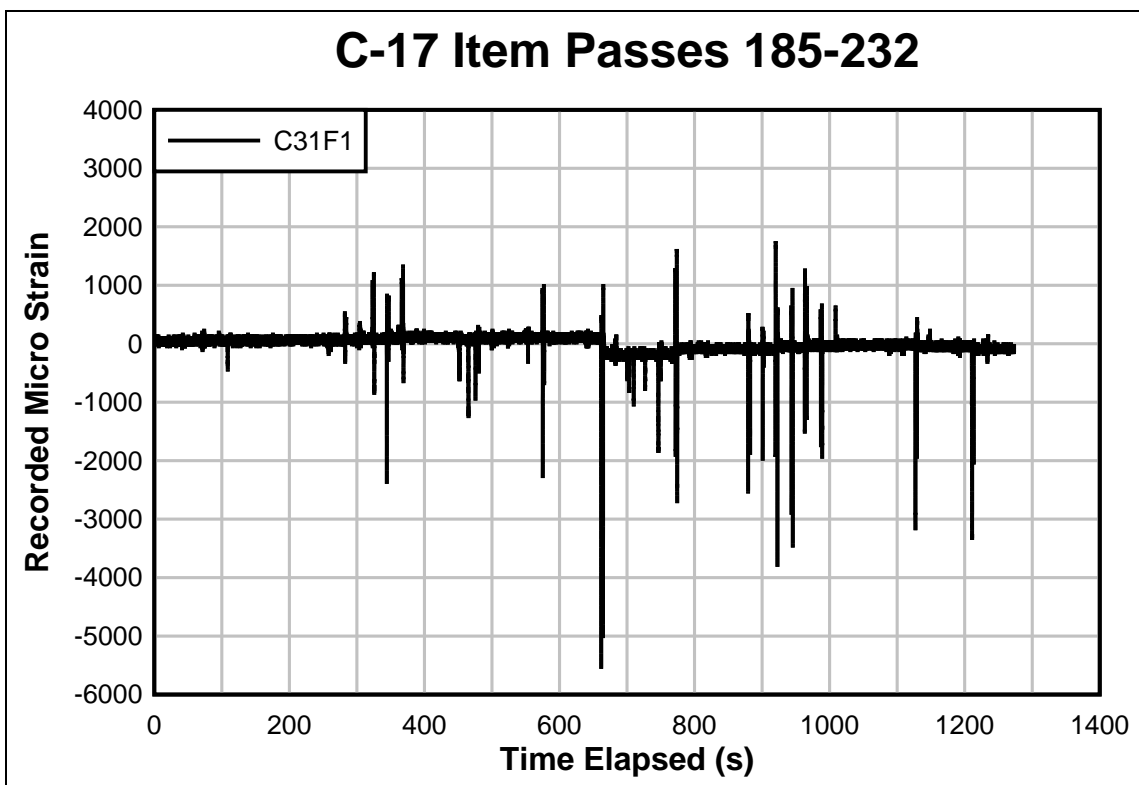


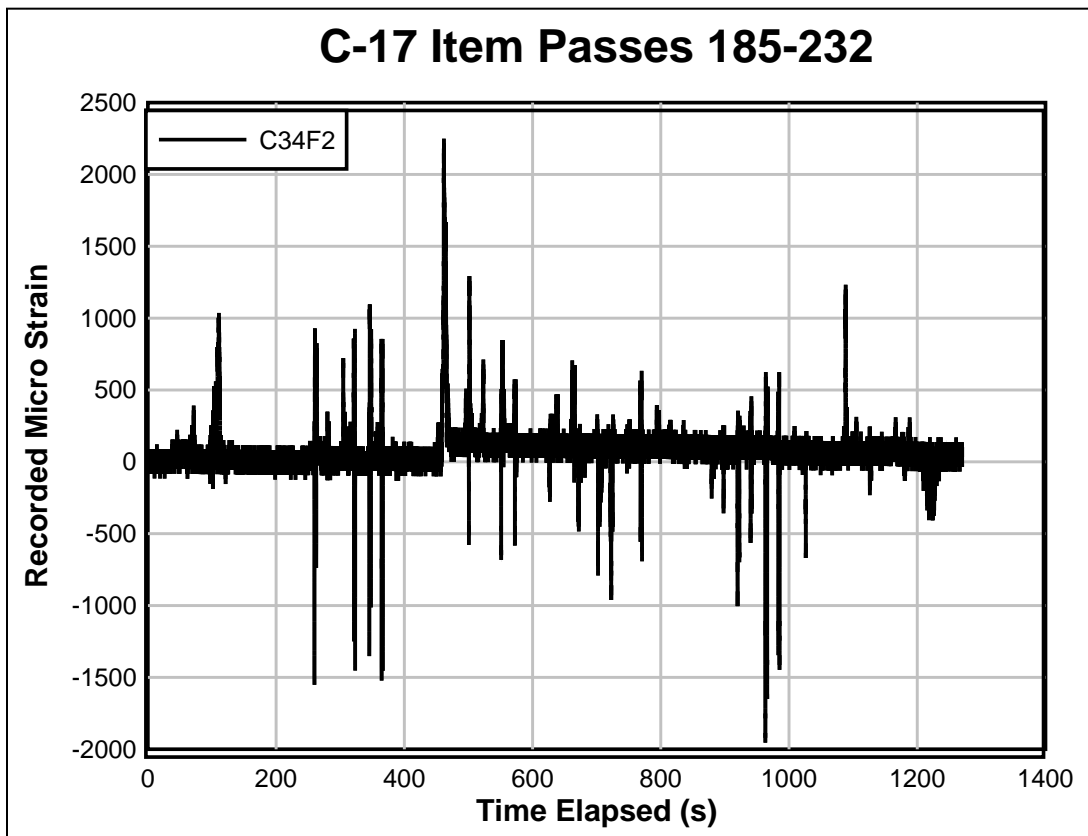
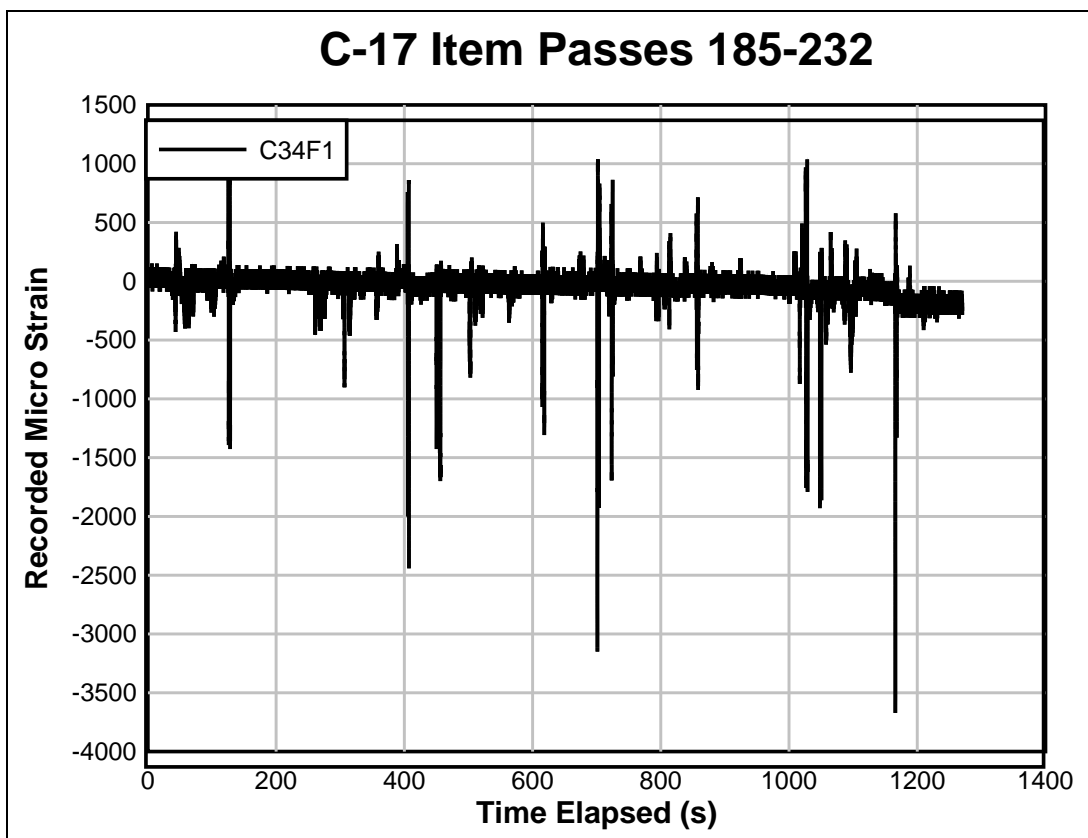


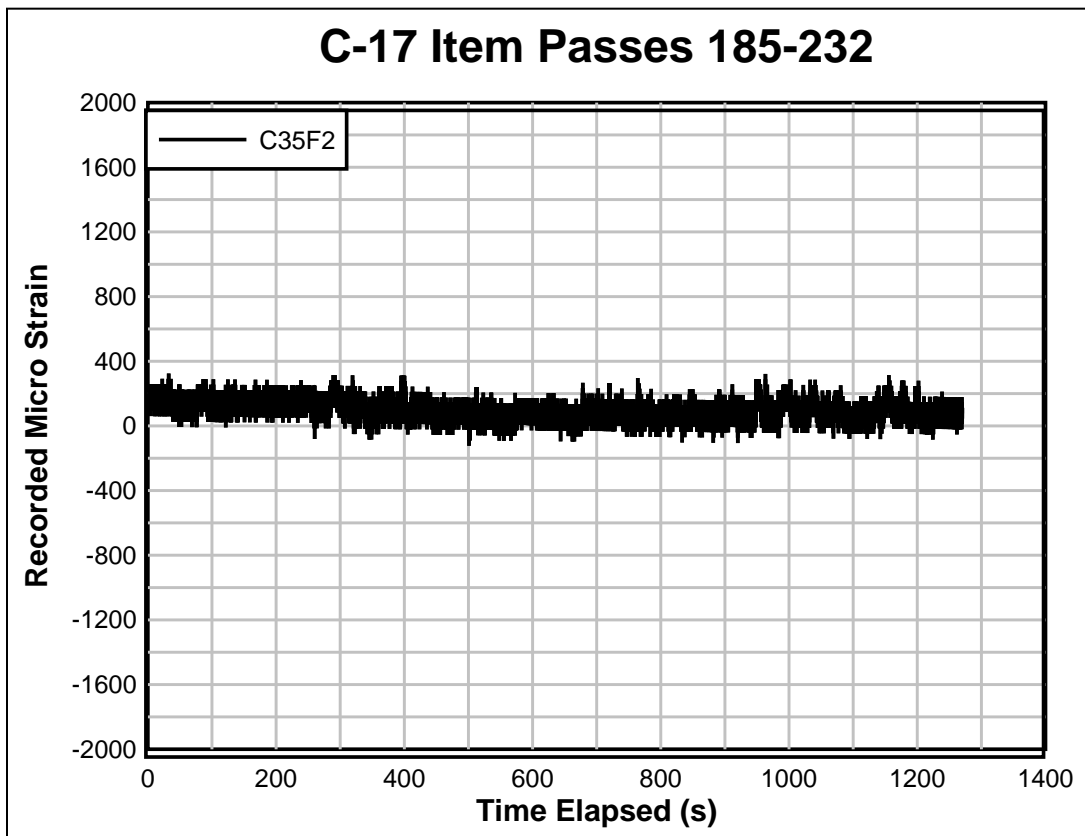
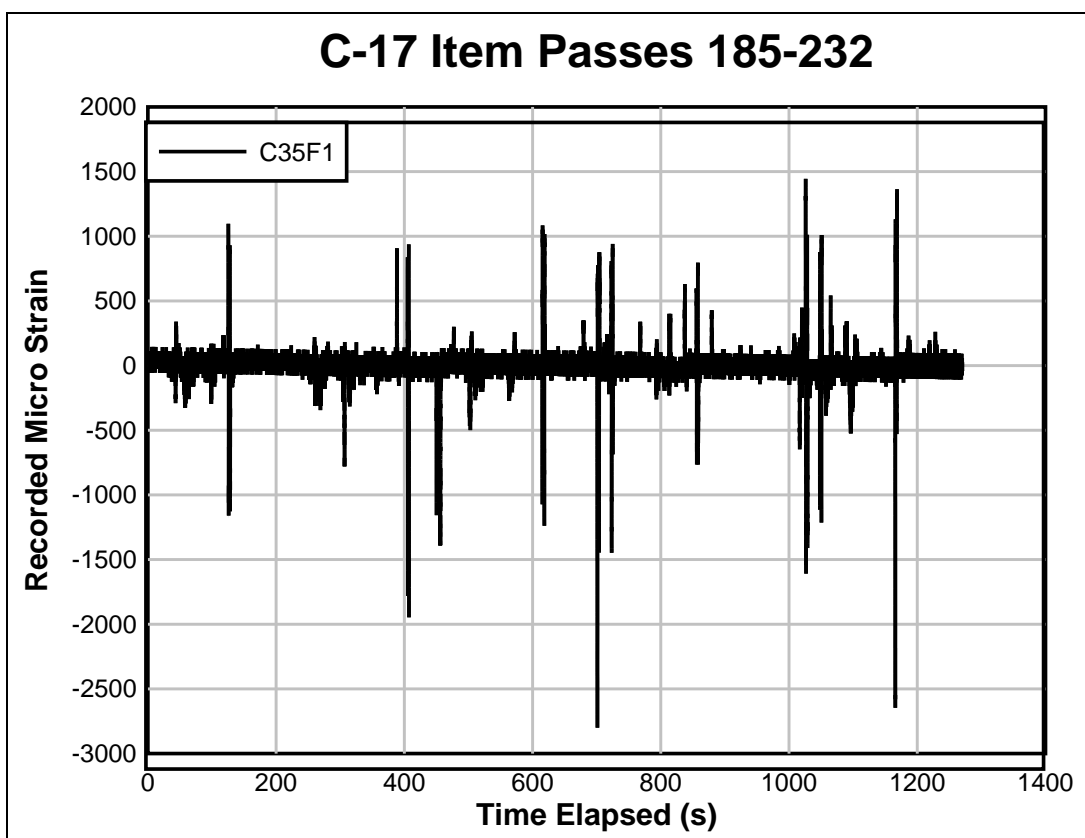


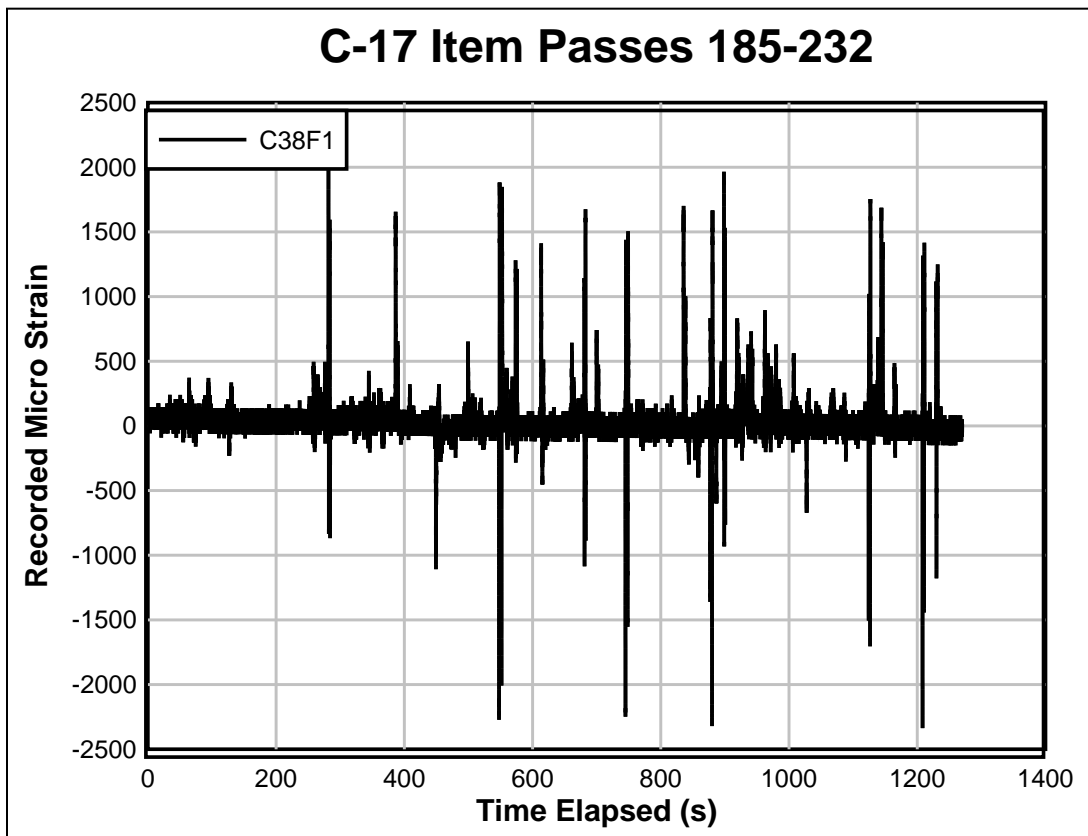
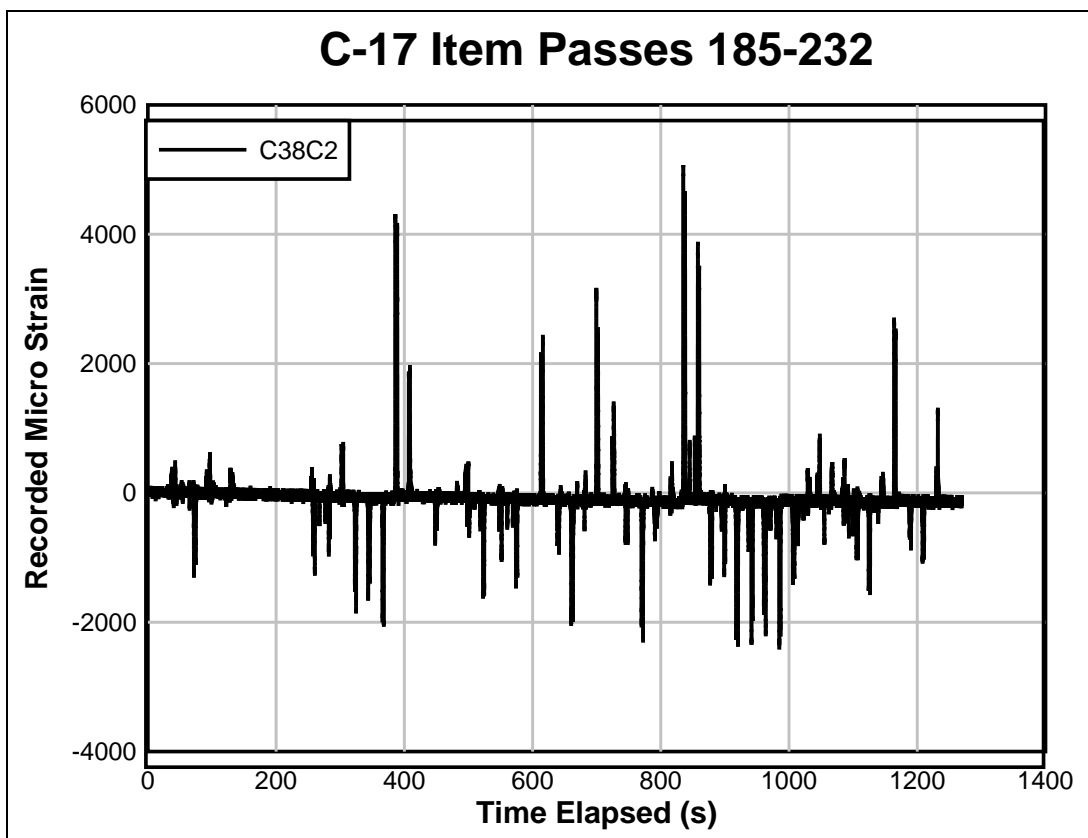


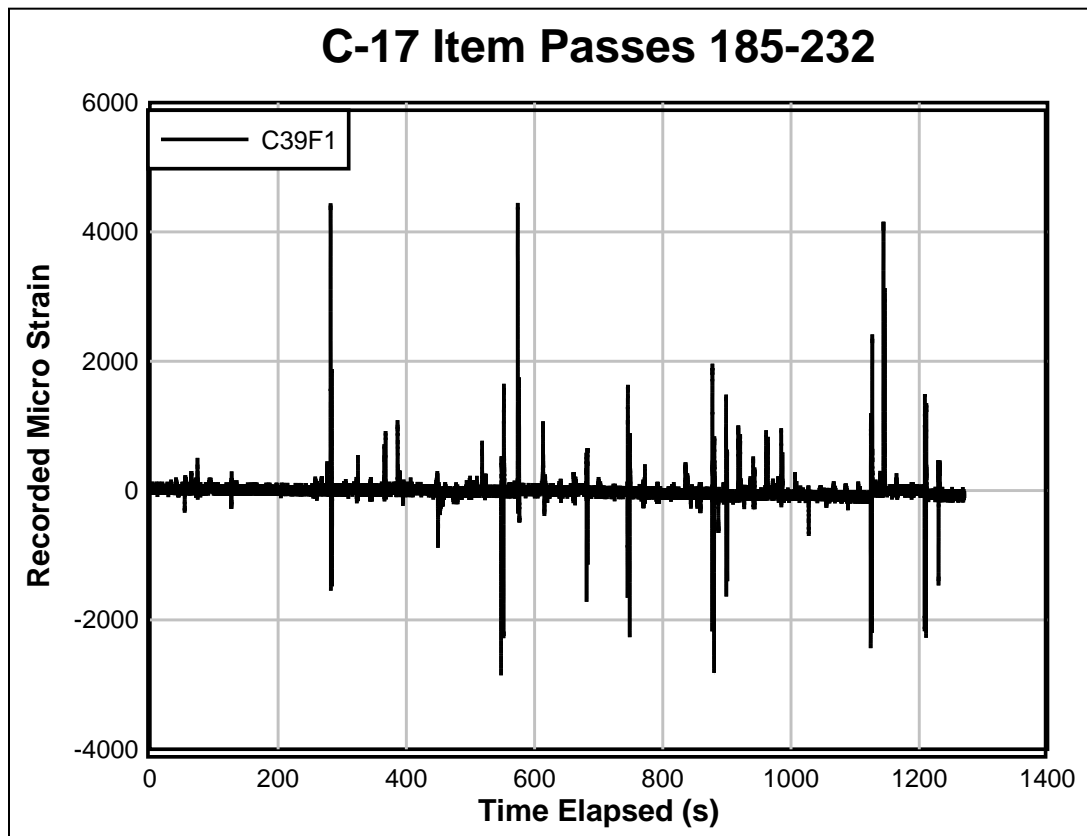
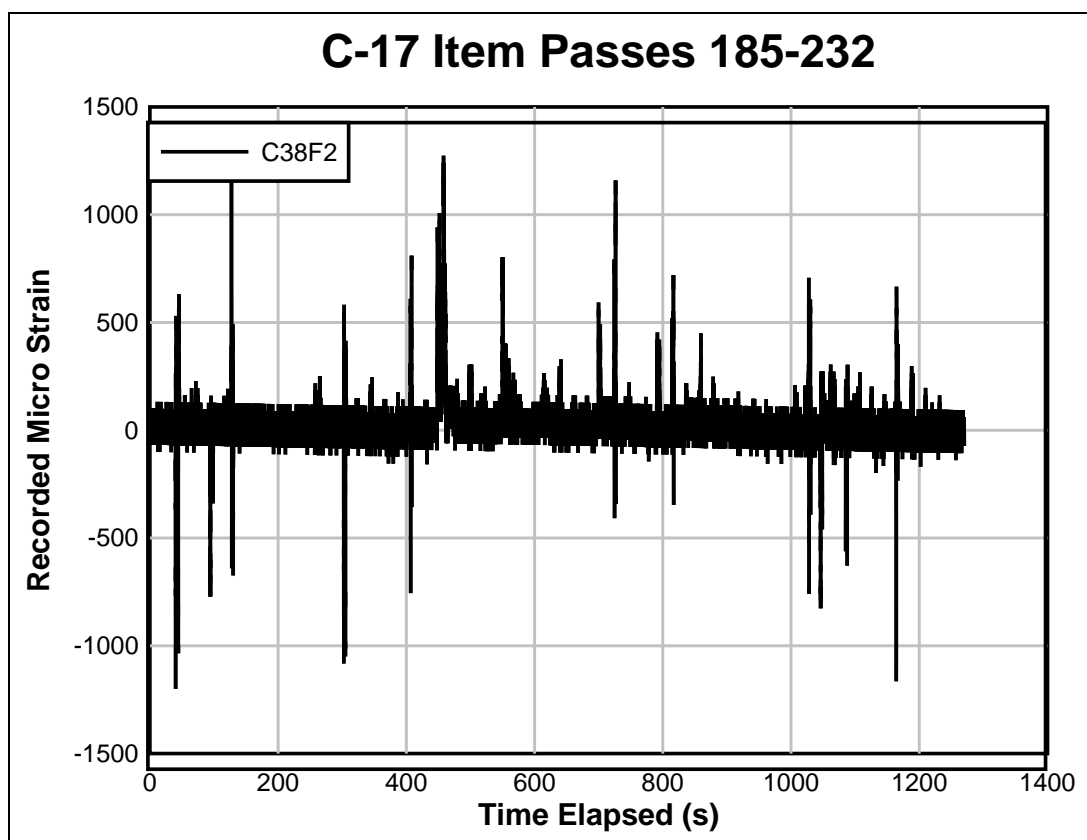


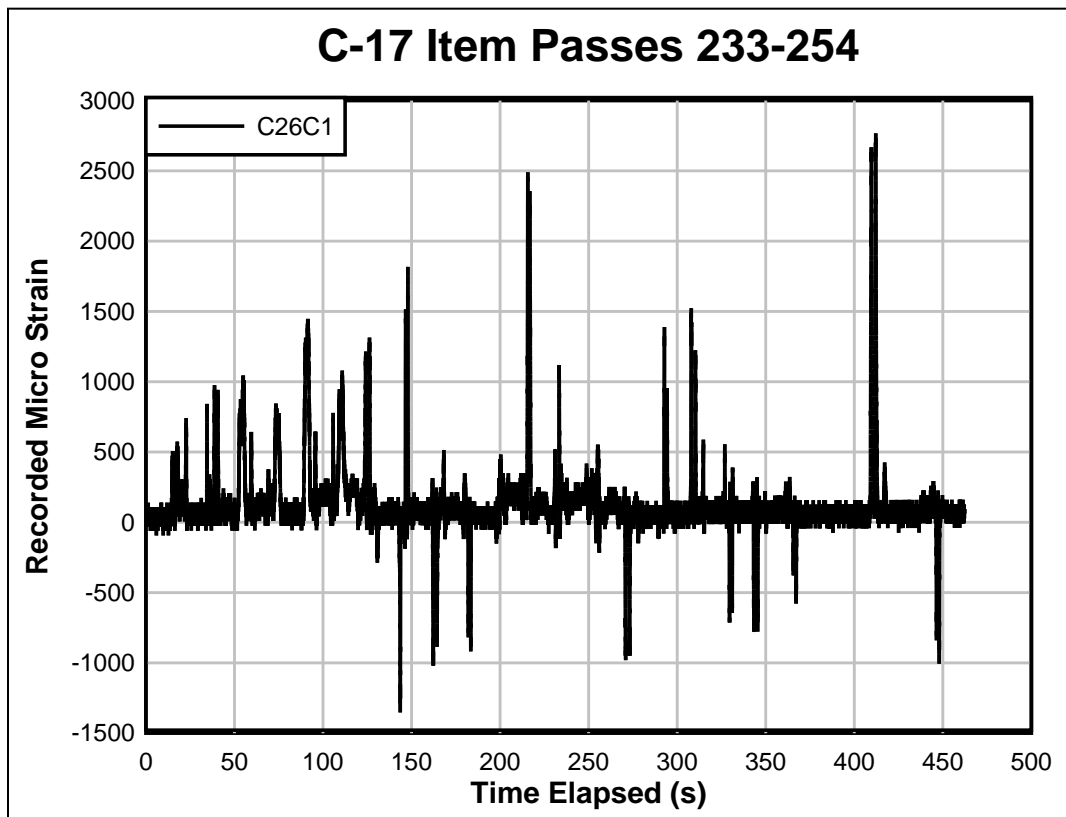
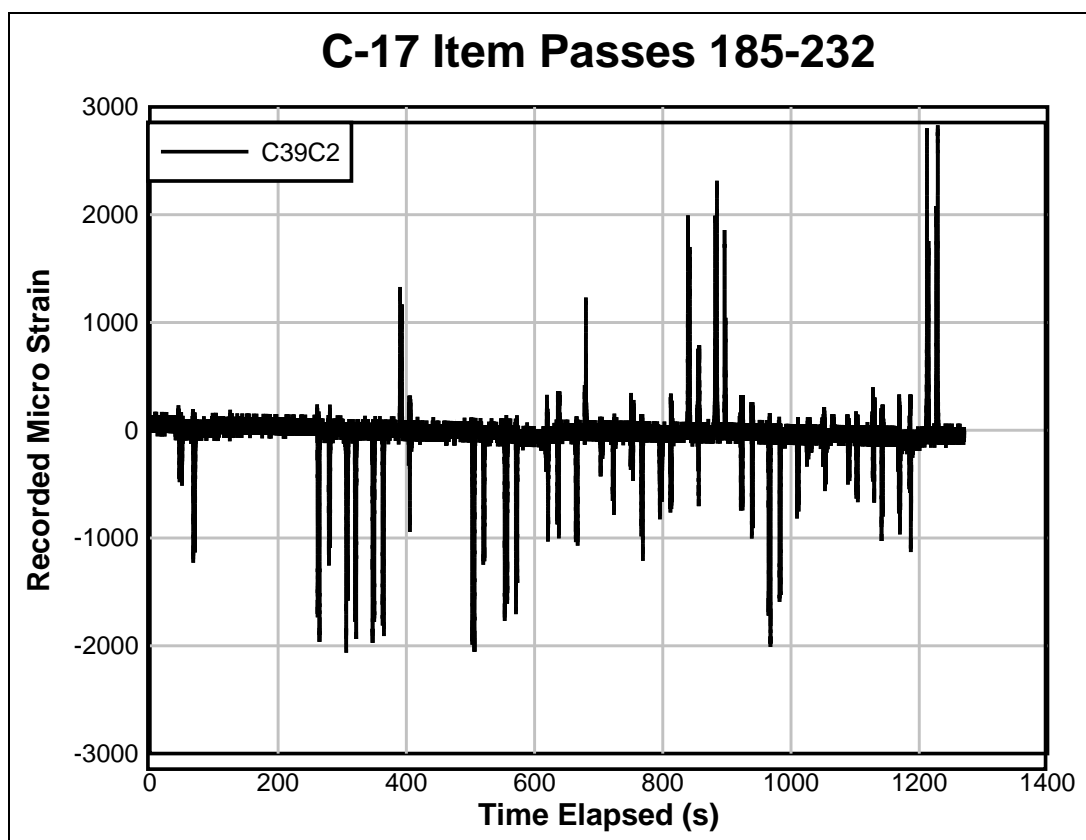


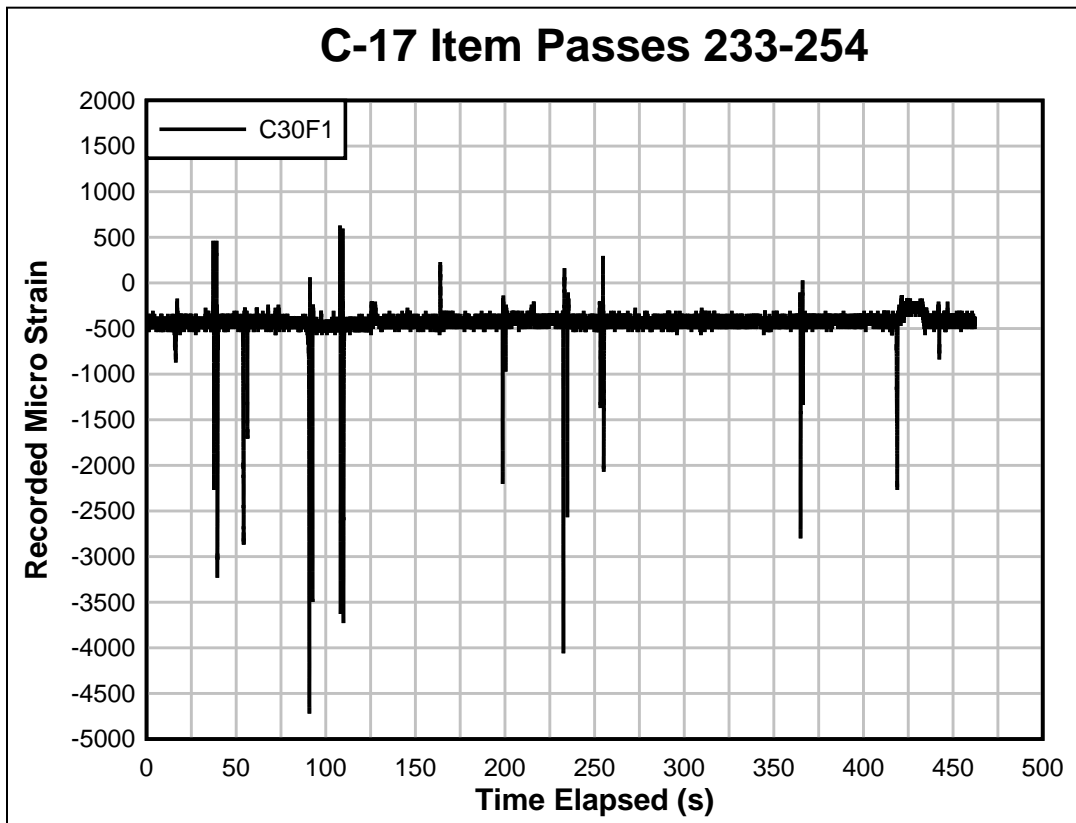
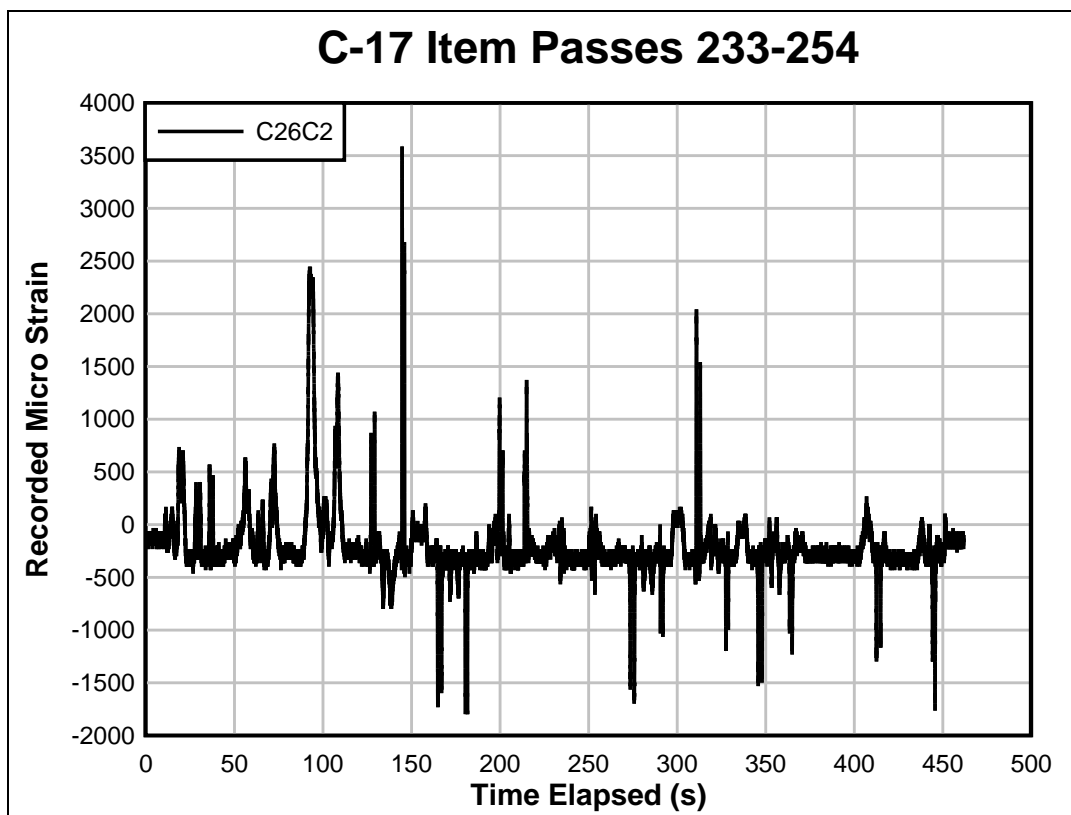


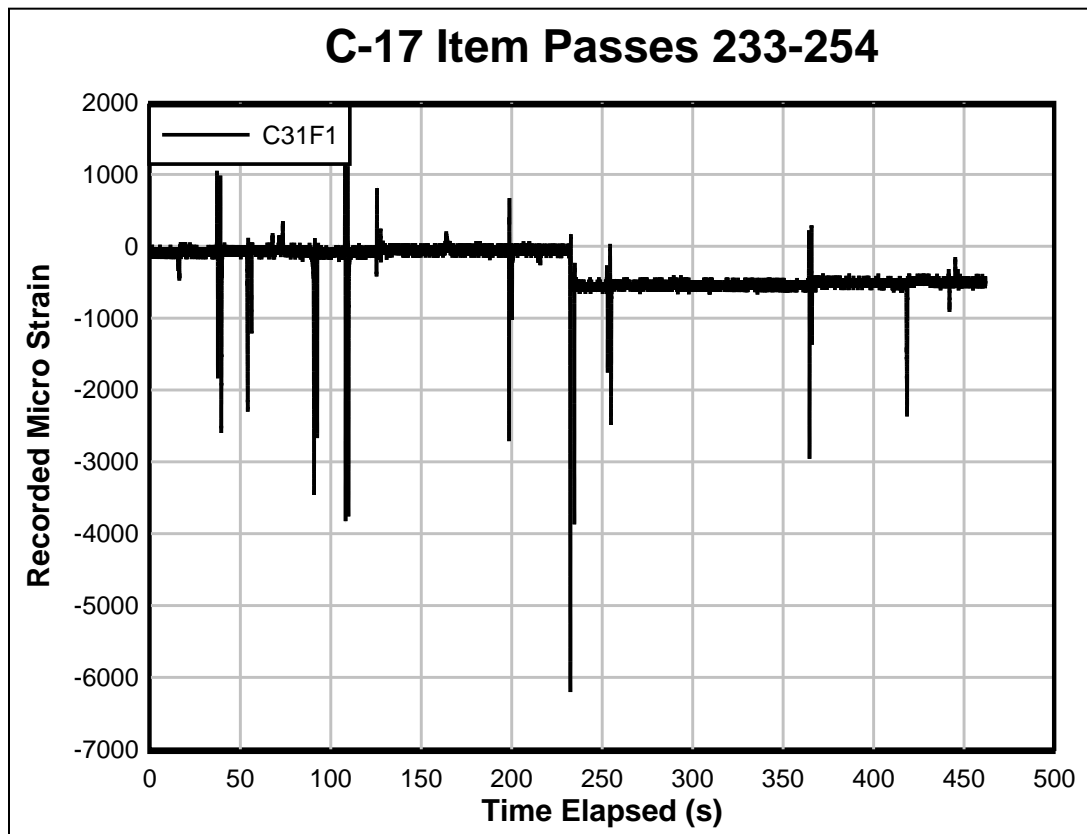
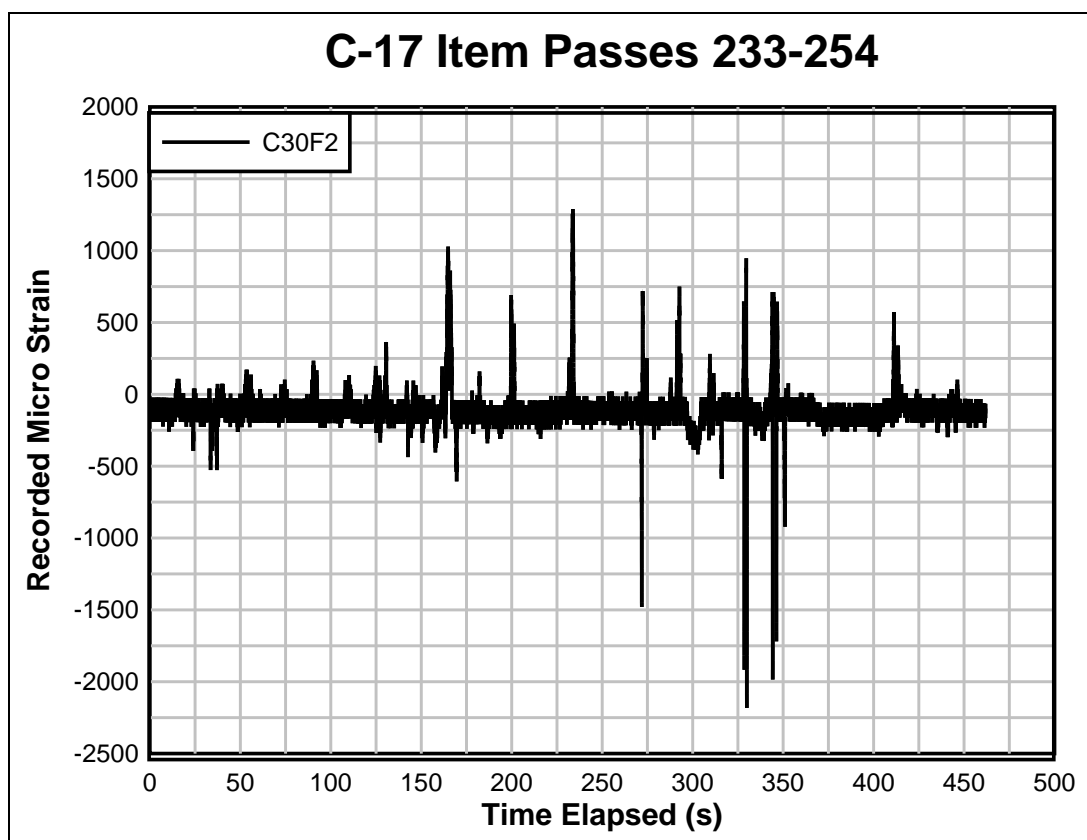


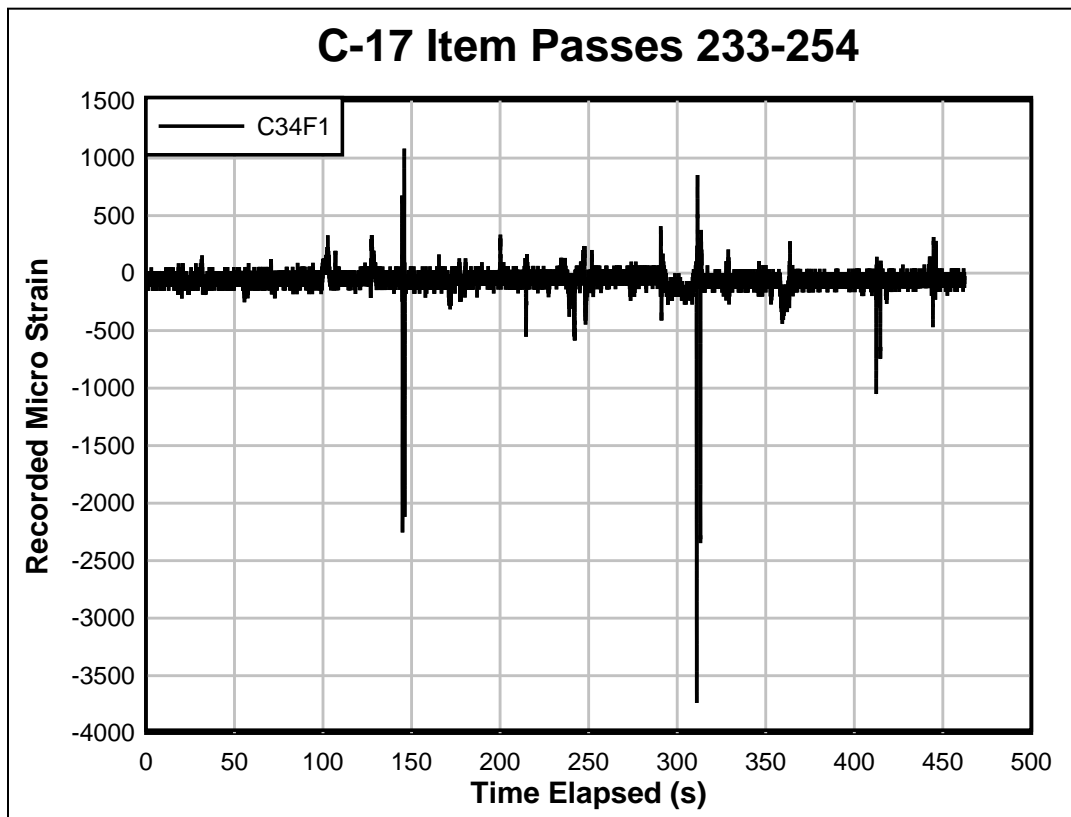
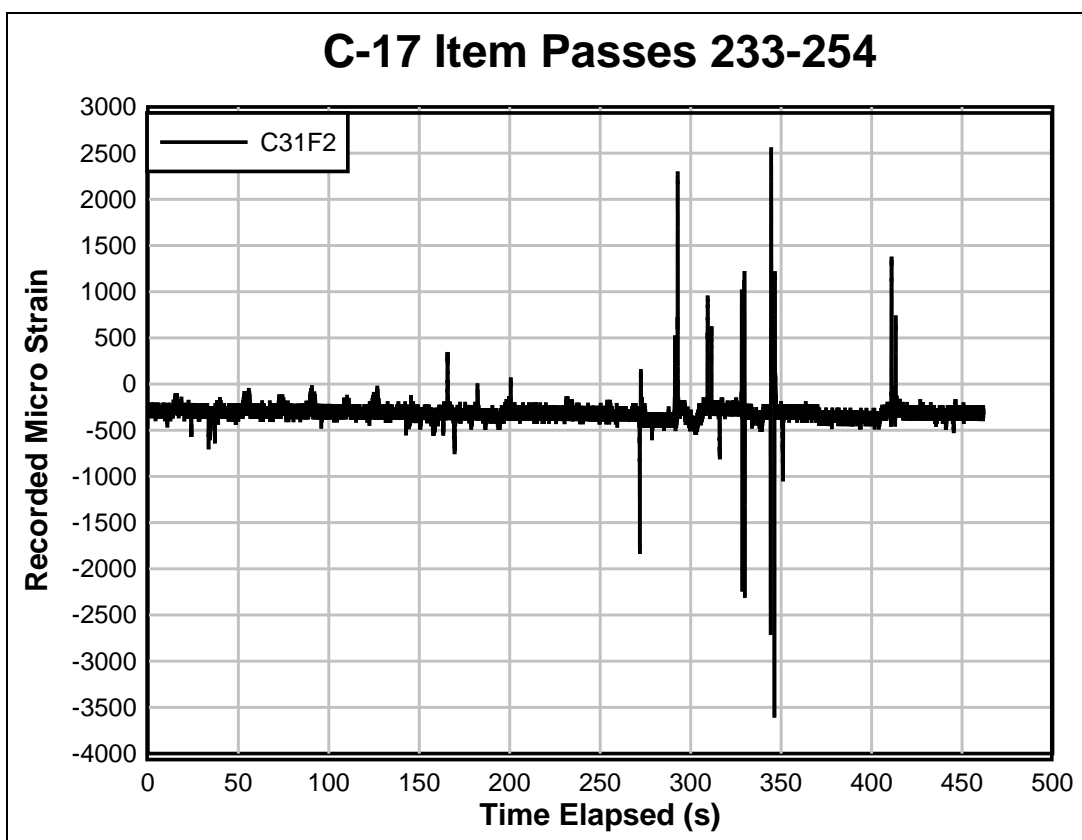


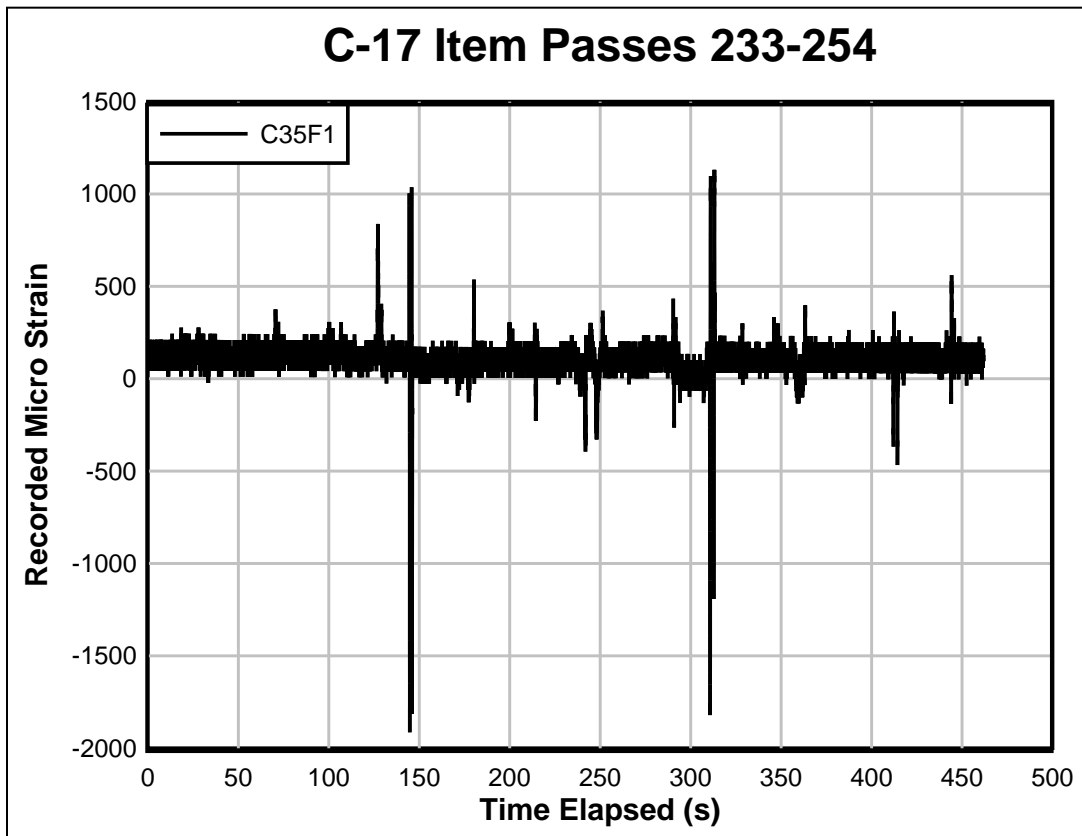
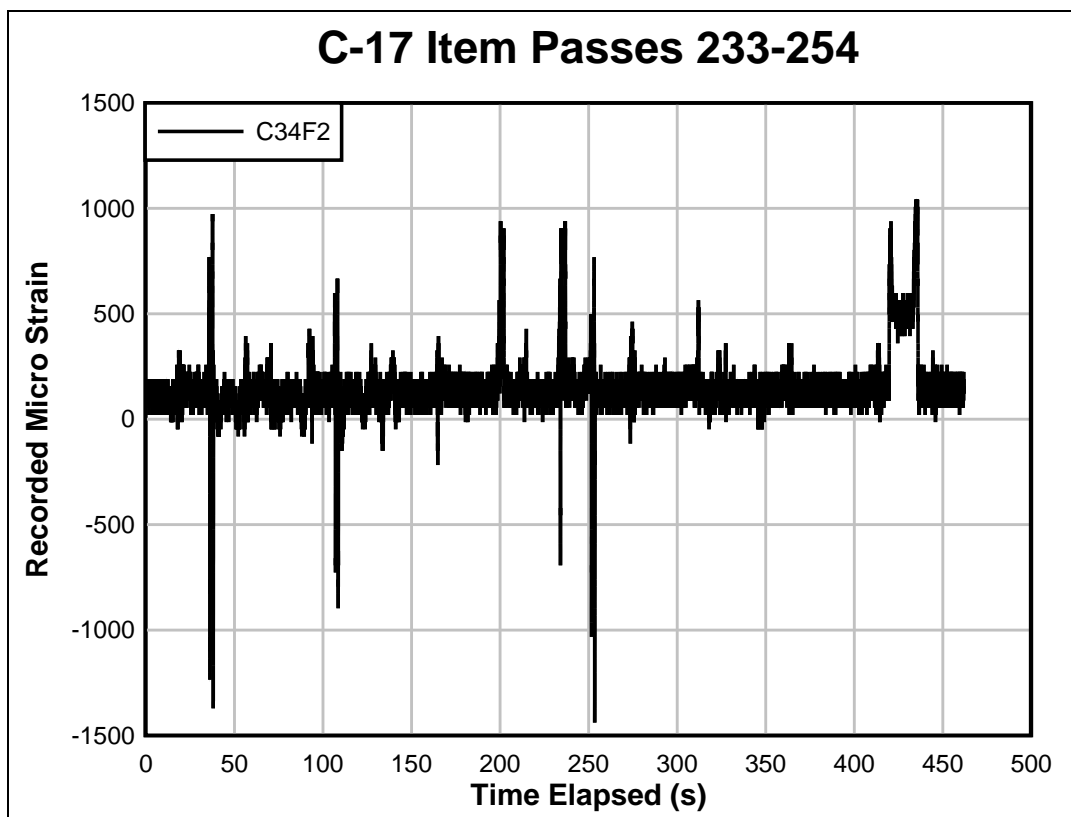


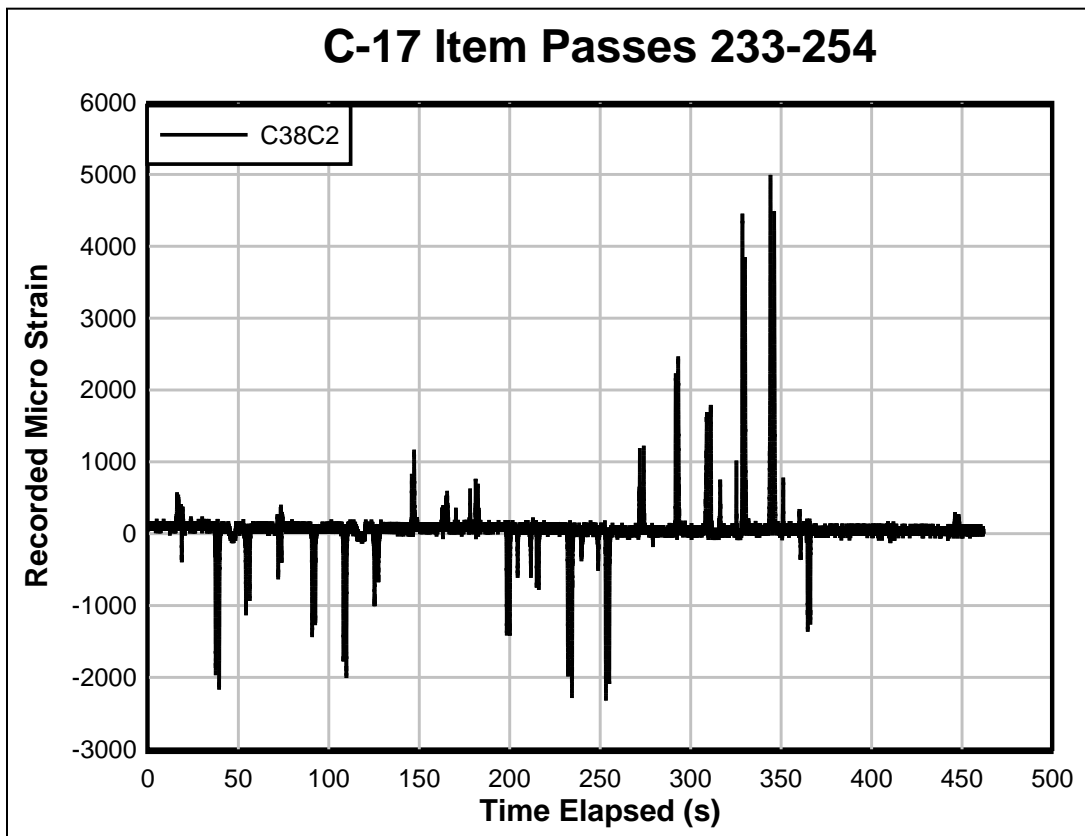
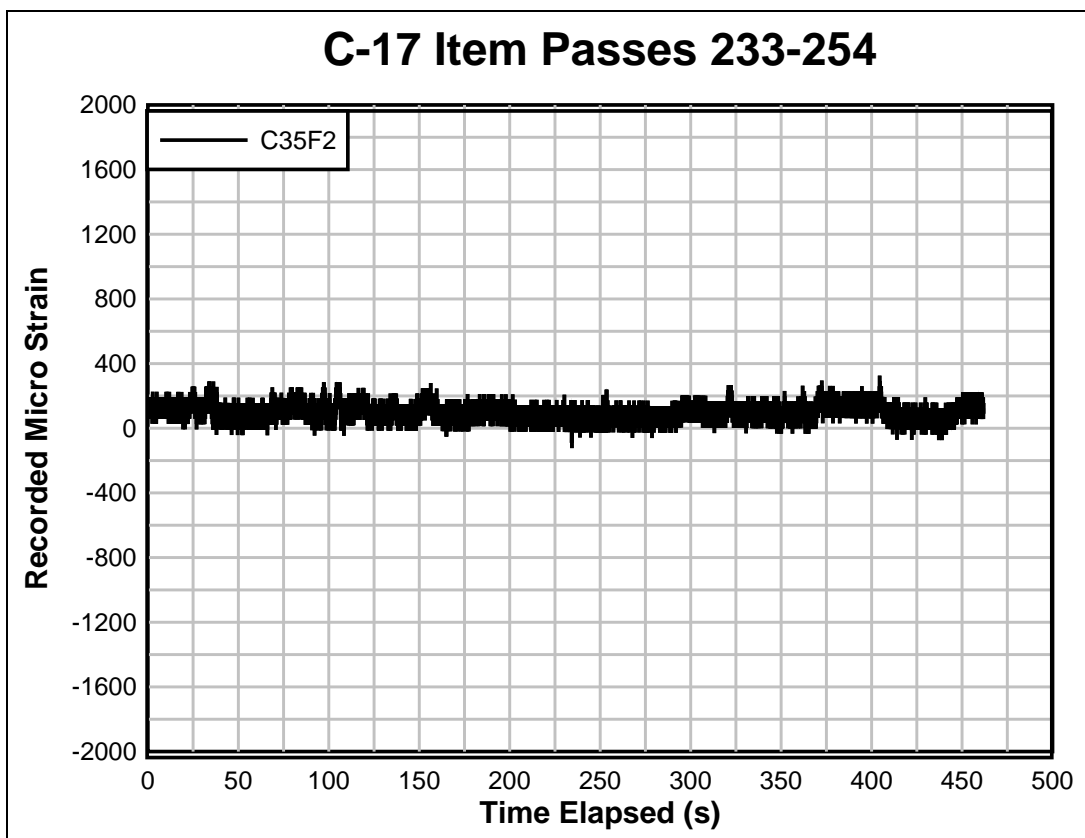


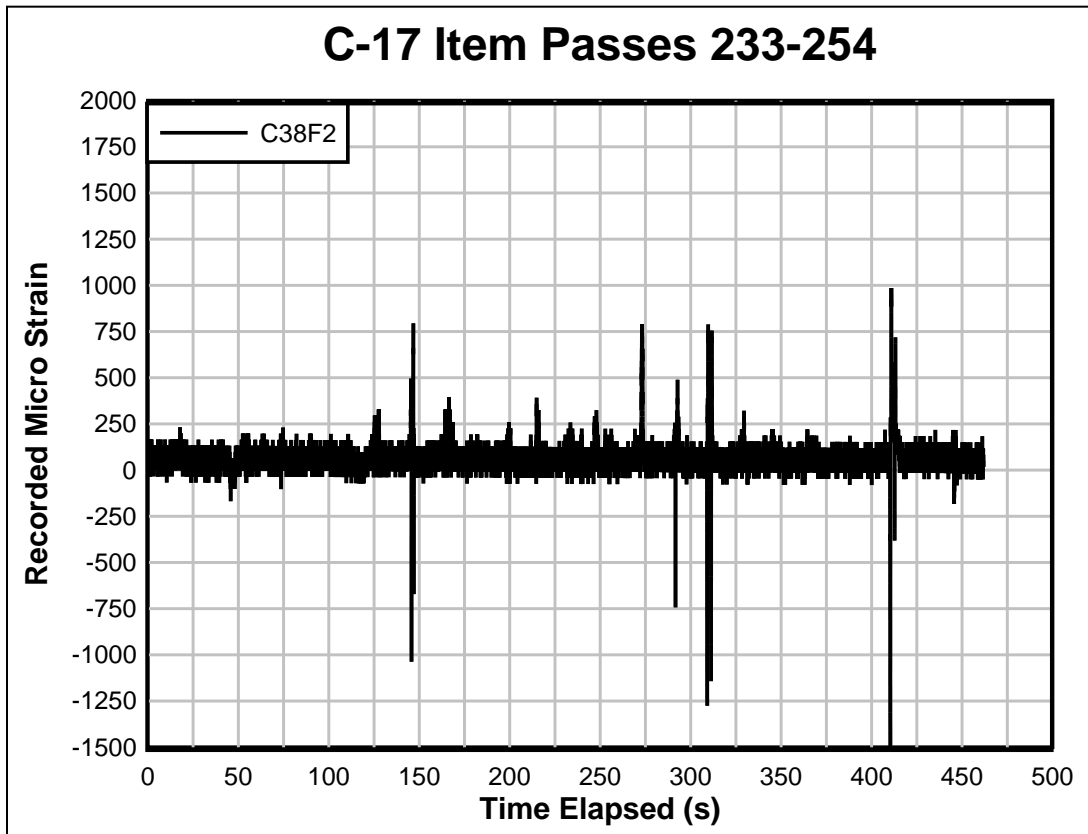
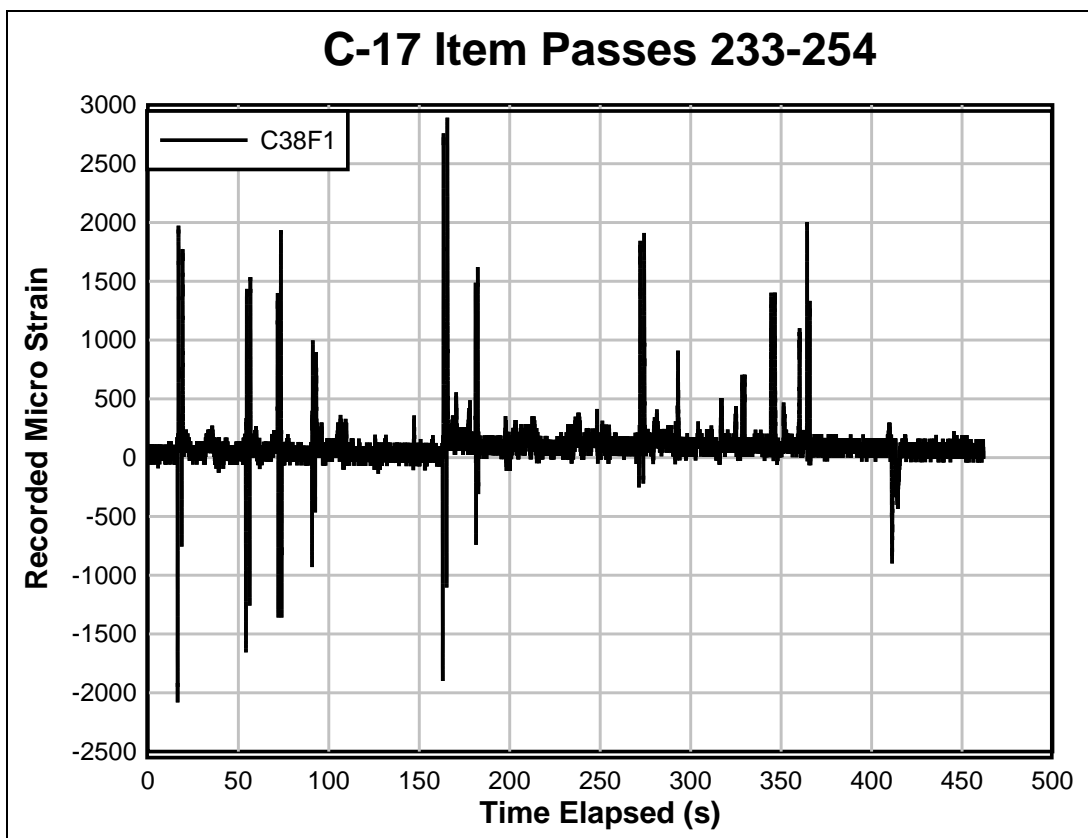


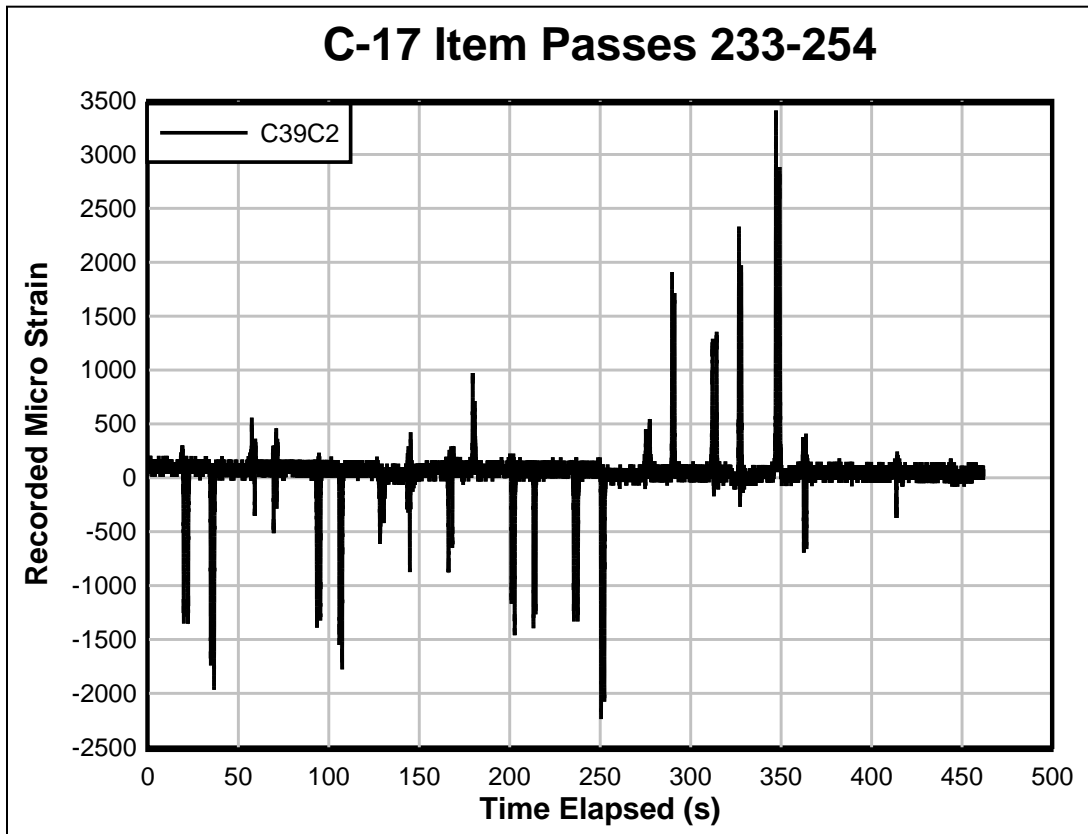
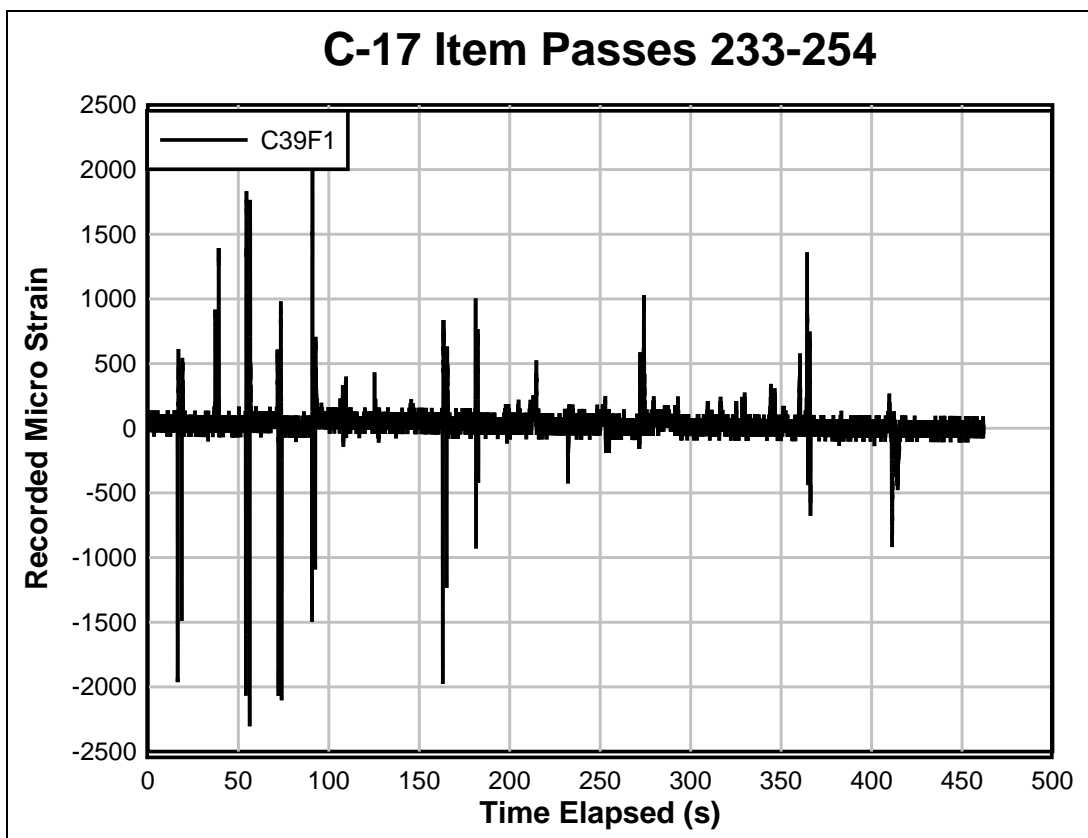


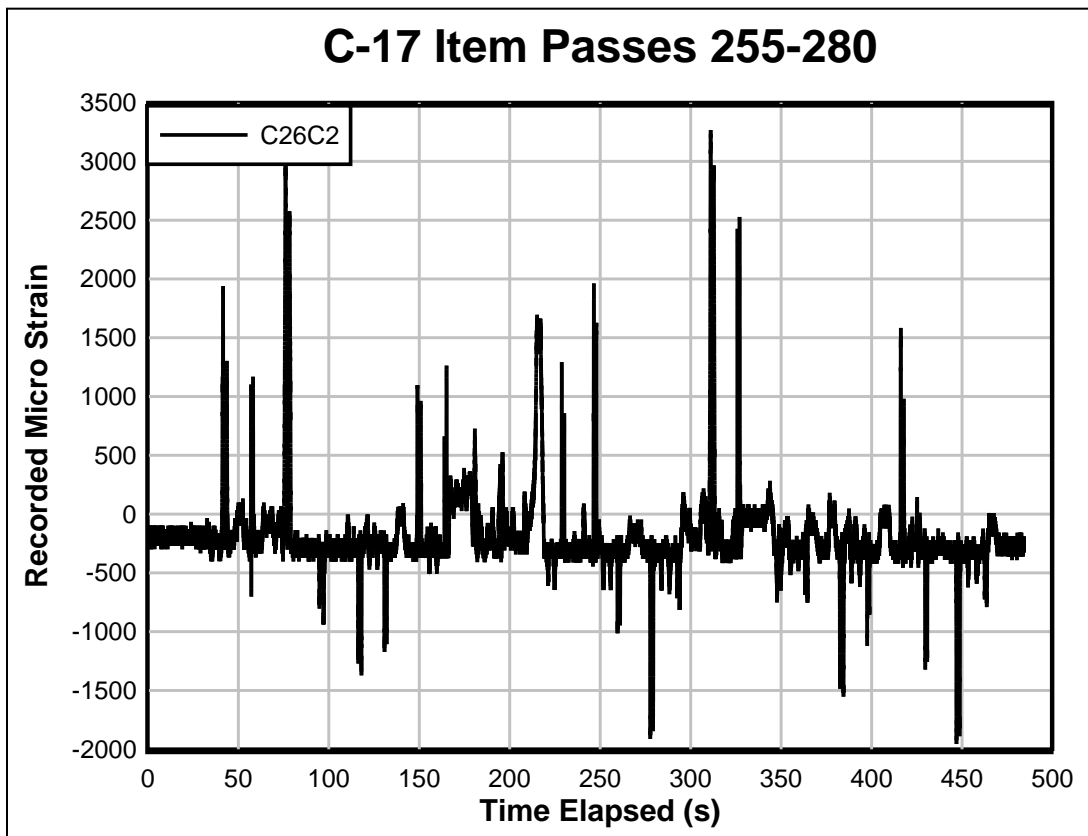
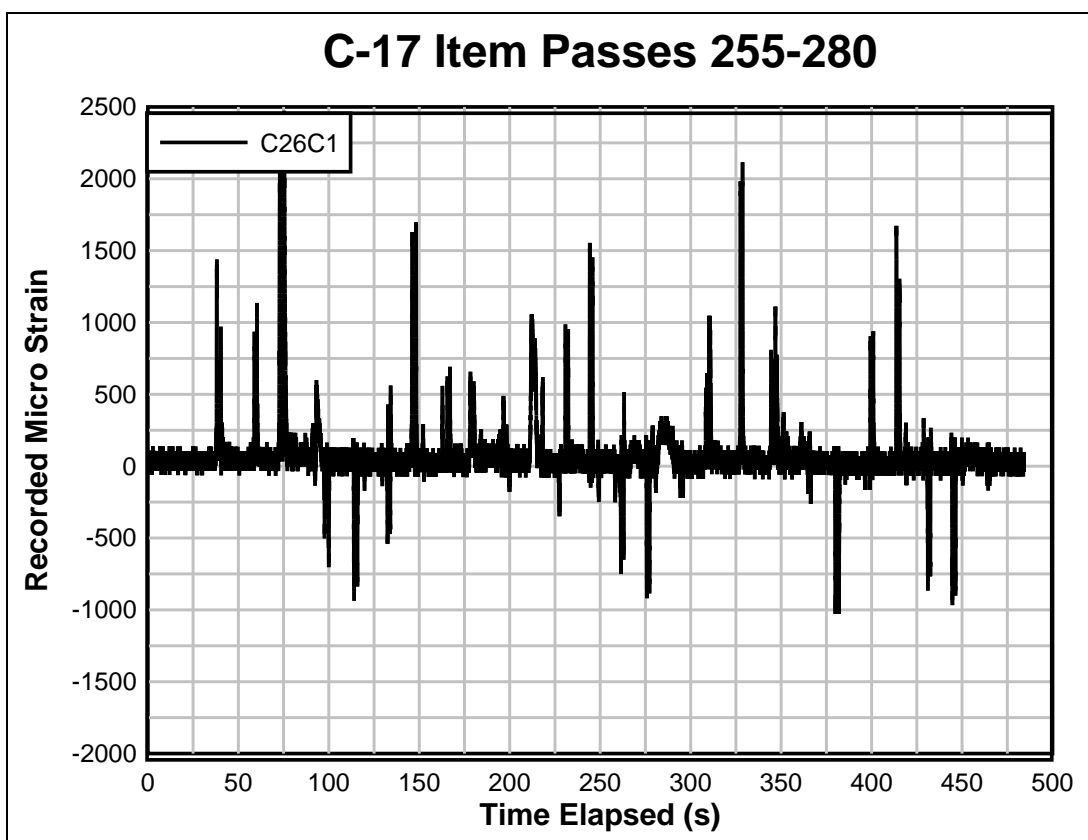


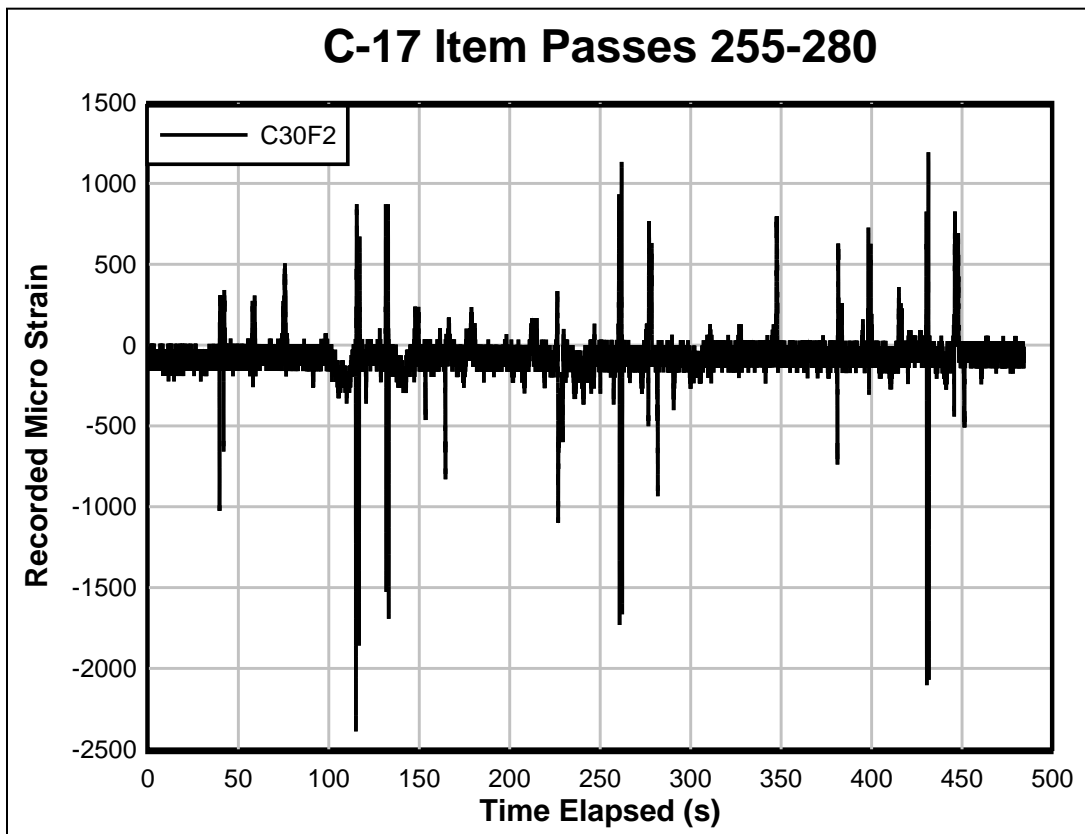
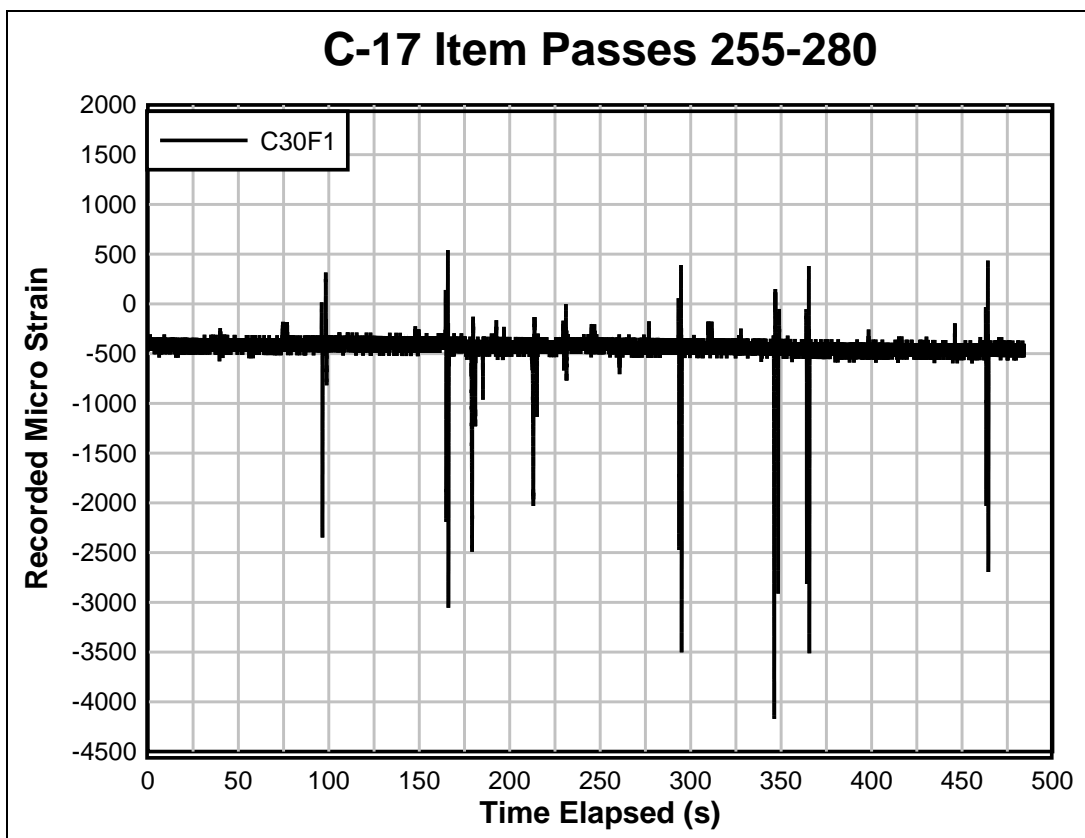


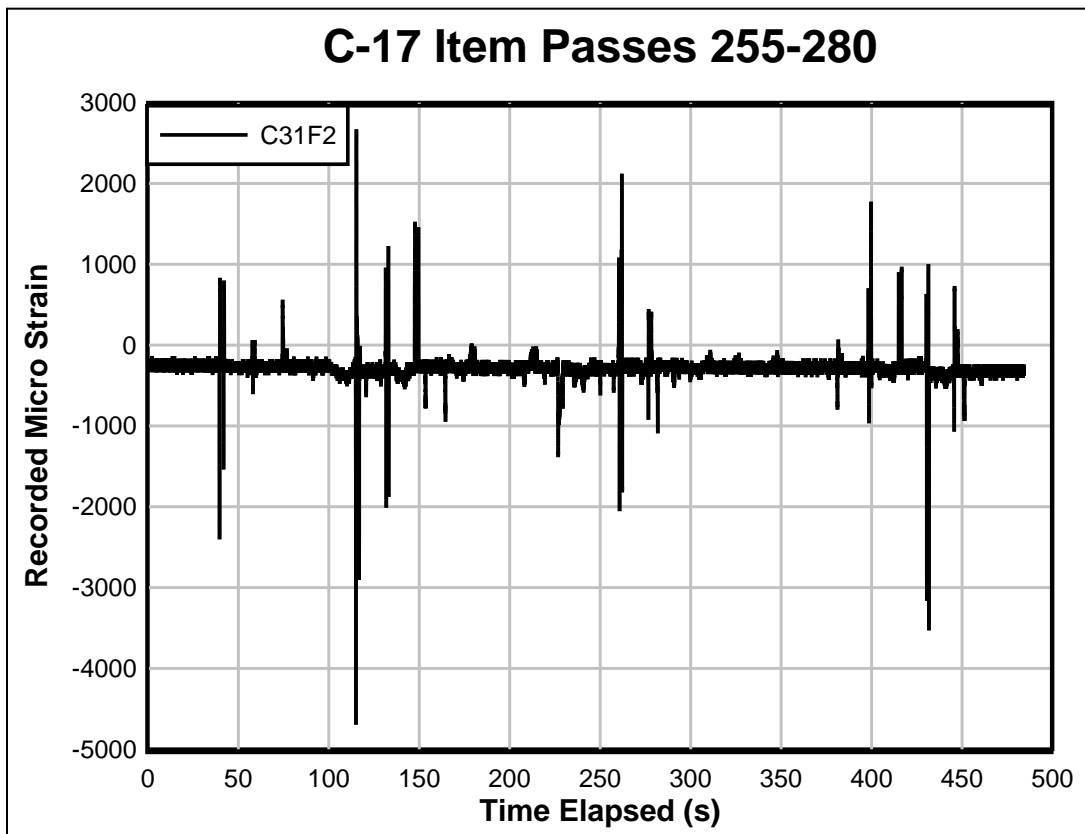
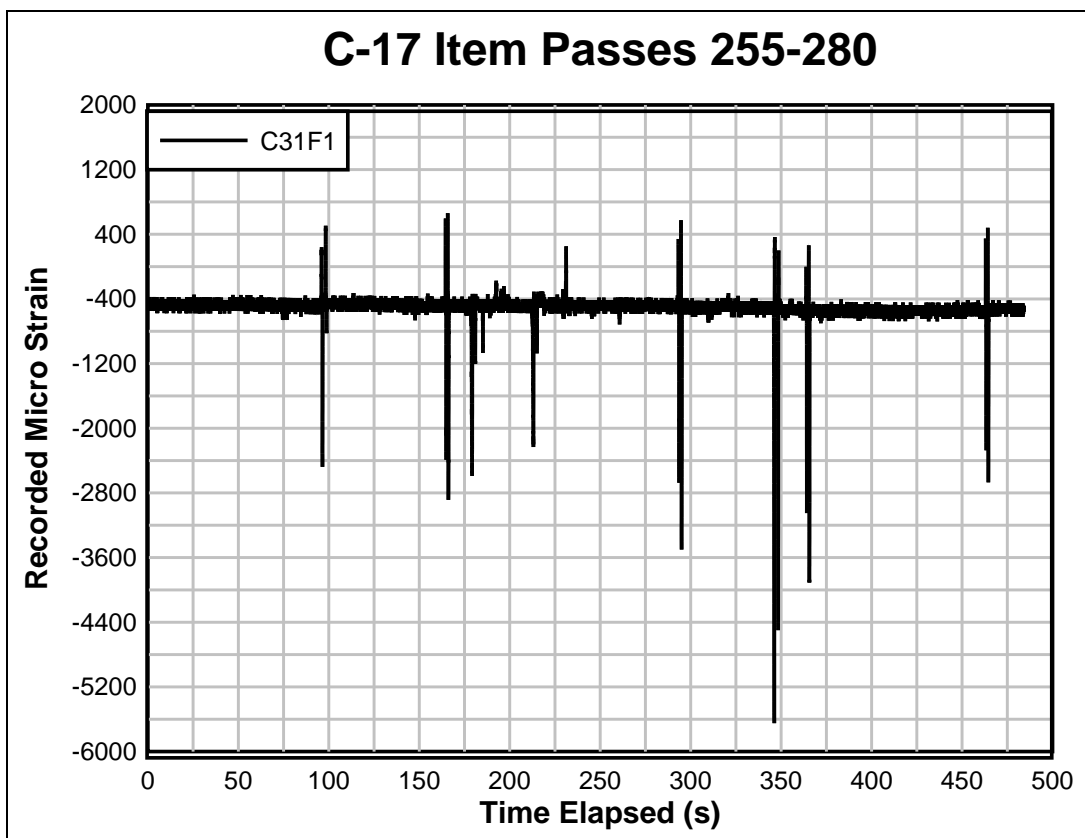


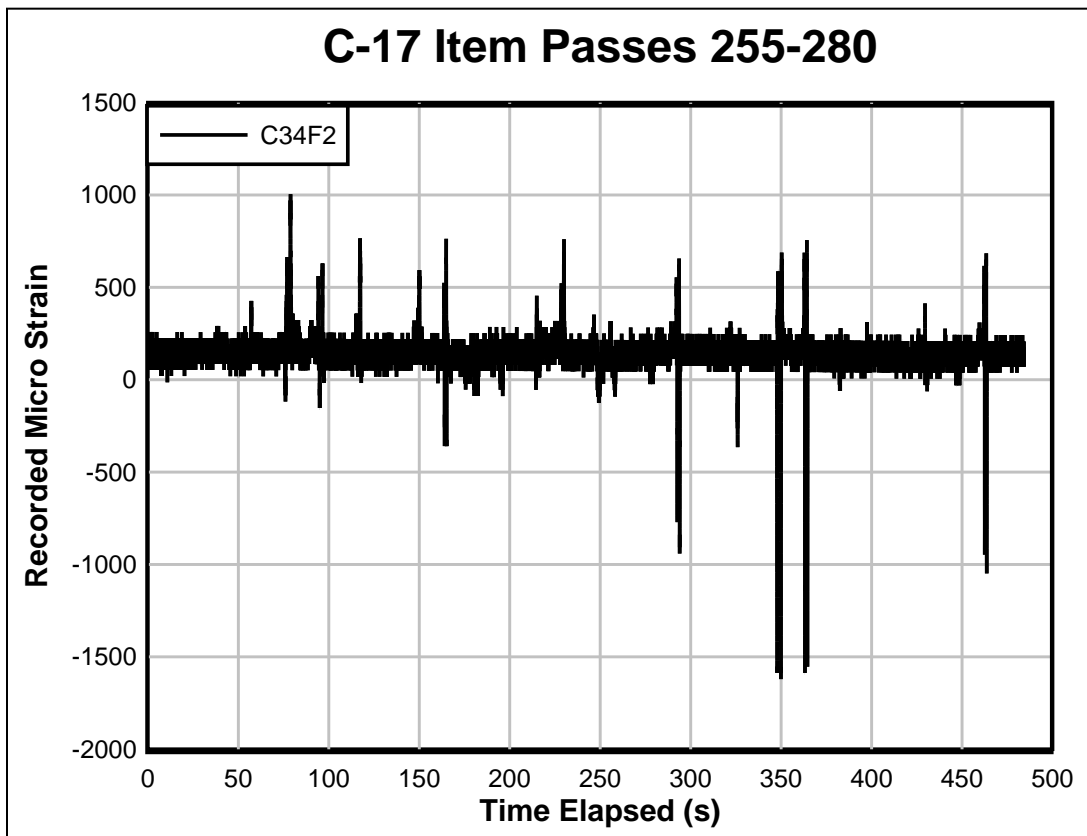
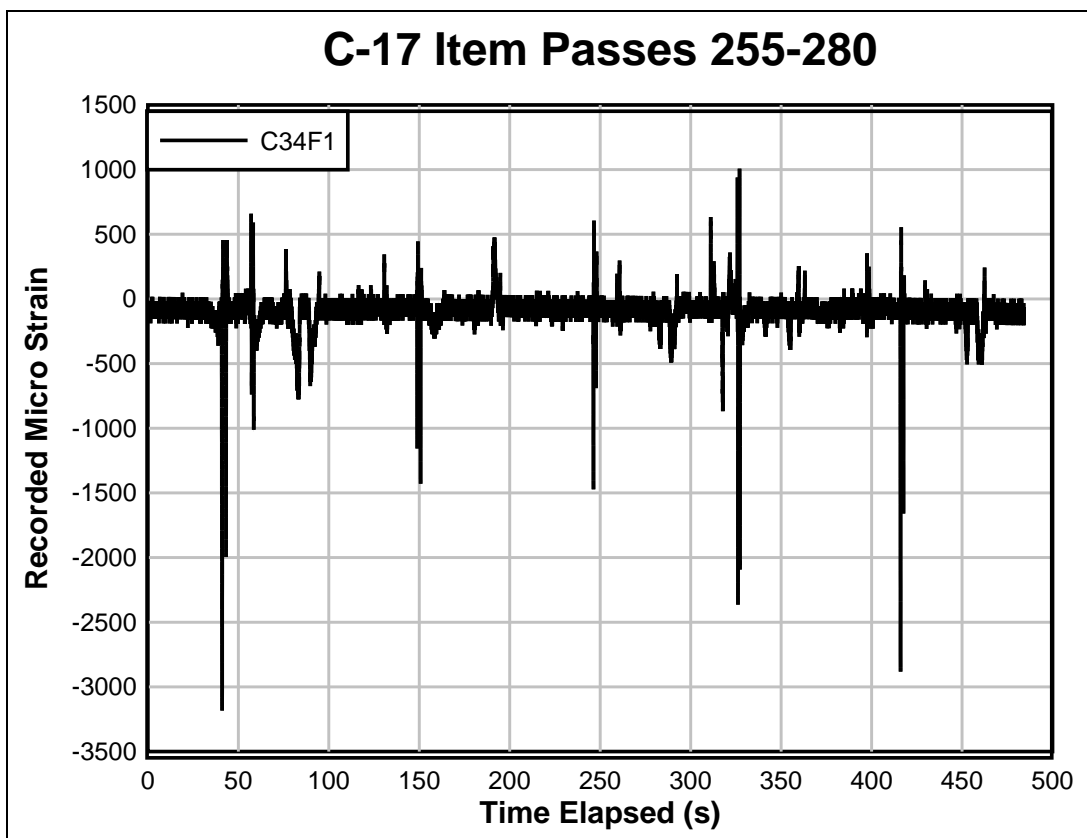


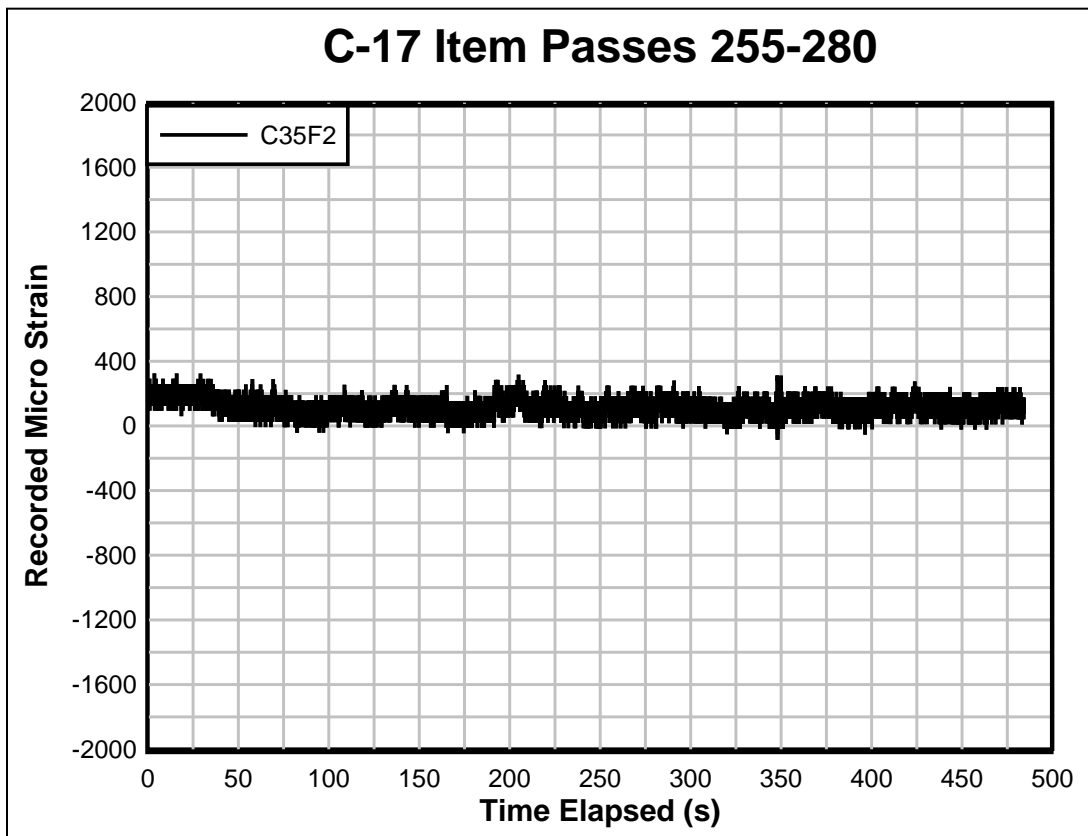
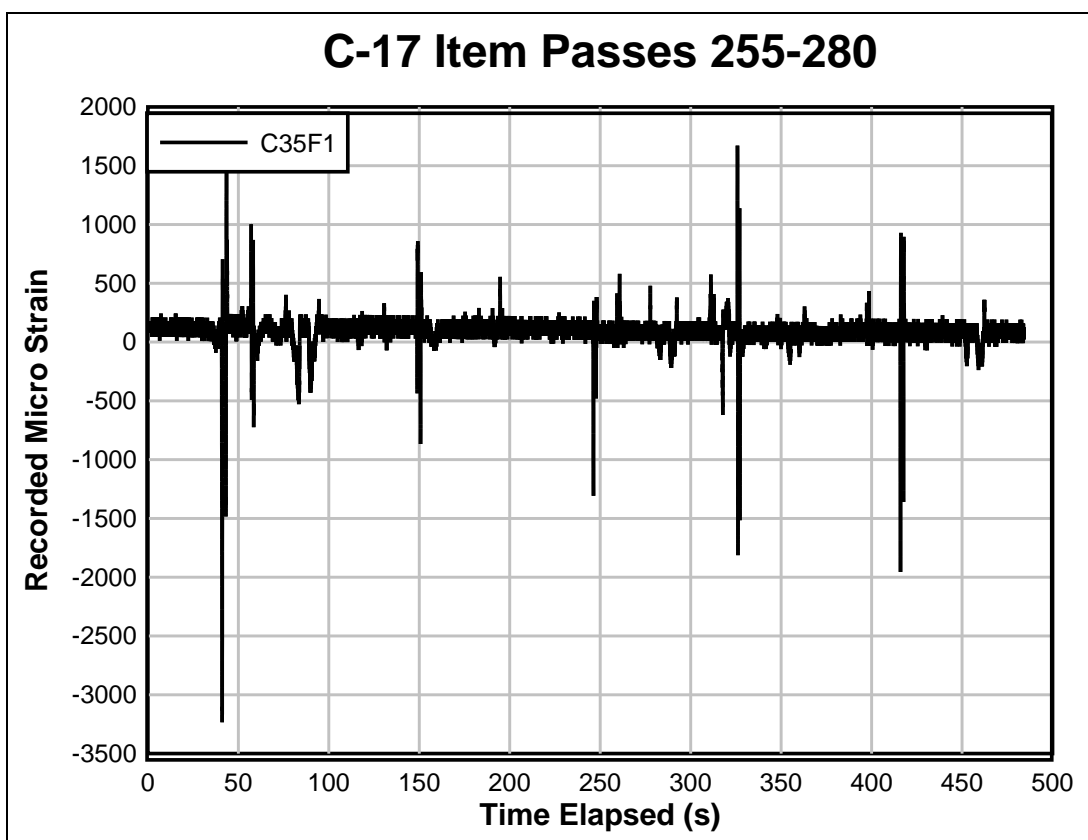


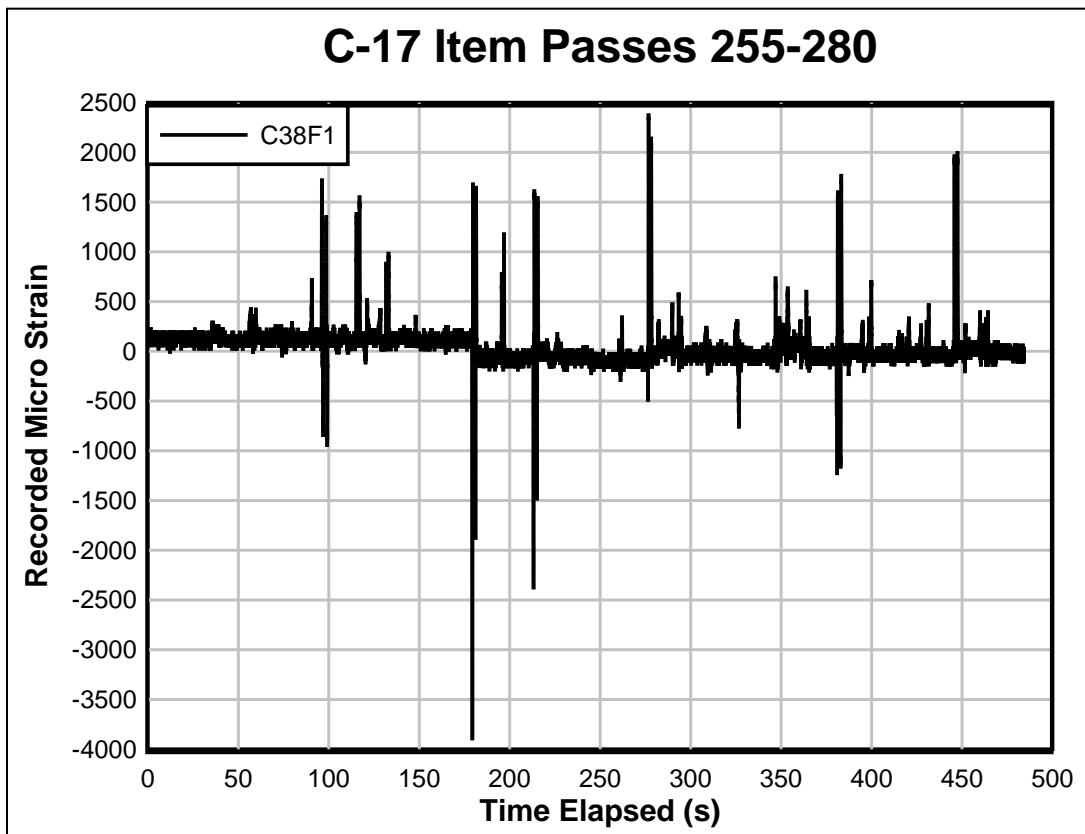
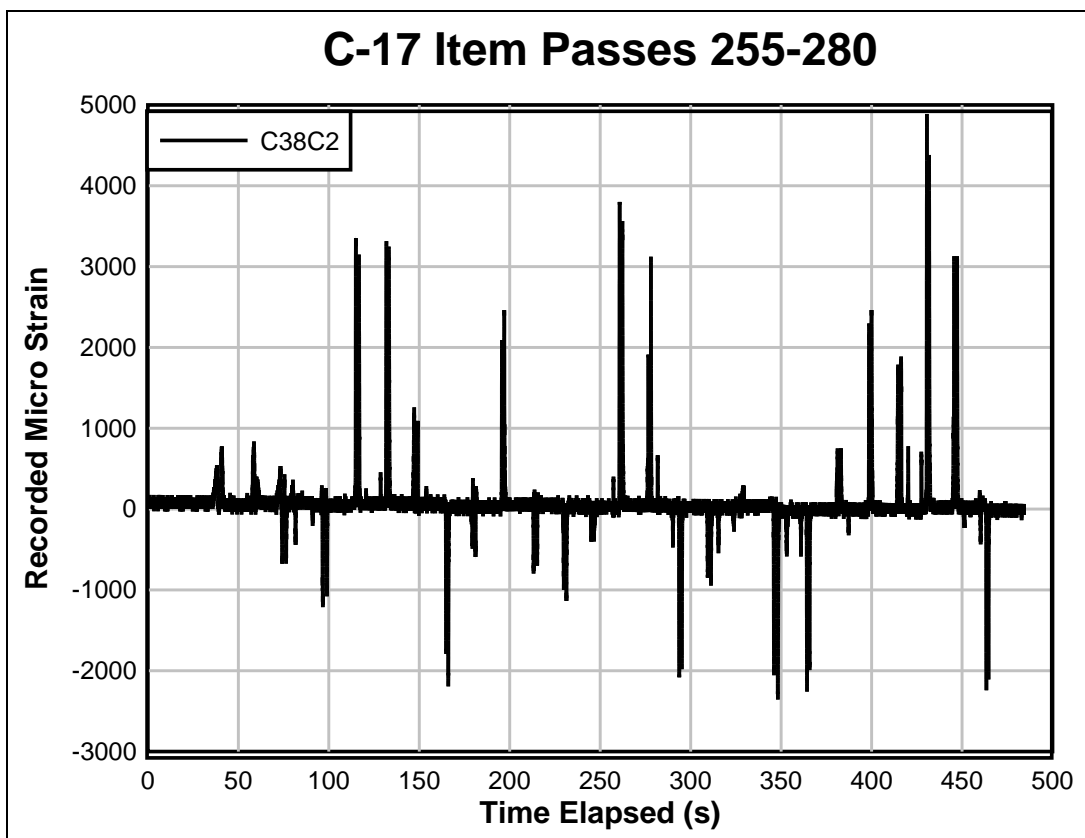


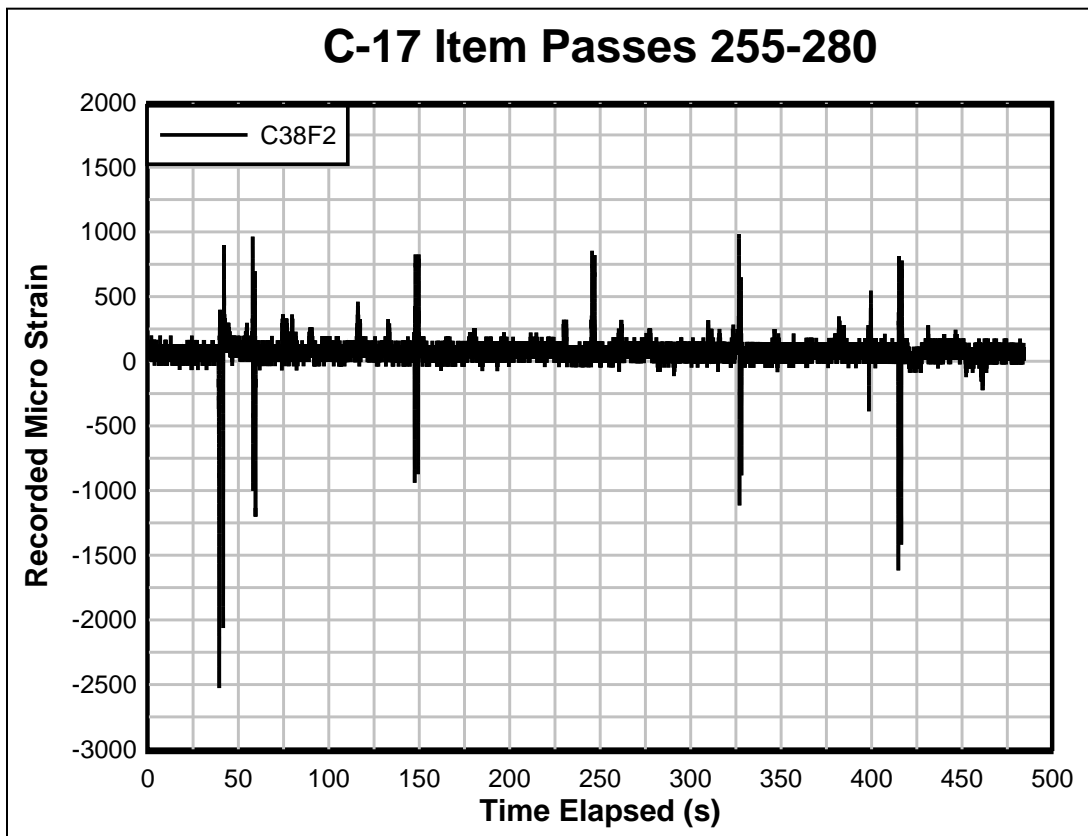
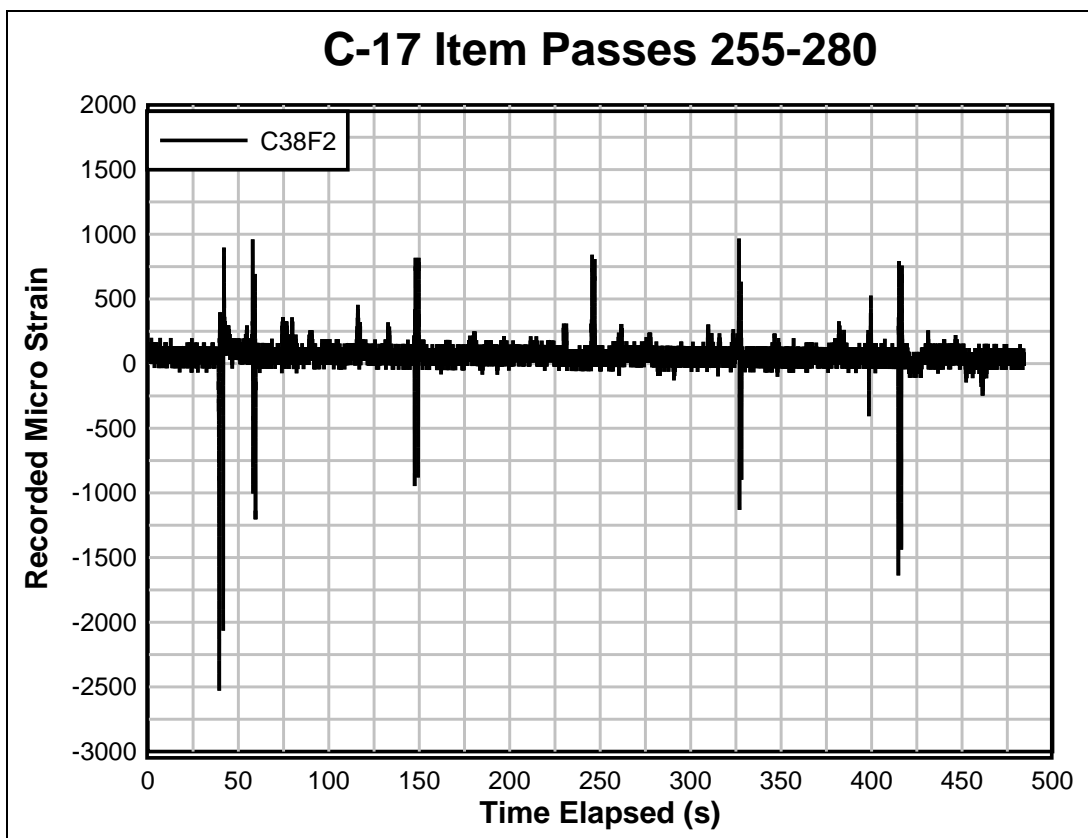


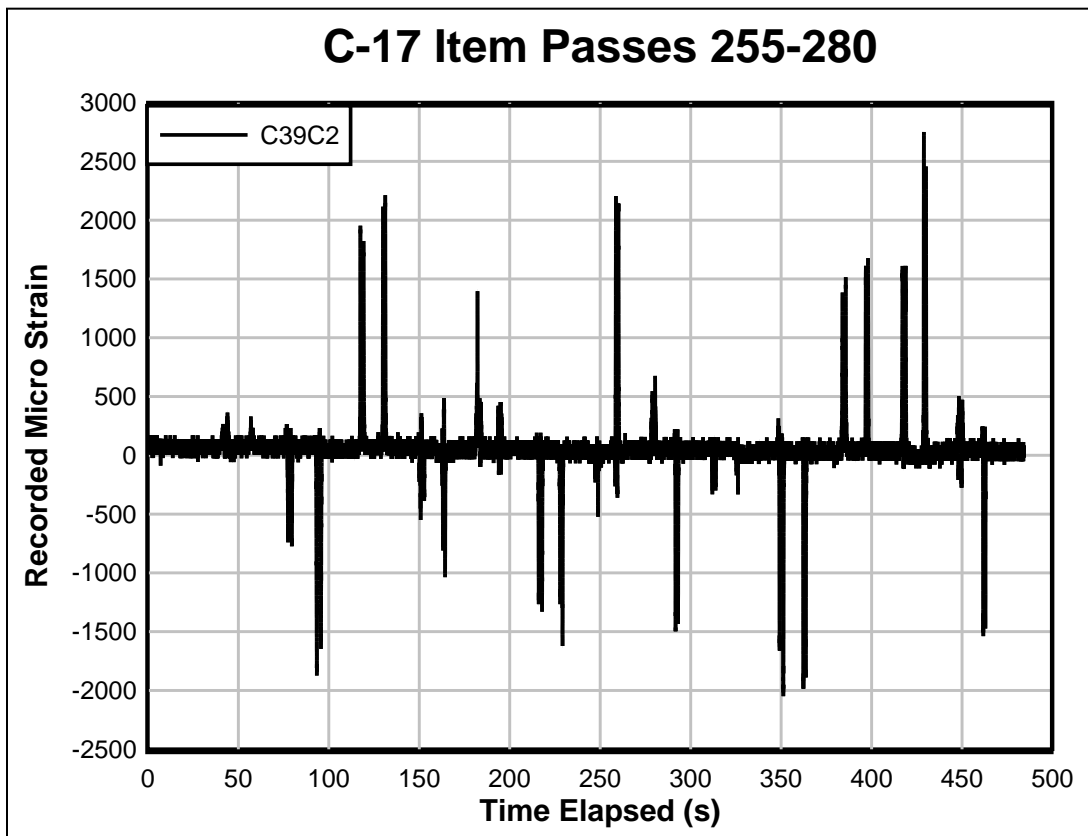
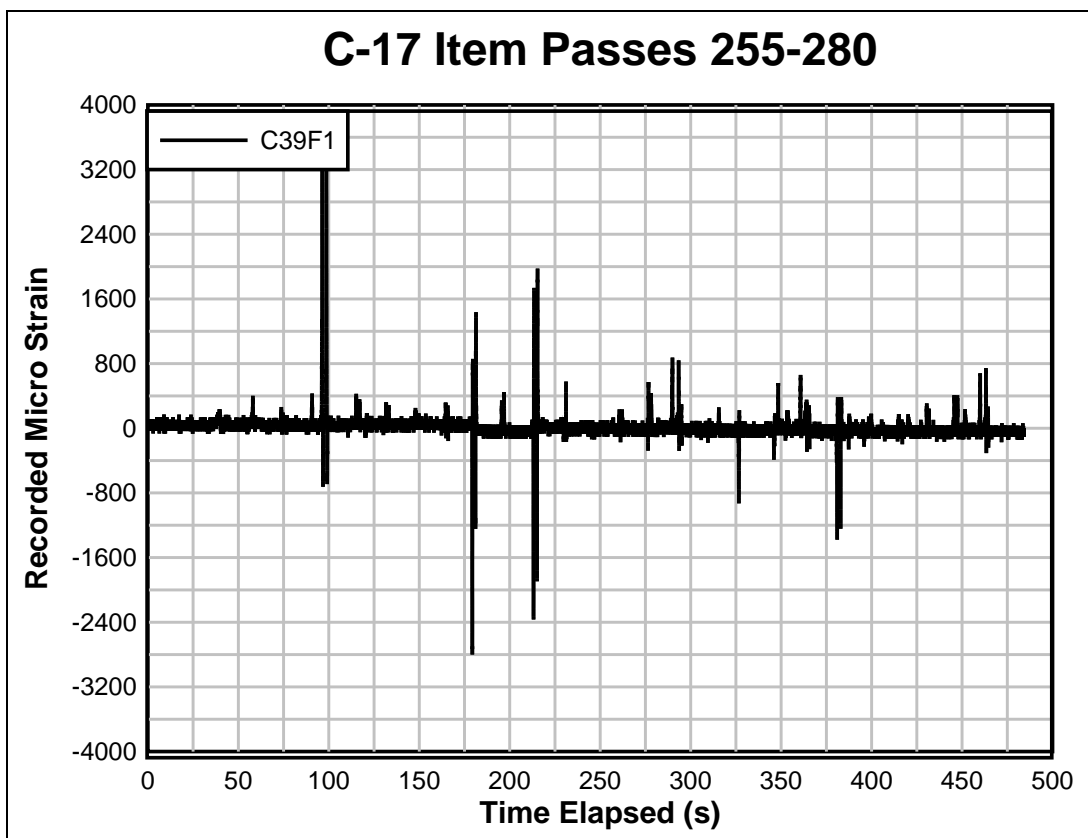


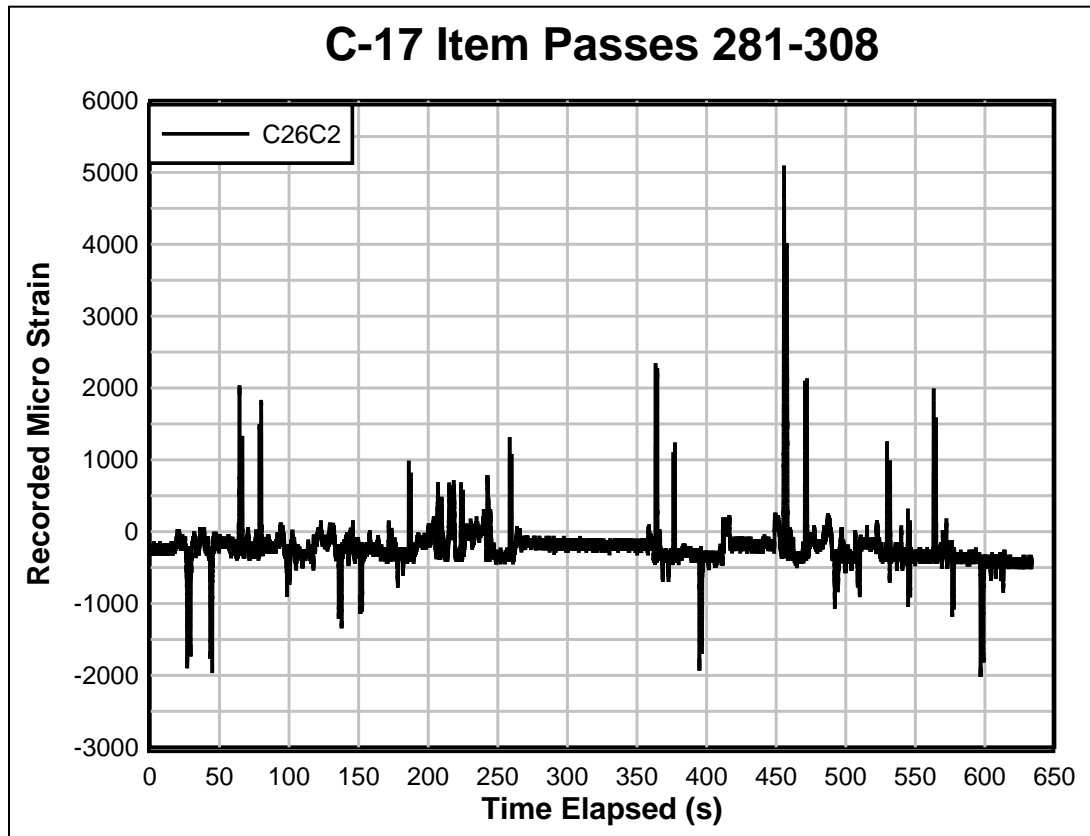
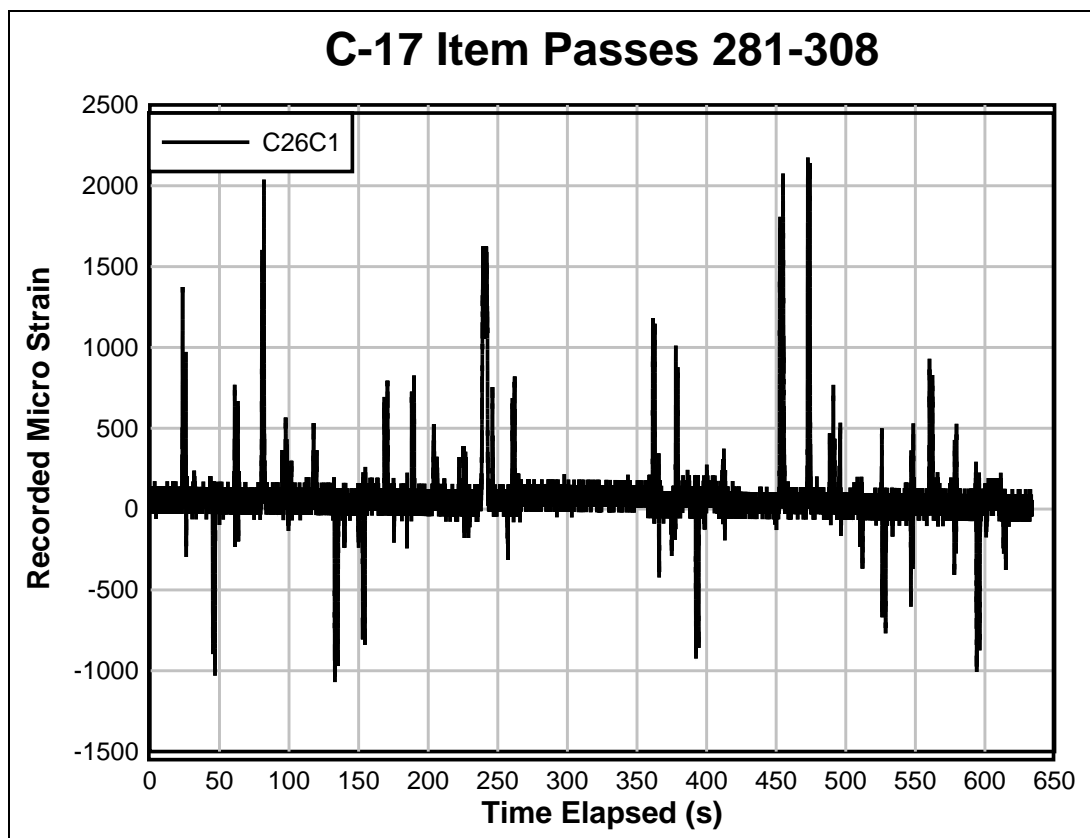


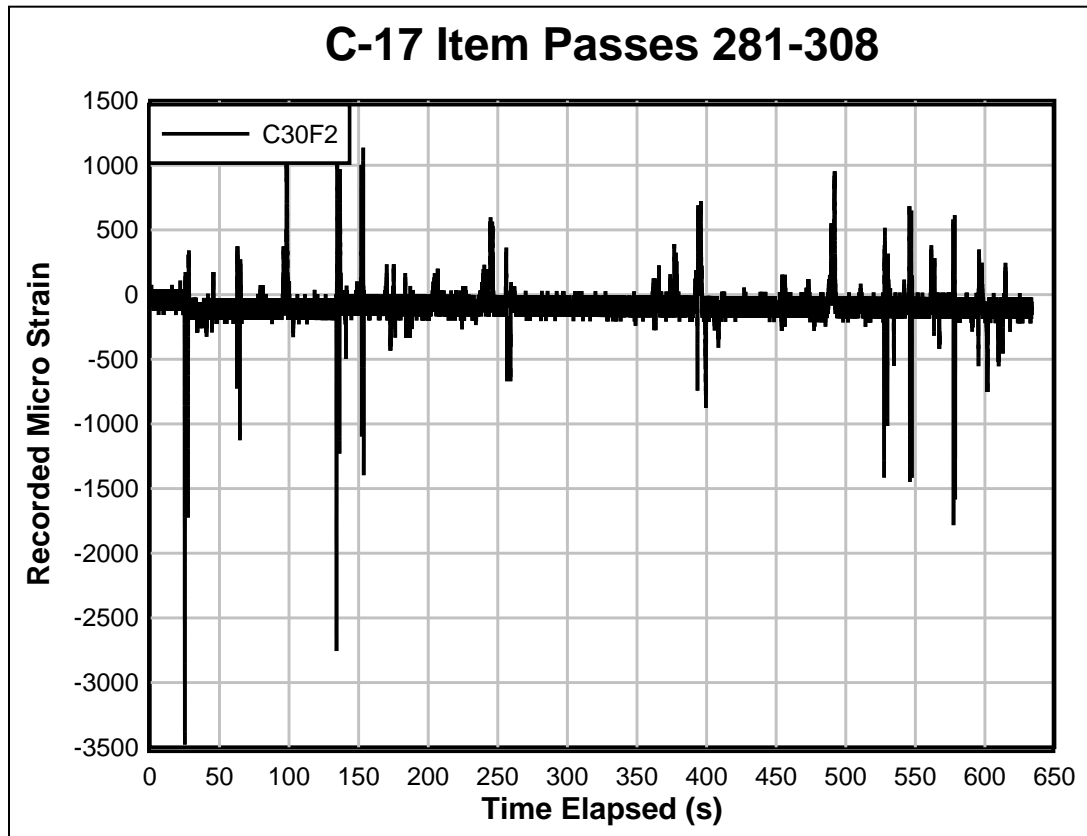
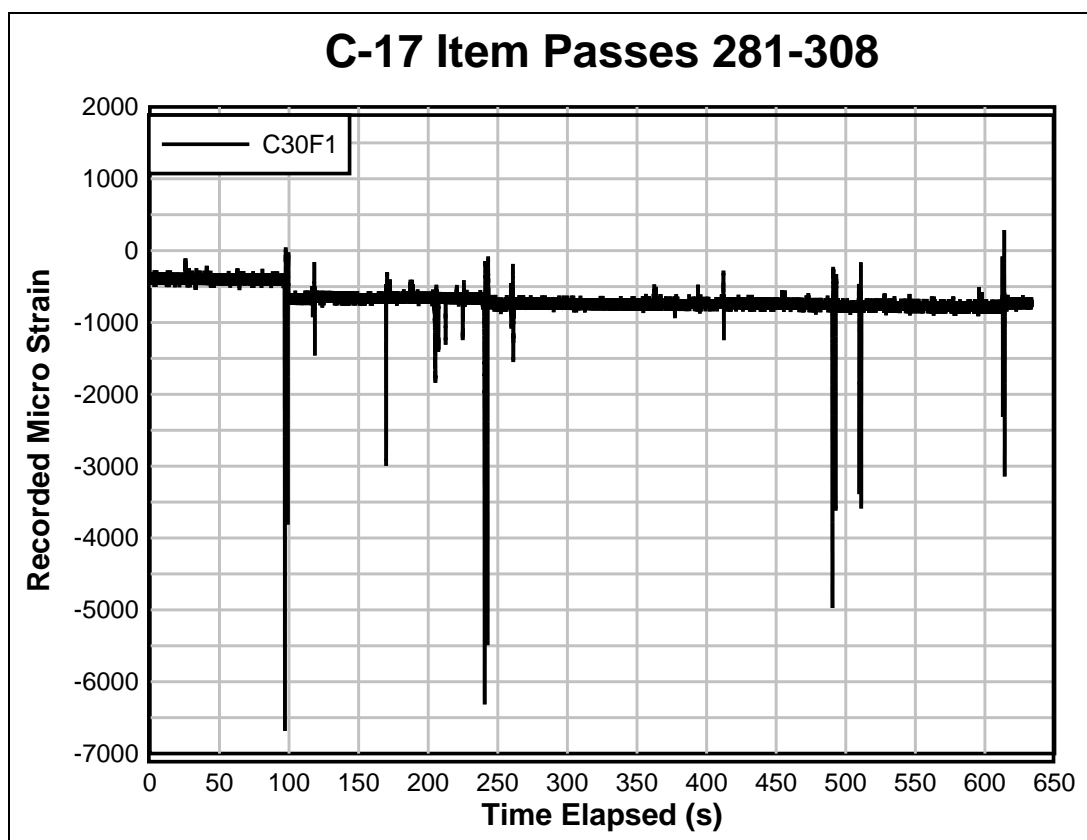


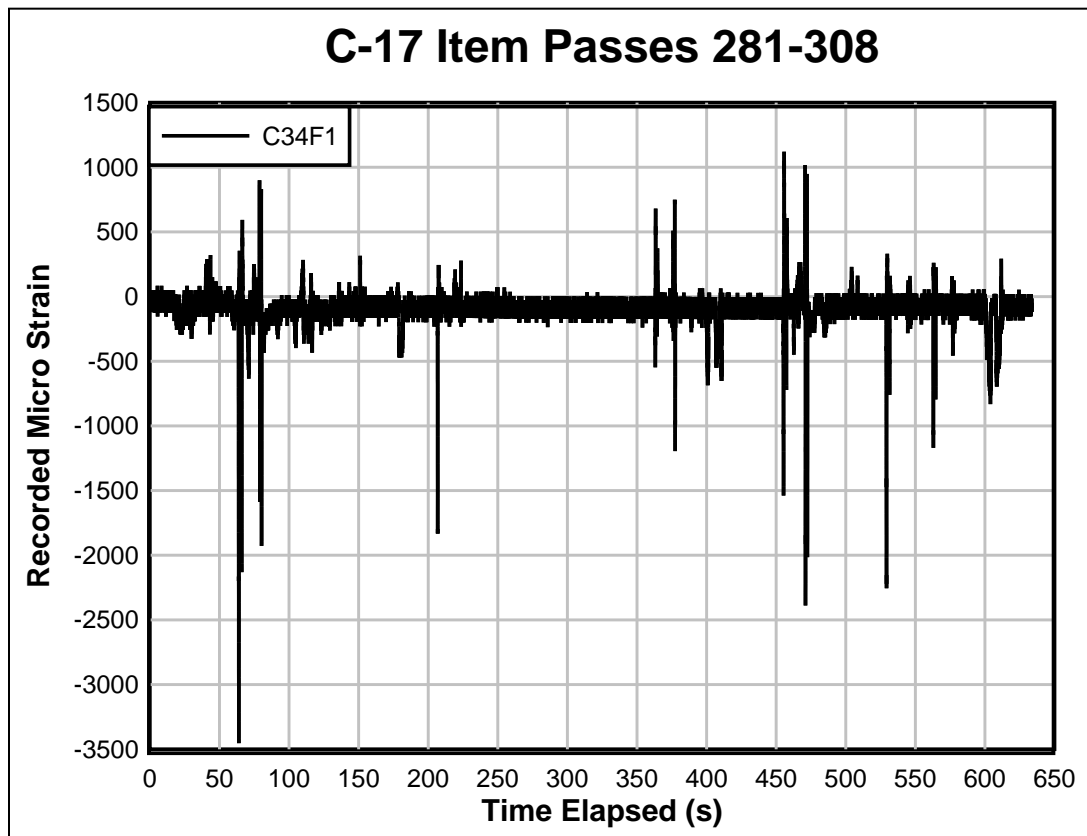
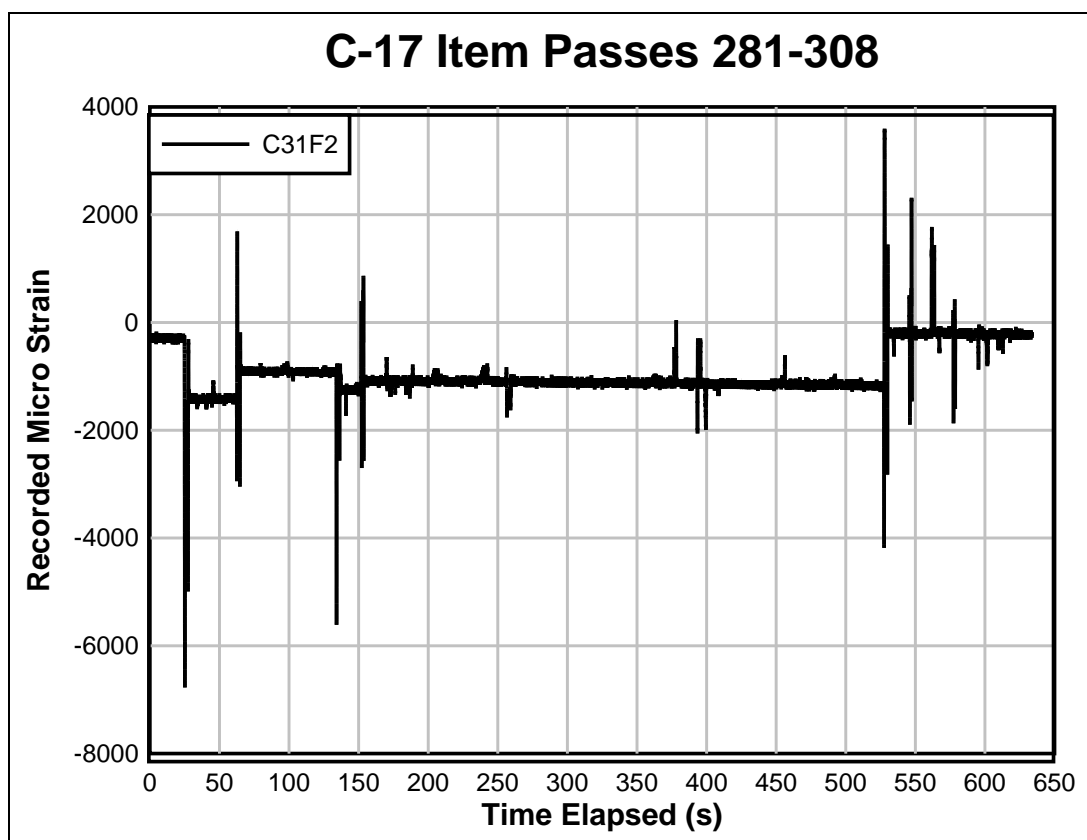


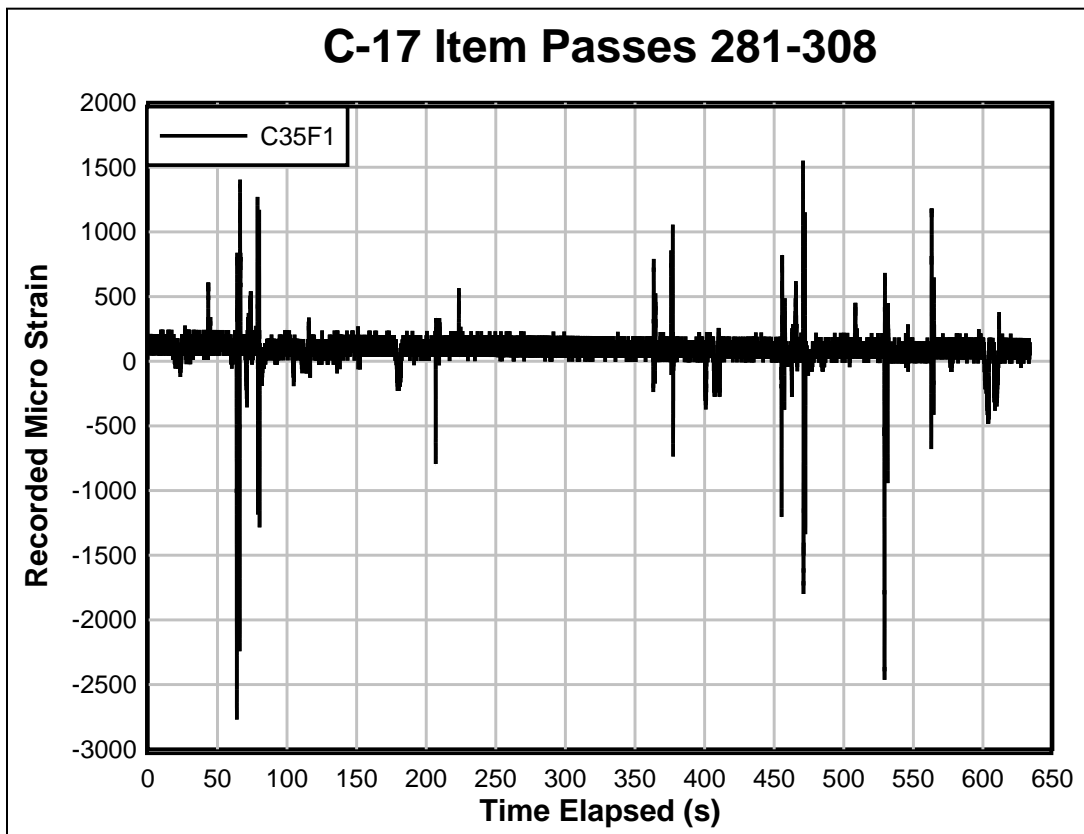
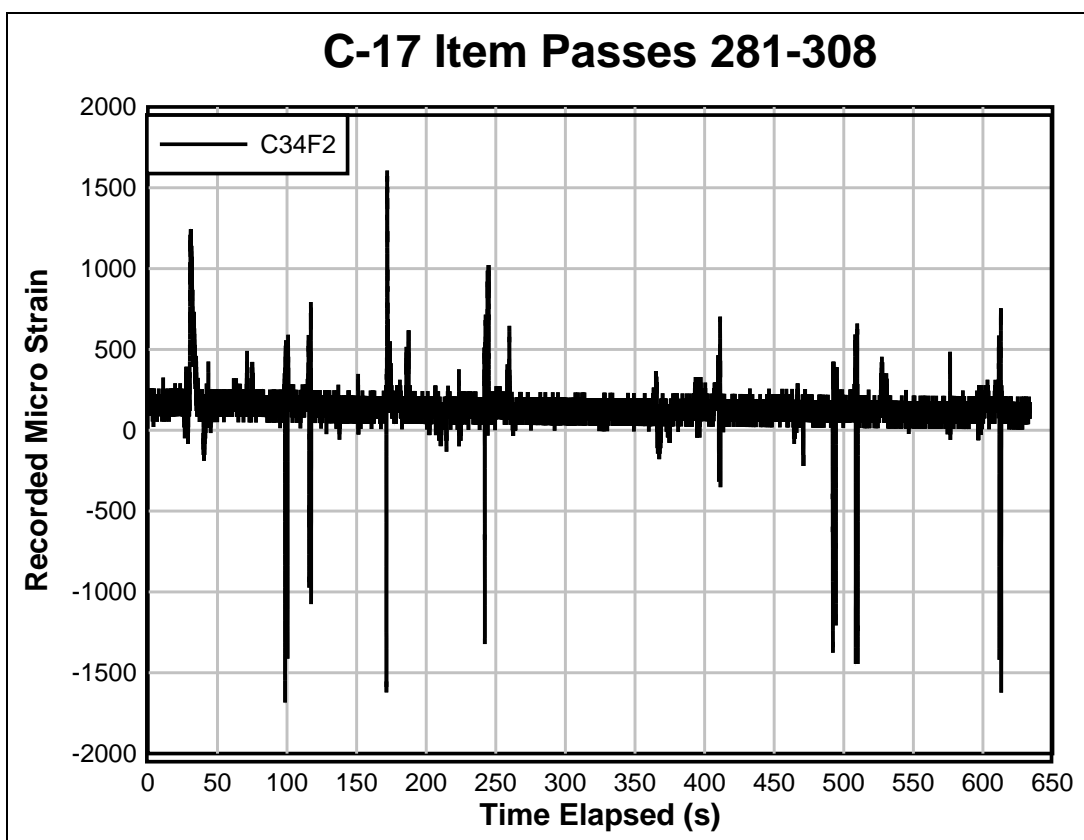


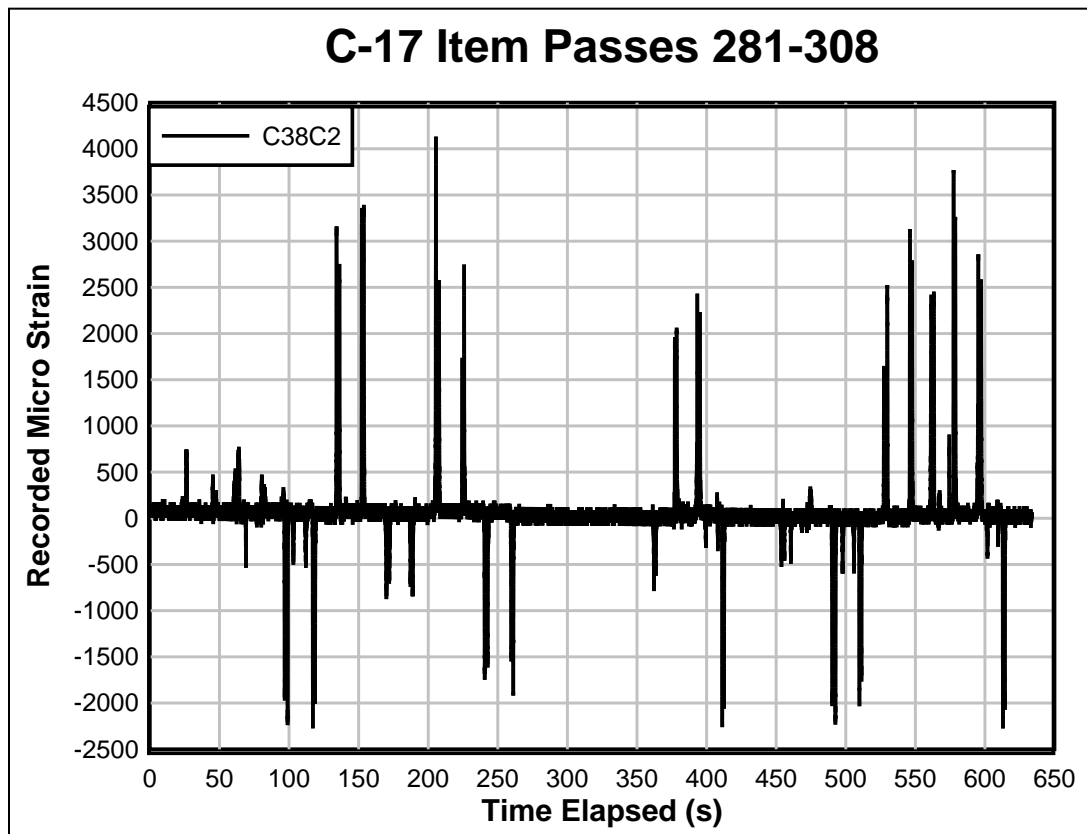
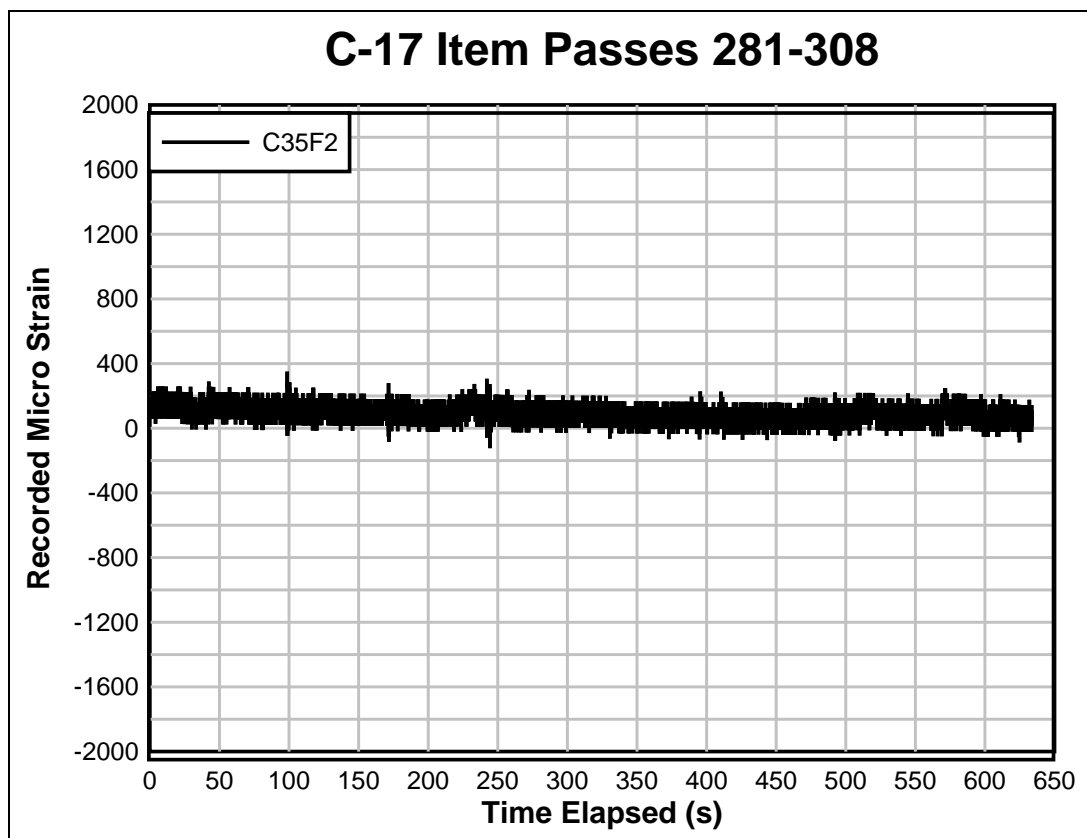


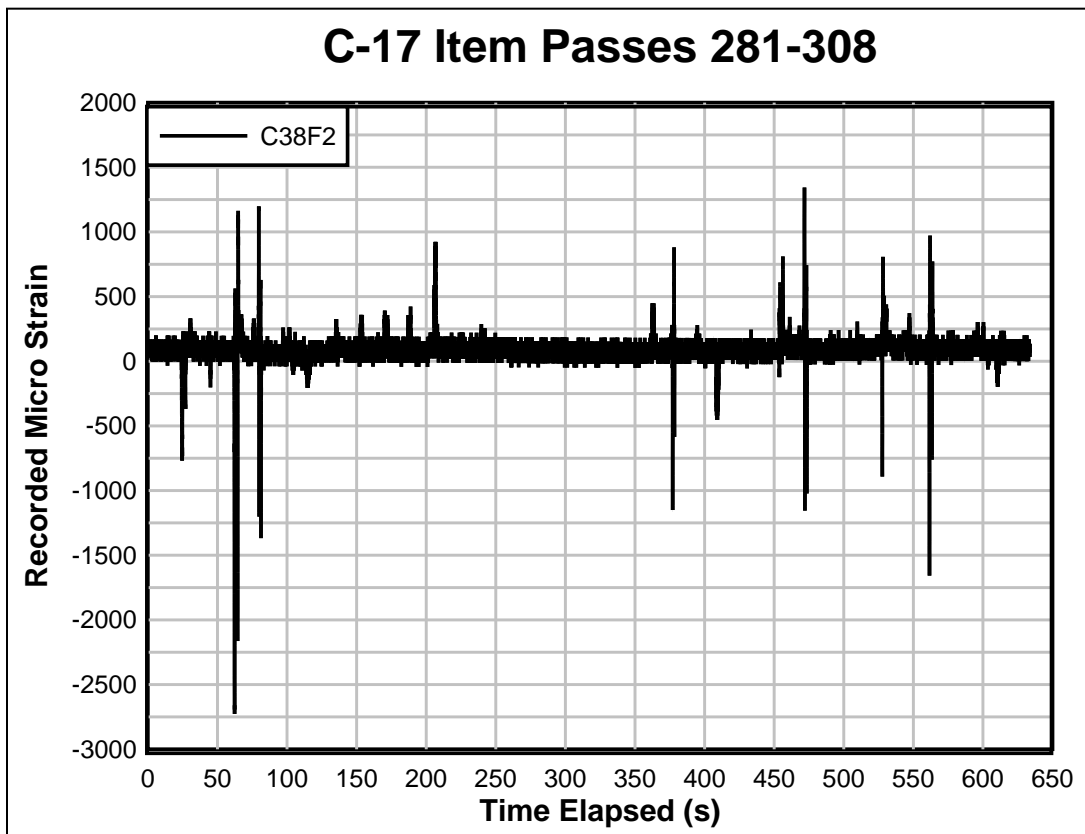
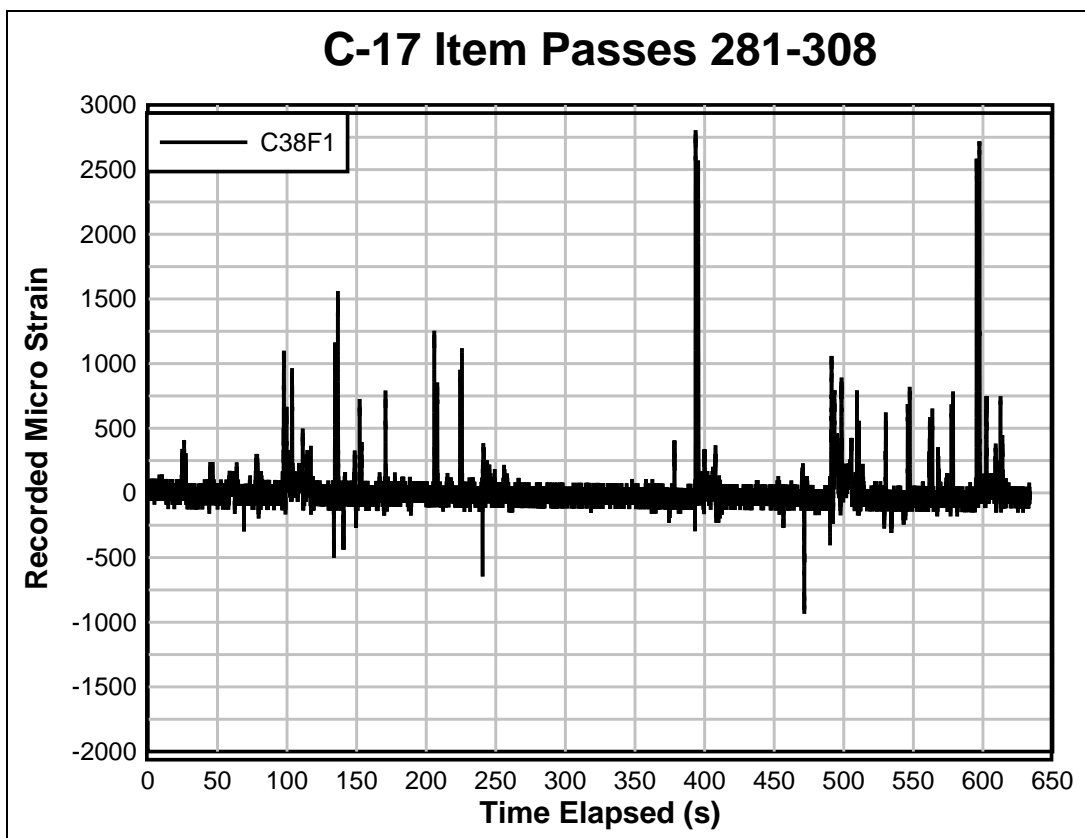


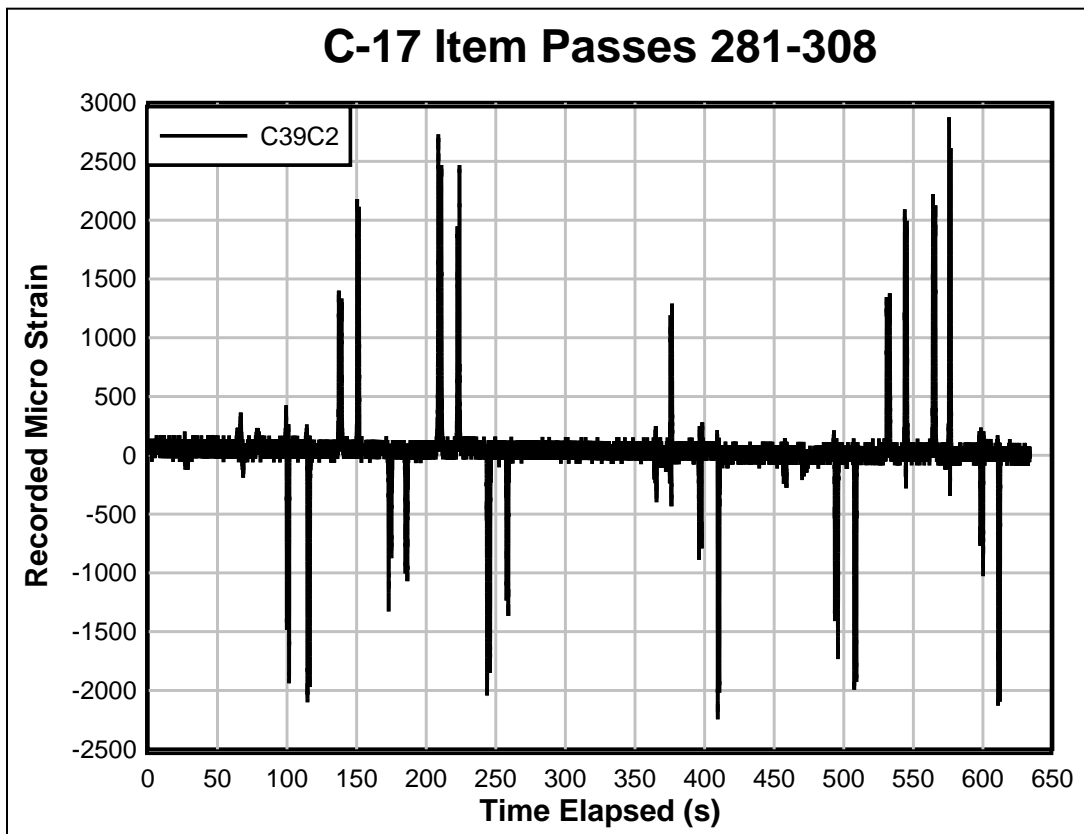
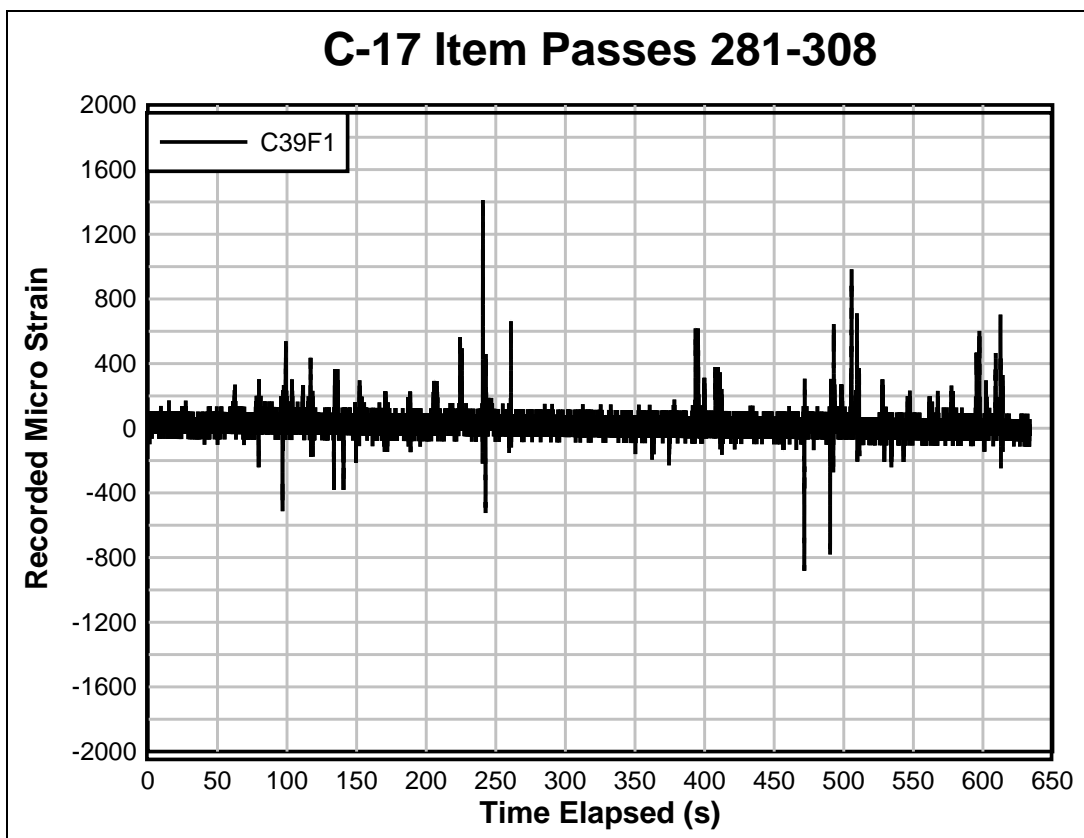


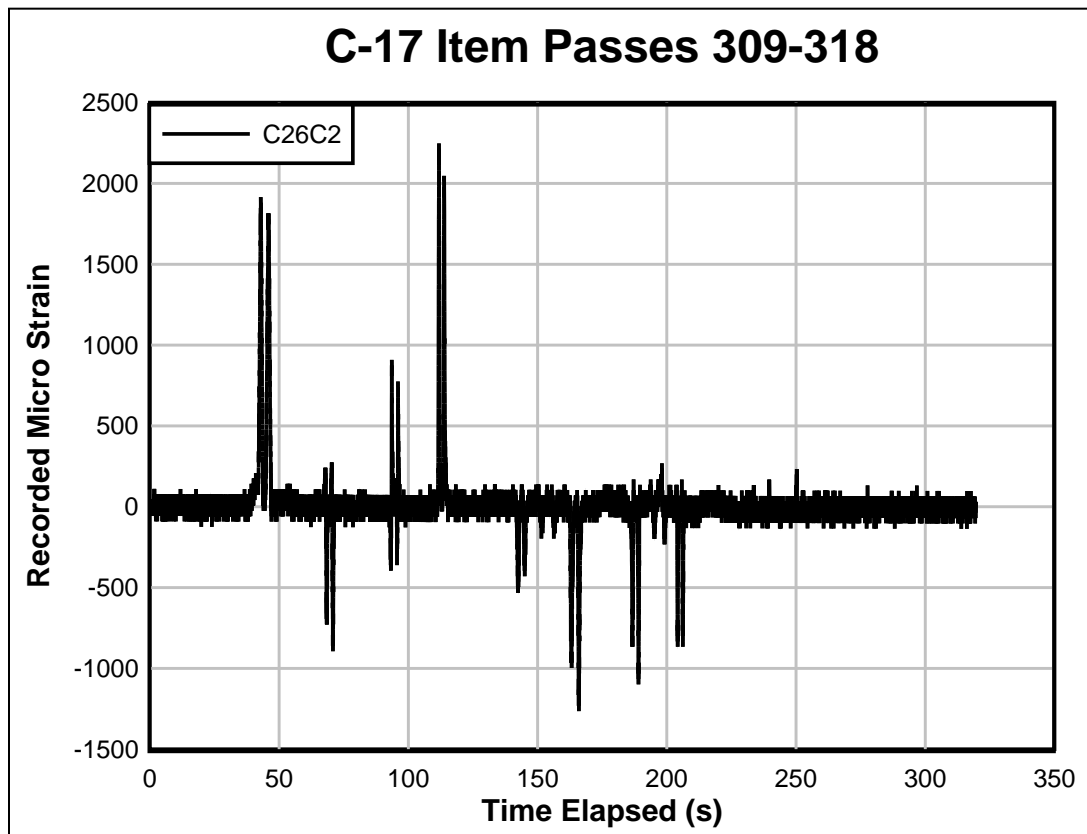
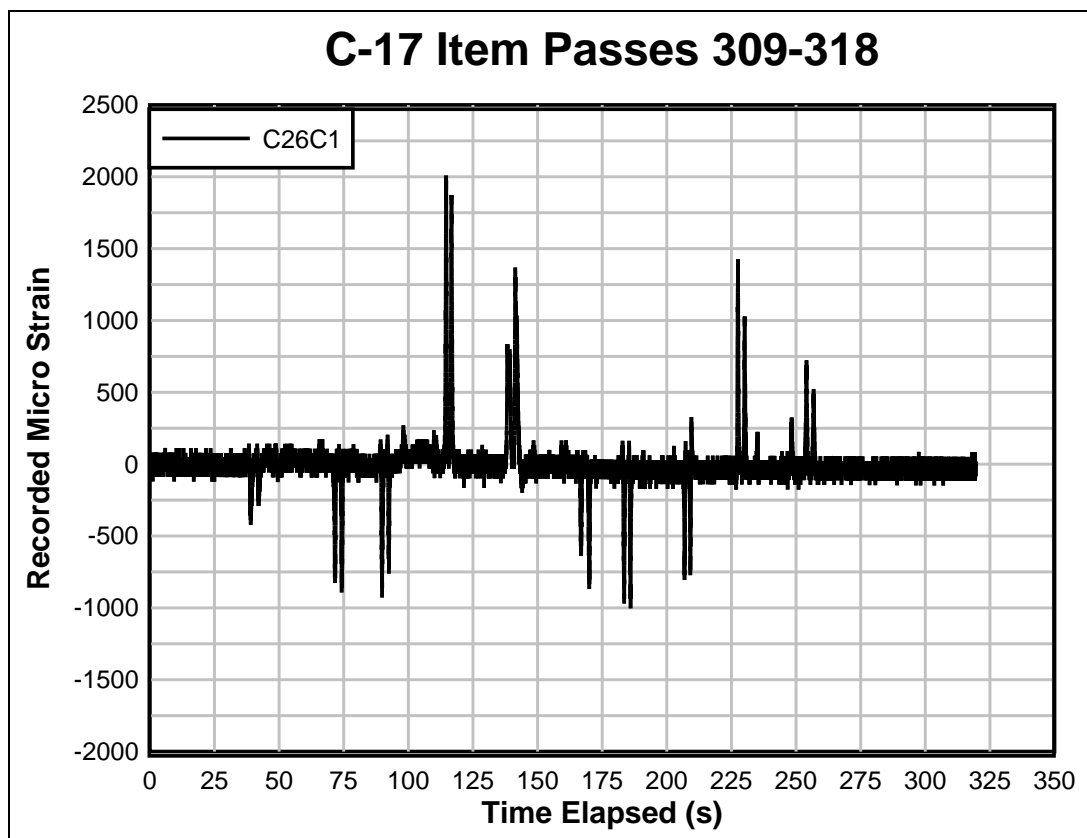


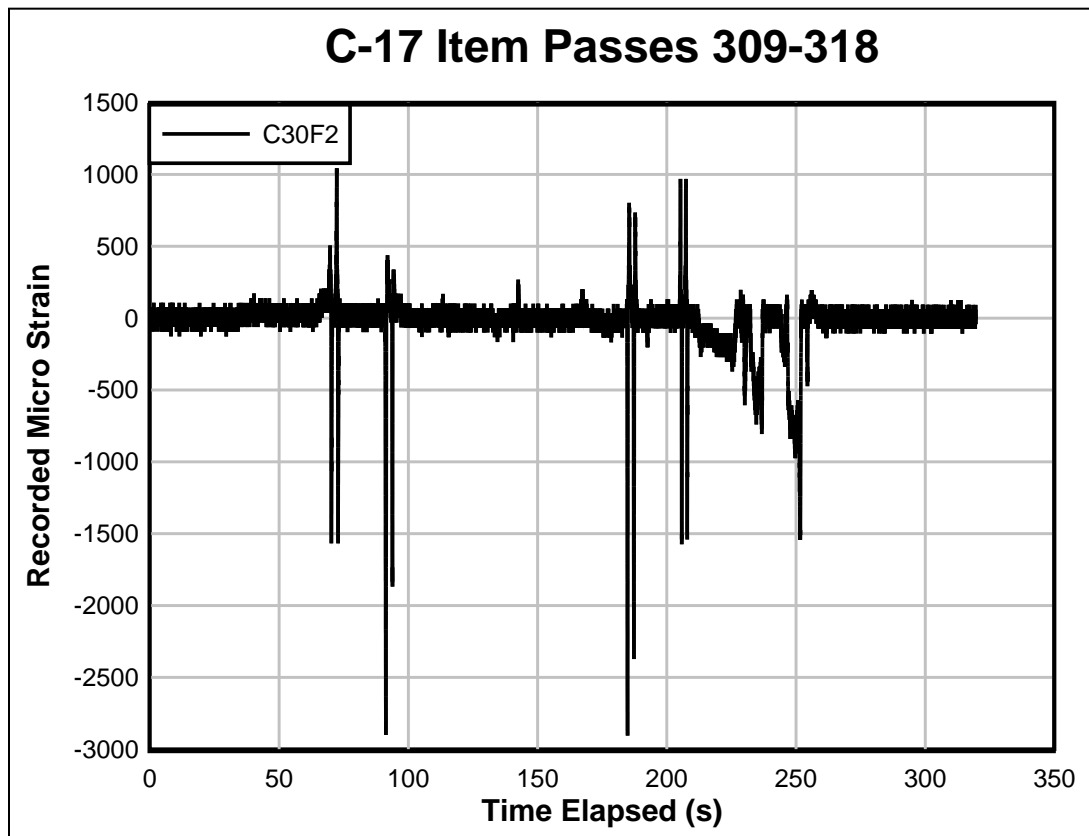
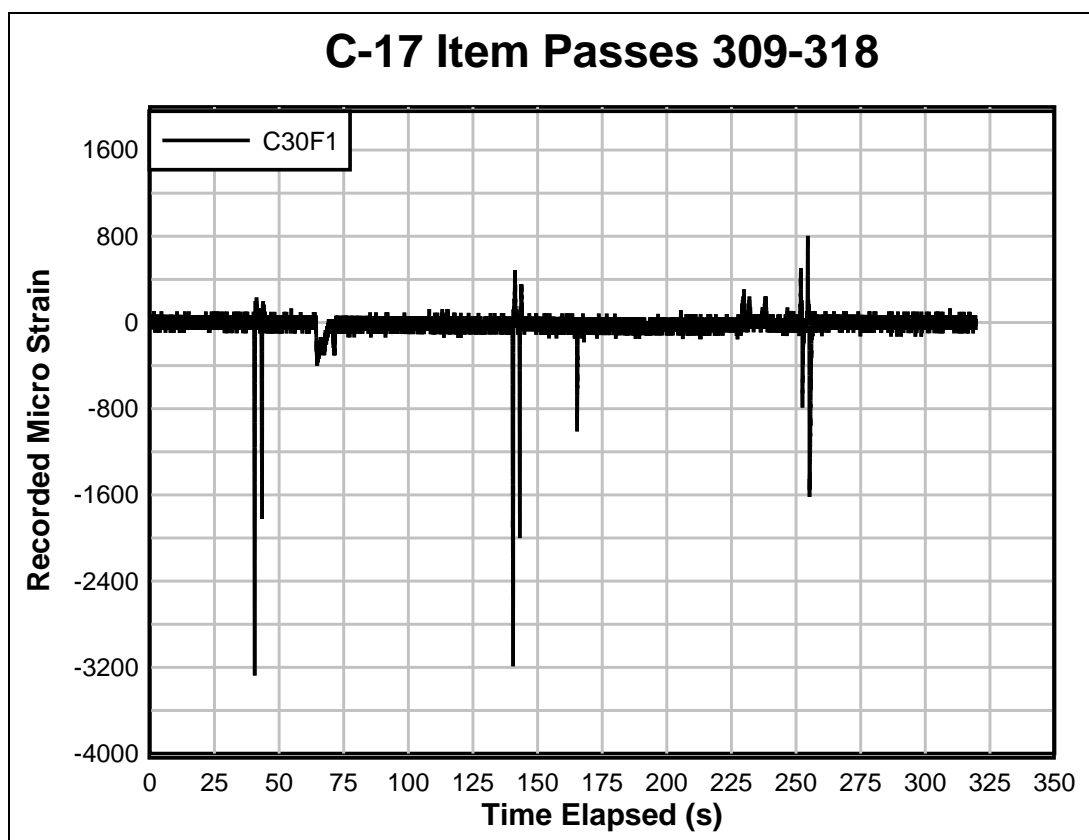


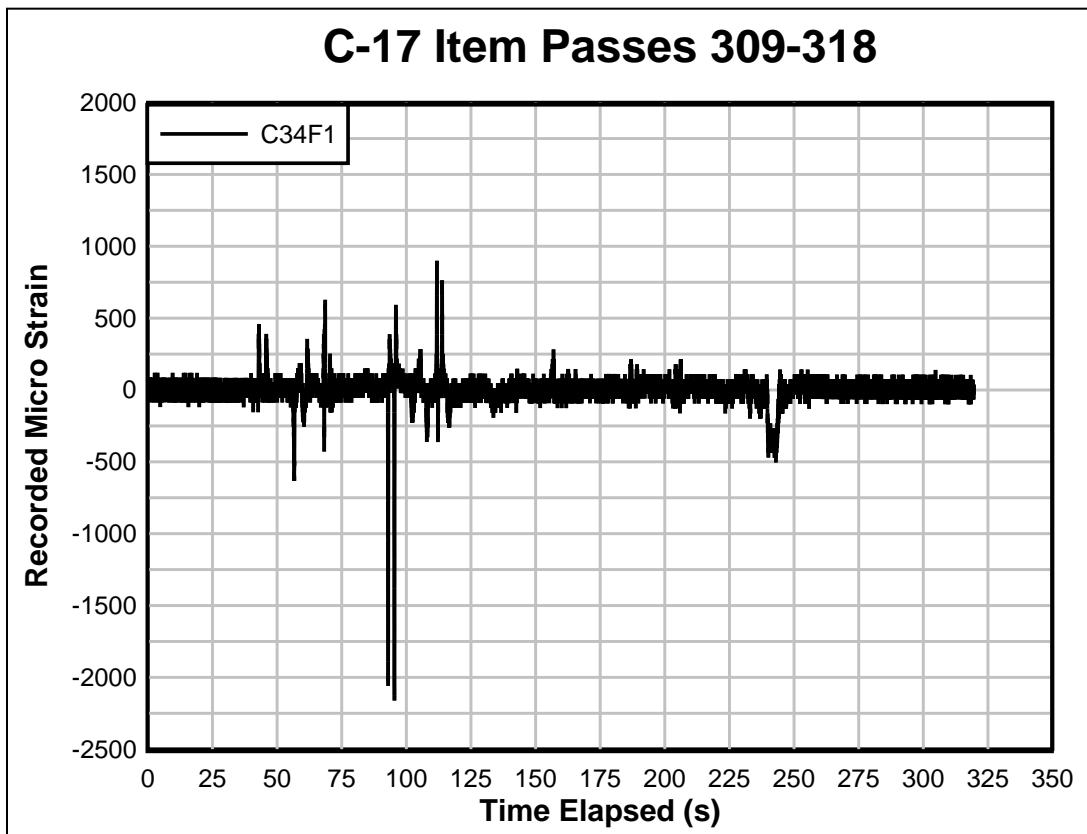
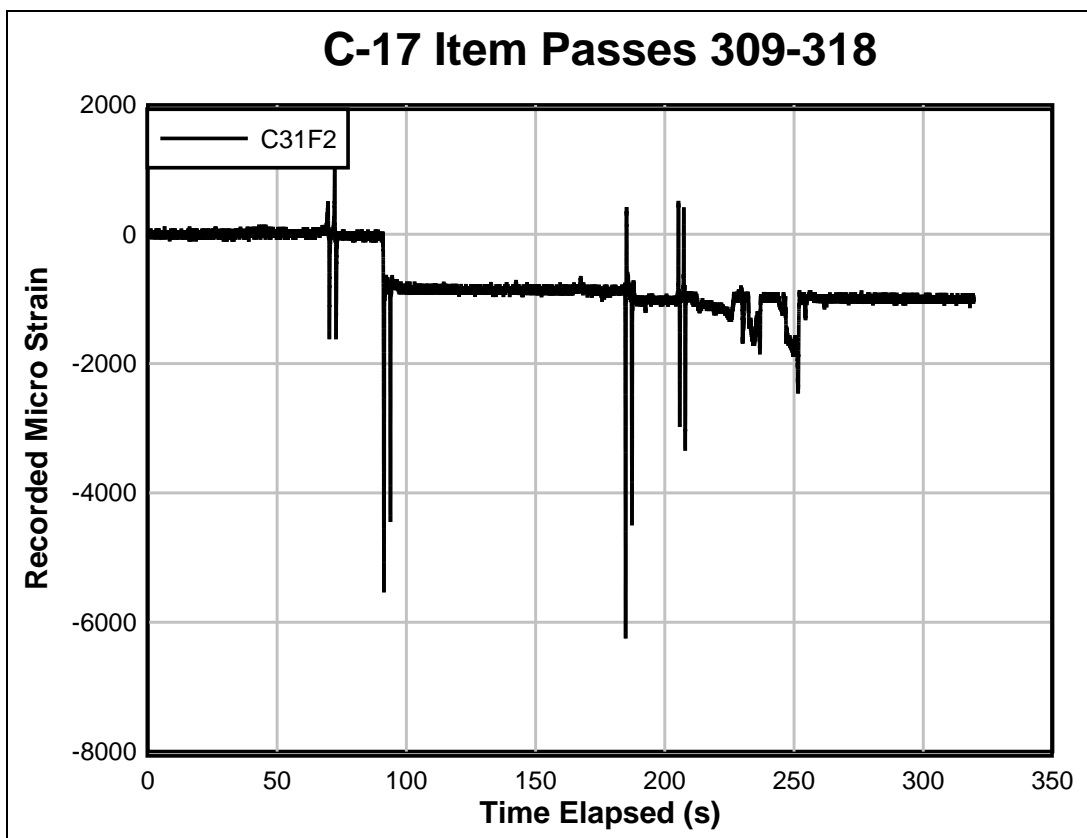


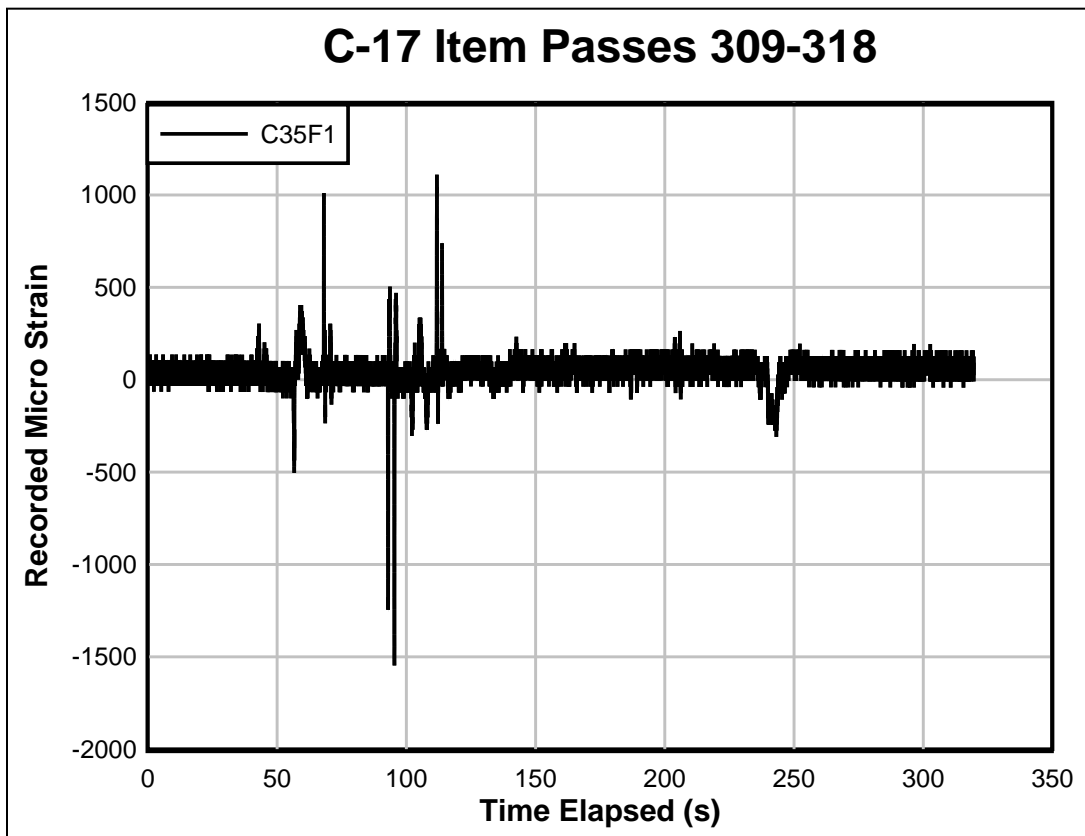
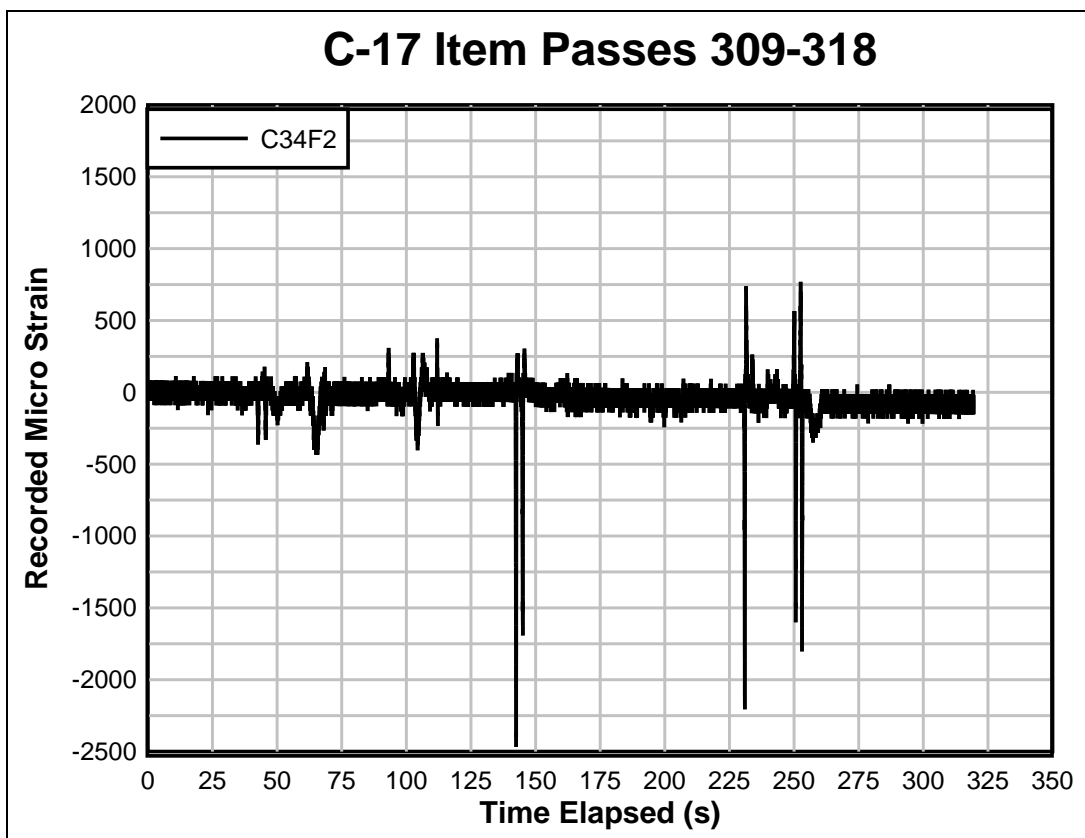


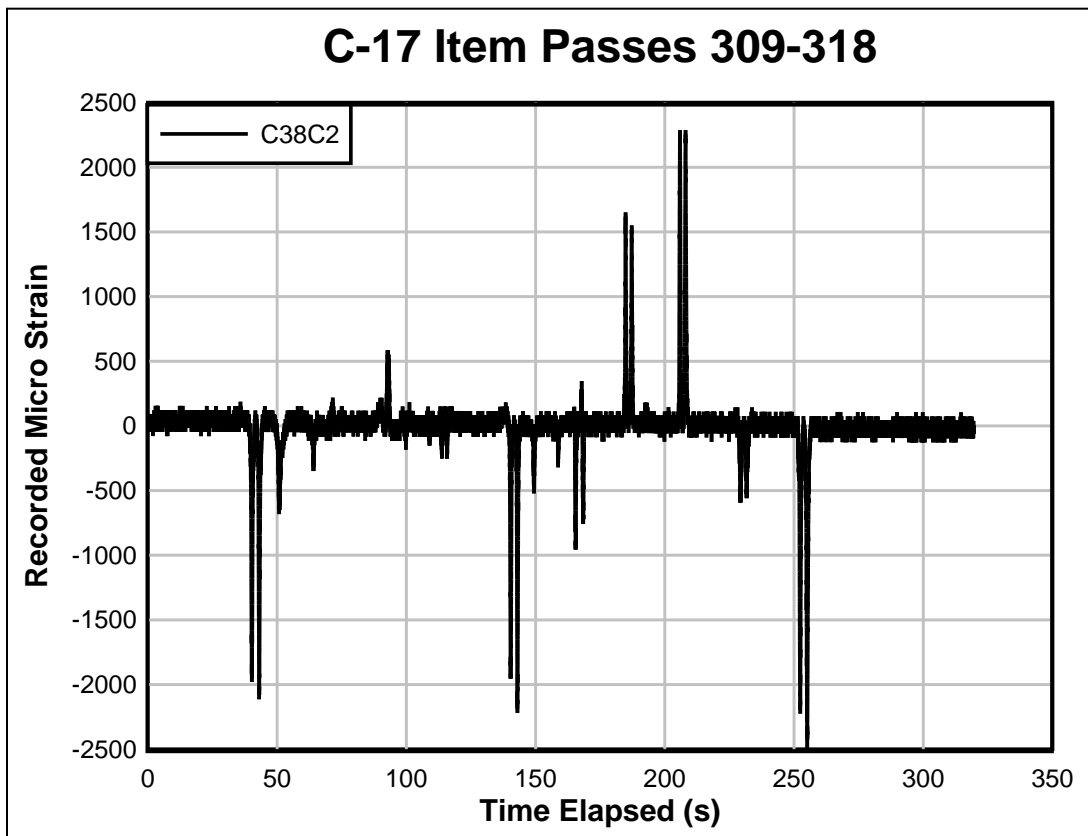
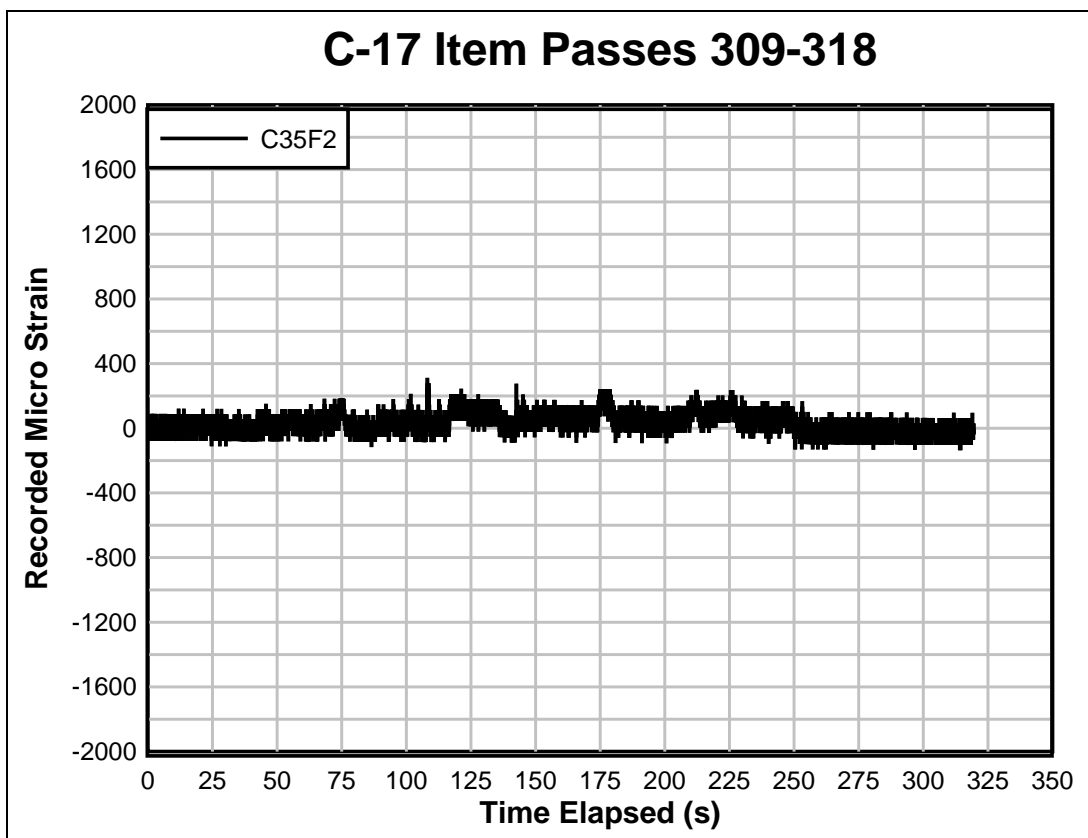


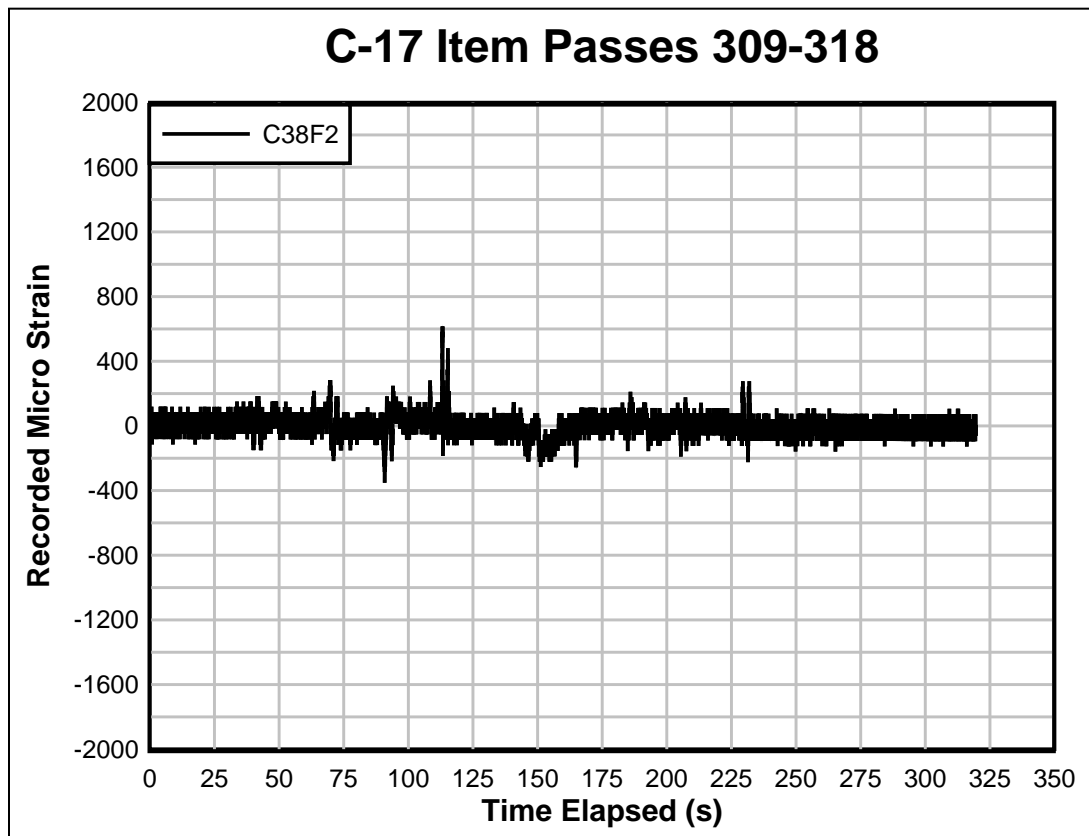
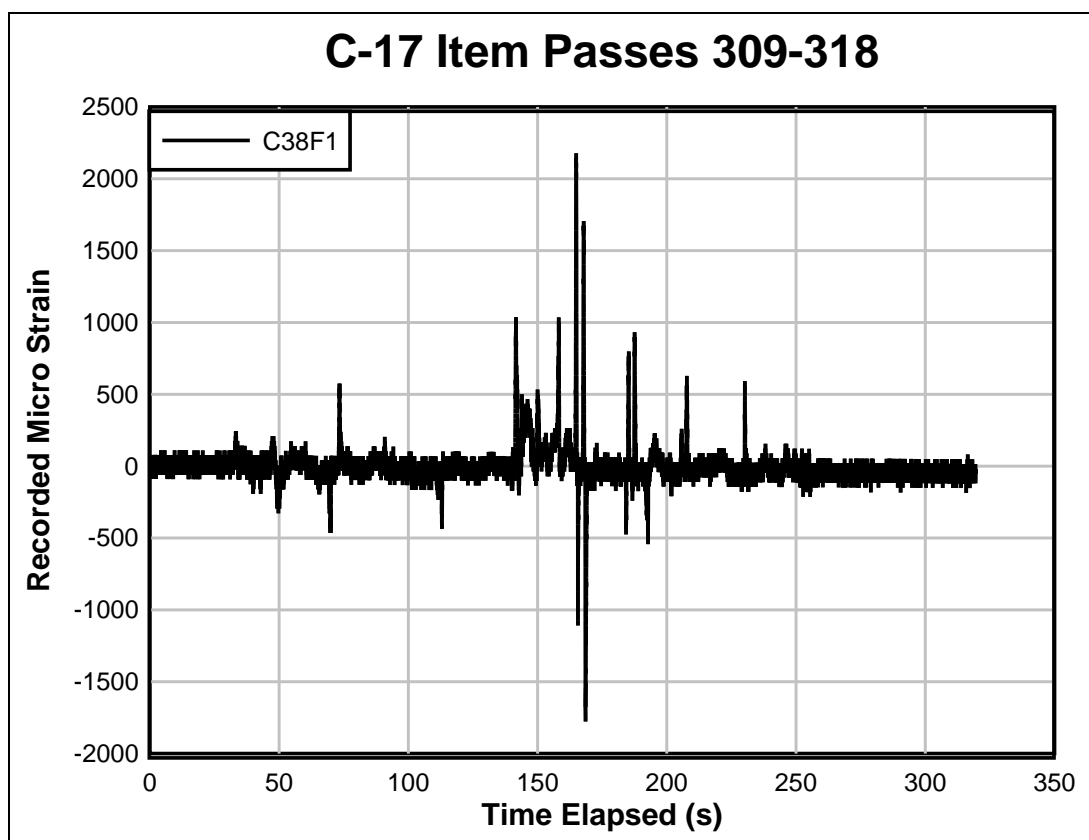


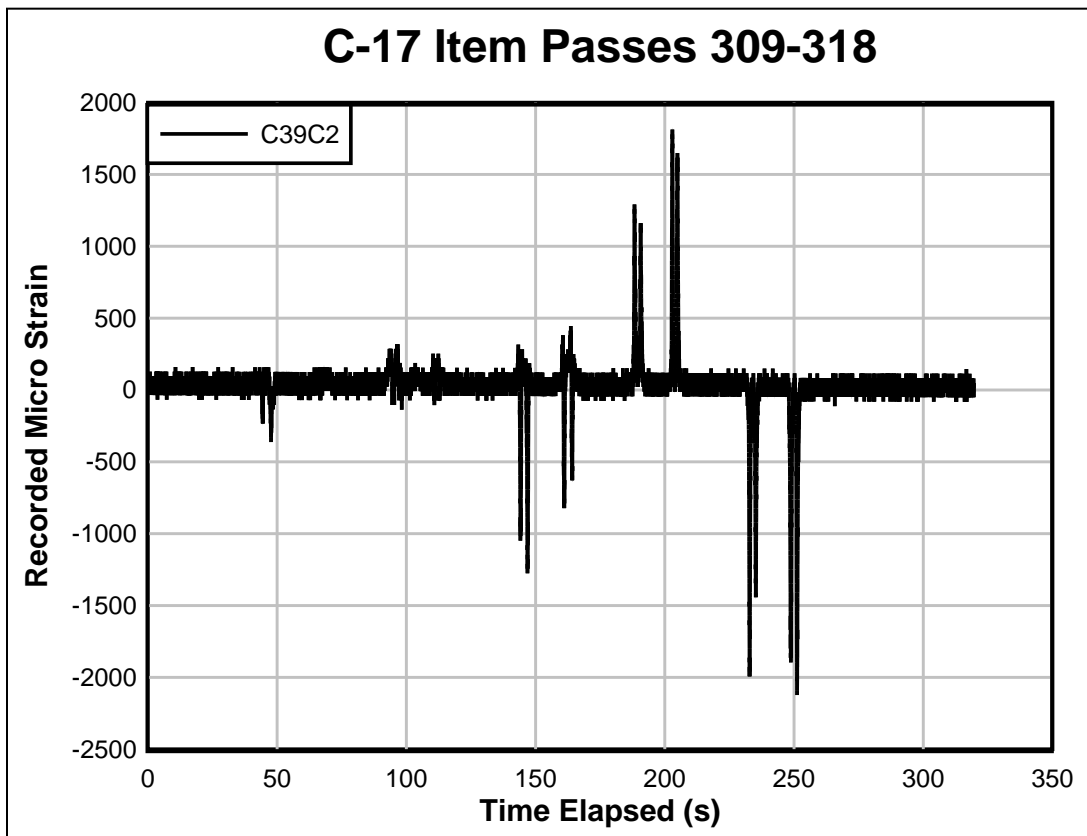
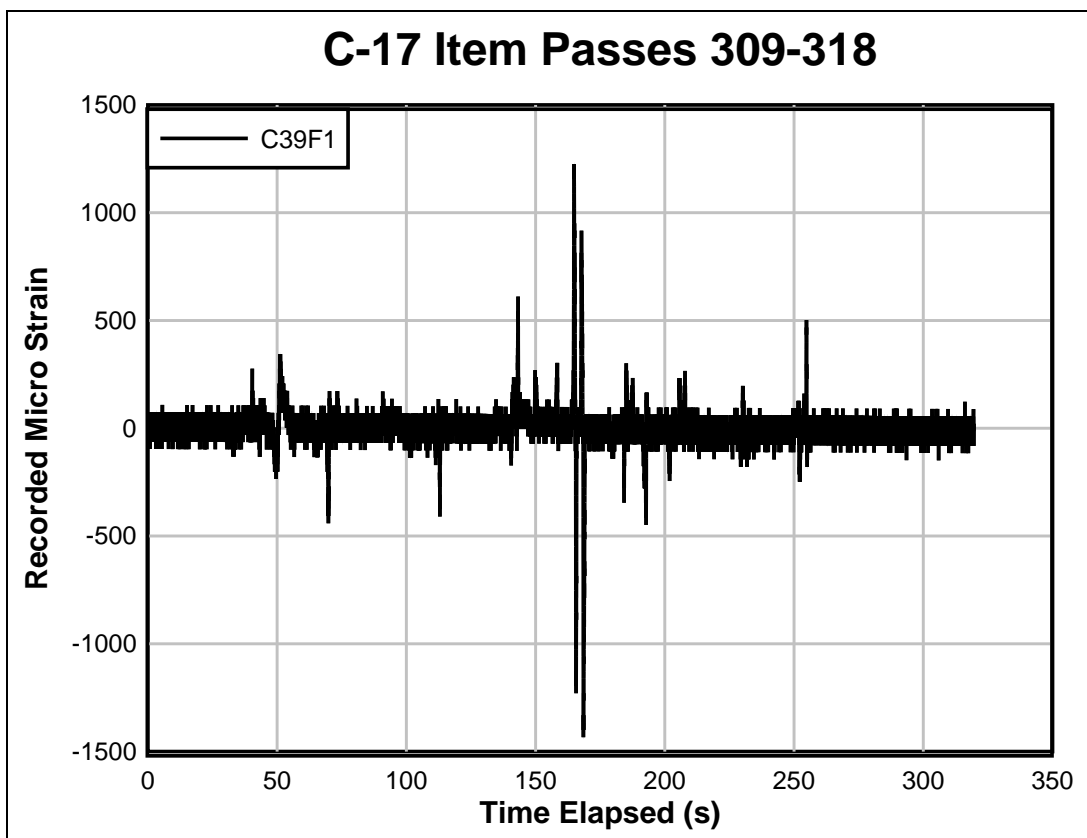


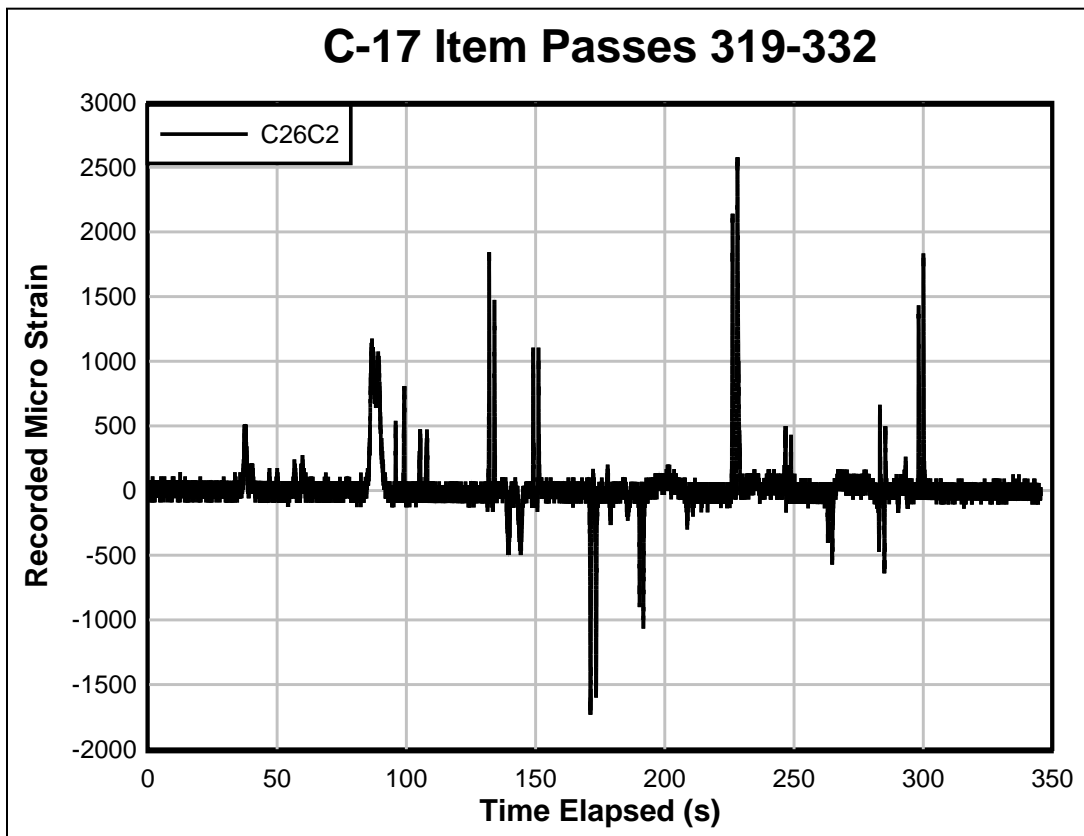
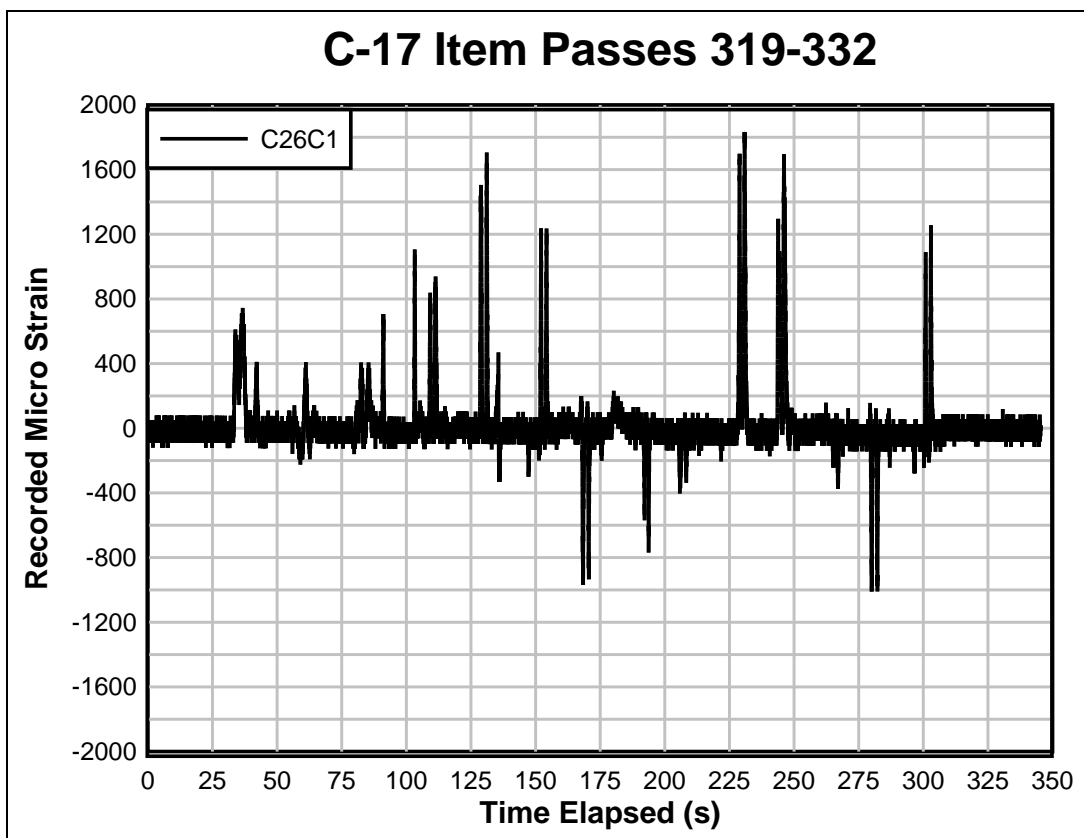


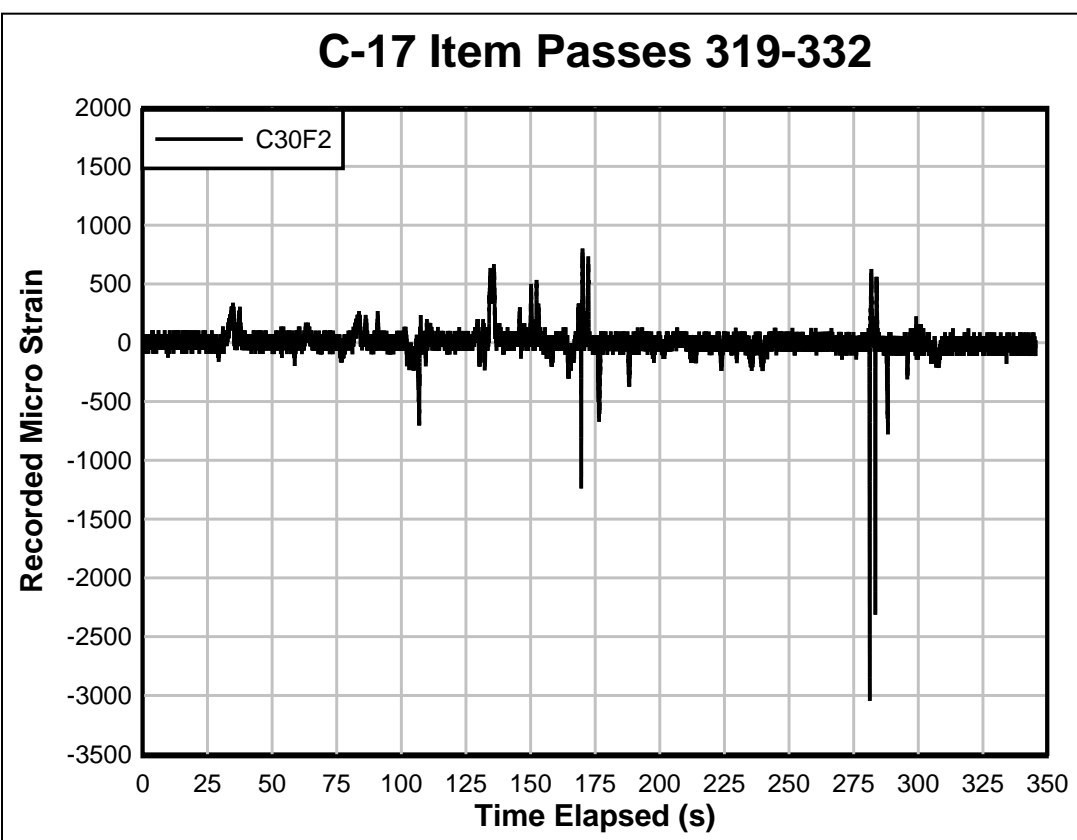
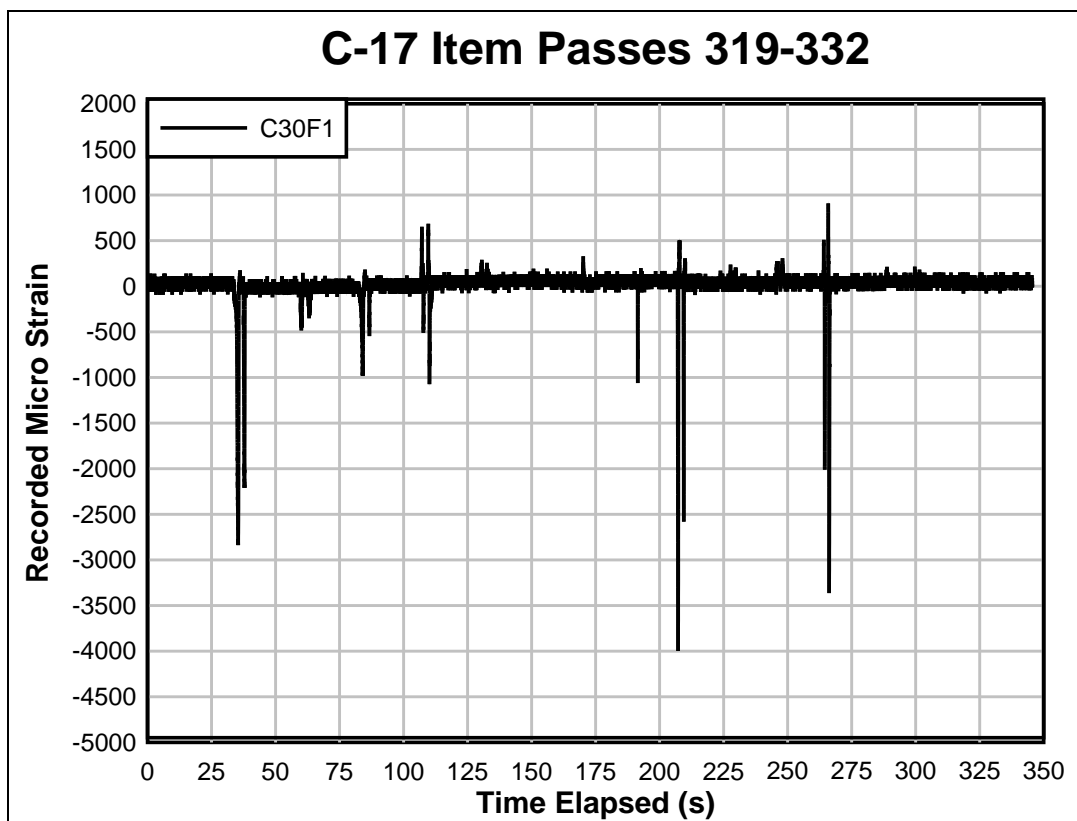


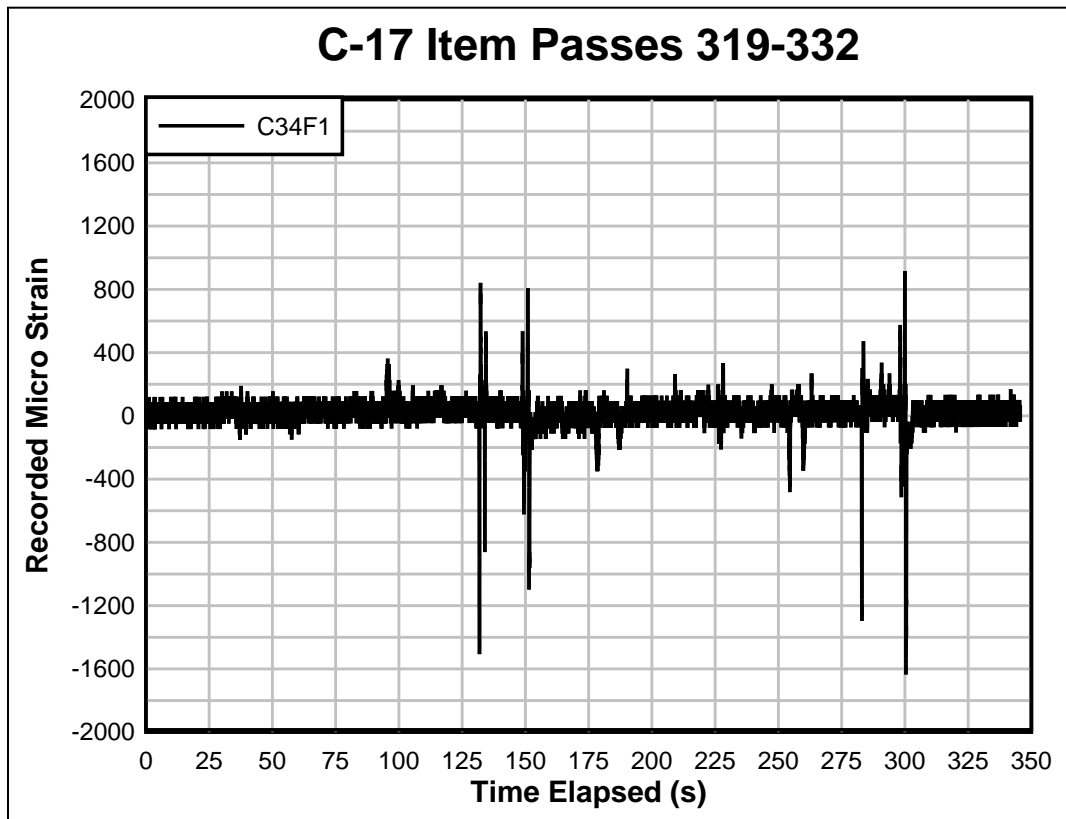
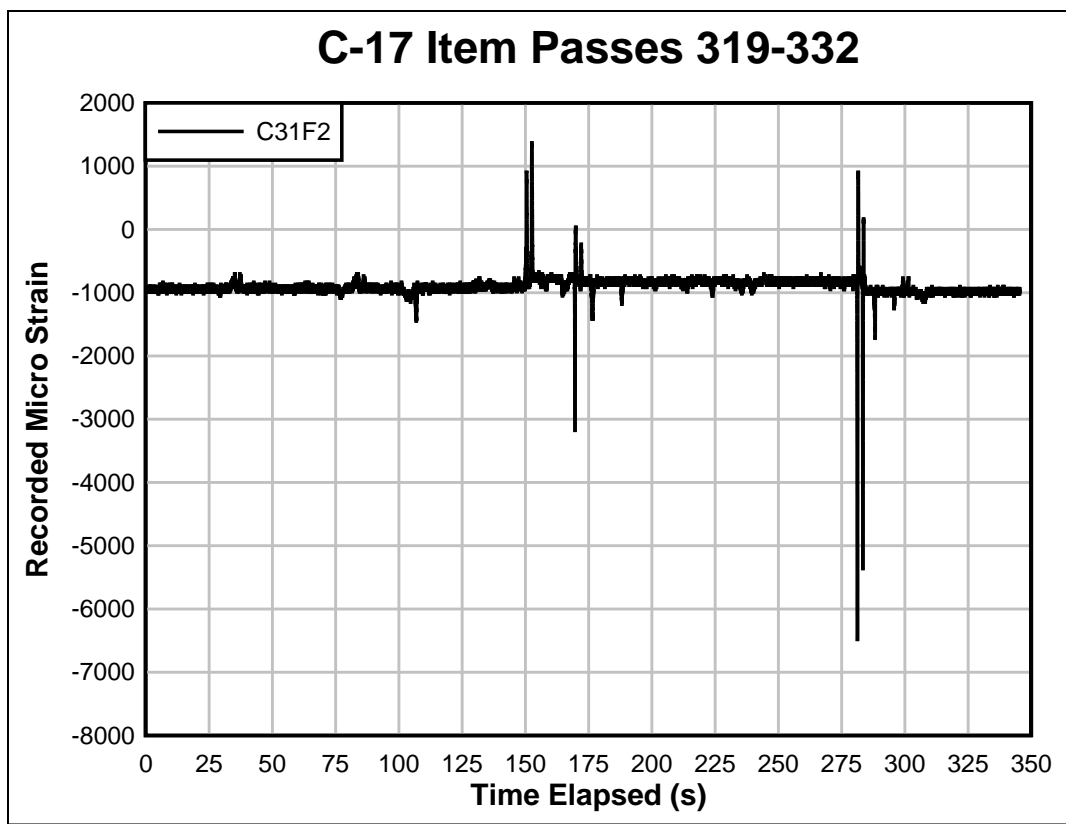


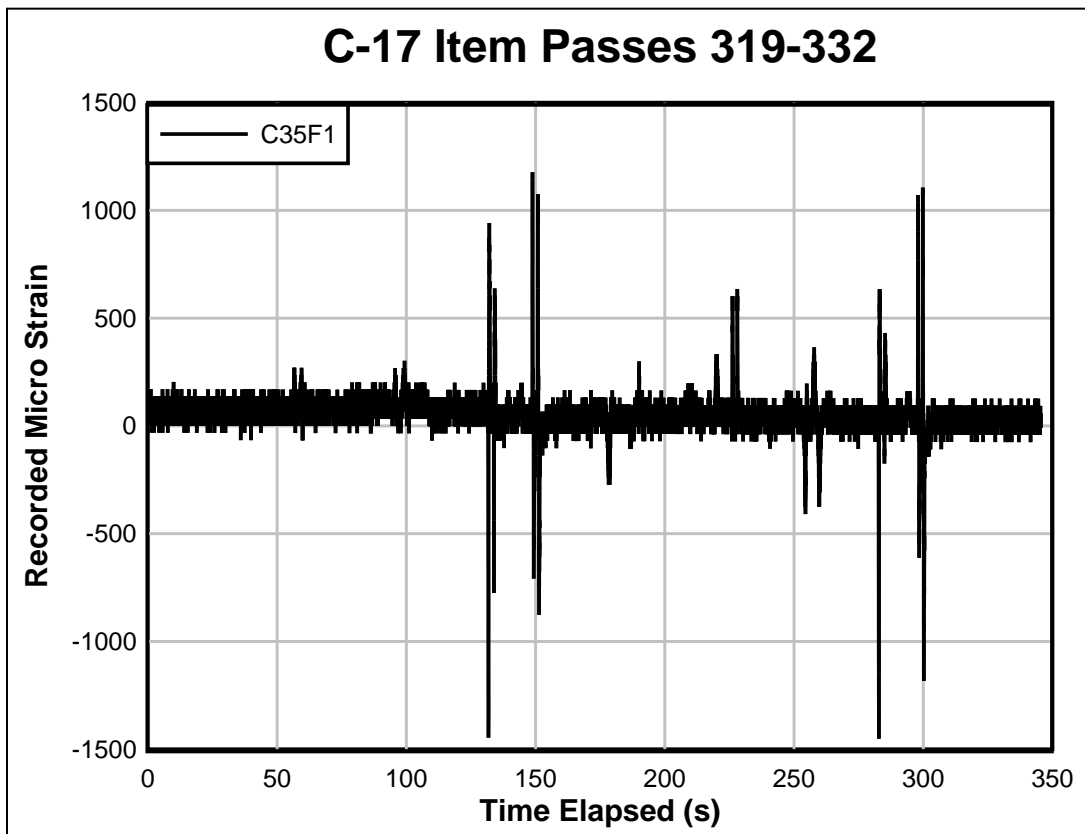
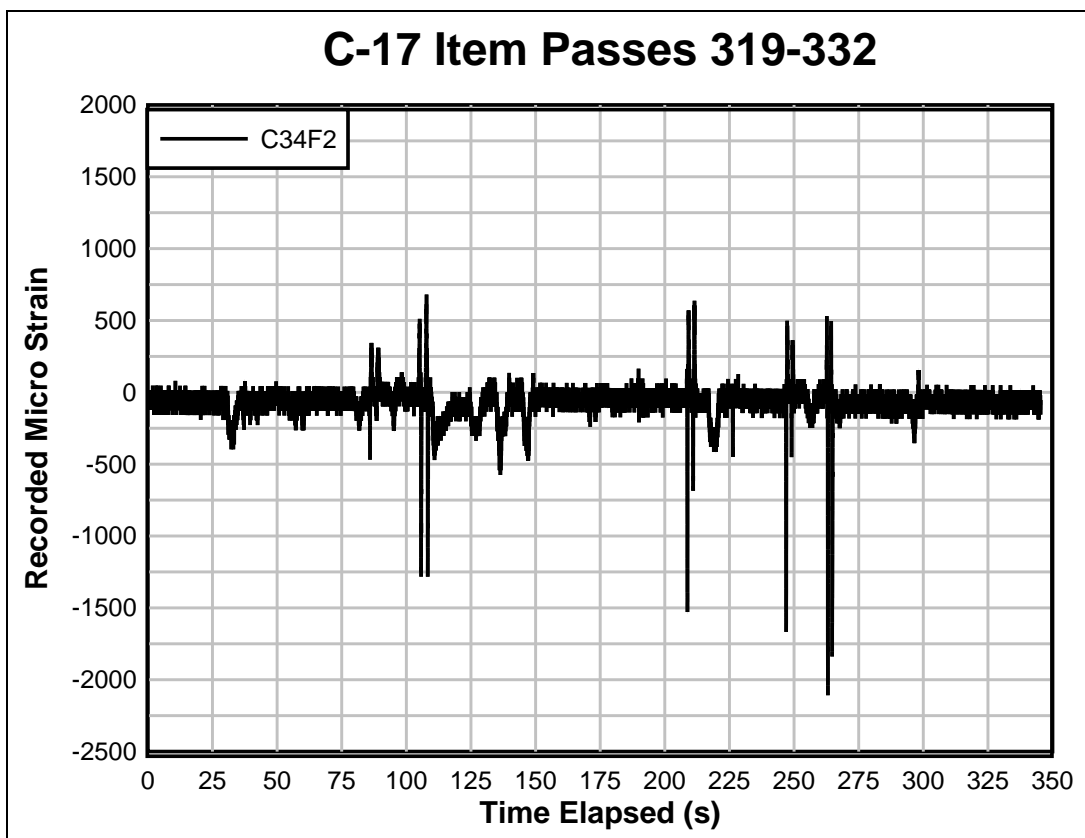


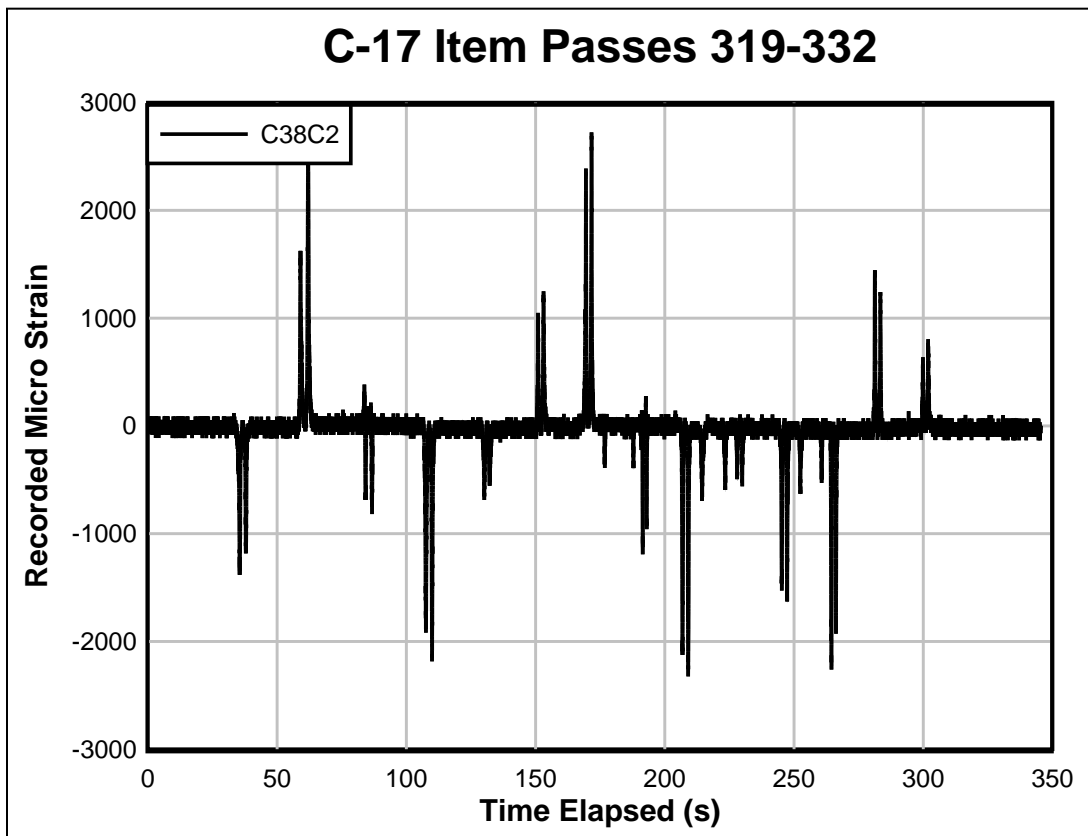
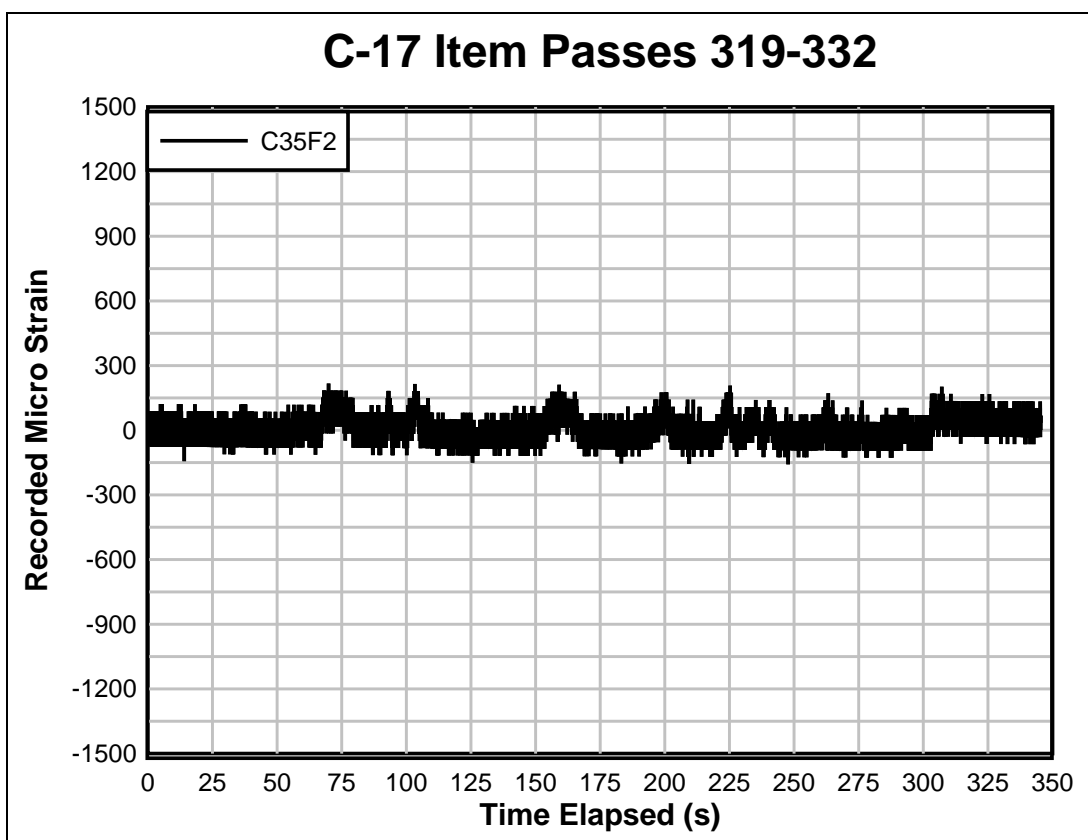


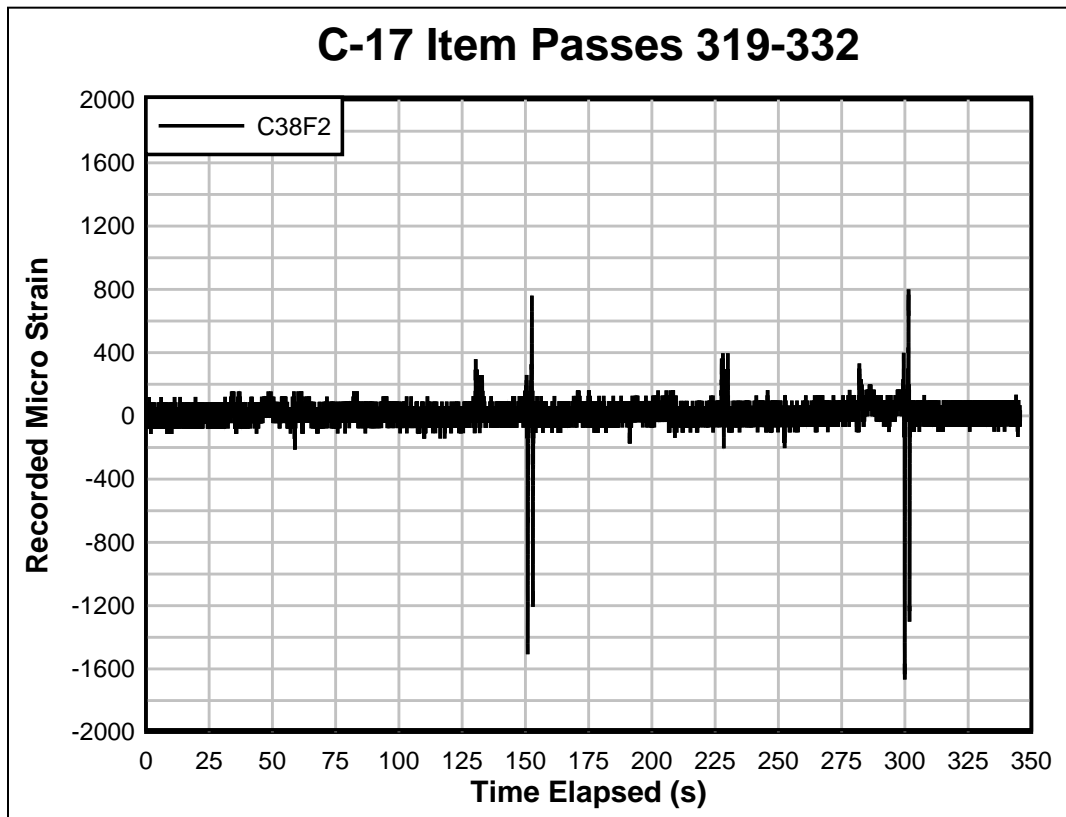
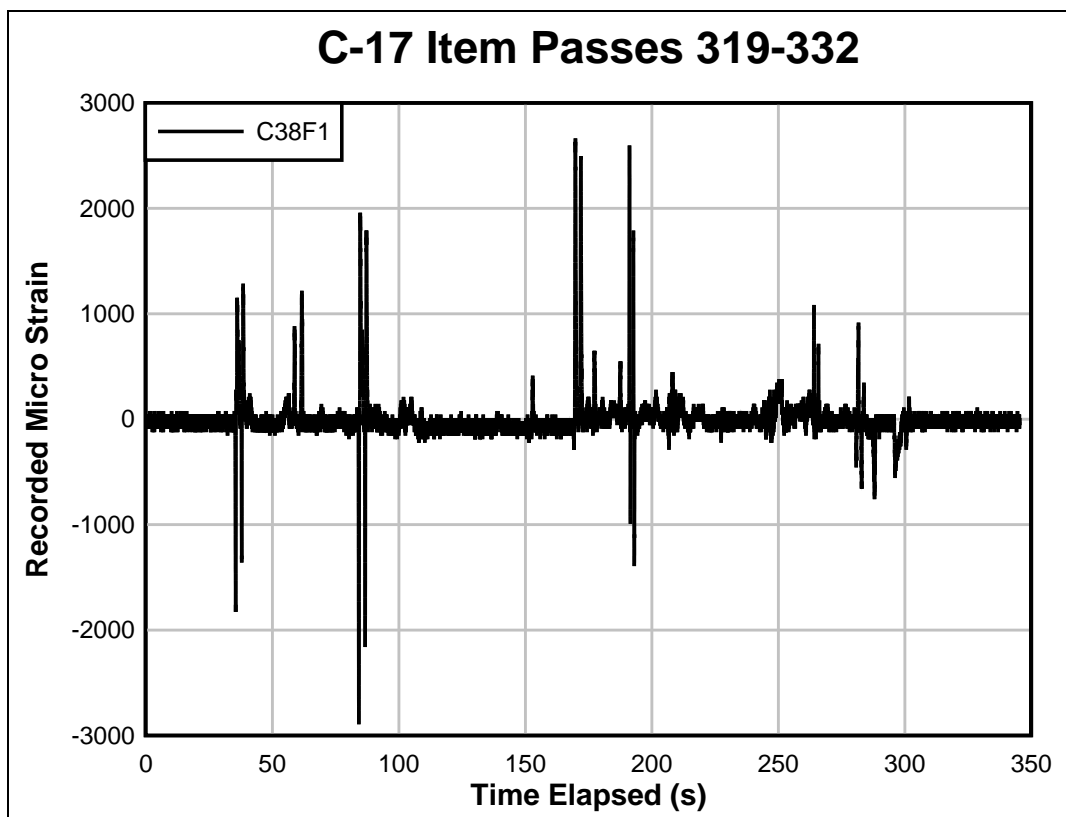


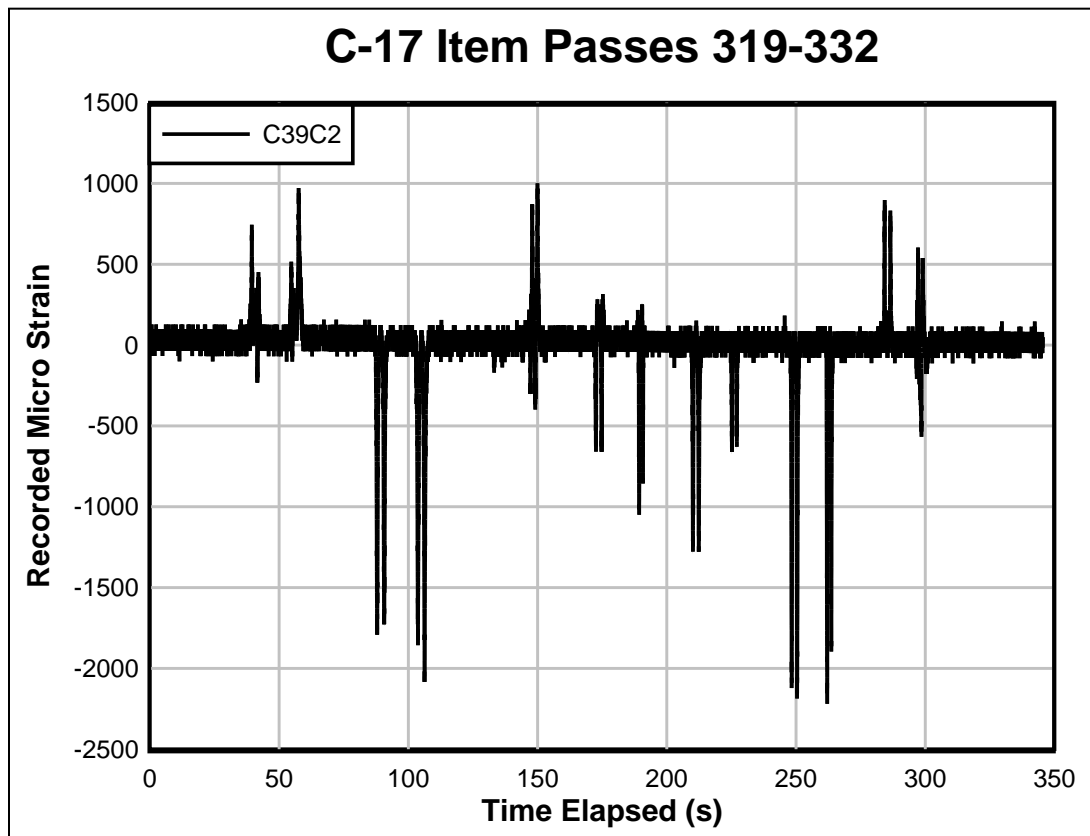
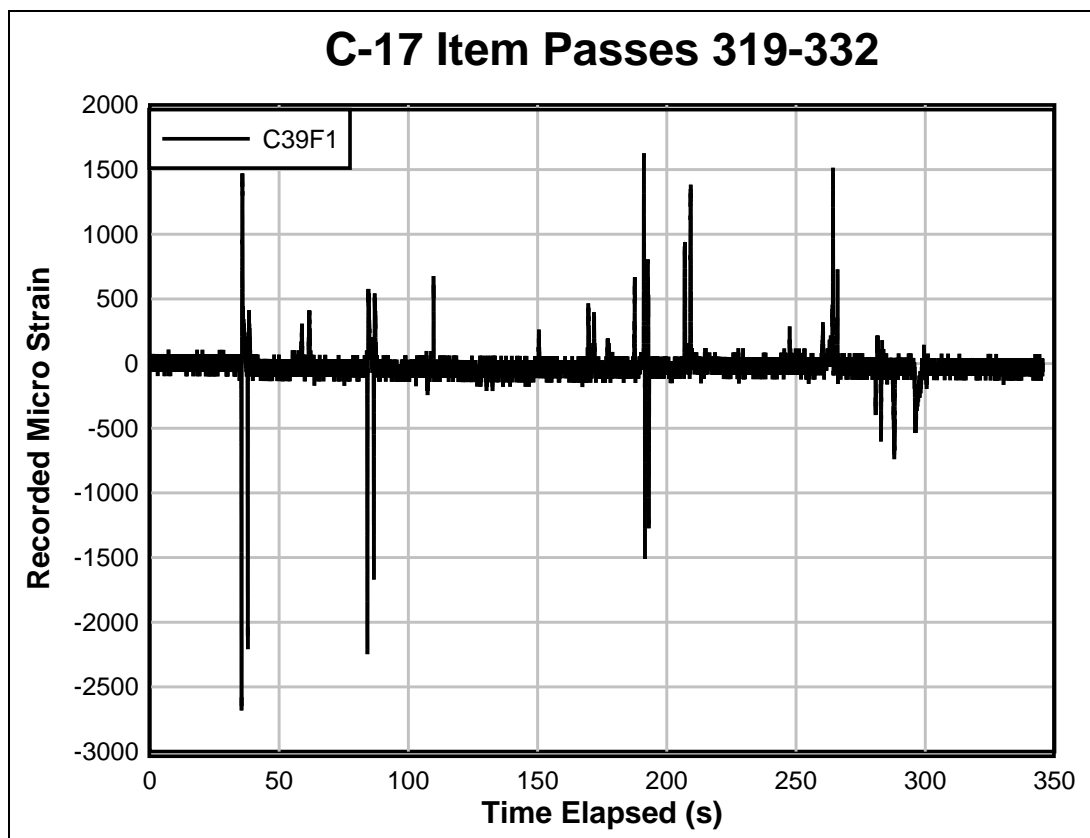


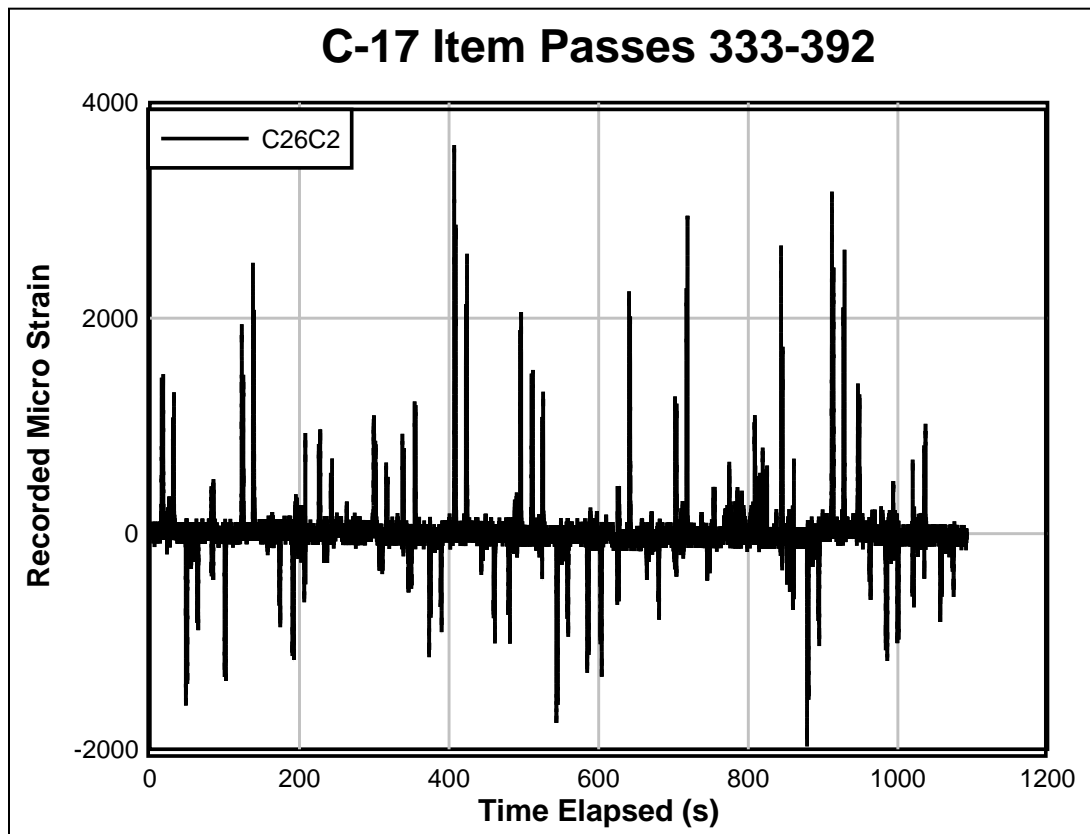
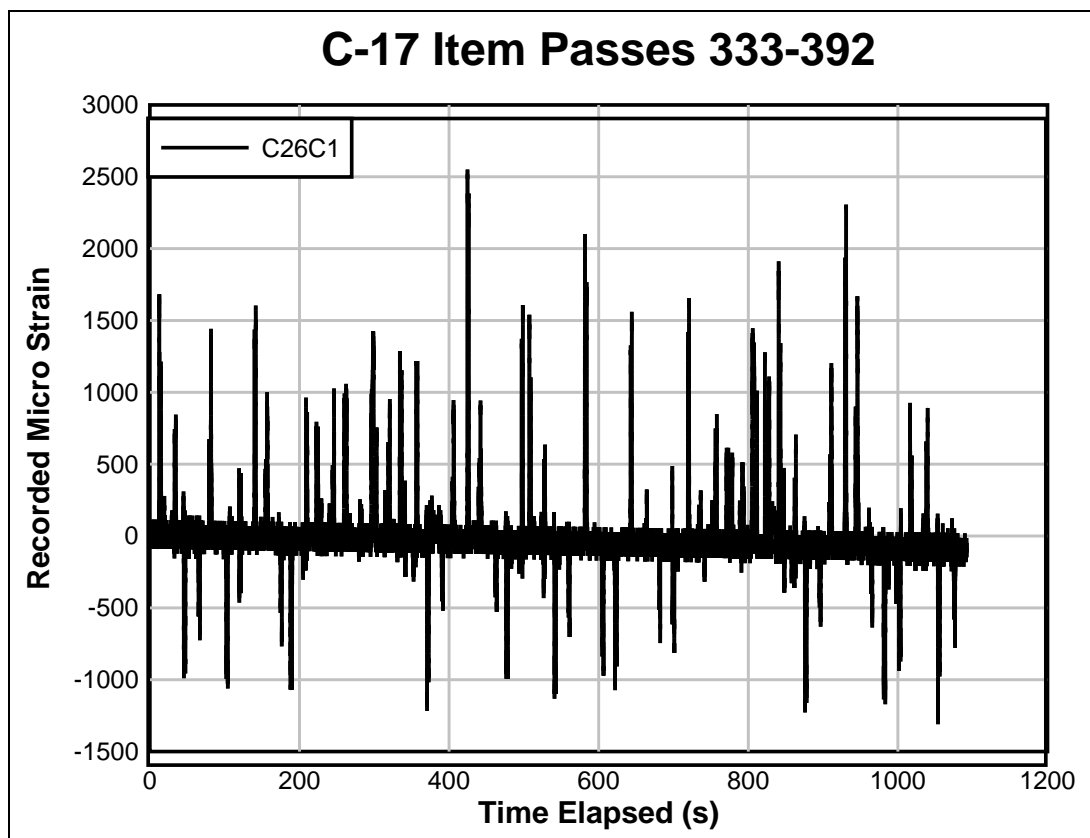


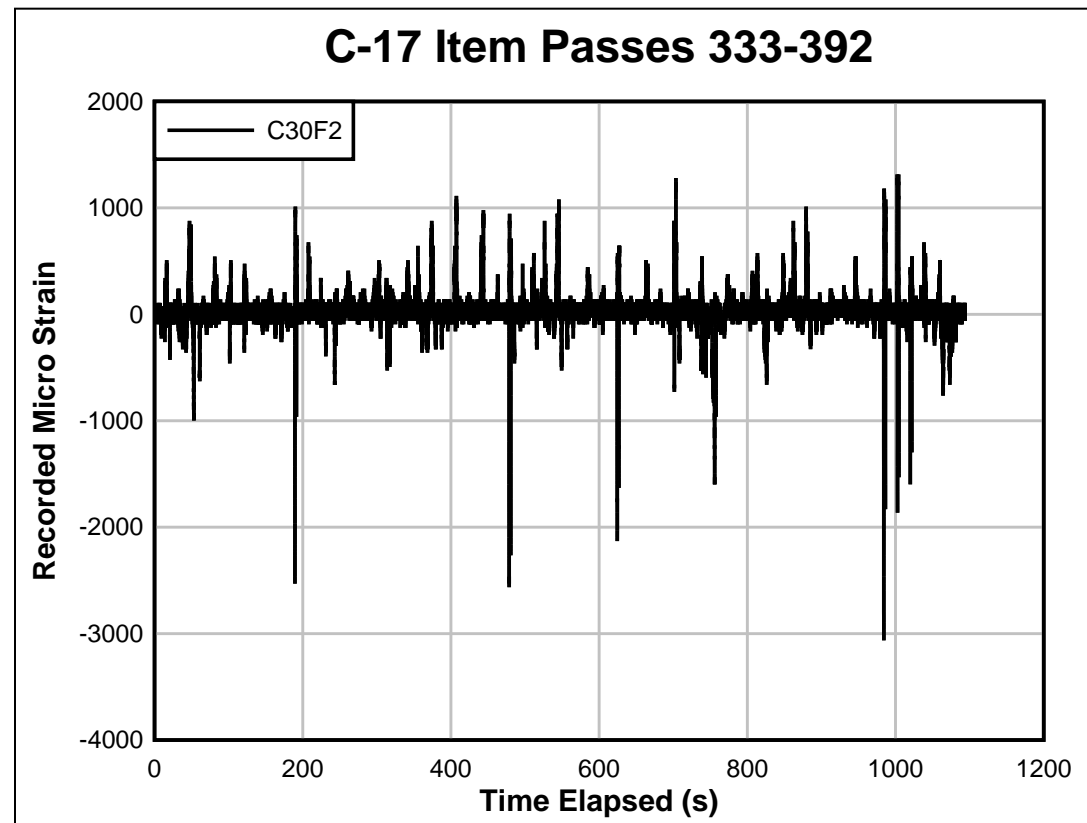
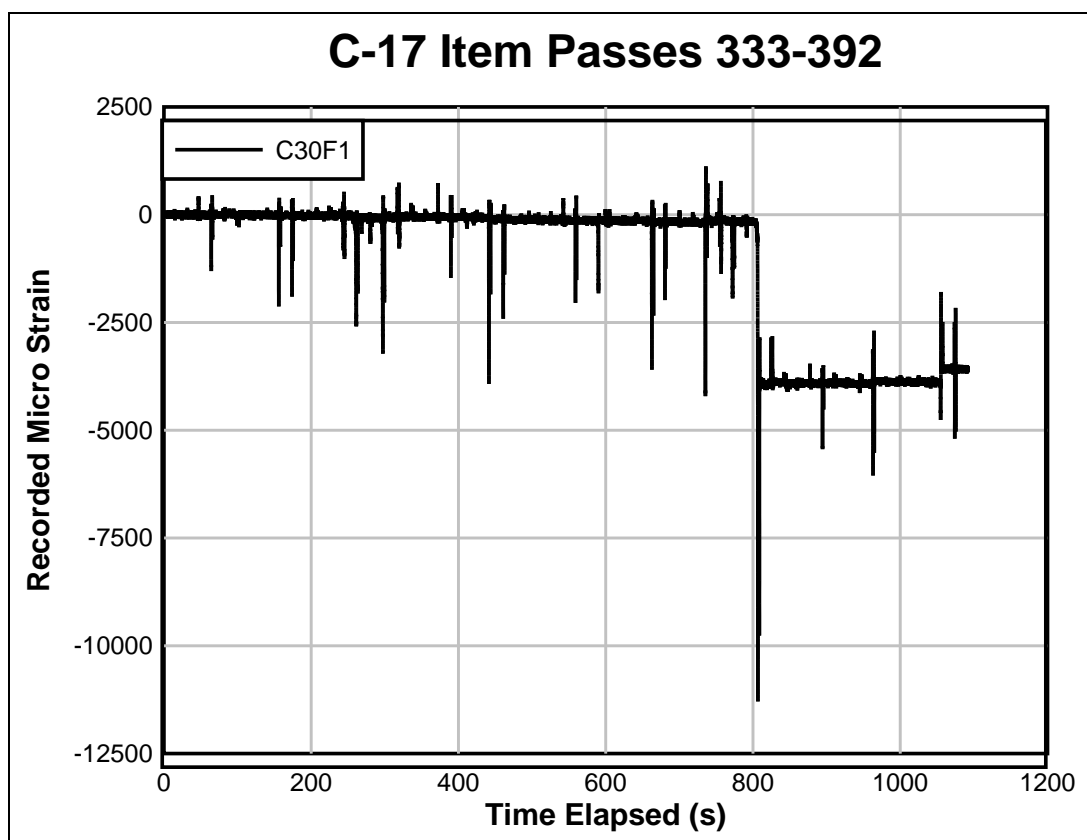


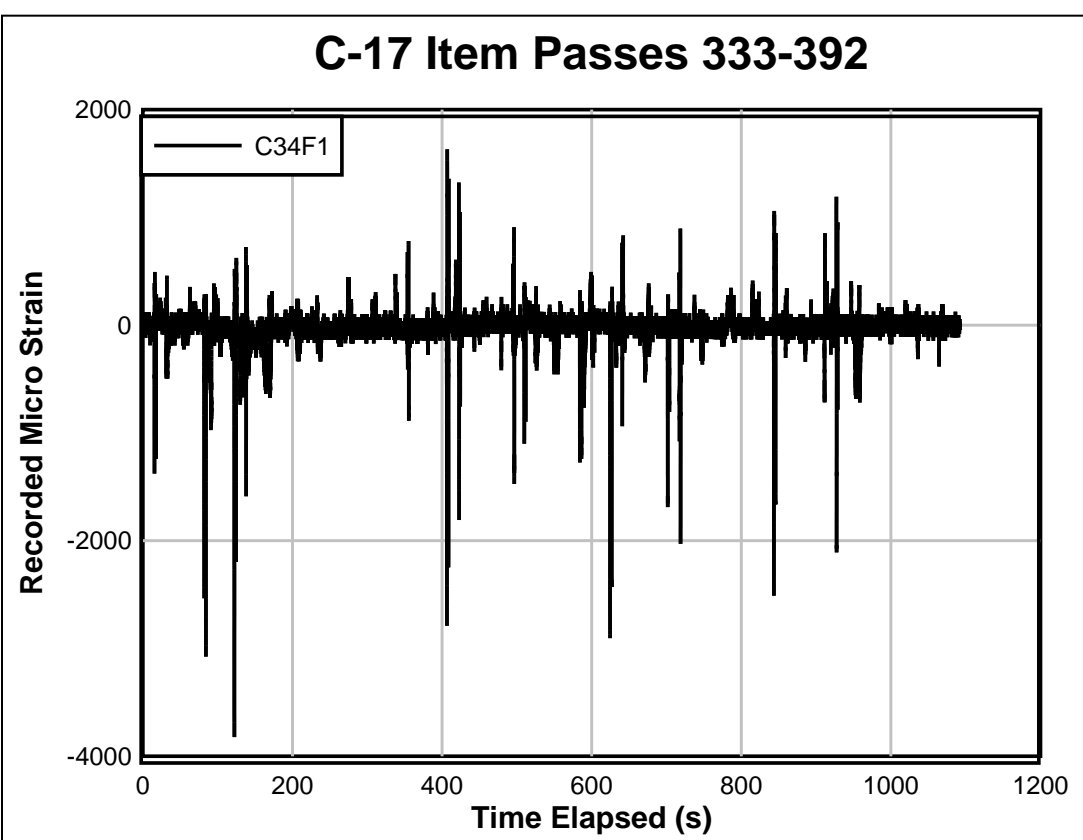
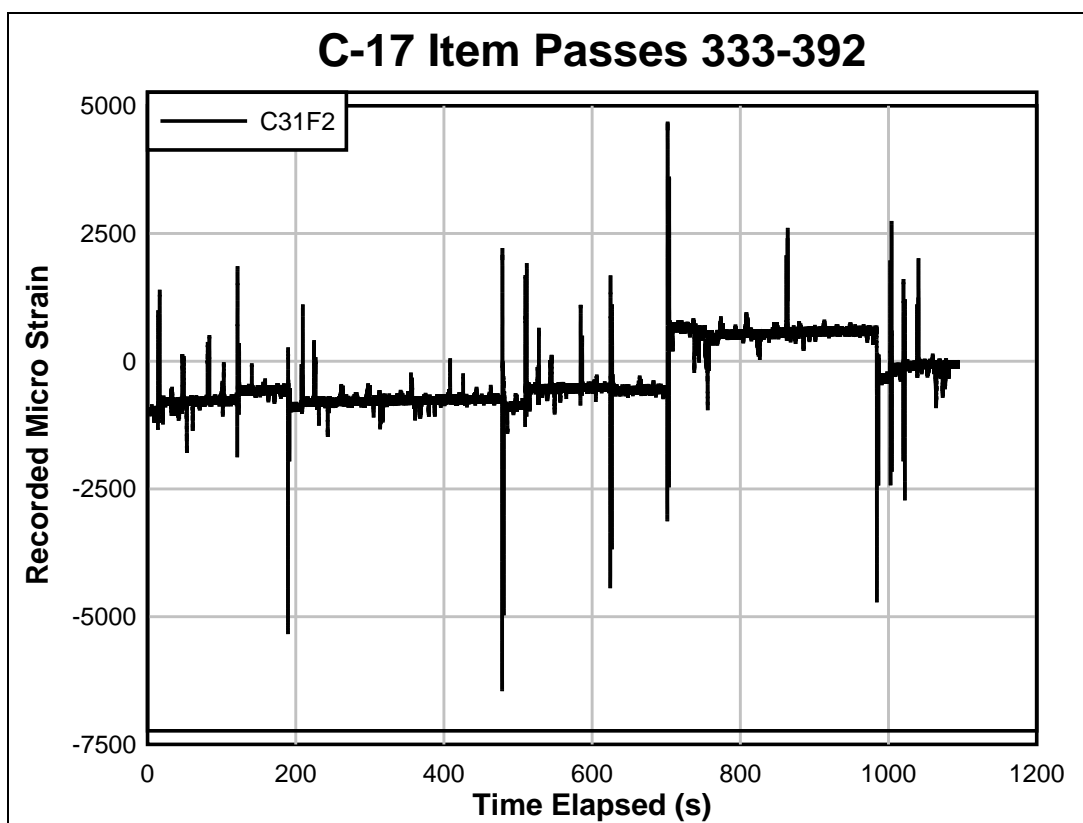


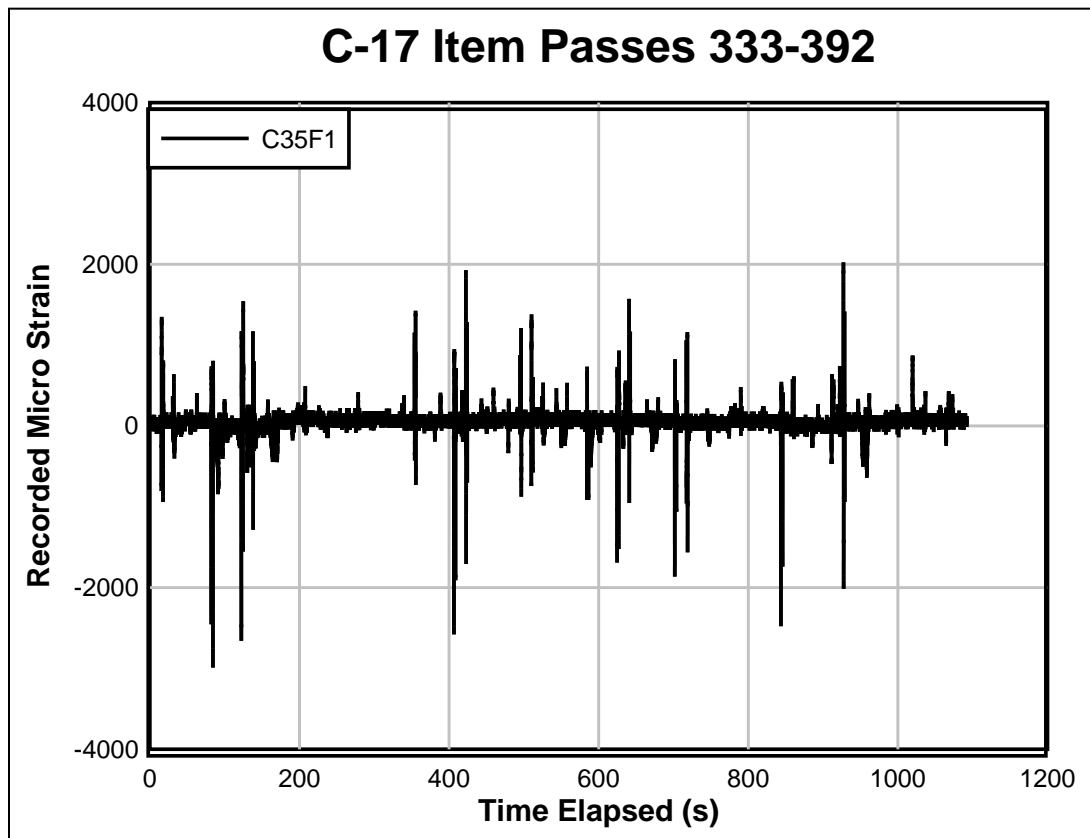
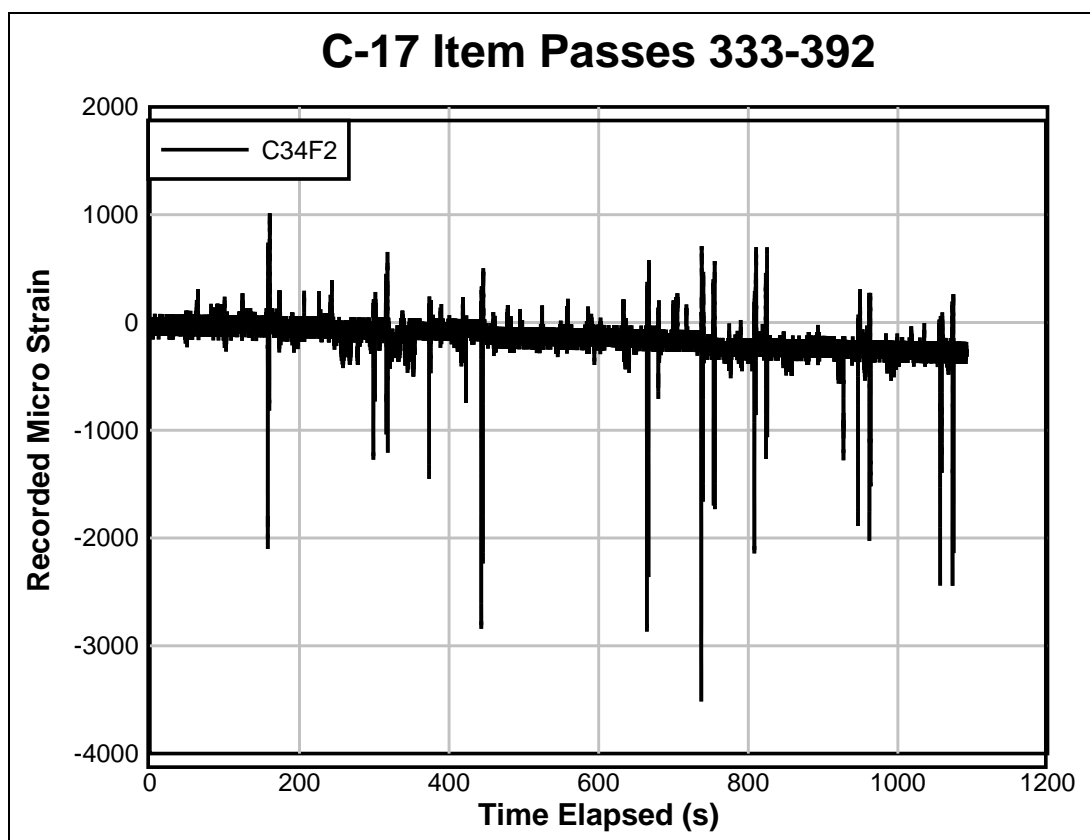


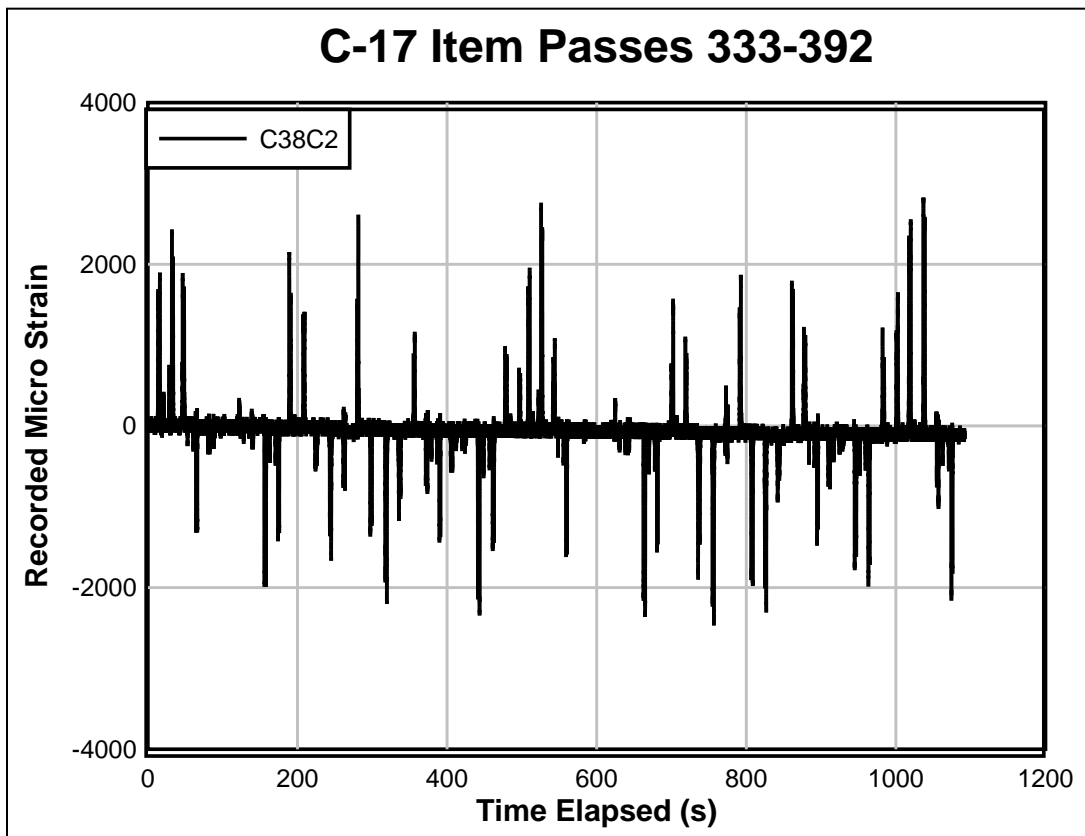
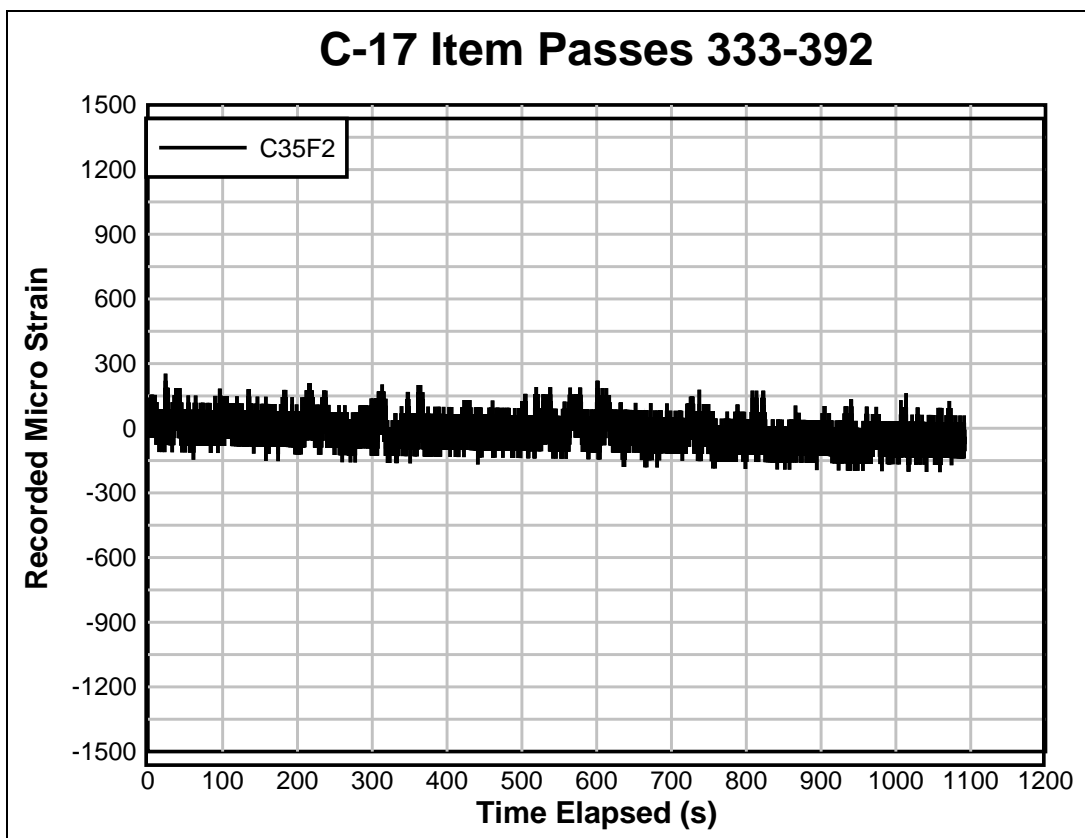


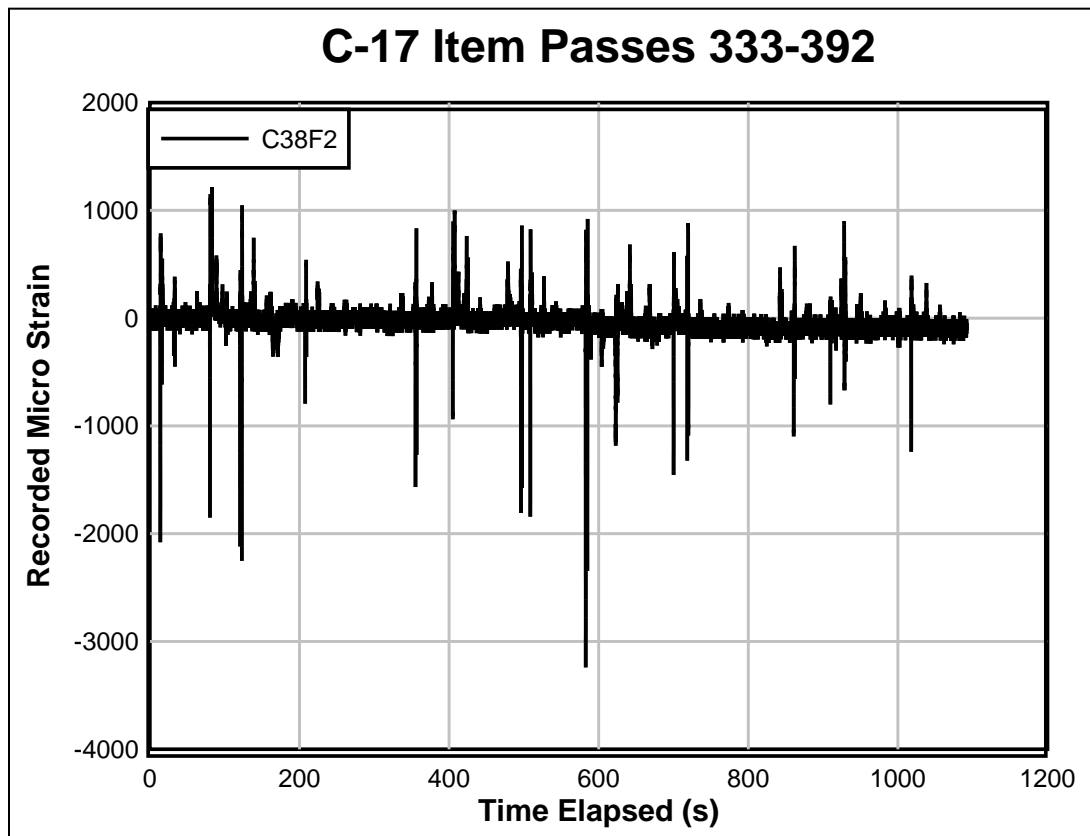
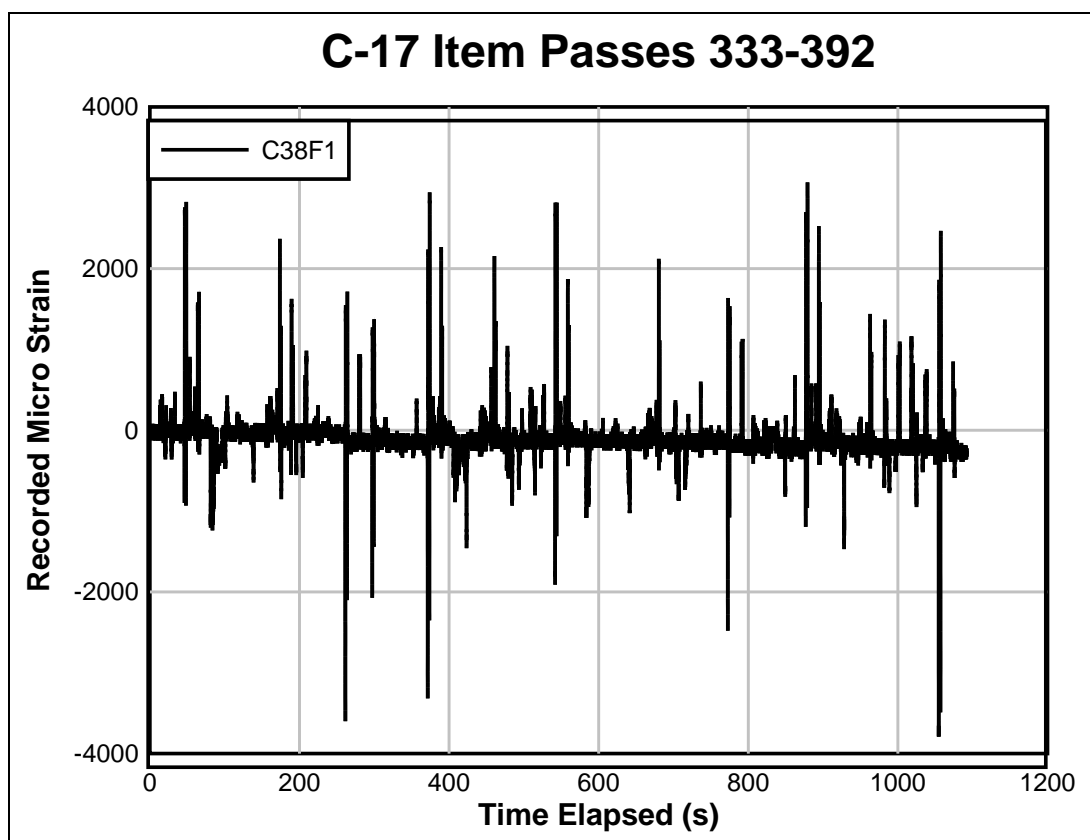


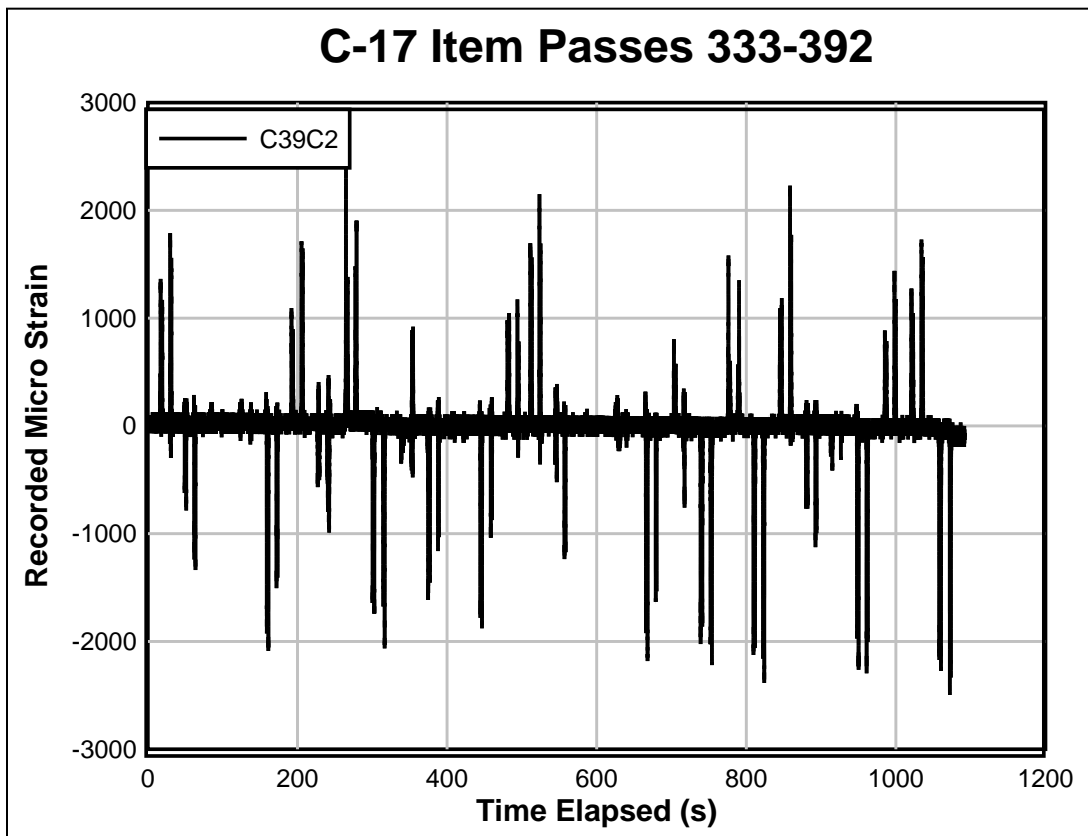
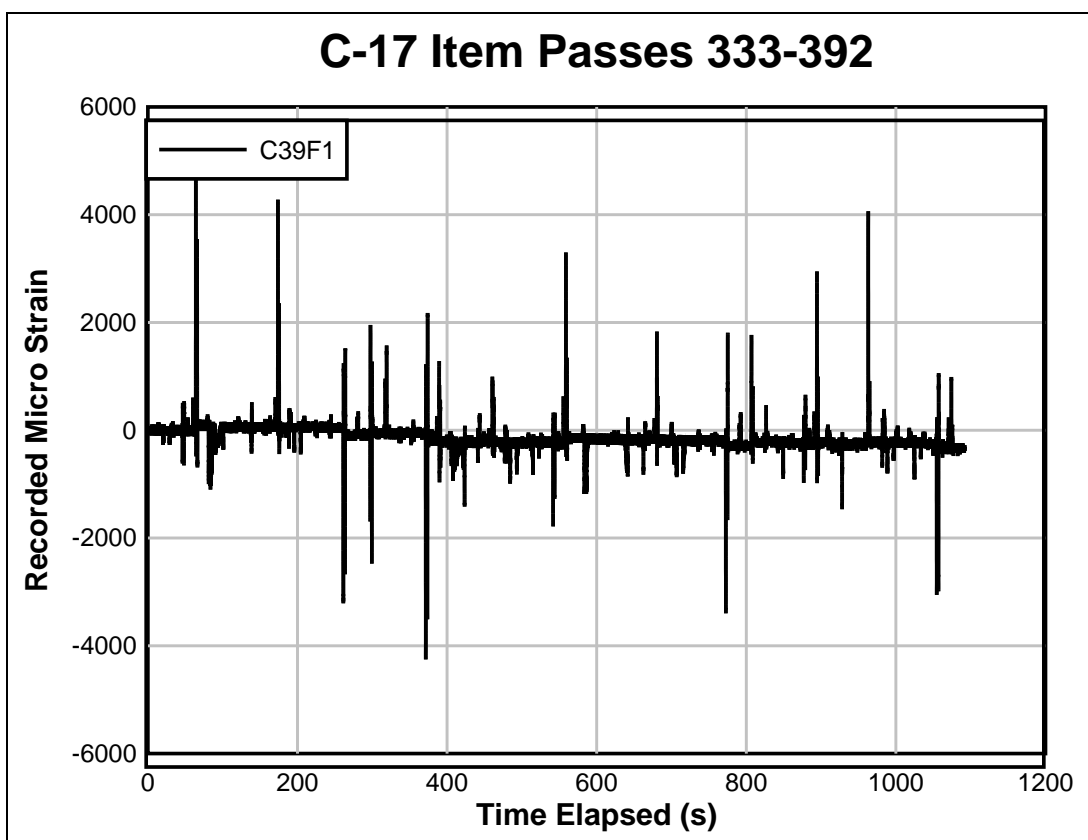












REPORT DOCUMENTATION PAGE

Form Approved
OMB No. 0704-0188

Public reporting burden for this collection of information is estimated to average 1 hour per response, including the time for reviewing instructions, searching existing data sources, gathering and maintaining the data needed, and completing and reviewing this collection of information. Send comments regarding this burden estimate or any other aspect of this collection of information, including suggestions for reducing this burden to Department of Defense, Washington Headquarters Services, Directorate for Information Operations and Reports (0704-0188), 1215 Jefferson Davis Highway, Suite 1204, Arlington, VA 22202-4302. Respondents should be aware that notwithstanding any other provision of law, no person shall be subject to any penalty for failing to comply with a collection of information if it does not display a currently valid OMB control number. PLEASE DO NOT RETURN YOUR FORM TO THE ABOVE ADDRESS.

1. REPORT DATE (DD-MM-YYYY) June 2015		2. REPORT TYPE Final		3. DATES COVERED (From - To)	
4. TITLE AND SUBTITLE AM2 Opposite Lay Evaluation				5a. CONTRACT NUMBER	
				5b. GRANT NUMBER	
				5c. PROGRAM ELEMENT NUMBER	
6. AUTHOR(S) Lyan Garcia, Wipawi Vanadit-Ellis, Timothy W. Rushing, Jeb S. Tingle, and Craig A. Rutland				5d. PROJECT NUMBER	
				5e. TASK NUMBER	
				5f. WORK UNIT NUMBER	
7. PERFORMING ORGANIZATION NAME(S) AND ADDRESS(ES) Geotechnical and Structures Laboratory U.S. Army Engineer Research and Development Center 3909 Halls Ferry Road Vicksburg, MS 39180-6199				8. PERFORMING ORGANIZATION REPORT NUMBER ERDC/GSL TR-15-14	
9. SPONSORING / MONITORING AGENCY NAME(S) AND ADDRESS(ES) Headquarters, Air Force Civil Engineering Center Tyndall Air Force Base, FL 32403-5319				10. SPONSOR/MONITOR'S ACRONYM(S) HQ-AFCEC	
				11. SPONSOR/MONITOR'S REPORT NUMBER(S)	
12. DISTRIBUTION / AVAILABILITY STATEMENT Approved for public release; distribution is unlimited.					
13. SUPPLEMENTARY NOTES					
14. ABSTRACT AM2 airfield matting has a long history of successful performance as an expeditionary airfield surfacing system. It has been used to form runways, vertical takeoff and landing pads, taxiways, and aircraft parking areas. A test program was initiated by the Naval Air Systems Command to evaluate and identify optimal AM2 lay patterns under different traffic conditions, and to validate a Dynamic Interface Model by feeding it mat breakage, deformation, and recorded strain data. The testing efforts discussed in this report focused on understanding the performance of AM2 when installed in the brickwork pattern on a weak subgrade and trafficked in a direction perpendicular to typical traffic operations. The mat test section was subjected to simulated F-15E and C-17 traffic until predetermined failure criteria were reached. The system became highly unstable after a limited number of F-15E and C-17 passes. Test results and discussions related to the stability of the system and structural integrity of the mat panels during traffic are provided.					
15. SUBJECT TERMS Mat AM2		Landing Mat Aluminum Mat Airfield Mat		Airfield Damage Repair Expeditionary Airfield	
16. SECURITY CLASSIFICATION OF: a. REPORT Unclassified			17. LIMITATION OF ABSTRACT	18. NUMBER OF PAGES 236	19a. NAME OF RESPONSIBLE PERSON
b. ABSTRACT Unclassified					c. THIS PAGE Unclassified